Journal of ATMOSPHERIC and TERRESTRIAL PHYSICS

EDITORIAL ADVISORY BOARD

H. O. G. ALFVEN–STOCKHOLM · **J. BARTELS**–GÖTTINGEN · **W. J. G. BEYNON**–ABERYSTWYTH
P. M. S. BLACKETT–LONDON · **H. G. BOOKER**–ITHACA, N.Y. · **E. G. BOWEN**–SYDNEY
SIR DAVID BRUNT–LONDON · **R. BUREAU**–BAGNEUX · **S. CHAPMAN**–ALASKA
J. EGEDAL–COPENHAGEN · **V. F. HESS**–NEW YORK · **E. O. HULBURT**–WASHINGTON, D.C.
H. ISRAEL–AACHEN · **D. K. MENZEL**–CAMBRIDGE, MASS. · **S. K. MITRA**–CALCUTTA
M. NICOLET–UCCLE · **E. H. NORINDER**–UPPSALA · **J. PATON**–EDINBURGH
N. V. PUSHKOV–MOSCOW · **J. A. RATCLIFFE**–SLOUGH · **O. E. H. RYDBECK**–GOTHENBURG
J. C. W. SCOTT–OTTAWA · **SIR GEORGE SIMPSON**–LONDON · **H. SOLBERG**–OSLO
J. VELDKAMP–DE BILT · **M. WALDMEIER**–ZÜRICH

OL.
21
961

EDITOR-IN-CHIEF
SIR EDWARD APPLETON, F.R.S.
EDINBURGH

VOLUME 21
1961

PERGAMON PRESS
OXFORD • LONDON • NEW YORK • PARIS

VOL.
21
1961

CONTENTS

No. 1

J. E. Titheridge: A new method for the analysis of ionospheric $h'(f)$ records . . 1
F. Horner: Narrow-band atmospherics from two local thunderstorms 13
J. W. King: Magnetic effects in the F-region of the ionosphere 26
J. W. King: Day-to-day and station-to-station correlation of ionospheric F-region critical frequencies 35
H. Unz: A solution of the integral equation $h'(f) = \int \mu'(f; f_0)\, dz(f_0)$ 40
V. I. Krassovsky, N. N. Shefov and V. I. Yarin: On the OH airglow 46
J. M. Malville: Excitation of helium in the aurora 54
Y. S. N. Murty and S. R. Khastgir: General expression for the group refractive index of the ionosphere 65
Book Review
"Selected Scientific Papers of Balthasar van der Pol". Edited by H. Bremmer and C. J. Bouwkamp. (Reviewed by Sir Edward Appleton) 70
Papers to be published in future issues 72

Nos. 2/3

Sir Edward Appleton and A. J. Lyon: Studies of the E-layer of the ionosphere—II. Electromagnetic perturbations and other anomalies. 73
A. J. Lyon, N. J. Skinner and R. W. Wright: Equatorial spread-F at Ibadan, Nigeria 100
O. Awe: The fading of radio waves reflected from the ionosphere at oblique incidence . 120
O. Awe: The fading of radio waves weakly scattered at vertical incidence from heights near 90 km 142
J. A. Lane: The radio refractive index gradient over the British Isles 157
R. Naismith, H. C. Bevan and P. A. Smith: A long term variation in the relationship of sunspot numbers to E-region character figures 167
J. A. Chalmers: A criterion for thunderstorm theories 174
B. P. Sandford: Aurora and airglow from colour film observations 177
B. P. Sandford: The behaviour of night-sky 6300, 5577 and 3914 Å emissions at Scott Base, Antarctica 182
G. H. Bazzard: A study of the variations in a daily ionospheric index of solar activity 193
Research Notes
J. N. Tandon: Cosmic ray increases during the sunspot minimum of 1953 . . 203
L. Thomas and R. E. Taylor: Sporadic-E phenomena associated with the high altitude nuclear explosions over Johnston Island 205
B. Ramachandra Rao and R. Raghava Rao: A new type of ionospheric drift recorder 208
J. P. Dougherty: The anisotropy of turbulence at the meteor level 210
G. R. Hébert and R. W. Nicholls: The λ2763 Å (0,9) band of the O_2 Schumann–Runge system 213
L. Thomas: Year-to-year changes in the winter anomaly in ionospheric absorption 215
Book Reviews
"Die Entstehung von Sternen", by G. R. Burbidge, F. D. Kahn, R. Ebert, S. v. Hoerner and St. Temesvary. (Reviewed by H. A. Brück) 218
"Ionization Phenomena in Gases", by G. Francis. (Reviewed by Sir Edward Appleton) 218
"Rival Theories of Cosmology", by H. Bondi, W. B. Bonnor, R. A. Lyttleton and G. J. Whitrow. (Reviewed by H. A. Brück) 219
Papers to be published in future issues 220
Errata
J. K. Hargreaves: Random fluctuations in very low frequency signals reflected obliquely from the ionosphere 220

No. 4

H. J. A. CHIVERS: A statistical study of ionospheric drifts measured by the radio star scintillation technique 221

U. HAUG: Zur Statistik der räumlichen Helligkeitsschwankungen der [OI]-Linie 5577 Å im Nachthimmelsleuchten 225

H. UNZ: On vertical drift velocities of the *F2*-layer 237

S. N. GHOSH and V. MALAVIYA: Microwave absorption in the earth's atmosphere . 243

W. STOFFREGEN: The east–west drift of auroral forms determined from all-sky camera films 257

J. S. GREENHOW and J. E. HALL: Attachment processes in meteor trails 261

S. A. BOWHILL: Rocket measurements of *F*-layer electron density and their interpretation 272

Research Notes

T. ONDOH: A possible explanation of *sc** observed at high geomagnetic latitudes . 284

D. R. BATES and M. NICOLET: Rate of ion–atom interchange 286

S.-I. AKASOFU: Thickness of an active auroral curtain 287

M. YASUHARA and H. MAEDA: Geomagnetic crochet of 15 November 1960 . . 289

M. J. BERAN: A note on non-equilibrium species concentrations in air . . . 293

Book Reviews

"Mathematical Tables for the Approximation of Geophysical Anomalies", by V. A. KAZINSKII. (Reviewed by A. C. AITKEN) 296

"Space Research by Rocket and Satellite", by R. L. F. BOYD. (Reviewed by Sir EDWARD APPLETON) 296

K-Indices of geomagnetic activity for January–April 1961 297

Papers to be published in future issues 300

VOL. 21 1961

AUTHOR INDEX

(B.R.) denotes a book review

AITKEN A. C. (B.R.) 296
AKASOFU S.-I. 287
APPLETON E. V. 73
(B.R.'s) 70, 218, 296
AWE O. 120, 142
BATES D. R. 286
BAZZARD G. H. 193
BERAN M. J. 293
BEVAN H. C. 167
BOWHILL S. A. 272
BRÜCK H. A. (B.R.'s) 218, 219
CHALMERS J. A. 174
CHIVERS H. J. A. 221
DOUGHERTY J. P. 210
GHOSH S. N. 243
GREENHOW J. S. 261
HALL J. E. 261
HARGREAVES J. K. 220
HAUG U. 225
HÉBERT G. R. 213
HORNER F. 13
KHASTGIR S. R. 65
KING J. W. 26, 35
KRASSOVSKY V. I. 46
LANE J. A. 157
LYON A. J. 73, 100
MAEDA H. 289
MALAVIYA V. 243
MALVILLE J. M. 54
MURTY Y. S. N. 65
NAISMITH R. 167
NICHOLLS R. W. 213
NICOLET M. 286
ONDOH T. 284
RAO B. R. 208
RAO R. R. 208
SANDFORD B. P. 177, 182
SHEFOV N. N. 46
SKINNER N. J. 100
SMITH P. A. 167
STOFFREGEN W. 257
TANDON J. N. 203
TAYLOR R. E. 205
THOMAS L. 205, 215
TITHERIDGE J. E. 1
UNZ H. 40, 237
WRIGHT R. W. 100
YARIN V. I. 46
YASUHARA M. 289

Journal of Atmospheric and Terrestrial Physics, 1961, Vol. 21, pp. 1 to 12. Pergamon Press Ltd. Printed in Northern Ireland

A new method for the analysis of ionospheric $h'(f)$ records

J. E. TITHERIDGE*
Cavendish Laboratory, Cambridge

(*Received* 10 *November* 1960)

Abstract—A method is given for calculating the real heights of reflection in the ionosphere, at a number of given frequencies, from the observed virtual heights at those frequencies. The complete real height curve is assumed to consist of a single smooth curve through the calculated points. This gives more accurate results than the lamination methods generally used, in which the real height curve is approximated to by a number of linear segments. So for routine calculations the present method requires less than half as many points as the lamination methods.

1. INTRODUCTION

OUR MAIN SOURCE of information about the ionosphere is the sweep-frequency virtual height records which are taken hourly at observatories all over the world. These $h'(f)$ records give the apparent or virtual heights of reflection (h'), of a vertically transmitted radio wave, as a function of the wave frequency f. The ordinary ray trace of these records can, subject to certain assumptions discussed in an earlier paper (TITHERIDGE, 1959), be used to calculate the variation of the electron density with height in the ionosphere. This calculation is however quite difficult. It consists essentially of the determination of the real height of reflection (h) as a function of frequency. The various methods which have been proposed for doing this have been reviewed by THOMAS (1959).

The routine analysis of $h'(f)$ records is now generally carried out on an electronic computer, using a lamination method of analysis. In this method the virtual heights are measured at a number of fixed frequencies, and the real heights at these frequencies are obtained from a set of simultaneous equations. These equations are based on the assumption that the real height varies linearly with the frequency (or with the square of the frequency) between the calculated points. Unless a large number of points are used in the analysis, this assumption can lead to considerable errors in the calculated real heights. An approximate relation for determining the size of this error is given in Appendix 1.

This difficulty is partly overcome in the method suggested by KELSO (1952). In this method the real height at any frequency is obtained simply by averaging the observed virtual heights at a number of given frequencies. If there are n of these frequencies, the results are equivalent to approximating to the $h'(f)$ curve by a polynomial of degree $2n - 1$ in f^2. For smooth virtual height curves this gives much greater accuracy than the lamination method. Thus for a parabolic layer, a Kelso analysis using five points is more accurate than a lamination method using thirty points. However the virtual height curves observed during the day generally have large cusps and discontinuities, so that they cannot be accurately represented by a polynomial. In this case the mean error given by a Kelso analysis is considerably increased, becoming equal to that of a lamination method using the same

* Now at the Seagrove Radio Research Station, University of Auckland, New Zealand.

number of points. The Kelso method has the further disadvantage that a different set of virtual heights must be measured for each calculated real height. This greatly increases the labour involved in the analysis, and leads to spurious irregularities in the calculated real height curve.

The polynomial method described in the present paper attempts to overcome these disadvantages. Only one set of virtual heights is measured, and the corresponding real heights are obtained on the assumption that the complete real height curve can be represented by a single polynomial in f. This is much preferable to assuming that the virtual height curve can be represented by a polynomial, since the real height curve is always smooth and continuous. The heights calculated by the polynomial method lie on the polynomial of lowest degree in f which can produce the observed virtual heights; in this sense the polynomial method produces the smoothest possible real height curve which can explain the experimental measurements.

When the virtual heights are measured at more than about eight frequencies, the simple polynomial method can, however, produce an irregular real height curve. This is because of the high degree of the polynomial used to represent the real height curve. So for the analysis of day-time $h'(f)$ records it is preferable, when calculating the real height at any frequency, to use a polynomial of lower degree to represent only that part of the real height curve near this frequency. The lower part of the curve can be adequately represented by the linear segments used in the lamination methods. With this modification, described in Section 3, the polynomial method is well suited to the rapid, routine analysis of large numbers of $h'(f)$ records. For a given accuracy this method requires less than half as many points as the lamination methods generally used, considerably reducing the time required for the analysis.

VOL. 21 1961

2. The Polynomial Method of Analysis

2.1. *The basic relations*

It will be assumed that the real height h is given as a function of the plasma frequency f_N by the relation

$$h = \sum_{j=1}^{n} \alpha_j f_N^{j+1}. \tag{1}$$

The constant term is omitted since the height is assumed, for simplicity, to be measured from the level at which $f_N = 0$. A term in $f_N{}^1$ has not been included since we normally require the rate of increase of height h with electron density N to be finite at $N = 0$, and this requires $dh/df_N = 0$ at $f_N = 0$.

The real heights $h_1, h_2, \ldots h_n$ at the plasma frequencies $f_1, f_2, \ldots f_n$ will then be given by

$$\begin{aligned}
h_1 &= \alpha_1 f_1{}^2 + \alpha_2 f_1{}^3 + \ldots + \alpha_n f_1^{n+1} \\
h_2 &= \alpha_1 f_2{}^2 + \alpha_2 f_2{}^3 + \ldots + \alpha_n f_2^{n+1} \\
&\cdot \\
&\cdot \\
&\cdot \\
h_n &= \alpha_1 f_n{}^2 + \alpha_2 f_n{}^3 + \ldots + \alpha_n f_n^{n+1}.
\end{aligned}$$

This set of equations will be written in matrix notation as

$$\mathbf{h} = \mathbf{A}\boldsymbol{\alpha} \tag{2}$$

where $\mathbf{A}$ is an n by n matrix with the typical element $a_{ij} = f_i^{j+1}$.

The virtual height h_i' at the frequency f_i is given by

$$h_i' = \int_0^{h_i} \mu'(f_i, f_N) dh \tag{3}$$

where $\mu'(f_i, f_N)$ is the group refractive index at the wave frequency f_i and plasma frequency f_N. Substituting the value of dh obtained from equation (1) gives

$$h_i' = \sum_{j=1}^{n} \alpha_j (j+1) \int_0^{f_i} \mu'(f_i, f_N) f_N^j df_N. \tag{4}$$

Writing

$$b_{ij} = (j+1) \int_0^{f_i} \mu'(f_i, f_N) \cdot f_N^j df_N \tag{5}$$

this becomes $h_i' = \sum_{j=1}^{n} b_{ij}\alpha_j$. The virtual heights $h_1', h_2', \ldots h_n'$ at the frequencies $f_1, f_2, \ldots f_n$ are therefore given by

$$\begin{aligned} h_1' &= b_{11}\alpha_1 + b_{12}\alpha_2 + \ldots + b_{1n}\alpha_n \\ h_2' &= b_{21}\alpha_1 + b_{22}\alpha_2 + \ldots + b_{2n}\alpha_n \\ &\cdot \\ &\cdot \\ &\cdot \\ h_n' &= b_{n1}\alpha_1 + b_{n2}\alpha_2 + \ldots + b_{nn}\alpha_n \end{aligned}$$

or, in matrix notation,

$$\mathbf{h}' = \mathbf{B}\boldsymbol{\alpha}. \tag{6}$$

This relation may be inverted to give $\boldsymbol{\alpha} = \mathbf{B}^{-1}\mathbf{h}'$, and substituting in equation (2) gives

$$\mathbf{h} = (\mathbf{A}\mathbf{B}^{-1})\mathbf{h}'. \tag{7}$$

For a given strength and direction of the magnetic field the values of a_{ij} and b_{ij} depend only on the frequencies f_i, and can be calculated rapidly by the method described in Appendix 2. The matrix $\mathbf{A}\mathbf{B}^{-1}$ can then be determined and used to calculate the real heights h_i at the frequencies f_i, from the virtual heights at those frequencies.

2.2. *The use of the polynomial method*

The elements of the matrix $\mathbf{A}\mathbf{B}^{-1}$, calculated for the frequencies 1–6 Mc/s at the magnetic equator, are shown in Table 1. They give the real heights at the six frequencies considered directly in terms of the virtual heights at those frequencies. Thus the real height at $f_N = 4$ Mc/s is

$$h_4 = 0{\cdot}2092h_1' + 0{\cdot}1198h_2' + 0{\cdot}3395h_3' + 0{\cdot}2800h_4' - 0{\cdot}0100h_5' + 0{\cdot}0007h_6'. \tag{8}$$

For ionospheric layers in which h varies linearly with f_N^2, or with any higher power of f_N up to f_N^7, the calculated heights are exact. For an arbitrary series of virtual heights the calculated real heights lie on the polynomial of lowest degree in f_N which is capable of explaining the observed virtual heights.

Table 1. The matrix $\mathbf{AB}^{-1}$ connecting the real and virtual heights at six frequencies at the magnetic equator

f (Mc/s)	Matrix $\mathbf{AB}^{-1}$					
1	0·7314	−0·1467	0·0755	−0·0300	0·0074	−0·0008
2	0·4510	0·4496	−0·0431	0·0119	−0·0024	0·0002
3	0·2166	0·3382	0·3650	−0·0296	0·0056	−0·0006
4	0·2092	0·1198	0·3395	0·2800	−0·0100	0·0007
5	0·1128	0·1915	0·0699	0·3314	0·2332	−0·0039
6	0·3239	−0·2005	0·4831	−0·1657	0·4072	0·1834

Table 2. A comparison of the accuracy given by different methods of analysis when applied to the $h'(f)$ curve calculated (at $I = 0°$) for a parabolic layer with a critical frequency of 6·4 Mc/s and a semithickness of 100 km

Method of analysis	Frequency interval (Mc/s)	Error (in km) in calculated height at f Mc/s						Mean error
		$f = 1$	$f = 2$	$f = 3$	$f = 4$	$f = 5$	$f = 6$	
Lamination	1·0	+0·34	+0·61	+0·89	+1·29	+1·76	+5·07	1·66
	0·5	+0·14	+0·25	+0·34	+0·50	+0·82	+2·29	0·72
	0·2	+0·04	+0·07	+0·10	+0·14	+0·20	+0·60	0·19
Polynomial	1·0	−0·10	+0·004	−0·006	+0·008	−0·037	+0·369	0·07
Modified polynomial	1·0	(0)	−0·001	−0·005	−0·002	−0·10	+0·1	0·04

Since a parabolic layer cannot be represented by a finite polynomial, the virtual heights calculated from such a layer can be used to test the accuracy of the present method when applied to smooth $h'(f)$ curves. Table 2 shows the errors in the heights calculated from Table 1 and from lamination methods using six, twelve and thirty points. The error in the polynomial method increases considerably at the highest frequency (the end point of the approximating polynomial). The mean error is however twenty-three times smaller than the error in the lamination analysis using the same frequency interval. This ratio is even greater at higher latitudes, where the virtual heights depend more on the exact gradient at the reflection point.

The polynomial method is thus very suitable for the analysis of smooth $h'(f)$ curves. Because of the small number of points required in the analysis, the matrices involved are small and can be calculated very rapidly on an electronic computor whenever they are required, and for any desired conditions.

2.3. *Disadvantages of the full polynomial analysis*

A minor disadvantage of the above method is that the real height at any frequency depends on the virtual heights at all the frequencies included in the

VOL. 21 1961

matrix. So all the virtual height curves analysed with a given set of coefficients must extend up to the same frequency (6 Mc/s, for the coefficients of Table 1). This offers no difficulties in practice, since curves with a lower frequency limit are simply extended by assuming some large value for the virtual height at higher frequencies. The exact value of this assumed height is not important; for the night-time F-layer a height of about 800 km is suitable, corresponding to a layer of normal size with a parabolic maximum.

A much more serious disadvantage of the polynomial method is that the calculations become inaccurate if the virtual heights are measured at more than ten frequencies. Thus a matrix extending up to 6 Mc/s in steps of 0·5 Mc/s, for conditions at the equator, gives the real height at $f_N = 4$ Mc/s as

$$h_4 = 1{\cdot}16h'_{0{\cdot}5} - 1{\cdot}65h_1' + 2{\cdot}37h'_{1{\cdot}5} - 2{\cdot}27h_2' + 2{\cdot}00h'_{2{\cdot}5} - 1{\cdot}06h_3' + 0{\cdot}74h'_{3{\cdot}5} + 0{\cdot}04h_4' + 0{\cdot}02h'_{4{\cdot}5}. \quad (9)$$

While the calculated heights are still accurate for layers in which h is any polynomial in f_N of degree less than thirteen they are obtained as the difference between comparatively large multiples of the virtual heights. With an arbitrary series of virtual heights this leads to an irregular real height curve. For example, adding 1 km to h_2' in equation (9) decreases the calculated height by over 2 km. This effect cannot be reduced by using different assumptions about the shape of the real height curve, in place of equation (1). So when analysing irregular $h'(f)$ curves, in which the virtual height must be measured at more than about eight frequencies, the polynomial analysis must be modified in the way described in the next Section.

3. A Modified Method for General Use

Experimentally observed $h'(f)$ curves are only accurate to a few kilometres, and often have an irregular structure showing several distinct layers. With such curves it is not necessary or desirable to use a single polynomial to cover the entire frequency range. In calculating the real height at any frequency it is sufficient to consider the exact shape of the real height curve near this frequency. The effect of the lower part of the real height curve can be allowed for to the required accuracy by using the usual approximation of a linear variation of h with f_N between the calculated points.

In the method to be described the real height at the frequency f_i is made to depend on the virtual height at the next higher frequency f_{i+1}, but not on the virtual heights at frequencies above this. This is sufficient to define the curvature of the real height curve up to f_i, and permit the use of a step-by-step method of calculating the successive real heights $h_1, h_2, \ldots h_n$. It would of course be possible to invert the relations obtained, to produce a matrix giving the real heights directly in terms of the virtual heights. However this considerably increases the time required to calculate the matrix coefficients and does not significantly speed up the real height calculation.

3.1. *The relations used*

In the step-by-step analysis of an $h'(f)$ record, suppose that the real heights

have been calculated up to the height h_{i-1} at $f_N = f_{i-1}$. Then in calculating the height h_i, the real height curve between the frequencies f_{i-2} and f_{i+1} will be approximated to by the polynomial

$$h = \alpha_{i0} + \alpha_{i1} f_N + \alpha_{i2} f_N^2 + \alpha_{i3} f_N^3 + \alpha_{i4} f_N^4. \tag{10}$$

The coefficients of this polynomial are calculated so that it goes through the points h_{i-2} and h_{i-1}, and gives the correct virtual heights at the frequencies f_i and f_{i+1}. In addition the polynomial will be required to give the correct virtual height at the frequency f_{i-1}. This ensures that the polynomial has the correct gradient at the height h_{i-1}, so that it will accurately represent a smooth continuation of the real height curve which has already been calculated up to this point.

The first two conditions give

$$h_{i-2} = \alpha_{i0} + \alpha_{i1} f_{i-2} + \alpha_{i2} f_{i-2}^2 + \alpha_{i3} f_{i-2}^3 + \alpha_{i4} f_{i-2}^4 \tag{11}$$

and

$$h_{i-1} = \alpha_{i0} + \alpha_{i1} f_{i-1} + \alpha_{i2} f_{i-1}^2 + \alpha_{i3} f_{i-1}^3 + \alpha_{i4} f_{i-1}^4. \tag{12}$$

If $H'_{i-1,i-2}$ is the virtual height at the frequency f_{i-1} due to the ionization above the height h_{i-2}, so that

$$H'_{i-1,i-2} = \int_{h_{i-2}}^{h_{i-1}} \mu'(f_{i-1}, f_N) dh \tag{13}$$

then we get from equation (10)

$$H'_{i-1,i-2} = \alpha_{i1} \int_{i-2}^{i-1} \mu' df_N + 2\alpha_{i2} \int_{i-2}^{i-1} \mu' f_N df_N + 3\alpha_{i3} \int_{i-2}^{i-1} \mu' f_N^2 df_N + 4\alpha_{i4} \int_{i-2}^{i-1} \mu' f_N^3 df_N \tag{14}$$

where $i - 1$, $i - 2$ have been written for f_{i-1}, f_{i-2} in the limits of integration. Similar relations hold for the "partial" virtual heights $H'_{i,i-1}$ and $H'_{i+1,i-2}$ at the frequencies f_i and f_{i+1}. Combining these relations with equations (11), (12) and (14) gives the matrix relation

$$\begin{pmatrix} h_{i-2} \\ h_{i-1} \\ H'_{i-1,i-2} \\ H'_{i,1-2} \\ H'_{i+1,1-2} \end{pmatrix} = \begin{pmatrix} 1 & f_{i-2} & f_{i-2}^2 & f_{i-2}^3 & f_{i-2}^4 \\ 1 & f_{i-1} & f_{i-1}^2 & f_{i-1}^3 & f_{i-1}^4 \\ 0 & \int_{i-2}^{i-1} \mu' df_N & 2\int_{i-2}^{i-1} \mu' f_N df_N & 3\int_{i-2}^{i-1} \mu' f_N^2 df_N & 4\int_{i-2}^{i-1} \mu' f_N^3 df_N \\ 0 & \int_{i-2}^{i} \mu' df_N & 2\int_{i-1}^{i} \mu' f_N df_N & 3\int_{i-1}^{i} \mu' f_N^2 df_N & 4\int_{i-1}^{i} \mu' f_N^3 df_N \\ 0 & \int_{i-2}^{i+1} \mu' df_N & 2\int_{i-2}^{i+1} \mu' f_N df_N & 3\int_{i-2}^{i+1} \mu' f_N^2 df_N & 4\int_{i-1}^{i+1} \mu' f_N^3 df_N \end{pmatrix} \begin{pmatrix} \alpha_{i0} \\ \alpha_{i1} \\ \alpha_{i2} \\ \alpha_{i3} \\ \alpha_{i4} \end{pmatrix} \tag{15}$$

This relation will be represented by

$$\mathbf{H}_i = \mathbf{G}_i \boldsymbol{\alpha}_i. \tag{16}$$

VOL. 21 1961

The real height h_i at the frequency f_i is given by

$$h_i = \alpha_{i0} + \alpha_{i1} f_i + \alpha_{i2} f_i^2 + \alpha_{i3} f_i^3 + \alpha_{i4} f_i^4.$$

Writing $\mathbf{F}_i$ for the row matrix $(1, f_i, f_i^2, f_i^3, f_i^4)$, and substituting the value of $\boldsymbol{\alpha}_i$ from equation (16), we get

$$h_i = \mathbf{F}_i \boldsymbol{\alpha}_i = (\mathbf{F}_i \mathbf{G}_i^{-1}) \mathbf{H}_i. \tag{17}$$

This relation replaces equation (7), and is used to determine the real height h_i at the frequency f_i from the real heights h_{i-2} and h_{i-1}, and the "partial" virtual heights at the frequencies f_{i-1}, f_i and f_{i+1}. These partial heights are the virtual heights due to the ionization above h_{i-2}. They are obtained by subtracting, from the observed virtual heights, the contribution due to the ionization below h_{i-2}. Thus

$$H'_{i,i-2} = \int_{h_{i-2}}^{h_i} \mu'(f_i, f_N) dh = h_i' - \int_{h_1}^{h_{i-2}} \mu'(f_i, f_N) dh. \tag{18}$$

The integral is evaluated by supposing that h varies linearly with f_N between the calculated heights $h_1, h_2, \ldots h_{i-2}$. The mean value of μ' over each of these intervals can then be calculated as in the lamination methods, and equation (18) becomes

$$H'_{i,i-2} = h_i' - \left[h_1 + \sum_{j=2}^{i-2} \overline{\mu}'_{i,j} (h_j - h_{j-1}) \right] \tag{19}$$

where

$$\overline{\mu}'_{i,j} = \frac{1}{f_j - f_{j-1}} \int_{f_{j-1}}^{f_j} \mu'(f_i, f_N) df_N. \tag{20}$$

3.2. *The method of calculation*

The use of an electronic computer to analyse an $h'(f)$ record, using the above relations, involves the following steps:

(i) The strength and direction of the magnetic field, and the frequencies to be used in the calculations, are used to calculate the matrices $\mathbf{FG}^{-1}$ and $\overline{\mu'}$ as described in Appendix 2.

(ii) The heights $h_0, h_1, h_1', h_2', \ldots h_n'$ are read into the machine; h_1' is the virtual height at the lowest frequency recorded (f_1), h_2', h_3', etc. are the values of h' at $f_1 + \Delta f, f_1 + 2\Delta f$, etc. where Δf is the sampling interval; h_0 and h_1 are the real heights at the frequencies $f_1 - \Delta f$ and f_1 and may be put equal to the first virtual height h_1'.

(iii) To determine h_i the stored numbers h_{i-2}, h_{i-1}, $H'_{i-1,i-3}$, $H'_{i,i-3}$, h_{i+1} are used to obtain the matrix $H_i = (h_{i-2}, h_{i-1}, H'_{i-1,i-2}, H'_{i,i-2}, H'_{i+1,i-2})$ by subtracting $\overline{\mu}'_{i-1,i-2}(h_{i-2} - h_{i-3})$, $\overline{\mu}'_{i,i-2}(h_{i-2} - h_{i-3})$ and $h_1 + \sum_{j=2}^{i-2} \overline{\mu}'_{i+1,j}$ $(h_j - h_{j-1})$ from the values of $H'_{i-1,i-3}$, $H'_{i,i-3}$ and h'_{i+1} respectively (equation 19).

The value of $h_i = (FG^{-1})_i H_i$ is then calculated and stored in place of $H'_{i-1,i-2}$.

The calculation is started by computing $h_2 = (FG^{-1})_2 H_2$, the matrix H_2 having elements h_0, h_1, H_{10}', H_{20}' and H_{30}', where $H_{10}' = h_1' - h_0$, $H_{20}' = h_2' - h_0$, and $H'_{30} = h'_3 - h_0$.

(iv) To calculate the height h_n, at the highest frequency f_n at which a virtual height was recorded, we require a value for h_{n+1}. For an ionospheric layer of normal size and with a parabolic maximum the correct value of h_n is obtained by taking $h'_{n+1} = h_n' + h'_{n-1}$. The exact value of h'_{n+1} is not important, since adding 100 km to h_{n-1} alters the calculated value of h_n by only about 1 km.

(v) The value of the critical frequency f_c of the highest layer is used to calculate the height h_m at the peak of the layer. This is done by fitting a parabola through the calculated heights h_{n-1} and h_n at the frequencies f_{n-1} and f_n. This gives

$$h_m = h_n + (h_n - h_{n-1})\left[\sqrt{\left(\frac{f_c^2 - f_{n-1}^2}{f_c^2 - f_n^2}\right)} - 1\right]^{-1}.$$

This procedure is used by several workers, and defines the peak of the layer more accurately than when measurements are confined to the fixed series of frequencies.

4. CONCLUSIONS

For the routine analysis of $h'(f)$ records, lamination methods with frequency intervals of 0·1 Mc/s (THOMAS *et al.*, 1958), 0·2 Mc/s and 0·4 Mc/s (SCHMERLING, 1957) have been used. The smaller frequency intervals increase the accuracy of the calculated heights, but they also increase the time required for measuring the experimental records and for carrying out the calculations. In developing a programme for use with an electronic computor, it was therefore decided to use the largest frequency interval which would give results at least as accurate as those given by a lamination method with $\Delta f = 0{\cdot}1$ Mc/s. An interval of 0·5 or 1 Mc/s was found to be sufficient except near large discontinuities on the $h'(f)$ record, when an interval of 0·25 Mc/s was sometimes required. Since these discontinuities seldom occur at frequencies above 5 Mc/s, a basic interval of 0·25 Mc/s was used from 1 to 5 Mc/s, with an interval of 0·5 Mc/s at higher frequencies.

Where the $h'(f)$ curve is reasonably smooth, even larger intervals can be used. This was made possible by separating the numbers on the data tape (giving the successive virtual heights) by an appropriate terminating symbol according as the frequency interval was 0·25, 0·5 or 1·0 Mc/s. The larger intervals are used whenever possible, the intermediate values being interpolated in the machine. The number of virtual heights which must be measured with this method of analysis is less than one quarter as large as if a lamination method with $\Delta f = 0{\cdot}1$ Mc/s is used.

The accuracy given by the modified analysis, when applied to a smooth $h'(f)$ curve, is shown at the bottom of Table 2. The errors are slightly less than for the full polynomial analysis, since with the modified method the analysis had to be started at 1 Mc/s, and the correct height was assumed at this frequency. The advantage of the present method is that these results are not altered when the calculations are extended to higher frequencies, to include several distinct layers.

To test the accuracy obtained with the present method when applied to irregular $h'(f)$ curves, three curves each showing two particularly large discontinuities were analysed. These curves were provided by Dr. J. O. THOMAS, who also supplied the corresponding real height curves calculated by a lamination method

VOL. 21 1961

with $\Delta f = 0{\cdot}1$ Mc/s. These heights are compared in Fig. 1 with the heights calculated by the present method. The overall agreement is quite good. The heights calculated by the lamination method at the highest recorded frequency are generally less than those given by the present method, which assumed an infinite virtual height at this frequency (Section 3.2 (v)). This difference is reduced when the exact critical frequency is used.

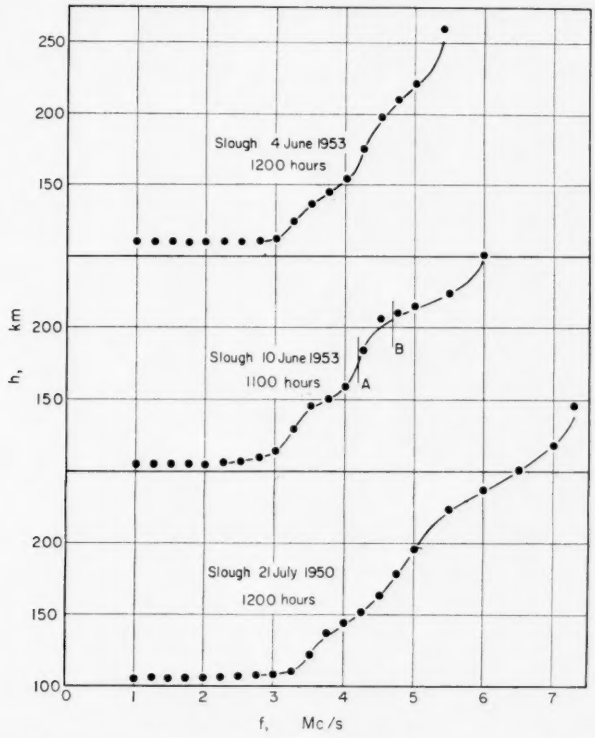

Fig. 1. Real heights calculated from irregular $h'(f)$ curves. —— lamination analysis with $\Delta f = 0{\cdot}1$ Mc/s; $\cdots$ present method with $\Delta f = 0{\cdot}25$ and $0{\cdot}5$ Mc/s.

The only other significant differences in the figure occur at frequencies which just penetrate the *E*- or *F1*-layers, when the heights calculated by the present method are slightly greater than those given by the lamination method. This difference is most marked in the centre curve, and can be explained by errors in the lamination analysis. Thus from A to B in Fig. 1 the value of dh/df decreases by about 30 per cent in each of the intervals $\Delta f = 0{\cdot}1$ Mc/s used in the lamination analysis. The calculated height increase from A to B will therefore be too small by about $0{\cdot}2 \times 30$ per cent $= 6$ per cent or 2 km (Appendix 1). This is just the difference between the heights at B calculated by the two methods. Thus the heights calculated by the present method are at least as accurate as those given by a lamination method with $\Delta f = 0{\cdot}1$ Mc/s. For smooth $h'(f)$ curves the present method is much more accurate than the lamination method. The modified polynomial analysis can therefore be used for all real height calculations, offering a considerable saving in time over lamination methods of comparable accuracy.

Acknowledgements—This work was carried out during the tenure of an Overseas Scholarship awarded by the Commissioners for the Exhibition of 1851. Thanks are also due to the Director of the Cambridge Mathematical Laboratory for permission to use the digital computor EDSAC II, and to Dr. J. O. Thomas for supplying the curves used in Fig. 1.

References

Kelso J. M.	1952	*J. Geophys. Res.* **57,** 357.
Lowan A. N., Davids N. and Levenson A.	1942	*Bull. Amer. Math. Soc.* **48,** 739.
Schmerling E. R.	1957	*Sci. Rep.* No. 94, Pennsylvania State University.
Thomas J. O.	1959	*Proc. Instn Elect. Engrs* **47,** 162.
Thomas J. O., Haselgrove J. and Robbins A. R.	1958	*J. Atmosph. Terr. Phys.* **12,** 46.
Titheridge J. E.	1959	*J. Atmosph. Terr. Phys.* **17,** 110.

Appendix 1

The Accuracy of the Heights Calculated by Lamination Methods

In the lamination methods it is normally assumed that the value of dh/df_N is constant between the calculated points. So for a general layer in which dh/df_N varies with f_N the calculated heights are incorrect. The size of the error depends on the rate at which dh/df_N changes, i.e. on the curvature of the layer. An approximate relation for determining the size of this error can be obtained by considering the step-by-step method of calculation. This relation will also apply to the matrix inversion method, since both methods give the same calculated heights from a given set of virtual heights.

Suppose that the solid line in Fig. A1 is the exact real height curve corresponding to the virtual height curve being analysed, and that the real heights have been correctly determined up to the point a. Then the next point b' is calculated so that the straight line ab' gives the same group retardation, at the frequency f_b, as the actual curve ab. If this curve is given by $dh/df_N = A + Bf_N$, the retardation is

$$R = \int_{f_a}^{f_b} \mu' dh = Af_b \int_0^{t_a} \frac{\mu' t dt}{\sqrt{(1 - t^2)}} + Bf_b{}^2 \int_0^{t_a} \mu' t dt$$

where $$t^2 = 1 - \frac{f_N{}^2}{f_b{}^2} \text{ and } t_a{}^2 = 1 - \frac{f_a{}^2}{f_b{}^2}.$$

At the magnetic equator, $\mu' t = 1$ and the integrals can be evaluated analytically. For a frequency interval $\Delta f = f_b - f_a$ of 0·1 Mc/s, at $f_a = 3$ Mc/s (or $\Delta f = 0{\cdot}2$ Mc/s at $f_a = 6$ Mc/s) the calculated value of R is the same as would be given by a constant gradient $dh/df_N = A + 0{\cdot}9894Bf_b$. This relation therefore gives the gradient of the calculated step ab'. It is greater than the mean gradient over the interval ab by 0·17 times the change in dh/df_N from a to b. So if the value of dh/df_N is x per cent greater at b than at a, the gradient of the broken line ab' (Fig. A1) is $0{\cdot}17x$ per cent greater than the gradient of the dotted line ab. The calculated height increase from a to b' is therefore $0{\cdot}17x$ per cent greater than the true increase from a to b.

For a magnetic dip angle I of 67° corresponding to conditions in S.E. England, the integrals were evaluated numerically. With $\Delta f = 0{\cdot}1$ Mc/s and $f_a = 3$ Mc/s, the percentage error in the calculated real height interval is 0·25 times the percentage change in dh/df_N over this interval. For $\Delta f = 0{\cdot}2$ Mc/s at $f = 6$ Mc/s the percentage error is 0·28 times the percentage change in dh/df_N.

These relations are approximately correct for all values of Δf between 0·05 and 0·5 Mc/s. This is borne out by Table 2, where halving the value of Δf, and so halving the amount by which dh/df_N changes over each interval, reduces the errors in the calculated heights by a factor of about 0·4.

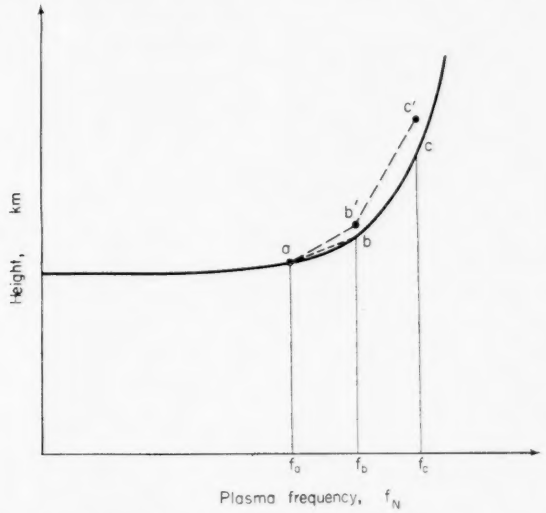

Fig. A1. Real heights calculated by lamination methods. —— true height curve; – – – – calculated curve.

The above calculations assumed that the lower part of the real height curve had been determined correctly. However, the fact that the point b' in Fig. A1 is already too high will tend to reduce the calculated size of the step $b'c'$. This effect is not very large, since the group retardation depends primarily on the value of dh/df_N at reflection. For a parabolic layer at $I = 67°$ this compensating effect reduces the errors by about 25 per cent. The percentage error in the calculated real height intervals is therefore about 0·2 times the percentage change in dh/df_N over each interval. This result can be used to determine the errors in a calculated real height curve, using the approximate values of dh/df_N given by this curve.

Appendix 2

The Calculation of the Coefficients

(a) *The polynomial method*

Writing $f_N^2/f_i^2 = 1 - t^2$, equation (5) becomes

$$b_{i,j} = (j + 1) \int_0^1 \mu'(f_i, t) f_N^{j+1} \frac{tdt}{1 - t^2}.$$

The integrand remains finite at all values of t. Evaluating the integral by an m point Gaussian formula gives

$$b_{ij} = (j + 1) \sum_{r=1}^{m} [\mu'(f_i, t_i) W_r] f_{N_r}^{j+1}$$

where $W_r = (\gamma_r t_r)/(1 - t_r^2)$ and $f_{N_r} = f_i \sqrt{(1 - t_r^2}$.) The values of $(1 - 2t_r)$ and the weighting function γ_r are given by LOWAN *et al.* (1942) for values of m up to 16.

At each frequency f_i the m values of $[\mu'(f_i, t_r) W_r]$ and of f_{N_r} are calculated from the known values of t_r and W_r. All the terms $b_{i1}, b_{i2}, \ldots b_{in}$ in the ith row of the matrix $\mathbf{B}$ can then be obtained. Finally the matrix $\mathbf{A}(= f_i^{j+1})$ is formed and $\mathbf{AB}^{-1}$ is calculated. Using a sixteen point integration the calculated coefficients are accurate to within one part in 10^6 when the dip angle I is small. The error increases at large dip angles, because of the rapid variation of $\mu' t$ near $t = 0$, becoming about 0·05 per cent at $I = 80°$ and 1 per cent at $I = 87°$. For $I = 0°$ the coefficients can be calculated from

$$b_{ij} = f_i^{j+1} \frac{[(j + 1)/2]! \, (-1/2)!}{(j/2)!} = f_i{}^2 \frac{j + 1}{2} \cdot b_{i,j-2} .$$

(b) *The modified method*

The integrals in equation (15) are (apart from the lower limits) the same as those used in the full polynomial method, and are calculated in the manner described above. For the analysis of experimental records an accuracy of 0·1 per cent is quite sufficient, and for dip angles less than 70° a five point integration can be used. At each frequency f_i $(i = 2, 3, \ldots n)$ the 5×5 matrix $\mathbf{G}_i$ is calculated and used to obtain the 5×1 matrix $\mathbf{F}_i \mathbf{G}_i^{-1}$.

The values of $\overline{\mu'_{ij}}$ (equation 20) are also required, for $i = 3, 4, \ldots n + 1$ and $j = 2, 3, \ldots i - 1$. For $j < i - 1$ these can be obtained to sufficient accuracy from $\overline{\mu'_{ij}} = \frac{1}{2}(\mu'_{ij} + \mu'_{i,j-1})$. At $j = i - 1$ the three point Simpson's rule is used to evaluate the integral in equation (20).

VOL. 21 1961

Journal of Atmospheric and Terrestrial Physics, 1961, Vol. 21, pp. 13 to 25. Pergamon Press Ltd. Printed in Northern Ireland

Narrow-band atmospherics from two local thunderstorms

F. HORNER
D.S.I.R. Radio Research Station, Slough, Bucks.*

(*Received* 11 *November* 1960)

Abstract—Atmospherics from two local storms at known distances have been recorded on magnetic tape. The frequencies of reception were 11 Mc/s for one storm and both 6 kc/s and 11 Mc/s for the other. The power bandwidths were in the range 200–300 c/s. Values of duration, peak amplitude, mean field strength and mean power flux have been deduced from the records, and estimates of the radiated power have been derived.

The waveforms of the atmospherics are partly explicable in terms of known characteristics of lightning discharges, but there are many features, particularly at 11 Mc/s, for which an adequate quantitative explanation is lacking. The results conflict with some theories of the origin of high-frequency atmospheric noise which have been advanced in recent years.

1. INTRODUCTION

MOST INVESTIGATIONS of electromagnetic radiation from lightning discharges have been in two main categories. In the first, the objective has been to elucidate the mechanism of the discharges; atmospherics from single flashes have been recorded with wideband receivers responding to a large part of the frequency range below 100 kc/s, in which most of the energy is radiated. In the other category have been studies of the interference to radio services by atmospheric noise; measurements have then been in narrow bandwidths and it has been the integrated noise from all sources which has been of interest.

Some recent investigations have been designed to bridge the gap between these two fields of study by recording single atmospherics in narrow-band receivers. This was first done at very low frequencies, where direct comparisons with wideband data could be made (HORNER, 1958; EDWARDS, 1956). There have also been attempts to explain the observed levels of narrow-band, integrated noise either from the experimental results on single atmospherics, or from assumed models of the lightning discharge (HILL, 1957; AIYA, 1955).

On the whole, frequencies above 100 kc/s have been neglected in the experimental work, and there is little information on the characteristics of atmospherics from single lightning discharges. Recently, records of single atmospherics have been obtained over a wide frequency range (MALAN, 1959), though the results have not all been quantitative. Calibrated records have now been obtained at the Radio Research Station, Slough, from nearby storms at known distances, and the characteristics of the atmospherics from two of these storms are here described, fully and in quantitative terms. Records were taken only at a high frequency for one storm, but on both high and very low frequencies for the other.

2. RECORDING TECHNIQUE

Techniques for studying atmospherics have been facilitated by the advent of

* Official communication.

magnetic tape recording (CLARKE, 1960b; HORNER and CLARKE, 1958; CHAPMAN and MACARIO, 1956), which has two main advantages over the older method of photographing traces on cathode ray tubes. First the signals may be played back through equipment designed to extract quantitative information in a quick and convenient manner; secondly the range of voltage fluctuations which may be faithfully recorded on tape is much greater than that which can be resolved on film. It is necessary to transfer the records from tape to film if they are to be examined visually, but the amplitude and time scales may be chosen at will and varied in successive replays if desired. Subsidiary advantages are economy and the facility for numbering the atmospherics by voice and adding spoken comments on the visible characteristics of the lightning discharges.

The records to be described were obtained at Slough during two storms, at 1100 G.M.T. on 19 July 1957 (Storm A) and 1400 G.M.T. on 12 August 1957 (Storm B). They were of a type often described as heat storms and appeared to be typical of summer afternoon storms in England.

During Storm A, atmospherics were recorded only at a frequency of 11 Mc/s. The frequency was changed to 10 kc/s by a beat-frequency technique and a band 300 c/s wide (power bandwidth) selected by means of three similar 10 kc/s tuned circuits in cascade. Thus the signal recorded on tape was a 10 kc/s oscillation, amplitude modulated with the same waveform as would have been obtained by the selection of a 300 c/s band at the original frequency of 11 Mc/s. The tape recorder was operated at a speed of 15 in/sec.

For Storm B a second channel was added to record the atmospherics received at 6 kc/s. The receiver was a tuned amplifier with two similar circuits in cascade, providing an overall bandwidth of 210 c/s. The 6 kc/s output was recorded on the same tape track as the 10 kc/s output derived from the 11 Mc/s atmospherics, and calibration signals from both channels were recorded. Vertical rod aerials were used at both frequencies.

The precise means for obtaining the restricted bandwidths have been mentioned because they materially affect the waveform of the atmospherics. At low frequencies particularly, but also to some extent at high frequencies, atmospherics consist largely of impulses, the shape of which is determined by the transient response of the receiver. The peak amplitudes would be different for receivers with differing numbers of tuned stages, even if the overall power bandwidths were the same.

Whenever possible the lightning flashes were observed visually and their distances determined from the delay of the thunder.

3. Analysis Technique and Form of Records

The atmospherics were first played back from tape onto film for visual examination. When 11 Mc/s and 6 kc/s atmospherics were recorded on the same track (Storm B) the tape was replayed through high and low pass filters to separate the two frequencies (10 and 6 kc/s). The filter cut-off frequencies were both 8 kc/s and on each replay channel the attenuation of the unwanted frequency was about 40 dB. The outputs were displayed simultaneously on a double-trace cathode ray tube and photographed, the time-sequence being obtained by movement of the

VOL. 21 1961

film at 5 in/sec. Figs. 3–8 illustrate the type of record obtained, and examples have also been shown in a previous publication (HORNER and CLARKE, 1958).

Calibration signals were also filmed and used, in conjunction with the known characteristics of the aerial, to derive the absolute peak amplitudes of the atmospherics, expressed in terms of field strength. In addition the films were used to measure the durations and to classify the waveforms.

Two other derived parameters were $\int e\,dt$ and $\int e^2\,dt$, taken over the atmospheric, where e is the instantaneous envelope field strength. These integrals are required in estimating the average field strength and average power of the noise as a whole, and they were calculated from graphs which showed the time for which various field strength levels were exceeded by e. The technique by which the graphs were obtained was to use the part of the envelope waveform which exceeded a given threshold to gate a uniform series of pulses, and to count these for a series of threshold levels (CLARKE, 1960a).

It should be emphasized that in the two storms discussed the intervals between any two atmospherics were so large compared with their durations, that each could almost certainly be attributed to a single discharge.

The spectral amplitude component $f(w)$, that is the modulus of the Fourier transform of the waveform, is related directly to $\int e^2\,dt$, since, if the spectrum is assumed to have constant amplitude over the receiver bandwidth,

$$f(w) = \frac{1}{2}\left[\frac{1}{B}\int e^2\,dt\right]^{\frac{1}{2}}$$

where B is the power bandwidth. The spectral component is listed as an additional parameter.

4. Amplitude Data

4.1. *Storm A*

Storm A, at an average distance of 4 km, was observed for 30 min, and seventy-five atmospherics received at 11 Mc/s were recorded on tape. The amplitudes of most of these were such that they can be assumed to have originated in the one storm. The discharge channels of twenty-eight flashes were seen, and all except one were seen to strike the ground. In the exceptional case the only visible part of the discharge followed a generally horizontal track, with both ends in the thundercloud. Distances of twenty-four flashes were measured and were between 1·5 and 6·5 km.

The main amplitude characteristics of the atmospherics from the visible flashes are summarized in Table 1.

No attempt has been made to normalize the data to a constant distance, because there was poor correlation between any one of the amplitude functions and the distance of the flash. Random variations evidently obscured any systematic trend. The amplitude data for the atmospheric from the flash which was not seen to strike the ground did not differ significantly from the others.

4.2. *Storm B*

Storm B was observed for 28 min, during which time seventy-four atmospherics were recorded on tape at 6 kc/s and 11 Mc/s. The general illumination from

forty-seven of these was seen and the distances of twenty-five were measured. Unfortunately the flashes were, with one or two exceptions, just too distant for the discharge channels to be seen, so no distinction could be drawn between ground flashes and possible cloud flashes. The basic data on amplitudes are given in Table 2, which has been compiled from twenty-two atmospherics known to be at ranges near to 10 km. Data for 6 kc/s have been normalized to the same bandwidth as was used at 11 Mc/s (300 c/s) and all 6 kc/s data subsequently quoted are for this bandwidth.

Table 1. 11 Mc/s atmospherics from Storm A
(Power bandwidth 300 c/s)

	Average	Minimum	Median	Maximum
Peak amplitude (μV/m)	970	340	850	1530
$\int e\,dt$ [(μV/m) sec]	25	4·3	25	48
$\int e^2\,dt$ [(μV/m)^2 sec]	9800	720	8500	26,500
Spectral component [(μV/m) sec]	2·9	0·78	2·7	4·7

Table 2. Atmospherics from Storm B
(Power bandwidth 300 c/s, distance 10 km)

		Average	Minimum	Median	Maximum
11 Mc/s	Peak amplitude (μV/m)	540	90	460	2100
	$\int e\,dt$ [(μV/m) sec]	20	5	18	45
	$\int e^2\,dt$ [(μV/m)^2 sec]	4000	270	1750	29,200
	Spectral component [(μV/m) sec]	1·8	0·48	1·2	4·9
6 kc/s	Peak amplitude (mV/m)	260	40	180	850
	$\int e\,dt$ [(mV/m) sec]	3·3	0·3	2·8	8·9
	$\int e^2\,dt$ [(mV/m)^2 sec]	310	22	100	2500
	Spectral component [(μV/m) sec]	510	140	290	1400

Although the discharge channels could not be seen, it is probable that most of the flashes struck the ground, since the peak fields at 6 kc/s were approximately those to be expected from a typical return stroke at 10 km (200 μV/m). The few which were seen to be ground strokes had amplitudes similar to the rest.

The peak amplitudes at h.f. and v.l.f. are compared in Fig. 1. The correlation is not well marked, but there is a general tendency for the amplitude at 6 kc/s to exceed that at 11 Mc/s by a factor of 500. There was a corresponding tendency for the total energy radiated at 6 kc/s to be higher than at 11 Mc/s by a factor of 10^5. This is less than the average ratio of the peak amplitudes squared, because h.f. atmospherics are more continuous and therefore have more energy for a given peak amplitude.

Other workers have presented amplitude data on v.l.f. atmospherics in recent years; these were obtained at longer distances, but may be compared by assuming an inverse distance law for the field strength variation. The most convenient basis of comparison is the spectral amplitude component, which avoids the necessity for specifying the bandwidth. TAYLOR and JEAN (1959) have expressed their data for distances of 150–600 km in this form and a range of values is plotted in Fig. 2,

VOL. 21 1961

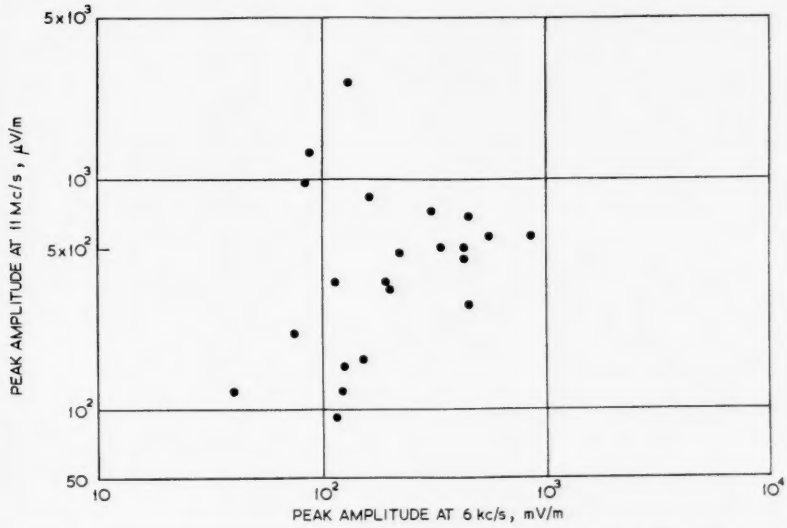

Fig. 1. Comparison between peak amplitudes at 6 kc/s and 11 Mc/s in Storm B. (Distance of storm, 10 km; bandwidth, 300 c/s).

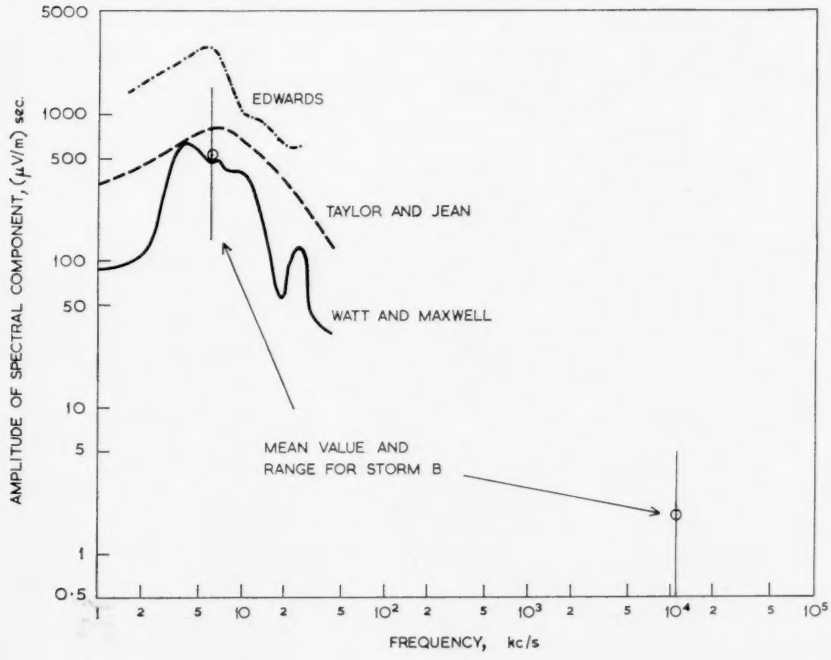

Fig. 2. Spectra of atmospherics.

after correction to 10 km distance. Values for 200 km, quoted by EDWARDS (1956) are also plotted in normalized form and are higher, but it may be noted that another storm which he studied at about 1600 km would have yielded lower values. WATT and MAXWELL (1957), expressed their data for 30–50 km in the form of field strengths in a 1 kc/s bandwidth. If it is assumed that this means the peak value of the r.m.s. field, and that the bandwidth was defined by at least two tuned circuits in series, values of the spectral amplitudes may be derived. They have been corrected for distance and plotted in Fig. 2. Values from the present study are also shown for both 6 kc/s and 11 Mc/s.

Table 3. Durations of atmospherics in milliseconds

	Average	Minimum	Median	Maximum
Storm A	200	30	210	320
Storm B	360	20	360	830

In comparing the data it must be borne in mind that the new results relate to complete atmospherics, many of them multiple, while the other values are for atmospherics from single return strokes. However it has been estimated that the new values at 6 kc/s would have been reduced by only about 30 per cent if each return stroke pulse had been treated as a separate atmospheric, so the agreement with previous data is satisfactory, except that EDWARDS' data are high.

Comparison between the data for 6 kc/s and 11 Mc/s shows a rather smaller difference than would result from an inverse frequency law, but the relationship is probably not a uniform power law over all the intermediate range.

VOL. 21 1961

5. DURATIONS

The accurate measurement of durations is dependent on all the significant features of the atmospherics being visible above the background noise. The background levels were 30 μV/m at 11 Mc/s and 12 mV/m at 6 kc/s.

On first inspection of the records from Storm B, it appeared that the durations were significantly different on the two frequencies. The 11 Mc/s atmospherics might, for example, be quasi-continuous while those at 6 kc/s consisted of one or more isolated pulses as in Fig. 4. Further examination of the largest atmospherics, however, by replaying at high enough gain to reveal the smaller details, suggested that energy was radiated for the same period on both frequencies. A common duration was therefore deduced by inspection of both records. In most cases the durations were well-defined, but those of a few atmospherics which were not much bigger than the background noise may have been underestimated.

The measured durations are shown in Table 3 compiled from twenty-six atmospherics from Storm A and fifty-two from Storm B.

6. WAVEFORMS

The waveforms of the atmospherics have been examined to determine whether they conform to the models of the lightning discharge which have been based on past low frequency observations, and whether they provide any new information

on the discharge processes. It should be borne in mind that owing to the restricted bandwidths of the receivers, the waveforms are smoothed to the extent that components lasting for times less than about 1 msec are not resolved.

Storm B is discussed first because the existence of records on both high and very low frequencies simplifies the task of relating the data to previous knowledge, and also enables a more comprehensive classification to be attempted.

6.1. *Storm B*

The discussion of peak amplitudes was restricted to twenty-two atmospherics whose distances were known with reasonable certainty to be about 10 km. In discussing waveforms, which are less critically dependent on distance, fifty-two atmospherics have been considered. There was strong evidence that most, if not all, of these originated in the same storm cell, although the distances were not all accurately known.

A classification can best be achieved by starting with waveforms containing large 6 kc/s pulses which could be attributed to the return strokes of ground discharges, considering first the simplest types and then introducing various complicating features. The basic sequence of an atmospheric from a discharge containing a ground stroke was a leader phase, a 6 kc/s return-stroke pulse and what will be called a follower phase. This last phase could be the final part of the atmospheric or could be part of the interval between two return strokes of a multiple flash. The term "follower phase" is appropriate because some features showed a definite relationship to the preceding return stroke rather than to any subsequent events.

The waveforms of Storm B have been classified into the following types.

6.1.1. *Type* I. An example of the simplest and commonest type of waveform is shown in Fig. 3 and is designated Type I. The leader was a short burst of 11 Mc/s noise of small amplitude, occupying a few of the 10 msec preceding the return stroke. On most records the return stroke followed this burst immediately, but on some, as in Fig. 3, there was an interval of a few milliseconds. Noise at 6 kc/s was rarely evident during the leader phase, and was never large. The 6 kc/s pulse resulting from the return stroke was unaccompanied by any simultaneous noise at 11 Mc/s. The 11 Mc/s component of the follower stage consisted of one or more pulses (most frequently two), usually in the range 10–20 msec after the return stroke, and these were the main part of the 11 Mc/s noise in the Type I waveforms. The follower stage often included small 6 kc/s pulses, mostly in the range 10–100 msec after the return stroke, which showed no apparent correlation with the 11 Mc/s pulses.

Although there was some variation in the relative amplitudes and times of occurrence of the main components of these waveforms, the example shown in Fig. 3 is about average in these respects.

Most of the Type I waveforms had no detectable energy other than in the components described, but one or two which have been included in this group had other small 11 Mc/s components barely visible above the background noise.

Fifteen waveforms were of Type I, including as special cases one in which the leader part was not visible and one in which no 11 Mc/s energy whatever was

detected, but which had characteristics at 6 kc/s almost identical with others of Type I. Nine other more complex waveforms included a portion of Type I form.

6.1.2. *Type* II. Waveforms classified as Type II had an 11 Mc/s leader of long duration but were otherwise similar to Type I. An example is shown in Fig. 4. Five waveforms of this type had leaders with durations ranging from 30 to 420 msec, with an average of 140 msec. The longest leader was in two parts with a quiescent intermediate phase. Only one had detectable energy at 6 kc/s in the leader phase, and this was small. Nine other more complex waveforms had a portion of Type II form.

In Type II waveforms the main part of the energy at 11 Mc/s occurred before the return stroke.

6.1.3. *Multiple atmospherics.* Ten waveforms had more than one large 6 kc/s pulse and were interpreted as resulting from discharges with more than one return stoke. Eight had two large pulses and the others had three and four. Intervals between the large pulses varied between 40 and 460 msec with an average of 160 msec. All these waveforms contained either Type I or Type II as part of their structure, and some had both types. Two examples are shown in Fig. 5. Each was interpreted as having two return strokes, although they may possibly have had more. In Fig. 5(a) the first return stroke was preceded by a large 11 Mc/s burst, the combined waveforms showing Type II characteristics, while the second large 6 kc/s pulse had little associated energy at 11 Mc/s. In Fig. 5(b) the first large 6 kc/s pulse is preceded by only small 11 Mc/s components and Type D characteristics are exhibited; the latter part of the waveform is more similar to Type II.

VOL. 21 1961

The ten waveforms in this category are those whose origin in multiple flashes was beyond reasonable doubt because they had pulses of similar amplitude (usually within 25 per cent). There were others which could have been attributed to multiple flashes, but with less certainty.

6.1.4. *Other Types.* To sum up the analysis so far, twenty waveforms were of either Type I or Type II, and these types also formed part of fifteen other waveforms including ten which were attributed to multiple flashes.

The remaining seventeen atmospherics had no common characteristics so well-defined as those already discussed, but they did fall into three groups on the basis of the relative amplitudes at the two frequencies.

Nine atmospherics had 6 kc/s amplitudes comparable with, though generally smaller than those of Types I and II, but the 11 Mc/s noise was of a quasi-continuous type with small amplitude and long duration, and lacked any obvious features which could be related to the 6 kc/s pulses. An example is shown in Fig. 6.

Three atmospherics had 6 kc/s amplitudes smaller than the average, but relatively large 11 Mc/s components. They can be identified on Fig. 1 as those with the largest 11 Mc/s amplitudes, and one is illustrated in Fig. 7.

The remaining four atmospherics had small amplitudes on both frequencies, and no outstanding features. It is possible that some of these were from more distant storms even though the illumination from the flash was visible. There were many others of this type which were not seen and which are therefore not discussed in this report.

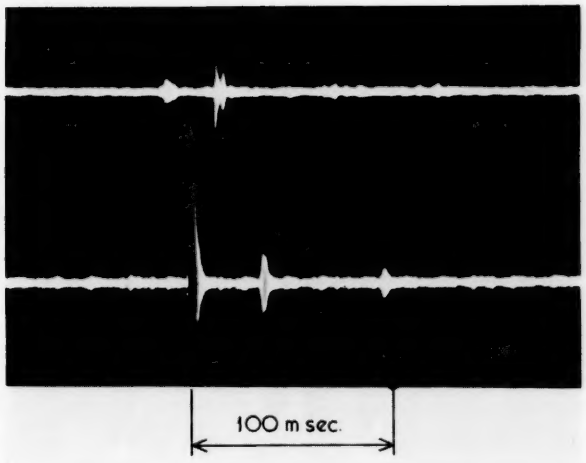

Fig. 3. Type I waveform. (a) 11 Mc/s, amplitude 270 μV/m. (b) 6 kc/s, amplitude 310 mV/m.

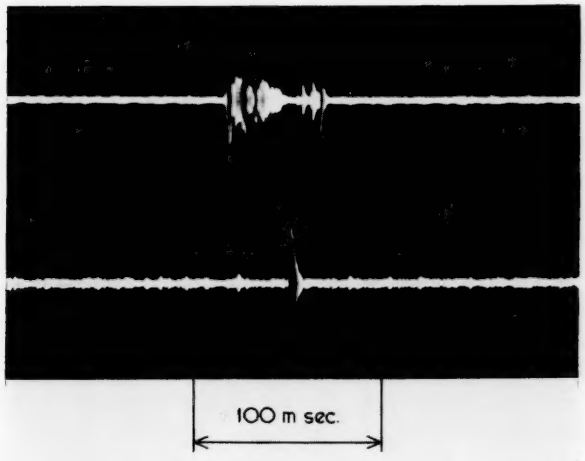

Fig. 4. Type II waveform. (a) 11 Mc/s, amplitude 350 μV/m. (b) 6 kc/s, amplitude 110 mV/m.

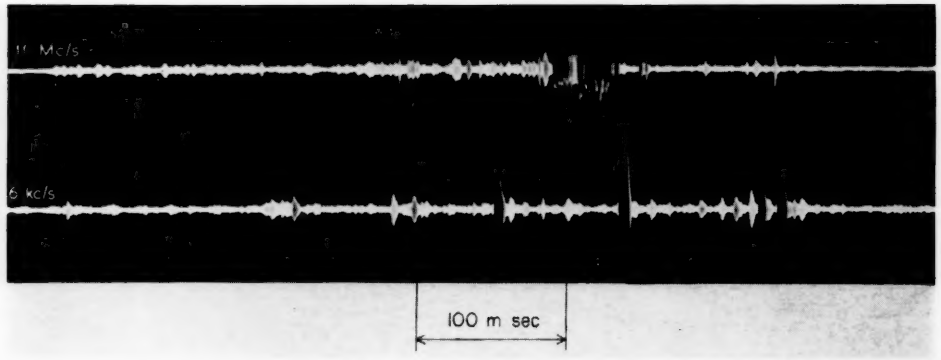

(a)

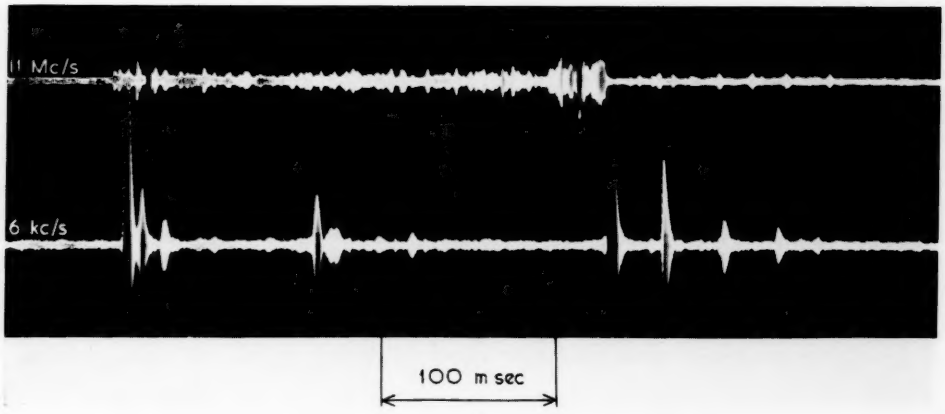

(b)

Fig. 5. Multiple atmospherics. Amplitudes: (a) 560 μV/m at 11 Mc/s, 720 mV/m at 6 kc/s; (b) 680 μV/m at 11 Mc/s, 450 mV/m at 6 kc/s. Owing to the limitations of reproduction the high-amplitude parts of the traces are obscure, particularly at 11 Mc/s. Their positions are indicated by the gaps in the baselines.

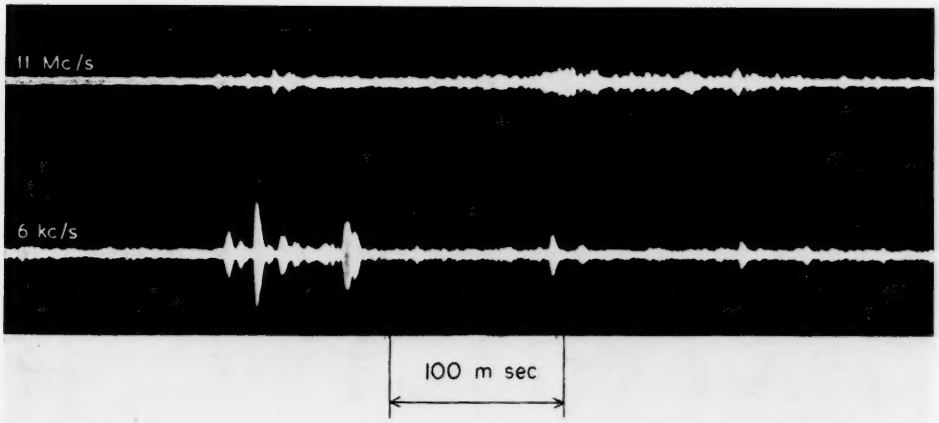

Fig. 6. Long atmospheric with small 11 Mc/s amplitude. Amplitudes: 120 μV/m at 11 Mc/s, 120 mV/m at 6 kc/s. See note in caption to Fig. 5.

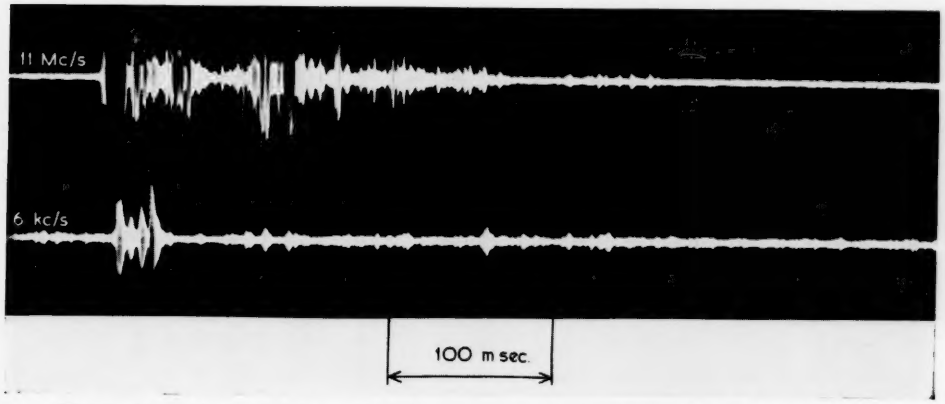

Fig. 7. Atmospheric with large 11 Mc/s component. Amplitudes: 2600 μV/m at 11 Mc/s, 130 mV/m at 6 kc/s.

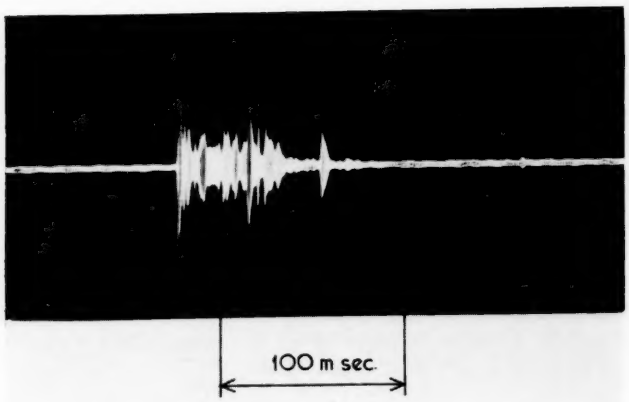

Fig. 8. 11 Mc/s atmospheric from Storm A. (Amplitude 800 μV/m).

6.2. *Storm A*

In the absence of a v.l.f. channel for Storm A, little can be said regarding the relationships between the 11 Mc/s features and the times of occurrence of the return strokes. The 11 Mc/s atmospherics were of somewhat shorter duration than those from Storm B, as shown in Table 3, but they showed similar characteristics. For example, that shown in Fig. 8 is similar to the 11 Mc/s part of Fig. 3, and since the Storm A atmospheric was known to have originated in a ground discharge, it is probable that the return-stroke occurred at the end of the quasi-continuous burst of 11 Mc/s noise. The general pattern of a burst, followed by a quiescent period, followed by either another burst or isolated pulses, was a common feature of the Storm A atmospherics. Many of the waveforms, such as that in Fig. 8, could reasonably be interpreted as being of the simple Type II, with durations in the range 20–100 msec. It is unlikely that any were of Type I, but it is not possible to say whether or not this type was present as part of a more complex waveform, as happened in Storm B.

One flash of particular interest was that which appeared visually to be an excellent example of a cloud flash (see Section 4.1). The waveform was examined to determine whether it had any features to distinguish it from the rest, but none were found. It is not possible to say with certainty that the flash did not strike the ground at a distance, possibly obscured by cloud, but the visible flash was no less bright than the ground flashes, and it is not surprising that it radiated atmospherics of similar intensity.

7. The Origins of Atmospherics

The question arises whether the amplitudes and forms of the atmospherics are consistent with currently-accepted models of the discharge processes in ground discharges. These models have been based on previous low-frequency observations and photographic records, of which full accounts have been given by Schonland (1956). The main features will be brought out in a discussion first of the waveforms illustrated in the figures and then of the results in general.

Type I waveforms (Fig. 3) arise from flashes with one return stroke. The average amplitude of the main 6 kc/s pulse was 260 mV/m at a range of 10 km. A value calculated from the Bruce–Golde (1941) model of the return stroke was 200 mV/m and the model proposed by Morrison (1953), and based on waveforms of Norinder leads to a similar value. The short burst of 11 Mc/s noise before the return stroke could be from the stepped-leader discharge to ground which is known to precede many return strokes, since its duration is within the range (4–30 msec) quoted for this process by Clarence and Malan (1957). There appears to be no simple explanation of the 11 Mc/s followers. They occur during the period when there may be the so-called *M*-components at low frequencies (Schonland, 1956), due to branches of the discharge channel, but it seems unlikely that these would give rise to noise at 11 Mc/s rather than at 6 kc/s. The followers may be associated with the redistribution of charge within the cloud, following the return stroke.

Type II waveforms may be explained similarly, except that the burst of 11 Mc/s noise preceding the return stroke is longer than the durations quoted for

the stepped-leader discharge alone. However, CLARENCE and MALAN (1957), and PIERCE (1955), have shown that the whole of the leader process may last for hundreds of milliseconds.

The atmospheric shown in Fig. 5(a) exhibits many of the features which would be expected in the radiation from a multiple discharge. For the moment it will be assumed to have originated in a discharge with two return strokes, corresponding to the two largest 6 kc/s pulses. The amplitudes and spacing (100 msec) of these pulses are within the limits to be expected.

The long burst of 11 Mc/s noise, lasting 400 msec, corresponds to the preliminary discharge of CLARENCE and MALAN (1957), and there is also 6 kc/s noise throughout this period. The high amplitude 11 Mc/s burst just before the return stroke may be associated with a stepped-leader discharge but is longer than would be expected (50 msec).

According to SCHONLAND (1956), the period between two return strokes is marked by the occurrence of "junction streamers" which progress upwards through the thundercloud, to link up with higher accumulations of charge. Fig. 5(a) shows no high noise levels at either frequency in the interval, except for a single pulse at 6 kc/s and, at 11 Mc/s, the follower pulses and the pulse preceding the second return stroke which might have been from a dart or a dart-stepped leader.

The two 6 kc/s pulses of medium amplitude have not been explained. The possibility that they were from strokes to ground cannot be excluded but it seems more probable that they were large-scale discharges in the cloud, occurring as part of the process leading to the initiation of the ground stroke. It has recently been suggested that noise pulses can be radiated from discharges in the cloud which encounter minor concentrations of charge as they progress (KITAGAWA, 1957).

Although the main features of Fig. 5(a) are consistent with current knowledge of lightning discharges, most of the waveforms could not be explained in such a straightforward manner. For example in Fig. 5(b), which has also been assumed to contain two ground stroke pulses, it is the first pulse which has a short leader phase and the second which is preceded by along burst of 11 Mc/s noise. This is contrary to what would be expected on the basis of the usual model. Also the large 6 kc/s pulses are followed by others of successively smaller amplitude. Those after the second main pulse have spacings similar to those quoted for intervals between return strokes but the later pulses are much smaller than the main return stroke pulses. The smaller 6 kc/s pulses may be discharges in the cloud to higher concentrations of charge.

The atmospherics shown in Figs. 6 and 7, which have smaller than average amplitudes at 6 kc/s, may have originated in cloud discharges.

The discussion of the waveforms shown in the figures has served to illustrate the possible relationships between the main features and the known characteristics of lightning discharges. The origins of the high frequency noise will next be discussed in relation to all the waveforms, with particular reference to the stepped leader as a possible source.

Most of the high frequency noise was contained in those atmospherics in which there were bursts of noise rather than isolated pulses. Considering the twenty-two atmospherics of Storm B which were known to have been received from discharges

at an approximate range of 10 km, 80 per cent of the total energy was contained in only six of the atmospherics. It appears therefore that most of the noise originated in some mechanism which occurred in only a small number of discharges. The return stroke contributed a negligible fraction of the energy. In Storm A, energy levels were more uniform, but 60 per cent of the total energy occurred in one third of the atmospherics.

The stepped-leader discharge has sometimes been assumed to be the main source of high-frequency noise (AIYA, 1955). It is true that in some atmospherics with intense bursts of noise, these occurred just before a return stroke but there were others in which the return stroke occurred first. In view of the limits of 4–30 msec quoted by CLARENCE and MALAN (1957) for the stepped leader process, the following data from the fifty-two atmospherics of Storm B are significant:

(a) The peak amplitude at 11 Mc/s occurred before the first large 6 kc/s pulse in only fourteen atmospherics, and in only ten of these did it occur within 30 msec of the 6 kc/s pulse;

(b) In thirty examples, including all these of Type I, the peak amplitude at 11 Mc/s occurred within 30 msec following the first large 6 kc/s pulse;

(c) In only sixteen examples did the whole of the leader phase contribute most of the energy at 11 Mc/s.

These results suggest that the stepped part of the leader contributed only a small part of the total noise at 11 Mc/s. This conclusion is contrary to that of AIYA (1955), who has calculated the expected intensity of high frequency noise on the assumption that it originates in stepped leaders having durations of the order of 1 msec. His calculations were based on a waveform in a paper by APPLETON and CHAPMAN (1937), and since they recorded only low-frequency energy their waveform contained no information about the high-frequency content of the atmospheric. AIYA's analysis therefore involves assumptions about the variations of discharge currents in stepped leaders for which experimental evidence is lacking.

There is no positive evidence to indicate whether any of the recorded atmospherics from Storm B originated in cloud discharges, although those of Figs. 6 and 7 may have done so. The range of peak amplitudes at 6 kc/s shown in Fig. 1, is similar to quoted values for the range of peak currents in return strokes, but all the atmospherics recorded in this plot were from discharges of which at least the general illumination was visible. There were a number of smaller atmospherics from discharges which were not visible, and these may have been either cloud discharges or more distant ground discharges. The ratio of the amplitudes on the two frequencies was not significantly different in these smaller atmospherics from those plotted in Fig. 1.

8. Power Radiated by Lightning Discharges

Many estimates have been made of the power radiated by lightning discharges, and these have usually referred to the total power in the whole of the range of radio frequencies. Here we will be concerned with the estimation of the power radiated within the relatively narrow pass bands of typical receivers.

Three powers are of interest:

(a) Peak power;

(b) Mean power during the discharge;

(c) Mean power from all discharges of a storm call.

To calculate the radiated power it is necessary to assume a distribution of energy over the hemisphere above the earth's surface, assumed perfectly reflecting. Although this distribution may vary widely according to the configuration of the discharge, it is reasonable to assume that for ground discharges, on the average, the power flux is proportional to $\cos^2 \phi$, where ϕ is the angle above the horizon. It is also assumed that the flux is independent of azimuth. Under these conditions, the relationship between the radiated power P (watts) and the envelope field strength E (V/m) at a horizontal distance r (metres) from the discharge is

$$P = E^2 r^2 / 180.$$

8.1. *Peak power*

The average value of the peak power is derived from the mean square values of the peak amplitudes. Using data for those discharges of Storm B which are known to have been at a range of 10 km, the peak power is found to have an average value of 56 kW in a bandwidth of 300 c/s at 6 kc/s, and 280 mW at 11 Mc/s. The average at 11 Mc/s is influenced considerably by the largest discharge which had a peak power of 3·8 W compared with an average value of 110 mW for all the rest. The average peak power for Storm A was 80 mW, at 11 Mc/s, assuming a mean distance of the storm of 4 km.

As the peak amplitude may be expected to be proportional to the bandwidth, over a wide range, the peak power will be proportional to the bandwidth squared.

8.2. *Mean power during the discharge*

The mean power is the total radiated energy divided by the duration. Using the average values of $\int e^2 \, dt$ and duration from Storm B, the calculated mean powers in the average discharge are 480 W at 6 kc/s and 5·4 mW at 11 Mc/s. For Storm A the average is 4·4 mW at 11 Mc/s. The mean power may be expected to be proportional to bandwidth.

8.3. *Mean power from a storm cell*

Atmospherics at a rate of nearly three per minute were recorded during both Storms A and B. Assuming that a few were from other more distant storms, the rate from those under investigation was probably about two per minute, and this seems to be typical of a storm cell in England.

Using this figure, the mean power from a storm cell derived from the Storm B data in Table 2 is about 6 W at 6 kc/s and 60 μW at 11 Mc/s. For Storm A the average at 11 Mc/s is 30 μW. These values will be proportional to bandwidth. In a typical storm cell in England, these powers will be substained for a time of the order of half an hour.

VOL. 21 1961

9. Conclusions

The recording of single atmospherics in narrow bandwidths can contribute to our knowledge of noise and of the mechanism of lightning discharges. Data can be readily derived by the analysis of records on magnetic tape.

Values of peak amplitudes and total energy of atmospherics at frequencies of 6 kc/s and 11 Mc/s have been obtained. From these values, and the known distances of the storms, the power radiated at these frequencies has been estimated.

A general conclusion from the waveform studies is that most waveforms showed some features which could be reasonably identified with known processes in lightning discharges, but few could be explained in terms of a regular sequence of events such as is envisaged in the models of the discharges which have been postulated. At 6 kc/s the largest pulses in most if not all the atmospherics, could be attributed to return strokes. Some of the smaller pulses may have been from return strokes also, but it seems more likely that many were from parts of the discharge within the cloud. If so, some of these discharge components evidently had characteristics comparable with those of return strokes.

At 11 Mc/s the return stroke radiates negligible energy, and although the stepped leader discharge appears to be a minor source of energy, the main sources have not been quantitatively identified with any of the well-known lightning processes. Most of the total energy from one storm occurred in only a small fraction of the atmospherics.

Acknowledgements—The work described was carried out as part of the programme of the Radio Research Board. The paper is published by permission of the Director of Radio Research of the Department of Scientific and Industrial Research. The recording of the atmospherics was carried out by C. Clarke, and P. A. Bradley assisted in the analysis.

References

Aiya S. V. C.	1955	*Proc. Inst. Radio Engrs, N.Y.* **43,** 966.
Appleton E. V. and Chapman F. W.	1937	*Proc. Roy. Soc.* **158,** 1.
Bruce C. E. R. and Golde R. H.	1941	*J. Instn Elect. Engrs* II **88,** 487.
Chapman F. W. and Macario R. C. V.	1956	*Nature, Lond.* **177,** 930.
Clarence N. D. and Malan D. J.	1957	*Quart. J. R. Met. Soc.* **83,** 161.
Clarke C.	1960a	*Electron. Techn.* **37,** 197.
Clarke C.	1960b	*Electron. Techn.* **37,** 346.
Edwards A. G.	1956	*J. Brit. Instn Radio Engrs* **16,** 31.
Hill E. L.	1957	*J. Franklin Inst.* **263,** 107.
Horner F.	1958	*J. Atmosph. Terr. Phys.* **13,** 140.
Horner F. and Clarke C.	1958	*Nature, Lond.* **181,** 688.
Kitagawa N.	1957	*Pap. Met. Geophys., Tokyo* **7,** 415.
Malan D. J.	1959	*Recent Advances in Atmospheric Electricity*, p. 557. Pergamon Press, London.
Morrison R. B.	1953	*Phil. Mag.* **44,** 980.
Pierce E. T.	1955	*Quart. J. R. Met. Soc.* **81,** 211.
Schonland B. F. J.	1956	*The Lightning Discharge.* Encyclopedia of Physics, Vol. 22. Springer, Berlin.
Taylor W. L. and Jean A. G.	1959	*J. Res. Nat. Bur. Stand.* D **63,** 199.
Watt A. D. and Maxwell E. L.	1957	*Proc. Inst. Radio Engrs, N.Y.* **45,** 787.

Journal of Atmospheric and Terrestrial Physics, 1961, Vol. 21, pp. 26 to 34. Pergamon Press Ltd. Printed in Northern Ireland

Magnetic effects in the *F*-region of the ionosphere

J. W. KING
Department of Physics, University of Natal, Pietermaritzburg, Union of South Africa

(*Received* 17 *November* 1960)

Abstract—Plots of f_0F2 vs. the equivalent planetary daily amplitude, A_p, show that at night f_0F2 decreases as the magnetic disturbance increases. During the midnight period an A_p of 35 is found to reduce the ionization below the value corresponding to zero magnetic disturbance by an amount within a few percent of 65 per cent in all seasons and for all the stations investigated.

The "half-life" of the ionization as deduced from critical frequency values during the night is shown to be dependent on the value of A_p, and decreases from 5·0 hr for nights of small magnetic disturbance to about 3·0 hr for disturbed nights. The amount of magnetic disturbance thus controls both the amount of ionization present before midnight and the fraction of this transferred to the next day. It is shown that this mechanism could be responsible for the day-to-day correlation of f_0F2 values.

A method for selecting ionospherically quiet and disturbed days is suggested, and it is shown that the magnetically selected 5*Q* days are not generally ionospherically quiet; the days immediately after the 5*Q* days are much more likely to be ionospherically quiet. It is shown that during the midday period the median critical frequency is the frequency corresponding to no magnetic disturbance, while days which are disturbed may have frequencies which are greater or smaller than the median, the amount greater or smaller depending on the value of A_p.

The greatest variability of the ionosphere is shown to occur at night rather than during the day; this, together with the fact that plots of f_0F2 before midnight unexpectedly form a set of divergent curves, is due to magnetic effects.

1. INTRODUCTION

THIS PAPER describes an analysis of f_0F2 data obtained during the International Geophysical Year at recording stations at Cape Town, Grahamstown and Johannesburg in South Africa, and at Tsumeb in South West Africa. Further information about these stations may be found in a companion paper (KING, 1961).

In Section 2 the relationship between f_0F2 and the equivalent planetary daily amplitude, A_p, and the appropriate geomagnetic planetary 3 hr range index, K_p, is discussed. Section 3 is concerned with the "half-life" of the ionization as deduced simply from f_0F2 results. The relationship between this half-life, and in consequence the amount of ionization remaining from one day to the next, and the degree of magnetic disturbance present is discussed. In Section 4 a method is used for the selection of days which are "quiet" ionospherically, and the relationship between such days and days which are quiet magnetically is indicated. Section 5 contains illustrations of some of the consequences of magnetic effects, e.g. the fact that f_0F2 plots before midnight form a set of divergent lines, and the fact that the greatest variability of the ionosphere occurs at night.

2. THE RELATIONSHIP BETWEEN f_0F2 AND THE DEGREE OF MAGNETIC DISTURBANCE

It is inadvisable to look for any relationship which may exist between f_0F2 and A_p by correlating corresponding values of the two quantities, because one grossly uncorrelated pair in the series will greatly reduce the value of the correlation coefficient which might otherwise be substantial.

The obvious method is to make monthly plots of A_p vs. f_0F2 for a particular station at a particular hour. Typical examples of such plots are shown in Fig. 1,

VOL. 21 1961

from which it is immediately apparent that f_0F2 depends on A_p, and increases as A_p tends to zero. Such plots show that this relationship exists during the night only; plots done for day hours indicate a relationship of some other form. In summer months the relationship becomes noticeable at about 2000 hours local time, and is evident for the ensuing hours.

We may use the best straight lines through the A_p vs. f_0F2 plots to calculate the change in critical frequency, and hence in the ionization at the maximum of

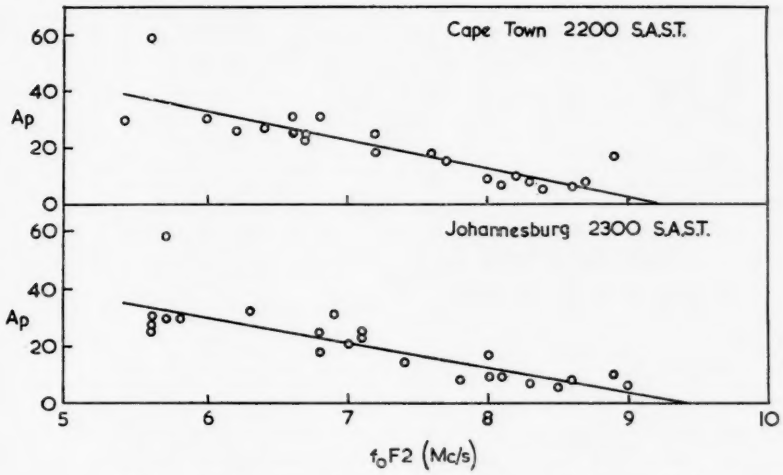

Fig. 1. Typical examples of A_p vs. f_0F2 plots. February 1958.

the layer, brought about by a change in A_p from zero to 35. If the ionospheric change is expressed in terms of ionization we can plot a graph of this change vs. the ionization pertaining to zero magnetic disturbance, i.e. we can plot

$$[f_0F2\ (A_p = 0)]^2 - [f_0F2\ (A_p = 35)]^2 \text{ vs. } [f_0F2\ (A_p = 0)]^2.$$

Such a plot is shown in Fig. 2 for the night-time A_p vs. f_0F2 plots. It appears that the change in ionization is proportional to the amount of ionization corresponding to the undisturbed ionosphere. In all cases an increase of A_p from 0 to 35 reduces the ionization by about 65 per cent. This fraction appears to be independent of the station, the time of night or the season.

We have seen that an A_p of 35 brings about a 65 per cent reduction of the ionization, and we may calculate the percentage reduction brought about by any other value of A_p. This reduction will be independent of the value of f_0F2 corresponding to $A_p = 0$, but it is of course not proportional to the value of A_p.

We may use the A_p vs. f_0F2 plots for the hours 2100–0000 inclusive in any month to calculate the average amount by which the ionization corresponding to the median f_0F2 values is reduced below the value corresponding to $A_p = 0$ for the month. Knowing this percentage we can predict, as indicated above, the median value of A_p for the month. This has been done for four months and the results are

shown in Table 1. The predicted A_p values are in excellent agreement with the actual values, indicating the validity of the f_0F2 ($A_p = 0$) values.

An entirely different type of investigation may be carried out to see whether f_0F2 is related to the values of the appropriate geomagnetic planetary 3 hr range

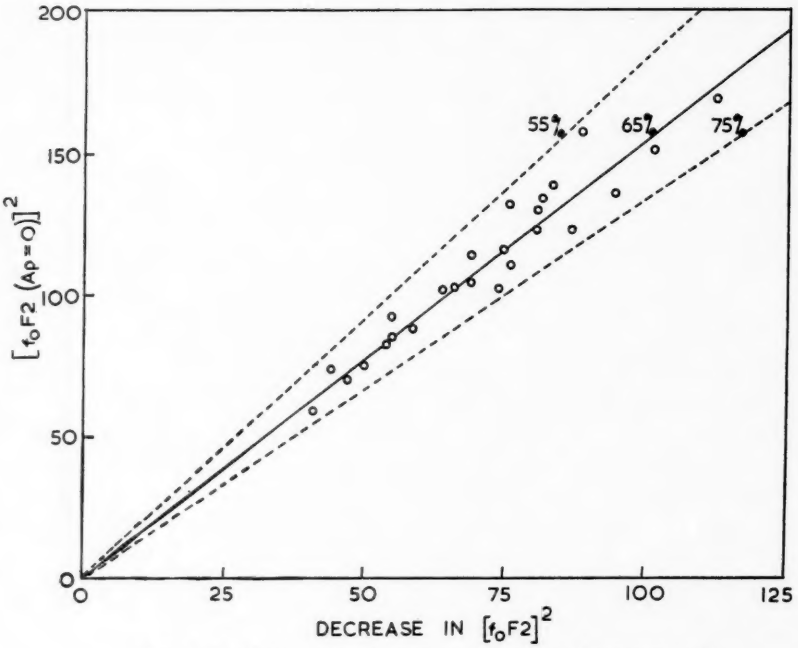

Fig. 2. Reduction in ionization as A_p increases from zero to 35.

Table 1. Predicted A_p values

Month	Amount by which median ionization is reduced below $A_p = 0$ ionization	Predicted A_p value	Actual median A_p value
October 1957	29 per cent	13	12
November 1957	36 per cent	17	16
December 1957	38 per cent	18	18
February 1958	40 per cent	20	23

index, K_p. For a particular station at a particular hour the daily values of K_p for the interval in which the chosen hour fell were used as follows: The days of the month were divided into groups having the same value of K_p for the interval, and the mean f_0F2 found for each group of days. Hence a plot of the K_p values vs. the corresponding f_0F2 is obtained for that hour. At night these plots are also found to be straight lines (Fig. 3) showing that f_0F2 decreases as K_p increases. It is found on average that a K_p of 5 corresponds to a reduction of the ionization below the

VOL. 21 1961

value corresponding to $K_p = 0$ by about 40 per cent. We conclude that a value of K_p (which pertains only to the relevant 3 hr interval of the day) of 5 corresponds to an A_p (which is calculated on a full day basis) of 20, since both produce an ionization decrease of 40 per cent.

During daylight hours this type of dependence of f_0F2 on A_p does not occur. It will be shown in Section 4 that at the middle of the day the monthly median value of f_0F2 corresponds to an A_p of zero, while larger A_p values cause local

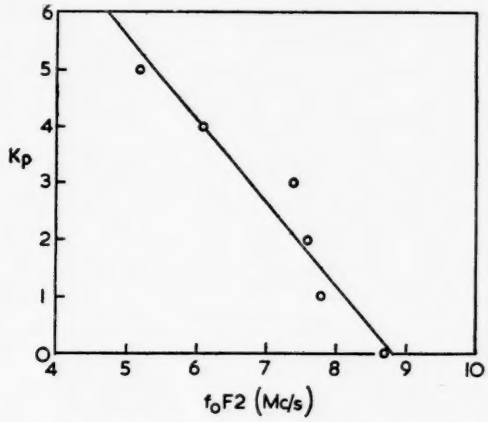

Fig. 3. Typical plot of K_p vs. f_0F2. Cape Town, February 1958, 2200 S.A.S.T.

ionospheric variability such that the critical frequency may be increased above or decreased below the median value. The larger the value of magnetic disturbance the greater, in general, is the departure of f_0F2 from the median value.

3. The Half-Life of the Ionization at Night

During the night the amount of ionization in the ionosphere decreases and we can imagine a simple "half-life" calculated from critical frequency values assuming an exponential decay

$$N = N_0 e^{-\lambda t}$$

where the half-life $T = 0{\cdot}693/\lambda$. This simple half-life cannot be applied to any particular height in view of the changes in the height of the maximum of the layer, but it is an interesting quantity which is found to be dependent on the value of A_p.

In the first instance we may use the values of f_0F2 at $A_p = 0$ obtained from the A_p vs. f_0F2 plots to calculate the half-life of the ionization under magnetically quiet conditions. For eight months for which plots were done a mean half-life of 4·9 hr is obtained for the period 2100–0000 hours. Using the corresponding monthly median values (which will correspond to some value of A_p greater than zero) we obtain a half-life of only 3·9 hr. The question immediately arises as to whether the half-life depends on the value of A_p in general. Individual day-to-day correlation is not a satisfactory method of investigating this problem because of isolated exceptional events which might affect only one day, and which are capable

of reducing a correlation coefficient of this type from 0·5 to zero. Thus the problem has been approached on a monthly basis instead. The half-life for each day was calculated from the values of f_0F2 at 2100 and 0400 hours the next day, and the mean half-life for the month thus found. This quantity is plotted against the mean value of A_p for the month in Fig. 4, and it is seen that longer half-lives occur during months of less magnetic disturbance. It will be seen from Fig. 4 that the

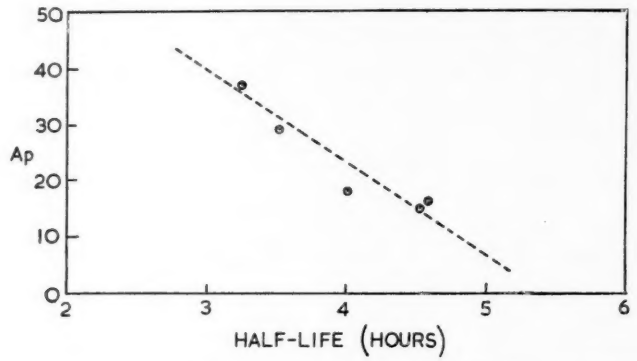

Fig. 4. Mean A_p plotted vs. mean half-life for five different months.

half-life predicted for very small values of A_p is just greater than 5 hr, while the half-life for a reasonably large A_p is about 3 hr. Nights having half-lives given by these values will yield very different critical frequencies at sunrise the next morning.

The effect of the half-life on the ionosphere was found as follows: Data from Tsumeb for the six months September 1957 to February 1958 were used to calculate the half-life during the period 2100 to 0400 hours for each night, and the days having the five longest and five shortest half-lives in each month were then investigated. For the thirty days of long half-lives the mean half-life was 5·1 hr and the critical frequency at 0400 hours next day was found in twenty-six cases to be greater than the appropriate monthly median critical frequency, the overall mean increase being 0·51 Mc/s. For the thirty days of short half-lives the mean half-life was 3·1 hr and in twenty-seven cases the critical frequency at 0400 hours next day was less than the appropriate median value, the overall mean decrease being 0·57 Mc/s. Thus the increase in half-life from 3·1 to 5·1 hr (which we saw from Fig. 4 were the values corresponding to disturbed and quiet magnetic conditions respectively) results in an increase of 1·08 Mc/s in the critical frequency at 0400 hours the next day.

The operation of the following mechanism has thus been established:

(a) Days of low A_p values have high critical frequencies (vide A_p vs. f_0F2 plots) during the evening and long half-lives during the night, so that the critical frequency at sunrise on the next day will be high.

(b) Days of high A_p values have low critical frequencies in the evening, and short half-lives, so that critical frequencies the next day will be low.

It seems reasonable to suggest that this double mechanism is responsible for the day-to-day correlation of f_0F2 values reported in a companion paper (KING, 1961). The extra ionization carried over after a long half-life would not be expected to be noticeable throughout the day because of changes in the height of the maximum of the layer, but its presence might well become noticeable again in the early evening. In this way the peaks centred at 0700 and 1900 hours in the diurnal variation of the auto-correlation coefficient of f_0F2 might be explained.

It is probable, if the day-to-day correlation depends on the amount of ionization transferred from one day to the next, that the correlation would be not so good in months when less ionization is transferred, i.e. in months of short half-lives i.e. in months of higher A_p values. This is borne out by the data given in Table 2.

Table 2. Values of A_p and corresponding auto-correlation coefficients

Month	Median A_p values	Mean auto-correlation coefficient
October 1957	12	0·41
November 1957	16	0·38
February 1958	23	0·32

4. Ionospheric Variability and the A_p of the Day before

In order to obtain some idea of the degree of ionospheric disturbance, as opposed to magnetic disturbance, pertaining to a particular day the following procedure is suggested: For each of several stations in the same geographical area the difference between the values of f_0F2 at noon (say) and the appropriate monthly median values are obtained, and the moduli of these differences added. The resulting figure may be used as a measure of the ionospheric disturbance over the area at the particular hour on the day concerned. This quantity will be referred to as the "disturbance parameter". The disturbance parameters may then be arranged in numerical order, with the day corresponding to the smallest value being the day which is ionospherically quietest in the month.

This procedure has been carried out for data from Cape Town, Johannesburg and Tsumeb, and it is found in general that the days officially listed as the $5Q$ days in the month (i.e. the days in the month having the five lowest A_p values) are by no means the five quietest days ionospherically. However, it is found that the days after the $5Q$ days are generally reasonably quiet ionospherically.

A typical example is September 1957, where the $5Q$ days are found to be the eighth, tenth, fifteenth, seventeenth and eighteenth quietest days ionospherically, whereas the five days after the $5Q$ days are the first, third, eighth, tenth and sixteenth quietest days ionospherically. It is obvious that if one chooses the $5Q$ days themselves one is not really choosing ionospherically quiet days at all. Similarly the $5D$ days do not include any of the three days most disturbed ionospherically, but the two days most disturbed ionospherically are days following

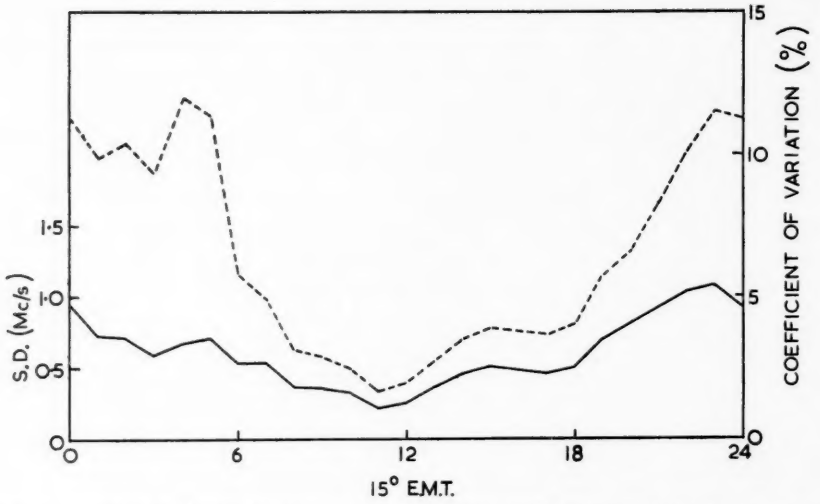

Fig. 5. Standard deviation (solid curve) and percentage coefficient of variation for Tsumeb, October 1957.

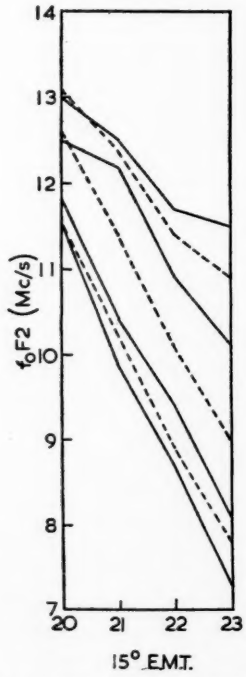

Fig. 6. f_0F2 plots during the late evening. Seven days from October 1957 (Tsumeb).

VOL. 21 1961

two of the 5 D days. These results, which are typical, may be presented in another way. The mean value of the disturbance parameter for:

(a) the month is . . . . 2·1 Mc/s
(b) the 5 Q days is . . . . 1·3 Mc/s
(c) the 5 D days is . . . . 2·6 Mc/s
(d) the five days after the 5 Q days is 0·9 Mc/s
(e) the five days after the 5 D days is 5·0 Mc/s

Two conclusions are immediately apparent:

(a) The disturbance parameter is less on the 5 Q days than on the 5 D days, but this effect is much more pronounced if the days following the magnetically selected days are used. There is other evidence which supports this conclusion viz: Six sets of ionospheric parameters and A_p for the same days during a month were correlated, and the mean value of the correlation coefficient found to be 0·24; for the same six series this value rises to 0·41 if the A_p values of the preceding days are used instead. This conclusion will be discussed more fully in a later paper.

(b) Magnetically quiet days lead to days with smaller than average disturbance parameters, and vice-versa, indicating that the median f_0F2 corresponds to a magnetically quiet day. Days with magnetic disturbance have critical frequencies which may be either above or below the median value. This is apparent from a cursory examination of data from stations several hundred kilometres apart, where, on a particular disturbed day, the critical frequency of one may be 1·5 Mc/s above the monthly median value and the other 1·5 Mc/s below the median value. It is because of this local variability that the moduli of the differences, and not the algebraic differences, must be added when finding the disturbance parameter as described above. In calculating the parameter care must be taken to avoid months with, or to avoid the effect of, a regular seasonal trend of the f_0F2 values. If such a trend is present departures from the median are not only an indication of ionospheric disturbance.

5. Behaviour of f_0F2 during the Early Evening

Fig. 5 shows plots, which are typical, of the standard deviation and the percentage coefficient of variation (i.e. 100 × standard deviation/mean) of f_0F2 for a month. The standard deviation curve exhibits a smooth diurnal variation which exhibits no sudden changes at sunset or sunrise. It seems probable that this variation has an explanation not entirely based on solar control, and it is probably partly explained in terms of magnetic effects. The actual standard deviation in megacycles per second is several times as great by night as by day, and simple calculation shows that the variability of the quantity of ionization present at the maximum of the layer is greater from night to night than from day to day. The increase in standard deviation during the early evening may be illustrated in another way which shows it to be the result of magnetic activity. Fig. 6 shows plots of f_0F2 at Tsumeb for seven days in October 1957. The curves obviously constitute a divergent set. It would be expected, in terms of current ideas of

electron loss in the $F2$-region, that the set of curves illustrated would be convergent. The rate of electron loss, omitting drift losses, is given by

$$\frac{\partial N}{\partial t} = -\beta N$$

and therefore we would not expect the standard deviation to increase during the evening.

The divergent set is produced, however, because days of low magnetic activity have high critical frequencies and long half-lives, while disturbed days have low critical frequencies and short half-lives. A high initial level of ionization therefore persists to a greater extent than a low level, thus explaining the increasing standard deviation.

The effect illustrated by the divergent set in Fig. 6 may be shown to apply for the days of any month by plotting the algebraic differences between the f_0F2 values at 2000 hours and the median for 2000 hours vs. the algebraic differences between the values at 2300 hours and the median at 2300 hours. In the resulting plot about 80 per cent of the points are found to lie in the first or third quadrants, and it appears on average that if the critical frequency on a particular day is n Mc/s greater than (or less than) the median frequency at 2000 hours it will be roughly $1{\cdot}5 \times n$ Mc/s greater than (or less than) the median frequency at 2300 hours on the same day.

Acknowledgements—The author is grateful to the S.A.C.S.I.R. for supplying him with bulletins of ionospheric data obtained at Cape Town and Johannesburg, and for a research grant which enabled him to obtain help with some of the calculations. He is also grateful to the Max-Planck-Institut für Physik der Ionosphäre for supplying him with data recorded at Tsumeb.

VOL. 21 1961

REFERENCE

KING J. W. 1961 *J. Atmosph. Terr. Phys.* **21**, 35.

Journal of Atmospheric and Terrestrial Physics, 1961, Vol. 21, pp. 35 to 39. Pergamon Press Ltd. Printed in Northern Ireland

Day-to-day and station-to-station correlation of ionospheric *F*-region critical frequencies

J. W. King
Department of Physics, University of Natal, Pietermaritzburg, Union of South Africa

(*Received* 17 *November* 1960)

Abstract—The cross-correlation of f_0F2 observed at different stations is found to have a diurnal variation with two maxima and two minima each day. The phase of this variation appears to exhibit a seasonal change with reversals of direction at the equinoxes. The mean cross-correlation coefficient is 0·5 for stations on the same north–south line and separated by 2000 km, and also for stations having the same latitude and a separation of only 1000 km. The diurnal variation of cross-correlation is shown to be unrelated to solar tidal effects.

The auto-correlation of critical frequencies from a single station indicates that there is an important relationship between the value of f_0F2 at a particular hour and the value at the same hour on the day before. The diurnal variation of the auto-correlation coefficient has maxima at 0700 and 1900 hours and minima at 1300 and 0100 hours, and exhibits no seasonal change. This correlation is probably due to magnetic effects which determine the amount of ionization carried over from one day to the next.

1. Introduction

During the International Geophysical Year several vertical incidence ionosphere recorders were operated in Southern Africa. The author has made a study of data from recorders operated by the S.A.C.S.I.R. at Johannesburg (26°04′S, 28°06′E) and Cape Town (34°08′S, 18°19′E), by Rhodes University at Grahamstown (33°17′S, 26°29′E) and by the Max-Planck-Institut für Physik der Ionosphäre at Tsumeb (19°14′S, 17°43′E) in South West Africa. Cape Town and Tsumeb have very similar longitudes; they are situated 1700 km apart.

In Section 2 are described the results of cross-correlating hourly values of f_0F2 at various pairs of stations, while in Section 3 the results of solar tidal investigations using Tsumeb and Cape Town data are discussed. Section 4 deals with the day-to-day correlation of f_0F2 at single stations.

2. The Cross-correlation of f_0F2 from Two Different Stations

The procedure adopted has been the correlation throughout a month of the values of f_0F2 obtained at a particular hour each day at the two stations. In this way the diurnal variation of station-to-station correlation (i.e. cross-correlation) is obtained. Fig. 1 shows the diurnal variation of this cross-correlation coefficient for Cape Town and Tsumeb for four consecutive months. The striking features of the results are:

(a) The diurnal variations are periodic, clearly having two maxima and minima in 24 hr, and

(b) The times at which the maxima and minima occur appear to undergo a regular seasonal change of about 4 hr per month. The existence of this seasonal change seems definite when it is noticed that the variations for September 1957 and November 1957 are almost completely out of phase. The sloping solid lines

in Fig. 1 indicate the phase changes of the maxima and minima which occur from month to month.

Apart from the results shown in Fig. 1, diurnal variations have been obtained for four other months for Cape Town–Tsumeb data. An idea of the seasonal variation may be obtained if a sinusoidal curve is superposed on the diurnal variation obtained each month and the best fit used to give an indication of the phase for the month. The results for the eight months August 1957–March 1958 are shown in Fig. 2. It will be seen that the seasonal variation undergoes reversals of direction at just about the times of the equinoxes.

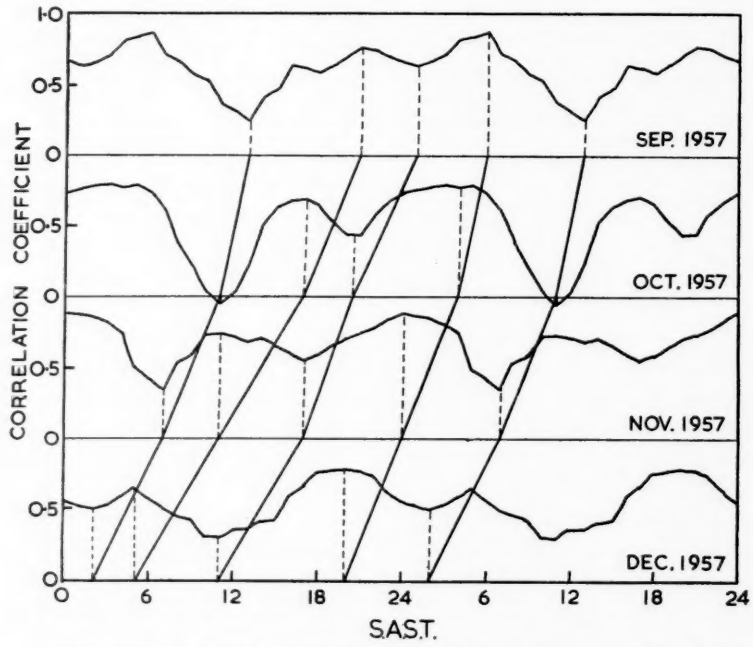

Fig. 1. Diurnal variation of Cape Town–Tsumeb cross-correlation for four consecutive months.

A similar seasonal variation is found in correlations of Cape Town and Johannesburg data, except that the maxima and minima occur about 1½ hr earlier. A time change in this direction is not unexpected in view of the fact that Johannesburg is east of the Cape Town–Tsumeb line.

It is tempting to suppose that the monthly variations, instead of following a seasonal trend, could all be fitted to a picture, for which one could readily suggest an explanation, in which maxima of correlation occur at about 0500 and 1700 hours, and minima at 1100 and 2300 hours. Fig. 1 shows that some months, e.g. September 1957 and December 1957, fit such a picture, but other months do not, e.g. November 1957 and January 1958 have maxima at about midday. The fact that the diurnal variations are reasonably periodic, yet some months are completely out of phase with other months, implies a seasonal change.

VOL. 21 1961

For Cape Town–Tsumeb data the mean value of the maxima of cross-correlation found in the eight months is 0·73 and the mean value of the minima is 0·34.

It is interesting to compare the cross-correlation coefficient obtained for two stations separated along a north–south line with that for two stations having the same latitude. For Cape Town and Tsumeb (same longitude, 1700 km apart) the mean value of the coefficient is 0·54, whereas for Grahamstown and Cape Town (same latitude, 750 km apart) the mean value is 0·65. From these figures we

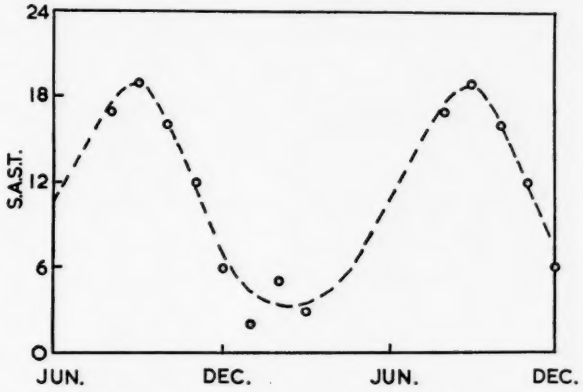

Fig. 2. Seasonal variation of the time at which a maximum of cross-correlation occurs.

estimate that the correlation between stations having the same longitude would be 0·5 if they were 2000 km apart, whereas for stations having the same latitude the value would be 0·5 if they were only 1000 km apart.

3. Solar Tidal Effects

It is obvious, in view of the large distances involved, that the cross-correlation reported in Section 2 cannot be caused by travelling ionospheric disturbances or ionospheric winds. It is not likely, in view of the apparent seasonal change, that the periodic diurnal variation is the result of solar tides. In fact, for the four months for which results are shown in Fig. 1, no evidence of solar tidal effects could be found by the usual (Mitra, 1952) means. Fig. 3 shows a plot of the differences between the mean f_0F2 values throughout the day at Cape Town and Tsumeb for September and October 1957. There is no sign of a semi-diurnal component indicating the presence of solar tidal effects; this component is very pronounced when such effects are important. In particular, since equinoctial months have been investigated in this way, asymmetrical tidal terms would be expected to be absent and the tidal effect therefore unobscured.

4. The Day-to-day Correlation of f_0F2 at a Single Station

Monthly plots of f_0F2 for a particular hour clearly show that the values are by no means arranged in random order, and that there appears to be some relationship between the values of f_0F2 on consecutive days. In order to investigate this relationship quantitatively the monthly values of f_0F2 at a particular hour have

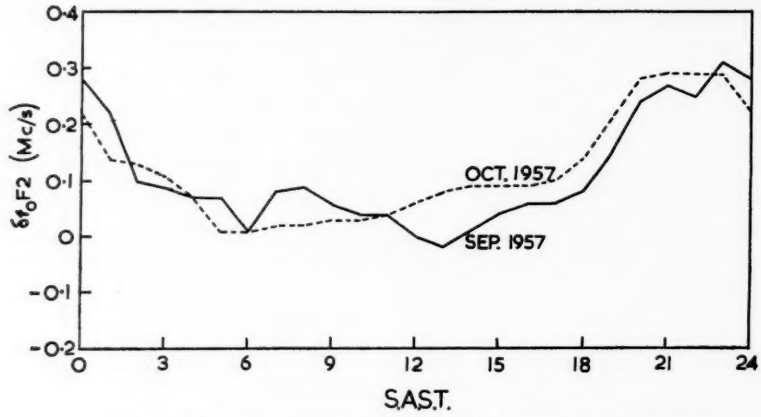

Fig. 3. Diurnal variations indicating the absence of tidal effects.

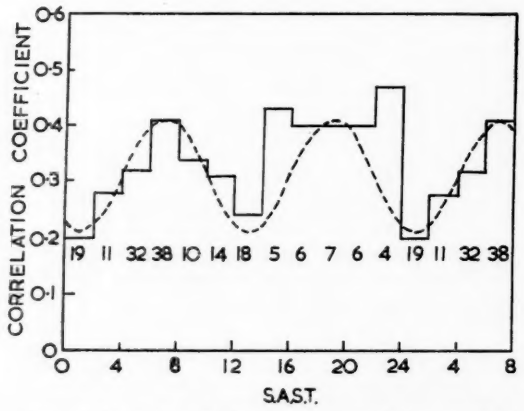

Fig. 4. Diurnal variation of auto-correlation coefficient.
The number of values in each interval is shown.

been auto-correlated, i.e. the series of values has been correlated with the same series displayed by one day. The values of auto-correlation coefficient obtained vary from 0·87 downwards, and indicate that there is an important relationship between the value of f_0F2 at a particular hour and the value at the same hour on the day before. In all, 170 values of auto-correlation coefficient have been obtained at different times of the day, in different months, and for different stations.

It is apparent from a study of the results that the diurnal variation of the auto-correlation coefficient has maxima at about 0700 and 1900 hours, and minima at 1300 and 0100 hours. There appears to be no seasonal variation of the auto-correlation coefficient. The 170 values are distributed as shown in Fig. 4. The values for the periods 1400–1600 and 2200–0000 hours are the least reliable because of the paucity of results in these intervals.

A histogram of the 170 values is given in Fig. 5 and indicates that, since almost three-quarters of the results are uniformly distributed between 0·10 and 0·55, there is a diurnal variation of the coefficient rather than some particular value at

VOL. 21 1961

which a peak occurs in the distribution. For four months complete diurnal variations were obtained and the average value of the minimum correlation coefficients is 0·10, and the average value of the maxima is 0·53. These values agree with those indicated by the histogram as the limits between which the diurnal variation occurs.

The mean value of the auto-correlation coefficient for f_0F2 with a displacement of one day is 0·33, and for a time shift of two days the mean value is 0·21. The former value should be regarded as being remarkably high in view of the large changes which often occur from day to day, as a result of an ionospheric storm for example, and which can drastically reduce the value of the correlation coefficient.

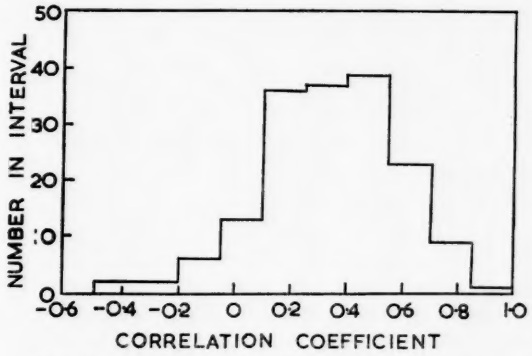

Fig. 5. Histogram of the 170 auto-correlation values.

It is suggested in a companion paper (King, 1961) that this auto-correlation is due to magnetic effects which are found to determine the amount of ionization present in the F-region on any day, and the fraction of this ionization which is carried over to the next day. The low minima in auto-correlation observed just after noon and midnight are presumably due to local ionospheric variability at these times. It is shown in the companion paper that the greatest variability of the ionosphere occurs in the middle of the night.

Acknowledgements—The author is indebted to the S.A.C.S.I.R. for supplying him with bulletins of ionospheric data obtained at Cape Town and Johannesburg, and for a grant which enabled him to obtain assistance with some of the correlation calculations. He is also grateful to the Max-Planck-Institut für Physik der Ionosphäre for supplying him with data recorded at Tsumeb. Mr. H. Helm assisted with the project at one stage, and some of the results were reported by Helm and King (1959).

References

Helm H. and King J. W. 1959 *The Morphology of the F2-region of the Ionosphere over Southern Africa.* Paper read to conference of S.A. Institute of Physics held at Stellenbosch in July.

King J. W. 1961 *J. Atmosph. Terr. Phys.* **21**, 26.

Mitra S. K. 1952 *The Upper Atmosphere*, 2nd Ed., p. 340. The Asiatic Society, Calcutta.

Journal of Atmospheric and Terrestrial Physics, 1961, Vol. 21, pp. 40 to 45. Pergamon Press Ltd. Printed in Northern Ireland

A solution of the integral equation $h'(f) = \int \mu'(f; f_0)\, dz(f_0)$*

H. UNZ
Electrical Engineering Department, University of Kansas, Lawrence, Kansas

(*Received* 18 *November* 1960)

Abstract—An alternative method for the solution of the integral equation $h'(f) = \int \mu'(f; f_0)\, dz\ (f_0)$ is given. The solution involves expansion of the functions in a power series. It is believed that this solution is superior in some respects to previous methods. We will assume that there are no collisions.

1. INTRODUCTION

THE virtual height h' in the ionosphere measurement is defined (THOMAS, 1959) as the height of a sharply bounded reflector, in free space, which would reflect pulses of mean frequency f with time interval τ between transmission and reflection by the reflector such that

$$h' = c\tau \tag{1}$$

h' is measured as a function of the frequency of the pulse f as $h'(f)$.

Actually the time delay of the pulse is due to the variation of the refractive index in the ionosphere:

$$\tau = \int_0^H \frac{dz}{v_g} \tag{2}$$

where v_g is the group velocity and H is the maximum height beyond which the pulse will not propagate. By defining the group refractive index $\mu' = c/v_g$ we get from (1) and (2):

$$h' = \int_0^H \mu'\, dz. \tag{3a}$$

Since h' depends on the transmitter frequency f and the electron density as function of height $N(z)$ may be written (RATCLIFFE, 1959) as $z(f_0)$ where $(2\pi f_0)^2 = \omega_0{}^2 = Ne^2/\varepsilon_0 m$ (using rationalized m.k.s. units). (3a) may be written as

$$h'(f) = \int_0^H \mu'(f;\ f_0) dz(f_0). \tag{3b}$$

H is the height of reflection; it is $X = (f_0/f)^2 = 1$ for the ordinary wave. Therefore (3b) may be rewritten as:

$$h'(f) = \int_0^f \mu'(f;\ f_0) \frac{dz(f_0)}{df_0}\, df_0\ . \tag{4}$$

(4) is the integral equation which we would like to solve.

* This work has been supported in part by Contract No. DA-44-009 Eng.-3769 at the Midwest Research Institute, Kansas City, Missouri.

VOL. 21 1961

In case of no magnetic field $Y_T = Y_L = 0$ we have (RATCLIFFE, 1959):

$$\mu' = \frac{1}{\mu} = \frac{1}{\sqrt{(1 - X)}} = \frac{1}{\sqrt{[1 - (f_0/f)^2]}}. \tag{5}$$

Substituting (5) in (4) we get:

$$h'(f) = \int_0^f \frac{f}{\sqrt{(f^2 - {f_0}^2)}} \frac{dz(f_0)}{df_0}\, df_0. \tag{6}$$

APPLETON (1930) and DE GROOT (1930) have shown that the solution of (6) may be written in closed form as:

$$z(f_0) = \frac{2}{\pi} \int_0^{f_0} \frac{h'(f)\, df}{\sqrt{({f_0}^2 - f^2)}}. \tag{7}$$

Another method of deducing this result based on the Laplace transform has been given by MANNING (1947).

2. THE CASE OF NO MAGNETIC FIELD

We are going to solve (6) by the expansion method, and use this solution as an alternative method for proving the equivalence of (6) and (7).

By using Weierstrass's theorem (COURANT and HILBERT, 1953) we can expand:

$$z(f_0) = \sum_{n=0}^{\infty} a_n {f_0}^n. \tag{8}$$

Since (8) is a uniformly convergent series we can substitute in (6) and interchange summation and integration signs:

$$h'(f) = \sum_{n=0}^{\infty} a_n n \int_0^f \frac{f}{\sqrt{(f^2 - {f_0}^2)}} {f_0}^{n-1}\, df_0 \tag{9}$$

the integral in (9) may be evaluated by putting $f_0 = f \sin \alpha$:

$$\int_0^f \frac{f}{\sqrt{(f^2 - {f_0}^2)}} {f_0}^{n-1}\, df_0 = f^n \int_0^{\pi/2} \sin^{n-1} \alpha\, d\alpha = f^n \beta_{n-1} \tag{10a}$$

where we define:

$$\beta_{n-1} = \int_0^{\pi/2} \sin^{n-1} \alpha\, d\alpha. \tag{10b}$$

Substituting (10) into (9) we obtain:

$$h'(f) = \sum_{n=0}^{\infty} (n a_n\, \beta_{n-1}) f^n. \tag{11}$$

We see that the formal solution of integral equation (6) could be found by expansion (11) of $h'(f)$ and using the coefficients a_n in (8) in order to find the solution. Expansion (11) is possible by different means, for example, by using the orthogonality properties of Legendre polynomials. In order to prove that (7) is a solution let us substitute (11) in the integral; after interchanging summation and integration sign we get:

$$z(f_0) = \frac{2}{\pi} \sum_{n=0}^{\infty} n a_n\, \beta_{n-1} \int_0^{f_0} \frac{f^n\, df}{\sqrt{({f_0}^2 - f^2)}} \tag{12}$$

evaluating the integral in (12) by substituting $f = f_0 \sin \alpha$ we get:

$$\int_0^{f_0} \frac{f^n df}{\sqrt{(f_0^2 - f^2)}} = f_0^n \int_0^{\pi/2} \sin^n \alpha \, d\alpha = f_0^n \beta_n \tag{13}$$

substituting (13) in (12) we get:

$$z(f_0) = \frac{2}{\pi} \sum_{n=0}^{\infty} (n\beta_{n-1}\beta_n) \, a_n f_0^n \tag{14}$$

using definition (10b) it can be shown (DWIGHT, 1954):

$$\beta_n = \int_0^{\pi/2} \sin^n \alpha \, d\alpha = \frac{\sqrt{\pi}}{2} \frac{\Gamma[n + 1)/2]}{\Gamma[(n/2) + 1]} \tag{15}$$

and from (15) we get:

$$n\beta_{n-1}\beta_n = n \frac{\pi}{4} \frac{\Gamma(n/2)\Gamma[(n + 1)/2]}{\Gamma[(n + 1)/2]\Gamma[(n/2) + 1]} = \frac{\pi}{2}. \tag{16}$$

Since $\Gamma(z + 1) = z\Gamma(z)$. From (16) and (14) we see that we get (8) which proves that (7) is the solution of (6).

3. The General Case

For the general case of the integral equation (4)—the case which includes the magnetic field but not collisions, several numerical methods of solution have been suggested (SCHMERLING, 1957; KELSO, 1954; JACKSON, 1956; BUDDEN, 1954). The method which we shall use here is original and it is believed that in certain respects is superior to previous methods. However the decision about this could be made after more experience in using this method for the reduction of h'–f records to N–h profiles. Unfortunately the author does not have time at present and will have a chance to use it only in the future. It is hoped that other workers in the field will take advantage of it.

Let us rewrite the integral equation (4) as follows:

$$h'(f) = \int_0^f \mu'(f;\ X) \frac{dz(f_0)}{df_0} df_0. \tag{17}$$

We write it in this form since it has been shown (UNZ, 1960) that in $\mu'(f;\ f_0)$ the value of f_0 always appears in the particular combination $X = (f_0/f)^2$. Let us substitute as above in (8):

$$z(f_0) = \sum_{n=0}^{\infty} a_n f_0^n \tag{18a}$$

$$\frac{dz(f_0)}{df_0} = \sum_{n=0}^{\infty} n a_n f_0^{n-1}. \tag{18b}$$

Since (18) is a uniform series we can substitute it in (17) and interchange summation and integration signs:

$$h'(f) = \sum_{n=0}^{\infty} n a_n \int_0^f \mu'(f;\ X) f_0^{n-1} \, df_0. \tag{19}$$

VOL. 21 1961

Let us rewrite the integral in (19) by substituting $f_0 = fy$ or $y = f_0/f$ and $X = y^2$ and we get:

$$\int_0^f \mu'(f;\ X) f_0^{n-1}\, df_0 = f^n \int_0^1 \mu'\ (f;\ y^2) y^{n-1}\, dy. \tag{20}$$

Let us denote the definite integral in (20) by:

$$\beta_{n-1} = \int_0^1 \mu'\ (f;\ y^2)\ y^{n-1}\, dy \tag{21}$$

where $y^2 = X$ and $n \geqslant 1$ since in (18b) we are not required to know β_{n-1} for $n = 0$. Substituting (20) in (19) and using notation (21) we get:

$$h'(f) = \sum_{n=1}^{\infty} n a_n \beta_{n-1}(f) f^n. \tag{22}$$

We see that (22) is practically identical with (11). The only difference is that in case of no magnetic field β_{n-1} does not depend on f since from (21) in case of no magnetic field:

$$\beta_{n-1} = \int_0^1 \frac{1}{\sqrt{(1 - y^2)}}\, y^{n-1}\, dy = \int_0^{\pi/2} \sin^{n-1} \alpha\, d\alpha \tag{23}$$

where (23) is identical with (10b). Equations (22), (8) and definition (21) represent the complete rigorous solution of the problem.

4. Discussion of the Solution

Before we indicate the practical way of using the solution let us summarize the results:

$$z(f_0) = \sum_{n=1}^{N} a_n {f_0}^n + a_0 \tag{24a}$$

$$h'(f) = \sum_{n=1}^{N} n \beta_{n-1}(f) a_n f^n \tag{24b}$$

$$\beta_{n-1}(f) = \int_0^1 \mu'(f;\ y^2) y^{n-1}\, dy \tag{24c}$$

$$n \geqslant 1, \quad y^2 = X, \quad y = \frac{f_0}{f}$$

The first step in the procedure will be to evaluate the definite integrals in (24c) in the form $\beta(f)$ for different parameters n. In this numerical integration we can use $\mu'(f;\ X)$ given in a previous paper (Unz, 1961). Every station with non-varying static magnetic field will have only one permanent set of curves $\beta_{n-1}(f)$ which could be plotted on one sheet of paper.

The second step will be to take the given $h'(f)$ record and from it evaluate a_n. One method of doing it will be to write (24b) for different points:

$$\begin{aligned} h'(f_1) &= \sum_{n=1}^{N} n\beta_{n-1}(f_1) f_1{}^n \, a_n \\ h'(f_2) &= \sum_{n=1}^{N} n\beta_{n-1}(f_2) f_2{}^n \, a_n \\ h'(f_3) &= \sum_{n=1}^{N} n\beta_{n-1}(f_3) f_3{}^n \, a_n \\ &\vdots \qquad\qquad\qquad \vdots \\ h'(f_N) &= \sum_{n=1}^{N} n\beta_{n-1}(f_N) f_N{}^n \, a_n \end{aligned} \tag{25}$$

We see that we have N equations with N unknown a_n. This could be rewritten in a matrix form:

$$h'(f_i)] = [n\beta f] \, a_j] \tag{26a}$$

$$a_j] = [n\beta f]^{-1} \, h'(f_i)] \tag{26b}$$

and by solving those N equations we can find the first N coefficients a_n. We see that we can take any number of points f_i at any positions we want; we might take them at the critical frequencies where we have jumps in the $h'(f)$ records. We can get any degree of accuracy we like—the more points we take, the larger the work we will have in inverting the matrix and calculating the coefficients, but the greater the accuracy of the result.

The last step will be to substitute the coefficients we found in (24a) and get the final result except for arbitrary additive constant. It must be noted that we could have normalized (24a) and (24b) by expanding the series in terms of $(f/f_N)^n$ instead of f^n where f_N is the maximum frequency used.

The advantages of the method of solution discussed above are as follows:

(a) The curves $\beta_{n-1}(f)$ could be calculated for every station by a central computer only once. These permanent curves could be plotted on one sheet of paper and sent to the field station.

(b) In the field station the reduction of the h'–f curves to N–h profiles could be calculated to any degree of accuracy, once the curves $\beta_{n-1}(f)$ are available. The degree of accuracy will depend only on the amount of work which the people are ready to do in the field on a simple hand computer. It involves only the simple solution of N linear equations with N unknown.

(c) The points f_i could be chosen at any place, in order to show critical discontinuities in the h'–f curve.

(d) For greater accuracy the curve h'–f could be divided into subcurves where each one could be analysed independently of the others.

(e) The method could be also used for much greater accuracies by inverting the matrix permanently for a large number of values.

In the near future we intend to use this method and publish a few examples. However, any initiative in using it will be appreciated. The author thinks that

VOL. 21 1961

there are certain advantages in this method over previous ones especially because this method is quite general and more accurate. In the Appendix we will show how to calculate the μ' required for the calculation of the $\beta_{n-1}(f)$ curves.

References

Appleton E. V.	1930	*Proc. Phys. Soc. Lond.* **42,** 321.
Budden K. G.	1954	*The Physics of the Ionosphere,* p. 332. Physical Society, London.
Courant R. and Hilbert D.	1953	*Methods of Mathematical Physics,* Vol. 1, p. 65. Interscience, New York.
Dwight H. B.	1954	*Tables of Integrals and other Mathematical Data,* p. 196. MacMillan, New York.
De Groot W.	1930	*Phil Mag.* **10,** 521.
Jackson J. E.	1956	*J. Geophys. Res.* **61,** 1.
Kelso J. M.	1954	*J. Atmosph. Terr. Phys.* **5,** 11.
Manning L. A.	1947	*Proc. Inst. Radio Engrs* **35,** 1203.
Ratcliffe J. A.	1959	*The Magneto-Ionic Theory and its Applications to the Ionosphere,* pp. 7, 103. Cambridge University Press.
Schmerling E. R.	1957	Ionosphere Research Laboratory, Penn. State University, State College, Pa. Report No. 96.
Thomas J. O.	1959	*Proc. Inst. Radio Engrs* **47,** 162.
Unz H.	1961	*J. Atmosph. Terr. Phys.* **20,** 189.

Appendix

In a previous paper μ' has been derived as follows:

$$\mu\mu' = 1 + \tfrac{1}{2}(1 - \mu^2)^2\, P \tag{A1}$$

$$P = \frac{2\alpha\beta/[X(1 - X)] + \gamma}{\alpha + \beta} \tag{A2}$$

$$\alpha = \frac{X}{1 - \mu^2} - 1 \tag{A3}$$

$$\beta = \frac{{Y_T}^2/2}{1 - X} \tag{A4}$$

$$\gamma = \frac{{Y_L}^2}{X} \tag{A5}$$

$$\mu^2 = 1 - X\left\{1 - \frac{{Y_T}^2/2}{1 - X} \pm \sqrt{\left[\left(\frac{{Y_T}^2/2}{1 - X}\right)^2 + {Y_L}^2\right]}\right\}^{-1} \tag{A6}$$

where

$$X = \left(\frac{f_0}{f}\right)^2, \qquad Y = \frac{f_H}{f}, \qquad Y_T = \frac{f_T}{f}, \qquad Y_L = \frac{f_L}{f}.$$

Journal of Atmospheric and Terrestrial Physics, 1961, Vol. 21, pp. 46 to 53. Pergamon Press Ltd. Printed in Northern Ireland

On the OH airglow

V. I. KRASSOVSKY and N. N. SHEFOV
Institute of Physics of the Atmosphere, USSR Academy of Sciences, Moscow
and V. I. YARIN
Yakut Branch of the Siberian Department of the USSR Academy of Sciences, Yakutsk

(*Received* 28 *June* 1960; *in revised form* 19 *November* 1960)

Abstract—An increase of the OH emission intensity with increasing rotational temperature, and seasonal variations of the intensity and rotational temperature of OH have been established by spectral observations at Yakutsk. No such behaviour has been observed at Zvenigorod. At both locations variations of the relative populations of the OH vibrational levels and a correlation between the OH and Hα airglow intensities have been observed.

OBSERVATIONS of the OH night airglow emission made in the USSR during the International Geophysical Year and International Geophysical Co-operation have made it possible to determine the relation between the rotational temperature, the intensity of the emission, and the geographical locality of its appearance. The

Table 1. Total intensities of the OH bands observed at Zvenigorod and Yakutsk*

V'	V''					
	0	1	2	3	4	5
3	3500 (2500)					
4	250 —	6000 (5300)				
5	35 (30)	900 —	12,000 —			
6	~5 (~10)	110 (90)	1300 —	15,000 —		
7		25 (20)	220 —	2500 (2100)	22,000 —	
8			60 (65)	400 —	3000 (3000)	
9			~15 (~10)	140 (120)	600 —	4500 (4000)
10					~3 —	

* The Yakutsk observations are given in parentheses.

instrumentation and techniques used in these studies have been described elsewhere (GERASIMOVA and YAKOVLEVA, 1956; GALPERIN *et al.*, 1957; VOLKOV *et al.*, 1959; SHEFOV, 1959; YARIN, 1960).

The total intensities of the OH bands observed at Zvenigorod and Yakutsk are given in Table 1. Here and throughout this report the Rayleigh has been used as the unit of intensity. These results differ somewhat from those previously published

VOL. 21 1961

(SHEFOV, 1959, 1960) in that they were obtained from a considerably larger number of observations. The Zvenigorod data are the average of all the observations so far processed. Of the Yakutsk observations only those corresponding to rotational temperatures of about 250°K were used because of the marked variation of the relative intensities observed at this station. This effect will be examined in more detail below.

The rotational temperatures of the OH bands were determined in the usual manner with the calculations based on Hill and van Vleck's formulas for the rotational energy levels (see HERZBERG, 1951a).

The relation between the rotational temperature and the total intensity of the (9,3) OH band is shown by filled circles in Fig. 1. The Yakutsk observations show clearly that at large intensity and rotational temperatures exceeding 250°K, an intensity increase is accompanied by a temperature increase. The Zvenigorod observations, however, show no such dependence. It should also be noted that the OH intensities at Zvenigorod have about the same value as those associated with temperatures less than 250°K at Yakutsk. Of the Zvenigorod data, only the two encircled values could be regarded as a suggestion of the dependence exhibited by the Yakutsk data.

The crosses in Fig. 1(a) indicate values obtained during nights of total cloudiness and occasionally with precipitation. The transparency at these times was very low but it was not measured, and as a result, it was impossible to correct these intensities for the low transparency. Still, the observed intensities on overcast nights are not much less than the mean of the values obtained on clear nights. This effect indicates an enhancement of the true OH intensity at Zvenigorod on cloudy nights.

If it is assumed that the hydroxyl emission is due to the ozone–hydrogen reaction (BATES and NICOLET, 1950; HERZBERG, 1951b), an OH intensity increase can be expected to be associated with an OH rotational temperature increase if this temperature reflects the ambient temperature. The straight line which best represents the Yakutsk data for temperatures in excess of 250°K is indicated in Figs. 1(a) and 1(b). This line shows the dependence which would result if the product of the ozone and hydrogen concentrations was constant and the activation energy was 2·7 kcal/mole. The scatter in the observational points is to be expected since it is hardly possible that the product of the ozone and hydrogen concentrations would remain constant in time.

It is evident from Fig. 2 that the relative intensities of the OH bands with high and relatively low initial levels also show changes with temperature. The Yakutsk data show a trend toward an increase of the population of the higher levels with increasing rotational temperature. The Zvenigorod data show a greater scatter in the population ratios at lower temperatures than do those for Yakutsk.

The relations indicated in Figs. 1 and 2 can be best explained by the assumption of a dual mechanism for the origin of the hydroxyl. At Yakutsk, for high rotational temperatures and intensities, the ozone–hydrogen reaction evidently plays the dominant role. The Yakutsk data for low rotational temperatures, and the Zvenigorod data for all rotational temperatures and for which the intensities are not too large, indicate that the excitation may be to a great extent due to a

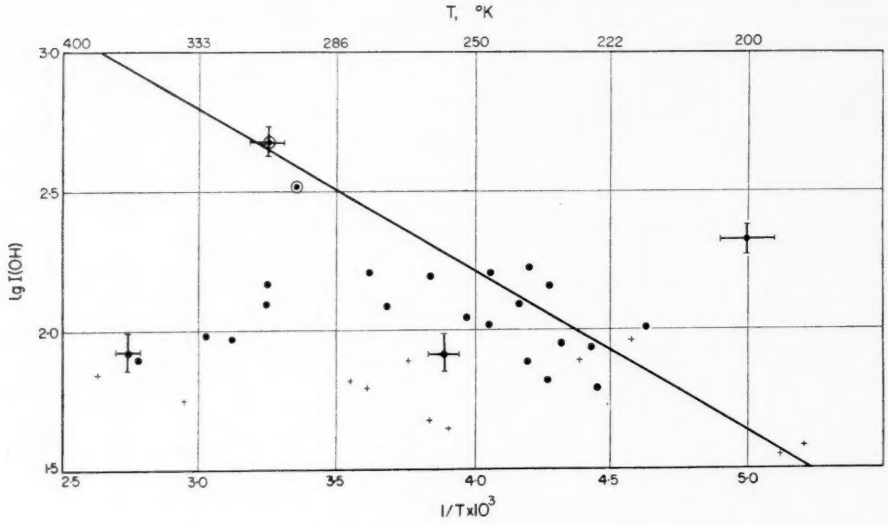

(a)

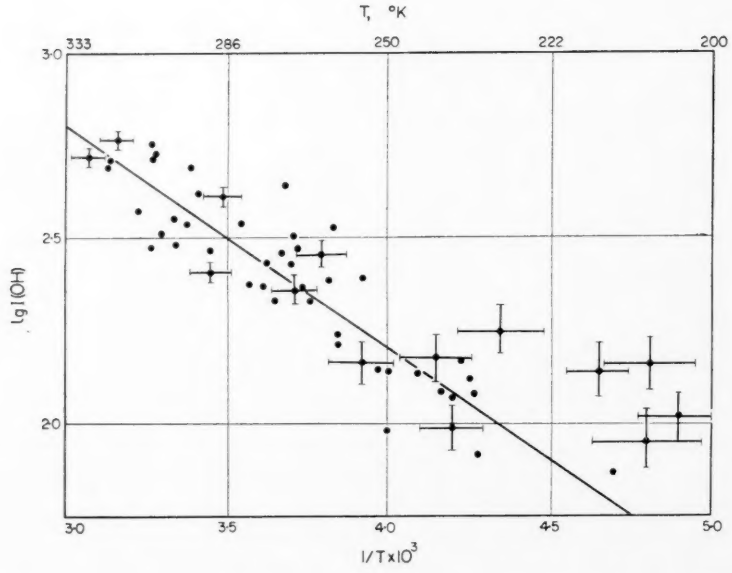

(b)

Fig. 1. Intensity an rotational temperature of the (9,3) OH band. (a) Zvenigorod (ϕ = 55° 43′, λ = 36° 51′, Φ = 51·0°, Λ = 120·3°). (b) Yakutsk (ϕ = 62° 3′, λ = 129° 40′, Φ = 51·0°, Λ = 193·8°). The filled circles represent clear nights whereas the crosses are for cloudy nights. For the sake of clarity only a few characteristic values of the errors are indicated.

VOL. 21 1961

reaction of vibrationally excited oxygen molecules with hydrogen atoms (KRASSOVSKY, 1951, 1956). As is well known, the rate of the latter reaction is not substantially temperature dependent. The scatter in the relative populations at Zvenigorod is quite reasonable since any change in the altitude at which the reaction takes place would change the efficiency of the collisional deactivation of

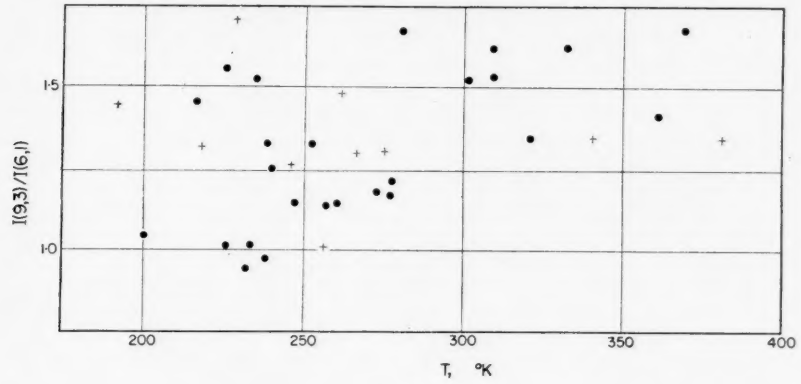

(a)

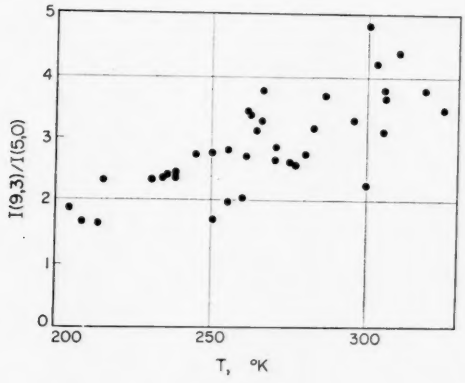

(b)

Fig. 2. Intensity ratio of the OH bands and the rotational temperature.
(a) Zvenigorod: $I(9,3)/I(6,1)$. (b) Yakutsk: $I(9,3)/I(5,0)$.

the excited OH states by the surrounding molecules and atoms. The decrease in the scatter of the relative populations at higher temperatures, exhibited by the Zvenigorod data, may point to an increased contribution of the ozone–hydrogen reaction which is characterized by a greater relative population of the ninth vibrational level.

It is of interest to note that there are in the Zvenigorod data cases in which a high rotational temperature ($T > 270°$K) was obtained for bands originating from the sixth to ninth vibrational levels when at the same time lower rotational temperatures were obtained from bands from the fourth and fifth levels. This may

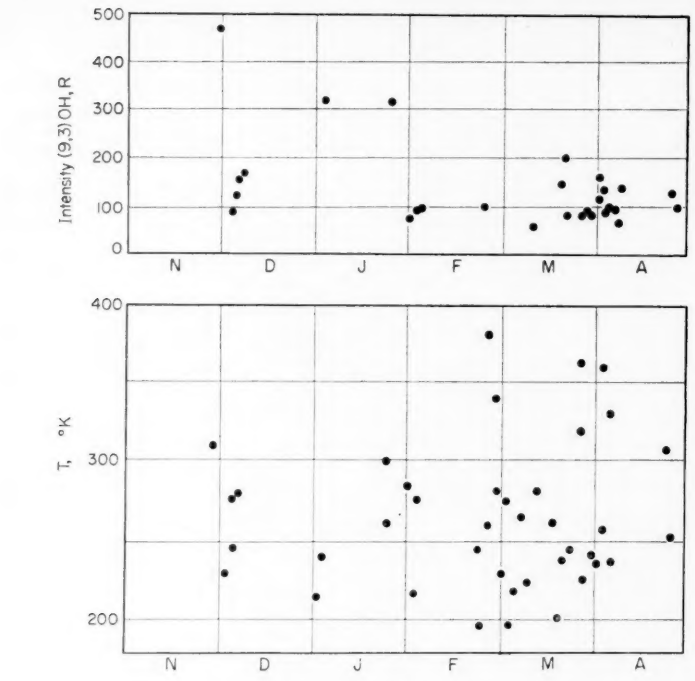

(a)

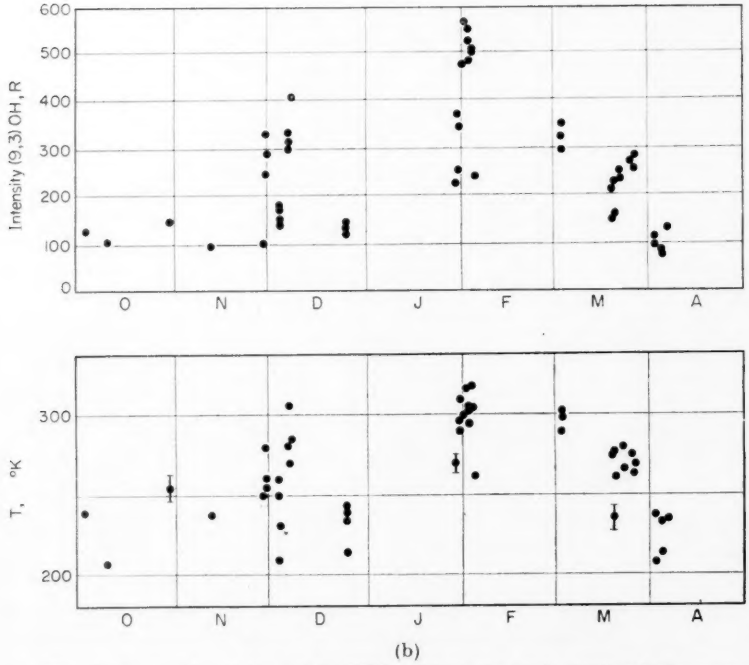

(b)

Fig. 3. Seasonal variation of the OH band intensity and rotational temperature. (a) Zvenigorod. (b) Yakutsk.

VOL. 21 1961

indicate that different mechanisms operating at different altitudes with different temperatures play significant roles in populating the relatively high and relatively low vibrational levels.

The change in the relative populations of the vibrational levels with time does not agree with the supposition made by CHAMBERLAIN and SMITH (1959) about the constant and equal production of hydroxyl molecules in all the vibrational levels.

Fig. 3 shows the data on the seasonal intensity and rotational temperature variations of the OH bands. No observations were gathered during the summer because of the long twilight. Seasonal intensity and rotational temperature variations are clearly seen in the Yakutsk observations but not in the Zvenigorod observations. At Yakutsk the OH temperature varies in a manner opposite to that of the ground temperature, i.e. the maximum OH temperature occurred at the time of minimum ground temperature. By means of short exposures it has been established at both Yakutsk and Zvenigorod that the variations in the intensity and rotational temperature from night to night, and occasionally even during a single night, are large and considerably exceed the errors of measurement.

It has been noted that vertical mixing in the upper atmosphere can increase the contact between O_3 and H and thus increase the OH emission (KRASSOVSKY, 1956). It is quite possible that the circulation of the air near the ground is accompanied by vertical mixing in the upper atmosphere which leads to the increased hydroxyl emission at Yakutsk due to the ozone–hydrogen reaction.

Fig. 4 shows the relation between the Hα and the OH intensities which was pointed out previously by SHEFOV (1959) and YARIN (1960). In each case there is a tendency for an increase in the intensity of the one emission to be accompanied by an increase in the other. The possible exceptions, indicated in the diagram by encircled dots, correspond to times when the Milky Way entered the field of view of the spectrograph.

If the OH rotational temperature reflects the ambient temperature it is apparent that the OH emission comes from considerably higher or considerably lower than the temperature minimum at about 85 km. In the first case the excited OH will be due to the reaction of vibrationally excited O_2 with H, and in the second case to the ozone–hydrogen reaction.

A change in the temperature of the upper atmosphere is not the only factor which can cause OH rotational temperature variation. It may that a change in the altitude of the reaction zone is also capable of producing these changes. In the region of great ozone concentration at altitudes of about 50 km where the temperature is high, the ozone–hydrogen reaction is possible only if a sufficiently large hydrogen concentration exists. Such a hydrogen concentration can be due, particularly in the high-latitude regions, to dissociation of water vapour by deeply penetrating corpuscles or X-radiation formed higher in the atmosphere by electrons with energies of tens of keV (KRASSOVSKY *et al.*, 1959a, b).

The Hα airglow intensity variations can be accounted for by the fact that the hydrogen and the hydroxyl intensities are proportional to the concentration of atomic hydrogen in the upper atmosphere. However, there is another explanation. Hydrogen can be excited in the upper parts of the atmosphere by electrons with energies of tens of keV (KRASSOVSKY *et al.*, 1959a, b). These electrons may produce

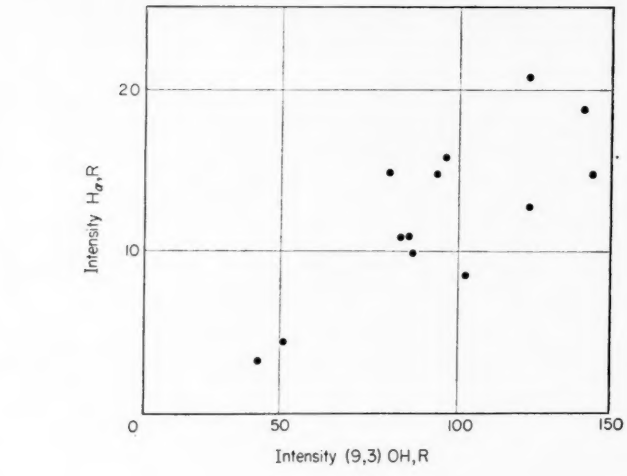

(a)

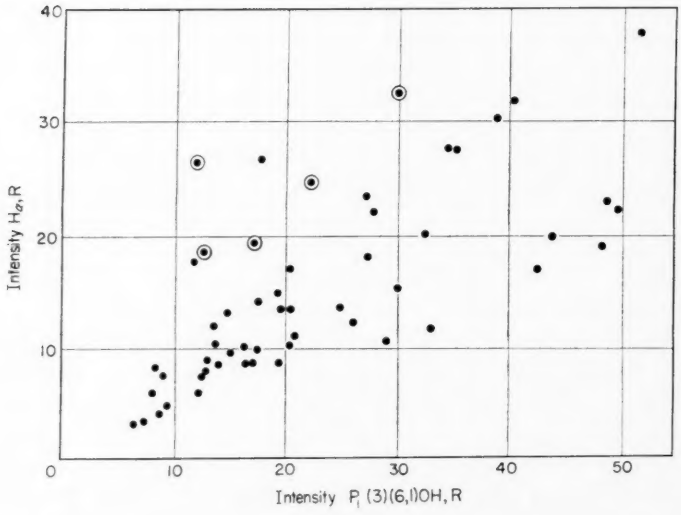

(b)

Fig. 4. Correlation between the nightglow Hα and OH intensities. (a) Zvenigorod: OH represented by the (9,3) band. (b) Yakutsk: OH represented by the $P_1(3)$ line of the (6,1) band.

atomic hydrogen by molecular dissociation either by direct collisions after penetrating to the lower layers or through their X-radiation.

Let us hope that the processing of the observational data obtained during the International Geophysical Year and International Geophysical Co-operation will completely elucidate the nature of the upper atmospheric hydroxyl emission.

REFERENCES

BATES D. R. and NICOLET M. 1950 *J. Geophys. Res.* **55,** 301.
CHAMBERLAIN J. W. and SMITH C. A. 1959 *J. Geophys. Res.* **64,** 611.

VOL. 21 1961

Galperin G. I., Mironov A. V. and Shefov N. N.	1957	*Mém. Soc. Sci. Liège* **18,** 68.
Gerasimova N. G. and Yakovleva A. V.	1956	*Instrumentation and the Methods of Experiments, USSR* **1,** 83.
Herzberg G.	1951a	*Spectra of Diatomic Molecules.* Van Nostrand, New York.
Herzberg G.	1951b	*J. R. Astr. Soc. Can.* **45,** 100.
Krassovsky V. I.	1951	*Dokl. Akad. Nauk SSSR* **80,** 735.
Krassovsky V. I.	1951	*Airglow and Aurorae,* pp. 86, 193, 197. Pergamon Press, London.
Krassovsky V. I., Shklovsky I. S., Galperin G. I. and Svetlitsky E. M.	1959a	*Izvest. Akad. Nauk SSSR, Ser. Geophys.* **8,** 1157.
Krassovsky V. I., Shklovsky I. S., Galperin G. I. and Svetlitsky E. M.	1959b	*Dokl. Akad. Nauk SSSR* **127,** 78.
Shefov N. N.	1959	*Spectral, Electrophotometrical and Radar Researches of Aurorae and Airglow, Acad. Sci. USSR* No. 1, 25.
Shefov N. N.	1960	*Spectral Electrophotometrical and Radar Researches of Aurorae and Airglow, Acad. Sci. USSR* No. 2/3, 57.
Volkov I. V., Esipov V. F. and Scheglov P. V.	1959	*Dokl. Akad. Nauk SSR* **129,** 228.
Yarin V. I.	1960	*Spectral, Electrophotometrical and Radar Researches of Aurorae and Airglow, Acad. Sci. USSR* No. 2/3, 72.

Journal of Atmospheric and Terrestrial Physics, 1961, Vol. 21, pp. 54 to 64. Pergamon Press Ltd. Printed in Northern Ireland

Excitation of helium in the aurora

J. M. MALVILLE
High Altitude Observatory,
Department of Astro-Geophysics,
University of Colorado, Boulder, Colorado

(*Received* 26 *November* 1960)

Abstract—The populations of the excited levels of a helium atom traversing the atmosphere with an original energy of 256 keV are calculated using the method of statistical equilibrium. Because of the present inadequate knowledge of helium cross-sections, the calculations are only an exploratory approach toward the problem of helium in aurorae. It is estimated that each 256 keV helium particle produces 450 photons of λ10830 and 40 photons of λ5876 during its passage through the atmosphere. The profile and luminosity curve of λ5876 and λ10830 are predicted. Observational data of helium emissions are discussed.

1. INTRODUCTION

SPECTRAL OBSERVATIONS of aurorae during the past two decades have left no doubt that high velocity protons penetrate to auroral heights in the atmosphere during times of auroral displays. Doppler shifted lines of the Balmer series appear in the majority of auroral forms and occasionally are observed in the absence of visible aurorae. Protons are, however, the only non-terrestrial heavy particles which have been definitely identified in the aurora.

It is of considerable importance to know whether or not the stream of auroral particles contains an appreciable fraction of heavier nuclei. If, for instance, the helium to hydrogen ratio can be determined, then one has available an additional fact concerning the conditions prevailing in the region of the solar atmosphere where auroral particles are generated. The mechanism for accelerating the particles undoubtedly operates only upon charged particles, and the helium to hydrogen ratio should give an indication of the relative degrees of ionization of helium and hydrogen in the region of acceleration. The smaller charge to mass ratio of helium ions may also play a significant role in establishing the helium abundance in auroral particles.

In the visible and ultra-violet portions of the auroral spectrum there is no evidence that helium lines have ever been observed. Some helium lines would be difficult to detect because of obscuration by strong auroral emissions. The lines HeI λ3889, and λ4713 would be blended with the first negative system of N_2^+. He λ6678 would blend with the λ6705 band of the first positive system of N_2. The D_3 line, λ5876, however, lies in a relatively unobscured portion of the auroral spectrum associated only with weak bands of the first positive system of N_2. As a result of his laboratory work at Yerkes Observatory, FAN (1955) suggested that He λ5876 should be observable if the ratio of helium to hydrogen in auroral primaries were 0·1 or greater. On ultra-violet spectra obtained at College, Alaska by BARBIER and WILLIAMS (1950) the line HeI λ3188 was clearly absent.

During the past few years Russian workers have had notable success observing the infra-red portion of the auroral spectrum with image converters. MIRONOV *et al.*

VOL. 21 1961

(1959) reported an enhancement of the Q branch of the OH 5,2 band, λ10830 relative to the R branch of that band and relative to other OH bands during the intense aurora of 10–11 February 1958. Observations of normal airglow OH emissions by MIRONOV *et al.* during eleven nights indicated the intensity of the Q branch varied between two and four times that of the R branch. During the aurora of 10–11 February, observed at Zvenigorod, the Q branch was nine times more intense than the R branch. MIRONOV *et al.* attributed the three-fold enhancement of the Q branch to the line He λ10830. The observations of FEDOROVA (1958) and

Table 1

Date	$\frac{\text{I}(5876)}{\text{I}(H\alpha)}$	$\frac{\text{I}(5876)}{\text{I}(H\beta)}$
17–18 July	<0·058	<0·18
29–30 August	—	<0·25

the calculations of CHAMBERLAIN and SMITH (1959) place the intensity of the OH λ10830 band at approximately 12,000 rayleighs. The enhanced λ10830 band observed by the Russians may then have had an intensity of some 24,000 rayleighs. By subtracting out the airglow Q branch of the OH 5,2 band, MIRONOV *et al.* obtained the profile of the enhanced emission which had a half width of 9 Å, equal to the resolution of the spectrograph.

Several aspects of the Russian observation are very striking. The apparent great intensity of He λ10830 ($2^3P - 2^3S$) demands that the population of the 3^3D state of He be very much less than that of the 2^3P state as the transition λ5876 ($3^3D - 2^3P$) is not observed in the aurora. In addition the 9 Å width of λ10830, corresponding to 125 km/sec (toward the observer), is less than half that of auroral $H\alpha$ at the magnetic horizon (GALPERIN, 1957). (The spectrograph at Zvenigorod was directed at a point 30° above the northern horizon).

In order to estimate the upper limit of the intensity of the D_3 line in the aurora, we have analysed two spectrograms which do not show λ5876 emission obtained with the IGY Patrol Spectrograph at Ellsworth Station, Antarctica, 1957. The results are presented in Table 1. The smaller value of I(5876)/I($H\beta$) of 17–18 July was possible because the N_2 first positive bands had an unusually small intensity relative to that of the hydrogen lines.

No absolute calibrations of the plates taken in the Antarctic are available; however, we may obtain a crude estimate of the absolute intensities by considering the maximum observed intensities of the auroral hydrogen lines. The photometric measurements of MONTALBETTI (1959) of $H\beta$ during February 1958 at Churchill place the maximum intensity of $H\beta$ at approximately 850 rayleighs. CHAMBERLAIN (1954) estimates the intensity of $H\alpha$ in a bright arc at some 3000 rayleighs. These values would place the D_3 threshold on the two Antarctic plates somewhere below 200 rayleighs. If the D_3 line intensity remains below 200 rayleighs throughout strong aurorae while He λ10830 rises as high as 24,000 rayleighs, the ratio I(5876)/I(10830) may be less than 8×10^{-3} in the majority of aurorae.

At present, the greatest uncertainty in detailed calculation on the excitation of helium in aurorae is the almost complete lack of appropriate cross-sections. Because of this lack, the calculations presented in this paper must be viewed, at best, as only exploratory. A really adequate solution of the problem must await the determination of more helium cross-sections.

2. CALCULATION OF CROSS-SECTIONS

The density of neutral particles at auroral heights in the atmosphere is some 10^6 that of free electrons. The encounters experienced by incident helium particles will be primarily with neutral oxygen and nitrogen atoms and molecules, and we need to take account only of collisional excitation and ionization by neutral particles.

We consider first the process of charge capture by helium ions from oxygen and nitrogen atoms. The two important parameters in charge capture collisions are conservation of spin (Wigner's rule) and energy resonance. Of the two apparently energy resonance is the dominant parameter in both gas-kinetic conditions and energetic collisions (MASSEY and BURHOP, 1952). Capture cross-sections for protons in hydrogen gas have been calculated using the Born approximation by BATES and DALGARNO (1953) and have been measured recently by FITE *et al.* (1958). Relative capture cross-sections of HeII in Ne have been observed by TRIFFELWITZ (1941) and WOLF (1937). In both these collisions, HI + HII and HeII + NeI, captures into the ground state are closest to resonance; capture cross-sections are greatest for capture into the ground state and fall off rapidly for captures into higher levels.

Considering only the energy resonance effect in the collision,

$$\mathrm{HeII}(1s) + \begin{matrix}\mathrm{NI}\\ \mathrm{OI}\end{matrix} \rightarrow \mathrm{HeI}(1s, n1) + \begin{matrix}\mathrm{NII}\\ \mathrm{OII}\end{matrix}$$

we see that HeI capture cross-sections in O or N should be quite different from proton capture cross-sections in hydrogen gas. Capture into the ground state and the first excited levels of HeI are equally out of resonance,

$$\mathrm{NI} + \mathrm{HeII} \rightarrow \mathrm{NII} + \mathrm{HeI}(1^1S) \qquad |\Delta E| \cong 10\ \mathrm{eV}$$

$$\mathrm{NI} + \mathrm{HeII} \rightarrow \mathrm{NII} + \mathrm{HeI}(2^1P) \qquad |\Delta E| \cong 11\ \mathrm{eV}$$

and the cross-sections should be strongly determined by the statistical weights of the levels. We adopt a six level helium atom with the following structure:

Helium level	Model atom level
1^1S	1
2^1S, 2^1P	2
2^3S	3
2^3P	4
3^3S, 3^3P, 3^3D	5
Continuum	k

We estimate the relative capture cross-sections by assuming that captures into each of the excited levels, except level 5, are determined only by the statistical weights of the levels. Such a method neglects effects due to the change of angular momentum of the p electron captured from O or N and, of course, the relative variation of cross-sections with energy. In the calculations of BATES and DALGARNO the largest cross-sections for captures into excited levels of hydrogen in the energy range below 100 keV were those of optically allowed transitions, i.e., $1s$ to $2p$ transitions. Because of this effect our scheme may tend to overestimate the cross-section for capture into the 2^3P level.

The energy difference between the 2^2P and 3^3D levels of helium is less than the difference between the $n = 2$ and $n = 4$ levels of hydrogen. The Born approximation used by BATES and DALGARNO for proton–hydrogen collisions appears to be satisfactory for energies above 10 keV (FITE *et al.*, 1958). In the range 10–120 keV the Born approximation gives the ratio of the cross-sections $\sigma k4/\sigma k2 > 0{\cdot}1$, gradually falling to 0·037 at 250 keV. Guided by this behaviour of the capture cross-section of hydrogen, we let the cross-sections for capture into the composite level 5 be 3/10 that for capture into level 4.

Absolute capture cross-section were obtained using the measurements of BARNET and STIER (1958) of total electron capture cross-sections of helium in air. If σ_{10} is the total capture cross-section, then the captures into the various levels were divided as follows:

$$\sigma_{k1} = 5{\cdot}26 \times 10^{-2}\,\sigma_{10}$$
$$\sigma_{k2} = 2{\cdot}11 \times 10^{-1}\,\sigma_{10}$$
$$\sigma_{k3} = 1{\cdot}58 \times 10^{-1}\,\sigma_{10}$$
$$\sigma_{k4} = 4{\cdot}74 \times 10^{-1}\,\sigma_{10}$$
$$\sigma_{k5} = 1{\cdot}42 \times 10^{-1}\,\sigma_{10}$$

Total electron loss cross-sections for helium in air have been measured (BARNET and STIER, 1958), however the interpretation of such cross-sections is difficult in the case of helium as a significant proportion of the atoms may be in the metastable state. The cross-section for electron loss would then be determined primarily by the ionization cross-section of the 2^3S level rather than that of the ground state. In the experiment of BARNET and STIER the electron loss cross-section varied with pressure in the sense that it increased toward lower pressures. At higher pressures an equilibrium was apparently established involving both the singlet and triplet states, and the cross-section remained relatively constant with pressure. The electron loss cross-section σ_{01}, increased monotonically with energy up to a value of 3×10^{-16} cm^2 at 200 keV. It is surprising that the near adiabatic region for ionization from the ground state would persist to such high energies and would attain such a large value. Rather it appears, as suggested by BARNET and STIER, that ionizations from the metastable levels make a significant contribution to the electron loss cross-section.

The measured maximum cross-section for the ionization of helium by electrons is 3×10^{-17} (SMITH, 1930). The equilibrium established in the experiment of SMITH appears to have had a smaller proportion of atoms in the metastable state

than in the experiment of BARNET and STIER. Consequently we have used the electron ionization cross-section for the ionization of the ground state by neutral particles. This approximation is justified as the cross-sections for ionization and excitation by electron impact and by heavy particle impact are in general identical for equal velocities. Actually, the maximum cross-section for heavy particle impact appears to occur at a slightly lower velocity than that for electron impact (MASSEY and BURHOP, 1952). We estimate the "equivalent electron velocity" to be 2·5 that of the helium atoms and use this factor in converting electron impact cross-section to neutral particle impact cross-sections.

For transitions from excited levels we have used for collisional excitation

$$\sigma = 3\pi e^4 f \frac{2}{mv}\left(\frac{1}{hv} - \frac{2}{mv^2}\right)$$

and for collisional ionization

$$\sigma = 4n\pi a_0^2(E - \chi)/E^2\chi \qquad \text{(ALLEN, 1955).}$$

The total cross-section for excitation of the 2^1P state of helium by collisions with hydrogen has been calculated by MOISEIWITSCH and STEWART (1954). It is important to note in connexion with their calculations that while the total excitation cross-section involving both single and double transitions has a maximum identical to that for excitation by electrons, it persists to much higher energies than either that for electron collisions or single transitions. In other words, the double transition encounter is the primary process at high energies and is neglected in approximating the total cross-section by the modified electron collision cross-section.

Collisions between helium and electrons which involve a change of multiplicity generally have a sharp peak at energies just above the threshold, followed by a flat-topped secondary maximum. The cross-section for excitations from the ground state falls off with energy approximately as E^{-2}, E^{-4}, and E^{-6} for excitation of the states ^3S, ^3P, and ^3D respectively (MOTT and MASSEY, 1949). The cross-section for electronic excitation of 2^3S calculated by MASSEY and MOISEIWITSCH (1954) has a flat-topped secondary maximum approximately equal to that for excitation of 2^1P. Accordingly we have used the double transition collision cross-section of 2^1P calculated by MOISEIWITSCH and STEWART for the excitation of the 2^3S level. Guided further by experimental cross-sections for electronic excitation of higher triplet levels (BATES *et al.*, 1950) we have set the cross-sections for excitation of the 4 and 5 levels to be respectively 1/10 and 1/100 that of the cross-section of the 2^1P level.

The collision de-excitation rates, important for de-populating the triplets, were obtained by balancing the collisional rates in thermodynamic equilibrium. Because of the high kinetic temperatures the de-excitation rates are

$$C_{ij} = \frac{\omega_j}{\omega_i} C_{ji}$$

where C_{ij} is the collisional rate from the i to the j level and ω_i is the statistical weight of the i^{th} level.

3. Equations of Statistical Equilibrium

The degree of excitation of helium atoms in the aurora is obtained by a solution of the equations of statistical equilibrium for a given velocity interval. In other words, we are assuming that for a given velocity of the helium atoms or for a given height in the atmosphere the populations of the levels remain constant with time. In all our calculations we neglect the HeIII content of the auroral stream. The five equations for the bound states may be written in terms of absolute rates

$$\sum_{\substack{i=1 \\ i \neq j}}^{n} n_i P_{ij} = n_j P_{jj} \qquad j = 1,2,3 \ldots . n - 1 \tag{1}$$

where P_{ij} is the total transition rate from i to j, P_{jj} is the sum of all ways out of the level, and n is the number of levels including the continuum. The collisional rates are

$$C_{ij} = N_n v \sigma_{ij}$$

where N_n is the density of neutral particles at the appropriate height of the atmosphere and v is the corresponding velocity of the helium atoms.

A sixth equation may be obtained assuming ionizational equilibrium. If F is the flux of helium particles outside the atmosphere then at any height in the atmosphere

$$\frac{F}{V} = N^+ + \sum_{j}^{n-1} N_j$$

where N^+ is the number density of singly and doubly ionized helium. The condition of ionizational equilibrium can be stated as

$$N^+ N_n V \sum_{j}^{n-1} \sigma_{kj} = N_n V \sum_{j}^{n-1} N_j \sigma_{jk}$$

assuming collisions involving neutral particles dominate, and we obtain the final form of the sixth equation:

$$\frac{F}{V} = \frac{\sum_{j}^{n-1} N_j \sigma_{jk}}{\sigma_{kj}} + \sum_{j}^{n-1} N_j. \tag{2}$$

Although auroral protons appear to possess a considerable dispersion in velocity (Chamberlain, 1957) we have carried out a solution for only one incident energy, namely 256 keV. The incident energy of 256 keV was used as it places the lower border of the hydrogen and helium auroral arc near 110 km. The lack of satisfactory cross-sections does not warrant at present the extention of the calculations to a range of energies. In applying these calculations to the ionosphere we have used Kallman's (1959) most recent model atmosphere which she obtained from satellite and rocket observations. This atmosphere was reduced to S.T.P. conditions and the helium velocities at each height were obtained from range–energy relations for helium in air (Cook *et al.*, 1953).

4. Results

The calculated luminosity curves for λ10830 and λ5876 are presented in Fig. 1.

According to the calculations, a helium particle with an initial energy of 256 keV produces 450 photons of λ10830 and 40 photons of λ5876 during its passage through the atmosphere. These values are to be compared to the figure of 50 $H\alpha$ photons emitted by each auroral proton of initial velocity greater than 90 keV (CHAMBERLAIN, 1954). If there is one helium atom for every ten hydrogen atoms in the solar corpuscular stream then we obtain for the ratio of the intensities:

$$\frac{\mathrm{I}(5876)}{\mathrm{I}(10830)} \simeq 0{\cdot}089 \qquad\qquad \frac{\mathrm{I}(10830)}{\mathrm{I}(H\alpha)} \simeq 1$$

The computed profiles of λ10830 and λ5876 at the magnetic horizon are shown in Fig. 2. The half-width of λ10830 is 1120 km/sec = 37 Å while that of λ5876 is 650 km/sec = 12·7 Å. The calculated half-width of auroral $H\alpha$ is 2500 km/sec

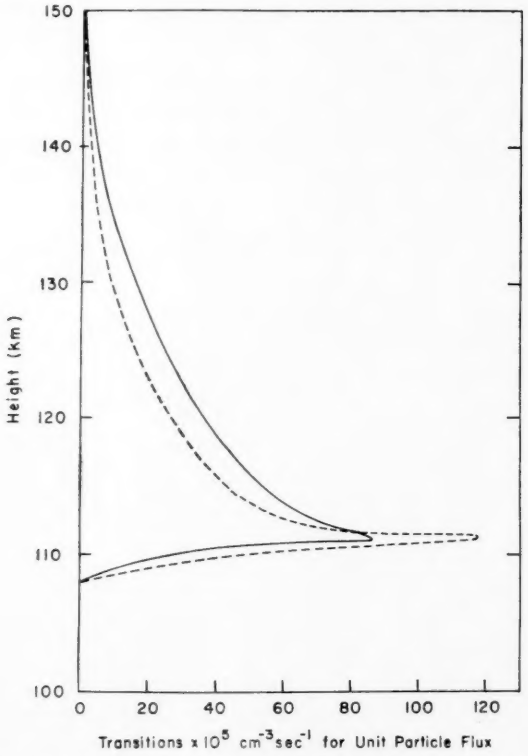

Fig. 1. Luminosity distribution of λ10830 and λ5876 for alpha-particles of incident energy 256 keV. ——— λ10830, — — — — λ5876($\times$10).

(CHAMBERLAIN, 1954). The predicted smaller half-widths of the helium lines appear to result from the metastability of the helium triplet levels. In the upper part of the helium "auroral arc" captures are the dominant process populating the 2^3P and 2^3D levels. At and below the brightest part of the arc collisional excitations from the triplet levels dominate. The maximum of the collisional cross-section for the transition 2^3S–2^3P of helium lies at a lower energy than that of the transition

VOL. 21 1961

$n = 1$ to $n = 3$ of hydrogen. The collisional rate populating the excited triplet levels of helium will reach a maximum at lower velocities than the corresponding rate populating the upper levels of the Balmer series. The helium emission will then tend to be concentrated more toward the lower part of the arc and will have a narrower profile than the hydrogen emission.

We noted earlier that the experimental electron loss cross-section of helium in air suggested that at high energies a large proportion of the helium atoms were in

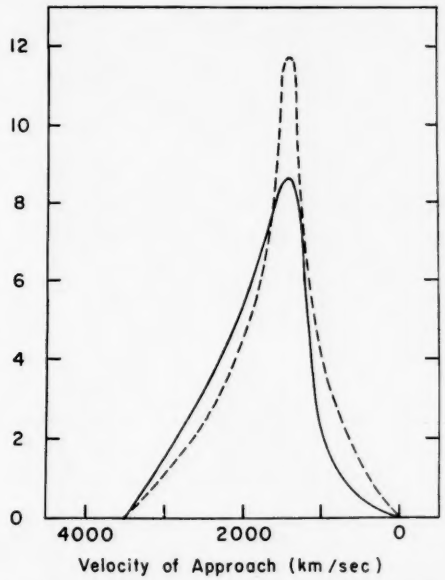

Fig. 2. Profiles of λ10830 and λ5876 for alpha-particles of incident energy 256 keV. ——— λ10830, – – – – λ5876($\times$10).

Table 2

Energy of helium atom (keV) $E_\infty = 256$ keV	10·4	20·8	41·6	82·2	166·4	208
$2^3S/1^2S$	0·003	0·013	0·14	0·55	1·2	1·4

the metastable state. In Table 2 we present the calculated variation with energy of the population of the 2^3S level relative to that of the ground state.

It is seen from Table 2 that the statistical equilibrium calculations also indicate that at high energies a large percentage of the helium atoms are in the metastable state. This remarkable behaviour of helium appears to be due to the increased coupling at high energies between the ground state and the triplets via the continuum. At low energies the cross-section for ionization of the ground state is small compared to that for ionization of the triplets. On the other hand, at high energies ionizations from the ground state increase sufficiently relative to that from the triplets so that charge capture becomes the dominant process determining

the relative populations of the singlets and the triplets. At such high energies when the dominant process populating both the singlet and triplet levels is charge capture, the true value of the ratio $2^3S/1^1S$ would depend upon the relative number of captures into all of the singlet levels and into all of the triplet levels. Our use of only one singlet level above the ground state tends to under-populate the singlets and the inclusion of more levels would bring the ratio $2^3S/1^2S$ closer to unity at high energies.

In the main part of the "helium arc" the upper level of the transition λ5876 is excited by collisions from the 2^3P level, while the 2^3P level is primarily populated from 2^3S. The metastability of the 2^3S level thus has a moderating influence on the 2^3P level so that the populating of 2^3P falls off less rapidly with increasing energy than that of 3^3D. As can be seen in Fig. 2, λ10830 has a larger half-width than λ5876.

The interpretation of the enhancement of λ10830 as auroral HeI requires that the ratio I(5876)/I(10830) be approximately 0·008 while the calculations indicate a value closer to 0·09. The computed value of the ratio rests, of course, upon several assumed values of cross-sections and may be significantly smaller if the values of certain cross-sections are altered. The ratio of the populations of the states may be calculated directly from the statistical equilibrium equations. Retaining only significant terms the ratio is

$$\frac{N_4}{N_5} = \frac{P_3(P_4C_{k5} + C_{k4}C_{45}) + C_{34}(C_{45}C_{k3} - P_{43}C_{k5}) + C_{35}(P_{43}C_{k4} + P_4C_{k3})}{P_3(C_{k4}P_5 + C_{k5}P_{54}) + C_{34}C_{k3}P_5}. \tag{3}$$

At the energy of the maximum emissivity of helium, ~40 keV, equation (3) gives the ratio $N_5/N_4 = 0{\cdot}0354$. In calculating the strength of the D_3 transition we have used the population of the composite level 5 modified according to the statistical weight of the 3^3D term. In using single level for the three terms 3^3S, 3^3P and 3^3D we have tended to overestimate the population of the upper level of the D_3 transition as the cross-section for the collisional excitation of 3^3D from 2^2S is small. If we set $C_{35} = 0$ in equation (3) we obtain the ratios $N(3^3D)/N_4 = 0{\cdot}0284$ and $\mathrm{I}(5876)/\mathrm{I}(10830) = 7{\cdot}1 \times 10^{-2}$.

The calculations predict that the maximum intensity of the D_3 line should be between 200 and 300 rayleighs. This value lies close to the threshold of detection of present spectrographs and in that sense is reasonable. The observed enhancement of λ10830 would then suggest an overpopulation of the 2^3P level relative to the physical conditions postulated in these calculations. We may estimate how greatly changes in rates will effect the populations of the 2^3P and 3^3D levels by using equation (3). We make the following alterations in rates:

$$\begin{aligned} C_{k3}' &= 3{\cdot}8 \times 10^4 = 0{\cdot}226\ \sigma_{10}N_nV \\ C_{k4}' &= 1{\cdot}14 \times 10^5 = 0{\cdot}68\ \sigma_{10}N_nV \\ C_{k5}' &= 2{\cdot}53 \times 10^3 = 0{\cdot}015\ \sigma_{10}N_nV \\ C_{34}' &= 1{\cdot}1 \times 10^7 \\ C_{45}' &= 9{\cdot}3 \times 10^4 \end{aligned}$$

VOL. 21 1961

where C' represents the new rate. These values most likely represent the greatest permissible alteration in cross-sections. They would mean that 68 per cent of all the electrons would be captured on the 2^3P level and the collisions proceeding from 2^3S to 2^3P would be more than 100 times more rapid than those from 2^2P to 3^3D. Using these values the ratio becomes $N(3^3D)/N(2^3P) = 2{\cdot}5 \times 10^{-3}$ or I(5876)/I(10830) $= 1{\cdot}7 \times 10^{-2}$. This value is reasonably close to that indicated by the observations. On the other hand BATES (1955) has pointed out that de-excitation of the metastable 2^3S level may be augmented by the process

$$\mathrm{HeI}(2^3S) + \mathrm{O} \rightarrow \mathrm{HeII} + \mathrm{O}^-$$

which may be rapid at moderate and low impact energies. Such a process, if effective, decreases the populations of all the triplet levels, thereby lowering the predicted intensity of λ10830.

5. CONCLUSIONS

The narrowness of the enhanced λ10830 line is reasonable if the observation by MIRONOV *et al.* is to be explained in terms of high velocity helium atoms. However it is more difficult to understand the great strength of the line. The observed enhancement cannot be due to an unusually high abundance of alpha-particles in the auroral stream as the lack of the D_3 line places an upper limit on the density of high velocity helium atoms in aurorae. We have seen that by adjusting certain cross-sections, the ratio of the intensities of the λ10830 and the D_3 lines may be close to that demanded by the observations. However, the reality of the modified cross-sections is questionable. Moreover, our method for obtaining relative capture cross-sections by the criterion of energy resonance is admittedly a very crude approximation at the energies concerned. Departures from our scheme of assigning relative capture cross-sections would most likely tend to make the capture cross-sections stronger inverse functions of the principal quantum number. Such modifications in the capture cross-sections and the inclusion of additional processes for de-populating the triplet levels would have the effect of decreasing the intensity of λ10830. Thus with our present knowledge of helium cross-sections, it appears difficult to explain the observed strength of λ10830 in terms of incident solar alpha-particles. Recently SHEFOV (1961) has suggested that the auroral λ10830 line results from resonance scattering from atmospheric helium. Although there are uncertain parameters in his theory, atmospheric helium may be a more satisfactory explanation for the observations than solar alpha-particles. The important problem of determining the helium abundance of the auroral stream nevertheless remains. It is clear that there is a particularly great need for additional observations of the enhancement of λ10830 and for a concentrated search for the D_3 line. There is an even greater need for measurements of additional helium cross-sections.

Acknowledgements—It is a pleasure to record my indebtedness to R. G. ATHAY, J. W. CHAMBERLAIN, and H. L. JOHNSON for discussions on this problem. During the course of this investigation the author held a fellowship from the Institute for Solar Terrestrial Research of the High Altitude Observatory.

References

Allen C. W.	1955	*Astrophysical Quantities*, p. 39. Athlone Press, London.
Barbier D. and Williams D. R.	1950	*J. Geophys. Res.* **55,** 401.
Barnett C. F. and Stier P. M.	1958	*Phys. Rev.* **109,** 385.
Bates D. R.	1955	*The Airglow and the Aurorae*, p. 251. Pergamon Press, London.
Bates D. R. and Dalgarno A.	1953	*Proc. Phys. Soc. Lond.* A **66,** 972.
Bates D. R., Fundaminsky A., Leech J. W. and Massey H. S. W.	1950	*Phil. Trans.* A **243,** 93.
Chamberlain J. W.	1954	*Astrophys. J.* **120,** 360.
Chamberlain J. W.	1957	*Astrophys. J.* **126,** 245.
Chamberlain J. W. and Smith C. A.	1959	*J. Geophys. Res.* **64,** 611.
Cook C. J., Jones E. and Jorgensen T.	1953	*Phys. Rev.* **91,** 1417.
Fan C. Y.	1955	*Astrophys. J.* **122,** 350.
Fedorova N. I.	1958	IAU Meeting, Moscow.
Fite W. L., Brackman R. T. and Snow W. R.	1958	*Phys. Rev.* **112,** 1161.
Galperin Iu. I.	1957	*Soviet Astronomy* **1,** 133.
Kallmann H. K.	1959	*J. Geophys. Res.* **64,** 615.
Massey H. S. W. and Burhop E. H. S.	1952	*Electronic and Ionic Impact Phenomena.* Chaps. 7 and 8. Clarendon Press, Oxford.
Massey H. S. W. and Moiseiwitsch B. L.	1954	*Proc. Roy. Soc.* A **227,** 38.
Mironov A. V., Prokudina V. S. and Shefow N. N.	1959	*Spectral, Electrophotometrical and Radar Researches of Aurorae and Airglow.* p. 10. Academy of Sciences of the USSR, Moscow.
Moiseiwitsch B. L. and Stewart A. L.	1954	*Proc. Phys. Soc. Lond.* A **67,** 1069.
Montalbetti R.	1959	*J. Atmosph. Terr. Phys.* **14,** 200.
Mott N. F. and Massey H. S. W.	1949	*The Theory of Atomic Collisions*, p. 260. Clarendon Press, Oxford.
Shefov N. N.	1961	*Planet. Space Sci.* **5,** 75.
Smith P. T.	1930	*Phys. Rev.* **37,** 1293.
Trittelwitz V. W.	1941	*Ann. Phys., Lpz.* **40,** 131.
Wolf V. F.	1937	*Ann. Phys., Lpz.* **30,** 313.

VOL. 21 1961

Journal of Atmospheric and Terrestrial Physics, 1961, Vol. 21, pp. 65 to 69. Pergamon Press Ltd. Printed in Northern Ireland

General expression for the group refractive index of the ionosphere

Y. S. N. Murty* and S. R. Khastgir
Calcutta University

(*Received* 12 *December* 1960)

Abstract—A general expression for the group refractive index of the ionosphere has been deduced. Considering the relevant quadrants for the phase-difference between the normal and the abnormal components of the magnetic vector of the radio wave, the general expression gives the values of the group refractive index for the ordinary and the extraordinary modes for different frequencies and for different electron-densities and electron-collisional frequencies of the ionospheric medium and also under different conditions of the earth's magnetic field.

Introduction

In a previous paper (Murty and Khastgir, 1960a), a general expression for the group refractive index of the ionosphere was worked out for low-frequency radio-wave propagation, where only the ordinary mode of propagation was considered (as the extraordinary mode of propagation is mostly absorbed for low frequencies). The expression was derived by making some approximations, which are applicable to low-frequency propagation. It was also shown that in the limiting case of low collisional frequency, this expression for group refractive index was reduced to that obtained by an elaborate method by Gibbons and Rao (1957).

In the present communication a general expression for the group refractive index has been developed. For different exploring wave frequencies, electron number densities and electron collisional frequencies of the ionosphere and under different conditions of the earth's magnetic field, the group refractive index for the ordinary and extraordinary modes of propagation can be obtained from the general expression with the help of the general phase-quadrant table given by Murty and Khastgir (1960b).

Deduction of the General Expression

For a frequency f, the group refractive index μ' is related to the phase refractive index μ by

$$\mu' = \mu + f\frac{\partial \mu}{\partial f}. \tag{1}$$

If M is the complex refractive index of the ionospheric medium, we can write

$$\mu' - \mu = f\frac{\partial \mu}{\partial f} = \mathscr{R}\left(f\frac{\partial M}{\partial f}\right) \tag{2}$$

where $\mathscr{R}$ denotes the "real part of". Let $M = (\mu - i\chi)$, where $\chi = ck/p$, $k =$ absorption coefficient, $p/2\pi =$ frequency f of the wave and c the velocity of light. If the complex polarization is expressed as:

$$R = \rho e^{i\phi} = r + is \tag{3}$$

* Defence Science Organisation, Delhi.

where ρ is the ratio of the normal to the abnormal components of the magnetic vector of the wave and ϕ the phase-difference between them, we have

$$r = \rho \cos \phi \quad \text{and} \quad s = \rho \sin \phi \tag{3a}$$

Putting

$$\tau = 1 + \chi^2 - \mu^2 \tag{4}$$

it has already been shown (Murty and Khastgir, 1960a) that

$$2(\mu' - \mu)(\mu^2 + \chi^2) = \mu(1 - \mu^2 - \chi^2) - \mu\tau^2\left(\alpha - \gamma_L f \frac{\partial s}{\partial f}\right) + 4\mu\chi^2(1 + \chi^2)\left(\alpha - \gamma_L f \frac{\partial s}{\partial f}\right) + \chi\gamma_L f \frac{\partial r}{\partial f}[\tau^2 + 4\mu^2(1 - \mu^2)]. \tag{5}$$

Here $\alpha = \dfrac{p^2}{{p_0}^2}$, $\gamma_L = \gamma \cos \theta'$, $\gamma = \dfrac{pp_H}{{p_0}^2}$, $p_H = \dfrac{eH}{mc}$, ${p_0}^2 = \dfrac{4\pi Ne^2}{mp^2}$

and θ' = angle between the direction of propagation and the earth's magnetic field H. (The other notations have their usual significance.)
Dividing (5) throughout by $2\mu(\mu^2 + \chi^2)$, we get

$$\frac{\mu'}{\mu} = 0{\cdot}5 + \frac{0{\cdot}5}{\mu^2 + \chi^2}\left\{1 - [\tau^2 - 4\mu\chi^2(1 + \chi^2)]\left(\alpha - \gamma_L f \frac{\partial s}{\partial f}\right)\right\} + \frac{0{\cdot}5\chi\gamma_L}{\mu(\mu^2 + \chi^2)}[\tau^2 + 4\mu^2(1 - \mu^2)]f \frac{\partial r}{\partial f}. \tag{6}$$

The quantities $f\,\partial s/\partial f$ and $f\,\partial r/\partial f$ in (6) are obtained as follows: It has already been proved (Murty, 1959; Murty and Khastgir, 1959) that the ratio of the normal to the abnormal components of the magnetic vector of the wave is given by

$$\rho = \frac{a'}{\nu_c}\left(\frac{\nu}{\cos \phi} - \frac{p'}{\sin \phi}\right) \tag{7}$$

and

$$\cos 2\phi = a' - \sqrt{[(1 + a')^2 - 4a'b']} \tag{8}$$

where

ν = electron collisional frequency

ν_c = critical collisional frequency

$$\left.\begin{aligned} a' &= \frac{{\nu_c}^2}{\nu^2 + p'^2} \\ b' &= \frac{\nu^2}{\nu^2 + p'^2} \end{aligned}\right\} \tag{9}$$

and

$$p' = p\left(1 - \frac{{p_0}^2}{p^2}\right).$$

Thus

$$r = \rho \cos \phi = \frac{a'}{\nu_c}(\nu - p' \cot \phi) \tag{10}$$

and

$$s = \rho \sin \phi = \frac{a'}{\nu_c}(\nu \tan \phi - p'). \tag{11}$$

VOL. 21 1961

From (9) we get,

$$\frac{\partial p'}{\partial a'} = \left(\frac{\partial a'}{\partial p'}\right)^{-1} = \left[-\frac{2p'{v_c}^2}{(v^2 + p'^2)^2}\right]^{-1} = -\frac{{v_c}^2}{2p'a'^2}. \tag{12}$$

From (11) we get

$$\frac{\partial s}{\partial a'} = \frac{s}{a'} + \frac{v_c}{2a'p'} - \frac{a'v}{v_c}\frac{\sec^2\phi}{2\sin 2\phi}\left(1 - \frac{1 + a' - 4b'}{a' - \cos 2\phi}\right) \tag{13}$$

and

$$\frac{\partial r}{\partial a'} = \frac{r}{a'} + \frac{a'}{v_c}\left[\frac{{v_c}^2}{2p'a'^2}\cot\phi - \frac{p'\,\mathrm{cosec}^2\,\phi}{2\sin 2\phi}\left(1 - \frac{1 + a' - 4b'}{a' - \cos 2\phi}\right)\right]. \tag{14}$$

Also

$$f\frac{\partial a'}{\partial f} = -\frac{2a'^2}{{v_c}^2}pp'\left(1 + \frac{{p_0}^2}{p^2}\right). \tag{15}$$

Therefore from (13) and (15) we get,

$$f\frac{ds}{\partial f} = \left(\frac{\partial s}{\partial a'}\right)\left(f\frac{\partial a'}{\partial f}\right) = -\frac{2a'^2}{{v_c}^2}pp'\left(1 + \frac{{p_0}^2}{p^2}\right) \times\left[\frac{s}{a'} + \frac{v_c}{2a'p'} - \frac{a'v}{v_c}\frac{\sec^2\phi}{2\sin 2\phi}\left(1 - \frac{1 + a' - 4b'}{a' - \cos 2\phi}\right)\right]. \tag{16}$$

Similarly from (14) and (15) we get,

$$f\frac{\partial r}{\partial f} = \left(\frac{\partial r}{\partial a'}\right)\left(f\frac{\partial a'}{\partial f}\right) = -\frac{2a'^2}{{v_c}^2}pp'\left(1 + \frac{{p_0}^2}{p^2}\right) \times\left[\frac{r}{a'} + \frac{v_c}{2a'p'}\cot\phi - \frac{a'p'}{v_c}\frac{\mathrm{cosec}^2\,\phi}{2\sin 2\phi}\left(1 - \frac{1 + a' - 4b'}{a' - \cos 2\phi}\right)\right]. \tag{17}$$

Hence on substituting the values of $f\,\partial s/\partial f$ and $f\,\partial r/\partial f$ from (16) and (17) in (6) we have

$$\frac{\mu'}{\mu} = 0{\cdot}5 + \frac{0{\cdot}5}{\mu^2 + \chi^2}\left(1 - (\tau^2 - 4\chi^2\sqrt{1 + \chi^2})\left\{\alpha - \gamma_L\left(-\frac{2a'^2}{v_c}pp'\sqrt{1 + \frac{{p_0}^2}{p^2}}\right) \times\left[\frac{s}{a'} + \frac{v_c}{2a'p'} - \frac{a'v}{v_c}\frac{\sec^2\phi}{2\sin 2\phi}\left(1 - \frac{1 + a' - 4b'}{a' - \cos 2\phi}\right)\right]\right\}\right) + \frac{0{\cdot}05}{\mu(\mu^2 + \chi^2)}(\tau^2 + 4\mu^2\sqrt{1 - \mu^2}) \times\left[-\frac{2a'^2}{{v_c}^2}pp'\left(1 + \frac{{p_0}^2}{p^2}\right)\right]\left[\frac{r}{a'} + \frac{v_c\cot\phi}{2a'p'} - \frac{a'p'\,\mathrm{cosec}^2\,\phi}{v_c 2\sin 2\phi}\left(1 - \frac{1 + a' - 4b'}{a' - \cos 2\phi}\right)\right]. \tag{18}$$

With the help of the general phase-quadrant table given by (Murty and Khastgir, 1960b; Appendix 1), equation (18) gives the group refractive index of the ionosphere for the ordinary and extraordinary modes of propagation for different wave frequencies, electron number densities, electron-collisional frequencies of the ionosphere and also under different conditions of the earth's magnetic field.

Group Refractive Index at Low Frequencies of the Exploring Wave for Places of Low Critical Collisional Frequency

In the case of low-frequency propagation, the ordinary mode only is considered, as the extraordinary mode is completely absorbed, Thus for places of low critical frequency and for low frequencies of the exploring wave and taking $f \approx 150$ kc/s, $p_H/p \approx 10$, $\nu_c/p \approx 0{\cdot}5$ and $\nu \approx 10^6$, it was already shown (Murty and Khastgir, 1960a) that

$$f\frac{\partial s}{\partial f} \approx -\frac{r}{\nu}p\left(1-\frac{1}{\alpha}\right). \tag{19}$$

Similarly for low frequency propagation and for low critical collisional frequencies, the term $f\ \partial r/\partial f$ in the expression (6) for the group refractive index can be approximately written as

$$f\frac{\partial r}{\partial f} = -\frac{2{\nu_c}^2}{\nu^4}pp'\left(1+\frac{{p_0}^2}{p^2}\right)\left(\frac{\nu}{\nu_c}+\frac{\nu}{2p'}-\frac{p'}{\nu}\right) \tag{20}$$

(*vide* Appendix II).

Substituting the approximate values of $f\ \partial s/\partial f$ and $f\ \partial r/\partial f$ in the expression (6) for the group refractive index we get,

$$\frac{\mu'}{\mu} \approx 0{\cdot}5 + \frac{0{\cdot}5}{\mu^2+\chi^2}\left\{1-[\tau^2-4\chi^2(1+\chi^2)]\left[\alpha+\gamma_L\frac{r}{\nu}p\left(1-\frac{1}{\alpha}\right)\right]\right\}$$
$$+\frac{0{\cdot}5\chi\gamma_L}{\mu(\mu^2+\chi^2)}[\tau^2+4\mu^2(1-\mu^2)]\frac{{\nu_c}^2}{\nu^4}\left(\frac{\nu}{\nu_c}+\frac{\nu}{2p'}-\frac{p'}{\nu}\right)$$
$$\times\left[-2pp'\left(1+\frac{{p_0}^2}{p^2}\right)\right]. \tag{21}$$

Since $\chi^2 \approx 0$ and $\nu_c \ll \nu$, the last term can be neglected. Thus we can write

$$\frac{\mu'}{\mu} \approx 0{\cdot}5 + \frac{0{\cdot}5}{\mu^2+\chi^2}\left\{1-\tau^2\left[\alpha+\gamma_L\frac{r}{\nu}p\left(1-\frac{1}{\alpha}\right)\right]\right\}. \tag{22}$$

Writing $\dfrac{pp_H}{{p_0}^2}\cos\theta'$ for γ_L, we get,

$$\frac{\mu'}{\mu} \approx 0{\cdot}5 + \frac{1}{\mu^2+\chi^2}\left[0{\cdot}5-\frac{\tau^2}{2}\left\{\alpha+(1-\alpha)p_H\cos\theta'\frac{r}{\nu}\right\}\right]. \tag{23}$$

This is the expression which Murty and Khastgir (1960a) derived earlier for low frequency propagation and for places of low collisional frequency.

References

Gibbons J. J. and Rao B. R.	1957	*J. Atmosph. Terr. Phys.* **11,** 151.
Murty Y. S. N.	1959	*Sci. & Cult.* **25,** 161.
Murty Y. S. N. and Khastgir S. R.	1959	*Proc. Nat. Inst. Sci. India* A **25,** 255.
Murty Y. S. N. and Khastgir S. R.	1960a	*J. Atmosph. Terr. Phys.* **17,** 309.
Murty Y. S. N. and Khastgir S. R.	1960b	*J. Geophys. Res.* **65,** 1449.

VOL. 21 1961

Appendix I

Phase-quadrant Table

Mode	Term	Northern hemisphere		Southern hemisphere	
		$p' > 0$	$p' < 0$	$p' > 0$	$p' < 0$
Ordinary	Amplitude-ratio	$\rho < 1$	$\rho < 1$	$\rho < 1$	$\rho < 1$
	Phase-quadrant	$0 < \phi < \frac{\pi}{2}$ First quadrant	$\frac{3\pi}{2} < \phi < 2\pi$ Fourth quadrant	$\pi < \phi < \frac{3\pi}{2}$ Third quadrant	$\frac{\pi}{2} < \phi < \pi$ Second quadrant
Extra-ordinary	Amplitude-ratio	$\rho > 1$	$\rho > 1$	$\rho > 1$	$\rho > 1$
	Phase-quadrant	$\frac{3\pi}{2} < \phi < 2\pi$ Fourth quadrant	$0 < \phi < \frac{\pi}{2}$ First quadrant	$\frac{\pi}{2} < \phi < \pi$ Second quadrant	$\pi < \phi < \frac{3\pi}{2}$ Third quadrant

Appendix II

The different terms within the square bracket in the expression (17) for $f\,\partial r/\partial f$ are reduced as follows:

(i) $$\frac{r}{a'} = \frac{\rho \cos\phi}{a'} = \frac{1}{v_c}(v - p' \cot\phi) \approx \frac{v}{v_c} \qquad (p' \ll v)$$

(ii) $$\frac{v_c}{2a'p'} \cot\phi = \frac{v_c}{2a'p'} \sqrt{\left(\frac{1 + \cos 2\phi}{1 - \cos 2\phi}\right)} \approx \frac{v_c}{2a'p'} \sqrt{\left(\frac{a'}{1 - a'}\right)}$$

$$\approx \frac{v_c}{2p'} \cdot \left(b' \approx 1 \text{ and } a' \approx \frac{{v_c}^2}{v^2} \approx 0\right)$$

(iii) $$\frac{a'p}{v_c} \frac{\operatorname{cosec}^2\phi}{2 \sin 2\phi} \left(1 - \frac{1 + a' - 4b'}{a' - \cos 2\phi}\right)$$

$$\approx \frac{a'p'}{v_c} \frac{1}{2(1 - a')\sqrt{[1 - (2a' - 1)^2]}} \left(1 - \frac{a' - 3}{1 - a'}\right)$$

$$\approx \frac{a'p'}{2v_c} \frac{1}{2a'^{\frac{1}{2}}} \cdot 2\left(\frac{2 - a'}{1 - a'}\right)$$

$$\approx \frac{a'^{\frac{1}{2}}p'}{v_c} \approx \frac{p'}{v}$$

Thus

$$f \frac{\partial r}{\partial f} = -\frac{2{v_c}^2}{v^4} pp' \left(1 + \frac{{p_0}^2}{p^2}\right)\left(\frac{v}{v_c} + \frac{v}{2p'} - \frac{p'}{v}\right) \qquad (20)$$

Journal of Atmospheric and Terrestrial Physics 1961, Vol. 21, pp. 70 to 71. Pergamon Press Ltd. Printed in Northern Ireland

BOOK REVIEW

Selected Scientific Papers of Balthasar van der Pol. Edited by H. BREMMER and C. J. BOUWKAMP, with an Introduction by H. B. G. CASIMIR; 2 volumes. North-Holland Publishing Company, Amsterdam, 1960. 1339 pp., £6.13s.

Dr. BALTH VAN DER POL, a revered figure in the world of radio-physics, died in October 1959. Within a year of that sad event there have been published, under the editorship of two of his Dutch colleagues, two handsome volumes of his collected scientific papers. Those of us who had the great privilege of enjoying the friendship of Dr. VAN DER POL must certainly feel that this kind of memorial is the one which would have pleased him most of all. His friends will be aware, too, that what VAN DER POL published was only a fraction of what he had achieved. Unlike some people, who publish faster than they think, he never allowed anything to see the light of publication until—to quote a favourite phrase of his—he had "got to the bottom of it". The loftiest standards in all his scientific work were indeed the mainspring of his many-sided genius.

One of VAN DER POL's outstanding achievements was to invest radio science, as it developed during the first half of the present century, with a mathematical basis and framework; though in his later years he also became much preoccupied with pure mathematics itself. He used frequently to quote, with warm approval, the famous remark of BOLTZMANN's that "there is nothing more practical than a good theory". In the field of radio we can divide his papers into two groups, one relating to electric wave propagation and the other to electrical circuit theory It was VAN DER POL who gave the first quantitative comparison between simple wave diffraction theory and practical reception results in long-distance radio communication round a spherical earth, which strikingly indicated the existence of a beneficent agent, favouring round-the-world radio transmission, which we now know to be the ionosphere. At the same time, in some elegant laboratory experiments, he demonstrated that ionized air at very low pressures possessed the necessary high-frequency properties to cause the ionic refraction of radio waves. The latter researches are the subject of his Utrecht University doctor's thesis, which is reprinted in full in the first of these two volumes.

In his investigations of electric circuits, VAN DER POL's outstanding achievement was to formulate the theory of relaxation oscillations and to explain the connexion between such oscillations and those of simple harmonic type. Both types of oscillations can be mathematically described by what, most appropriately, has come to be known as VAN DER POL's equation:

$$\frac{d^2v}{dt^2} - \varepsilon(1 - v^2)\frac{dv}{dt} + v = 0.$$

Solutions of this non-linear equation for $\varepsilon \gg 1$ describe relaxation oscillations; while, for $\varepsilon \ll 1$, they describe the more familiar harmonic vibrations.

It is fascinating to note, from the sequence of memoirs now published, how VAN DER POL's interest in electric circuit theory led him to a major preoccupation in the operational calculus, on which subject, in collaboration with a distinguished Dutch colleague, H. BREMMER, he wrote a treatise of enviable lucidity and originality.

Those of us who, in the past, read most of VAN DER POL's original papers, as they appeared, will be grateful for this new and convenient opportunity of refreshing our acquaintance with

VOL. 21 1961

them, and also of reading those which, somehow, we may have missed. But perhaps an older scientific worker may take the liberty of drawing the attention of the younger generation of scientific radio-physicists to this record of one man's achievement, and of predicting that they will not fail to find in it both encouragement and inspiration. Many of these young folk may have met the man himself; for VAN DER POL was a great traveller and much in demand as a lecturer in the world's centres of radio research. He loved young people; and, like all really great men, always treated them as equals.

E. V. APPLETON

Journal of Atmospheric and Terrestrial Physics, 1961, Vol. 21, p. 72. Pergamon Press Ltd. Printed in Northern Ireland

Papers to be published in future issues

A. J. Lyon, N. J. Skinner and R. W. Wright: Equatorial spread-*F* at Ibadan, Nigeria

O. Awe: The fading of radio waves reflected from the ionosphere at oblique incidence

O. Awe: The fading of radio waves weakly scattered at vertical incidence from heights near 90 km

B. P. Sandford: Aurora and airglow from colour film observations

B. P. Sandford: The behaviour of night-sky 6300, 5577 and 3914 Å emissions at Scott Base, Antarctica

Sir Edward Appleton and A. J. Lyon: Studies of the *E*-layer of the ionosphere—II. Electromagnetic perturbations and other anomolies

H. J. A. Chivers: A statistical study of ionospheric drifts measured by the radio star scintillation technique

H. Unz: On vertical drift velocities of the *F2*-layer

U. Haug: Zur Statistik der räumlichen Helligkeitsschwankungen der [OI]-Linie 5577 Å im Nachthimmelsleuchten

R. Naismith, H. C. Bevan and P. A. Smith: A long term variation in the relation of sunspot numbers to *E*-region character figures.

J. A. Lane: The radio refractive index gradient over the British Isles

J. A. Chalmers: A criterion for thunderstorm theories

W. Stoffregen: The east–west drift of auroral forms determined from all-sky camera films

G. H. Bazzard: A study of the variations in a daily ionospheric index of solar activity

J. S. Greenhow and J. E. Hall: Attachment processes in meteor trails

K. V. V. Ramana and B. Ramachandra Rao: Investigation of ionospheric absorption on 5·65 Mc/s at Waltair

S. N. Ghosh and V. Malaviya: Microwave absorption in the earth's atmosphere

M. S. V. Gopala Rao and B. Ramachandra Rao: Nocturnal and seasonal variations of equatorial spread-*F*

VOL. 21 1961

Journal of Atmospheric and Terrestrial Physics, 1961, Vol. 21, pp. 73 to 99. Pergamon Press Ltd. Printed in Northern Ireland

Studies of the *E*-layer of the ionosphere—II

Electromagnetic perturbations and other anomalies

Sir Edward Appleton
University of Edinburgh

and

A. J. Lyon
University College, Ibadan

(*Received* 2 *April* 1960)

Abstract—An extended, and more detailed, account is given of a result, first described by the authors some years ago: namely, that the electromagnetic influence of the S_q system of currents can be detected in studies of *E*-layer morphology. This result has been subsequently confirmed by Beynon and Brown, and by Shimazaki.

Part I of this paper was devoted to the derivation of various quantitative relations by which the experimentally observed behaviour of the *E*-layer could be explained in terms of current theories of ionized layer formation and variation. It was there shown that two valuable criteria in this connection are (a) the nature of the diurnal asymmetry of $N_m(E)$ when corresponding forenoon and afternoon values are compared and (b) the dependence of the mean level of $N_m(E)$, the layer maximum electron density, on $\cos\chi$, where χ is the solar zenith distance.

Departures from the predictions of simple theory have been identified by comparing *E*-layer characteristics observable at different times at a given station, and at the same time at different stations. For example, studies of diurnal asymmetry in f_0E and $h'E$ indicate departures from theoretical predictions; and, moreover, disclose opposite trends in high and low latitudes which we identify as geomagnetic perturbations arising from the motor effect of the S_q system of currents flowing in the *E*-layer. The same geomagnetic distortion is identified as one main reason why f_0E is not a unique function of $\cos\chi$ under comparable conditions. For example, at a solstice noon, the maximum value of f_0E does not occur at the sub-solar point, but on the equatorial side of it. This and other phenomena suggest that, quite generally, the motor effect of the S_q current is to raise f_0E in low latitudes, and reduce it in high latitudes, with reference to its basic value produced by solar radiation.

Simple theory suggests that, in the *E*-layer, N_m should be, substantially, proportional to $(\cos\chi)^{1/2}$ at all times when N_m is not changing too rapidly, as is the case over the greater part of the hours of daylight. Experimental evidence, however, shows that for the diurnal variation at constant latitude, and also for a latitude variation at constant time (such as noon), N_m varies approximately at $(\cos\chi)^{2/3}$. This and other anomalies, such as the considerable variation of f_0E at constant χ, and the anomalous asymmetry observed at low $\cos\chi$, are also discussed.

1. Introductory

In Part I of this paper we have given an account of a number of theoretical relationships by which the correspondence between ionospheric behaviour and ionospheric theory can be examined. The relative simplicity of these relationships derives from the assumption that quasi-stationary conditions obtain in the case of the ionospheric layer under consideration; we therefore consider them relevant to the case of the *E*-layer. In this continuation of our paper we describe an investigation of *E*-layer experimental data in the light of the results set out in Part I, to which the reader is referred for a fuller discussion. We shall therefore use the formulae of that paper, with only the minimum of explanation, below.

2. The Experimental Material

Most of our knowledge of the *E*-layer comes from routine ionosonde measurements which are now yielding very extensive series of values of *E*-layer critical

frequency, f_0E (and hence of its maximum electron density N_m), and also of $h'E$, the minimum equivalent height, for all parts of the world. In favourable cases it is also possible to determine the $N(h)$ profile of the lower E-region from the experimental $h'(f)$ curve, though this is not usually done as a routine matter. Quite independent evidence concerning the E-region $N(h)$ profile is now also available from a limited number of rocket measurements.

With regard to the determination of the critical frequency f_0E from ionograms, several sources of uncertainty unfortunately exist. First there is often ambiguity due to stratifications in the region. Bibl (1951), in an attempt to solve this difficulty, proposed that f_0E be defined by the first major discontinuity of equivalent height (of, say, more than 15 km) corresponding to a layer of normal thickness, as indicated by the shape of the $h'(f)$ curve. This definition has not, however, been generally accepted, and may indeed be considered somewhat arbitrary. At any rate in cases of ambiguity there is no agreed convention, and at some stations f_0E may tend to be read high and at others low. Second, in the presence of E_s the normal discontinuity may degenerate into a cusp and the lower part of the F trace may be obscured. If f_0E is then read at the cusp it will have too low a value. Third, the E trace may be obscured in the neighbourhood of f_0E by spread echoes, transparent E_s or absorption. In such cases f_0E is liable to be determined from the F trace and the value may then be too high.

In general the magnitude of the uncertainty arising from these causes is of the order of 0·1–0·2 Mc/s. One of the main reasons for the frequent occurrence of such ambiguities is clear from a study of $N(h)$ profiles obtained from rocket measurements (e.g. Jackson and Seddon, 1958). These show that there may often be no clear maximum in the E-region at all but rather a region of 20 km or more over which the electron density N increases rather slowly with height. Relatively small, and unimportant, variations of electron density may therefore cause considerable changes in the appearance of the $h'(f)$ curve in the region of the transition from E-region to F-region echoes.

The critical penetration frequency of the E-layer may, then, not always be a sharply defined quantity and the search for a precise "true f_0E" in such cases is meaningless. We shall have to deal in this paper with perturbations which are of the same order of magnitude as these ambiguities, and the greatest care has therefore been required to ensure that any conclusions are not invalidated by uncertainties of this kind. There are broadly two ways of doing this: firstly by averaging data from many stations and many months so that random variations are largely eliminated, and, secondly, by considering whether any regularities found could reasonably be attributed to some trend in the mode of measurement—for example as due to a prevalence of E_s.

3. Methods of Analysis

Assuming that electrons disappear according to a simple recombinative law, and also assuming, for the moment, that there is no electron transport, the variations of electron density are governed by the continuity equation

$$\frac{\partial N}{\partial t} = q(h, t) - \alpha N^2 \qquad (1)$$

VOL. 21 1961

where the rate of electron production q is a function of height h and of time t, and the effective recombination coefficient α is assumed constant.

If now q has the form appropriate to a simple Chapman layer and if, further, conditions are "quasi-stationary", that is, if $\partial N/\partial t$ is small compared to αN^2 in the neighbourhood of the layer maximum (and it is clear from diurnal curves of N_m that this condition is in fact satisfied for the E-layer except quite near sunrise and sunset), then, according to APPLETON and LYON (1955), the maximum value of electron density N_m at a given time satisfies the equation:

$$\frac{dN_m}{dt} = q_0 \cos\chi(1 - \tfrac{1}{2}a^2) - \alpha N_m^2 \tag{2}$$

where a is the difference in the heights at which q and N respectively have their maximum value, a being expressed as a fraction of the scale height H. a is given by:

$$a = \frac{dN_m/dt}{\alpha N_m^2} \tag{3}$$

and h_m, the height of maximum q, is given by

$$h_m = H \log \sec\chi + h_0. \tag{3a}$$

In principle, equation (2) determines N_m in terms of q_0, α and χ (or t). The ratio q_0/α is readily determined from the values of N_m near noon, when dN_m/dt is zero, but the effective value of α in the E-region is not accurately known, and may vary with height, time of day, season, latitude, etc. However the evidence available (e.g. MINNIS, 1956) suggests that, in general, for the E-region

$$\alpha \sim 1 \times 10^{-8} \text{ cm}^3/\text{sec}.$$

If this is so, then, except within about an hour of sunrise and sunset, the quantity a is a small fraction, and equation (2) can be solved by successive approximations. Indeed, for many purposes and certainly near noon the completely stationary approximation

$$N_m = \left(\frac{q_0}{\alpha}\right)^{1/2} (\cos\chi)^{1/2} \tag{4}$$

is sufficiently accurate; and to test this equation α need not be known.

Since N_m is proportional to the square of the critical frequency we should thus find:

$$\frac{(f_0E)^4}{\cos\chi} = \text{const.} = K \text{ say}, \tag{5}$$

K being sometimes referred to as the "character figure" (APPLETON and NAISMITH, 1939). The constancy of K is then a test of the validity of simple Chapman theory.

In studies of the actual relationship between f_0E and $\cos\chi$, it has been common practice to write

$$f_0E = K_p(\cos\chi)^p \tag{6a}$$

or

$$\cos\chi = K_n(f_0E)^n \tag{6b}$$

where, obviously, p is equal to $1/n$ and the relation between the two constants K_p and K_n is given by

$$K_n K_p^{\,n} = K_p K_n^{\,p} = 1. \tag{6c}$$

Usually the experimental data are employed to determine the value of the exponent p (or n), for which purpose we write (6a) and (6b) in their more convenient logarithmic form

$$\log (f_0 E) = \log K_p + p \log (\cos \chi) \tag{7a}$$

and

$$\log (\cos \chi) = \log K_n + n \log (f_0 E). \tag{7b}$$

In what follows we shall usually take $\cos \chi$ as the independent variable, and employ equations (6a) and (7a) for the determination of p.

Strictly, in investigations of this kind one should make corrections for the dN_m/dt term which is neglected in equation (4) and the subsequent equations. A simple way of doing this, which does not require a knowledge of α, is to use, instead of f_0E (or N_m), the average $\overline{f_0E}$ (or $\overline{N_m}$) of the values at the two times, in the morning and afternoon respectively, when χ has the same numerical value. This method depends on the theoretical conclusion—borne out by experiment—that, at two such times, the values of dN_m/dt for the E-layer are opposite in sign and almost exactly equal in magnitude (except possibly near to sunrise and sunset). In most of our studies based on equations (7) we have therefore adopted this procedure.

Equation (2) can also be tested, in principle, by studying the asymmetry in the diurnal curve which arises from the presence of the dN_m/dt term. This will cause afternoon values to be slightly higher than morning values for the same χ and, using (4) as a first approximation, it is readily seen that ΔN_m, the difference between afternoon and morning values at the same χ, is given (Appleton, 1937) by

$$\Delta N_m = \frac{dN_m/dt}{\alpha \overline{N}_m} = \frac{\tan \chi \, d\chi/dt}{2\alpha}. \tag{8}$$

It can also be shown (Appleton, 1953) that the maximum value of N_m will occur at a time Δt after local noon, where

$$\Delta t = \frac{1}{2\alpha N_0} \tag{9}$$

N_0 being the noon value of N_m.

There will also be an asymmetry in the predicted diurnal variation of h_m due to the "height-lag" already mentioned, morning values being higher than afternoon values by an amount $2a$, where a is given by equation (3).

Insertion of typical values for χ, $d\chi/dt$ and N_0 in equations (8) and (9) shows that these predicted asymmetries in the diurnal variations of height and critical frequency will be readily detectable if the effective α is numerically of the order of 1×10^{-8}; but would be rather difficult to detect if α were, say, 5×10^{-8} or greater. For example, if we take $\alpha = 10^{-8}$ cm^3/sec, and consider the equator, the estimated difference ΔN_m between the values at 0800 hours and 1600 hours would be $0{\cdot}63 \times 10^{-4}$ cm^{-3}, which would correspond to a difference in f_0E of 0·08 Mc/s;

for 0700 hours and 1700 hours that difference would increase to 0·2 Mc/s. The corresponding values of $2a$ would be 0·5 and 1 km respectively. Differences of this order should be measurable.

The investigations recorded in this paper have been mainly directed towards discovering how far the basic equations, (7), (8) and (9), agree or disagree with the observed behaviour of the E-layer.

4. Anomalies in the (f_0E, cos χ) Relationship

There have been numerous investigations of the dependence of f_0E on cos χ, chiefly based on the semi-empirical equations (6) or (7). Such studies have used

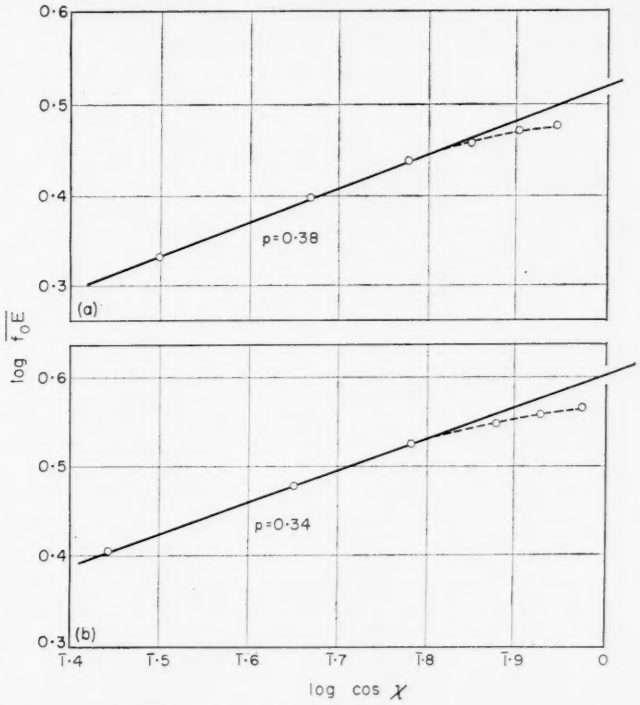

Fig. 1. Variation of log $\overline{f_0E}$ with log cos χ showing midday summer depressions. (a) Slough, June 1954; (b) Christchurch, December (1947–1953).

(a) the diurnal variation at specific places and seasons, or (b) the seasonal variation at specific places and fixed times of day (often at noon), or (c) the latitude variation at specific seasons and times of day; and in general the results are derived from routine published data, accepted at their face value.

(a) *Diurnal variations*

It has been stated (e.g. by Menzel and Wolbach, 1955, and Harnischmacher, 1950) that the exponent p of equation (6a) tends to have values around 0·3 for the diurnal variation, with both K_p and p tending to decrease slightly with increasing latitude. The variation of log f_0E against log cos χ is, however, not always linear, but may, for example, show a downward deflection (Fig. 1) at high cos χ: this

anomaly which we shall refer to as the "noon depression" is usually present in summer months (and sometimes in equinox months) at middle latitudes. Thus at Slough (51° N) in June and July we find a mean depression in f_0E of about $1\frac{1}{2}$ per cent at noon, at Washington (39° N) a depression of about $2\frac{1}{2}$ per cent, and at Christchurch (44° S) a mean noon depression of about 4 per cent in December and

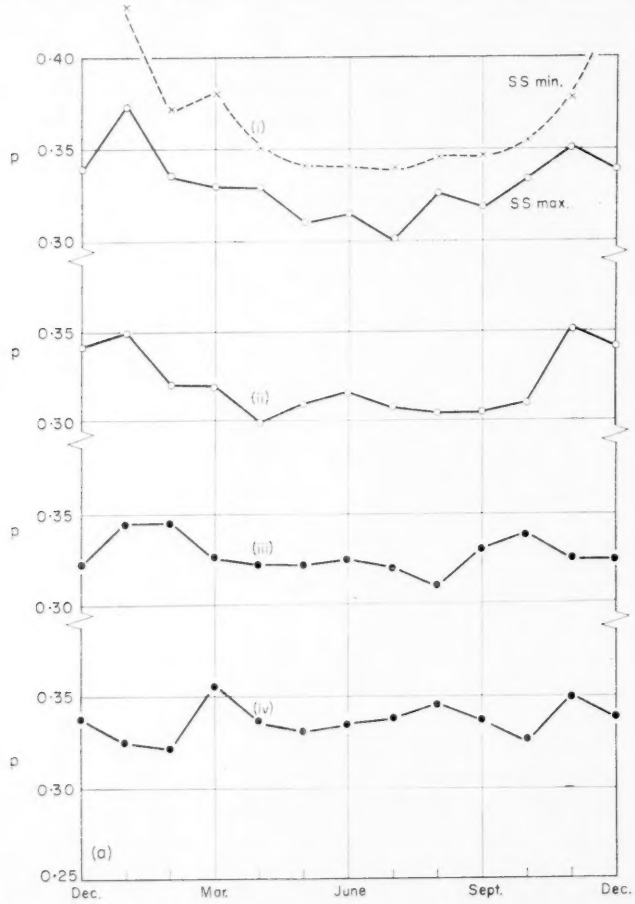

Fig. 2(a). Variation of diurnal exponent p with month of the year, showing a small winter increase in some cases. (i) Slough; (ii) Washington (1949–1953); (iii) Singapore (1951–1953); (iv) Christchurch (1947–1953).

January. No noon depression is observed, however, at Falkland Islands (52° S).

Obviously the value of p obtained will depend on whether we use the linear portion of the curve or (as Menzel and Wolbach did) use a best-fitting straight line through all the points. If we adopt the former alternative and if the data are averaged over a number of years, then the exponent p shows little or no variation with latitude: p in fact remains close to 0·30 at sunspot maximum and close to 0·32 at sunspot minimum. Some seasonal variation was found at northern temperate stations (thus for Washington (1949–1953) p varied from about 0·31 in summer to

VOL. 21 1961

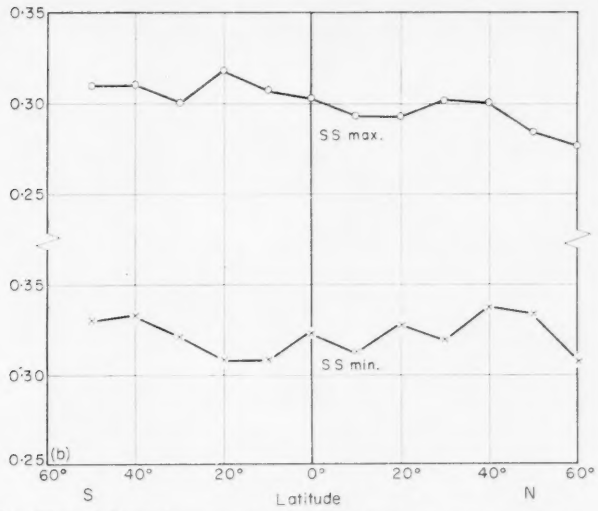

Fig. 2(b). Plot of diurnal exponent p with latitude, showing general constancy.

about 0·35 in winter): but no corresponding variation has been found at southern temperate stations (e.g. Christchurch). These results are illustrated in Fig. 2.

(b) *Latitude variations*

For the study of the latitude variation of f_0E with cos χ a number of methods, largely but not completely equivalent to each other, are available. Perhaps the

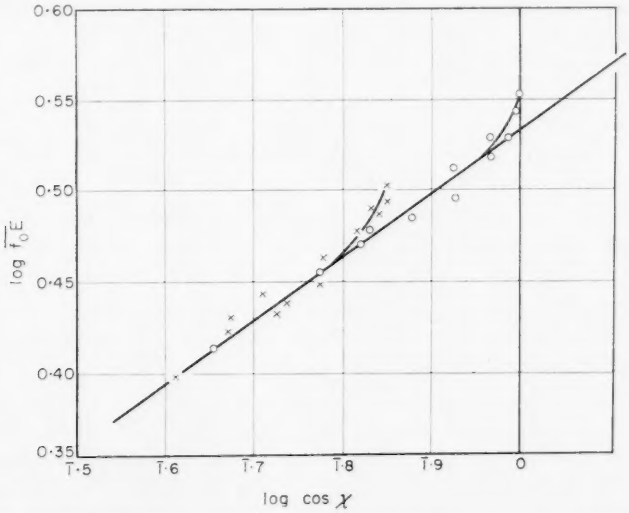

Fig. 3. Meridional variation of $\log \overline{f_0E}$ with $\log \cos \chi$ at equinox, showing the equatorial enhancement. March 1953 (various stations). ○ Noon values; × Mean of values for 0900 and 1500 hours.

simplest is to plot $\log f_0E$ against $\log \cos \chi$ somewhat as we did in the previous section, but this time using values for a series of different stations at a fixed hour, say noon. Such a plot is shown in Fig. 3 for fourteen stations covering a wide range

of latitudes, the data used being monthly medians for March 1953. Two points are worthy of note: the value of the exponent is of the same order of magnitude as for the diurnal variation (in the present case 0·35); and secondly there is a marked upwards inflection near the equator which is present both for noon values and for means of 0900 and 1500 hours. This is typical of equinox conditions, and appears to indicate an anomalous enhancement of f_0E of magnitude 5 per cent at the equator.

A second method which gives a more comprehensive picture is to plot contours of the "region character figure" K, defined by equation (5) on a world map with

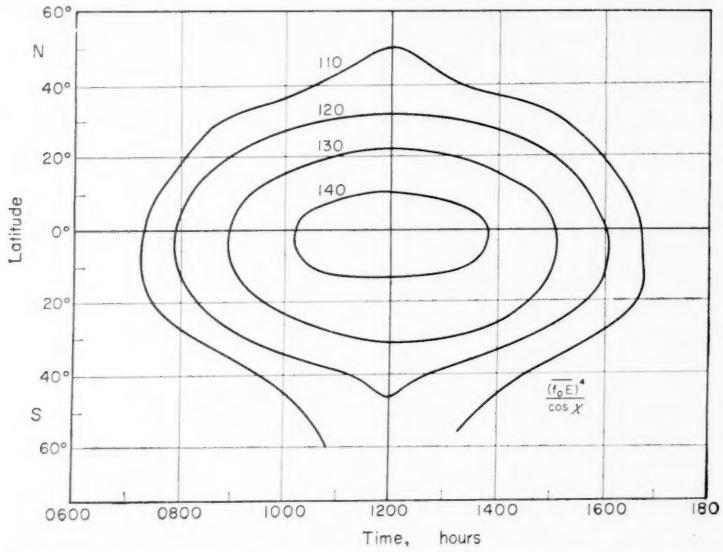

Fig. 4. World contours of character figure K for equinox months at sunspot minimum, showing the marked ellipticity.

latitude for the vertical axis and local time on the horizontal axis. Such a plot, for equinox months at sunspot minimum, is shown in Fig. 4. The rising values, with the summit at the origin (i.e. equator at noon), express the fact that the exponent n is less than the Chapman value of 4 used for the character figure. The marked ellipticity is an expression of the equatorial enhancement, for it implies that at a given cos χ (contours of which are circles with centre at the origin) f_0E increases with latitude. The actual value of f_0E for a particular value of χ is plotted against latitude in Fig. 5; the percentage increase from latitude 50° N to the equator is 5 per cent (both at sunspot maximum and sunspot minimum)—in agreement with the value obtained from Fig. 4. We must remember, of course, that the high latitude value refers to a time near noon and the equator value to about 0830 hours and it might be suggested that we are dealing again with the noon depression at mid-latitudes rather than with an equatorial enhancement. However we know that at equinox the noon depression at 50° N is quite small—less than 1 per cent—and moreover the marked ellipticities of the K-contours over areas where no noon depression has been observed confirm that this is in fact a new and separate anomaly.

VOL. 21 1961

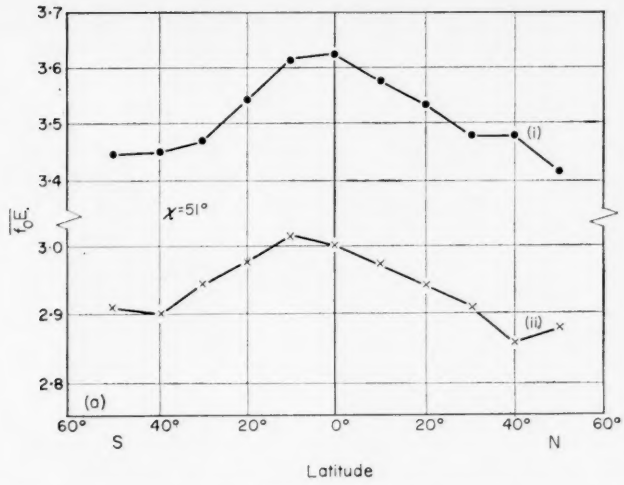

Fig. 5(a). Variation with latitude of $\overline{f_0E}$ at constant χ showing the equatorial enhancement; Equinox; (i) Sunspot maximum; (ii) Sunspot minimum.

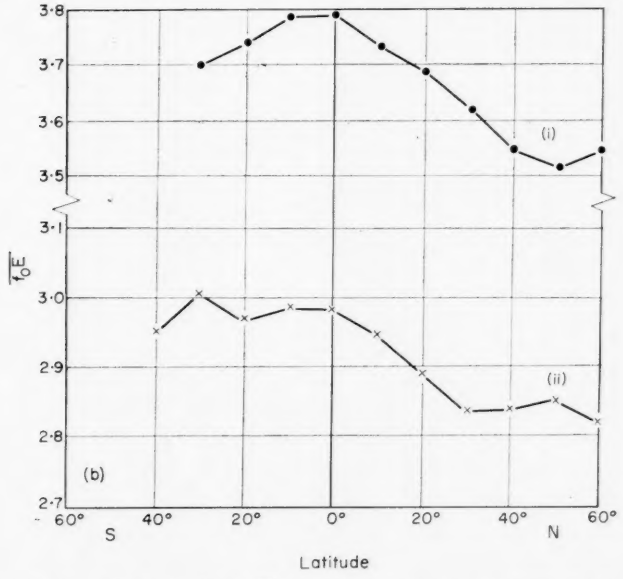

Fig. 5(b). Variation with latitude of $\overline{f_0E}$ at constant χ showing the equatorial enhancement; Northern summer; (i) Sunspot maximum; (ii) Sunspot minimum.

Fig. 5 also shows that in summer the enhancement appears to be about 6 per cent at sunspot minimum and about 8 per cent at sunspot maximum. However if we remember that the noon depressions are greater in summer (about 2 per cent or more) it seems likely that the true equatorial enhancement is about the same in all seasons. We note also that the peak of the curve in summer occurs at the equator or even to the south of it, although the sun is some 20° to the north of the equator.

Thus the equatorial enhancement is not, at least directly, under solar control, but remains tied to the neighbourhood of the equator regardless of the position of the sun.

Still another and very simple way of examining the situation at the solstices is to plot noon values of f_0E against latitude as in Fig. 6. The maximum of the curve occurs not, as we should expect, at the sub-solar point, but some 12° or 14° south of the sun (for the data used the mean position of the sun was about 20° N)—again demonstrating the equatorial enhancement.

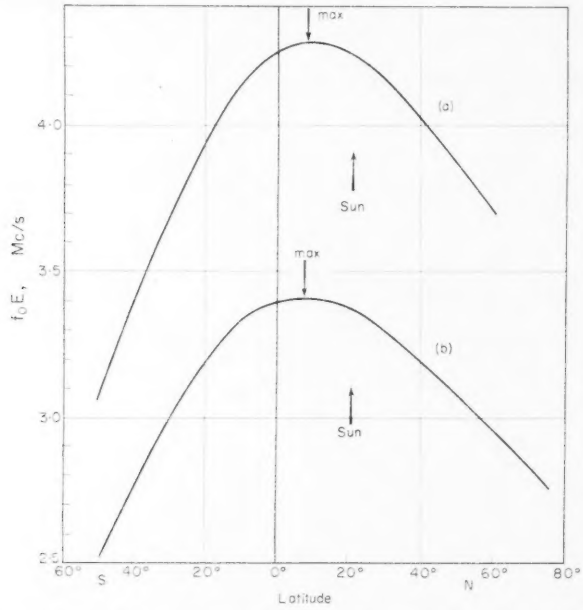

Fig. 6. Noon values of f_0E at northern solstice, showing maxima 12° to 14° south of the sun, data averaged over all available stations. (a) Sunspot maximum; (b) Sunspot minimum.

(c) *Seasonal variations*

If we plot log f_0E against log cos χ, at noon say, for all months of the year at a given station, we can now obtain seasonal values of the exponent p (or n) just as we have obtained diurnal and latitude (or meridional) values. Here we shall follow Beynon and Brown (1959) and deal with n rather than p, in this case. In dealing with the seasonal variation we face a new problem, namely correcting for the irregularly varying intensity of the sun's radiation from month to month. To do this we use the well-known correlation between f_0E and the sunspot number R which may be written

$$f_0E = f_z(1 + bR) \tag{10}$$

where b has the value 16×10^{-4} in the northern hemisphere. This, however, is a statistical relationship and not necessarily valid for a single month. This difficulty can be minimized either by averaging over a large number of years (as we can do for example with stations like Slough and Washington) or by working at sunspot minimum where the variations from this cause are small.

VOL. 21 1961

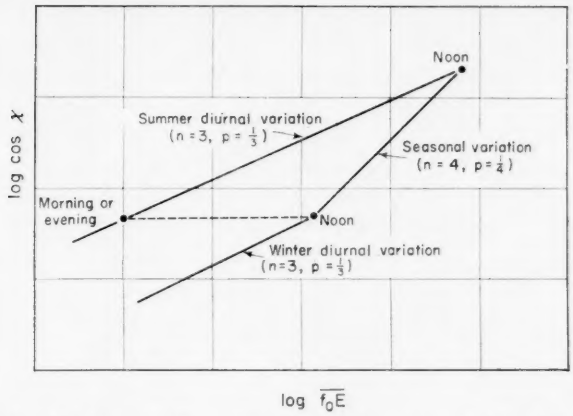

Fig. 7. Relationship between diurnal and seasonal variations of log f_0E with log cos χ.

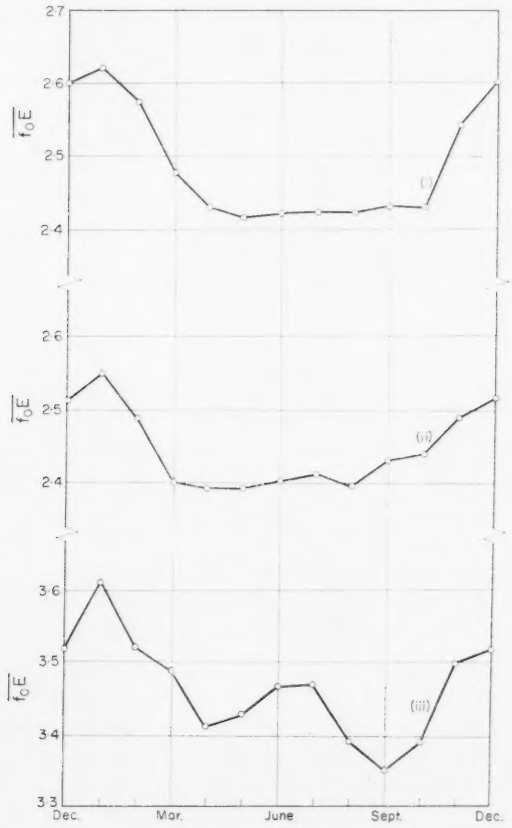

Fig. 8. Variation with month of the year of $\overline{f_0E}$ at constant χ at three stations, showing the winter anomaly at temperate stations. (Data corrected for sunspot number and varying distance of the sun.) (i) Slough (1947–1953); (ii) Washington (1949–1953); (iii) Maui (1947–1949).

For Slough we find that the exponent n for seasonal variation always has a value close to 4, as against the diurnal value of about 3 (Appleton *et al.*, 1937). Since the annual range of log cos χ at Slough is about 0·517 this implies that, for the same χ, f_0E is some $10\frac{1}{2}$ per cent greater in winter than in summer. The relationship between the diurnal and annual variations is illustrated diagrammatically in Fig. 7. Of this difference about $1\frac{1}{2}$ per cent can be attributed to the noon depression already discussed and about $1\frac{1}{2}$ per cent to the fact that the sun is some 3 per cent nearer in winter than in summer. This leaves a "seasonal anomaly" amounting to some $7\frac{1}{2}$ per cent in f_0E.

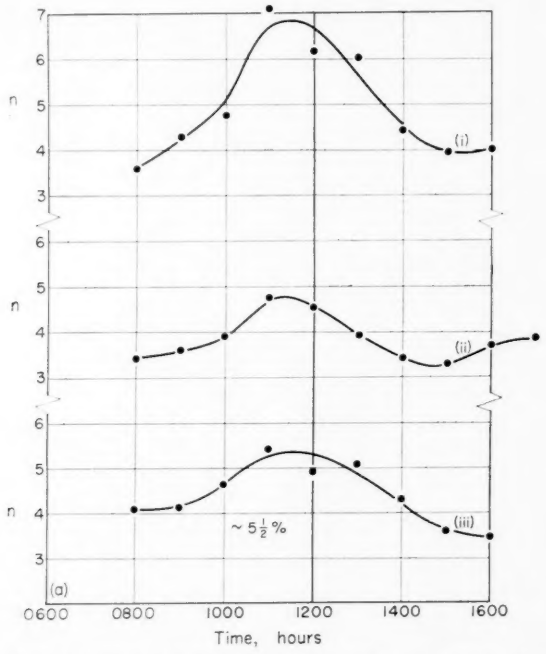

Fig. 9(a). Diurnal variations of the seasonal exponent n at various stations, showing the pre-noon maxima. Sunspot minimum (1951–1953), (i) Tokyo (35° N), (ii) Watheroo (30° S), (iii) Washington (39° N).

We can also measure this anomaly, as we measured the equatorial anomaly, by plotting f_0E at constant χ, in this case against months of the year. This has been done in Fig. 8 for Slough, Washington and Maui, corrections in each case having been made for the variation of the sun's distance. At Slough we again find a difference of about 8 per cent between summer and winter: in this case winter values refer to midday, but summer values to the mean of 0600 and 1800 hours or thereabouts. This confirms that the seasonal anomaly is not to be explained in terms of the summer noon depression.

The other stations show that the anomaly is consistently present at northern temperate stations even as far south as Maui (21° N) but in the southern hemisphere the occurrence of the anomaly is not quite so clear or consistent. Indeed a comparison between the different results obtained in the two hemispheres suggests that

VOL. 21 1961

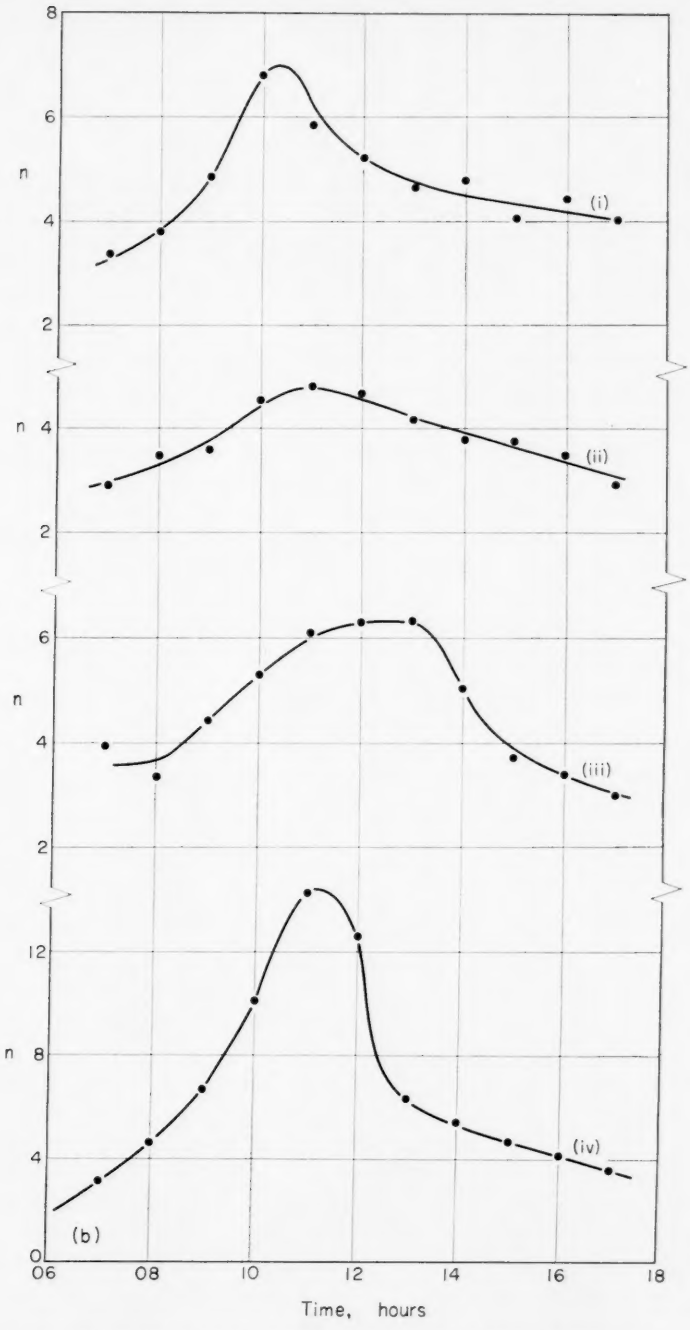

Fig. 9(b). Diurnal variations of the seasonal exponent n at various stations, showing the pre-noon maxima. Sunspot maximum (1947–1949), (i) Tokyo (35° N), (ii) Slough (51° N), (iii) Washington (39° N), (iv) Maui (21° N).

we must, at this stage, leave open the question whether the effect is really a seasonal one or an annual one.

In this connection Beynon and Brown (1956, 1959) have demonstrated two important properties of the exponent n. First when n is plotted against latitude for stations near one meridian (150° E) two peaks are observed, one at 35° N (Tokyo) and the other at 30° S (Watheroo). Secondly n also shows a diurnal variation—most marked, of course, near the peak latitudes—with a maximum about an hour before noon. As this has an important bearing on our studies of diurnal asymmetry in the next Section we have made a number of independent determinations of this diurnal variation of n which we show in Fig. 9. These confirm that at northern temperate stations n tends to a value close to 4 away from noon. Secondly they confirm the finding of Beynon and Brown (1959) that the peaks occur before noon. (It should be noted that at sunspot maximum the numerical values of n are doubtful because of the difficulty of correcting for variations of solar activity from month to month, but the trend of the curve and the position of the maximum should still be reliable).

To explain these peaks wholly in terms of summer depressions around midday (with a maximum depression around 1100 hours) would require maximum depressions of about $3\frac{1}{2}$ per cent at Slough, 5 per cent at Watheroo, $5\frac{1}{2}$ per cent at Washington and 7 per cent at Tokyo. These are somewhat larger than the depressions we have estimated by the method of Fig. 1. This may be because the latter method is inaccurate (the placing of the straight line is necessarily somewhat arbitrary); or it may be that there are inverse effects (small pre-noon enhancements) in winter.

5. Anomalies in the Asymmetry Relations

We have seen that N_m (or f_0E) should reach its maximum value not exactly at noon (when cos χ is a maximum) but at Δt seconds after noon, where Δt is given by equation (9). In a diurnal curve of f_0E the maximum is generally so flat that it is not possible to measure the time of maximum directly. However with the aid of a formula due to Aitken (quoted by Appleton and Lyon, 1957) it is possible to determine Δt on the basis of the best-fitting parabola for the seven hourly values between 0900 and 1500 hours. Δt determined in this way is effectively a measure of the asymmetry of the curve relative to noon over this period. It should not be confused with Δt determined from the axis of symmetry of the diurnal curve as a whole, a method used, for example, by Rawer (1955).

First it is a useful test of the accuracy and consistency of the f_0E data and of the present method to plot Δt against month of the year but without making correction for the equation of time (cf. Rawer, 1955). This has been done in Fig. 10(a) for a 12 month period of the IGY using data from Slough (51° N) and Ibadan ($7\frac{1}{2}$° N). The annual variation of Δt shows a marked correlation with the equation of time, shown in Fig. 10(b), demonstrating that Δt, as we have computed it, can be significant even to the order of a few minutes.

In Fig. 10(c) the corrected values of Δt are shown for Ibadan (same data as above) and for Slough (values averaged over the 7 years 1947–1954). In summer and autumn the Slough values of Δt are considerably greater than would be expected from equation (9) with $\alpha = 10^{-8}$, but in winter they are too small and indeed

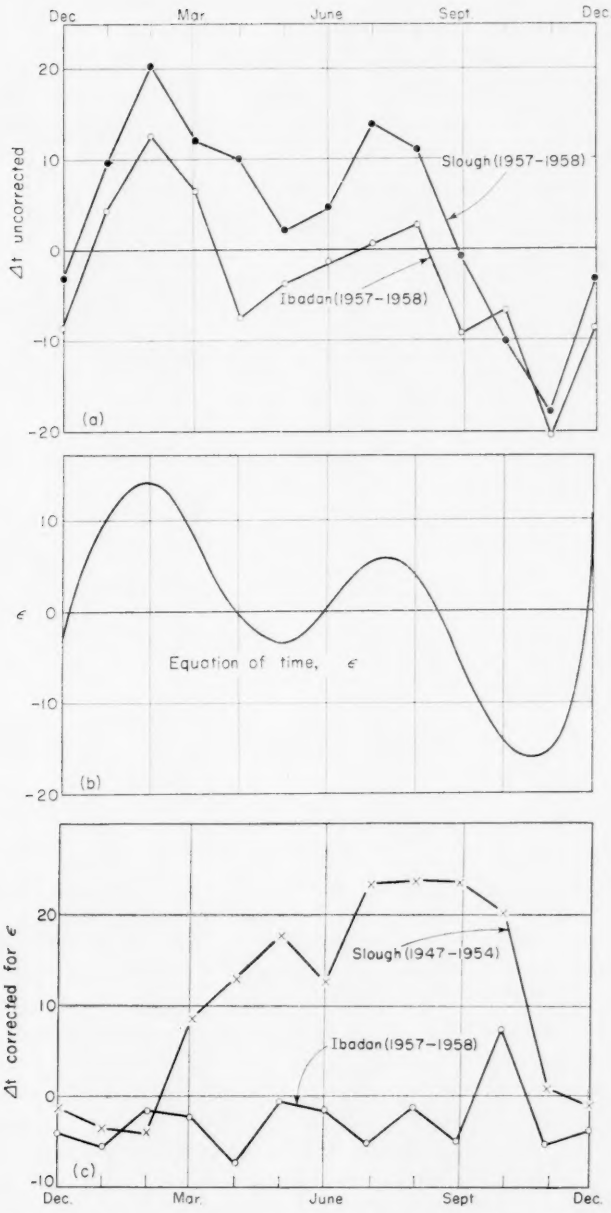

Fig. 10. Variation of Δt, representing the diurnal asymmetry of f_0E, with month of the year.

become negative. At Ibadan Δt is slightly, but consistently, negative for the year as a whole. This is characteristic of equatorial stations.

The diurnal asymmetry can also be studied using equation (8), by which we can obtain values of effective α for any pair of times in the morning and afternoon for which χ is the same. The result of doing this at hourly intervals for a typical summer diurnal curve of f_0E is shown in Fig. 11. Near noon α appears to have very low values of around 2×10^{-9} cm^3/sec and at low cos χ it has very high values of about 8×10^{-8} cm^3/sec.

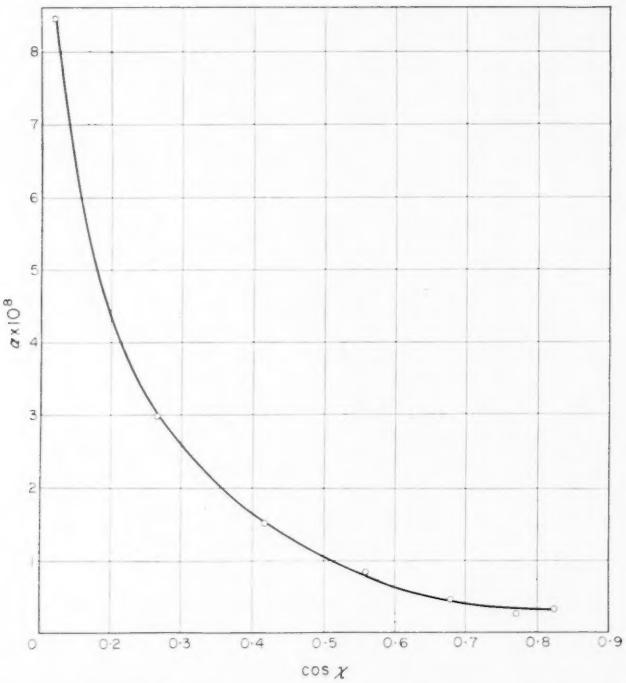

Fig. 11. Diurnal variation of apparent α in summer at Slough, Summer 1952.

The large summer values of Δt might also be taken as indicating very small values of α (around 2×10^{-9} cm^3/sec) but there are strong theoretical arguments against such low values of effective α in the E-region, and of course no value of α could account for the negative values found in winter, or in low latitudes. Moreover the rapid apparent diurnal variation of α cannot be considered genuine, if only because it would require similar and even less acceptable variations of q_0.

It is important to remember that, as pointed out by Bates and McDowell (1957), we are probably dealing, in the E-region, with an *effective* recombination coefficient resulting from two processes, affecting the ions NO and O_2 respectively, and having different recombination rates. The effective α will thus change as the proportion of the different ions present changes, but since this proportion becomes constant under quasi-stationary conditions, it does not seem possible to account for the rapid variation of apparent α in this way either.

VOL. 21 1961

However it is easy to see that relatively small perturbations in the diurnal curve can produce the observed effects, and indeed we have seen in the previous Section that there is evidence for summer depressions around midday and also evidence that these depressions are greatest an hour or so before noon. A perturbation of this kind is precisely what is required to explain the large Δt and the small apparent α in summer shown in Figs. 10 and 11. The magnitudes are also of the right order: thus a depression of only 2 per cent at 1000 hours (say 0·06 Mc/s) is sufficient to make the apparent α about 3×10^{-9} cm^3/sec when the true α is 10^{-8} cm^3/sec.

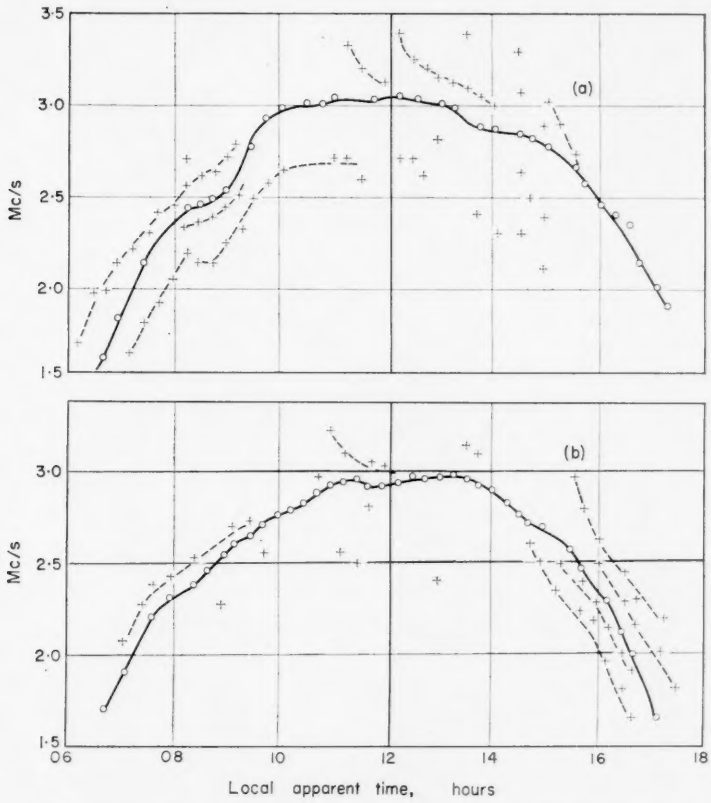

Fig. 12. f-plots for the E-region at Slough showing multiple stratifications. (a) 27 September 1955; (b) 30 September 1955.

We can frequently find more direct evidence of the pre-noon depression from the diurnal variation of f_0E on particular days. Such a case for 27 September 1955 at Slough is shown in Fig. 12(a). The open circles indicate the values that would most probably be taken as f_0E; values shown with a plus sign indicate additional cusps or penetration frequencies. Records were taken every 15 min using an expanded time base (Lyon and Moorat, 1956), to permit easier identification of E-region characteristics.

This "E-plot" is fairly typical of E-region variations at Slough, and is instructive

in a number of respects. First there is a marked pre-noon depression, centred, in this case, just before 0900 hours, and detectable in all the four stratifications present at this time. Obvious pre-noon depressions like this are quite common at Slough and, though their exact timing is variable, they result in the average in the abnormally high asymmetry relative to noon which we have noted in the two previous figures, both based on monthly mean values.

Secondly there are three main strata whose penetration frequencies (or cusp frequencies) increase in a regular way with cos χ for the early part of the day, running at first on roughly parallel lines, but later tending to merge together in the midday period. The occurrence of two or three such regular strata is very common in the morning period at Slough.

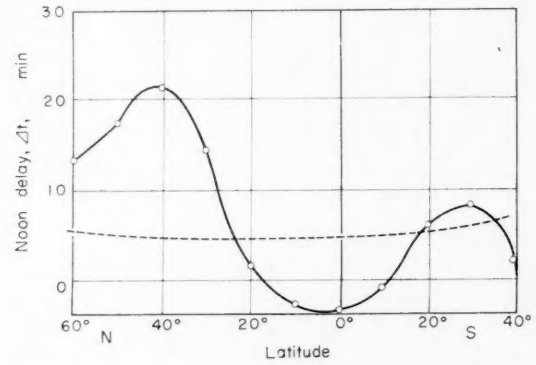

Fig. 13. Variation of Δt with latitude showing the reversal of phase between high and low latitudes.

Thirdly, stratifications occur later in the day also, but these are much more irregular and not under solar control, but are presumably to be connected with sporadic disturbances in the layer. Regular strata do sometimes appear in the evening, as in Fig. 12(b), but evening stratifications are rather less common than morning ones. In this second E-plot only two strata were visible in the morning, and there is no sharp pre-noon depression, though there is a quite marked asymmetry relative to noon.

Finally the latitude variation of this phenomenon may be studied by plotting Δt (determined as above) against latitude, and the result of doing this for the northern solstice (mean of sunspot maximum and sunspot minimum) is shown in Fig. 13 from Appleton *et al.* (1955a). Generally speaking at temperate latitudes Δt is considerably greater than would be expected for $\alpha = 10^{-8}$ (a dashed line on the curve shows the expected values); but in equatorial regions Δt is less than expected, and indeed becomes negative.

It seems then that over the midday period we have, in temperate latitudes, a depression of f_0E in the summer months (and to a lesser extent in equinox months) with a maximum before noon, but in equatorial latitudes an enhancement of f_0E in the pre-noon period. Whether this is related to the general equatorial enhancement noted in the previous section we shall discuss below. In any case it is clear from

VOL. 21 1961

Fig. 13 that we have a perturbation which has opposite phases in low and temperate latitudes, changing phase near 20° N or S; and from numerous cases studied it is clear that this perturbation is most marked, in the case of temperate latitudes, in local summer, and that it is stronger, in both phases, at sunspot maximum than at sunspot minimum.

In addition to this main perturbation there is also a "low cos χ anomaly" seen for example in the very high apparent values of effective α at low cos χ in Fig. 11. It is typical of diurnal curves of f_0E at all latitudes that they do not show the expected asymmetry at low cos χ (which should normally give a Δf_0E of the order of 0·3 Mc/s for the extremes of the diurnal variation) but instead Δf_0E usually tends to zero or even sometimes becomes negative.

Finally there is also an "anomalous winter asymmetry" shown by the negative Δt's in winter in Fig. 10. Fig. 13 also shows negative Δt's in the winter hemisphere, and we have found this to be most marked at sunspot minimum. This seems to suggest that the main daytime perturbation may be reversed in phase in winter at temperate latitudes. If this happens it will clearly accentuate the peaks in the diurnal curve of the seasonal exponent n and may explain why these peaks are found to be greater than might have been expected from the summer depressions alone.

6. Anomalies in the Height Variations

The value of h_mE is not normally determined in routine measurements but, as noted by Appleton (1937), the minimum height $h'E$ should correspond pretty closely to the level of the point of inflection in the Chapman profile, and this follows the same variation with sec χ as does h_mE. The observed variations of $h'E$ therefore provide a simple means of testing the validity of equations (3) and (3a). In general the variation is undoubtedly of the form predicted, i.e. proportional to log sec χ, though it has to be remembered that, at low cos χ, $h'E$ is usually read at a point where appreciable group retardation is bound to be included. If allowance is made for this, both the diurnal and seasonal variations yield values of H consistent with the generally accepted values of about 7 or 8 km for the E-region.

However the predicted asymmetries relative to noon have not been observed. On the contrary at Slough we find an asymmetry in the opposite sense, morning values around 0900 and 1100 hours being lower than the corresponding afternoon values. This effect has been reported by a large number of observers, e.g. Martyn (1948), Findlay (1951) and Robinson (1957), and can be considered well-established. The corresponding effect at low latitudes is more difficult to establish, partly because of contamination by E_s and partly because of the relative paucity of data. However there can be little doubt that, as with the midday perturbations in f_0E, the phase of the height perturbation is reversed in low latitudes. Our results for Slough and Singapore are shown in Fig. 14. We may note that Martyn (1948), using different data, also found a reversal of phase between high and low latitudes.

7. E-layer Anomalies and the S_q Current-system

We have now demonstrated the existence of a number of anomalous features in the behaviour of the E-layer—anomalous, that is, in relation to the behaviour

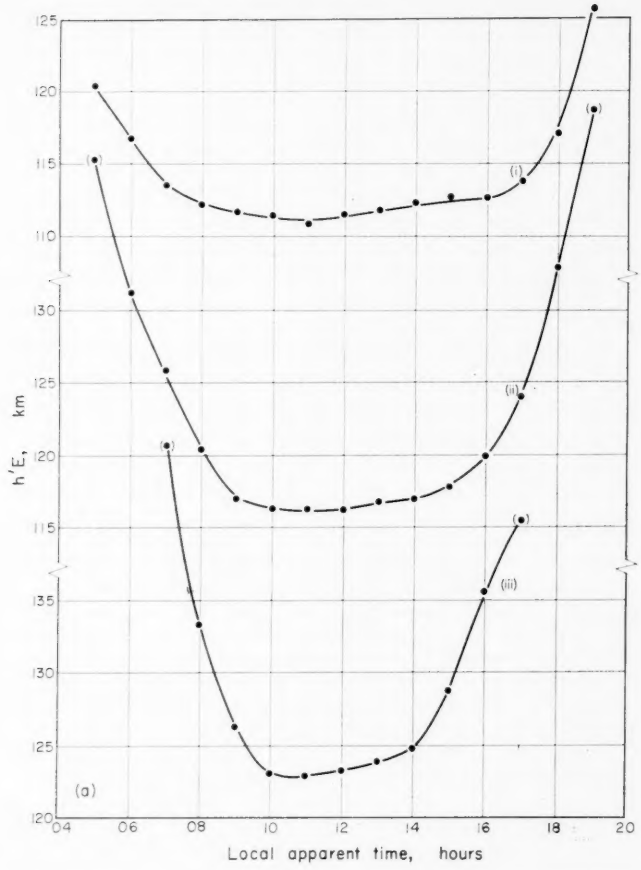

Fig. 14(a). Diurnal variations of $h'E$; at Slough (1947–1954) in the three seasons, showing pre-noon depressions, (i) Summer, (ii) Equinox, (iii) Winter.

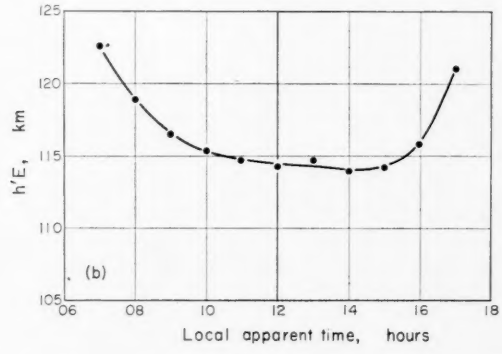

Fig. 14(b). Diurnal variations of $h'E$; at Singapore (1949–1955), showing pre-noon enhancement, average over year.

VOL. 21 1961

predicted for a simple Chapman layer. We must now consider possible explanations for these anomalies. That vertical drifts of ionization, associated with tidal movements in the atmosphere, might have important effects on the heights and critical frequencies of ionospheric layers was first suggested by MARTYN (1947). APPLETON *et al.* (1955) then showed that a number of the E-layer anomalies we have been considering might indeed be explained by such vertical drifts, more specifically by drifts associated with the well-known S_q current-system. This has been confirmed in subsequent work by BEYNON and BROWN (1956, 1959) and SHIMAZAKI (1957, 1958).

According to the quantitative theory of ionospheric drift effects in a quasi-stationary layer put forward by APPLETON and LYON (1955, 1957) the effects of a vertical drift of velocity v, having a gradient dv/dh (v and h being measured positive upwards), on the height of the layer maximum h_m and its maximum electron density N_m are given by

$$\delta h_m = \frac{v}{2\alpha N_m} \tag{11}$$

and

$$\frac{\delta N_m}{N_m} = -\frac{dv/dh}{2\alpha N_m} - \left(\frac{\delta h_m}{2H}\right)^2 \tag{12}$$

where H is the scale height, and it is assumed of course that the same unit of distance (e.g. the kilometre) is used for h_m, H and v.

The relationship between vertical drift and the associated ionospheric electric current has been derived by MARTYN (1953) in the following very simple manner. Vertical drift arises from the elementary law that an electric current perpendicular to a magnetic field experiences a mechanical force at right angles to both. In the ionospheric case the current is carried by positive ions and electrons, and hence, whenever the current has a component towards the magnetic east, of density j_y say, there must be a drift of neutral ionization in the direction of the mechanical force. If v is the velocity of this vertical drift, N the ion density, m_e, m_i, and ν_e, ν_i the masses and collision frequencies of electrons and positive ions respectively, then equating the electro-magnetic force to the rate at which momentum is absorbed, we have

$$j_y H = (m_i\nu_i + m_e\nu_e)Nv \tag{13}$$

$$\approx m_i\nu_i Nv. \tag{13a}$$

(The ratio of the two terms inside the bracket is estimated by MARTYN to be 1650:1, and the second term is therefore generally negligible.)

Now the values of v and dv/dh at the layer maximum will depend critically on the position of this maximum relative to the S_q current sheet (or sheets) and this is not in general known. However to the extent that this position remains roughly constant, j_y (to the magnetic *east*) will be roughly proportional to its height-integrated value which, in turn, is proportional to the magnetic *north* component of the S_q variation in horizontal magnetic intensity at the ground. The latter variation is of course well known, at least in general form, and VESTINE *et al.* (1947) give data for the geomagnetic north component, X_q say, of the S_q magnetic variation. For detailed studies at particular stations the component parallel to the local magnetic north might be preferable, but this distinction will not be important for our present

purpose. We note also that these data are averaged over a sunspot cycle (1922–1933), and may not always represent the true situation in individual years.

Fig. 15(a) shows the diurnal variations of X_q first for latitude 50° N in the three seasons separately, and second for the equator averaged over the year (there being little annual variation). At 50° N the maximum depression is around 1000 hours in

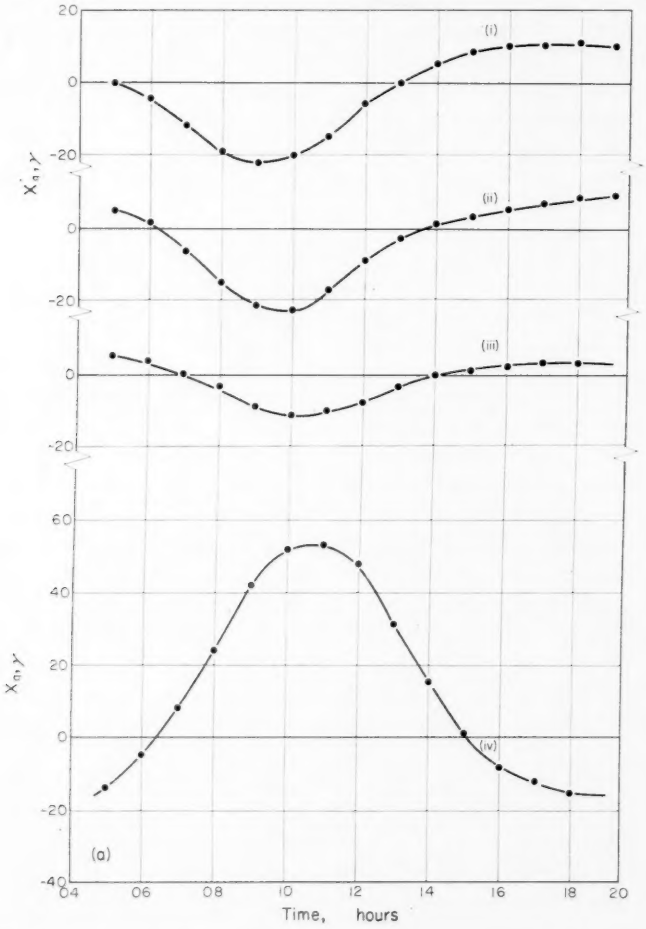

Fig. 15(a). Diurnal and meridional variations of X_q, representing the effective strength of the S_q current-system for vertical drift effects; (i) Summer, 50° N, (ii) Equinox, 50° N, (iii) Winter, 50° N, (iv) Equator (average for year).

equinox and winter, and at about 0900 hours in summer. At 0° the maximum increase occurs rather later, at about 1100 hours. Fig. 15(b) shows the variation, with latitude, of X_q at 1000 hours, averaged over the year. The change of phase occurs at about 30° N or S.

Now according to equation (13) and our discussion above, the sign of v is the same as that of j_y and hence of X_q, so we expect that in the regions where the S_q

VOL. 21 1961

currents flow there will be vertical drifts in the middle of the day, upwards at low latitudes and downwards at high, with maximum amplitude between 0900 and 1100 hours. In accordance with equation (11) we should therefore expect corresponding changes in h_mE and $h'E$, also upwards at low latitudes and downwards at high; and we have seen that Fig. 14 gives evidence of just such perturbations.

The magnitude of the changes in $h'E$ appear to be of the order of 1–2 km and substitution in equation (11) with $\alpha = 10^{-8}$ and $N_m = 10^5$ say, gives values of drift velocity of 2–4 m/sec.

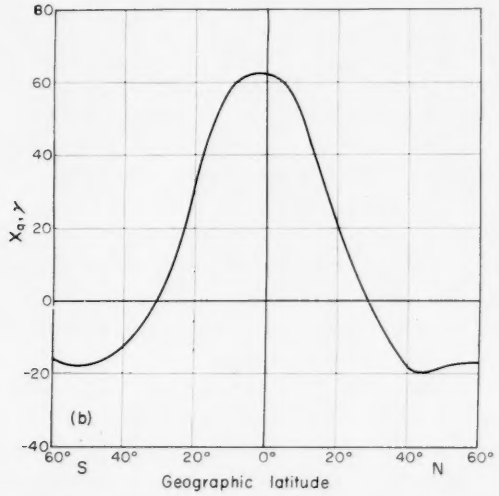

Fig. 15(b). Diurnal and meridional variations of X_q representing the effective strength of the S_q current-system for vertical drift effects; X_q at 1000 hours, average for year.

Now we have seen that the midday perturbations of f_0E consist of depressions at high latitudes and enhancements at low latitudes, with maximum amplitude near to 1000 hours. This can be accounted for, in accordance with equation (12), by supposing that at midday the layer maximum should be at a level where the magnitude of v is decreasing with height (which requires, by (13), that the current density is also decreasing with height). This means that dv/dh is positive at high latitudes and negative at low. We note that the second term of (12) will by itself always give a depression: but for $\delta h_m = 2$ km and $H = 8$ km, the depression in f_0E is still rather less than 1 per cent. We may also note that without any gradient of v, a decreasing gradient of α could have a similar effect. The equation for this case (given by ROBINSON, 1959) is easily seen to be

$$\frac{\delta N_m}{N_m} = -\frac{1}{2\alpha}\frac{d\alpha}{dh}\delta h_m - \left(\frac{\delta h_m}{2H}\right)^2. \qquad (14)$$

To determine accurately the magnitude of the perturbations in f_0E is not easy, because we have no reference points of clearly unperturbed conditions; but the difference Δf_0E between morning and afternoon values at the same χ (in the sense, a.m. minus p.m.) should give a good indication, provided allowance is made for the

natural difference given by equation (8). If we assume that the perturbation follows X_q as shown in Fig. 15(a) the difference for (1000 hours — 1400 hours) should be about equal to the maximum perturbation at higher latitudes. At the equator the X_q variation is more nearly symmetrical about noon, and the maximum perturbation may be substantially greater than the difference for (1000 hours — 1400 hours). We must also note that there will be a certain delay (at least of order $1/2\alpha N$) between the X_q variation and the corresponding changes in N_m. If this delay is 20 min the perturbation at noon will be about twice the difference $\Delta f_0 E$ for (1000 hours — 1400 hours).

The variation of $\Delta f_0 E$ in summer and equinox months at sunspot minimum and sunspot maximum for (1000 hours — 1400 hours) is shown in Fig. 16. The corresponding differences ΔX_q are also shown (by dashed lines); and the general excellence of the correlation (except for equinox at sunspot minimum) is apparent. The maximum depression (for these averaged data) is 0·16 Mc/s at sunspot maximum and 0·06 Mc/s at sunspot minimum, corresponding to 4 per cent and 2 per cent respectively. We have seen that up to about 1 per cent of this may be accounted for by drift alone without any gradient, so that relatively small velocity gradients are required: thus to make the dv/dh term of equation (12) amount to 2 per cent in $f_0 E$, we require dv/dh to be about 0·1 m/sec/km. To produce the same depression by a gradient of α if $\delta h_m = -1$ km would by (14) require α to decrease by about 8 per cent per km.

At the equator the maximum of $\Delta f_0 E$ is about 0·1 Mc/s corresponding to about $2\frac{1}{2}$ per cent, and we have seen that this may represent a maximum enhancement near noon of about 5 per cent. This would agree with the magnitude of the equatorial enhancement we have noted in Figs. 3, 5 and 6. Allowing for the second term of equation (12), this would require dv/dh to be about 0·2–0·3 m/sec/km. It is of course quite reasonable (as a glance at Fig. 15 shows) that v and dv/dh should be 2–3 times greater at the equator than at, say, 50° N. We note also that, as the geomagnetic data show, the enhancement due to S_q currents should remain approximately constant at all seasons at the equator, thus explaining the asymmetry relative to the sun at the solstices (Fig. 6).

We have seen that negative Δt's, suggesting a pre-noon enhancement, often occur at mid-latitudes in winter (see Figs. 10 and 13). This may mean that in winter conditions the level of the layer maximum (which is then higher) may be such that dv/dh is negative, giving a reversal in phase of the perturbation compared to summer.

From Fig. 15 we might expect that detectable perturbations in $f_0 E$ may also occur in the late evening when X_q is reversed in sign. Now we have seen that at low cos χ the expected asymmetry of the diurnal curve does not as a rule occur, or is substantially reduced. This could be due to depression of $f_0 E$ in the late evening. To account for this at the higher latitudes would mean postulating a reversal in sign of the velocity gradient as the layer rises (similar to the reversal we have suggested may occur in winter). At the equator however no change in sign of dv/dh would be required. The suggestions of this and the previous paragraph must, however, be regarded as speculative in the present state of our knowledge.

We have seen then that the major midday anomalies at high and low latitudes are very satisfactorily explained as effects of S_q current-system; and low cos χ

VOL. 21 1961

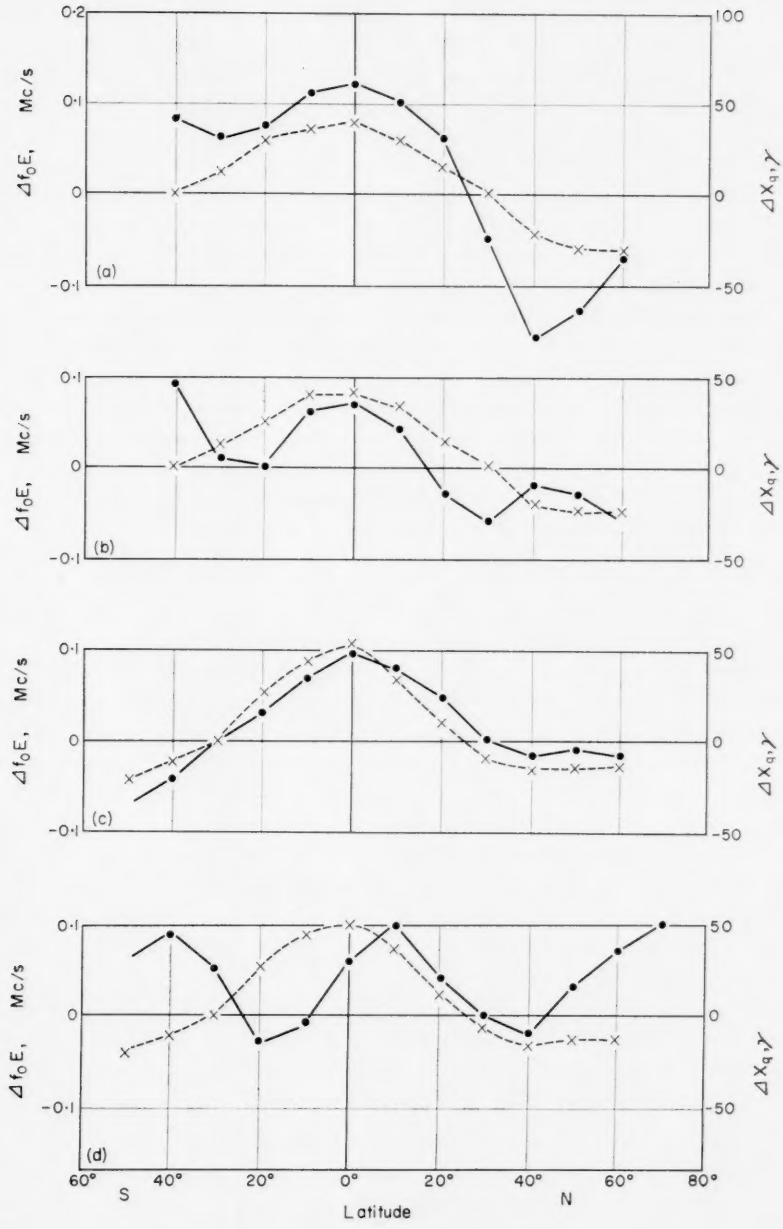

Fig. 16. Variations of Δf_0E(●——●), the difference for (1000 hours − 1400 hours) with latitude, compared with the corresponding differences ΔX_q(×– – –×). (a) Northern Summer, Sunspot maximum, (b) Northern summer, Sunspot minimum, (c) Equinox, Sunspot maximum, (d) Equinox, Sunspot minimum.

anomalies may be. The two remaining major anomalies are probably not so explained. Thus the winter enhancement shown in Fig. 8 appears rather large (7 or 8 per cent) to be accounted for by S_q effects alone, and it seems likely that some other factor, such as a smaller α or scale height in winter, is involved. Equally the rather high values of the exponent p can hardly be attributed to S_q effects since they are characteristic of all latitudes and seasons. The effect is also rather large to be accounted for by a temperature gradient which would have to be of the order of 10° per km. Perhaps effects associated with the complex structure of the E-region (of which its numerous stratifications give evidence) are involved here.

Finally we return for a moment to the possibility mentioned in Section 2 that spurious "anomalies" might arise from ambiguities of measurement. One such source is a possible effect of E_s leading to too low values of f_0E and so giving spurious "depressions". BEYNON and BROWN (1959) have, however, examined this question carefully for temperate stations, and give convincing evidence that any such effects are on the average very small indeed and can be neglected. At low latitudes we have seen that an opposite effect—an apparent enhancement of f_0E—might occur due to the blanketing of the E trace by equatorial type of E_s. Data for Ibadan, however, show no evidence that f_0E is smaller on days when E_s is absent, and again it seems unlikely that this factor is important.

8. E-LAYER BEHAVIOUR DURING IONOSPHERIC STORMS

Since ionospheric currents are also believed to be induced by magnetic storms, it is natural, following the preceding evidence of S_q effects, to enquire whether magnetic storm effects are detectable in f_0E. The depression of f_0E during magnetic storm conditions was first noted during the Second International Polar Year; and recently BEYNON and BROWN (1959) have used a superposed epoch method to confirm this effect. Indeed, even a simple comparison of the values of f_0E on magnetically disturbed (D) days and on magnetically quiet (Q) days using a large quantity of data shows that the effect of an ionospheric storm is slightly to depress the value of f_0E during the middle of the day in temperate latitudes. An examination of Lindau data, for example, has shown that all three critical frequencies f_0F2, f_0F1 and f_0E are lower on D days than on Q days. If Δf represents the depression, relative to the median value f_0, typical values for $\Delta f/f_0$ are 0·3, 0·1 and 0·04 for the $F2$, $F1$ and E layers respectively.

Since the evidence of the preceding section suggests that, under normal conditions, an east–west current in the E-layer causes a depression in f_0E, we conclude the additional ionospheric currents associated with storm conditions also flow in an east–west direction over the midday period.

Acknowledgement—We wish warmly to acknowledge our indebtedness to Mrs. A. G. TURNBULL, of Edinburgh University, for her expert assistance in many of the statistical data studies recorded in this paper.

REFERENCES

APPLETON E. V.	1937	*Proc. Roy. Soc.* A **162,** 451.
APPLETON E. V.	1953	*J. Atmosph. Terr. Phys.* **3,** 282.
APPLETON E. V. and LYON A. J.	1955	*Physics of the Ionosphere*, p. 20. Physical Society, London.

Appleton E. V. and Lyon A. J.	1957	*J. Atmosph. Terr. Phys.* **10,** 1.
Appleton E. V., Lyon A. J. and Pritchard A. G.	1955	*J. Atmosph. Terr. Phys.* **7,** 292.
Appleton E. V., Lyon A. J. and Turnbull A. G.	1955	*Nature, Lond.* **176,** 897.
Appleton E. V. and Naismith R.	1939	*Phil. Mag.* **27,** 144.
Appleton E. V., Naismith R. and Ingram I.	1937	*Phil. Trans.* A **236,** 191.
Bates D. R. and McDowell M. R. C.	1957	*J. Atmosph. Terr. Phys.* **10,** 96.
Beynon W. J. G. and Brown G. M.	1956	*Nature, Lond.* **177,** 583.
Beynon W. J. G. and Brown G. M.	1959	*J. Atmosph. Terr. Phys.* **14,** 138.
Bibl K.	1951	*Ann. Géophys.* **7,** 208.
Findlay J. W.	1951	*J. Atmosph. Terr. Phys.* **1,** 353.
Harnischmacher E.	1950	*C.R. Acad. Sci., Paris* **230,** 1301.
Jackson J. E. and Seddon J. C.	1958	*J. Geophys. Res.* **63,** 197.
Lyon A. J. and Moorat A.	1956	*J. Atmosph. Terr. Phys.* **8,** 309.
Martyn D. F.	1947	*Proc. Roy. Soc.* A **189,** 241.
Martyn D. F.	1948	*Proc. Roy. Soc.* A **194,** 429, 445.
Martyn D. F.	1953	*Phil. Trans.* A **246,** 306.
Menzel D. H. and Wolbach J. G.	1955	*Proc. Mixed Comm. on Ionosphere, 4th Meeting,* p. 17.
Minnis C. M.	1956	*J. Atmosph. Terr. Phys.* **9,** 36.
Rawer K.	1955	*Proc. Mixed Comm. on Ionosphere, 4th Meeting,* p. 107.
Robinson A. K.	1957	Ph.D. thesis, Cambridge University.
Robinson A. K.	1959	*Rep. Progr. Phys.* **22,** 241.
Shimazaki T.	1957	*J. Radio Res. Lab.* **4,** 37.
Shimazaki T.	1958	*J. Radio Res. Lab.* **5,** 35.
Vestine E. H., Laporte L., Lange I. and Scott W. E.	1947	*The Geo-magnetic Field, its Description and Analysis.* Carnegie Institution, Washington, D.C.

Journal of Atmospheric and Terrestrial Physics, 1961, Vol. 21, pp. 100 to 119. Pergamon Press Ltd. Printed in Northern Ireland

Equatorial spread-*F* at Ibadan, Nigeria

A. J. Lyon*, N. J. Skinner* and R. W. Wright†
*University College, Ibadan, Nigeria, and †University College of Ghana, Legon, Ghana

(*Received* 14 *October* 1960)

Abstract—The characteristics of equatorial spread-*F* at Ibadan (magnetic latitude 3°S) are investigated including nocturnal, seasonal, solar-cycle and magnetic disturbance variations; and all of these are found to show marked correlations with corresponding changes in the height of the layer. For example spreading begins shortly after the evening rise in the layer, and becomes less intense and more restricted to the higher frequencies as the layer descends later in the night. Also at Ibadan spread-*F* incidence on quiet days is found to increase with solar activity; and this corresponds to a marked increase in the evening rise of the layer as the solar cycle advances. A possible interpretation of these and earlier results is that the irregularities responsible for spread-*F* are due to hydro-magnetic disturbances which are increasingly attenuated at lower heights.

1. Introduction

In a companion paper (Lyon *et al.*, 1960), which we shall refer to as Paper I, we have shown that at sunspot maximum near the magnetic equator the phenomenon of spread-*F* occurs with great regularity under magnetically quiet conditions and is present for the greater part of the night. At American low magnetic latitude stations this is true for most of the year but not for the months of local winter (May–August) when there is little spread-*F* even on quiet days: at African stations it is true throughout the year and the quiet day incidence of spread-*F* shows no significant seasonal variation. It was shown in Paper I that throughout the belt of equatorial spread-*F* there is (a) an inverse correlation between spread-*F* incidence and magnetic activity and (b) a positive correlation between spread-*F* incidence and the prior height rise of the layer just after local ground sunset. In the present paper we examine these characteristics in greater detail as they are observed at Ibadan, Nigeria.

By confining our attention, in the main, to a single station it is possible to extend the analysis in a number of ways. In the first place it is possible by reference to the ionograms to investigate how the directly observed characteristics of spread-*F* vary, for example, in the course of the night and the corresponding height variations can be analysed. Secondly annual variations can be studied in more detail, e.g. month by month, instead of using "seasonal" groupings whose significance in equatorial regions may be doubtful. Thirdly since data for Ibadan are available from December 1951 the variations through the greater part of a solar cycle can now be examined. We shall examine these various aspects of spread-*F* behaviour in turn.

2. Equatorial Spread-*F* as Observed on the Ionogram

The appearance of the *F*-region trace as observed on the ionogram under spread-*F* conditions is very variable, but Figs. 1–3 show typical examples of what is observed at Ibadan. Figs. 1 and 2 illustrate the phenomenon of "doubling" that

VOL. 21 1961

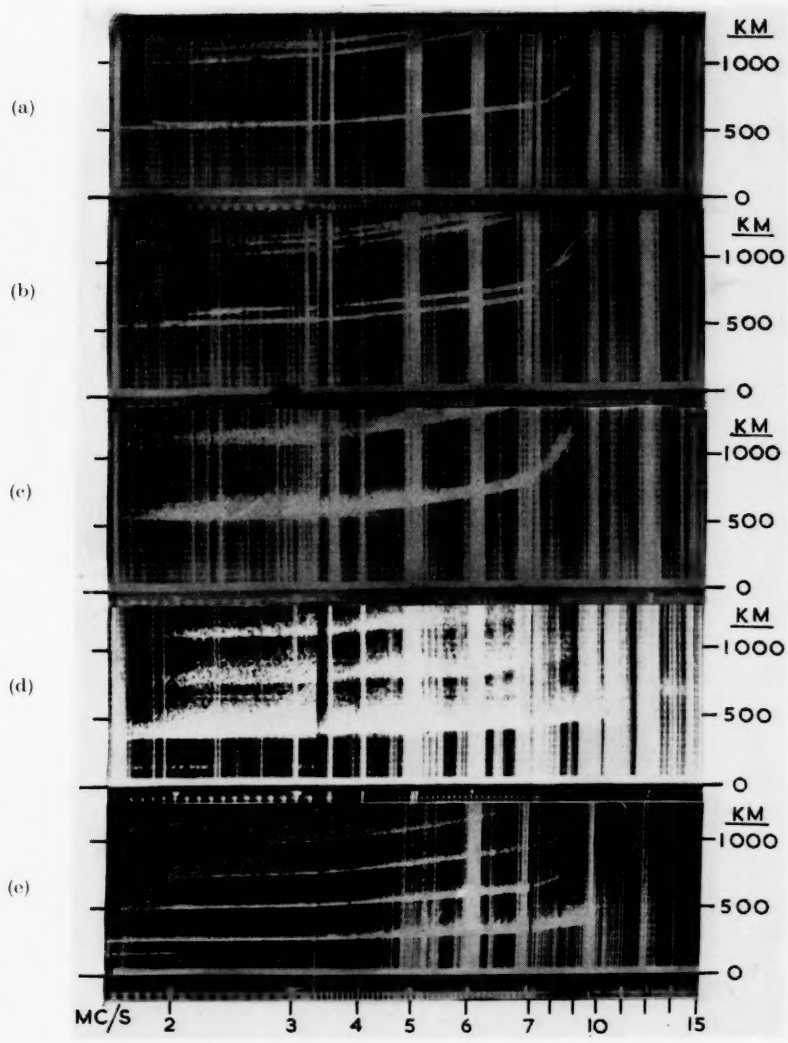

Fig. 1. (a)–(e) Ionograms showing the phenomenon of doubling and the subsequent spreading of the layer. (d) Fully developed equatorial spread-*F*. (e) Pseudo-critical frequencies (see text).
(a) 1900 hours, 1 May 1958; (b) 1915 hours, 1 May 1958; (c) 1945 hours, 1 May 1958; (d) 2200 hours, 26 February 1958; (e) 0000 hours, 7 December 1959.

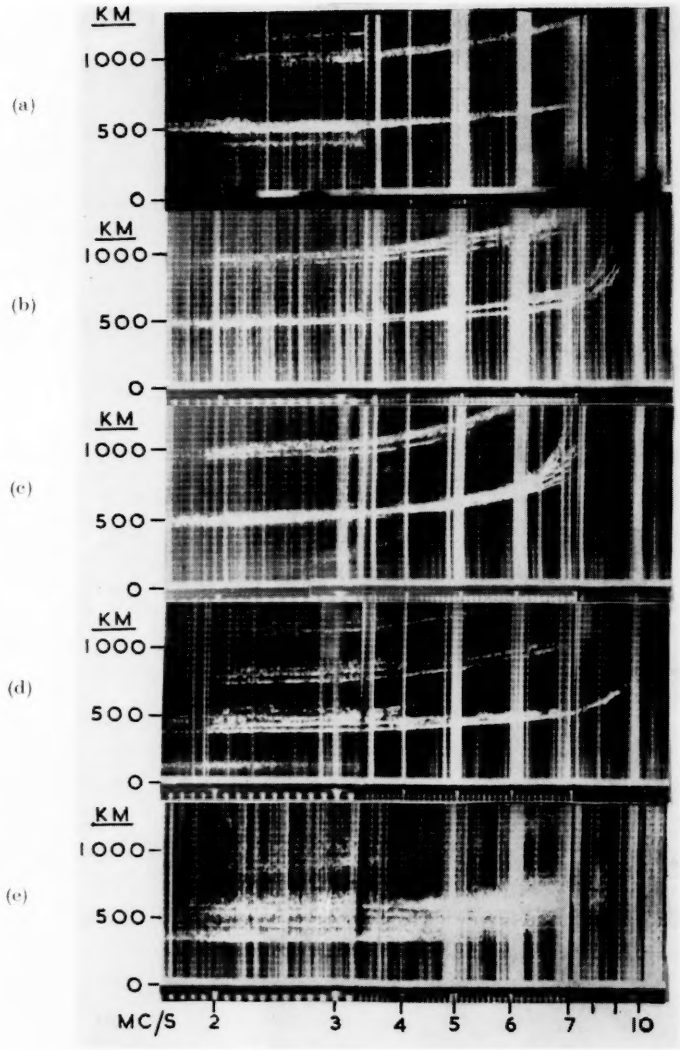

Fig. 2. (a)–(e) Further examples of satellite traces associated with the development of spread-*F*. (d) and (e) "Stratification" in spread-*F*.
(a) 1910 hours, 24 April 1958; (b) 1945 hours, 30 May 1958; (c) 1910 hours, 1 June 1958; (d) 1835 hours, 15 May 1958; (e) 2230 hours, 18 April 1958.

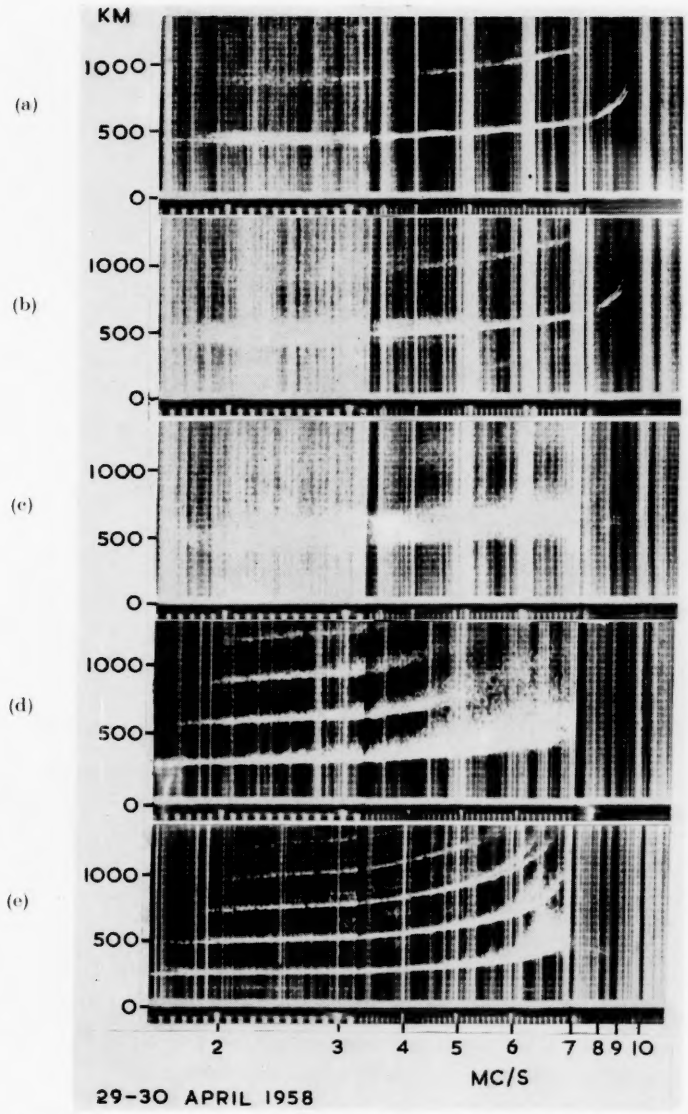

Fig. 3. A typical sequence showing the changes in spread-*F* characteristics during the night.

(a) 1845 GMT; (b) 1915 GMT; (c) 2230 GMT; (d) 0300 GMT; (e) 0500 GMT.

VOL.
21
1961

is, the appearance of discrete "satellite" traces additional to the main trace, which is almost invariably observed just before the development of spread echoes at Ibadan. We shall first examine this phenomenon in some detail.

2.1. *The phenomenon of doubling*

The first three ionograms in Fig. 1 show a typical sequence in which a satellite trace first appears on the second echo and 15 min later is seen on the first echo, whilst two satellites now appear on the second echo. In the third ionogram, taken 45 min after the first, the satellites are not visible, but there is considerable spreading along the whole trace.

The occurrence of satellites cannot be studied satisfactorily with hourly, or even quarter-hourly, records, and so from 24 April to 1 June 1958 continuous recordings were made on most nights between 1800 and 2000 hours G.M.T. In every one of twenty-three cases in which spread-*F* occurred and continuous records were available over the whole of this period, at least one satellite trace was observed prior to the development of spread-*F*. The time of the first appearance of a satellite trace varied between 1836 and 2045 hours with a mean time of 1915 hours which is 80 min after local ground sunset. The time between the first appearance of a discrete satellite trace and the first appearance of continuous spreading of echoes varied between zero and +45 min with a mean time difference of 15 min, i.e. the mean time of onset of spread-*F* on these days was 1930 hours. The satellite trace remained clearly visible for times ranging up to $\frac{1}{2}$ hr and on the average for about 10 min.

The height difference between the main trace and the satellite on the first echo varied between 25 and 160 km with an average of about 80 km. In almost all cases the satellite traces were above the main trace but occasionally they appear below: such an exceptional case, where the satellite was about 80 km below the main trace, is shown in Fig. 2(a). The height difference seems usually to remain fairly constant during the time for which it is observable, but in one case there was a steady increase from 40 to 60 km in 20 min. The variations in height difference are best studied by $h't$ recordings at a fixed frequency. A number of such recordings have been made and these also show that in many cases the satellite is nearly stationary, but again in one case there was a clear and steady increase from 100 to 125 km in 10 min. If the satellite trace is assumed to represent oblique echoes from a large, moving irregularity situated say to the east of the observing station, then the horizontal speeds indicated by the variations in the two apparently rather special cases mentioned are of the order of 50 or 100 m/sec.

Often three or four separate satellite traces (but rarely more) are observed simultaneously, as in the ionograms of Fig. 2(d), and the remnants of this "stratification" of the echoes sometimes persist for several hours even after spread-*F* is fully developed as in Fig. 2(e). The satellite traces we have been discussing up to now are those which run parallel to the main trace and their situation and length along the frequency axis are variable, but they usually stop short of the critical frequency. A different type of discrete satellite trace, which appears as forking near the critical frequency, is also quite common during the period when spread-*F* conditions are developing. A case where two quite separate traces appear at the high frequency

end of the trace, and show separate apparent critical frequencies, is shown in Fig. 2(b). Fig. 2(c) shows a more complex case of multiple forking at the critical frequency.

The occurrence of doubling at other stations has not been examined in detail but the phenomenon is also observed at Maiduguri, Nigeria, (magnetic latitude, 2°N), and on the ionograms for Huancayo and Singapore available at World Data Centre C at Slough. The latter show that doubling is observed with about the same frequency at these stations as at Ibadan: thus for Huancayo, out of 10 days in various seasons for which 5 min soundings were made and on which spread-F developed, in all but one case, at least one satellite trace could be observed prior to the full development of spreading. It therefore seems likely that doubling is a characteristic precursor of spread-F over the whole equatorial belt.

2.2. *Changes in spread-*F *during the night*

As the night proceeds a number of rather systematic changes are observed in the appearance of the spread echoes on the ionograms. These changes are illustrated in Fig. 3. The middle ionogram in this figure, for 2230 hours, is a typical example of fully developed equatorial spread-F. Spreading over a range of 200–300 km occurs more or less uniformly at all frequencies, and there is no sign of a normal critical frequency, and the lower edge of the trace is rather rough and indistinct. This roughness of the lower edge, which is characteristic of the early stages of spread-F, is even more pronounced on the earlier record for 1915 hours.

In the post-midnight records however the lower edge is sharp and distinct, spreading is much reduced at the lower frequencies and at higher frequencies group retardation is again observable. It is to be noted that even at 0300 hours the appearance is still not entirely similar to that observed at temperate latitudes, and in particular there is no sharp inner edge nor does the critical frequency show up more clearly on the multiple echoes. These latter characteristics do however begin to appear in the last record, that for 0500 hours.

In order to have a rough quantitative measure of these nocturnal changes we have used several indices representing the various characteristics of spread-F which change during the night. Thus the index f indicates the range of frequencies over which spreading occurs, h indicates the average amount of height spreading and g the maximum group retardation visible at the high frequency end of the trace. These three indices were each assigned a value between 0 and 3 by inspection without detailed measurement: thus for h, 3 represents height spreading of over 200 km or so for a substantial range of frequencies; for f, 3 represents substantial spreading over the whole frequency range; and for g, 3 represents full group retardation as for a normal layer and 0 represents full equatorial spread-F with no group retardation visible, and so on. In addition two two-value indices were adopted, one for the presence of roughness on the base, and one for the presence of "stratification": thus r denotes the percentage of cases of roughness and s the percentage of cases of stratification at each hour. Several months were analysed using these indices, and the results for March 1957, which are typical, are shown in Fig. 4, where the various indices are plotted against time throughout the night.

The figure shows that frequency-range and height-range of spreading both

VOL. 21 1961

have a maximum between 2000 and 2200 hours and decrease for the rest of the night except for, in this case, a small increase between 0400 and 0500 hours. It may be noted that a similar small secondary maximum in spread-*F* incidence at this time is commonly observed in equinox months at Ibadan. The index *g* for group retardation shows an inverse variation as would be expected. The percentage

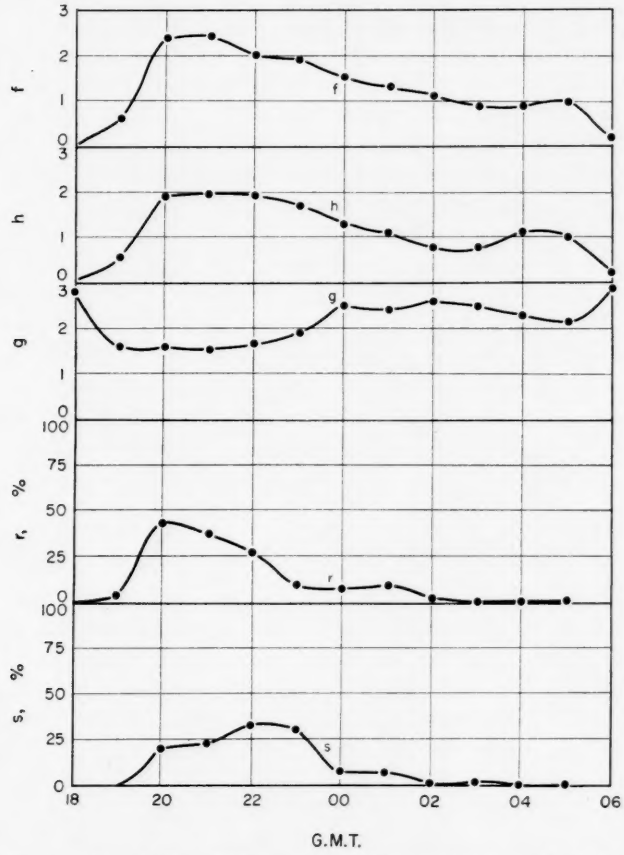

Fig. 4. Nocturnal variation of indices representing various spread-*F* characteristics in March 1958.
f = index of frequency range of spreading.
h = index of mean height range of spreading.
g = index of group retardation visible.
r = percentage frequency of "roughness" on lower edge of trace.
s = percentage frequency of "stratification."

occurrence of roughness, *r*, has a maximum between 2000 and 2100 hours and has fallen almost to zero by midnight. The percentage occurrences of stratification, *s*, shows a rather broader maximum between 2100 and 2300 hours, and also has very low values from midnight onwards. Other months show similar trends and in general these results show that the nocturnal variation illustrated by the sequence of records in Fig. 3 is typical of equatorial spread-*F* at Ibadan.

A type of satellite trace which occurs occasionally during the later part of the night is illustrated in Fig. 1(e) where a whole series of "wispy" pseudo-critical-frequency traces are seen emerging from the main trace, as though there were a series of "windows" in the ionosphere of maximum electron density less than the maximum of the main layer.

A rough indication of the reflecting properties of the layer is given by the strength of the multiple echoes observed on the ionogram. In some cases, as in Fig. 3(b), there are no multiple echoes, or only very weak ones at lower frequencies, and the layer appears to have a considerably lower effective reflection coefficient under spread-F conditions than under normal conditions. In other cases, as in Fig. 1(d), the second, and even the third multiples are quite strong, and the effective reflection coefficient is comparable with that under normal conditions. Measurements with standard ionospheric absorption equipment confirm these observations.

Most of the evidence given above is from ionograms taken at sunspot maximum but an examination of records at sunspot minimum has shown that there is no essential difference in the directly observed characteristics of spread-F behaviour at different phases of the solar cycle. The interpretation of these results will be further considered below but they clearly imply that early in the night, when the layer is high, the irregularities producing spread-F are very numerous in the lower part of the layer and that later in the night when the layer is descending (cf. Fig. 7 below), these irregularities become concentrated higher in the layer and ultimately near the layer maximum.

VOL. 21 1961

3. Spread-F and the Height of the Layer

3.1. *The post-sunset rise of the* F*-layer*

At Ibadan and at other stations near the magnetic equator the minimum virtual height of the F-layer $h'F$ begins to rise sharply just after local ground sunset, reaches a maximum as a rule between 1900 and 2000 hours and then falls again steadily during the remainder of the night. Since $h'F$ is in some cases a rather misleading parameter it is important before using it as an index of the rise of the layer to examine some $N(h)$ profiles during the period of the rise. Where the magnetic dip angle is very small (as at Ibadan where it is 6°) the ordinary-wave refractive index for vertical propagation is unaffected by the earth's magnetic field. Moreover there are rarely any *F1* or other intermediate cusps at the relevant times and the Kelso method of true height determination (Kelso, 1952) gives results of adequate accuracy for our purpose.

Fig. 5 shows the average variations of $h'F$ and h_mF (the true height of maximum electron density as determined by the Kelso method) for groups of days in the equinox period during 1957–1958, (a) under magnetically quiet conditions (10 days), (b) under moderately disturbed conditions (5 days of mean A_p about 50) and (c) under very disturbed conditions (5 days of mean A_p about 150). The corresponding curves are marked Q, D_1 and D_2 respectively. This figure shows that at this time for quiet or moderately disturbed conditions the variation of $h'F$ is very similar to the corresponding variation of h_mF. Fig. 6, which shows $N(h)$ profiles for the period 1700–1900 hours on a typical equinox day at Ibadan,

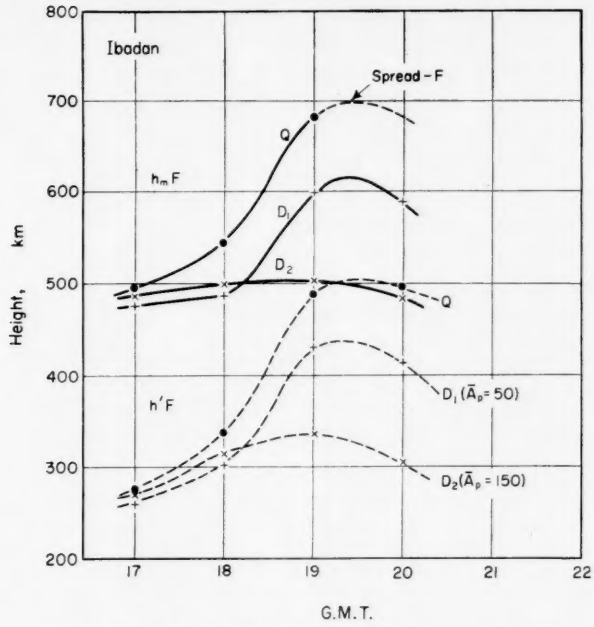

Fig. 5. Variations of $h'F$ and h_mF during the post sunset rise of the layer at sunspot maximum.
Q = quiet conditions.
D_1 = moderately disturbed conditions (mean A_p of 50)
D_2 = very disturbed conditions (mean A_p of 150)

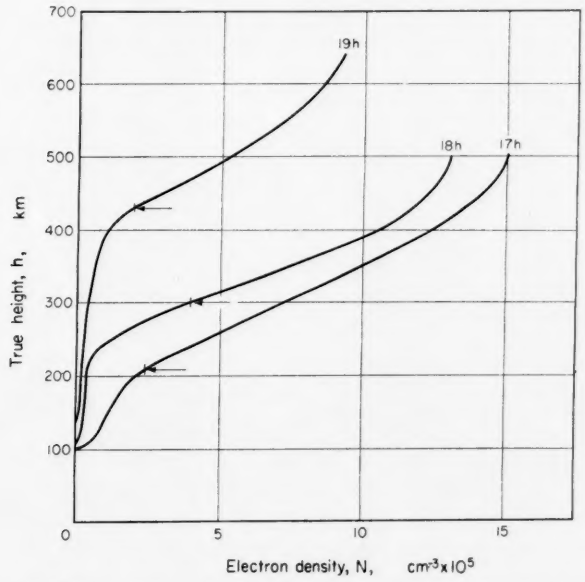

Fig. 6. Typical $N(h)$ profiles during the post sunset rise of the F-layer at sunspot maximum. Ibadan, 2 March 1958. The arrows indicate the corresponding values of $h'F$.

confirms that the rise of $h'F$ (indicated by arrows) does correspond to a rise of the layer as a whole. Under very disturbed conditions h_mF may, as Fig. 5 shows, remain practically constant despite a small rise in $h'F$. For most purposes however and in most cases we can use $h'F$ as quite a satisfactory index of the behaviour of the layer as a whole.

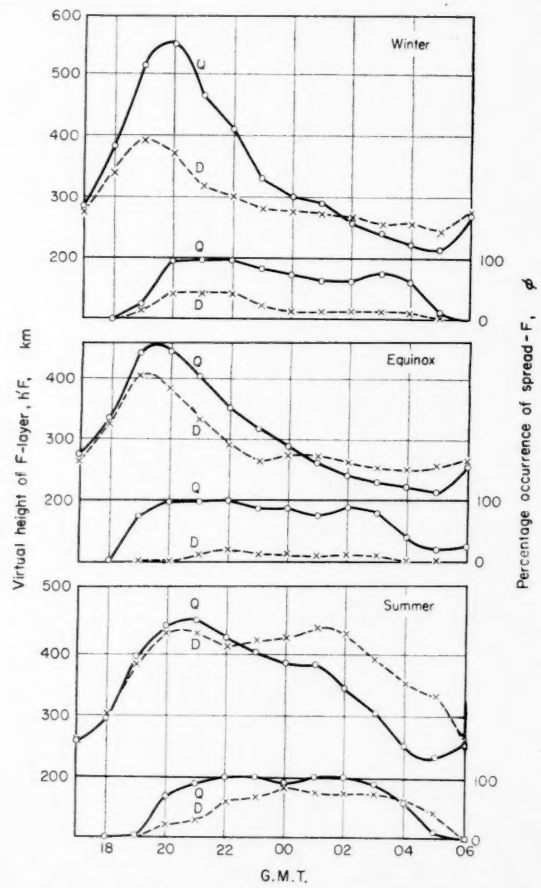

Fig. 7. Variations during the night of the occurrence frequency of spread-F (ϕ) and of $h'F$ on magnetically quiet nights (Q) and magnetically disturbed nights (D).

3.2. *Nocturnal variations of* h'F *and of spread-*F *incidence* ϕ

As we have noted in Paper I spread-F usually develops shortly after the rapid post-sunset rise of the layer which we have just described. This is illustrated by the curves of Fig. 7 which show the variations of $h'F$ and of spread-F incidence ϕ throughout the night in the three seasons, for quiet and disturbed days, and gives further evidence of the correlation between them. ϕ was determined as described in Paper I and the data used refer to the 12 months from November 1957 to October 1958 at sunspot maximum. We shall consider how the situation changes during the solar cycle in Section 4.

VOL. 21 1961

The modal (i.e. most frequent) time of onset of spread-F may be taken to be approximately the time of maximum slope of the ϕ variation and so is easily estimated from Fig. 7. The same method can be used with data for separate months and the results of doing this for the 2 years 1957 and 1958 and then averaging for each month are shown in Fig. 8. The quiet day variation shows that spread-F starts as a rule between 1 and 1½ hr after local ground sunset (the time of which is also shown in Fig. 8) and the delay tends to be least in the equinox months and greatest in the summer months. These results are in agreement with Fig. 7 which in addition shows that the onset of spread-F occurs about ½ hr after

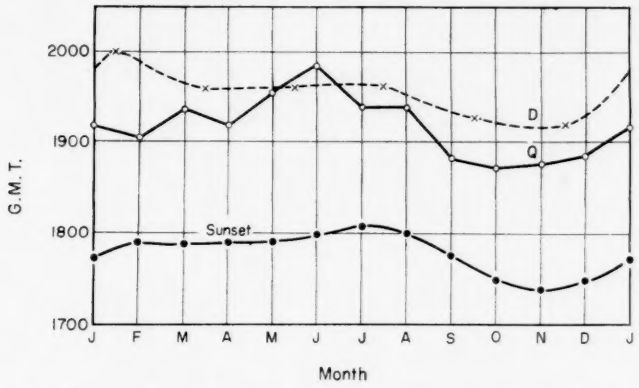

Fig. 8. Modal times of onset of spread-F. The average of the 1957 and 1958 values are used for each month for Q days and for each pair of months in the case of D days. The curve marked Sunset shows the variation of the time of local ground sunset.

the time of steepest rise of $h'F$ in equinox, and about an hour after the time of steepest rise in summer and winter. Also maximum ϕ is reached within ½ hr or an hour of the time of maximum $h'F$. The cases of occurrence of spread-F on disturbed days are of course rare and for these we have taken successive pairs of months together. Fig. 8 shows that when spread-F does occur on disturbed days it tends to start about ½ hr later than on quiet days.

In view of theories which make the actual height of the layer, rather than its vertical movement, the controlling factor it is of interest to compare the hour-by-hour values of ϕ and $h'F$. As we have seen ϕ reaches its maximum ½–1 hr after $h'F$ but it is also clear from Fig. 7 that spreading begins to develop as soon as the minimum virtual height of the layer exceeds about 375 km and starts to decrease again as soon as the height falls below this figure. It is interesting to note that a critical height of about 375 km for the sunspot maximum period was also obtained from the morphological study of Paper I. It is true that the post-midnight decrease in ϕ in winter and equinox seems small compared with the sharp drop in height during the same period. It should be remembered however that the statistic ϕ takes little account of the intensity of the spreading, and comparison of the curves of Fig. 4 with the equinox height curve of Fig. 7 shows that the intensity of spread-F as measured by indices such as f, h and r does indeed decrease substantially as the height decreases. We may therefore claim that in its nocturnal,

as well as other variations spread-F shows a remarkable degree of correlation with the height of the layer.

Fig. 7 also illustrates the difference between summer and the other seasons at Ibadan. In the first place whereas in winter and equinox the layer falls rather rapidly after 2000 hours, in summer it remains high until well after midnight. This corresponds to somewhat higher incidence of spread-F in summer, as compared with the other seasons, after midnight. In the second place whereas in winter and equinox the height-rise is much reduced on disturbed days as compared with quiet days, in summer the height-rise is negligibly reduced on disturbed days, and in the post-midnight period the layer is actually higher on disturbed days than

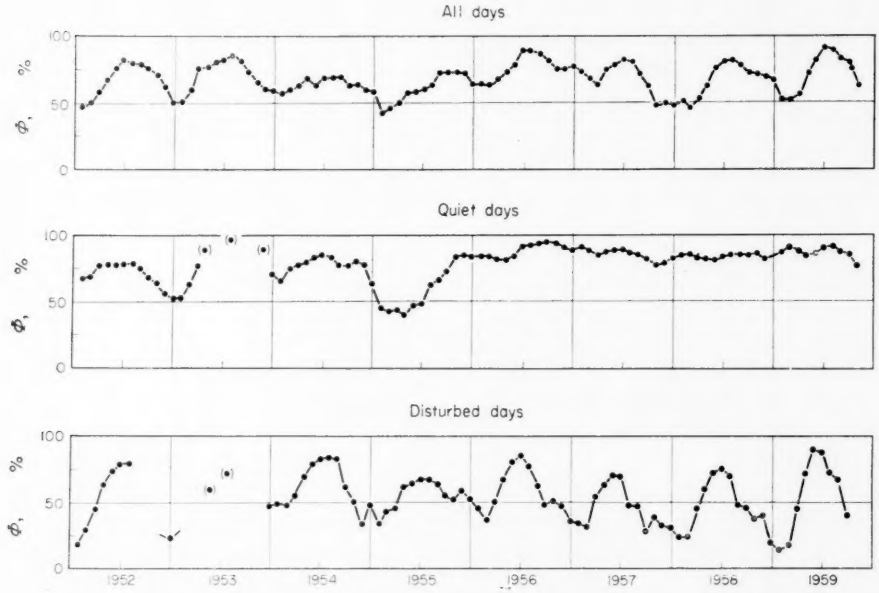

Fig. 9. Three-monthly running means of the occurrence frequency of spread-F (Φ) from 1952 to 1959, on all days, quiet days (Q) and disturbed days (D). The points in brackets represent doubtful values.

on quiet days. This corresponds to the maintenance of a high incidence of spread-F in summer on disturbed days, especially after midnight, as the figure clearly shows. In the other two seasons the reduced height-rise on disturbed days as compared to quiet days corresponds to substantially reduced incidence of spread-F.

The existence of a correlation between spread-F and the height-rise has already been demonstrated in Paper I where in particular it was shown that the morphologies of the two phenomena are very similar—both showing a maximum near the magnetic equator and falling to low values between 20 and 30°N or S. The decrease of both on disturbed days was also noted. We may remark however that a considerable height-rise can occur with virtually no spread-F, as in equinox on disturbed days in the case shown in Fig. 7. We shall return to this point in Section 5.

VOL. 21 1961

4. Solar Cycle Variations in Spread-F

4.1. *Seasonal variations throughout the solar cycle*

Fig. 9 shows the variations of the 3-monthly running means of spread-F incidence Φ respectively on all days, quiet days and disturbed days during the period 1952–1959. The mean annual variations over the whole period are shown

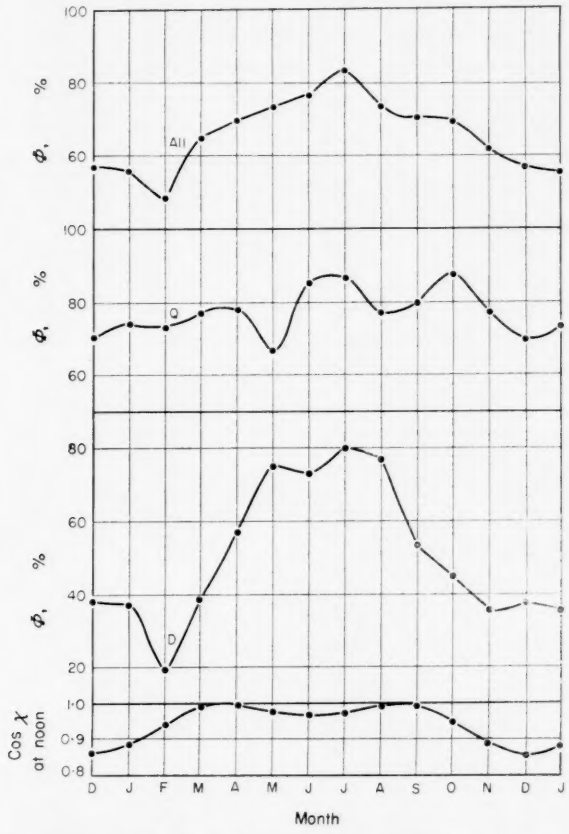

Fig. 10. Mean annual variations of spread-F incidence (Φ) using (a) all days, (b) quiet days (Q) and (c) disturbed days (D), averaged over the 8 years, 1952–1959. The lower curve (d) shows the annual variation of cos χ at noon.

in Fig. 10. The curves marked D in these figures show that disturbed day incidence has a marked seasonal variation with a maximum in the summer months May–August and a minimum in the winter months November–February, and that this variation occurs in every year of the period under review.

The curves marked Q in Figs. 9 and 10 give the quiet day variation. In the years of sunspot maximum and in the mean curve no significant annual variation is detectable. From October 1955 to October 1959 spread-F incidence remains between 75 and 95 per cent and the small variations which occur appear to be quite random. In the sunspot minimum period 1952–1954 however a seasonal

variation similar to the disturbed day variation is clearly present. Since the levels even in summer tend to be somewhat lower at sunspot minimum, this suggests that the absence of any seasonal variation at sunspot maximum may be due to a "saturation" phenomenon, i.e. that spread-*F* incidence is at saturation level on quiet days in all seasons at sunspot maximum, and that seasonal variations only occur when the general level is lower, as at sunspot minimum or under disturbed conditions.

The curves marked "All" in Figs. 9 and 10 give the mean variation of Φ on all days which, as we might expect, shows a similar seasonal variation to that for disturbed days but of smaller amplitude. At sunspot maximum the all-days seasonal variation is clearly due solely to the variation on disturbed days.

The curves of Figs. 8–10 show that the "seasonal" grouping which we have used in Paper I and elsewhere—namely May–August for "summer", November–February for "winter" and the other months for "equinox"—is well justified by the mean annual variation of spread-*F* at Ibadan, despite the fact that they do not correspond to the variations in the "relative declination", $\delta - \lambda$, of the sun, δ being the true declination and λ the latitude. $\delta - \lambda$ is of course equal to the noon value of χ, the solar zenith distance. The annual variation of cos $(\delta - \lambda)$, equal to noon cos χ, is shown in Fig. 10 at the bottom of the figure. If the local intensity of solar radiation were the decisive factor clearly March, April and September ought to be more summer-like than May–August but the *D* curve of Fig. 10 makes it plain that this is not so, and we may regard our "seasonal" groupings, related to the absolute and not relative solar declination, as being the valid and significant ones at any rate for spread-*F* studies.

Finally it is noteworthy that in summer in the 2 years 1954 and 1955 when sunspot activity was low Φ was greater on disturbed days than on quiet days. This underlines the exceptional character of the summer months at Ibadan which we noted in Section 3.2: at high sunspot number spread-*F* incidence is only slightly reduced by magnetic activity in summer and at low sunspot number the normal inverse correlation can even be reversed.

4.2. *Solar cycle variation of spread-*F *incidence*

A number of authors have published data on the solar cycle variations of spread-*F* incidence. Most of the available evidence is summarized in Fig. 11 which shows the mean annual occurrence frequency of spread-*F* at seven low-latitude stations for periods in the interval 1938–1959. Because of different methods of analysis the levels of incidence are not inter-comparable. At three stations, Maui, Rarotonga (Reber, 1954, 1955) and Ahmedabad (Kotadia, 1959) spread-*F* is more prevalent at sunspot minimum than at sunspot maximum, whereas the reverse is true at Dakar (Reber, 1955) and Baguio (Marasigan, 1960). At Ibadan and Huancayo (Wells, 1954) there is no clear correlation on the evidence of these results. It should also be mentioned that Shimazaki (1959) has found that at middle and low latitude stations spread-*F* incidence was greater in the sunspot minimum year 1954 than during the I.G.Y. at sunspot maximum.

These results would suggest that for equatorial stations there is either no consistent solar cycle variation in spread-*F* incidence, or that if there is, it is

VOL. 21 1961

liable to be masked by adventitious circumstances such as varying sensitivity of the ionosondes. However, the evidence already presented here and in Paper I has shown the importance in many studies of spread-F incidence of separating the incidence under magnetically quiet from that under magnetically disturbed conditions, and we shall now show that the same is true for the solar cycle influence.

Fig. 12 gives the variations of the mean annual spread-F incidence Φ at Ibadan for magnetically quiet and disturbed days—respectively labelled Q and D—for

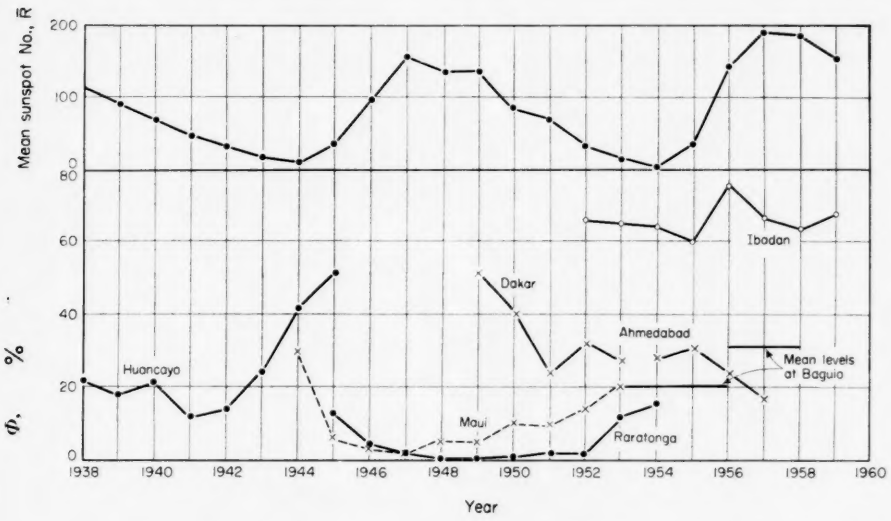

Fig. 11. Solar cycle variation of spread-F occurrence on all days at Huancayo (after WELLS), at Maui, Dakar and Raratonga (after REBER), at Ahmedabad (after KOTADIA), at Baguio (after MARASIGAN), and at Ibadan, Nigeria. The upper curve shows the variation of the annual mean Zurich sunspot-number $\bar{R}$.

the period 1952–1959. Each point represents the average percentage occurrence of spread-F in the night-time hours, 1900–0500 hours inclusive, for the 60 international quiet (or disturbed) days in the corresponding year. (In Paper I it was convenient because of local time variations to use the longer time period 1800–0600 hours. Since spread-F is rare at Ibadan at 1800 and 0600 hours the figures given here for quiet day incidence are greater by a factor 6/5 than those of Paper I.) Comparing the Q curve with the corresponding curve of mean annual sunspot number R shown in the same figure, it is evident that under quiet conditions spread-F incidence is substantially greater in years of high sunspot activity. To put it quantitatively, in the 4 years during which the sunspot number is greater than 100, Φ is some 20 per cent greater than in the 4 years when it is less than 50: or, corresponding to a mean R of 22 we have a mean Φ of 68 per cent and corresponding to a mean R of 168 we have a mean Φ of 86 per cent. After re-investigating much of the data and the original ionograms we are convinced that this fairly large and consistent difference does not arise from variations of ionosonde sensitivity or of reduction procedure, but represents a real influence of solar activity. The

fact that spread-F incidence on quiet days increases with solar activity, demonstrated here for Ibadan, may be of considerable importance for theories of equatorial spread-F. Similar investigations for other equatorial stations are therefore highly desirable.

The variation of Φ on disturbed days shows no clear dependence on solar activity, but comparing the D and Q curves of Fig. 12 it is clear that the difference Q–D is much greater at high values of $\bar{R}$. This is shown more explicitly in the

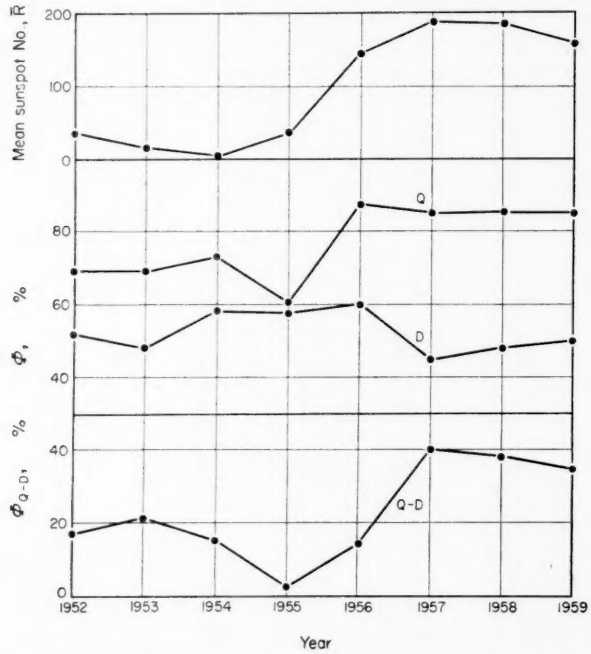

Fig. 12. Solar cycle variation of spread-F occurrence frequency at Ibadan on quiet days (Q) and on disturbed days (D), and of the difference between quiet and disturbed days (Q–D). The annual mean Zurich sunspot number ($\bar{R}$) is also shown.

bottom, Q–D, curve of Fig. 12. In other words the decrease of Φ on disturbed days is greater at sunspot maximum than at sunspot minimum. This is readily interpreted as a simple consequence of the fact that the mean level of magnetic activity on the selected international disturbed days is naturally much greater at sunspot maximum than at sunspot minimum (cf. Fig. 14 below).

We now consider whether these solar cycle variations are to be observed equally in all seasons or not. Fig. 13(a) shows the solar cycle variations of Φ in each of the three seasonal groupings winter (W) equinox (E) and summer (S), as explained above. Each value represents the mean Φ for the 20 quiet (or disturbed) days in the 4 month period of the corresponding year.

The quiet day increase of Φ with solar activity clearly occurs in all seasons but is greatest in winter and in that season Φ on quiet days has a mean value of 61 per cent for the period 1952–1955 and 85 per cent for the period 1956–1959. The increased difference between quiet and disturbed days as solar activity increases

VOL. 21 1961

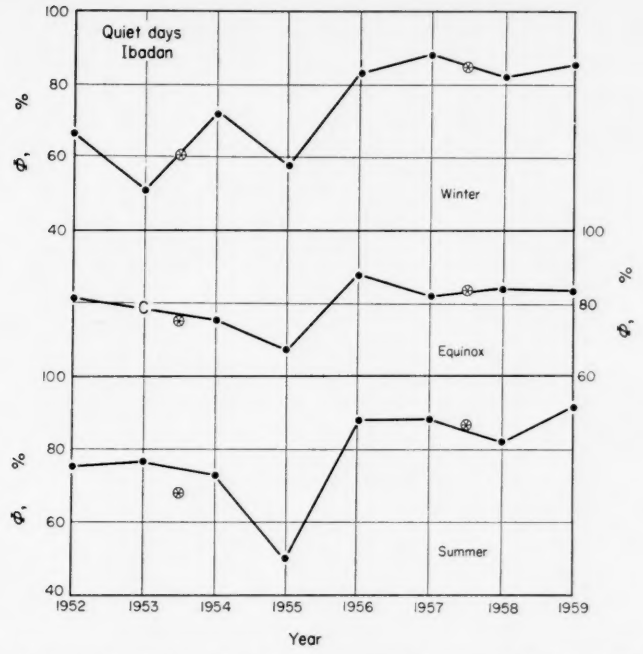

Fig. 13(a). Solar cycle variation of spread-F occurrence frequency at Ibadan on quiet days in the three seasons. The asterisks indicate averages over the years 1952–1955 and over the years 1956–1959.

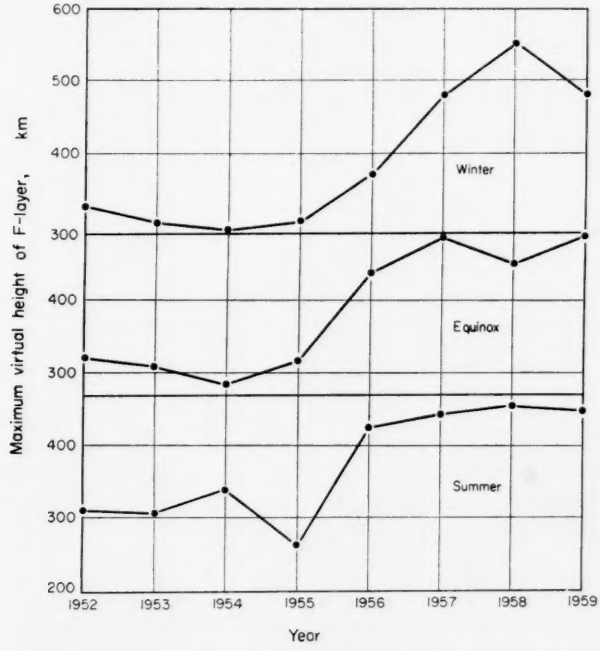

Fig. 13(b). Solar cycle variations of $h'_{\max}F$ at Ibadan on quiet days in the three seasons.

is also observed in all three seasons. This is shown in Fig. 14(a) where the difference between Φ on Q and D days is shown (a) for winter and equinox combined together (the separate variations are very similar) and (b) for summer, and we also show for comparison the variation of the mean A_p on disturbed days in the same years. The increased inhibiting effect of magnetic activity as the solar cycle advances is

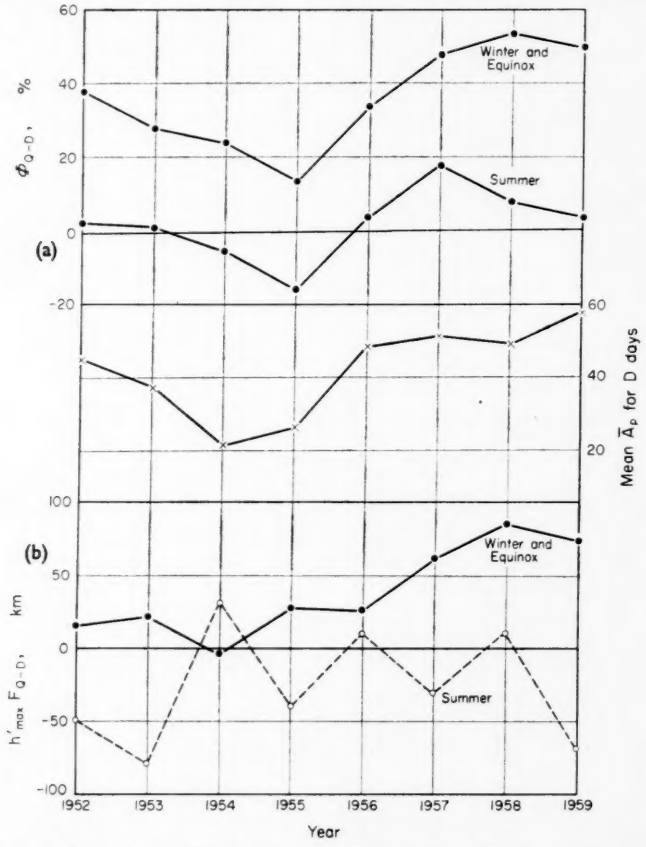

Fig. 14. (a) Solar cycle variations of the difference $\Phi_Q - \Phi_D$ in winter and equinox (averaged together) and in summer, compared with the mean A_p on disturbed days. (b) Solar cycle variations of the difference $(h'_{max}F)_Q - (h'_{max}F)_D$ in winter and equinox (averaged together) and in summer.

clear in both cases. In summer as we have already noted the inhibiting effect is much lower at all periods of the sunspot cycle and there is even a reversal of sign in 1954 and 1955, i.e. at sunspot minimum. It may be remarked however that the difference in the level of magnetic activity between quiet and disturbed days at sunspot minimum is very small.

4.3. *Correlations with* F*-layer heights in the solar cycle variations*

As we have shown in Paper I, and mentioned again in Section 3 of this paper, the occurrence of spread-F correlates very well with the height of the F-layer

VOL. 21 1961

and particularly with $h'_{\max}F$, the maximum virtual height reached in the early evening, usually between 1900 and 2000 hours. It is therefore of interest to consider how the solar cycle variations just described correlate with the corresponding variations in layer heights. Fig. 13(b) shows the solar cycle variation of $h'_{\max}F$ from 1952 to 1959 in the three seasons on magnetically quiet days. It is at once evident that there is a remarkable correlation between these and the Φ variations of Fig. 13(a). Thus $h'_{\max}F$, like Φ, increases with solar activity on quiet days in every season, and in winter when the increase in Φ is greatest the increase in $h'_{\max}F$ is also greatest. Also there is a pronounced minimum of both in summer 1955.

Fig. 14(b) shows the solar cycle variations of the Q–D difference in heights, i.e. $(h'_{\max}F)_Q - (h'_{\max}F)_D$ in winter and equinox together and in summer for comparison with the corresponding Q–D difference in spread-F incidence shown in Fig. 14(a). It is clear from this figure that in winter and equinox the depression of height increases with solar activity just as the inhibiting effect of magnetic activity also increases. In summer on the other hand we find that the F-layer usually reaches greater heights under disturbed than under quiet conditions and the difference varies in an erratic manner. This corresponds to the much reduced magnetic control of spread-F in summer which as we have already noted is shown in Fig. 14(a).

4.4. *Nocturnal variations and the solar cycle*

Fig. 15 compares the nocturnal variation of ϕ and of $h'F$ on quiet days at sunspot maximum (1957–1958) and at sunspot minimum (1954–1955). Since the variations in winter and equinox are similar, the mean variations for these two seasons together are shown in Fig. 15(a) and (b): and the variations for summer are shown in Fig. 15(c) and (d). In winter and equinox the layer is high only in the pre-midnight period and there is then a large difference between the height at sunspot maximum and that at sunspot minimum. After midnight the layer is rather low generally and there is little difference between sunspot minimum and sunspot maximum. Indeed from 0300 to 0500 hours the heights are lower at sunspot maximum. So far as spread-F incidence (ϕ) is concerned the difference between sunspot maximum and sunspot minimum is also large in the pre-midnight period but is maintained at least until 0200 hours, i.e. for at least 2 hr after there has ceased to be any difference in the heights of the layer.

In summer, as Fig. 15(d) shows, at sunspot maximum $h'F$ remains high until well after midnight, but at sunspot minimum the rise in the layer height does not occur until after midnight, the maximum being reached between 0200 and 0300 hours. Again spread-F incidence behaves similarly: at sunspot maximum ϕ increases early and remains at almost 100 per cent until well after midnight whereas at sunspot minimum it remains low in the pre-midnight period and reaches a maximum around 0200–0300 hours.

5. Discussion and Conclusions

Theories of spread-F require fuller investigation than is possible here, but some implications of the above results may be considered briefly. In the first place the

evidence of this paper and of Paper I makes it very clear that either the height of the layer, or possibly, as suggested by Martyn (1959), its upward motion, plays a very important role in the formation of equatorial spread-F. The suggestion of Marasigan (1960) that downward motion of the layer produced the irregularities would clearly not be consistent with the evidence we have presented. On the other hand spread-F can occur at very low heights (even below 300 km) as it does at sunspot minimum, and it can fail to occur at great heights (over 400 km) as on

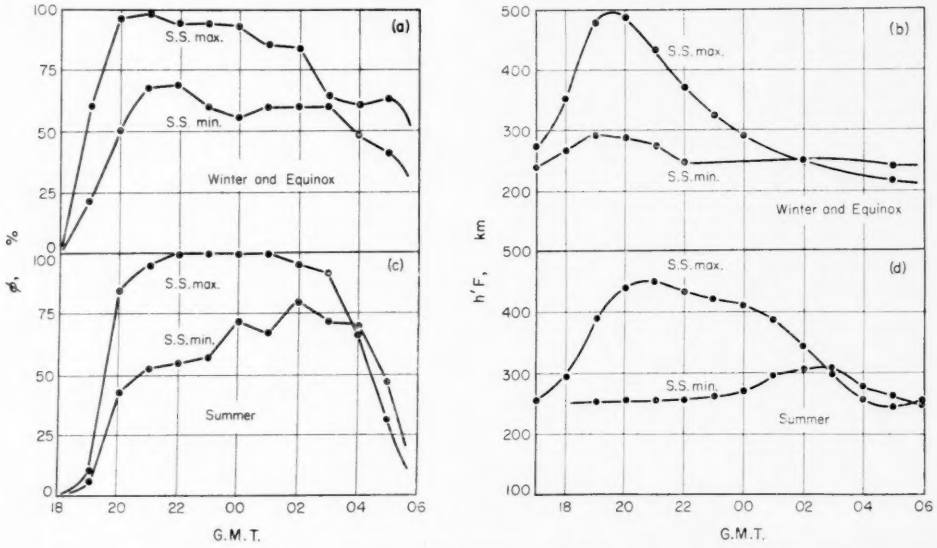

Fig. 15. Nocturnal variations of spread-F incidence (ϕ) and of $h'F$ at sunspot maximum and at sunspot minimum, (a) and (b) in winter and equinox months together and (c) and (d) in summer.

disturbed days at sunspot maximum; but in the equatorial belt when both conditions are satisfied, height over 400 km and conditions magnetically quiet, the occurrence of spread-F is virtually certain at any time of the year and in any phase of the solar cycle.

We have already noted in Paper I that the hypothesis that hydro-magnetic disturbances, perhaps of extra-terrestrial origin, are the source of equatorial spread-F is an attractive one. It was originally proposed, though not in a fully satisfactory form, by Dessler (1958). The existence of a critical height could be accounted for on this hypothesis by the well-known fact that the attenuation of hydro-magnetic disturbances increases as the height decreases and the collision frequency increases, and below a certain level they degenerate into electromagnetic disturbances in which motion of the ionization no longer occurs.

On such a theory almost all the variations of equatorial spread-F incidence which we have noted here and in Paper I, and also the nocturnal changes in the character of equatorial spread-F, could be explained as consequences of corresponding changes in the height of the layer. The origin of the height changes would be quite independent of the disturbances, and could lie for example in variations

VOL. 21 1961

of electro-magnetic drifts or of the horizontal diffusion which is probably important in equatorial regions.

Taking the nocturnal variations first, when the base of the layer is above about 400 km, which occurs mainly between 2000 and 2200 hours, and especially at sunspot maximum, the disturbances reach the lowest parts of the layer and we observe typical fully-developed equatorial spread-F, in which there is a wide range of roughly uniform spreading in virtual height (200–300 km or more) at all frequencies for which echoes occur.

The source of the great range of spreading is not clear from the evidence at our disposal: it could be due (a) to oblique echoes from the highly irregular lower surface of the layer, or (b) to deep "holes" in the layer even at nearly vertical incidence, or (c) to multiple echoes, i.e. to echoes reflected a number of times from widely separated irregularities, or (d) to multiple paths, i.e. to the existence, because of the intense inhomogeneity of the layer, of numerous paths, some of them highly group retarded, to and from a given level of electron density. Whatever the mechanisms involved it is clear that at least the base of the layer is normally—even under the quietest magnetic conditions—subjected to disturbances of a very violent nature whenever it rises to heights above about 400 km.

As the layer descends later in the night fewer and fewer disturbances reach the lower parts of the layer and hence waves of the lower frequencies are reflected coherently without spreading. Even near the critical frequency where spreading does occur the normal group retardations suffered lower in the layer are clearly visible and the critical frequency can usually be measured, at least approximately. It is of interest to note that this latter situation, where irregularities are confined to the neighbourhood of the layer maximum (and perhaps above), and spreading is confined to the neighbourhood of the critical frequency, is also typical of temperate and higher latitudes where the height of the layer remains relatively low under almost all conditions.

As to the phenomenon of "doubling", the evidence suggests that the formation of large isolated irregularities just east of the sunset meridian is an initial phase in the development of the intensely disturbed layer which the phenomena of equatorial spread-F imply.

Turning now to the solar cycle variations we have shown that quiet day incidence of equatorial spread-F at Ibadan increases as the level of solar activity rises and the maximum height $h'_{\max}F$ also increases correspondingly. On the other hand it might seem that the change in Φ is less than would be expected from the large change in $h'_{\max}F$ between sunspot minimum and sunspot maximum. To account for this it may be necessary to suppose that the critical height is lower at sunspot minimum, due perhaps to a lower scale height. In support of this suggestion we may note that at Ibadan y_m the semi-thickness of the F-layer (as determined by an Appleton–Beynon technique) is substantially smaller at sunspot minimum than at sunspot maximum, rising from about 80 km to about 120 km or more as the solar cycle advances.

Magnetic disturbance changes in spread-F also show good correlation with corresponding height changes. In many cases however (cf. the equinox curves of Fig. 7 for example) there seems to be almost complete elimination of spread-F for

a relatively small decrease in heights. Other evidence of such a discrepancy has been given earlier from a morphological analysis (cf. Fig. 7 of Paper I). This suggests that in addition to the height changes the source of the irregularities itself, or some additional factor affecting their development is also diminished by magnetic disturbance. Clearly there is a large increase in sources of hydro-magnetic disturbances during periods of high magnetic activity, but it may be that the conditions which allow them to be propagated into equatorial regions are disrupted under magnetically disturbed conditions.

Finally in regard to seasonal variations of spread-F at Ibadan two outstanding features, both affecting the summer months, call for comment, namely first the tendency to greater incidence of spread-F in summer as compared with the other seasons even on quiet days, and secondly the reduced magnetic control in the summer months. As we have already mentioned the latter may be in part a consequence of the former. However both phenomena correspond again to peculiarities of the layer heights in summer. Thus the layer remains high for a longer period (and so over a larger area of the ionosphere) in summer than in the other seasons, and there is also reduced magnetic control of heights in summer.

One important feature of spread-F incidence which does not at first sight agree with the general rule that spread-F invariably occurs at great heights under quiet conditions is the restriction of spread-F to the night, for h_mF2 regularly exceeds 400 km in the day time and sometimes reaches 600 km and yet no spreading is observed near the critical frequency in the day time. This can hardly be due to absorption since the related phenomenon of radio-star scintillation at a frequency of 45 Mc/s (where absorption would be very small) is also restricted to the night (Koster, 1958) and the same is true for the scintillation fading of radio signals at 108 Mc/s from the Explorer satellites (Kent, 1960).

It may however be significant that a phenomenon of somewhat similar nature does occur in the day time in equatorial regions—namely equatorial E_s. Points of obvious similarity are the diffuse spreading (though over a smaller range in the case of E_s), the fast fading associated with echoes both from E_s and from spread-F and the negative correlation with magnetic activity in both cases (cf. Skinner and Wright, 1957), though this negative correlation is much less marked with E_s than with spread-F. These similarities would suggest that the disturbances give rise to major irregularities only at the base of the ionized regions, where there would be a discontinuity in the hydro-magnetic refractive index, (i.e. at the bottom of the E-layer in the daytime, and at the bottom of the F-layer at night).

To summarize our discussion then it seems that most of the variations which occur in equatorial spread-F—in particular the nocturnal changes in character, the increase in quiet day incidence with solar activity and the reduced or even reversed magnetic control in summer are closely related to and probably explained by corresponding changes of height. In the case of the reduced incidence on disturbed days, although there is some reduction in heights, there is often such a dramatic elimination of spread-F for a relatively small drop in heights that some additional factor may be involved. The theory that hydro-magnetic disturbance of extra-terrestrial origin produce the irregularities which lead to equatorial spread-F appears to give a reasonable account at least qualitatively of this correlation.

VOL. 21 1961

References

Dessler A. J.	1958	*J. Geophys. Res.* **63,** 507.
Kelso J. M.	1952	*J. Geophys. Res.* **57,** 357.
Kent G. S.	1960	Personal communication.
Koster J.	1958	*J. Atmosph. Terr. Phys.* **12,** 100.
Kotadia K. M.	1959	*Proc. Ind. Acad. Sci.* **50,** 259.
Lyon A. J., Skinner N. J. and Wright R. W. H.	1960	*J. Atmosph. Terr. Phys.* **19,** 145.
Marasigan V.	1960	*J. Atmosph. Terr. Phys.* **18,** 257.
Martyn D. F.	1959	*Proc. I.R.E.* **47,** 147.
Reber G.	1954	*J. Geophys. Res.* **59,** 257.
Reber G.	1955	*J. Geophys. Res.* **61,** 157.
Shimazaki T.	1959	*J. Radio Res. Lab.* **6,** 669.
Skinner N. J. and Wright R. W.	1957	*Proc. Phys. Soc. Lond.* B **70,** 833.
Wells H. W.	1954	*J. Geophys. Res.* **59,** 273.

OL.
21
961

Journal of Atmospheric and Terrestrial Physics, 1961, Vol. 21, pp. 120 to 141. Pergamon Press Ltd. Printed in Northern Ireland

The fading of radio waves reflected from the ionosphere at oblique incidence

O. AWE*
Cavendish Laboratory, Cambridge

(*Received* 7 *December* 1960)

Abstract—The fading of radio waves reflected from the ionosphere at oblique incidence is studied by the use of pulse transmissions on frequencies near 2 Mc/s. It is found that echoes reflected from a height of about 90 km have a fading period of about 1 min. Echoes from a greater height of about 120 km, which usually appear only during or immediately after magnetic disturbances, have a shorter fading period of about 6 sec. A clear distinction between reflections from these two levels is urged for an understanding of the fading of echoes from the *E*-region. The spatial characteristics of the diffraction pattern on the ground are studied by the use of three spaced receivers. Possible models for the ionospheric irregularities which would explain the results are considered. It is suggested that the irregularities at heights near 90 km have the form of horizontal discs, that the irregularities near 120 km are spherical, and that the irregularities near 300 km are elongated along the direction of the earth's magnetic field, with an axial ratio of about 3 : 1

1. INTRODUCTION

SEVERAL WORKERS have made observations of pulses from transmitters of the Loran navigational system, reflected obliquely from the ionosphere (YABSLEY, 1945; PIERCE *et al.*, 1948; PIERCE, 1946; NAISMITH and BRAMLEY, 1951). In all cases, the first echo received was found to correspond to a height of reflection of about 90 km. The characteristics of this echo were found to depend on the distance of the transmitter. As this distance increased, so that incidence on the ionosphere became more oblique, the echo was found to become stronger and its fading became slower and less variable from one occasion to another.

These results indicate that there is usually a distinct echo from some height near 90 km. In the experiments described in this paper, there was no ground wave reference and the results of the above workers, who had a ground wave reference, have been used to identify the echoes received. The fading of the echoes from around 90 km is studied. In another paper (AWE, 1961), the author has suggested that the 90 km layer is distinct from the normal *E*-region. Additional evidence is presented here to show that only such a separation can explain the experimental results and those of previous workers.

The effect of magnetic disturbances is discussed in Section 4.

Due to the difference in obliquity, echoes are usually obtained from 90 km and from the *F*-region simultaneously during the night, and the fading characteristics of the echoes from the *F*-region are also studied.

The spatial properties of the diffraction pattern formed on the ground by the downcoming waves are discussed in Section 6. Possible theories which might explain the results are then considered in Section 7. In Section 8, the horizontal drifts of irregularities at various heights are discussed. Finally, the significance of all the results and their relation to those of other workers are discussed in Section 9.

* Now at University College, Ibadan, Nigeria.

VOL. 21 1961

2. Experimental Techniques

Signals from three Loran transmitters were used for most of these investigations. They are all on a frequency of 1·95 Mc/s. The pulse width is 40 μsec and the peak power 100 kW. The pulse repetition rate, which is crystal-controlled, is about 25 per second. The transmitting aerials are inverted-L aerials with a circular polar diagram in the horizontal plane and a $\cos\theta$ polar diagram in the vertical plane. The master station is at Skuvanes (61°27′N, 06°49′W) on Faroes Island and the two slave stations are at Mangersta (58°11′N, 07°05′W) in the Hebrides and at Vik (63°24′N, 19°02′W) in Iceland. Two pulses of slightly different repetition rates are transmitted from the master station and each of the slave stations. Reception was at Cambridge (52°13′N, 00°06′E). The distances of the transmitters from Cambridge are 800 km for Mangersta, 1110 km for Skuvanes and 1670 km for Vik. In this paper they are referred to as Tx_{800}, Tx_{1110} and Tx_{1670}. Their bearings from Cambridge are 30°, 20° and 40° West of North respectively (see Fig. 1).

Short vertical dipoles were used for reception. The receivers used were the Admiralty model of the Loran receiver, type Das/2. They have a bandwidth to half power of 75 kc/s, use stabilized power supplies, and have no automatic gain control so that gain changing is manual. An indicator unit displays the echoes on an oscilloscope whose time base is locked to a crystal oscillator. By the use of a station selector switch on the indicator unit, a master-slave pair can be made stationary on the oscilloscope trace and the other pair is then seen to drift across the tube.

Minor modifications carried out on the receiving equipment included a mechanism to change the gain of a receiver at an out-station a few kilometers away from the central receiving station by remote control; this enabled the gain to be changed in steps. The output of the receiver was disconnected from the input to the oscilloscope plates and taken to two cathode followers connected in parallel. The output from one of these was taken to a strobe unit which was used to select an echo for recording. The other output was connected to the input of an anode follower whose output was now taken to the oscilloscope input. Also connected to the anode follower input was the strobe pulse so that both the strobe pulse and the receiver output appeared on the oscilloscope tube. The strobe pulse at the central station was generated from a 25 cycle square waveform from the indicator unit. Its width could be varied and it was locked to the oscilloscope time base. A left–right switch on the indicator unit could be used to make a stationary echo drift towards the left or the right of the trace until it was inside the strobe. Thereafter, the slow drift of the echo out of the strobe, which inevitably occurred because the transmitter and the time base were locked to different crystals, was controlled by a small condenser on the indicator unit labelled "phase shift".

In the spaced receiver experiments described in Section 7, it was necessary to select for recording the same echo at each of the receiving sites. This was achieved by sending strobe generating pulses from the central receiving station to the outstations by the use of telephone lines. A strobe unit at each of the outstations generated a strobe pulse of variable width at the site by the use of the distorted pulse from the telephone line. All the strobe pulses could be moved relative to the echoes from the central receiving hut. In the initial adjustment, the strobes at the

outstations and the central site were arranged to fall on the same echo. The selected echo was taken to a peak amplitude rectifier which gave a d.c. output proportional to the echo amplitude. The d.c. outputs from the outstations were transmitted to the central hut by telephone lines where they operated a three-track pen recorder. In this way, the fading of the echoes at the three spaced receivers was recorded on a single chart.

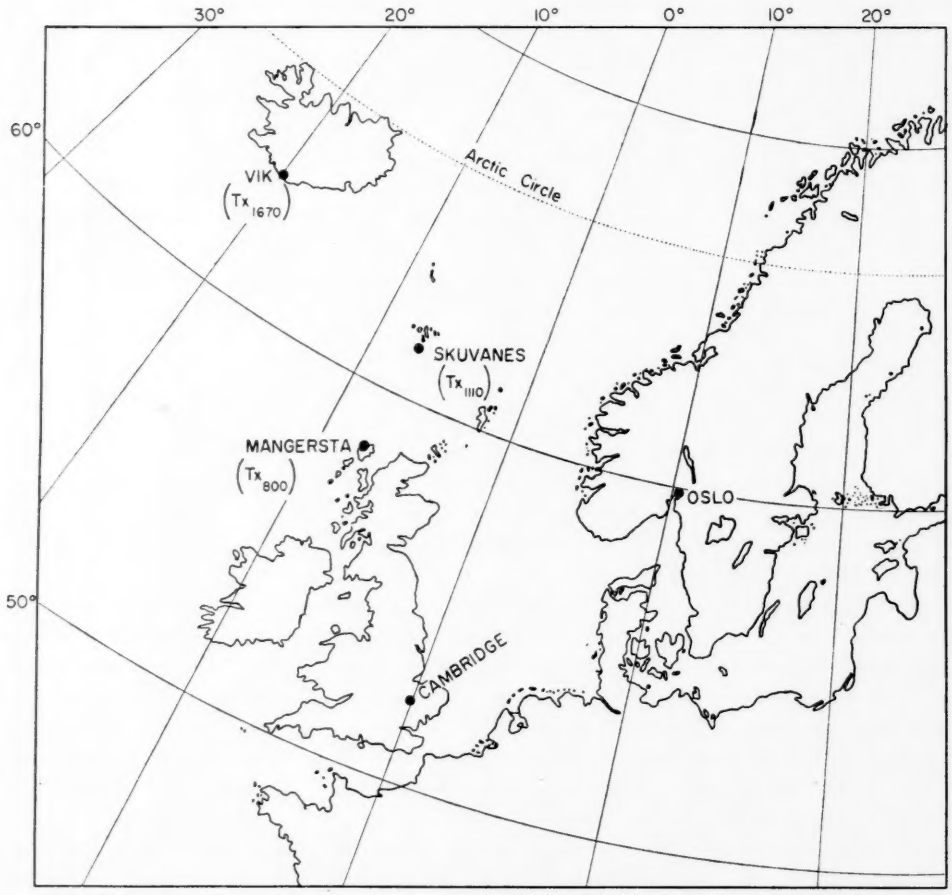

Fig. 1. Map showing the positions of the transmitters used in the experiments. Reception was at Cambridge.

3. Fading Speeds of the 90 km Echo

3.1. *The counting of maxima*

One measure of the speed of fading of the echoes was obtained by counting the number of maxima of amplitude in a fading record per unit time. This analysis was

VOL. 21 1961

carried out on records of the echoes from the three transmitters. Each record was divided into $\frac{1}{2}$ hr lengths and the number of maxima/hour evaluated.

Fig. 2 shows the results obtained for the 90 km echo on the three transmitters. Fewer results were obtained on Tx_{1670} due to the fact that the echoes from this transmitter are often absent; a probable explanation for this is suggested in Section 4. The records were obtained mostly at night because the echoes were too weak during the day. However, during the winter months, day-time records could be obtained and these are included.

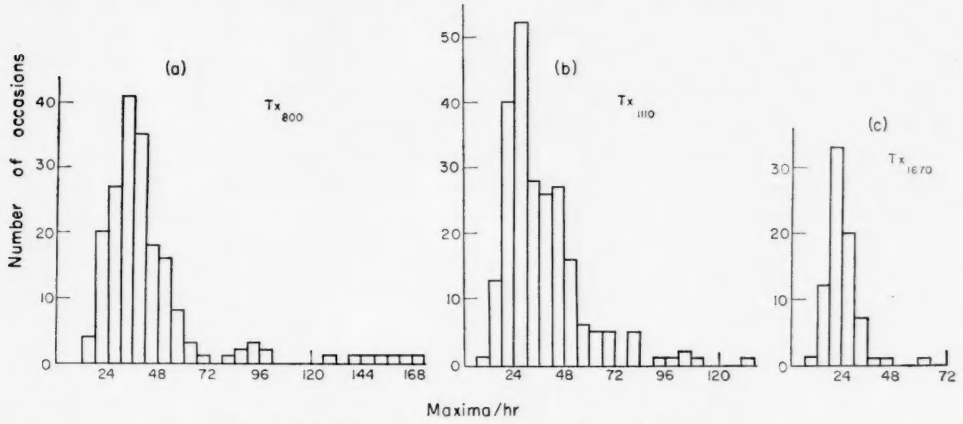

Fig. 2. Distribution of fading speeds of the 90 km echoes.

From the figure, it is at once evident that not only does the speed of fading decrease as the receiver–transmitter separation increases, but also the spread in the values for the speed of fading also decreases.

3.2. *Auto-correlation analysis of fading records*

The period of fading of the echoes may be defined in a different way by the use of the auto-correlation function of the amplitude. If $R(t)$ denotes the amplitude at a time t, and $R(t + \tau)$ the value at time τ later, the time auto-correlation function $\rho(\tau)$ is defined as

$$\rho(\tau) = \frac{\overline{R(t)R(t+\tau)} - \left[\overline{R(t)}\right]^2}{\left[\overline{R(t)}\right]^2 - \left[\overline{R(t)}\right]^2} .$$

To evaluate this function, the fading record was sampled at regular time intervals much less than the mean time between maxima. The lengths of records analysed varied between 24 min for the shortest to $1\frac{1}{2}$ hr for the longest.

We may define a time $\tau_{\frac{1}{2}}$ such that $\rho(\tau_{\frac{1}{2}}) = 0{\cdot}5$, and $\tau_{\frac{1}{2}}$ may then be used as a measure of the fading period.

The period of recording was from January 1958 to January 1960, and the auto-correlation functions of 135 records obtained during this period were calculated by the use of an electronic computer. The values of $\tau_{\frac{1}{2}}$ obtained from these auto-correlation functions are shown in Table 1.

Table 1. Fading period: 90 km echoes

Transmitter	Day (sec)	Night (sec)	Summer night (sec)	Winter night (sec)
Tx_{800}	47 (29)	31 (31)	31 (7)	31 (24)
Tx_{1110}	50 (31)	44 (27)	56 (11)	32 (15)
Tx_{1670}	48 (3)	63 (24)	95 (5)	54 (19)

The figures in brackets are the number of independent values of the fading period from which the mean values are determined.

The results obtained at night confirm the increase of fading period with transmitter–receiver separation. The results obtained by day are inconclusive in this respect, owing to the small number of results obtained by day for Tx_{1670}. There are indications of possible diurnal and seasonal variations of fading period, but these cannot be regarded as well established with the present limited number of observations.

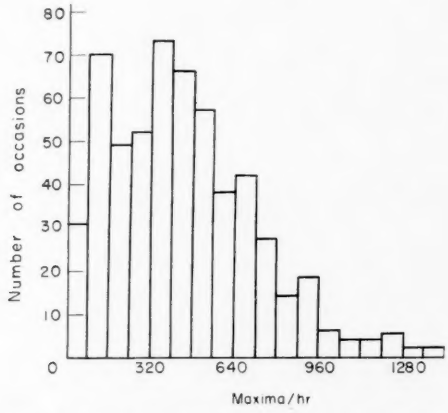

Fig. 3. Distribution of fading speeds of echoes from the E-region at vertical incidence.

King (1958) has suggested that there is a linear variation of fading speed (defined for example, as the number of maxima per hour) with $f \cos i$, where f is the frequency and i the angle of incidence on the ionosphere. The period of fading would then be proportional to $\lambda \sec i$ where λ is the wavelength. To test this relationship, recordings were made at vertical incidence on a frequency of 2·4 Mc/s. On this frequency, echoes from the normal E-region are only obtained in the daytime. Fig. 3 shows the histogram of fading speeds obtained during 2 weeks of observations from April to May 1959. When this is compared with Fig. 2, it is evident that there is a much greater spread of values. Auto-correlation analysis of fifteen different records gave a mean value of $\tau_{\frac{1}{2}}$ of 6·3 sec. In comparing this value with the results in Table 1, it should be noted that the values of sec i are approximately 4·0 for Tx_{800}, 4·9 for Tx_{1110}, and 5·7 for Tx_{1670}. There is agreement only in order of magnitude with the law proposed by King; this point is discussed further in Section 9.

VOL. 21 1961

4. Effect of Magnetic Disturbances

4.1. *The effect of magnetic disturbances on the height of reflection*

Lindquist (1953) gives evidence to show that one of the effects of a disturbance on the lower E-region at night is to reduce the electron density at heights near 90 km. This is attributed to an increased recombination coefficient due to the impact of high energy charged particles during such disturbances. During some disturbances, 150 kc/s waves were found to penetrate the 90 km region at vertical incidence and were reflected from new virtual heights between 120 and 150 km. Watts and Brown (1951) also obtained evidence which supports this. Lindquist remarks that the intermediate layer at about 120 km is invariably present during disturbances and that 150 kc/s waves never succeed in getting to the F-layer. It is important to determine whether the disturbance gives rise to this new layer or whether the effect of the disturbance is to reduce the electron density near 90 km which normally screens off this higher layer. A study of the echo patterns obtained from Tx_{1110} and Tx_{800} is of help here.

Fig. 4(a) shows a typical echo pattern obtained on a quiet night. The top trace is the echo pattern on Tx_{1110} and the first echo is the 90 km echo which is followed after about 500 μsec delay by an echo from the F-region which corresponds to a virtual height of 300 km. The lower trace is the echo pattern for Tx_{800}, the first echo being the 90 km echo and the second the echo from the F-region with a time delay of about 550 μsec which corresponds to a virtual height of 280 km.

On the lower trace of Fig. 4(b), the 90 km echo is followed after a time delay of about 50 μsec by another echo of about the same amplitude. This corresponds to a virtual height of 120 km. While this echo appears for brief periods only on quiet nights, it is invariably present on disturbed nights. In Fig. 4(c) it is considerably stronger than the 90 km echo and it occurs at a time delay of 100 μsec, corresponding to a virtual height of 140 km. A weak echo at 100 μsec delay can also be seen on the upper trace. The 90 km region was thus in this instance almost completely penetrated by the signals from the nearer transmitter, but still reflected quite well the signals from the more distant transmitter. This can be attributed to the difference in the equivalent frequencies, which are 400 kc/s for the long path and 490 kc/s for the short path. During very severe storms, all echoes disappear soon after the onset of the storm due to the high absorption which accompanies such storms. This high absorption persists for a few nights after the storm. This "after effect" has been studied in some detail by Lauter (1950) and also by Belrose (1957) who report that the "after effect" lasts for one to six nights depending on the magnitude of the storm. In the present experiments this behaviour has been noted for eight different storms. The geomagnetic latitude of the midpoint of the path from Tx_{1670} is 59°N which is only 6° South of the maximum of the auroral zone, and it is believed that the frequent occasions on which echoes from this transmitter are absent is connected with this absorption phenomenon.

The fact that the echo with a delay of 50–150 μsec behind the 90 km echo appears for short periods even on quiet nights suggests that the reflecting layer near 120 km is not created by the storm but rather that it is present all the time, being revealed only when the 90 km layer suffers a depletion of its electron content. It is believed

that this upper layer is the residual night-time E-region, and that the 90 km layer is quite separate from it.

4.2. *The effect of magnetic disturbances on the fading speed of the* 90 *km echo*

As an index of magnetic activity, the 3-hourly K-indices of the Hartland observatory were used, and a disturbed period was defined as one with $K \geqslant 4$.

It is simplest to consider first results obtained during the day-time, for which the complications discussed in the previous Section do not arise. Daytime results obtained in the winters of 1959 and 1960 showed that the speed of fading of the 90 km echo was unaffected by magnetic disturbances. This conclusion is based upon seventeen records analysed by the auto-correlation method. Belrose (1957) obtained the same result in a study of the fading of 200 kc/s c.w. signals reflected at near vertical incidence, which showed that the degree of magnetic activity had no effect on the fading of the signals provided the disturbance occurred during the day. The work of Lindquist (1953) shows that waves of 150 kc/s would be reflected from about 90 km during the day, and so the results of Belrose refer to the same region as the echoes studied in the present work.

At night, complicated changes occur as discussed previously. However, it was possible to obtain three records of the fading of the 90 km echo from Tx_{800} just before it disappeared due to the occurrence of a disturbance. These records gave a mean value of $\tau_{\frac{1}{2}}$ of 19 sec. This shows that the fading was about 1·5 times faster than the normal night-time value for this echo.

VOL. 21 1961

5. The Fading Speeds of Echoes from the E- and F-Regions

5.1. *The* E*-region*

As explained in Section 4.1, the echo from the E-region was obtained consistently only during a period of magnetic disturbance, or during a few days following such a disturbance. Ten records were obtained for the fading of the echo from Tx_{800} reflected from a height of about 120 km during the days following a disturbance and when the disturbance itself, according to the magnetic K-figures, was over. The mean value of $\tau_{\frac{1}{2}}$ obtained from these records was 5·8 sec.

Recordings made when a storm was actually in progress, after the 90 km echo had disappeared, showed that the fading speed was then much higher than normal. The fading period was usually of the order of 1 sec. Thus the fading speed of this echo increases by a factor of about six during a magnetic disturbance.

5.2. *The* F*-region*

Recordings were made on the echo from the F-region for Tx_{800}. Auto-correlation analysis gave the mean of twenty-nine values for the period $\tau_{\frac{1}{2}}$, obtained for quiet conditions, as 6·3 sec.

During a storm, the speed of fading of this echo increased greatly. For example, during a magnetic storm on 21 January 1960, the mean of six values of $\tau_{\frac{1}{2}}$ obtained during the night was 0·43 sec. The fading speed thus increased by a factor of more than ten during this storm.

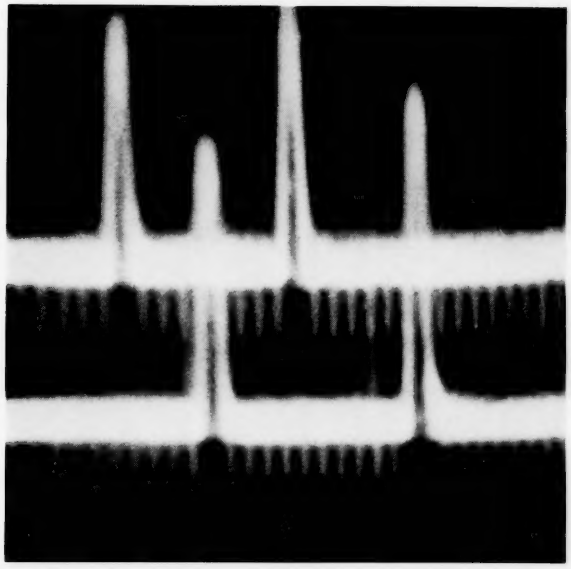

(a)

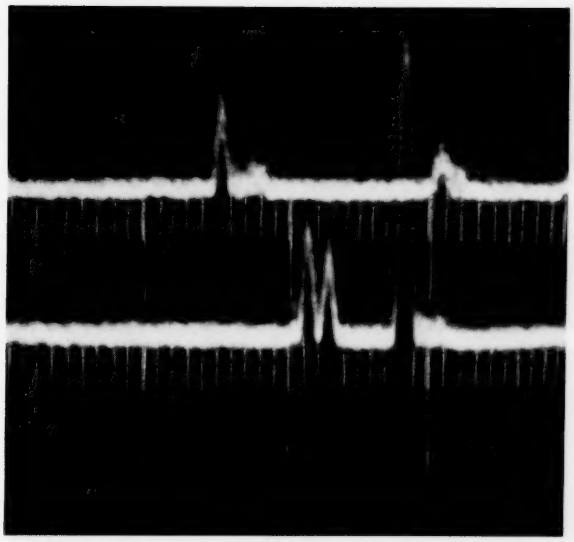

(b)

Fig. 4. Photographs of Loran echoes. The short time marks are at 50 μsec intervals and the long time marks at 500 μsec intervals. (a) 10 November 1959, (b) 17 December 1959.

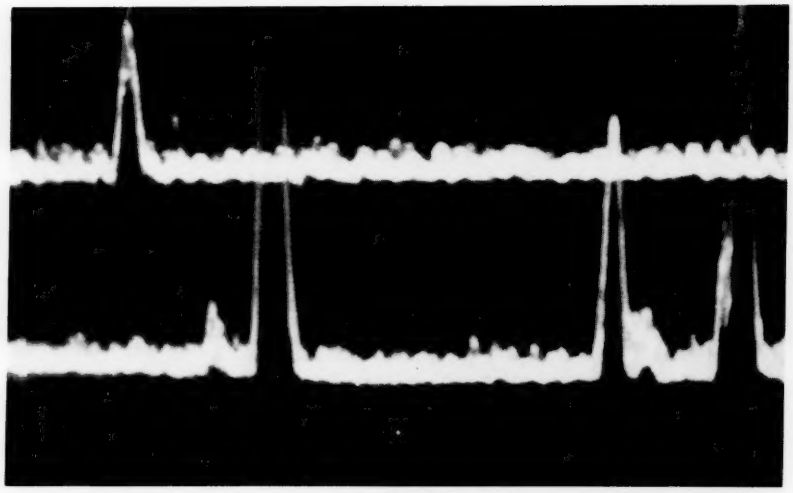

(c)

FIG. 4 (*cont.*) Photographs of Loran echoes. The short time marks are at 50 μsec intervals and the long time marks at 500 μsec intervals. (*c*) 24 December 1959.

6. The Spatial Characteristics of the Pattern Formed on the Ground by the Downcoming Waves

6.1. *Definitions and method of measurement*

Recordings of the amplitude of a wave reflected from the ionosphere show that similarity between records taken at two receivers decreases as the separation of the receivers increases. This is a consequence of the diffractive reflection suffered by the wave in passing through the ionosphere which contains irregularities of electron density embedded in a background ionization. The downcoming wave is spread into a cone of downcoming rays, the angle of the cone depending on the size of these irregularities. On reaching the ground a diffraction pattern is formed. We can describe this pattern by means of the space auto-correlation function of signal amplitude $\rho(\xi)$ defined as

$$\rho(\xi) = \frac{\overline{R(x)R(x+\xi)} - \left[\overline{R(x)}\right]^2}{\overline{[R(x)]^2} - \left[\overline{R(x)}\right]^2}$$

We may define a distance $\xi_{\frac{1}{2}}$ such that $\rho(\xi_{\frac{1}{2}}) = 0{\cdot}5$ and regard $\xi_{\frac{1}{2}}$ as the average size of the irregularities in the pattern. In the practical determination of $\xi_{\frac{1}{2}}$ it is usual to record simultaneously the amplitudes at two stations separated by ξ_1, say, and to evaluate the cross-correlation between the records. This is assumed to give the value $\rho(\xi_1)$. The $\rho(\xi)$ curve is then obtained by assuming a shape for this correlation function and inferring the rest of the curve from this one value and, of course, the value 1 for $\xi = 0$. Bowhill (1956) and King (1958) assumed a Gaussian form for $\rho(\xi)$. A different assumption, made by Briggs *et al.* (1950) was that the time and the space correlation functions had the same shape. An entirely different approach has been made in the results described in this Section and no assumption is made regarding the shape of the space correlation function. Instead an arrangement of three aerials suitably spaced along a straight line was used and simultaneous recordings were taken on the three. Cross-correlation analysis on the three records taken in pairs then gave three points on the $\rho(\xi)$ curve and of course the fourth point at $\rho(0) = 1$. Through these four points, a best fit curve was drawn by eye.

6.2. *Experimental results*

The method described above was used only for the 90 km echo. The two outstations were at distances 1·8 km and 5·1 km from the recording hut which was at one end of the straight line. These distances gave four values of ξ viz: 0, 1·8, 3·3 and 5·1 km. The centrally controlled strobe was used to select for recording the same echo at each station.

Recordings on a three-track pen recorder were made on thirty-one nights from May to October 1958, and correlation coefficients evaluated for lengths of records about 1 hr in duration.

Fig. 5 shows the scatter plots of the variation of correlation coefficient with the receiver separation for the three transmitters. The crosses show the mean values of the correlation coefficients for each value of ξ and the dotted curves are the estimated space correlation functions. The scatter in the values of the coefficients for Tx_{1110} is much larger than on the other two. The reason for this is not known.

The mean values of $\xi_{\frac{1}{2}}$ obtained from Fig. 5 are 4·1 km for Tx_{800}, 5·0 km for Tx_{1110} and 7 km for Tx_{1670}. This shows that the size of the irregularities in the ground pattern increases as the transmitter–receiver separation increases.

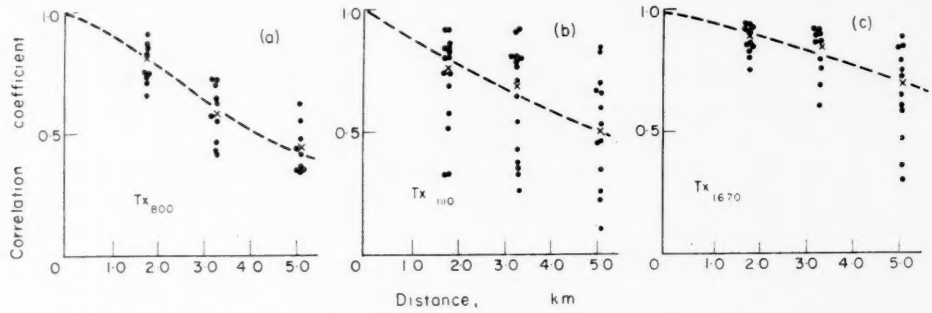

Fig. 5. Scatter plot of the variation of correlation coefficient with receiver separation for 90 km echoes.

6.3. *The relation between the scale of the pattern and the fading period*

For each set of records analysed by the method outlined above, a space and a mean time correlation function is obtained. We may now define a distance $\xi_{\frac{1}{2}}$ and a time $\tau_{\frac{1}{2}}$ such that

$$\rho(\xi_{\frac{1}{2}}) = \rho(\tau_{\frac{1}{2}}) = 0{\cdot}5.$$

A scatter plot of $\xi_{\frac{1}{2}}$ against $\tau_{\frac{1}{2}}$ is shown in Fig. 6. It includes results obtained for all three transmitters. It is at once obvious that a high degree of correlation exists

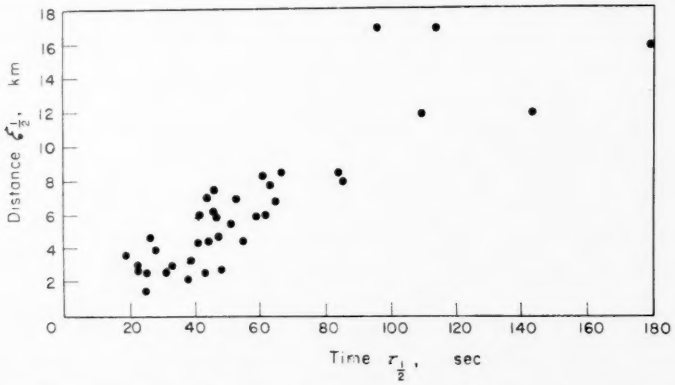

Fig. 6. Variation of the size of the irregularities in the ground pattern with the fading period for 90 km echoes.

between the two quantities; the coefficient of correlation is 0·87. If the fading of the received signals is the result of a drift of the diffraction pattern over the ground, the slope of the straight line of best fit gives a velocity of 120 m sec^{-1}. If this explanation is correct, it must follow that the drift velocity does not change much, but that the size of the irregularities in the pattern varies quite a lot from time to time. Alternatively, if the fading is due to random changes of the diffraction

VOL. 21 1961

pattern, the same result shows that the velocity of the random movements of the irregularities in the pattern is fairly constant.

6.4. *The shapes of the space and the time correlation function*

Some individual cases will now be examined in order to see to what extent the space and the time correlation functions can be regarded as having the same shape. Fig. 7 shows three different examples. The full lines in the lower diagrams are the time correlation functions and the dotted lines the space correlation functions. The space correlation functions, on which only four points are known, namely $\rho(\xi)$ for $\xi = 0$, 1·8, 3·3 and 5·1 km are plotted as follows: the correlation coefficient for the spacing of 1·8 km was fitted to the time correlation curve and this determined the scale for ξ on the abscissae of the lower diagrams. The values of the correlation coefficients for the distances 3·3 and 5·1 km were then plotted. The dotted curves were fitted to the four points by eye.

The agreement between the space and the time correlation functions is seen to be good in Fig. 7(i b); it is only fair in Fig. 7(ii b), and is considered poor in Fig. 7(iii b). Of the thirty-eight individual cases, the agreement between the space and the time correlation functions was considered fair to good in twenty-six cases and poor in the remaining twelve cases. The individual results suggest that the time correlation function falls off more rapidly than the space correlation function.

6.5. *The shape of the irregularities in the pattern on the ground*

Following PHILLIPS and SPENCER (1955) we may use recordings at the corners of a triangle to investigate the average size and shape of the irregularities in the pattern on the ground. In this analysis, it is necessary to assume that the time and space correlation functions have the same shape. It is then possible to determine for each pair of the three spaced aerials the distance at which correlation falls to a certain value (0·5 say) in the three directions defined by the triangle. A radial plot of these distances in the three directions then gives three points which determine an ellipse with centre at the origin. The major axis of the ellipse, its axial ratio (i.e. the ratio of the major to the minor axis) and the orientation of the major axis can then be determined. This characteristic ellipse gives the simplest "first-order" description of the size and degree of elongation of the irregularities in the pattern.

The shape of the characteristic ellipse has been determined in this way for the 90 km echo for the three transmission paths and for the *E*- and *F*-echoes on Tx_{800} only.

Table 2 shows the mean results obtained for the parameters of the characteristic ellipse determined with the value $\rho(\xi) = 0{\cdot}5$. The values for the major axis are $2\xi_{\frac{1}{2}}$ (i.e. the length of the whole major axis, not the semi-major axis).

For the 90 km echoes a small systematic elongation is found; this is believed to be genuine because the direction of the major axis is very nearly the same for the three transmission paths. Further, when the individual ellipses are examined, it is found that all except one have their major axes in the NW–SE quadrants.

Echoes from the *E*- and *F*-regions give somewhat larger values of axial ratio but with similar directions for the major axis. For the echo from the *E*-region, all

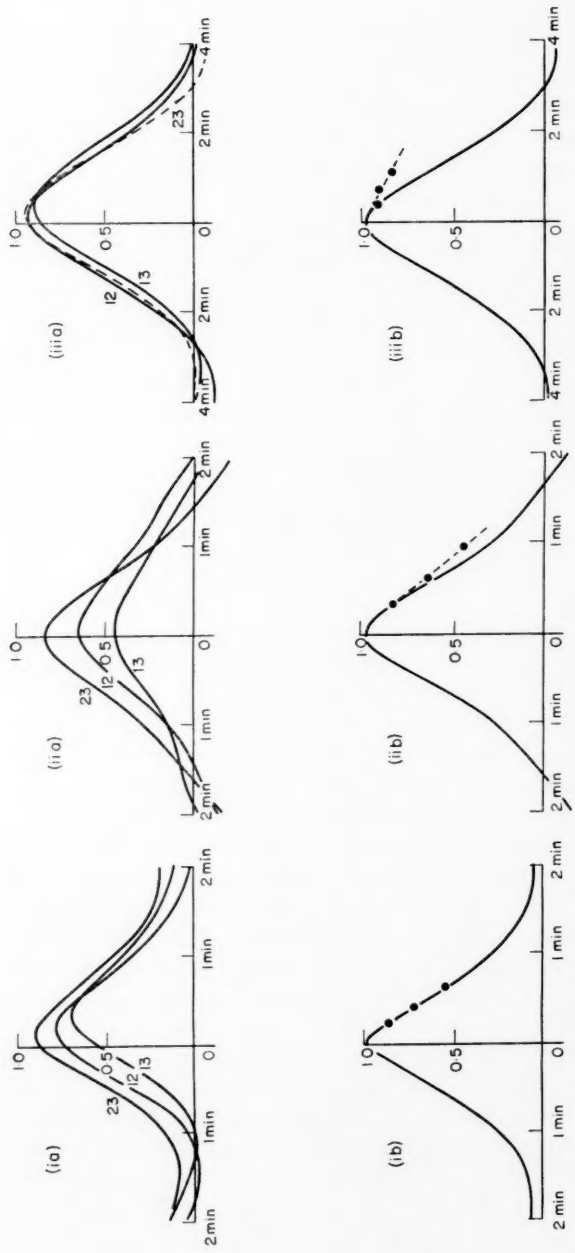

Fig. 7. Graphs of correlation functions. The upper curves (a) are cross-correlation functions and the lower curves (b) are time (full lines) and space (dotted lines) correlation functions.

VOL. 21 1961

Table 2. Measurements of the ground patterns

Echo	Transmitter	No. of observations	Major axis (km)	Axial ratio	Direction of major axis
90 km	Tx_{800}	21	7·9	1·6	37° W of N
	Tx_{1110}	12	7·8	1·6	33° W of N
	Tx_{1670}	11	13·1	2·3	38° W of N
E	Tx_{800}	10	5·4	3·1	31° W of N
		3(D)	5·8	2·4	42° W of N
F	Tx_{800}	29	6·7	3·9	29° W of N

(D) indicates results obtained during magnetic storms.

ellipses have their major axes in the NW–SE quadrants, and for the *F*-region, all except one are in these same quadrants.

It will be noted that in all cases, the mean direction of the major axis is close to the line joining the transmitter and receiver. In other words, the irregularities in the pattern are elongated in the plane of propagation. The significance of this result will be discussed in the next Section.

7. Theories of Reflection and Scattering at Oblique Incidence

Fejer (1953) has developed a theory of scattering at oblique incidence and finds that the characteristics of the diffraction pattern formed on the ground depend on the shape of the irregularities of electron density responsible for the scattering. The theory is limited to small angle forward scattering in a medium in which the departures of the refractive index from its mean value are small. If the irregularities are in the form of horizontal discs with a horizontal scale much larger than their vertical scale, then the diffraction pattern on a plane parallel to the diffracting screen has no tendency to be elongated, but if the irregularities are spherical, the irregularities in the pattern are elongated in the plane of incidence by a factor which is equal to the secant of the angle of incidence of the wave on the diffracting screen.

If these results are applied to the present observations at oblique incidence, it is found that the results for the 90 km echoes can be explained on the assumption of disc-like irregularities. The small but significant elongation in the NW–SE quadrants would then be explained as due to the small but finite angle between the horizontal plane at the point of reflection in the ionosphere and that at the receiver. The elongation in the plane of incidence which we would expect on this account would be given by

$$r = \frac{\sin(\pi/2 - i + \theta)}{\cos i} = \frac{\cos(i - \theta)}{\cos i}$$

where 2θ is the angular separation of the transmitter and receiver, and i is the angle of incidence on the ground (Fig. 8).

This gives expected axial ratios of 1·3 for Tx_{800}, 1·7 for Tx_{1110} and 3·2 for Tx_{1670} for a reflecting layer at 95 km. The agreement between these values and the

experimental values is good, but the direction of elongation is 7° away from the plane of incidence for Tx_{800} and 13° away for Tx_{1110}. These differences may be attributed to the difficulty of determining the direction of the major axis for ellipses which are only slightly elongated.

This factor of elongation will decrease as the height of reflection increases so that this mechanism alone can not explain the elongation for the echoes from the *E*-region or for the echoes from the *F*-region with Tx_{800} (Table 2). For spherical irregularities, however, the expected axial ratio is 3·2 for a layer at 120 km and 2·6 for 150 km. The experimentally determined values of axial ratio for the echoes returned from heights between 120 km and 150 km are in good agreement with

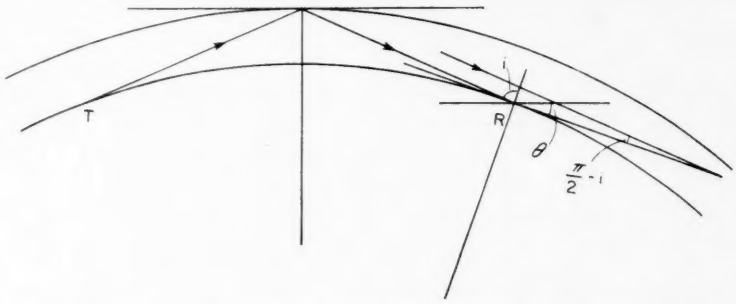

Fig. 8. Diagram to illustrate the elongation of the ground pattern due to the finite angle between the tangent planes at the ionosphere and at the receiver. (Not drawn to scale).

these values and the mean direction of the major axis is within a degree of the plane of propagation. The results therefore, suggest that near 120 km the irregularities are spherical.

In considering the results for the *F*-region, it is found that the elongation which results from scattering from spherical irregularities is inadequate to account for the experimentally determined axial ratio. For a layer at 300 km this factor is 1·6, while the observed axial ratio is 3·9. This suggests that the irregularities in the *F*-region must be elongated.

The scattering from elongated irregularities is considered in the Appendix. It is there assumed that the irregularities are elongated in the form of prolate spheriods lying with their long axes along the lines of force of the earth's magnetic field. Observations on radio star scintillations show that this is a reasonable assumption for the *F*-region (Spencer, 1955; Jones, 1960). The bearing from Cambridge of the transmitter (Tx_{800}) used to observe reflections from the *F*-region at oblique incidence was 30°W of N, while the magnetic declination at the midpoint of the path is 12°W of N. If it is assumed that the magnetic elements are not greatly different in the *F*-region from their values on the ground, then the plane of propagation is close to the magnetic meridian plane, and S_2 is close to zero. The magnetic dip at the midpoint of the path is 70°.

In travelling from the transmitter to the receiver, the upgoing and the downcoming portions of the transmission path make different angles with the earth's field. We assume that the irregularities are situated below the level of reflection so that the rays suffer little deviation in travelling through the region in which the

VOL. 21 1961

irregularities are situated. The direction cosines S_1, S_2, S_3 have values 0·50, 0·31 and 0·84 respectively for the upgoing ray, and 0·92, 0·31 and 0·34 for the downcoming ray, and these rays make angles $\chi = 142°$ and 38° respectively with the horizontal plane. The analysis thus becomes complicated in this case of reflection from the ionosphere as opposed to the case of transmission through the ionosphere. If we make the approximation that S_2 is zero, then we see from Fig. 9(b) that the experimentally determined value of the axial ratio of the characteristic ellipse could be accounted for by irregularities at about 300 km which were elongated by a factor of the order of 3.

In order to test the above theory of propagation at oblique incidence for a direction which is not identical with the magnetic meridian plane, transmissions were arranged from Oslo on a frequency of 2·75 Mc/s during a fortnight from November to December 1959. The bearing of Oslo from Cambridge is 39°E of N and this direction makes an angle of 51° with the magnetic meridian (Fig. 1).

The mean value of the length of the major axis of the characteristic ellipse for seven records was 1·3 km and the mean axial ratio was 2·3. The mean direction of the major axis was 10° E of N. This direction, lying as it does between the magnetic meridian and the plane of incidence, is just what would be expected and the axial ratio, which is smaller than was obtained for the Loran transmitter Tx_{800}, is also in agreement with the predictions of the theory.

8. Horizontal Drifts in the Ionosphere

8.1. *The determination of drift velocities*

The drift velocity V of the ground pattern was determined by the method described by Briggs *et al.* (1950), as extended by Phillips and Spencer (1955). It should be noted that the ionospheric irregularities drift with half the velocity of the ground pattern and in the same direction. The values given below refer to the velocity of the ionospheric irregularities (i.e. $\frac{1}{2}V$).

The importance of random changes relative to pure drift as a cause of fading was also estimated from the ratio $(V_c)_v/V$, where V_c is as defined by Briggs *et al.* and $(V_c)_v$ is the value appropriate to the direction of drift (Fooks and Jones, 1961). The results are for night-time only.

8.2. *Observations*

For the 90 km echo, a total of twenty-nine records were analysed; thirteen were for the transmitter Tx_{800}, eight for Tx_{1110} and eight for Tx_{1670}. There was no preferred direction of drift. The mean value of the drift velocity was 28 m sec^{-1} and the value of $(V_c)_v/V$ was 1·6. For the E-region, seven records obtained during quiet conditions gave a mean drift velocity of 117 m sec^{-1} and the value of $(V_c)_v/V$ was 0·9. There was no preferred direction of drift. A further three records were obtained during magnetic disturbances, and these gave a mean velocity of drift of 384 m sec^{-1}, and a value of $(V_c)_v/V$ of 0·8. On two of the occasions, the direction of drift was within 10° of the West direction, while on the third occasion it was 128°W of N.

For the F-region, nineteen records were analysed, and these gave a mean velocity of 190 m sec^{-1}, and a value of $(V_c)/_vV$ of 0·7. If the velocities are resolved

into NS and EW components, the two components are of the same order of magnitude and the EW component is, except for one occasion, always directed towards the West.

9. Discussion

Some features of the results will now be discussed in more detail and compared with the results of other workers.

Two inseparable effects occur as the transmitter–receiver separation increases; the ionosphere is illuminated more and more obliquely, and the height at which reflection takes place decreases. Any variation of the sizes of electron density irregularities with height would therefore tend to obscure the changes (if any) of the ground pattern due to the effect of obliquity alone. Comparison of the fading characteristics of the Loran signals with vertical incidence results runs up against this difficulty. Vertically incident waves of frequencies in the neighbourhood of 2 Mc/s are reflected from heights of about 105–120 km, while the Loran echoes usually come from near 90 km. Any simple law of the type proposed by King (see Section 3.2) depends on the assumption that the irregularities have the same properties at all heights. However, Bowhill (1956) suggested that the sizes of the irregularities decreases with increase in height in the *E*-region and that the irregularities near 90 km had a size of the order of 6 km, decreasing to less than 0·5 km at a height of 100 km. We should therefore compare the present results for 90 km with results obtained by other workers for low frequencies reflected at about the same level. Similarly, the results obtained on the 120–150 km echoes which appear during and for a few nights after a magnetic storm should be compared with the results obtained at vertical incidence with frequencies near 2 Mc/s.

VOL. 21 1961

Previous measurements of the scale of the pattern for radio waves reflected from near 90 km differ by a factor of the order of 3 for different workers. Thus, Bowhill (1956) gives a space correlogram (Fig. 7 in the paper) for 85 kc/s which falls to 0·5 at a separation of 4 km. On the other hand, Cilliers (1960) obtained a value of 10 km on a frequency of 113 kc/s. These two results are at near vertical incidence. King (1958) in observations at oblique incidence, using a transmitter at a distance of 1500 km and on a frequency of 845 kc/s, found that the correlation fell to 0·5 at a separation of 13 km. In this experiment, the vertical incidence equivalent frequency was 150 kc/s. Brennan and Phillips (1957) also working at oblique incidence on a frequency of 543 kc/s, and with a vertical incidence equivalent frequency of 150 kc/s, found that the correlation fell to 0·5 at a separation of 12 km. By Martyn's theorem, we would expect the signals received by King and by Brennan and Phillips to be from the same heights in the ionosphere and slightly above the level of reflection of the signals received by Cilliers and Bowhill. The equivalent vertical incidence frequencies for the Loran transmissions used in the present work are 490 kc/s for Tx_{800}, 400 kc/s for Tx_{1110} and 340 kc/s for Tx_{1670}, and it is unlikely that the electron density in the night-time 90 km layer is high enough to reflect these frequencies by a gradual bending process. Naismith and Bramley (1951) have ascribed the reflections to partial reflections from irregularities at these heights. Although the values obtained for the ground pattern sizes for the Loran transmissions are smaller than those obtained

by CILLIERS, KING and BRENNAN and PHILLIPS, they are of the same order as the value obtained by BOWHILL.

It has been shown (Table 2) that there is a small increase in the scale of the pattern as the transmitter distance increases from 800 to 1110 km and a larger increase as the distance increases from 800 to 1670 km.

FEJER (1953) has shown that in traversing a scattering medium an incident wave of power density Q_0, say, is progressively scattered until on traversing the whole thickness z_0 of medium, the power density is reduced to Q, which is given by

$$Q = Q_0 \exp(-B_0)$$

where $B_0 = Az_0$ and A is a constant for the medium.

If $B_0 \gg 1$, so that the undeviated portion of the emerging wave is very small, then the diffraction pattern on the emerging wave front has a scale of the order of $L/(B_0)^{\frac{1}{2}}$, where L is the size of the irregularities in the medium. KING (1958) reported that for frequencies greater than about 150 kc/s, the ratio of the undeviated to the deviated component in the downcoming wave is negligible. We would therefore expect the size measured on the ground to be much smaller than the size of the irregularities in the ionosphere.

The drifts in the 90 km region are lower in magnitude than those obtained at vertical incidence on frequencies of about 2 Mc/s (see for example, BRIGGS and SPENCER, 1954). However, these low values are in satisfactory agreement with the values obtained by BOWHILL (1956) for 85 kc/s. BOWHILL also found that the random component of velocity was often of the order of twice the drift velocity and in agreement with the present results. These values for the drift velocity and for the ratio of random velocity to drift velocity also agree with those obtained by the present author in the study of the fading of weak backscatter echoes from the 90 km region at vertical incidence (AWE, 1961).

The echoes from the E-region which is exposed after a magnetic storm, fade at the same rate as the echoes from the E-region observed at vertical incidence; that is with a fading period of the order of 6 sec (see Sections 3.2 and 5.1). At the time of the storm, the echoes fade much faster. The drift velocity is also of the same order of magnitude as that obtained at vertical incidence at about 2 Mc/s.

The fading law suggested by KING (1958) is based on results obtained on the fading of c.w. signals in which no resolution into 90 km and E- and F-regions is possible, although all but two of the results were thought to refer to heights below the F-region because of the low frequencies of the signals. The fine resolution which the narrowness of the Loran pulses makes possible shows that a distinction is necessary between the echoes which come from the residual night-time E-region and those from the 90 km layer. The two fading speeds reported by BOWHILL (1956) in his study of the fading of c.w. signals are probably due to simultaneous reflections from the 90 km layer and the residual E-region. When this distinction between reflections from the 90 km layer and the E-region is made, the result obtained by BELROSE (1957) in his study of c.w. 200 kc/s signals is easily explained. BELROSE observed that the 200 kc/s waves faded rapidly during a magnetic disturbance and that the fast fading continued for the next few nights depending on the strength of the disturbance, provided that the disturbance took place at

night. For a magnetic disturbance during the day, no such increase of fading speed was observed. The experiments on the Loran transmissions reveal that for a disturbance taking place at night, the slow fading 90 km echo disappears, due to the depletion of the electron content at the 90 km level, and in its place there is a faster fading echo from the *E*-region, which increases in fading speed by a factor of about five at the time of the storm. The daytime behaviour of the signals received on the 200 kc/s transmissions during a magnetic storm is explicable if the depletion of the 90 km layer is not sufficiently great to enable the signals to penetrate the layer and be reflected from the *E*-region, due presumably to the much higher daytime electron density in the layer.

We consider next the shapes of the characteristic ellipses for the pattern on the ground. It has already been shown that the results for the 90 km echoes are explicable in terms of disc-like irregularities near 90 km in the ionosphere. King (1958) also came to the same conclusion in his oblique incidence experiments. The slight elongation (of the order of 2) of the ground pattern which he obtained for a transmitter distance of 1500 km is in good agreement with our results and can be explained, as in our case, by the small but finite angle between the horizontal planes at the reflection point in the ionosphere and that at the receiver.

For the echo from the *E*-region (120 to 150 km) the elongation of the ground pattern was ascribed to oblique illumination of spherical irregularities at these heights. In this case, the minor axis of the ellipse should be of the same order of size as the scale of the pattern obtained from experiments at vertical incidence. The mean value of the minor axis is 1800 m, so that the correlation falls to 0·5 for a receiver separation of 900 m. This is rather larger than the value of 400 m obtained for vertical incidence, by Briggs and Phillips (1950), but the agreement is regarded as fair considering the scatter of the experimental values of the pattern size at vertical incidence as presented in histogram form by Briggs and Phillips (1950). Also the present results refer to night-time, while those of Briggs and Phillips were for day-time.

If the irregularities at these heights are spherical, no preferred direction of elongation of the pattern should be observed at vertical incidence, and this is in agreement with experiment (Phillips and Spencer, 1955; Fooks and Jones, 1961).

For the *F*-region, the present results indicate the presence of irregularities which are somewhat elongated along the direction of the earth's field. Such irregularities would also account for the vertical incidence results obtained by Fooks and Jones (1961) in which there was a small but significant elongation of the pattern with the major axis of the ellipse in the NW–SE quadrants in which the magnetic meridian plane also lies.

If the irregularities in the ionosphere are the result of turbulence, we see that the earth's magnetic field has little control over the turbulence which remains isotropic up to 150 km. This is in agreement with the predictions of the theory of turbulence in the ionosphere in the presence of the earth's magnetic field (Golitsyn, 1959; Howells, 1959). There have been reports of the existence of field aligned irregularities in the *E*-region (Peterson *et al.*, 1955; Booker *et al.*, 1955; Heritage *et al.*, 1959; Dyce *et al.*, 1959; Nichols, 1959). These irregularities are

VOL. 21 1961

however special in the sense that they are not in continuous existence and are therefore distinct from the irregularities which are there all the time. The field aligned irregularities might arise from ionization due to bombardment of the ionosphere by charged particles, which, moving along the earth's field could create such irregularities in much the same way as a meteor creates a trail of ionization along its path.

Acknowledgements—I am indebted to the University College, Ibadan, for a Scholarship which enabled me to do this work at the Cavendish Laboratory, Cambridge.

The correlation functions were calculated by the use of the EDSAC computer in the Mathematical Laboratory, Cambridge, by kind permission of the Director.

Thanks are due to the Norwegian Defence Research Establishment for providing pulse transmissions on a number of occasions during the experiments.

I also wish to thank Mr. J. A. Ratcliffe and Dr. B. H. Briggs for their advice and criticism in the course of this work.

The work forms part of a programme for the investigation of ionospheric irregularities, supported by a grant from the Department of Scientific and Industrial Research.

References

Awe O.	1961	*J. Atmosph. Terr. Phys.* **21,** 142.
Belrose J. S.	1957	Ph.D. thesis, Cambridge University.
Booker H. G., Gartlein C. W. and Nichols B.	1955	*J. Geophys. Res.* **60,** 1.
Bowhill S. A.	1956	*J. Atmosph. Terr. Phys.* **8,** 129.
Brennan D. G. and Phillips M. L.	1957	MIT Technical Report No. 93.
Briggs B. H. and Phillips G. J.	1950	*Proc. Phys. Soc. Lond.* B **63,** 907.
Briggs B. H., Phillips G. J. and Shinn D. H.	1950	*Proc. Phys. Soc. Lond.* B **63,** 106.
Briggs B. H. and Spencer M.	1954	*Rep. Progr. Phys.* **17,** 245.
Cilliers W.	1960	*J. Atmosph. Terr. Phys.* **19,** 102.
Dyce R. B., Dolphin L. T., Leadbrand R. L. and Long R. A.	1959	*J. Geophys. Res.* **64,** 1815.
Fejer J. A.	1953	*Proc. Roy. Soc.* A **220,** 455.
Fooks G. F. and Jones I. L.	1961	*J. Atmosph. Terr. Phys.* **20,** 229.
Golitsyn G. S.	1959	*J. Geophys. Res.* **64,** 2212.
Heritage J. L., Weisbrod S. and Fay W. J.	1959	*J. Geophys. Res.* **64,** 1235.
Howells I. D.	1959	*J. Geophys. Res.* **64,** 2198.
Jones I. L.	1960	*J. Atmosph. Terr. Phys.* **19,** 26.
King J. W.	1958	*J. Atmosph. Terr. Phys.* **12,** 26.
Lauter E. N.	1950	*Z. Met.* **4,** 234.
Lindquist R.	1953	*J. Atmosph. Terr. Phys.* **4,** 10.
Naismith R. and Bramley E.	1951	*Wireless Engr* **28,** 271.
Nichols B.	1959	*J. Geophys. Res.* **64,** 2200.
Peterson A. M., Villard O. G. and Gallagher P. B.	1955	*J. Geophys. Res.* **60,** 497.
Phillips G. J. and Spencer M.	1955	*Proc. Phys. Soc. Lond.* B **68,** 481.
Pierce J. A.	1946	*Electronics* **19,** No. 5, 146.
Pierce J. A., McKenzie A. A. and Woodward R. H.	1948	"Loran". MIT Radiation Lab. Series No. 4.

Spencer M.	1955	*Proc. Phys. Soc. Lond.* B **68,** 493.
Watts J. M. and Brown J. N.	1951	*J. Geophys. Res.* **56,** 403.
Yabsley D. E.	1945	CSIRO Report R.P.264/1.

Appendix

Small Angle Scattering from Ellipsoidal Irregularities

The treatment of this problem is an extension of the relevant parts of the paper by Fejer (1953).

In a rectangular system of co-ordinates XYZ, we may represent the auto-correlation function of the irregularities as

$$\rho(x, y, z) = \exp\left[-\left(\frac{x^2}{a^2} + \frac{y^2}{b^2} + \frac{z^2}{c^2}\right)\right]$$

where a, b and c are constants.

A monochromatic electromagnetic wave incident on the medium in which these irregularities are embedded is spread into an angular spectrum $F(s_1, s_2, s_3)$, where s_1, s_2, s_3 are the direction cosines of the direction of scattering. The functions $F(s_1, s_2, s_3)$ and $\rho(x, y, z)$ are Fourier transforms. We therefore have

$$F(s_1, s_2, s_3) = \pi^{3/2}\, abc \exp\left[-(a^2 {s_1}^2 + b^2 {s_2}^2 + c^2 {s_3}^2)^3\right.$$

This leads to the following expression for P, the power scattered per unit solid angle per unit volume per unit incident power density:

$$P \propto \exp\left\{-\frac{\pi^2}{\lambda^2}\left[a^2(s_1 - S_1)^2 + b^2(s_2 - S_2)^2 + c^2(s_3 - S_3)^2\right]\right\}$$

where S_1, S_2, S_3 are the direction cosines of the direction of incidence.

If we have prolate ellipsoids of revolution, so that $a = b = c/r$, then r is the factor of elongation of the ellipsoids so that for spherical irregularities, $r = 1$. We then have

$$P \propto \exp\left\{-\frac{\pi^2 l^2}{\lambda^2}\left[(s_1 - S_1)^2 + (s_2 - S_2)^2 + r^2(s_3 - S_3)^2\right]\right\}.$$

We may transform our Cartesian co-ordinate system (x, y, z) to (x', y', z') such that $x = x'$, $y = y'$, $z = z'/r$, and s_1', s_2', s_3', S_1', S_2', S_3' are such that $s_1 = s_1'$, $s_2 = s_2'$ $s_3 = s_3'/r$, with similar relations for the S.
Then

$$P \propto \exp\left\{-\frac{\pi^2 l^2 \phi^2}{\lambda^2}\right\}$$

where

$$\begin{aligned}\phi^2 &= (s_1 - S_1)^2 + (s_2 - S_2)^2 + r^2(s_3 - S_3)^2 \\ &= (s_1' - S_1')^2 + (s_2' - S_2')^2 + (s_3' - S_3')^2.\end{aligned}$$

If we suppose that the scattering from a thick medium is equivalent to successive scattering from a series of thin layers such that the fraction of the power lost due to

VOL. 21 1961

scattering is the same at successive planes (FEJER, 1953), then it can be shown that after multiple scattering in the thick layer the angular power spectrum is given by

$$W \propto \exp\left\{-\frac{\pi^2 l^2 \phi^2}{B_0 \lambda^2}\right\}$$

where B_0 is a constant for the medium.

If the angle of scattering is small so that $s_1 - S_1$, $s_2 - S_2$ and $s_3 - S_3$ are small, then

$$s_3 - S_3 = -(s_1 - S_1)S_1/S_3 - (s_2 - S_2)S_2/S_3$$

$$\text{and } \phi^2 = (s_1 - S_1)^2\left(1 + \frac{r^2 S^2{}_1}{S_3{}^2}\right) + (s_2 - S_2)^2\left(1 + \frac{r^2 S_2{}^2}{S_3{}^2}\right) + 2\frac{S_1 S_2}{S_3{}^2}(s_1 - S_1)(s_2 - S_2).$$

For simplicity, we limit consideration to the case where $S_2 = 0$. Then

$$\phi^2 = (s_1 - S_1)^2\left(1 + \frac{r^2 S_1{}^2}{S_3{}^2}\right) + s_2{}^2$$

and

$$W \propto \exp\left\{-\frac{\pi^2 l^2}{B_0 \lambda^2}\left[(s_1 - S_1)^2\left(1 + \frac{r^2 S_1{}^2}{S_3{}^2}\right) + s_2{}^2\right]\right\}.$$

The auto-correlation function of the diffraction pattern in a plane perpendicular to the Z-axis is then obtained by taking the Fourier transform of W so that

$$|\rho(\xi,\eta)| \propto \int_{-\infty}^{+\infty}\int_{-\infty}^{+\infty} W \exp\{ik(s_1 - S_1)\,x + s_2 y\}\,ds_1 ds_2$$

where $k = 2\pi/\lambda$.

This gives

$$|\rho(\xi, \eta)| = \exp\left\{-\frac{B_0}{l^2}\left[\frac{S_3{}^2}{S_3{}^2 + r^2 S_1{}^2}\right]x^2 - \frac{B_0}{l^2}y^2\right\}$$

showing that the auto-correlation function drops to e^{-1} in absolute value at a distance

$$\xi = \frac{1}{[B_0 S_3{}^2/(S_3{}^2 + r^2 S_1{}^2)]^{\frac{1}{2}}}$$

in the X-direction and $\eta = 1/(B_0)^{\frac{1}{2}}$ in the Y-direction. Thus the distance at which the auto-correlation function has a given value in a plane perpendicular to the axis of elongation of the irregularities is longer by a factor of

$$\left(1 + \frac{r^2 S_1{}^2}{S_3{}^2}\right)^{\frac{1}{2}}$$

in the plane of incidence than at right angles to it.

If the direction of incidence makes an angle α with the long axis of the ellipsoids, then $S_1 = \sin\alpha$ and $S_3 = \cos\alpha$ so that the factor of elongation of the pattern in a plane perpendicular to the long axis is $\epsilon = (1 + r^2 \tan^2\alpha)^{\frac{1}{2}}$. If we consider the pattern formed in a plane making an angle δ with the long axis of the irregularities, then the elongation ratio of the pattern in this plane is

$$R = \operatorname{cosec}\chi\,(r^2 \sin^2\alpha + \cos^2\alpha)^{\frac{1}{2}}$$

where χ is the angle which the direction of propagation makes with the plane in which the pattern is formed. In the diagram (Fig. A1a), which illustrates the scattering model we are considering here, $\alpha + \delta + \chi = \pi$ so that

$$R = \operatorname{cosec} \chi \, [r^2 \sin^2 (\chi + \delta) + \cos^2 (\chi + \delta)]^{\frac{1}{2}}.$$

The variation of R with χ is shown in Fig. A1(b), for the case $\delta = 70°$, and for several values of r. The restriction of consideration to the case of $S_2 = 0$ amounts to

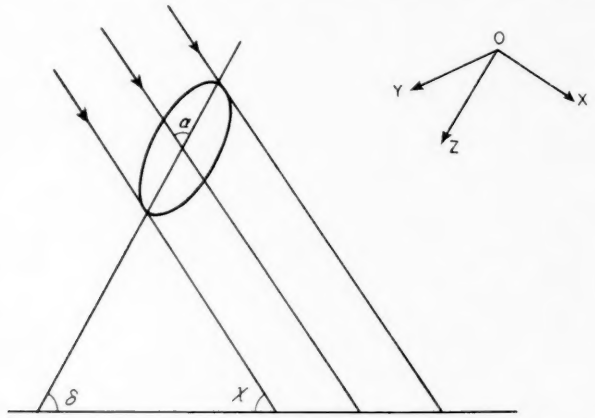

Fig. A1(a). Diagram illustrating the scattering model for elongated irregularities.

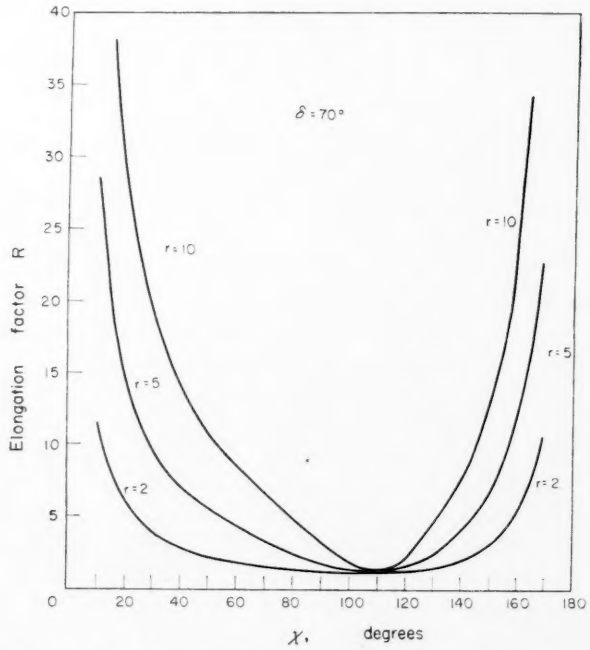

Fig. A1(b). Variation of the elongation of the ground pattern with the elevation of the source and the elongation of the irregularities.

VOL. 21 1961

limiting the result to cases where the plane of propagation contains the long axis of the ellipsoid.

For propagation in any other direction with $S_2 \neq 0$, the long axis of the elongated pattern formed on a plane perpendicular to the long axis of the irregularities is rotated through an angle θ given by $\theta = \tan^{-1}(-S_2/S_1)$ from the OXZ plane and the elongation factor ϵ is now modified to

$$\epsilon = \left[\frac{1 + (S_2^2/S_1^2) + (2S_2^2/S_3^2) + (r^2S_1^2/S_3^2) + (r^2S_2^4/S_1^2S_3^2)}{1 + (S_2^2/S_1^2) - (2S_2^2/S_3^2) + (2r^2S_2^2/S_3^2)}\right]^{\frac{1}{2}}.$$

Journal of Atmospheric and Terrestrial Physics, 1961, Vol. 21, pp. 142 to 156. Pergamon Press Ltd. Printed in Northern Ireland

The fading of radio waves weakly scattered at vertical incidence from heights near 90 km

O. AWE*
Cavendish Laboratory, Cambridge

(*Received* 7 *December* 1960)

Abstract—The fading of radio waves weakly scattered at vertical incidence from heights near 90 km has been studied. Frequencies between 2 and 3 Mc/s were used. The fading rate was found to be of the order of 20 maxima per min, considerably faster than the fading rate for echoes from the normal E-region observed with the same frequency. The correlation between fading records obtained with aerials separated by about one wavelength was found to be small. The shape of the echo was found, on some occasions, to be approximately that expected for reflection from a completely rough screen. These results imply that appreciable energy is returned from directions well away from the vertical. It is shown that the fading is mainly due to random movements of the scattering elements, rather than a steady drift, and the root mean square velocity of the scatterers is found to be about 13 m sec^{-1}.

1. INTRODUCTION

WITH a high-power transmitter and a low-noise receiving site, weak echoes may be observed from the ionosphere down to heights as low as 50 km. Most workers who have studied these echoes have used frequencies near 2 Mc/s, so that in the daytime an echo is also obtained from the normal E-region near 110 km. The weak scatter echoes therefore extend from 50 km up to the echo from the normal E-region. They are usually weak at the lowest heights, and become stronger at greater heights, with a tendency to occur most strongly near 90 km (GARDNER and PAWSEY, 1953). In the present experiments, only this 90 km group of echoes could be observed consistently because, although a transmitter of 180 kW peak power was used, the receiving site had a relatively high noise level. The fading rate of the 90 km echoes is studied in some detail, as well as the spatial characteristics and drift velocity of the diffraction pattern formed on the ground by the downcoming waves. The average shape of the echo is also studied, both experimentally and theoretically.

2. EXPERIMENTAL TECHNIQUES

2.1. *Apparatus*

Transmitter:

Peak power	180 kW
Pulse length	52 μsec
Pulse repetition rate	25 per sec
Aerial	Delta
Frequency	Fixed frequencies of 2·28, 2·33, 2·75 Mc/s

Receivers:

Three receivers were used during the course of the experiments although some of the experiments required the use of only two receivers and some the use of only one. The receivers consisted of three identical converters whose outputs at a frequency of 1·95 Mc/s were fed into separate Loran receivers. Two of these were the

* Now at The University College, Ibadan, Nigeria.

VOL. 21 1961

airborne model AN/APN 4, and the third was the Admiralty model DAS/2. Slight modifications were made to the Loran receivers to obtain satisfactory operation for the conditions of the experiments. The gain of the receivers was changed manually and no automatic gain control was used.

Overall bandwidth	60 kc/s
Receiving aerials	Centre fed horizontal half-wave dipoles resonant at 2·4 Mc/s

Gating unit:

This consisted of two units, a square wave generator whose square wave output had one of its edges coincident with the start of the ground pulse from the transmitter, and a strobe generator which gave a pulse of variable width and variable delay phase-locked to the transmitter ground pulse.

2.2. *Experimental arrangement*

The receiving site was 1 km away from the transmitter, so that incidence on the ionosphere was very nearly vertical. In the spaced aerial experiment described in Section 5 three identical horizontal dipoles were used. These aerials ran parallel to one another and their centres were at the corners of a right-angled triangle whose short sides were 110 m in length. Some simple tests were carried out to see if there was appreciable coupling between the aerials, but these appeared to show that any coupling or interaction was negligibly small. The signals from two of the aerials were taken by coaxial cable to two receivers in a central receiving hut A, and the third had signals from it taken to a second hut B, close to the aerial. The huts A and B were separated by a road, but telephone lines ran underneath the road from one to the other. One of these lines took the square wave from hut A to hut B. From the slightly distorted square wave obtained at the end of the line, a strobe pulse was generated with which the particular echo to be studied could be selected. A similar strobe unit in hut A was used to select the same echo from the other two receivers. The fading signals from the third receiver in hut B were taken back along another line to hut A as a slowly varying voltage produced by peak rectification of the strobed video output. Similar peak rectifiers were used with the two receivers in hut A and the three varying voltages were applied to a three-track pen recorder in hut A. This recorder had a response time of about $\frac{1}{2}$ sec and a maximum chart speed of 12 in/min.

For the faster fading echoes the pen recorder was found to be unsuitable, and recourse was had to photographic recording. Such records were obtained for a pair of spaced receivers by applying the varying voltages from the peak rectifiers to the plates of a double beam oscilloscope. A camera was mounted on this oscilloscope and was provided with a continuously moving film. A film speed of about 8 in/min was normally used, and time marks at 1 sec intervals were produced by the momentary application of a timing pulse to one of the plates. (A typical record obtained in this way is shown in Fig. 5). Fading records at a single receiver could also be obtained photographically by displaying a selected echo on a Loran indicator tube, and arranging a photographic film to move in a direction perpendicular to the deflection. (A typical record of this type is shown in Fig. 2.)

3. Occurrence of the 90 km Echoes

Fig. 1 shows a typical A-scan display of the echoes. In the summer months of June–September 1959, the echoes occurred regularly at virtual heights of about 95 km. The echo from the normal E-region was at a virtual height of about 110 km. In the winter months from October 1959 to February 1960, the echoes were spread in range down to about 90 km, and occasionally to 85 km. Recordings were started on a frequency of 2·33 Mc/s. This was changed to 2·75 Mc/s in the middle of September 1959.

On a few of the days in summer, the 90 km echoes were entirely absent but on most of the days they were present and were about 40 dB weaker than the main echo from the E-region. On very few of the occasions on which records were taken was the mean amplitude of the 90 km echoes comparable with that of the echo from the normal E-region. The echoes persisted until after penetration of the normal E-region, and were then about 20 dB weaker than the echo from the F-region.

In the winter months, the 90 km echoes became stronger and the echo from the normal E-region became weaker due to deviative absorption as the critical frequency of the E-region decreased and approached the working frequency of 2·75 Mc/s. When the presence of an echo from the normal E-region was essential for the investigations, the frequency of the transmitter was changed to 2·28 Mc/s. On all other occasions during the winter, a frequency of 2·75 Mc/s was used.

VOL. 21 1961

4. The Fading Speed of the 90 km Echoes

4.1. *Introduction*

As remarked in Section 3, the 90 km echo has a spread appearance. Fig. 2 shows the fading within the group and it is clear that separate echoes within the group fade independently. At first, an attempt was made to select an echo from within the group. This attempt was however, abandoned due to the fact that echoes from different apparent heights were not resolved. This overlapping of echoes within a group has been reported by Gregory (1956), who remarked that changes of virtual heights of up to 10 km in the course of a fading cycle often occur.

A peak amplitude rectifier, as used in the present work, will pick out the greatest amplitude occurring within the selecting strobe at each instant. Fig. 3 shows simultaneous recordings taken (a) before and (b) after peak rectification.

4.2. *Counting of maxima*

One measure of the fading speed of the group is the number of maxima of amplitude per unit time recorded by a peak amplitude recorder. In the case of a spread echo, this quantity does not have the direct significance which it would have for a discrete echo, since it may be expected to depend to some extent on the number of individual echoes with the strobe pulse at any one time, and also on the duration of the transmitter pulse. Nevertheless, it is of interest to compare the order of magnitude of the fading speed determined in this way with that for normal ionospheric layers. (The effect of the duration of the transmitter pulse is considered further in Section 7.)

In counting maxima on the fading records, it was found to be necessary to use photographic recording, since the smaller maxima were not reproduced on the

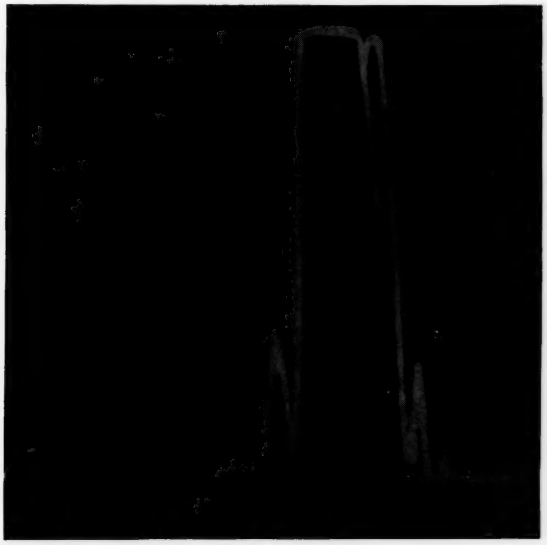

Fig. 1. Photograph showing the 90 km echo and the echo from the normal E-region, on 23 October 1959. The ground pulse is suppressed. Height marks are at 7·5 km intervals.

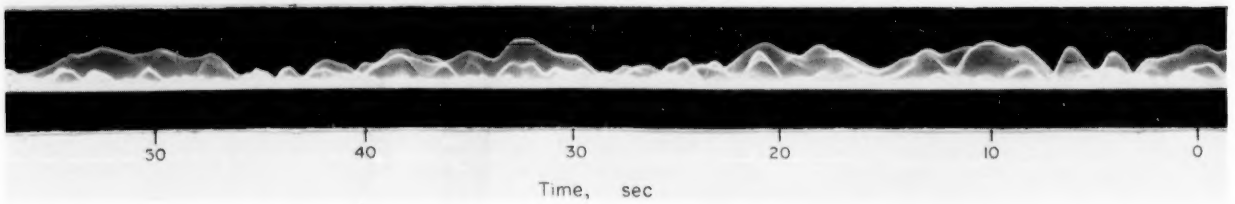

Fig. 2. The fading of the 90 km echoes, 1 February 1960.

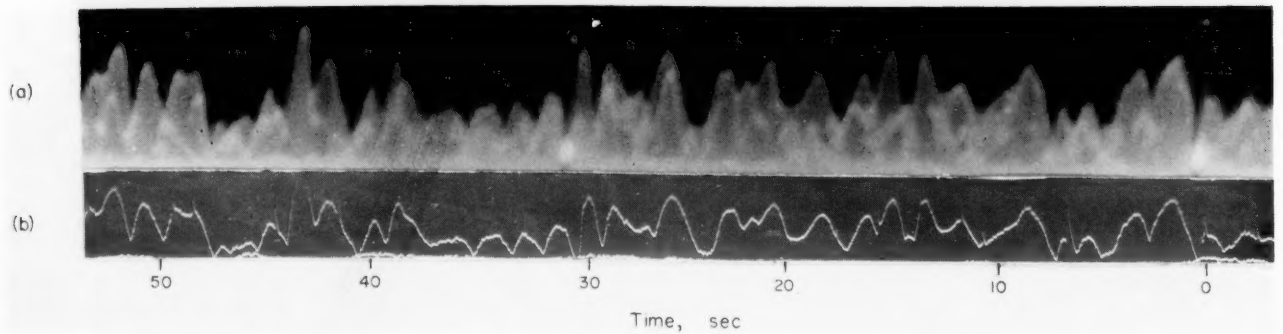

Fig. 3. Fading records to show the effect of peak rectification of 90 km echoes.

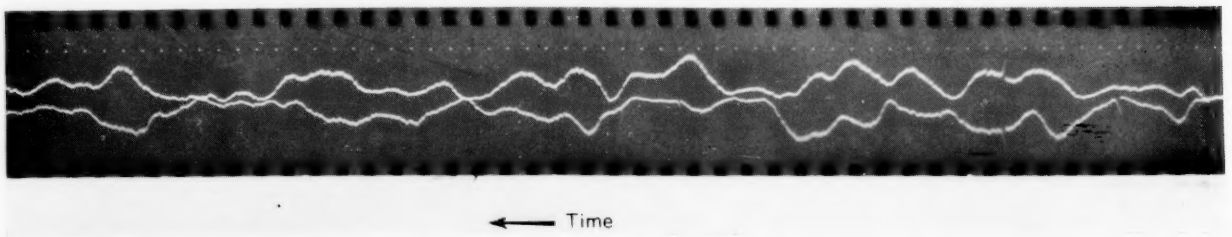

Fig. 5. Fading record for two aerials spaced 110 m apart, 16 November 1959. White spots are 1 sec time marks

pen-recorder. The records used were of the type shown in Fig. 5, which is typical of many obtained from October 1959 to January 1960.

Fig. 4 shows a histogram for the number of maxima per minute observed on different occasions. The mean fading speed was 31 maxima/min. There was some tendency for the fading speed to be higher in winter than in summer. This may be related to the greater spread of the echoes in winter.

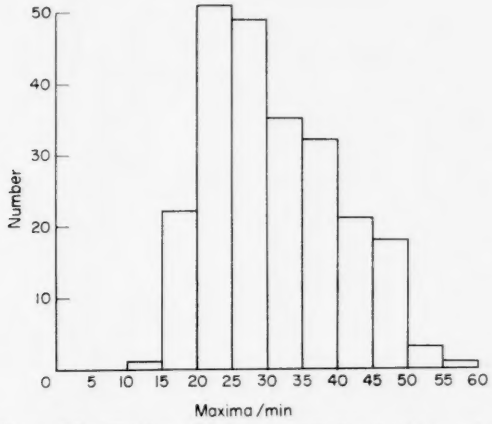

Fig. 4. Distribution of fading speeds for the 90 km echoes.

4.3. *The time auto-correlation function*

A different definition of the fading speed (or its inverse, the fading period) can be obtained by the use of the time auto-correlation function.

This is defined as

$$\rho_R(\tau) = \frac{\overline{R(t)R(t+\tau)} - \left[\overline{R(t)}\right]^2}{\overline{R(t)^2} - \left[\overline{R(t)}\right]^2} \tag{1}$$

where $R(t)$ is the voltage from the peak amplitude rectifier at an instant t, and $R(t + \tau)$ the value at a time τ later. The bars denote averaging over time t. The auto-correlation function measures the average correlation between values of the amplitude measured a time interval τ apart. For a random function of time, $\rho_R(\tau)$ decreases from unity for $\tau = 0$ towards zero as τ increases to large values. For the evaluation of the auto-correlation functions it was again necessary to use photographic recording. Some typical auto-correlation functions are shown in Fig. 6. They were normally of Gaussian form near the origin, but showed oscillations for larger values of τ. These oscillations are within the sampling error limits and are probably not significant.

Since a Gaussian function of the form

$$\rho_R(\tau) = \exp\left(-\tau^2/2\tau_0^2\right) \tag{2}$$

is usually a good fit to the observed auto-correlation functions at any rate down to a correlation of about 0·3, it is convenient to use the parameter τ_0 as a measure of the fading period. Thus we define τ_0 such that $\rho_R(\tau_0) = 0{\cdot}61$, and this definition can

still be used even if the curves depart somewhat from the Gaussian form. The mean of forty-nine independent values of τ_0 evaluated from records taken in the winter months from October 1959 to January 1960 was

$$\bar{\tau}_0 = 0{\cdot}49 \pm 0{\cdot}18 \text{ sec.}$$

It is of interest to compare these results with those obtained for echoes from the normal E-region. The speed of fading of the echo received vertically from the E-

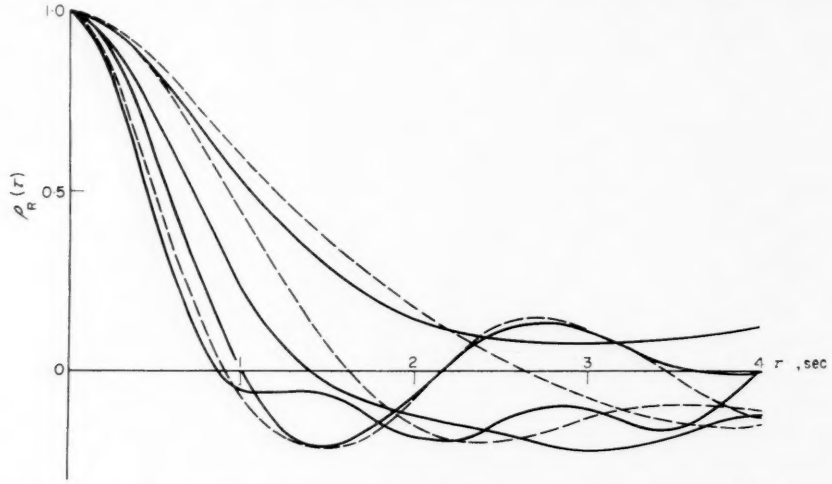

Fig. 6. Time auto-correlation functions of signal amplitude, obtained on several different occasions.

region on a frequency near 2·4 Mc/s was determined in a separate series of experiments, and the results are shown in Fig. 7. Comparison with Fig. 4 shows that the 90 km echo fades much more rapidly than the echo from the E-region. A few simultaneous records of the fading of the 90 km echo and the echo from the E-region were

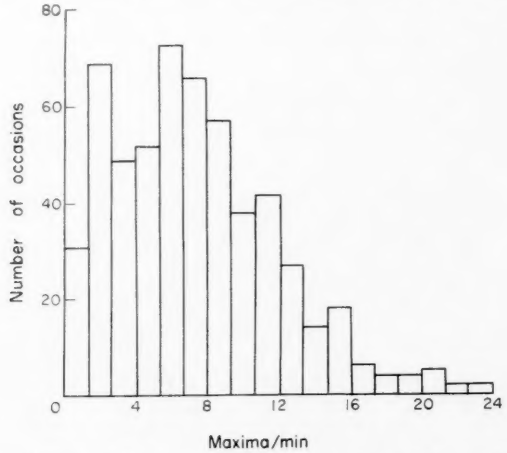

Fig. 7. Distribution of fading speeds for waves reflected from the normal E-region at vertical incidence.

VOL. 21 1961

also made; a typical record showing the marked difference in fading speed is reproduced in Fig. 8. This difference supports the view that the 90 km echo has a separate identity and is quite distinct from the echo from the normal *E*-region.

4.4. *Comparison of the results of* 4.2 *and* 4.3

BOWHILL (1956) has shown that if the auto-correlation function is Gaussian in shape, there is a simple relation between the value of τ_0 in equation (2) and the mean

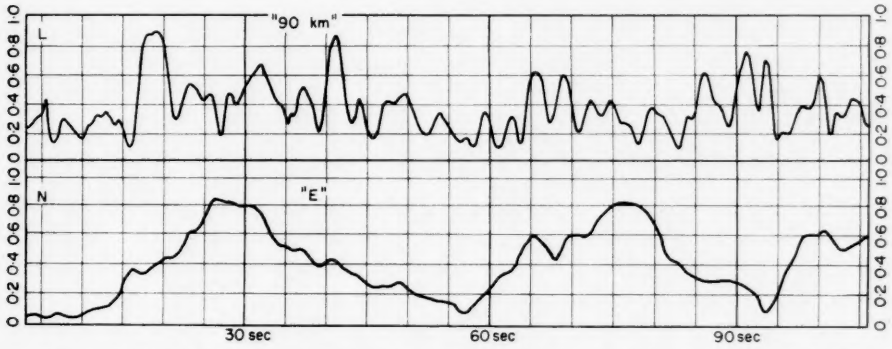

Fig. 8. Fading of the 90 km echoes and the echo from the normal *E*-region recorded simultaneously on the Local (L) and the North (N) aerials, 21 October 1959.

time interval between maxima T. If the amplitude has a Gaussian probability distribution, $T = 3{\cdot}62\ \tau_0$, and if the amplitude has Rayleigh probability distribution, then $T = 3{\cdot}52\ \tau_0$. The difference between these two cases is too small to be important in the present work. It is of interest to apply the results to the values obtained in the proceeding sections. With $\tau_0 = 0{\cdot}5$ sec, we have $T \simeq 1{\cdot}8$ sec, and the number of maxima per minute should therefore be approximately 33. The mean value obtained from the histogram of Fig. 4 is 31 maxima per min, so that there is quite good agreement between the two measures of fading speed.

4.5. *The r.m.s. turbulent velocities of irregularities*

If the fading of the backscattered waves is due entirely to the turbulent motion of irregularities with a Maxwellian distribution of velocities whose r.m.s. velocity has a value v_0, then BOOKER *et al.* (1950) have shown that the time auto-correlation function of signal amplitude is given by

$$\rho_R(\tau) = \exp\left(-16\pi^2 v_0^2 \tau^2/\lambda^2\right)$$

where λ is the wavelength of the incident radiation in the medium. Now if μ is the refractive index of the medium at the frequency of the waves whose free space wavelength is λ_0, then $\lambda = \lambda_0/\mu$ and the normalized auto-correlation function is

$$\rho_R(\tau) = \exp\left(-16\pi^2 \mu^2 v_0^2 \tau^2/\lambda_0^2\right). \qquad (3)$$

A comparison of equations (2) and (3) shows that v_0 and τ_0 are related by the equation

$$v_0 = \frac{\lambda_0}{4\sqrt{2}\pi\mu\tau_0} \tag{4}$$

from which v_0 can be determined if the refractive index μ is known.

While the exact value of the refractive index for a wave frequency of 2·75 Mc/s in the neighbourhood of 90 km is not known, it is believed that this value is near unity. The reasons for this belief are as follows:

Total reflections from these heights are only obtained at low frequencies. Brown and Watts (1954) in their sweep frequency investigations in the low frequency region report the presence of a reflecting stratum in the height range 85–90 km whose upper frequency limit is in the range of 800–900 kc/s. They also mention that another stratum in the height range 98–110 km is sometimes detectable through the lower stratum and that the amplitude of the echo reflected from this upper stratum depends on the shielding provided by the 90 km stratum. Thus the critical frequency of the 90 km stratum is lower than 1 Mc/s.

Another indication of the order of magnitude of the background ionization at these heights is given by the fact that all medium wave backscatter work reported so far shows the presence of a strong echo from the normal *E*-region which is seen through this 90 km region. Table 1 shows the different frequencies used by these workers. The background ionization must be considerably less than critical for all these frequencies. The only results in conflict with this conclusion are those obtained by Titheridge (1959) about an hour before and after noon during which period he considered that waves of frequencies 700 kc/s and 1·42 Mc/s are totally reflected from around 90 km. This claim is however, difficult to reconcile with his other claim of significant stratification above this height during this 2 hr period.

It therefore seems that the critical frequency at this height is less than 1 Mc/s for most of the time and is probably not above about 1·4 Mc/s at any time.

Table 1

Author	Frequency
Dieminger (1954)	Sweep 1·4–4 Mc/s
Gardner and Pawsey (1953)	2·28 Mc/s
Gnanalingam and Weekes (1954)	1·42 Mc/s
Gregory (1956)	1·75 Mc/s
Fejer and Vice (1959)	1·83, 2·63 Mc/s
Titheridge (1959)	70 kc/s, 1·42 Mc/s

The bulk of the fading records were taken within 4 hr centred around noon. It can be shown from the work of Gardner and Pawsey (1953) that at these times the echoes from the 90 km region may be expected to consist almost entirely of the "ordinary" magneto-ionic component. As the working frequency of 2·75 Mc/s is about three times the probable plasma frequency for this component it follows that the refractive index will be very nearly unity.

VOL. 21 1961

With the assumption that the refractive index μ in equation (4) is unity, this equation can be used to determine the value of v_0. The mean value obtained in this way was

$$v_0 = 13 \text{ m sec}^{-1}.$$

This result will only be correct if the velocity of random motion of the irregularities is considerably larger than any uniform velocity of drift which they may possess. It will be shown in Section 5.2 that this is the case.

5. Spatial Characteristics of the Pattern Formed on the Ground by the Downcoming Waves

5.1. *Introduction*

In this section, the observations on spaced receivers will be used to investigate the spatial properties of the irregular diffraction pattern formed over the ground by the downcoming waves from the 90 km region.

Consider first a pair of receivers placed along a fixed line. A space auto-correlation function can be defined for these two receivers, in a manner which is analogous to that used for the time auto-correlation function, viz:

$$\rho_R(\xi) = \frac{\overline{R(x)R(x+\xi)} - \left[\overline{R(x)}\right]^2}{\overline{R(x)^2} - \left[\overline{R(x)}\right]^2}.$$

In this equation, the averaging should strictly be over all possible positions of the pair of receivers along the line. It is impracticable to average in this way, and instead a pair of receivers in a fixed position are used, and the averaging is carried out over time, instead of over space. In other words, the correlation between the two fading records is assumed to give the value of $\rho_R(\xi_1)$ if the receiver separation is ξ_1. The justification of this method for experiments of the present type has been discussed by Briggs (1961).

The auto-correlation function $\rho_R(\xi)$ may depend upon the orientation of the line joining the pair of receivers. In this case, the pattern is said to be anisometric. Briggs *et al.* (1950) and Phillips and Spencer (1955) have shown how the properties of such a pattern may be described by a number of parameters. The complete description includes the mean drift velocity V, and a parameter V_c, of the dimensions of velocity, which is a measure of the rate at which the pattern changes randomly. The spatial properties alone are described by a "correlation ellipse" whose radius gives the separation required for a fixed correlation in different directions. The actual scale of the correlation ellipse is not simply related to the size of the ionospheric irregularities, but its axial ratio will indicate the degree of elongation, if any, of the irregularities which produce the scattering.

Phillips and Spencer (1955) have described a convenient graphical method by which the parameters of the theory can be determined from observations made at three spaced receivers, and this method was used in the present work.

5.2. *Observations*

Most of the observations were made with the photographic method of recording (see Section 4.2 and Fig. 5). With this method only two receivers could be used and

it was therefore not possible to determine the shape of the correlation ellipse. However, the results give a useful measure of the scale of the pattern in one fixed direction. For a receiver separation of 110 m the mean of fourteen independent values of the correlation coefficient was found to be $0{\cdot}14 \pm 0{\cdot}17$. Thus at a separation of one wavelength, the correlation is small. The measured correlation of the ground pattern will be influenced by the aerial polar diagrams used to measure it. With isotropic aerials, the correlation would be less than the value given above which therefore represents an upper limit to the true correlation.

For echoes from the normal E-region, Briggs and Phillips (1950) showed that the correlation was about 0·5 for an aerial separation of 400 m, which, at their frequency of 2·4 Mc/s, is about three wavelengths. Thus we find again a marked difference between results for the 90 km echoes and for the echoes from the E-region. The correlation is much smaller for the echoes from the 90 km region, which implies a much larger spread of angles in the downcoming waves.

Not only is the correlation small for zero time shift between the records but also the cross-correlation functions do not rise to high values for any value of time shift, as would be expected if a drift of the ground pattern was the main cause of the fading. This suggests that drifts of ionization in the 90 km region are not the main cause of fading of the backscattered signals.

Although small correlation existed between the records for most of the time, there were brief periods during which visual inspection of the records suggested a higher correlation than usual. During such periods the echoes also faded rather more slowly, and the three-track pen recorder could be used. By taking records simultaneously on the three spaced aerials, characteristic ellipses were determined.

Eleven specially selected parts of the fading records were analysed. The characteristic ellipses had a mean axial ratio of 1·3 and there was no preferred direction of orientation of the major axes. This was also confirmed by comparing the values of the correlation coefficients for the two perpendicular directions of the short sides of the aerial arrangement which were equal within the errors of measurement. We conclude therefore that the ground diffraction pattern was isometric, and that the scattering irregularities had no systematic elongation on these occasions. Of the eleven records, six showed evidence of drifts in the diffraction pattern, the mean velocity of drift being 40 m sec^{-1} corresponding to a velocity in the ionosphere of 20 m sec^{-1}. The ratio of V_e to V had a mean value of 1·7, indicating again that irregular movements are more important than horizontal drifts in the production of fading for these echoes.

6. The Shape of the Echo

6.1. *The shape expected theoretically for a completely rough scattering layer*

The small scale of the ground pattern found in the preceding Section shows that the downcoming wave is spread through a wide range of angles so that important contributions to the received power come from directions far from the vertical. Fejer and Vice (1959) have also come to this conclusion by a different method of investigation. An extreme example of a scattering screen which will give a wide cone for downcoming wave is the perfectly rough screen. It is of interest to consider the shape of the echo which would result from backscatter from a two-dimensional

VOL. 21 1961

perfectly rough screen at a height h from the ground and to compare the result with the echo shape actually observed.

In Fig. 9 the origin O represents the foot of the perpendicular from the transmitter to the screen. We take an annular element at a distance x from the origin and of width dx. R is the distance of the element from the transmitter and θ the angle OTP. Let $t(\theta)$ represent the transmitting aerial polar diagram for power, and $r(\theta)$ that of the receiving aerial. The completely rough screen scatters power equally

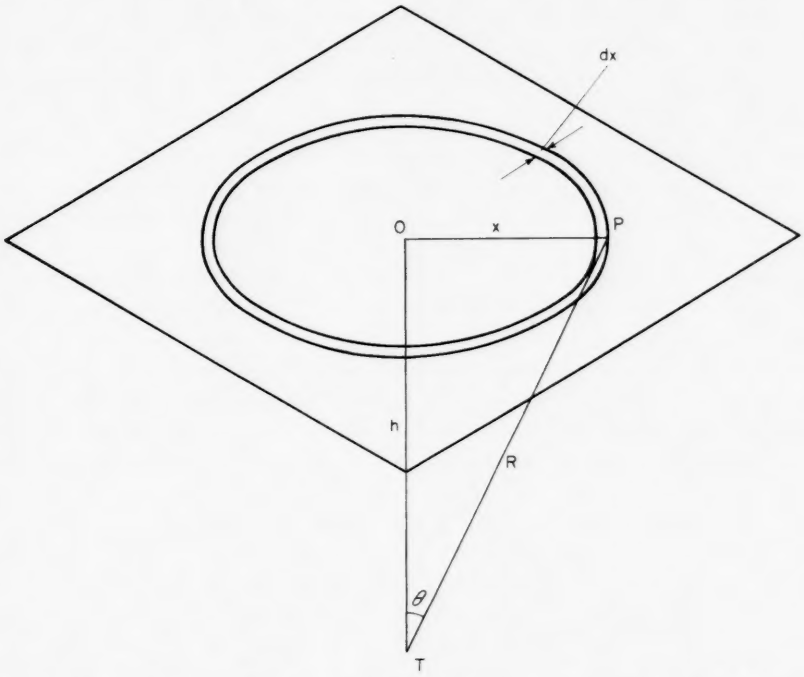

Fig. 9. Diagram to illustrate scattering from a two-dimensional completely rough screen.

in all directions and its polar diagram is therefore independent of θ. Let the screen scatter a fraction σ of the power falling on it per unit solid angle. The area of the element is $2\pi x\,dx$ and the power received by a detector R near the transmitter is

$$dW = \sigma \frac{t(\theta)\cos\theta}{R^2} 2\pi x\,dx \cos\theta \frac{r(\theta)}{R^2}.$$

But $R^2 = x^2 + h^2$, so that $R\,dR = x\,dx$.

Also $\cos\theta = h/R$ and hence

$$dW = kt(\theta)r(\theta)R^{-5}\,dR$$

where k is a constant independent of θ. If we have transmitting and receiving

aerials with isotropic polar diagrams, then $dW = K\,R^{-5}\,dR$ where K is also independent of θ. The energy arriving in the interval of time between t and $t + dt$ is obtained by writing

$$R = \tfrac{1}{2}ct \quad \text{and} \quad dR = \tfrac{1}{2}c\,dt$$

where c is the velocity of the wave.

Hence $$dW \propto t^{-5}\,dt.$$

The mean amplitude which is obtained after smoothing out the fluctuations is proportional to the square root of the energy. In pulse operation therefore, an A-scan display will show a ground pulse followed after a time delay of $2h/c$ by a sharply rising echo whose mean amplitude then decays according to the curve

$$A \propto t^{-5/2}$$

where t is the time delay after the start of the ground pulse.

In the present experiments, the polar diagrams of the aerials were not isotropic. The receiving aerial, a half wave dipole, would, if in free space, have a $\cos^2\theta$ polar diagram in a plane containing the aerial and a circular polar diagram in the perpendicular plane. The presence of the ground introduces an additional $\cos^2\theta$ variation in both planes. We may therefore take an average value of $\cos^3\theta$ for the polar diagram of the receiving aerial.

The transmitting aerial was a delta whose polar diagram was not known exactly. According to Cones (1948), a delta aerial behaves like a loop at low frequencies, and at high frequencies, it behaves like a V antenna. A loop, which is a magnetic dipole, has an average $\cos\theta$ polar diagram and the ground had no effect on its polar diagram.

The effect of the polar diagrams of the aerials is therefore to modify the mean amplitude–time relation to $A \propto t^{-4.5}$.

The above results for the shape of the echo would apply if the transmitter pulse had an infinitely short duration. The actual echo shape is obtained by taking a convolution with a rectangular pulse of duration equal to the duration of the transmitter pulse. The resulting echo shapes are shown in Figs. 10(a) and (b). Fig. 10(a) is for scattering from a single perfectly rough screen of negligible thickness. Fig. 10(b) is for scattering from two such screens separated by a small distance. It is assumed in this case that only a small fraction of the incident radiation is scattered by the first screen, so that little power is lost in transmission through it. The final decay of the echo in all cases follows approximately the law $A \propto t^{-4.5}$ deduced above, because the finite duration of the transmitter pulse has little effect on this part of the curve.

6.2. *Observations*

Due to the fading of the individual echoes within the group as mentioned in Section 4, an averaged echo shape is best obtained by taking a long exposure photograph of the A-scan display. The time of exposure must be several times longer than τ_0 the period of fading as determined in Section 4.2. Because the spread of the 90 km echoes might be obscured by the presence of an echo from the normal E-region, the photographs were taken when this echo was absent.

VOL. 21 1961

Fig. 11(a) shows one such photograph. Many of the photographs so obtained show this characteristic spread in range, although the amount of spreading varied from one photograph to the other. We note the sharp rise of the echo at a delay corresponding to a height of 90 km and the gradual decay after the maximum of the echo is passed.

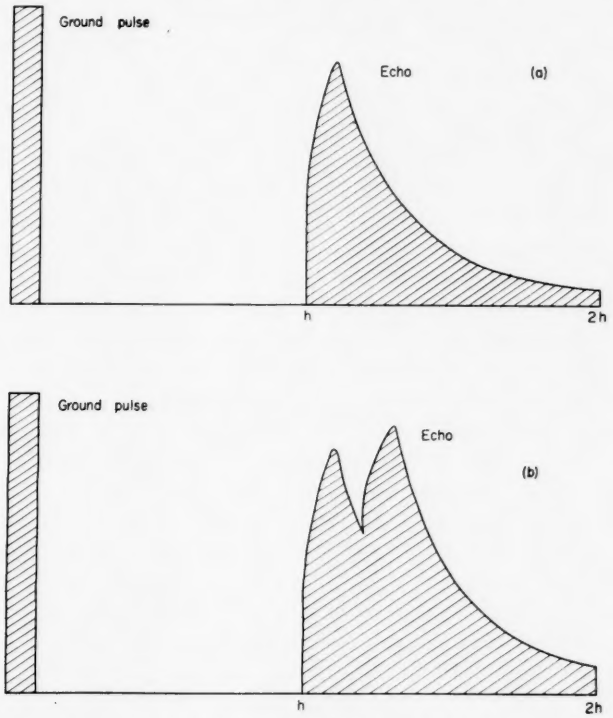

Fig. 10. Theoretical shape of the echo. (a) The shape of the echo expected for scattering from a single, thin, completely rough screen. (b) The shape of the echo when two such screens are present at different heights.

The decaying part of the echo in Fig. 11(a) is found to follow a relation

$$A \propto t^{-n}, \quad \text{where} \quad n = 4{\cdot}3.$$

The approximate agreement with the preceding theory suggests that on this occasion the scattering region behaved like a completely rough screen. It implies that important contributions to the received signals came from far away from the vertical direction. The alternative explanation would be to suppose that the echoes came from the actual heights indicated by the time delays. With this assumption, important scattering would exist up to 170 km, which seems unlikely.

Fig. 11(b) shows an occasion where spreading is superimposed on a stratification of the echoes while Fig. 11(c) shows an occasion where the evidence points to a clear case of stratification in two distinct layers.

Changes from one form into another were frequent.

7. Discussion

Some of the results obtained in the present work may be dependent upon the particular duration of transmitter pulse which was used. This point will therefore be considered in some detail.

Consider first the results relating to fading speeds. If the fading were due mainly to horizontal drifts, it might be expected that the fading speed would vary with the duration of the transmitter pulse. This can be seen most simply by considering the fading to be due to Doppler shifts of frequency produced by the moving scatterers (Ratcliffe, 1948). The maximum Doppler shift would be produced by those scatterers which are at a maximum angle from the vertical. Thus the strongest part of the echo, which is due to scatterers nearly overhead, would fade slowly and the falling "tail" of the echo, which is due to scatterers at a greater range, would fade more rapidly. Since a peak rectifier is used, the fading will tend to be dominated by the strongest part of the echo, and the fading speed will therefore be less than it would be if all the scatterers could contribute simultaneously. If now, the duration of the transmitter pulse is increased, there will come a time when these contributions all overlap and the fading record will be equivalent to that which would be obtained by the use of continuous waves. Thus the fading speed might be expected to increase as the duration of the transmitter pulse is increased. On the other hand, if there is no horizontal drift, and the Doppler shifts are due to irregular movements of the scatterers, with equal horizontal and vertical components, then the Doppler shifts for scatterers nearly overhead will be the same as for those far away from the vertical direction. In this case, the fading speed would be expected to be independent of the duration of the transmitter pulse, provided only that this is long enough for the contributions from several individual scatterers to overlap in time. Since it has been shown that the effect of random movements predominates over the effect of horizontal drifts, there is reason to believe that the results for the fading speeds will not depend greatly on the duration of the transmitter pulse. The value of 13 m sec^{-1} for the root mean square velocity of the scatterers should therefore be fairly reliable.

It could be objected that the random movements might be mainly in the horizontal direction, as has indeed been suggested by some workers. In this case, the above discussion about the effect of a horizontal drift would apply. The value of 13 m sec^{-1} would then be a lower limit to the possible velocity of the scatterers. Further information on this point could probably be obtained by finding out whether the fading speed does vary with the duration of the transmitter pulse.

We consider next the results for the scale of the diffraction pattern formed on the ground by the downcoming waves. The smallest scale structure of this pattern will be produced by those components of the downcoming waves which lie at a maximum angle from the vertical. Thus by arguments similar to those used above, it may be concluded that the scale of the pattern might be expected to decrease as the duration of the transmitter pulse is increased.

Finally, we consider the measurements of horizontal drifts. It has been shown that, although random movements predominate, there are occasions when horizontal drifts can be measured. The method is therefore a potentially valuable one for the investigation of drifts, and if a low noise site were available, it might be possible

VOL. 21 1961

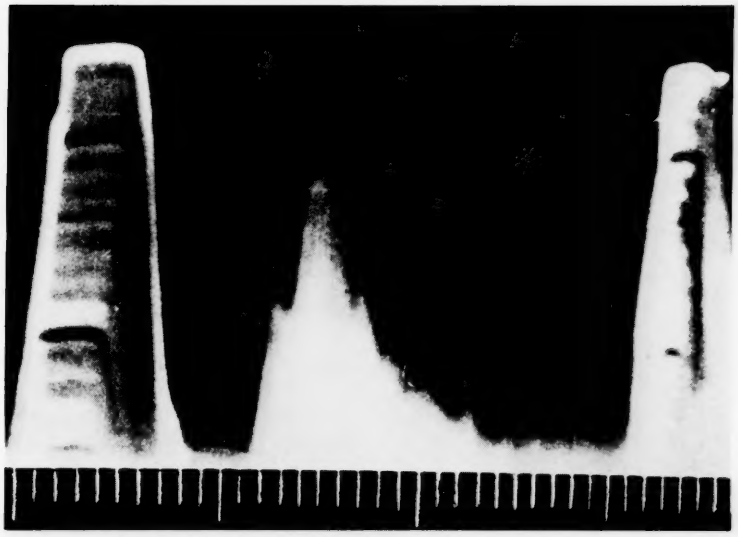

(a)

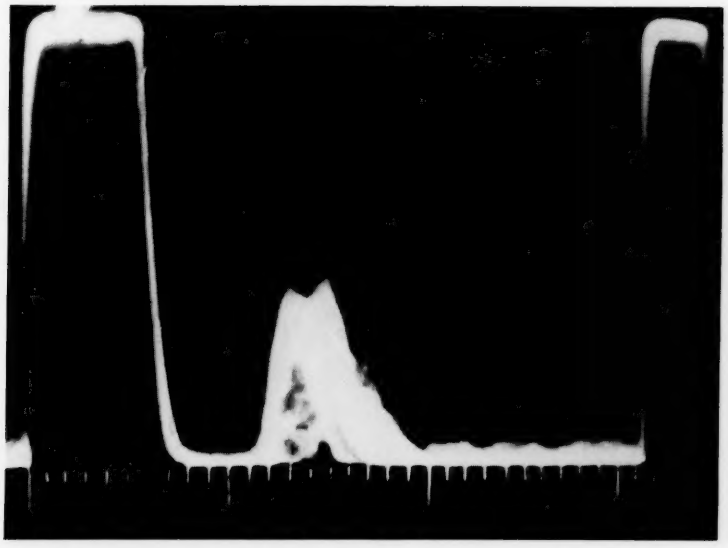

(b)

Fig. 11. The observed shape of the echo. Height marks are at 7·5 km intervals. Photographs taken on (a) 3 February 1960; (b) 14 January 1960;

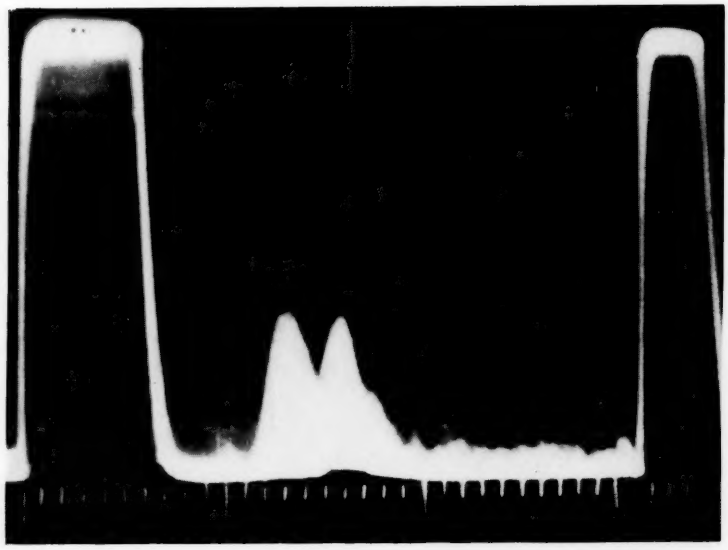

(c)

Fig. 11 (*cont.*). The observed shape of the echo. Height marks are at 7·5 km intervals. Photograph taken on 14 January 1960.

to measure drifts down to heights as low as 55 km. It is therefore of some interest to note that the above uncertainties about the effect of the duration of the transmitter pulse do not apply to the measurement of drifts. It is a feature of the method of drift measurement with spaced receivers that it does not matter what characteristic of the signal is measured at each receiver, provided that the same thing is measured at each point. There is, however, a practical point which might be important. If the duration of the transmitter pulse were very great, the receiving aerials might have to be very close together because of the small scale of the pattern, and this might introduce difficulties due to coupling between them. A spacing of about one wavelength, as used in the present work, is probably about the closest which could be used with safety.

It is of interest to compare the value of 13 m sec^{-1} for the turbulent velocity of the scatterers with the values obtained by other workers. It is in fair agreement with the value of 10 m sec^{-1} obtained by HAGFORS (1959) in his work on oblique incidence scatter transmissions at a frequency of 46·8 Mc/s. KENT (1959) obtained a value of 10–20 m sec^{-1} in similar scatter experiments on a frequency of 37·15 Mc/s. HAGFORS considered that the signals received in his experiments came from heights near 85 km. The agreement between the present results and those from v.h.f. scatter experiments suggests that the same irregularities are responsible for the weak scattered signals observed at medium frequencies and obliquely at very high frequencies. GREGORY (1957) has made the same suggestion from his study of the heights of occurrence and seasonal variations of the two types of signals.

Acknowledgements—The author wishes to thank the University College, Ibadan, for a Scholarship which enabled him to carry out the work described in this paper at the Cavendish Laboratory, Cambridge. The advice and encouragement of Dr. B. H. BRIGGS is gratefully acknowledged. The correlation functions were calculated by the use of the EDSAC electronic computer at the Mathematical Laboratory of the University of Cambridge, by kind permission of the Director. The work forms part of a programme for the investigation of ionospheric irregularities, supported by a grant from the Department of Scientific and Industrial Research.

REFERENCES

BOOKER H. G., RATCLIFFE J. A. and SHINN D. H.	1950	*Phil. Trans.* A **262,** 579.
BOWHILL S. A.	1956	*J. Atmosph. Terr. Phys.* **8,** 129.
BRIGGS B. H.	1961	*Proc. Phys. Soc. Lond.* In press.
BRIGGS B. H. and PHILLIPS G. J.	1950	*Proc. Phys. Soc. Lond.* B **63,** 907.
BRIGGS B. H., PHILLIPS G. J. and SHINN D. H.	1950	*Proc. Phys. Soc. Lond.* B **63,** 106.
BROWN J. N. and WATTS J. M.	1954	*J. Geophys. Res.* **59,** 71.
CONES H. N.	1948	NBS Report CRPL–5–3.
DIEMINGER W.	1954	Cambridge Conference Report, p. 53. Physical Society, London.
FEJER J. A. and VICE R. W.	1959	*J. Atmosph. Terr. Phys.* **16,** 291.
GARDNER F. F. and PAWSEY J. L.	1953	*J. Atmosph. Terr. Phys.* **3,** 321.
GNANALINGAM S. and WEEKES K.	1954	Cambridge Conference Report, p. 63. Physical Society, London.
GREGORY J. B.	1956	*Aust. J. Phys.* **9,** 324.

Gregory J. B.	1957	*J. Geophys. Res.* **62,** 383.
Hagfors T.	1959	*Geofys. Publ.* **21,** 1.
Kent G. S.	1959	*J. Atmosph. Terr. Phys.* **19,** 272.
Phillips G. J. and Spencer M.	1955	*Proc. Phys. Soc. Lond.* B **68,** 481.
Ratcliffe J. A.	1948	*Nature, Lond.* **152,** 9.
Titheridge J. E.	1959	Ph.D. thesis, Cambridge University.

VOL.
21
1961

Journal of Atmospheric and Terrestrial Physics, 1961, Vol. 21, pp. 157 to 166. Pergamon Press Ltd. Printed in Northern Ireland

The radio refractive index gradient over the British Isles

J. A. LANE
D.S.I.R. Radio Research Station, Slough*

(*Received* 13 *January* 1961)

Abstract—Reference atmospheres, specifying the average change of refractive index at radio frequencies with height, are derived from basic meteorological data. The atmospheres are represented by the equation $N_h = N_s.e^{-bh}$, where N_s and N_h are the average values of $(n - 1)\ 10^6$ at the surface and at a height h respectively, n being the refractive index. This exponential relation is in agreement with the results of a series of measurements with a microwave refractometer.

The variations in N_s and b over the British Isles are relatively small in comparison with the changes observed in other areas (e.g. over the United States); however, some local effects are evident which are illustrated in maps of N_0, the average value of $(n - 1)\ 10^6$ at sea level.

A high correlation is found between N_s and ΔN (the average decrease in the first kilometre) but ΔN for a given N_s is slightly smaller for the region of the British Isles than for the United States.

1. Introduction

The importance of a knowledge of the refractive index gradient of the earth's atmosphere has been recognized in studies of tropospheric wave propagation for many years, especially in investigations of non-optical paths. Ideally, a satisfactory explanation of the measured field strength variations on a given link requires a detailed knowledge of the refractive index structure over the whole path throughout the period of observation. Such information can occasionally be obtained by soundings with an airborne microwave refractometer, but the extensive facilities which are required limit the applications of the technique. Many problems, therefore, can only be analysed at present on a long-term statistical basis using meteorological data; a typical example being the study of the seasonal variation of v.h.f. field strength at points beyond the horizon. In such analysis, the radio engineer needs a knowledge of the average gradient of the refractive index above the earth's surface, as a function of location and season. It is the purpose of this paper to provide this information for the area of the British Isles. Apart from their importance in propagation studies, the results have valuable applications in the calculation of possible errors in range and elevation angle which may be experienced with precision radar equipment (Bean and Thayer, 1959; Fannin and Jehn, 1957).

2. Exponential Reference Atmospheres

The effect of atmospheric refraction on the propagation of radio waves has frequently been discussed in terms of an effective earth radius which is greater than the actual value. This concept leads to considerable simplification in the calculation of field strengths on a given path, since the problem reduces to one of rectilinear propagation over a hypothetical spherical earth having a radius of say k times the actual value. k is given by:

$$k = \left(1 + \frac{a}{n} \cdot \frac{dn}{dh}\right)^{-1} \tag{1}$$

where a = radius of the earth
n = refractive index (about 1·0003 at ground level)
dn/dh = vertical gradient of refractive index.

* Official communication.

Putting $a = 6300$ km, and $dn/dh = -40 \times 10^{-6}$/km, we find $k = 1{\cdot}33$, the value generally adopted. This procedure involves an assumption that n decreases linearly with height, and unrealistic values of n are consequently obtained at heights of several kilometres. Fortunately, no serious error results in many applications since, as BEAN and THAYER (1959) have pointed out, a large fraction of the total bending of a ray occurs in the first kilometre above the earth's surface (especially for rays leaving the earth tangentially). However, there is now considerable evidence that a model atmosphere defined by an exponential variation of n with height gives good agreement with experimental data at heights up to several kilometres at least (BEAN and THAYER, 1959). In fact, a standard reference atmosphere, based on this model has been formulated by the International Radio Consultative Committee (C.C.I.R.) for use in studies of tropospheric wave propagation.

An exponential reference atmosphere has the form:

$$N_h = N_s e^{-bh} \tag{2}$$

where N_s and N_h are the values of $(n - 1)\ 10^6$ at the surface and at a height h respectively. N_s and b can be determined statistically for various climatic regions.

The C.C.I.R. basic reference atmosphere is specified by:

$$N_s = 289;\ b = 0{\cdot}136.$$

However, the monthly mean values of N_s and b over the earth's surface (say $\bar{N}_s$ and $\bar{b}$) range from 250 to 400 and from 0·12 to 0·19 respectively (BEAN and HORN, 1959). The determinations of appropriate local values of these parameters is consequently of interest, not only in relation to refraction effects but also in general studies of climatology.

It may be mentioned here that an independent confirmation of the validity of the exponential form of reference atmospheres is provided by the results of soundings made with a microwave refractometer over Southern England in 1959 (LANE *et al.*, 1961). Fig. 1 illustrates a comparison between the experimental measurements, derived from thirty profile flights with a refractometer during the period June–September 1959, and calculated values based on an exponential atmosphere. Also shown is the gradient of refractive index corresponding to an effective earth radius of 1·33 times the actual value. The measured values of N at a given height, and the initial gradient, are somewhat greater than those given by the C.C.I.R. standard atmosphere; however, they can still be represented by a relation of the form $N_h = N_s e^{-bh}$. The experimental technique followed in the airborne measurements has been described by LANE *et al.* (1961).

2.1. *Derivation of $\bar{N}_s$ and $\bar{b}$*

The reference atmospheres were calculated from the data obtained from the radio sonde stations of the Meteorological Office. Monthly mean values of N_s and b, $(\bar{N}_s, \bar{b})$, were derived from the individual readings of pressure, temperature and dew-point, the final figures being the mean for the period 1951–1955. In order to facilitate comparisons with other results, the mean value of N at a height of 1 km was first determined, and this was then used with the surface value, N_s, to determine the parameter b.

VOL. 21 1961

Most of the calculations were based on the soundings made at the 850 mb level ($h \simeq 1{\cdot}3$ km), these values then being reduced on a linear basis to give initial values for a height of 1 km. The latter were then modified by a small correction term to allow for the non-linearity in the N vs h relationship. We have the equation:

$$\left(\frac{db}{dN}\right)_{1\text{ km}} = -\left(\frac{1}{N}\right)_{1\text{ km}} \tag{3}$$

derived from the exponential profile. Examination of the data showed that the linear reduction process gave a value of N at a height of 1 km which was too large

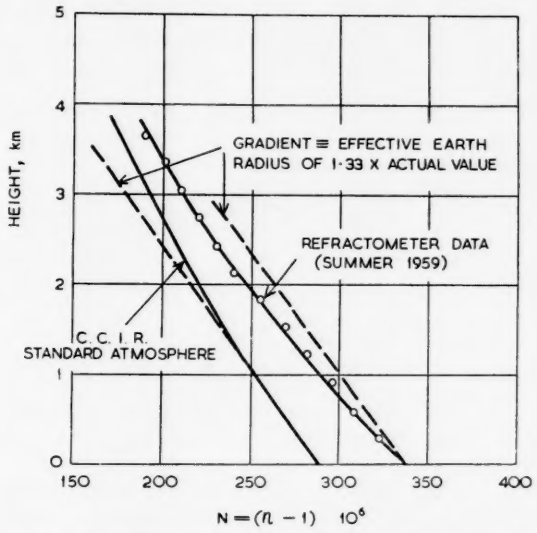

Fig. 1. Comparison of exponential reference atmospheres with refractometer soundings over Southern England.

by 1 N unit, on the average. From equation (3) this change ($dN = 1$) corresponds to a value of db of 0·0036.

Table 1 summarizes the final values of $\bar{N}_s$ and $\bar{b}$ for February, May, August and November for the period 1951–1955, for the various radio sonde stations, at 0200 and 1400 hours G.M.T. Although the variations in the surface value and gradient shown in the table are relatively small in comparison with the corresponding changes observed in say equatorial or monsoon climates, the values given exhibit several features of interest which are discussed in detail below.

2.2. *Variation in average gradient*

The results quoted by Bean and Thayer (1959) suggest that a high correlation exists between $\bar{N}_s$ and $\overline{\Delta N}$, the average decrease in the first kilometre. The nature of the correlation for the area of the British Isles is shown in Fig. 2, in which each point is a mean value for one month (February, May, August or November) for one year in the period 1951–1955. The full line shown is that giving the best fit to the data (determined by the method of least squares) and corresponds to a linear

Table 1. Exponential reference atmospheres derived for British Isles

	Station		0200 hours				1400 hours			
			Feb.	May	Aug.	Nov.	Feb.	May	Aug.	Nov.
1	Lerwick	N_s	318	327	336	323	318	325	336	323
	60°08′N, 01°11′W	b	0·135	0·144	0·147	0·139	0·136	0·142	0·147	0·139
2	Stornoway	N_s	322	330	339	326	322	329	338	326
	58°13′N, 06°20′W	b	0·133	0·139	0·143	0·136	0·135	0·136	0·144	0·135
3	Leuchars	N_s	321	330	339	326	319	330	337	325
	56°23′N, 02°53′W	b	0·132	0·138	0·139	0·135	0·130	0·135	0·136	0·135
4	Aldergrove	N_s	320	328	339	325	320	325	337	325
	54°39′N, 06°13′W	b	0·137	0·138	0·145	0·140	0·133	0·133	0·141	0·138
5	Fazakerly	N_s	322	331	342	328	321	327	339	327
	53°28′N, 02°55′W	b	0·134	0·135	0·142	0·138	0·133	0·131	0·138	0·136
6	Hemsby*	N_s	322	332	345	328	321	329	340	328
	52°41′N, 01°41′E	b	0·137	0·137	0·146	0·140	0·136	0·134	0·140	0·141
7	Valentia	N_s	324	332	345	330	323	332	345	330
	51°56′N, 10°15′W	b	0·134	0·140	0·148	0·140	0·133	0·140	0·147	0·140
8	Crawley†	N_s	319	329	341	326	316	326	337	325
	51°05′N, 00°12′W	b	0·141	0·146	0·157	0·145	0·136	0·136	0·146	0·144
9	Camborne	N_s	322	333	346	328	321	333	345	328
	50°13′N, 05°19′W	b	0·138	0·149	0·157	0·142	0·141	0·149	0·154	0·144
10	Weathership "J"	N_s	326	333	343	330	326	332	343	330
	52°30′N, 20°00′W	b	0·134	0·139	0·146	0·137	0·132	0·140	0·144	0·137
11	Weathership "I"	N_s	322	330	337	324	322	330	336	325
	59°00′N, 19°00′W	b	0·133	0·137	0·145	0·134	0·136	0·137	0·143	0·135
	Average for above stations	N_s	322	331	341	327	321	329	339	327
		b	0·136	0·140	0·147	0·139	0·135	0·137	0·144	0·138

* Soundings taken at Downham Market (52°37′N, 00°22′E) before 19 November 1951.
† Soundings taken at Larkhill (51°12′N, 01°48′W) before 19 April 1953.

regression of $\overline{\Delta N}$ on $\bar{N}_s$ over the range indicated. The correlation coefficient determined from Fig. 2 is 0·85.

Part of the logarithmic line given by BEAN and THAYER (1959) for the more varied conditions of the United States is also shown in Fig. 2. For a given value of $\bar{N}_s$, the average values of $\overline{\Delta N}$ over the British Isles and the United States differ by a small but significant amount. The reduction in the average lapse rate found for the British Isles may be regarded as a characteristic of the temperate maritime climate of the area: in fact, this feature is confirmed by data derived from a paper

VOL. 21 1961

by Du Castel and Misme (1957). Their results for $\bar{N}_s$ and $\overline{\Delta N}$ for Trappes (near Paris) are represented by the lower dotted line in Fig. 2. Over the range of $\bar{N}_s$ given (from 310 to 330) the mean line is close to, but slightly below, that given for the British Isles.

These results emphasize the fact that care should be exercised in specifying reference atmospheres for regions of the earth's surface for which adequate measurements of refractive index gradient are not available.

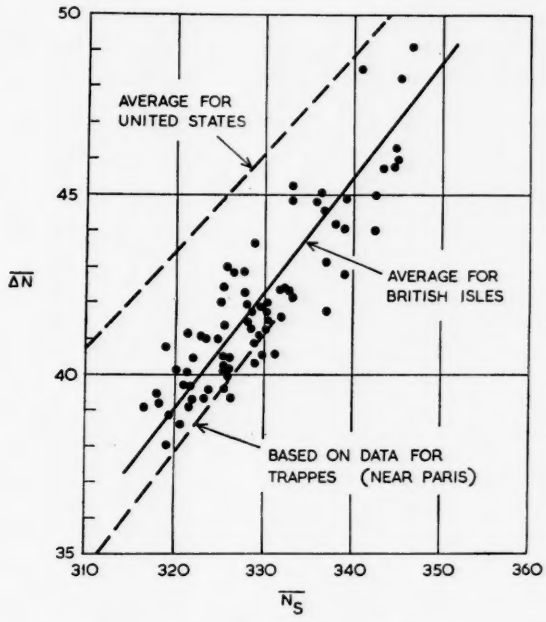

Fig. 2. Correlation of average surface value, $\bar{N}_s$, with average decrease in first kilometre, $\overline{\Delta N}$.

2.3. *Seasonal changes*

The correlation between the seasonal variation of $\bar{N}_s$ and $\bar{b}$ is illustrated in Fig. 3, in which the monthly mean values for 1400 hours are shown for February, May, August and November. Both the surface value and the gradient exhibit maximum values in the summer months, examination of the original data showing that the highest values are reached in either July or August. However, the annual range of $\bar{N}_s$ for both the land and sea stations is relatively small ($\sim$20 N units), and may be compared with the following values for other regions given by Bean and Horn (1959) and by Du Castel and Misme (1957):

Oslo, Norway:	approximate annual range,	18 N units
Paris, France:	approximate annual range,	19 N units
Washington, D.C., U.S.A.:	approximate annual range,	50 N units
Jodphur, India:	approximate annual range,	85 N units

2.4. *Diurnal changes*

There is some evidence of small diurnal changes in the results given in Table 1, and Fig. 4 illustrates the magnitude of these changes. The values of [$\bar{N}_s$ (0200 hours) $-$ $\bar{N}_s$ (1400 hours)] and [$\bar{b}$ (0200 hours) $-$ $\bar{b}$ (1400 hours)] are plotted for the stations given in Table 1, the land stations being arranged in order of decreasing latitude. The results show that:

(1) There is a general correlation between the changes in $\bar{N}_s$ and the changes in $\bar{b}$.

(2) With a few exceptions (e.g. Lerwick and Stornoway), $\bar{N}_s$ and $\bar{b}$ are greater at 0200 hours than at 1400 hours in February, May and August.

(3) Diurnal changes are small for all stations in November.

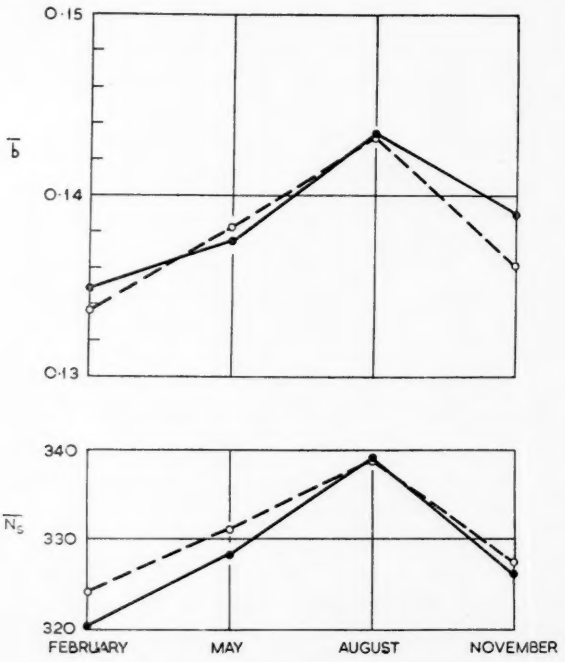

Fig. 3. Seasonal change of $\bar{N}_s$ and $\bar{b}$ for British Isles, for 1400 hours. ($\bar{N}_h = \bar{N}_s e^{-\bar{b}h}$). Land stations, ●; Weather ships, ○; see Table 1.

There is a marked similarity in the refractive index characteristics given for Valentia (7), Camborne (9) and the two Weather Ships (10) (11), in that the diurnal variation for these stations is relatively small. In contrast, marked changes are observed at an inland station (8) in every month except November.

The above examples of local variations can be clarified by a general summary of the geographical changes of refractive index characteristics over the British Isles, and these are discussed in the next Section.

VOL. 21 1961

3. Geographical Variation of Refractive Index at Sea Level

In the previous Sections, reference atmospheres have been discussed in terms of N_s the surface value. In a more general study, it is desirable to remove the dependence of N_s on the height of the ground above sea level in order to clarify the effect

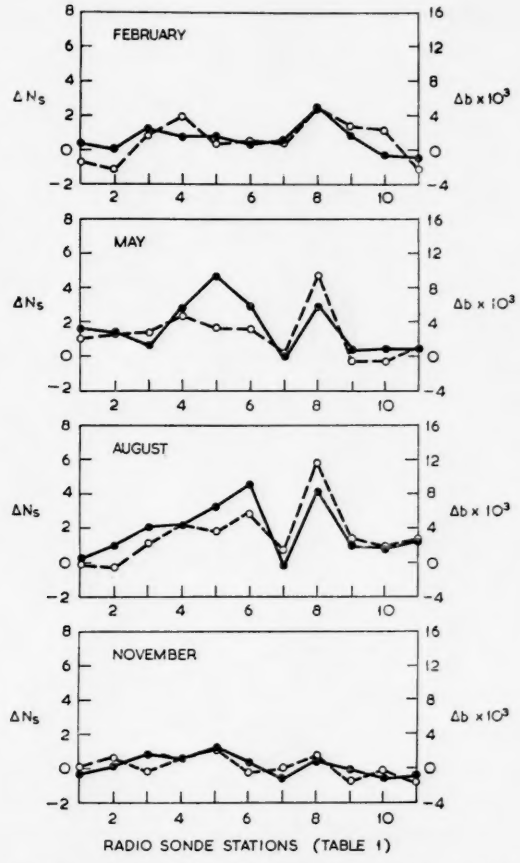

Fig. 4. Diurnal changes in $\overline{N_s}$ and $\bar{b}$ for stations in Table 1 (1951–1955).
●, $\overline{N_t}$ (0200 hours) − $\overline{N_s}$ (1400 hours) = $\overline{\Delta N_s}$.
○, $\bar{b}$ (0200 hours) − $\bar{b}$ (1400 hours) = $\Delta\bar{b}$.

of various climatic conditions. This problem has been considered in detail by Bean and Horn (1959) who derived a reduction formula, based on data obtained in the United States, as follows:

$$N_0 = N_s\, e^{0.1056h}$$

where

N_0 = sea level value of $(n - 1)\, 10^6$ (4)

N_s = surface value of $(n - 1)\, 10^6$

h = altitude of station, in km.

The maximum height of a station in Table 1 is only 144 m and consequently the derivation of a realistic correction factor from the original data is not possible. This is not a serious problem in the present study, however, since the terrain of the British Isles is such that $(N_0 - N_s)$ is generally small, having values of a few N units in S.E. England and about 30 N units in parts of Wales and Western Scotland. In the following discussion, the procedure followed in the *Climatological Atlas of the*

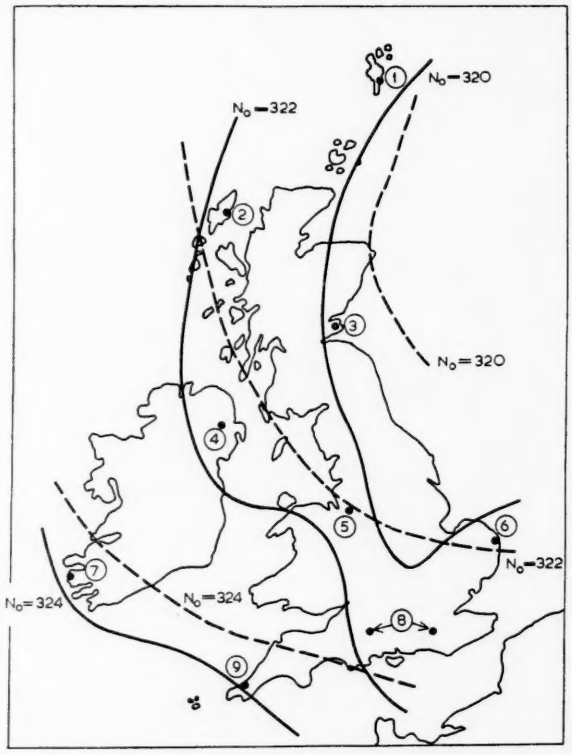

Fig. 5. Variation of $\overline{N_0}$ over British Isles for February (1951–1955).
— — — — 0200 hours. ———— 1400 hours.

British Isles 1952 (H.M.S.O., London) for reducing meteorological readings to sea level values has been used to calculate a reduction formula:

$$N_0 = N_s e^{0.100h}. \tag{5}$$

In the case of the radio sonde station at Crawley ($h = 0{\cdot}144$ km), the corrected N_0, given by equations (4) and (5), differ by 1 N unit.

Fig. 5 shows the variation of $\bar{N}_0$ (the monthly mean value) over the British Isles for 0200 and 1400 hours G.M.T. for February, and Fig. 6 illustrates the corresponding values for August. In both months $\bar{N}_0$ increases from a minimum value in N.E. Scotland to a maximum value in Cornwall and S.W. Ireland, but the range of $\bar{N}_0$ values is greater in August. Furthermore, the direction of the $\bar{N}_0$ isopleths tends

VOL. 21 1961

to change, over much of the area, from S.E.–N.W. in February to E.–W. during August. The displacement between the two isopleths of a given value in either month (i.e. the diurnal change) is generally relatively small in the West and South-West; however, the effect is noticeable in E. and S.E. England in both months and, in addition, in E. Scotland in August.

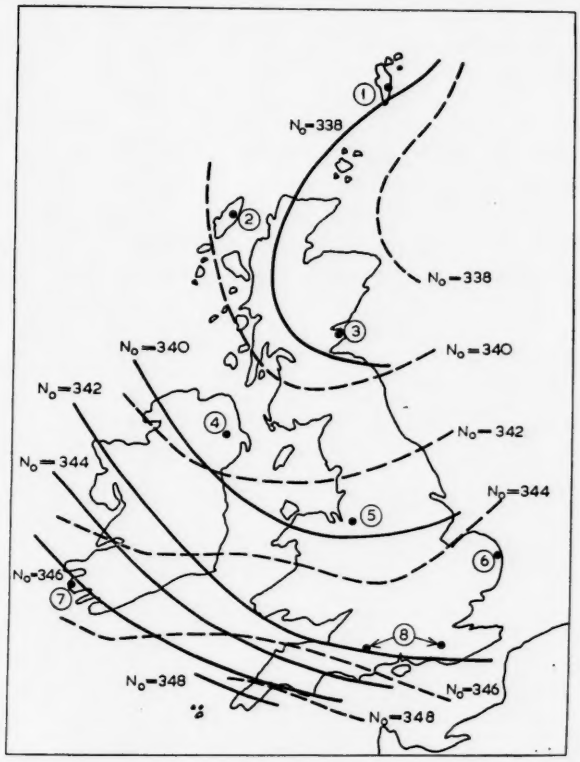

Fig. 6. Variation of $\overline{N_0}$ over British Isles for August (1951–1955).
— — — — 0200 hours; ———— 1400 hours.

4. Conclusions

The results given above enable reference atmospheres to be determined for any region of the British Isles for any season. As might be expected, the climatic conditions over the area are such that the local variations are relatively small in comparison with those observed over say Central Europe or the United States. However, some diurnal effects are evident in the case of the inland stations.

It is of interest, in conclusion, to indicate the magnitude of the changes in average field strength which would arise on a given path as a result of the variations in average refraction discussed above. As an extreme example, the value of k in equation (1) varies from about 1·32 in N.E. Scotland in February to about 1·45 in Cornwall in July or August, the corresponding value of $\bar{N}_s$ being approximately 318 and 346. From some calculations made by Saxton (1951), it can be shown that the

change in mean field strength, ΔE say, produced by the above change in average refraction over a smooth earth at, for example, a frequency of 90 Mc/s, is given by:

$\Delta E_{(db)}$, for terminal heights of 30 m, $\simeq$ 4·5 *db* at 200 km distance
$\Delta E_{(db)}$, for terminal heights of 30 m, $\simeq$ 6 *db* at 300 km distance
$\Delta E_{(db)}$, for terminal heights of 30 m, $\simeq$ 9·5 *db* at 400 km distance

The calculations assume, of course, that the average conditions specified prevail over the whole path.

Acknowledgements—The author is indebted to Dr. J. A. SAXTON for helpful comments on the preparation of the paper. The assistance of Mr. G. W. GARDINER in the analysis of the meteorological data is also gratefully acknowledged.

The work described was carried out as part of the programme of the Radio Research Board. The paper is published by permission of the Director of Radio Research of the Department of Scientific and Industrial Research.

REFERENCES

BEAN B. R. and HORN J. D.	1959	*J. Res. Nat. Bur. Stand.* D **63,** 259.
BEAN B. R. and THAYER G. D.	1959	*Proc. Inst. Radio Engrs, N.Y.* **47,** 740
DU CASTEL F. and MISME P.	1957	*Onde Élect.* **37,** 1049.
FANNIN B. M. and JEHN K. H.	1957	*I.R.E. Transactions on Antennas and Propagation* AP-5, p. 71.
LANE J. A., FROOME D. S. and MCCONNELL G. J.	1961	*Proc. Instn Elect. Engrs* In press.
SAXTON J. A.	1951	*Proc. Instn Elect. Engrs* III **98,** 360

VOL. 21 1961

Journal of Atmospheric and Terrestrial Physics, 1961, Vol. 21, pp. 167 to 173. Pergamon Press Ltd. Printed in Northern Ireland

A long term variation in the relationship of sunspot numbers to *E*-region character figures

R. NAISMITH, H. C. BEVAN and P. A. SMITH
D.S.I.R. Radio Research Station, Slough, Bucks.*

(*Received* 20 *January* 1961)

Abstract—During the last 25 years there has been a progressive increase in sunspot numbers at the maximum of each cycle. Over the same period ionospheric measurements indicate that the *E*-region ionization corresponding to a given sunspot number has decreased. This change has necessitated an adjustment of the empirical constants in the expression relating sunspot numbers to *E*-region character figures which is used in forecasting *E*-region critical frequencies.

1. INTRODUCTION

A DECREASE in *E*-region ionization at noon at Slough corresponding to a fixed sunspot number has been observed in the period 1933–1957. The work described is based upon a consideration of the formation of a layer ionized by monochromatic radiation from the sun (CHAPMAN, 1931). At noon, the rate of production of ionization can be equated to the rate of loss, resulting in the expression:

$$\frac{(f_0E)^4}{\cos\chi} = \frac{\beta S_\infty}{K\alpha H \exp 1} \tag{1}$$

where α = recombination coefficient
H = scale height
K = a constant
χ = zenith distance of sun
S_∞ = intensity of radiation outside the ionosphere
β = number of ions produced per unit intensity of radiation
f_0E = noon *E*-region critical frequency.

The use of the index 4 assumes that the dissipative process is recombination and this value has been used in the following discussion. The expression $(f_0E)^4/\cos\chi$ is referred to as the *E*-region character figure (Ch_E)(APPLETON and NAISMITH, 1939). By using monthly mean values of f_0E the day-to-day irregularities are eliminated and Ch_E, which contains no seasonal term, is proportional to the intensity of solar radiation, provided α, β and H are constant.

A good correlation exists between Ch_E and sunspot number (R) which may be expressed in the form:

$$Ch_E = mR + c \tag{2}$$

where m = slope of regression line of Ch_E with respect to R
c = intercept of Ch_E where $R = 0$.

Predictions of f_0E made at the Radio Research Station, Slough are based on this linear relationship (MITRA 1947) and during almost three sunspot cycles

* Official communication.

(1933–1957) it has been necessary to adjust the constants "m" and "c" mainly in one direction so that for a given sunspot-number the corresponding Ch_E has decreased. This could be due to a long term change in any of the parameters in equation (1). Although it has been shown that the value of the index is a function of the magnetic S_q variation by APPLETON *et al.* (1955) and by BEYNON and BROWN (1956) no known long term changes occur in S_q. There is also no established long term variation in α, β or H. The possibility remains that a change in solar radiation may have occurred. The value of R has steadily increased at the maxima of successive cycles but the decreases of the regression line intercept is confirmed by changes in the measured Ch_E at sunspot minimum. The early measurements of f_0E have been re-checked (and particular attention was given to the elimination of sporadic-E measurements) and no errors which could account for the observed effects were discovered.

2. OBSERVATIONS

2.1. *At Slough*

The available data extending over 25 years have been divided into epochs corresponding to the rising and falling parts of each sunspot cycle. It is convenient

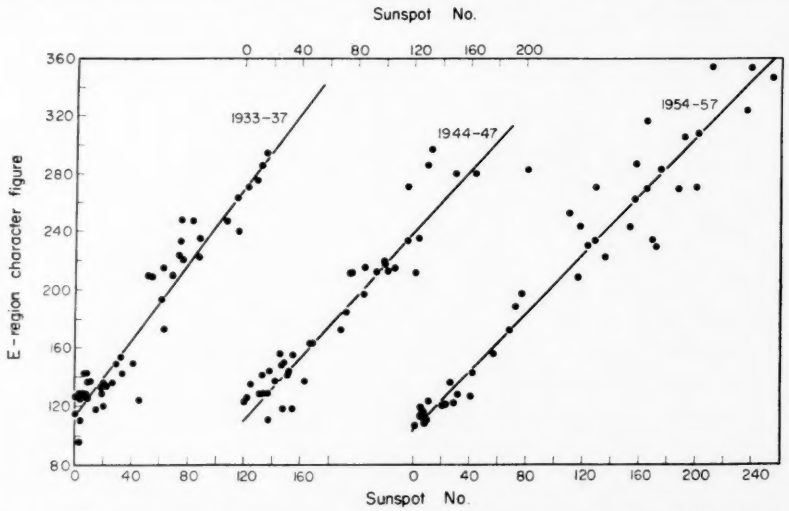

Fig. 1. Monthly average values of E-region character figures for Slough plotted against sunspot numbers and the calculated regression lines.

to call these epochs "half sunspot cycles". The scatter diagrams and the regression lines for the half cycles 1933–1937, 1944–1947 and 1954–1957 are shown in Fig. 1 and the regression lines for all available half sunspot cycles have been calculated and plotted in Fig. 2(a). They indicate that for any given sunspot number the corresponding Ch_E decreases in successive epochs. Thus, for a sunspot number of 100 the Ch_E corresponds at Slough to 243, 223, 217, 207 and 204 in successive half sunspot cycles.

The constants in equation (2) for the period considered are summarized in Table 1 and plotted in Fig. 3 together with the 95 per cent confidence limits.

VOL. 21 1961

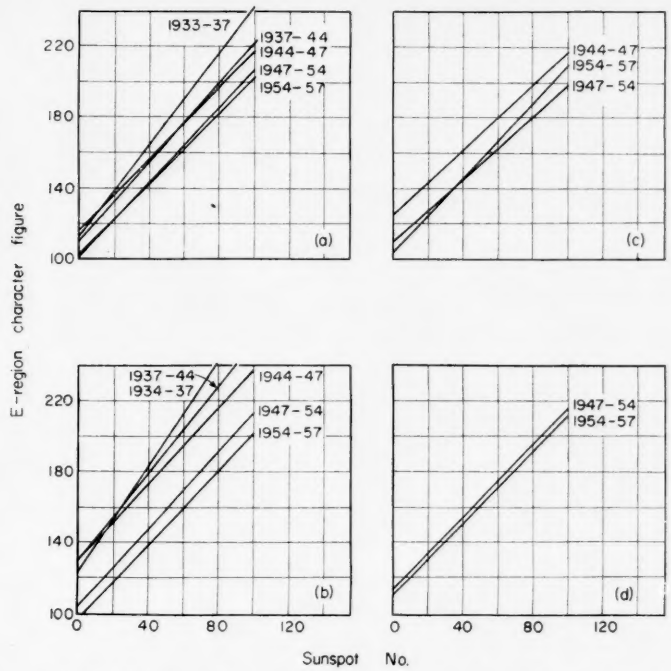

Fig. 2. Calculated regression lines for (a) Slough, (b) Washington, (c) Christchurch and (d) Port Stanley.

Table 1. Intercepts and slopes of Slough regression lines (equation 3)

Epoch	Intercept (c)	Slope (m)
1933–37	113	1·30
1937–44	111	1·12
1944–47	116	1·03
1947–54	103	1·05
1954–57	104	1·00

If this downward trend in both "c" and "m" is significant it should be observed in measurements made in other parts of the world.

2.2. *Other observations*

Washington is the only other ionospheric observatory for which data covering approximately the same period are available. The corresponding regression lines are drawn in Fig. 2(b) and the values for "c" and "m" are plotted in Fig. 4 together with the 95 per cent confidence limits. This diagram shows that a significant reduction in both the slope and the intercept of the regression line has been recorded at Washington over this same 25 year period.

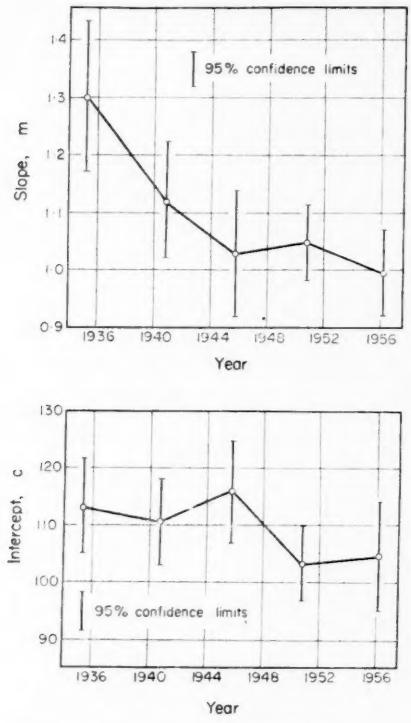

Fig. 3. Variation of slopes and intercepts of regression lines at zero sunspot number and 95 per cent confidence limits for Slough.

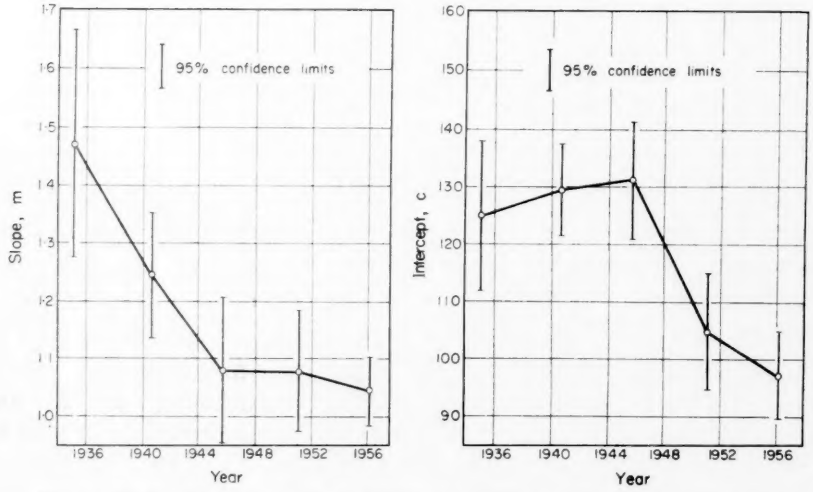

Fig. 4. Variation of slopes and intercepts of regression lines at zero sunspot number and 95 per cent confidence limits for Washington.

VOL. 21 1961

It is desirable to extend this comparison to the southern hemisphere and some measurements are available from Christchurch, New Zealand and from Port Stanley, Falkland Islands. The corresponding regression lines are drawn in Figs. 2(c) and 2(d).

These additional comparisons show that the effect observed at Slough is, in the main, demonstrated in three other widely different parts of the world. The latest measurements from all stations show a decrease in Ch_E when compared with the

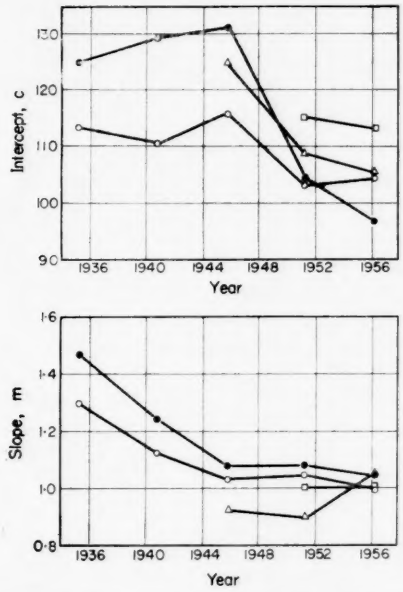

Fig. 5. Relative variation of slopes and intercepts of regression lines at zero sunspot number at Slough (○), Washington (●), Christchurch (△) and Port Stanley (□).

measurements at corresponding earlier points in the sunspot cycle. A plot of all slopes and intercepts (Fig. 5) shows a general decrease in both quantities with time. The progressively slower rate of decrease suggests that it may have a long period cyclic variation and an increase in both the slopes and intercepts may eventually be observed.

3. Critical Frequencies at Sunspot Minimum

Since the intercept is the regression value of the Ch_E when $R = 0$ it is expected that, for a given value of cos χ, f_0E will decrease at successive sunspot minima. This is demonstrated in Table 2 where the noon values are compared for nine stations in February 1944 and February 1954 when the monthly mean sunspot number was very low (0·5). It is calculated from this table that f_0E dropped by an average of 6 per cent in two successive minima.

4. Significance

The predictions referred to in Section 1 may be used to illustrate the significance of the change discussed above. Calculations of the Ch_E corresponding to sunspot

numbers measured in 1954–1957 can be made using separate regression equations in turn. Comparison of these calculated values (which can also be viewed as predictions) with those actually measured show a decrease in the standard deviations with time (Fig. 6). This demonstrates the need to adjust the constants in the regression equation during the period discussed.

Table 2. Critical frequencies for months in which the sunspot number was 0·5

Observatory	February f_0E		
	1944	1954	Difference
Canberra	3·3	3·1	−0·2
Christchurch	3·3	3·1	−0·2
Churchill	2·8	2·5	−0·3
Fairbanks	2·3	2·0	−0·3
Ottawa	2·9	2·8	−0·1
Huancayo	3·6	3·4	−0·2
Slough	2·7	2·6	−0·1
Washington	3·1	2·9	−0·2
Watheroo	3·1	3·1	0

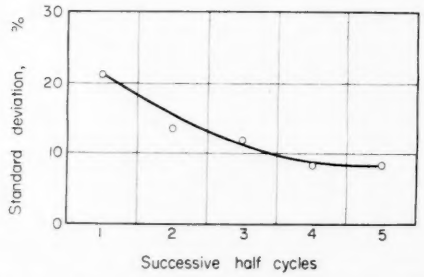

Fig. 6. Comparison of E-region character figure from measured f_0E at Slough with E-region character figure computed from actual sunspot numbers according to the relationships given in Table 1. (Relationships used: 1 = 1933–1937; 2 = 1937–1944; 3 = 1944–1947; 4 = 1947–1954; 5 = 1954–1957).

The 95 per cent confidence limits (Fig. 4) show that the downward trend observed at Washington in both "c" and "m" is significant. Fig. 3 confirms this in regard to "m" for Slough. The computed value of "c" for Slough also shows that there has been a steady reduction although the magnitude of the confidence limits makes the observed decrease less definite. However, this should be considered also in relation to Fig. 6 which shows a steady reduction and it is concluded, therefore, that the reduction is significant at Slough as well as Washington.

5. Conclusions

A study of the relationship of sunspot numbers to E-region character figures reveals a long term variation which is not directly associated with any of the recognized changes in solar activity.

VOL. 21 1961

The average value of the E-region character figure corresponding to a sunspot number of 100 decreased by 16 per cent from 243 in 1933–1937 to 204 in 1954–1957.

The application of the latest known regression line results in more accurate predictions of f_0E.

Acknowledgements—The work described was carried out as part of the programme of the Radio Research Board. The paper is published by permission of the Director of Radio Research of the Department of Scientific and Industrial Research.

References

Appleton E. V., Lyon A. J. and Turnbull A. G.	1955	*Nature, Lond.* **176,** 897.
Appleton E. V. and Naismith R.	1939	*Phil. Mag.* **27,** 144.
Beynon W. J. G. and Brown G. M.	1956	*Nature, Lond.* **177,** 583.
Chapman S.	1931	*Proc. Phys. Soc. Lond.* **43,** 26.
Mitra S. K.	1947	*The Upper Atmosphere*, p. 253. The Asiatic Society of Bengal.

L.
1
61

Journal of Atmospheric and Terrestrial Physics, 1961, Vol. 21, pp. 174 to 176. Pergamon Press Ltd. Printed in Northern Ireland

A criterion for thunderstorm theories

J. A. CHALMERS
Department of Physics, Durham Colleges in the University of Durham

(*Received* 1 *February* 1961)

Abstract—It is shown that thunderstorm theories of the classical type would predict a charging current greater than the external currents, but the reverse is true for theories of the convection type. Such results as are available favour the classical type of theory, but more measurements are required.

1. INTRODUCTION

THE MAIN electrical features of a thunderstorm are the upper positive and lower negative charges, and there have been numerous theories to account for these; such theories have to consider both the origin of the charges and also the mechanism by which they get to the parts of the cloud where they are observed.

There are a number of ways in which these thunderstorm theories can be classified, but in the present discussion we shall consider only a classification in terms of the place of origin of the charges.

In most of the theories proposed, the charges are considered to originate within the cloud; in some theories, e.g. WILSON (1929), the charges are those on ions produced in the region of the cloud; in others, e.g. SIMPSON (1927), it is the precipitation particles from which the charges arise; and in yet others, e.g. WORKMAN and REYNOLDS (1950), it is the interaction of precipitation particles and cloud droplets that is concerned. We shall not discuss the details of these theories, and we can group them all together under the title of "classical" theories.

On the other hand, there are two more recent theories, one due to GRENET (1947, 1959) and, independently, VONNEGUT (1955), and the other to WILSON (1956), in which the charges originate outside the cloud and are brought into the cloud by mechanical and electrical forces. We shall not be concerned with the details of, or differences between, these two theories, but will describe them both as "convection" theories.

2. PRINCIPLE OF BALANCE

Electrical conditions in a thunderstorm vary rapidly, but if averages are taken of the charges and currents over periods of time several times the interval between lightning flashes, it is probable that the values would not differ much between one time during the active period of a storm and another; at any rate, the changes in the average charges would correspond to currents considerably smaller than the average currents. In the further discussion, it will be convenient to use the terms "current" and "charge" for these average values.

If the charges do not alter rapidly, we must consider that there is a balance between the charging current, whatever may be its mechanism, and dissipating currents, including those of lightning discharges.

Also, if there is little accumulation of charge, there must be nearly the same

VOL. 21 1961

current above, within and below the cloud, although there will be different ways in which the current is carried in the three regions.

3. Classical Theories

In those theories we have termed "classical", the charging process consists of positive charges moving upwards in the cloud and negative charges moving downwards, from where these charges have become attached to whatever particle carries them. The charging current is balanced by dissipating currents of various kinds, namely a conduction current above the cloud, a conduction current and lightning flashes within the cloud and point-discharge current and lightning flashes below the cloud. There are certainly a conduction current and usually lightning flashes within the cloud so that the resultant current within the cloud is less than the charging current, and since the currents above and below the cloud are nearly the same as that within the cloud, it follows that the external currents, above and below the cloud, are each less than the charging current.

4. Convection Theories

In the convection theories, the positive charge in the top of the cloud has been drawn up from below the cloud and through it. The negative charge in the base has come from above the cloud and round or through it. If all the positive charge from below reached the top of the cloud and all the negative charge from above reaches the base, then the charging current would be the sum of these two. Above the cloud, there must be, in addition to negative charge coming down, also positive charge moving up, and since the two polar conductivities are about equal, the two contributions to the current above the cloud will be about equal. Although the point-discharge current below the cloud is uni-polar near the ground, there is a negative-ion conductivity below the cloud and at the base of the cloud the current cannot be carried entirely by positive ions; in addition there is a current carried by lightning discharges. So, at most, the whole charging current cannot be much greater than the current above or below the cloud, even if it all reaches its destination. But it is certain that a part of the current of positive ions moving upwards will be used in neutralizing negative charge in the base of the cloud and will not get to the top of the cloud, and the same applied to the negative charge coming downwards; also there are certainly lightning discharges and conduction currents within the cloud. We can therefore conclude without much doubt that the charging current must be less than the external currents, above or below the cloud.

Thus, if it is possible to measure the relative magnitudes of the average charging current in a thunderstorm and the average external current, above or below the cloud, it should be possible to discriminate between the two types of theory. If the charging current is greater, this agrees with classical theories, if external currents then with convection theories.

5. Charging Current

A lightning flash neutralizes all or part of the charges in the cloud and immediately afterwards the charges begin to build up again; if, at that time, there are no dissipating currents, then the initial rate of build up gives the charging current,

and if the charging current remains constant while the dissipating current is proportional to the charge built up, then the recovery of charge, and of external field, follows an exponential law. Wormell (1939), investigating the recovery of field after lightning flashes, found results agreeing with these predictions and deduced that the average value of the charging current for storms in England is about 3 A. It would be most desirable to obtain similar results for storms in other places.

6. External Currents

Measurements of the potential gradient and conductivity at various situations over thunderstorms in the central United States have been made by Gish and Wait (1950) and the integration of the currents gave an average value of 0·5 A. Similar measurements of thunderstorms in Florida by Stergis *et al.* (1957) gave a value of 1·3 A.

Schonland (1928) gave an estimate of 2·2 A for the total current below a thunderstorm in South Africa, but Wormell (1953) has given reasons for thinking this an overestimate and has preferred a value of 0·5 A.

Chalmers (1953) assumed the total current below a thunderstorm in England to be 0·5 A and used this, with values of potential gradients below a typical thundercloud and the relation of point-discharge current to potential gradient, to obtain a value of the effective separation of discharging points; the value obtained was rather less than by other methods. Reversing this procedure and assuming the separation obtained otherwise, the conclusion would be that the total current below a typical English thunderstorm is less than 0·5 A.

VOL. 21 1961

7. Conclusion

There are not yet sufficient results for the charging and external currents of the same thunderstorms to be able to use the criterion suggested here with any certainty. But the results to date are in favour of the classical type of theory and against the convection theories.

It is to be hoped that more measurements will be made to confirm or contradict these results.

References

Chalmers J. A.	1953	*J. Atmosph. Terr. Phys.* **3,** 346.
Gish O. H. and Wait G. R.	1950	*J. Geophys. Res.* **55,** 473.
Grenet G.	1947	*Ann. Géophys.* **3,** 306.
Grenet G.	1959	*Météorologie* **53,** 45.
Schonland B. F. J.	1928	*Proc. Roy. Soc.* A **118,** 252.
Simpson G. C.	1927	*Proc. Roy. Soc.* A **114,** 376.
Stergis C. G. Rein, G. C. and Kangas T.	1957	*J. Atmosph. Terr. Phys.* **11,** 83.
Vonnegut B.	1955	Air Force Cambridge Research Center *Geophysical Research Papers* **42,** 169.
Wilson C. T. R.	1929	*J. Franklin Inst.* **208,** 1.
Wilson C. T. R.	1956	*Proc. Roy. Soc.* A **236,** 297.
Workman E. J. and Reynolds S. E.	1950	*Phys. Rev.* **78,** 254.
Wormell T. W.	1939	*Phil. Trans.* A **238,** 249.
Wormell T. W.	1953	*Quart. J. R. Met. Soc.* **79,** 3.

Journal of Atmospheric and Terrestrial Physics, 1961, Vol. 21, pp. 177 to 181. Pergamon Press Ltd. Printed in Northern Ireland

Aurora and airglow from colour film observations

B. P. SANDFORD
DPL Auroral Station, Private Bag, Omakau, New Zealand

(*Received* 13 *December* 1960)

Abstract—Colour photography with an all-sky camera is a powerful tool for systematic studies of the night-sky emissions. Extensive auroral glows that are not observable visually or on black-and-white film can easily be detected. Type A aurora, usually considered a rare form, may indeed be quite common. The colour of aurora shows some interesting relationships with height effects and magnetic activity.

1. INTRODUCTION

DURING 1959, an Alaskan IGY all-sky camera was operated by SANDFORD and HEISER (1959) at Scott Base, Antarctica (Lat. 77° 51′S, Long. 166° 47′E, Geomag. Lat. 79·0°S). Records were taken on Super Anscochrome colour film on all clear nights from 12 June till the end of the Antarctic night on 8 September.

The term visual aurora used in this paper refers to auroral forms, not close to the horizon, which can be observed by the naked eye or which can be detected on an all-sky camera, recording with black-and-white film, with an exposure giving a sensitivity equal to the naked eye. There is an extensive type of glow which becomes bright enough for naked eye observation only during magnetic storms when it can be observed near the horizon but not high in the sky where its brightness appears less and its contrast low. This type of glow has not been classified as visual aurora even though it is visible to the naked eye on some occasions. Its behaviour at Scott Base is reported in a companion paper by SANDFORD (1961).

During the season June–September 1959, only one aurora was observed visually which showed any other than the usual white or greenish-white colour. This aurora was a brilliant display during the magnetic storm on 17 July 1959. It consisted of very bright white active rayed forms with stationary patches of red glow which appeared among the rayed display but seemed to have no direct connexion with the rayed forms.

On the other hand, the colour film records, during the whole period of observation, showed considerable amounts of colour. These colours were not observed visually, presumably because they were below the threshold for colour vision.

Variations in the density of the night-sky pictures can arise from changes in various factors, i.e. atmospheric extinction, scattering, night-sky emission, moonlight, twilight. A great advantage of colour photography lies in its ability to detect the different colour of the night-sky emissions, the behaviour of which can thus be studied independent of the other factors.

2. REALITY OF COLOUR ON THE FILM

With the long exposures and special processing methods used by SANDFORD and HEISER (1959) it is necessary to be sure that the colours recorded are "real" and not a false representation arising from inadequacies of the film and the processing.

As colour is rarely observed visually at Scott Base, one must check with spectrograms of aurora to find what the colour would be were it only bright enough for the eye to perceive. Sandford (1961) has shown that a major part of the night-sky emissions in the visible spectrum arises from subvisual glows, which are normally too weak to be recorded on the colour film. It is therefore necessary to determine that the spectrum is definitely due to some identifiable feature on the colour film before a comparison can be made.

Occasionally an isolated auroral arc would remain almost stationary and cause a localized intensity enhancement on the spectrogram which could be definitely identified with that arc. In these cases comparison of relative spectral intensities and the colour film records indicated that the colours recorded were a correct representation.

The red observed visually in the 17 July display looked the same red on the colour film. The Milky Way is also recorded as a whitish colour.

The evidence thus indicates that the response of the film is accurate. Recent extensive laboratory tests on the response of Super Anscochrome colour film supports these field observations.

3. Colour of Auroral Forms

The analysis of the colour film shows there are quite distinct types of aurora on a colour classification. Since these colours cannot be observed visually, distinctions of this type have not previously been possible. Four classifications have been recognized.

The first is a white or blue-white type with no trace of any red coloration in or near the form. At Scott Base, most auroral bands and some rays and arcs are this colour. The auroral emissions at 5577 Å and 3914 Å are greatly enhanced in this type.

The second, and most common, is the Type A aurora which has a white lower border and red upper edges. This is considered a rare form by Vegard (1956) and on visual observations alone it certainly is. The colour film observations show that it may actually be the most common type, the upper edges only becoming bright enough for visual colour observations in major magnetic storms.

The third type is the extensive red glow always associated with high magnetic activity. This type can be observed visually only in the biggest magnetic storms. The red glows on 17 July 1959 discussed above are of this type, and Hatherton and Midwinter (1960) also report this type and recognized its association with intense magnetic activity. During smaller magnetic storms the colour film shows this type on many occasions when it is too weak to be seen visually as a coloured form, and of too low a contrast to be observed visually or to be identified from black-and-white all-sky camera records. Colour photography is a very useful tool to study this aspect of the night-sky emission. Such emissions have been reported in spectroscopic studies by Krassovsky (1960) and Sandford (1959, 1961).

The fourth type is coloured red or orange only, with no suggestion of white areas, and is rather rare. Unlike the third type it shows structure, which is usually rayed, and is not closely associated with magnetic activity.

VOL. 21 1961

4. Colour and Auroral Heights

On occasions the white lower border and the red upper section of Type A aurora showed considerable enhancement independent of each other. A section of red would sometimes brighten considerably without any change in the white border below the red enhancement, and vice versa. Sometimes a red arc developed into a Type A, and on other occasions the white lower border of a Type A disappeared to leave a red arc.

On 25 July a red homogeneous arc running in a north–south direction was a prominent stationary feature for many hours. A seemingly independent display of active white aurora was also present on this night. At 1628 hours U.T. there was the red arc running north–south and a white rayed arc running normal to it in an east–west direction. At 1710 hours the red arc developed a white lower border at its southern end which rapidly developed northward along the arc. The white lower border then drifted away from the red arc as a band.

These observations show that one cannot always assume that changes of colour with height in aurora are only height effects of one emission process. The apparently independent motions of different auroral types in the sky at the same time suggest that they either occur at very different heights or originate from different agencies.

5. Colour and Magnetic Activity

Any one auroral colour type could not be uniquely identified with any one auroral form. The colour types have similar diurnal variations. Some association of colour types with magnetic activity was found however.

It has already been mentioned that the extensive red glow is only associated with magnetic storms.

In Fig. 1 the probability of occurrence of white aurora and Type A aurora in the zenith (zenith angle less than 45°), and for quarter-hourly observations for clear moonless nights, is plotted as a function of the Scott Base K-index. The Type A aurora predominates at low magnetic activity and the white aurora predominates at high magnetic activity.

If these types are assumed to be associated randomly with magnetic activity a distribution with K-index can be predicted. The χ^2 test can then be applied to find if the observed distributions differ significantly from a random or chance distribution. It was found that the random and observed distributions differed to a highly significant degree so we can say, positively, that in the zenith at Scott Base Type A aurora are much more likely to be observed at low K-indices and the white aurora are more likely to be observed at high K-indices.

The expansion of the auroral zone during high magnetic activity is expected to cause a decrease of auroral occurrence at a station inside the auroral zone. The decreasing occurrence of Type A aurora at Scott Base with increasing K-index can be attributed to this effect, which implies that the Type A aurora is in some way associated with the agency responsible for the expansion of the auroral zone.

The increase in occurrence of white aurora might be associated with the inner auroral zone. Hatherton and Midwinter (1960) and Hatherton (1960) present evidence which questions the existence of an inner auroral zone at Scott Base. It is possible that the agency responsible for white aurora just becomes more efficient

at high magnetic activity and this effect may or may not be confined to a zone inside the "normal" auroral zone; only more extensive observations can answer this question.

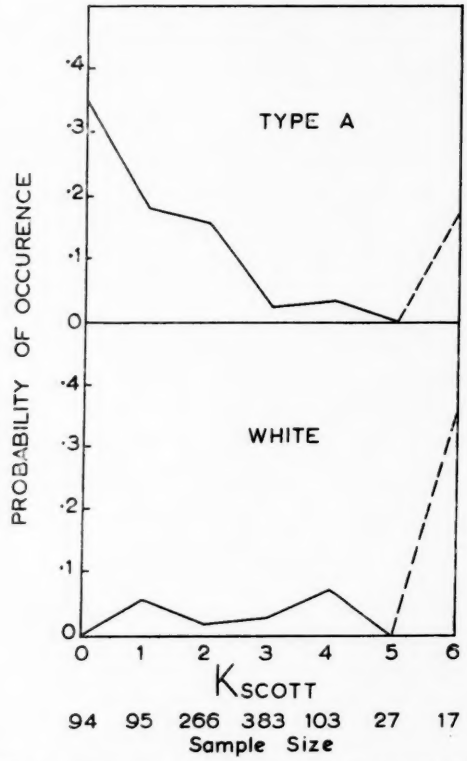

Fig. 1. Probability of occurrence of Type A and white auroral forms in the zenith as a function of the Scott Base magnetic K-index.

6. Conclusions

Routine recording on colour film is clearly a powerful and useful method of studying the aurora. This study has shown that:

There are very distinct auroral types if classified by their colour.

These auroral types exhibit differing behaviour with magnetic activity.

Type A aurora, previously considered a rare form, may be very common.

An extensive red glow is observable which, because of its low contrast, cannot be detected by visual observations or by black-and-white photography, except in the greatest magnetic storms.

The change of colour with height in an auroral form does not seem always to be a simple height effect of one emission process.

It seems quite possible that different agencies are responsible for the different night-sky emissions.

This last observation suggests that the question "Are aurora and airglow the same?" should be restated as, "How many different types of night-sky emission are there?"

VOL. 21 1961

References

Hatherton T.	1960	*Nature, Lond.* **186,** 288.
Hatherton T. and Midwinter G. G.	1960	*J. Geophys. Res.* **65,** 1401.
Krassovsky V. I.	1960	*Vest. Akad. Nauk SSSR* **5,** 10.
Sandford B. P.	1959	*Ann. Géophys.* **15,** 445.
Sandford B. P.	1961	*J. Atmosph. Terr. Phys.* **21,** 182.
Sandford B. P. and Heiser P.	1959	*Nature, Lond.* **184,** 540.
Vegard L.	1956	*Geofys. Publ.* XIX, No. 9.

Journal of Atmospheric and Terrestrial Physics, 1961, Vol. 21, pp. 182 to 192. Pergamon Press Ltd. Printed in Northern Ireland

The behaviour of night-sky 6300, 5577 and 3914 Å emissions at Scott Base, Antarctica

B. P. SANDFORD
DPL Auroral Station, Private Bag, Omakau, New Zealand

(*Received* 13 *December* 1960)

Abstract—The diurnal and seasonal variations and the correlations with magnetic activity of the 6300, 5577 and 3914 Å emissions from the zenith at Scott Base are discussed. There is a marked twilight enhancement of 3914 Å emission. Most of the emissions at these wavelengths do not originate from visible auroral forms but from extensive glows that can only be observed visually or with all-sky cameras during major magnetic storms.

1. INTRODUCTION

FROM May to September 1959, during the Antarctic night, at Scott Base, a patrol spectrograph was operated. The spectrograph is on loan from the Air Force Cambridge Research Centre.

The spectrograph images onto the film a thin strip of sky, from horizon to horizon through the zenith, along a true bearing of 348° at Scott Base. The spectra were recorded on Kodak 103a-F(3) emulsion with a normal exposure time of 2 hr which was reduced to 1 hr or to $\frac{1}{2}$ hr in twilight.

The forbidden oxygen lines OI at 6300 and 5577 Å and the first negative band of molecular nitrogen, N_2^+ at 3914 Å are the only spectral features consistently bright enough to provide data for an extensive statistical study of diurnal and seasonal variations and of correlations with magnetic activity.

2. REDUCTION OF DATA

The equipment and method of analysis is similar to that described by SANDFORD (1959) but with the original automatic exposure control replaced by a mechanical timing system so that exposures of constant length were obtained.

Because of the difficulties involved no corrections for atmospheric extinction or scattering have been applied, but errors arising from these causes have been kept to a minimum by taking measurements in the zenith on clear nights only. Only the central portion of the spectral image emanating from night-sky radiation in the region with a zenith angle of less than 20° has been measured.

As the majority of spectra were obtained with constant 2 hr exposures there is no reciprocity error to consider when comparing these measurements. The $\frac{1}{2}$ hr and 1 hr exposures have been corrected for reciprocity errors using data determined by RUMSEY (1960) from original Kodak data. These corrections agree with the more complete information provided by ROACH *et al.* (1960). ROACH *et al.* criticize photographic measurements of spectral intensities, but with careful control of exposures, development, etc., as has been done in these experiments, very consistent results can be obtained. In SANDFORD'S (1959) original work there is no significant error in the final result even if reciprocity failure is not allowed for.

The density of the spectral lines were measured on a microdensitometer and converted to intensities using the characteristic curve of the emulsion. The characteristic curve was obtained from the tungsten wedge calibration spectrum

which is recorded automatically after each night-sky exposure. From the known spectral distribution of energy from the tungsten lamp producing the wedge calibration spectra it was possible to convert the intensities at various wavelengths to the same intensity scale. In the intensity scale used equal energies at the various wavelengths are denoted by the same intensity.

The intensity scales are in arbitrary units as an absolute calibration of the instrument has not been possible. If we assume that the 5577 Å intensity versus geomagnetic latitude from ROACH (1960) is correct, the median value for Scott Base 5577 Å intensity would be about 1·3 kR, thus the intensity scales in this paper would be in kilo-rayleighs.

Often the intensity of the 3914 Å emission is below the lower limit of measurable intensity. On clear moonless nights there is no background continuum visible and in these cases if 3914 Å emission is too weak to be measured or even detected on the emulsion, the intensity can be recorded as less than 0·15 on the scale used.

3. Influence of Twilight

The zenith intensity of the 6300, 5577 and 3914 Å emissions are plotted in Fig. 1 as a function of the minimum angle of solar depression during the exposure. The intensities have been plotted only from spectra obtained when the Scott Base K-index is not greater than 3 because at higher K-indices there is a considerable enhancement of these emissions.

The twilight enhancement of 6300 Å emission is apparent in both the evening and morning twilights. As aurora is sometimes present during twilight the 6300 Å radiation does not all arise from twilight enhancement and the large scatter of observations is to be expected. The variation of the median values for 6300 Å emission agrees well with MEGILL'S (1960) determination. The evening and morning twilights show the same variation unlike MEGILL'S results, but as he made measurements on only one night and as there is evidence of a considerable night-to-night variation in these results this difference may be of little significance.

No twilight enhancement at 5577 Å is observed. Observations do not extend sufficiently far into twilight to observe the enhancement reported by MEGILL.

There is a very large enhancement of zenith 3914 Å emission in twilight. The enhancement is much greater in the morning than it is in the evening which is possibly due to the presence of visual auroral forms. These have a maximum of occurrence in the morning hours and are responsible for a considerable portion of the night-sky emission at 3914 Å as will be shown later. These observations indicate that N_2^+ ions are present in the region from 100 km to above 300 km and are present at all times at this location inside the auroral zone. The enhancement is very similar to that reported by LYTLE and HUNTEN (1960), REES (1959a) and WEILL (1960).

4. Diurnal and Seasonal Variations

To minimize magnetic influences the diurnal and seasonal variations are plotted only from spectra obtained during periods when the Scott Base K-index is not greater than 3. The medians of the intensities of 6300, 5577 and 3914 Å emissions are plotted in Fig. 2 for each month against Universal Time. (Local time is U.T. plus 11·1 hr.)

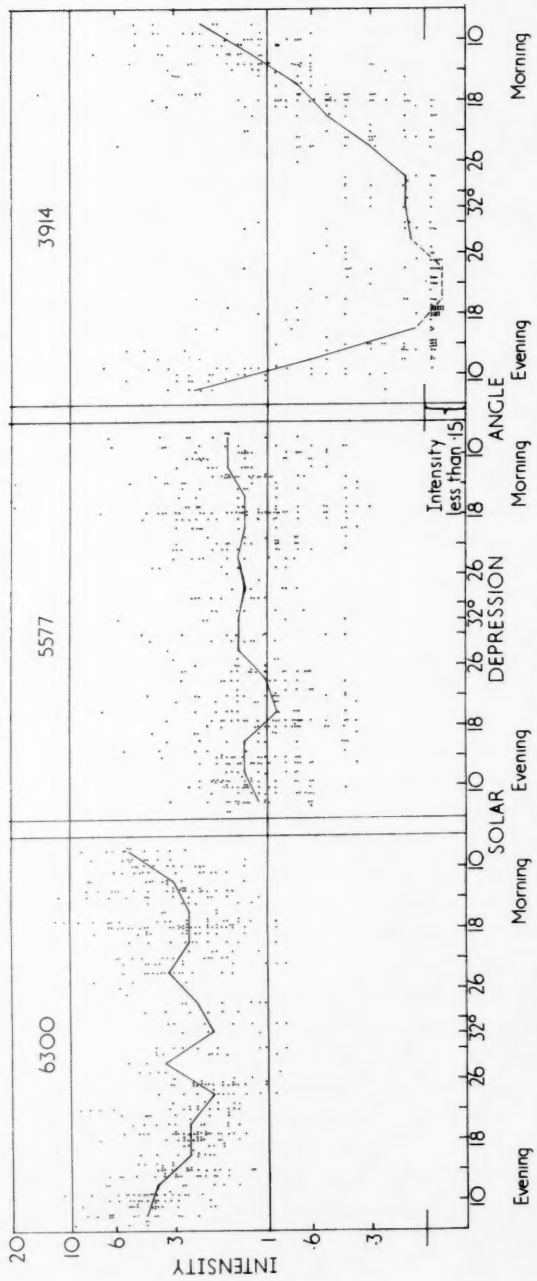

Fig. 1. The zenith intensity at Scott Base of 6300, 5577 and 3914 Å emissions as a function of the minimum solar depression angle during the exposure. Twilight enhancements at 6300 and 3914 Å are evident. Values are given only when the Scott Base K-index is not greater then 3.

VOL. 21 1961

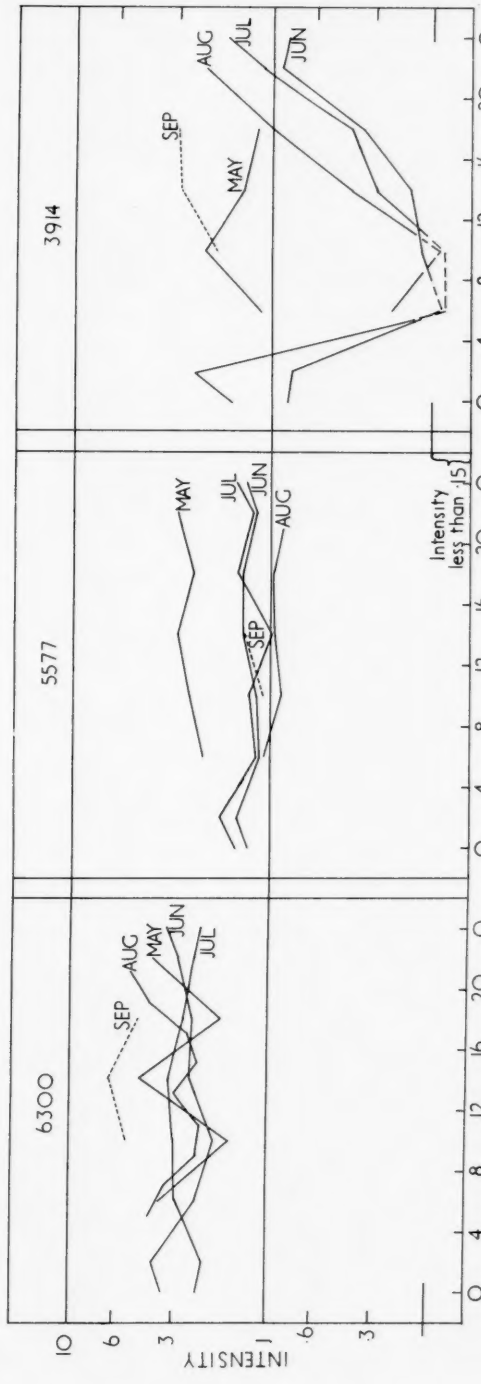

Fig. 2. Medians of the zenith intensity of 6300, 5577 and 3914 Å emissions at Scott Base for each month, as a function of the time of day to indicate seasonal and diurnal variations. Values are given only when the Scott Base *K*-index is not greater than 3.

8—(20 pp.)

The twilight enhancement at 6300 Å tends to be hidden in these plots, because the time of twilight varies considerably in a month at these high latitudes. There is no significant diurnal or seasonal variation of 6300 Å emission additional to the twilight enhancement.

The 5577 Å emission exhibits no diurnal variation but from May till August the median value of intensity drops by a factor of three. The intensity rises again in September but the number of measurements in this month is too small to consider this rise significant.

The 3914 Å emission exhibits a considerable diurnal and seasonal variation which is due to the twilight enhancement already discussed. The evening–morning asymmetry is again very evident.

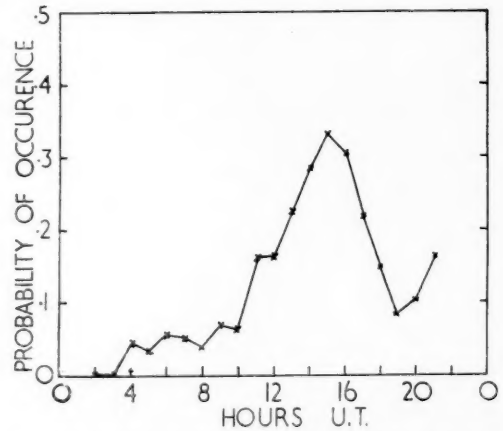

Fig. 3. The diurnal variation of the probability of occurrence of aurora in the zenith at Scott Base.

A significant factor in these three emissions is the apparently independent behaviour of each, particularly the seasonal change in 5577 Å emission which does not occur with the 6300 Å emission. All three are known to be the main features of visual aurora, and yet here they behave as though they were independent. This will be considered further after the magnetic dependence of these emissions has been discussed.

In Fig. 3 the diurnal variation for visual aurora in the zenith (zenith angle less than 40°) at Scott Base for the observing season of 1959 shows a single maximum centred on 1500 hours U.T. (The diurnal variation is the same for all levels of magnetic activity). These observations are taken from all-sky camera records using Tri-X film, an f 1·4 camera and exposures in a cycle varying from 5 sec to 2 min. The evening (local time) maximum reported by HATHERTON and MIDWINTER (1960) and others is not apparent.

The diurnal variations of zenith 6300 and 5577 Å emissions show no tendency towards increased values at the time of the visual auroral maximum of occurrence. This very surprising observation will be considered later. The asymmetry in the 3914 Å diurnal variation can however be explained if the morning increase in

VOL. 21 1961

3914 Å emission is associated with the presence of visual aurora. Evidence to support this will be considered later.

5. Magnetic Variations

Examination of the relationship between the magnetic activity and the spectral intensities of night-sky emissions helps considerably in the understanding of the apparent lack of correlation between visual aurora and spectral intensities.

The term visual aurora referred to in this work is aurora that can be observed with the naked eye or with an all-sky camera using black-and-white film recording

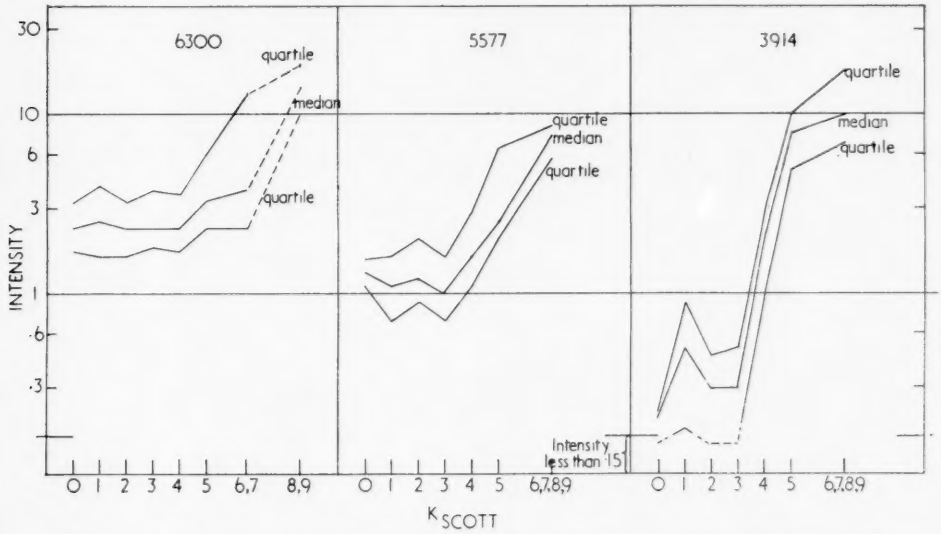

Fig. 4. The medians and upper and lower quartiles of the zenith intensity of 6300, 5577 and 3914 Å emission at Scott Base, plotted as a function of the Scott Base magnetic K-index. Only intensities obtained when the solar depression angle is not less than 18° are included to remove twilight enhancement effects.

with a sensitivity similar to that of the naked eye. Extensive glows sometimes visible near the horizon would not be visible in the zenith due to lack of contrast and intensity. These glows have not been considered as visual aurora although colour film observations and careful visual experiments in the zenith show them to be above the visual threshold on occasions.

The zenith intensities of 6300, 5577 and 3914 Å emissions for Scott Base are plotted in Fig. 4 as a function of the Scott Base magnetic K-index. Twilight enhancement effects have been removed by plotting intensities from spectra obtained when the solar depression angle was not less than 18°. The medians and upper and lower quartiles are given to indicate the general law of the relationship as well as the scatter in the observations. In contrast with Roach and Rees (1960) low values of intensity are rarely recorded at the high K-indices which is probably due to the integrating properties of the photographic recording employed here. The twilight spectra show the same results but at a higher level of intensity for the emissions that are enhanced in twilight.

For all the emissions very little variation of intensity occurs with K-indices below 4. At higher K-indices the emissions steadily increase in intensity, the increase at 3914 Å being particularly large.

Plots of intensity against planetary K-index, instead of the Scott Base K-index, have considerably more scatter which indicates that local rather than world-wide geomagnetic effects are related to the night-sky emissions. It was considered that current systems in the southern auroral zone and consequently geomagnetic activity near the maximum of the southern auroral zone may be associated closely

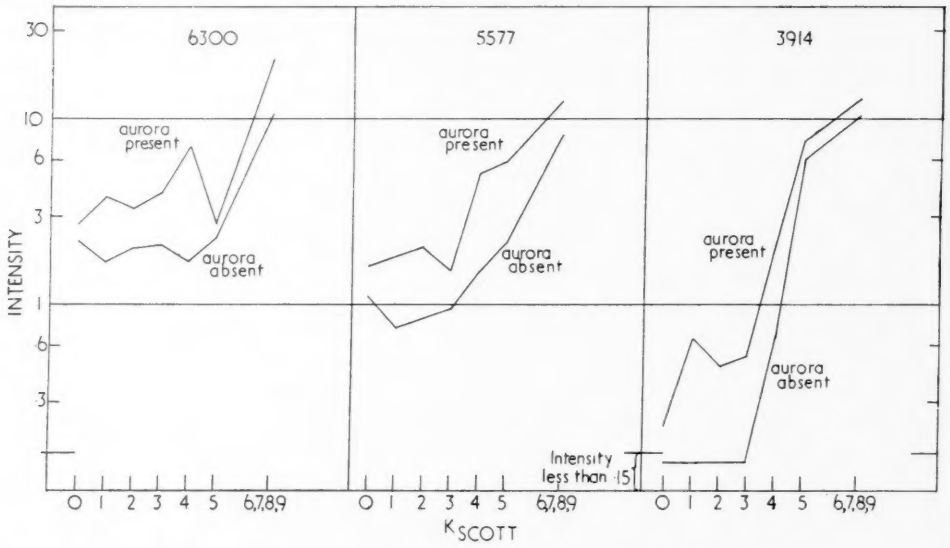

Fig. 5. The same data as used for Fig. 4 showing medians of the intensity when visual aurora were or were not present in the zenith during the spectrum exposure. Only clear moonless nights are considered.

with aurora inside the auroral zone. As a test of this hypothesis the intensity of the Scott Base night-sky emissions were plotted against the K-index for Byrd Station which is situated very close to the southern auroral zone. The scatter is much less than is obtained when using the planetary K-index but the best correlation remains with the local Scott Base K-index.

McCAULLEY *et al.* (1960) find that the 5577 Å intensity correlates better with the departure, ΔH, of the magnetic horizontal intensity from the quiet day variation than it does with K-index. For Scott Base only a very small correlation with ΔH was observed.

Instead of using the K-index the maximum change of the horizontal intensity, H, during the period of the exposure of the spectrum was tried, but this shows no closer correlation than does the K-index.

It has been shown that the night-sky spectral emissions exhibit no obvious correlation with visual auroral behaviour. The zenith intensity of the spectral emissions are again plotted as a function of the Scott Base K-index in Fig. 5 for solar depression angles of not less than 18° and for clear moonless nights only.

VOL. 21 1961

Here a distinction is made between spectral exposures during which visual aurora were or were not observed in the zenith region.

For the 6300 Å emission the presence of aurora during an exposure gives spectral intensities about one and a half times brighter than when no aurorae are observed. A difference of this nature but of an even greater magnitude would be expected because the intrinsic brightness of aurora is so great. The significant fact is that even when aurora is not observed the night-sky emission of this feature is still very high and moreover it is very much enhanced during magnetic storms.

The 5577 Å emission exhibits an almost identical behaviour. In this case spectra obtained in the presence of visual aurora are about twice as bright as those obtained in the absence of visual aurora.

The 3914 Å emission is again similar. Here at low K-indices spectra obtained in the absence of aurora are normally too weak to measure. The spectra obtained in the presence of aurora are up to four times brighter than those obtained in the absence of aurora at all K-indices with a possibly higher ratio during quiet or average magnetic conditions.

This indicates that a major portion of the 3914 Å emission is due to or associated with the presence of visual aurora. It is thus concluded that the assymetry of the twilight enhancement of the 3914 Å zenith intensity is due to radiation from visual auroral features which have a maximum of occurrence in the morning hours.

In a recent paper WEILL (1960) examines the behaviour of the 3914 Å emission at Adelie Land, Antarctica. He finds an asymmetry in the diurnal variation very similar to that reported in this paper. WEILL explains the asymmetry as due to the presence of a strong geomagnetic latitude dependence of N_2^+ ions, there being a high concentration in the auroral zone which falls to much lower values inside the auroral zone. In this paper observations have been made in the zenith, that is, at a fixed geomagnetic location, so that a latitude dependence cannot explain the asymmetry. Although WEILL'S interpretation is reasonable the observations at Scott Base show that it is not complete. The results suggest that there is an actual diurnal variation in the number of N_2^+ ions in the upper atmosphere in addition to any latitude variation.

In all the emissions considerable enhancement is observed at high magnetic activity even in the absence of visual aurora. This enhancement gives rise to the extensive red glows discussed by HATHERTON and MIDWINTER (1960). They are a prominent feature on all-sky camera colour films examined by SANDFORD (1961).

In Fig. 6 the probability of occurrence of visual aurora is given as a function of the Scott Base K-index for zenith aurora in 1959 and for all-sky aurora in 1957–1958 (after HATHERTON and MIDWINTER, 1960). The higher occurrence of aurora in 1957–1958 at high K-indices is due to the ease of observation of the extensive glows near the horizon which are not observable in the zenith region. Thus at Scott Base visual auroral occurrence is essentially independent of K-index whereas the extensive glow-type emission is closely associated with magnetic activity.

6. Intensity Ratios

There was found to be no constant ratio of intensity between the emissions examined. The zenith intensity ratios, $I6300/I5577$ and $I5577/I3914$ were deter-

mined from each spectrum with solar depression angle not less than 18°. The ratios are plotted in Fig. 7 as a function of the Scott Base K-index. The scatter of these ratios is large which does not contradict the conclusion made earlier that these emissions are essentially independent of each other.

It has been shown that visual aurora is not the main source of these emissions except perhaps for 3914 Å. From one night's observation only REES (1959b) finds a constant intensity ratio of $I5577/I3914$. We can conclude from Scott Base

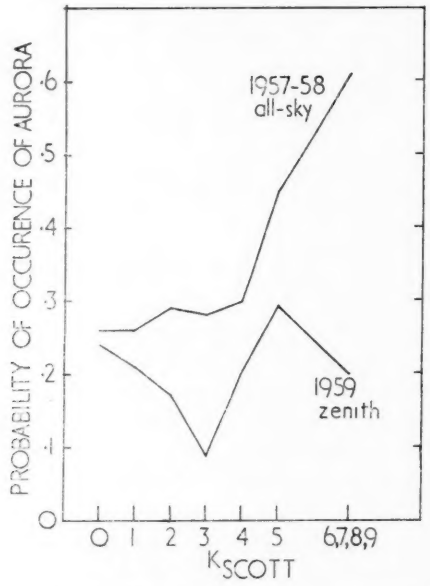

Fig. 6. The probability of occurrence of visual aurora in the whole sky for 1957–1958 (HATHERTON and MIDWINTER, 1960) and in the zenith only for 1959 at Scott Base as a function of the Scott Base magnetic K-index.

observations that the ratio is not constant at all times. These observations involve the comparison of a line and band intensity so that, although attempts have been made to determine the actual intensity of these features and so get the correct ratio of intensities, the only thing we know for certain is that the ratio does not remain constant but decreases with increasing magnetic activity.

The median of the intensity ratio $I6300/I5577$ tends to remain fairly constant except at the higher K-indices.

Since the 6300 and 5577 Å emissions originate from closely related energy levels of OI one would not be surprised to find a close relation between them. Recent height determinations with the use of rockets reported by TOUSEY (1958) indicates that the 6300 Å emission originates mostly from the ionosphere F-region heights and that the 5577 Å emission originates mainly from the E-region heights. As the major portion of these emissions comes from different heights then the lack of correlation is not so surprising.

Night-time 3914 Å emission, if it does arise predominantly from visual aurora will originate mainly in the E-region heights. A lack of a close correlation with the

VOL. 21 1961

5577 Å emission may arise from the fact that the 3914 Å emission is associated mostly with visual aurora whereas the 5577 Å emission, even in the presence of visual aurora, is mainly due to non-visual sources. It is not possible from the observations to determine the $I5577/I3914$ ratio in visual aurora alone.

It is clear that observations on visual aurora with instrumental methods must be made in the shortest possible time, to take advantage of the relatively high

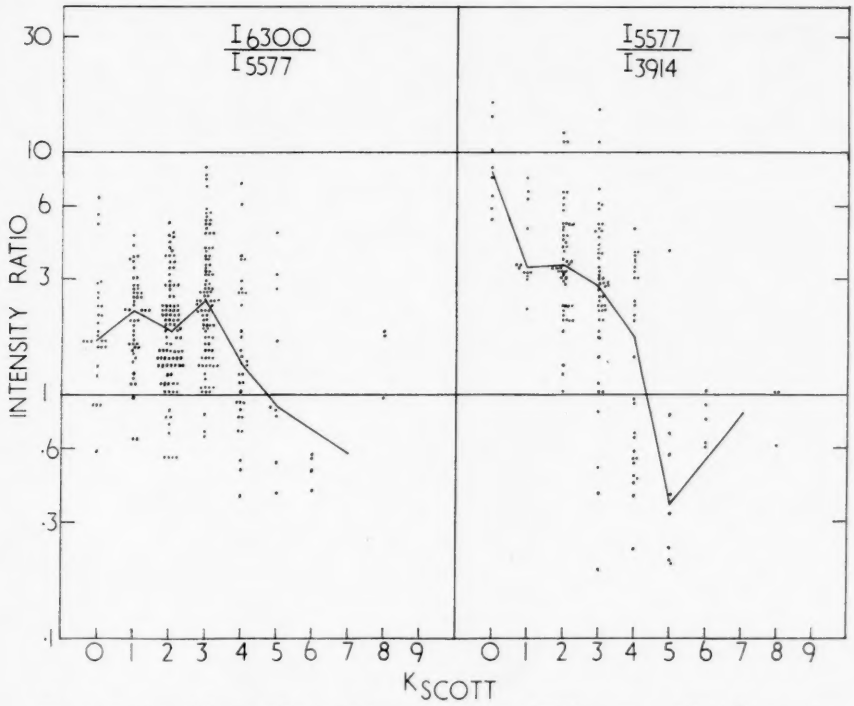

Fig. 7. Ratios of the zenith intensities and medians of 6300, 5577 and 3914 Å emissions at Scott Base as a function of the Scott Base K-index.

intrinsic brightness of the visual aurora above the extensive but relatively weak night-time glow. The influence of background glows on observations made on visual forms should always be considered.

7. Conclusion

At Scott Base there was at all times sufficient N_2^+ ions present up to heights of at least 300 km to cause a strong twilight enhancement of 3914 Å emission. There is evidence of a diurnal variation of N_2^+ ion concentrations.

There is no diurnal or seasonal variation of 6300 Å emission outside the twilight enhancement. There is no diurnal variation of 5577 Å emission but during the observing season the intensity of this emission exhibited a seasonal variation. The 3914 Å emission shows a strong diurnal and seasonal variation attributable to twilight enhancement and to the presence of visual aurora.

The source of a major part of the 6300, 5577 and 3914 Å emissions at Scott Base does not originate from visual aurora but apparently from weak extensive glows. Since visual aurorae are not the main source of night-sky radiation these observations cannot be applied to visual auroral behaviour.

References

Hatherton T. and Midwinter G. G.	1960	*J. Geophys. Res.* **65,** 1401
Lytle E. A. and Hunten D. M.	1960	*Canad. J. Phys.* **38,** 477.
McCaulley J. W., Roach F. E. and Matsushita S.	1960	*J. Geophys. Res.* **65,** 1499.
Megill L. R.	1960	*J. Atmosph. Terr. Phys.* **17,** 276.
Rees M. H.	1959a	*J. Atmosph. Terr. Phys.* **14,** 338.
Rees M. H.	1959b	*J. Atmosph. Terr. Phys.* **14,** 325.
Roach F. E.	1960	*J. Geophys. Res.* **65,** 1495.
Roach F. E., McCaulley J. W., Marovich E. and Purdy C. M.	1960	*J. Geophys. Res.* **65,** 1503.
Roach F. E. and Rees M. H.	1960	*J. Geophys. Res.* **65,** 1489.
Rumsey N. J.	1960	Dominion Physical Lab. Technical Note TN. 139.
Sandford B. P.	1959	*Ann. Géophys.* **15,** 445.
Sandford B. P.	1961	*J. Atmosph. Terr. Phys.* **21,** 177.
Tousey R.	1958	*Ann. Géophys.* **14,** 186.
Weill G.	1960	*Ann. Géophys.* **16,** 223.

VOL. 21 1961

Journal of Atmospheric and Terrestrial Physics, 1961, Vol. 21, pp. 193 to 202. Pergamon Press Ltd. Printed in Northern Ireland

A study of the variations in a daily ionospheric index of solar activity

G. H. Bazzard
D.S.I.R. Radio Research Station, Ditton Park, Slough, Bucks.*

(*Received* 3 *February* 1961)

Abstract—Values of a daily index of solar activity, based on the ionization of the *E*-layer, are presented for the period of I.G.C. 1959 as a continuation of values already published for the I.G.Y.

Variations in the index during the whole period of 2½ years were examined statistically and evidence has been obtained of periodicities resulting from localized active areas on the sun and its rotation. The variations in the ionospheric index have also been shown to be partially correlated with coronal green line activity which suggests that solar conditions conducive to the excitation of the green line are also favourable to the emission of *E*-layer ionizing radiation.

1. Introduction

A method of constructing a daily index of solar activity, based on the density of ionization in the *E*-layer, has recently been described by Minnis and Bazzard (1959) who have tabulated this index (J_E) for the period of the I.G.Y. The same technique has now been applied to observations of the *E*-layer critical frequencies made at Slough during the period of I.G.C. 1959 and values of J_E for this period are presented in Table 1. The procedure followed and the accuracy of measurement described in the earlier work also apply to these later figures. The erratic fluctuations, which remain in the index and which are due to observational errors of critical frequency, are estimated to have a standard deviation of about 2 per cent.

The set of index figures, which is now available for the period July 1957–December 1959 inclusive, is examined here to ascertain whether the variations present in it are representative of changes in ionizing radiation produced by localized areas of activity on the sun and by the effect of the sun's rotation. Beynon and Brown (1951) have shown, over a limited period, that the 27-day Fourier component of the *E*-layer critical frequency coincides with the corresponding component of sunspot number. If J_E is a reasonably accurate index of *E*-layer ionizing flux, it should be possible to demonstrate that it contains similar periodic variations which can be correlated with short-term variations in solar activity.

2. Methods of Analysis

2.1. *General*

If it is assumed that an isolated active area on the sun is a strong source of ionizing radiation, it would be expected that the value of J_E would be greater than average during that half of the period of solar rotation when the active area was on the visible disk. Such an increase in J_E would last for about 13 days if the radiation was emitted with equal intensity in all directions. If, however, the radiation was restricted to a narrow cone whose axis was normal to the surface of the sun, a peak in the value of J_E would occur near the c.m.p. of the active area and the duration of such a peak would be related to the angular width of the cone.

* Official communication.

8A—(4 pp.)

Table 1. Daily values of E-layer index J_E

Date	Jan.	Feb.	Mar.	Apr.	May	June	July	Aug.	Sept.	Oct.	Nov.	Dec.
1	(312)	327	235	269	(288)	(294)	(274)	(263)	(344)	237	202	(253)
2	335	343	230	280	256	268	(261)	270	346	259	199	232
3	308	316	244	308	(268)	(262)	(277)	303	(328)	233	—	(215)
4	349	351	265	(275)	282	—	—	(301)	307	187	213	(275)
5	(325)	285	250	288	(286)	—	—	(305)	287	204	207	218
6	327	289	278	310	294	—	(256)	(284)	286	208	215	(226)
7	270	272	237	(313)	—	(267)	292	—	291	224	218	186
8	298	C	263	(304)	(329)	264	284	(275)	(287)	220	239	—
9	288	303	302	275	319	(303)	(305)	(312)	276	231	248	—
10	260	288	299	268	C	312	(288)	—	258	234	214	242
11	287	295	(312)	278	(333)	357	C	(281)	275	244	235	(237)
12	288	264	313	261	298	(324)	C	303	272	(241)	(235)	228
13	313	261	293	304	(321)	—	(338)	275	(270)	247	(228)	219
14	(276)	233	C	294	(305)	(308)	—	—	284	262	228	230
15	315	243	314	271	(295)	—	—	(289)	289	252	228	—
16	316	251	(318)	293	C	(317)	—	C	264	(223)	267	—
17	(285)	225	(282)	(304)	C	—	—	257	269	(256)	240	232
18	—	274	319	269	(349)	302	—	—	280	240	198	210
19	(287)	277	312	320	—	—	—	(268)	285	—	230	210
20	291	258	(313)	321	(303)	(284)	—	(289)	294	—	208	C
21	374	274	352	301	303	(284)	—	299	260	223	205	(237)
22	(319)	294	372	312	268	—	—	—	253	(222)	216	(273)
23	(288)	287	346	326	270	(296)	—	348	250	211	206	223
24	—	294	(361)	283	248	(284)	(301)	286	247	222	260	246
25	—	287	351	(295)	—	(279)	—	(331)	—	—	253	240
26	—	271	311	297	291	290	(287)	—	(265)	(228)	265	—
27	(397)	277	245	(278)	(274)	299	—	(342)	251	231	268	—
28	365	274	(222)	294	(287)	279	—	(365)	258	233	215	221
29	320		(238)	287	(267)	—	(286)	338	249	246	242	—
30	(304)		279	295	(275)	—	(287)	C	266	228	(258)	—
31	320		268		272		(268)	342		213		231

This simple model will be more complicated near the epoch of maximum solar activity because of the presence of many active areas on the sun. If, however, there is any association between the short-term changes in J_E and the presence of active areas, it should still be possible to detect it by statistical methods.

If solar flares are excluded, active areas on the sun often retain their activity, at least in visible light, for several days or longer. It is also not unusual for the same active area to reappear on several successive rotations of the sun. When these facts are considered, there are several ways in which the variations in J_E may be examined for evidence of an association between them and solar active areas and these are discussed in Section 2.2.

VOL. 21 1961

2.2. *Statistical tests*

2.2.1. If it is assumed that positive and negative deviations in J_E are associated respectively with the presence or absence of active areas on the sun's disk, long sequences of days having deviations of the same sign would occur more frequently than would otherwise be expected. The observed frequency distributions of sequences of days showing positive and negative deviations are discussed in Section 3.2.

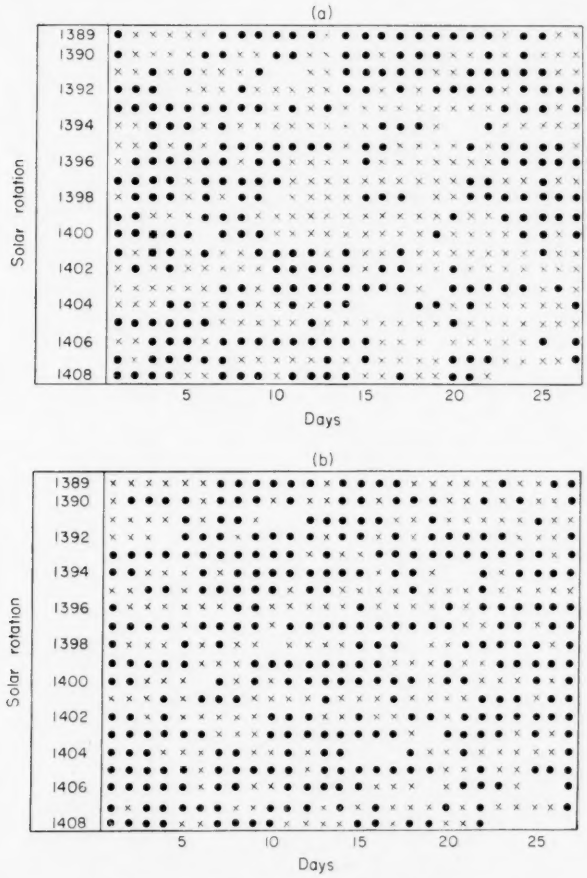

Fig. 1.(a) Daily changes in sign of ΔJ_E. ● Positive, × Negative.
(b) Daily changes in coincidence of signs of ΔJ_E and ΔJ_G. ● Same sign, × Different sign.

2.2.2. If the areas of activity tend to remain active during one or more solar rotations, deviations in J_E of the same sign ought to recur at intervals which are integral multiples of 27 days, the approximate synodic rotation period of the sun. If this is the case, a deviation of a given sign will be followed by deviations of the same sign 27, 54, 81, etc. days later with probabilities which exceed 0·5, $(0{\cdot}5)^2$, $(0{\cdot}5)^3$, etc., which would be expected if positive and negative deviations were

equally probable. The observed recurrences of deviations of the same sign are discussed in Section 3.3.

2.2.3. It has already been pointed out that the radiation from the active areas may be either omnidirectional or confined to a narrow cone. In the latter case, increases in J_E caused by a very narrow beam would last for only 1 or 2 days as compared with periods of up to 2 weeks if they were due to a very wide beam. A superposed epoch test has been devised to provide information on the directional properties of the radiation from active areas and is discussed in Section 3.4.

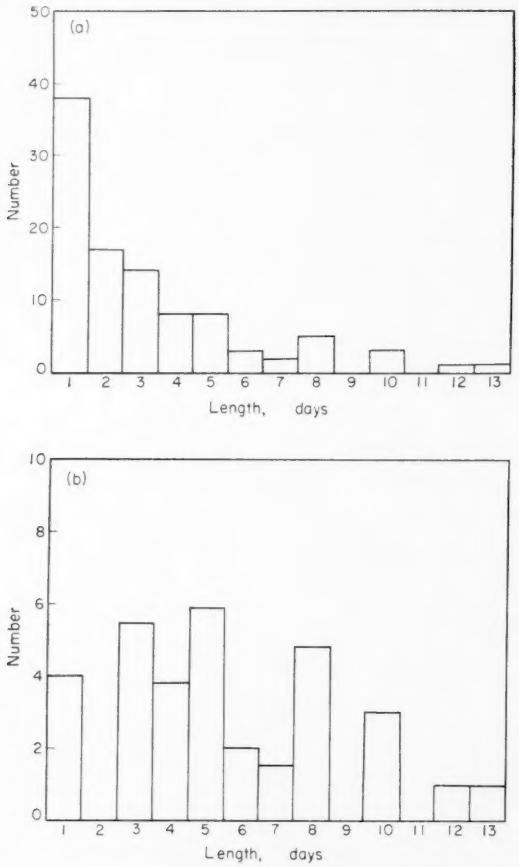

Fig. 2. Lengths of sequences of days for which the signs of ΔJ_E and ΔJ_G coincide. (a) All sequences, (b) Sequences not due to chance.

2.2.4. The frequency distributions of sequences of positive and negative deviations in J_E, which are examined in Section 3.2, do not by themselves provide evidence of a link with solar activity. It is necessary to demonstrate also an association between the deviations in the ionospheric index and directly observed changes on the sun. In order to provide evidence for such an association, the coincidences in sign of simultaneous deviations in both the ionospheric and the solar indices of activity could be examined. If there is no association between the

VOL. 21 1961

two, the frequency distributions of the lengths of sequences of both coincidences and non-coincidences would be proportional to 0·5, $(0{\cdot}5)^2$, $(0{\cdot}5)^3$ . . . . If, however, there is a partial association, the longer sequences of coincidences ought to occur more frequently than expected but the occurrence of sequences of non-coincidences should still be in the above proportion. The observed occurrences of such sequences are described in Section 4.

3. The Periodic Variations in J_E

3.1. *Arrangement of the data*

The values of J_E were arranged to correspond to consecutive groups of 27 days commencing with 1 July 1957. The mean value of J_E for each 27-day period was calculated and the deviation (ΔJ_E) of each individual value from the mean was determined. These deviations can be represented symbolically by a diagram, of the kind used by Bartels (1932), which is shown, for the period of the I.G.Y. only, in Fig. 1(a). In the figure, the 27-day periods represent the solar rotations from No. 1389 beginning on 6 July 1957, but the symbols represent the signs of deviations from 27-day means calculated beginning on 1 July 1957.

3.2. *Sequences of the same sign in* ΔJ_E

The observed lengths of unbroken sequences of positive and negative values of ΔJ_E are shown in Table 2 together with the numbers expected assuming that positive and negative values are equally probable.

Table 2. Distribution of sequences of the same sign in ΔJ_E

Length of sequence	Number of sequences			
	Positive deviations		Negative deviations	
	Observed	Expected	Observed	Expected
1	66	79·0	71	73·0
2	39	39·5	30	36·5
3	20	19·8	19	18·3
4	6	9·9	10	9·1
5	12	4·9	9	4·6
6	3	2·5	4	2·3
7	3	1·2	5	1·1
8	3	0·6	1	0·6
9	4	0·3	2	0·3
10	1	0·2	2	0·2
11	0	0·1	2	0·1
12	0	0·04	0	0·04
13	1	0·02	0	0·02
14	0	0·01	1	0·01

The observed distributions for both positive and negative deviations are found to differ significantly from the expected ones when the χ^2 test is applied. The difference is obviously due to the unexpectedly large numbers of longer sequences which occur. It is concluded that the day-to-day variations in J_E are not chance

occurrences but are controlled by some external cause which is, presumably, the variation in solar radiation incident on the E-layer.

3.3. *Recurrence of signs of ΔJ_E in successive solar rotations*

The numbers of occasions on which ΔJ_E recurred with the same sign after one, two and three solar rotations are shown in Table 3 together with the observed and expected probabilities of such recurrences.

Table 3. Recurrence of ΔJ_E with the same sign after $27n$ days

n	Observed	Expected	Probability of occurrence	
			Observed	Expected
1	412	372	0·55	0·50
2	218	207	0·32	0·30
3	108	102	0·18	0·17

The observed number of recurrences after an interval of 27 days corresponds to a probability of 0·55. Statistical tests show that the observed occurrence is significantly greater than the number which would be expected assuming that positive and negative deviations are equally likely. It is concluded that some areas of activity retain their ability to emit unusually intense ionizing radiation for at least 27 days.

If the probability of single recurrence is 0·55 and, if it is assumed that the probability of recurrence depends only on the sign of the immediately preceding deviation, the probabilities of two and three successive recurrences will be $(0{\cdot}55)^2$ and $(0{\cdot}55)^3$ respectively. The expected numbers of recurrences based on these probabilities are also given in Table 3. Although they are less than the observed numbers of recurrences, they are found not to differ significantly from them when statistical tests are applied. Hence there is no conclusive evidence in the data examined to show that many active areas continue to emit ionizing radiation for as long as 54 days.

Additional evidence of the periodic nature of the recurrences of deviations of the same sign is provided by Fig. 3 where the observed probability of occurrence of coincidences of the signs of deviations is plotted as a function of the time interval between the deviations. The expected probability will be 0·5 if it is assumed that there is an equal chance of the occurrence of a positive or negative deviation. It can be seen that the probability of coincidences falls to a level which is not significantly different from 0·5 after about 7 days but rises above this level to a peak around 27 days. There is a similar increase in probability after 54 days although this is not statistically significant. It is interesting to note that after about 13 days the probability of coincidences is less than that of non-coincidences. This is probably due to an asymmetry in the distribution of activity across the sun's disk; a fact which can be noted from Fig. 1(a) where the occurrence of positive deviations is much greater than negative deviations on the left-hand half of the diagram while the reverse is true of the right-hand half. An autocorrelation analysis

VOL. 21 1961

of the magnitudes of the deviations has also been made. The autocorrelogram is shown in Fig. 4 and closely resembles the curve of Fig. 3 in its characteristics.

3.4. *The beam width of radiation from active areas*

In order to obtain some information on the probable beam width of radiation from active areas a superposed epoch test was made using values of ΔJ_E. From

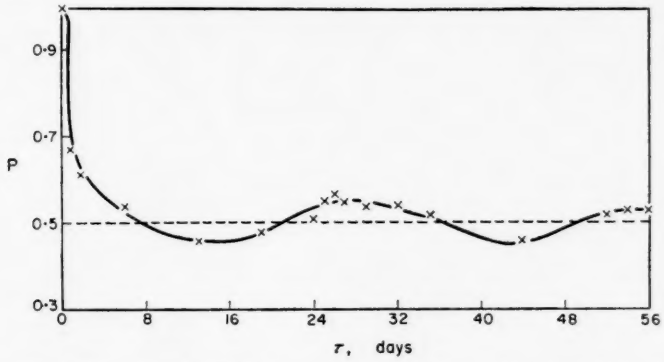

Fig. 3. Probability (P) of coincidences of sign of ΔJ_E as a function of time interval (τ).

data reported by TROTTER and ROBERTS (1958, 1959) the dates of c.m.p. of intensely active areas (Category a) were noted and the day of c.m.p. was taken as the reference epoch. Mean values of ΔJ_E for this day and for the remaining days of the 27-day period were obtained for twenty-three such epochs.

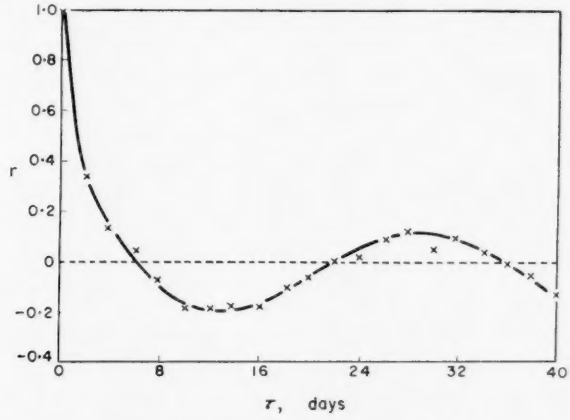

Fig. 4. Autocorrelation function of ΔJ_E.

However, statistical tests showed that some of the mean values obtained for individual days did not differ significantly from the mean value for the 27-day period so that it was only possible to obtain useful information by considering groups of days. When this procedure was adopted, it was found that the mean value of ΔJ_E for the 13-day period when the active area was on the visible solar

disk was significantly greater than that for the remainder of the 27 days. A similar result was obtained for a 9-day period which included the c.m.p. but a visual examination of the data suggested that any period of less than 9 days would not yield a statistically significant result. With the available data, therefore, there does not seem to be any evidence to show that the radiation from active areas is sharply focused. This conclusion is consistent with the nature of the curve of Fig. 3 which rises to a maximum and then falls over a period of about 13 days and does not peak sharply as would be the case if the radiation from the active areas was sharply beamed.

4. The Association of ΔJ_E with Changes in the Intensity of the Coronal Green Line (λ5303 Å)

The directly observed index of solar activity, which has been used for the comparison with the ionospheric index, is the intensity (J_G) of the green coronal line (λ5303 Å) integrated over the visible disk of the sun and reported by Trotter and Roberts (1958, 1959). These data were available only for the period of the I.G.Y. and the analysis described below is, therefore, limited to that period.

Values of ΔJ_G were derived in the same way as described in Section 3.1 for ΔJ_E. For most days of the I.G.Y., therefore, a pair of values of ΔJ_E and ΔJ_G is available for examination. The coincidence of signs in ΔJ_E and ΔJ_G is indicated in Fig. 1(b) by a circle and the non-coincidence by a cross. The distribution of lengths of sequences of coincidences is shown in Fig. 2(a) and statistical tests show that the number of long sequences is significantly greater than would be expected if there was no association between the signs of ΔJ_E and ΔJ_G. On the other hand, the lengths of sequences of non-coincident days are distributed in a way which indicates that such days are equally likely to be followed by a coincidence or a non-coincidence.

There is not a complete association between the signs of ΔJ_E and ΔJ_G and hence the occurrence of some of the sequences of coincident days must be due to chance. Assuming that it is equally likely that a coincidence will be followed by a second coincidence or a non-coincidence, the expected probability of occurrence of a sequence of n coincidences will be $(0{\cdot}5)^n$. An attempt has been made to estimate roughly the number of the sequences in Fig. 2(a) which cannot be attributed to chance by subtracting $K(0{\cdot}5)^n$ from the observed frequencies; the constant, K, was arbitrarily adjusted to ensure that there were no negative differences. The distribution thus obtained is shown in Fig. 2(b). It seems reasonable to conclude from this distribution that when active areas are present on the sun, and when they influence both the ionization of the E-layer and the solar corona, the mean duration of this control is about 6 days. The days which show no coincidence are presumed to occur either when the errors in ΔJ_E or ΔJ_G are large or when the E-layer is partially controlled by some other unidentified influence which is not correlated with the intensity of the coronal green line.

5. Conclusions

The day-to-day variations in the intensity of solar ionizing radiation which is absorbed in the E-layer are assumed to be represented reasonably accurately by

VOL. 21 1961

the daily index figure $J_E(=f_E{}^4 \sec \chi)$ when precautions are taken in measuring the E-layer critical frequency, f_E. The daily values of J_E for thirty-three solar rotations (July 1957–December 1959) have been examined statistically. The conclusions reached, which are summarized below, indicate that J_E contains periodic variations which correspond to variations in solar ionizing radiation.

5.1. The ionization of the E-layer, as indicated by J_E, often tends to remain consistently above or below its average value for periods of about a week or more. The distribution of the frequencies of occurrence of these periods indicates that they are not due to chance and it is suggested that they may result from variations in the incident ionizing radiation which arise from the presence on the sun of localized active areas which strongly emit ionizing radiation.

5.2. It is found that the sign of the deviation of J_E from its average value, on a given day, tends to recur after an interval of 27 days with a frequency of occurrence which statistical tests show to be significantly greater than would be expected by chance. This observation could result from the existence of active areas on the sun having a lifetime of at least 27 days, the period of rotation of the sun, providing a connexion can be shown to exist between short-term changes in J_E and visible changes in solar activity. The observation is also consistent with the earlier work of Beynon and Brown (1951) which has been mentioned previously.

5.3. There is no evidence in the data examined to suggest that there is any marked focusing of the radiation emitted by the localized areas of activity on the sun.

5.4. It has been shown that days on which J_E is greater or smaller than average tend to coincide with days on which the integrated solar coronal green line intensity also shows the same deviation from its average value. It seems likely, therefore, that conditions on the sun which are favourable to the excitation of the green line in the coronal spectrum also tend to be associated with enhanced emission of the ionizing radiation which contributes to the formation of the E-layer.

It is interesting to note that the solar eclipse studies of Waldmeier (1947), Osawa (1950) and Minnis (1952, 1955) have also led to the suggestion that there may be a common factor between changes in E-layer ionizing radiation and the excitation of the coronal green line. In addition, the rocket measurements made by Byram *et al.* (1956) have indicated an enhancement of short wavelength X-radiation, a component of E-layer ionizing radiation, during periods when coronal green line activity is high. However, it is emphasized that neither the present analysis nor the results of these other workers prove the existence of a direct connexion between E-layer ionizing radiation and coronal activity.

Acknowledgements—The author is indebted to Dr. B. Briggs of the Cavendish Laboratory, Cambridge for the autocorrelation analysis described in Section 3.3 of the work.

The author acknowledges the assistance of Mrs F. P. Vickers in much of the statistical analysis described. The work described above was carried out as part of the programme of the Radio Research Board. The paper is published by permission of the Director of Radio Research of the Department of Scientific and Industrial Research.

References

Bartels J.	1932	*Terr. Magn. Atmos. Elect.* **37,** 1.
Beynon W. J. and Brown G. M.	1951	Proc. Second Meeting Mixed Comm. Ionos. I.C.S.U., p. 156.
Byram E. T., Chubb T. A. and Friedman H.	1956	*J. Geophys. Res.* **61,** 251.
Minnis C. M.	1952	*Nature, Lond.* **170,** 453.
Minnis C. M.	1955	*J. Atmosph. Terr. Phys.* **6,** 91.
Minnis C. M. and Bazzard G. H.	1959	*J. Atmosph. Terr. Phys.* **17,** 57.
Osawa K.	1950	*Rep. Ionos. Res. Japan* **4,** 53.
Trotter D. E. and Roberts W. O.	1958	Univ. Colorado Rep., HAO Nos. 39, 40, 42.
Trotter D. E. and Roberts W. O.	1959	Univ. Colorado Rep., HAO Nos. 43, 44, 45.
Waldmeier M.	1947	*Terr. Magn. Atmos. Elect.* **52,** 333.

VOL. 21 1961

Journal of Atmospheric and Terrestrial Physics, 1961, Vol. 21, pp. 203 to 217. Pergamon Press Ltd. Printed in Northern Ireland

RESEARCH NOTES

Cosmic ray increases during the sunspot minimum of 1953

(*Received* 12 *January* 1961)

CORPUSCULAR RADIATIONS from the Sun are the main cause of geomagnetic storms, aurorae and cosmic ray variations. TANDON (1957) has studied the association of geomagentic storms with various solar features and classified the whole geomagnetic activity in three different groups, viz. intense storms, disturbed M-storms and quiet M-storms. The quiet M-storms which are of interest here, are associated with quiet solar regions (low coronal line intensity regions, etc.) and hence do not possess large "frozen-in" magnetic fields. They generally occur near the sunspot minimum and form long sequences of annual variation lasting for about thirty to fifty solar rotations. The period of recurrence is found to be exactly 27 days. They show their maximum development on about 1–3 days after the central meridian passage of a weak coronal line region. When a solar-ion stream possesses large "frozen-in" fields, they give rise to intense storms or disturbed M-storms depending upon the complexity of the magnetic field of the solar region. These storms are generally associated with the Forbush decreases in cosmic rays.

Analysis of cosmic ray data for meson intensity at Huancayo and Cheltenham and of quiet M-storms for the period 1950–1954 has been made to study the effect of low "frozen-in" fields of solar-ion streams on cosmic ray variations. The cosmic ray data have been taken from LANGE and FORBUSH (1957) and the geomagnetic data from various issues of the *Journal of Geophysical Research*. Here we have selected as zero day the dates of the active period of four sequences (A, B, A_1 and B_1) of quiet M-storms. These storm sequences have been discussed in detail by TANDON (1956, 1957). Taking these dates as zero day the Chree type of analysis was done for -7 to $+9$ days around zero day. To obtain the smoothed effect 3 days running mean values of meson intensity and geomagnetic data were used. The analysis showed that three of the sequences (A, B and A_1) are accompanied by an increase of 0·3–0·4 per cent in cosmic ray intensity after about 2–3 days when the magnetic storm is over, i.e. when the C-fig. value goes below 1·0 (Fig. 1). However, sequence B_1 does not show such increases. This sequence shows no storminess on Chree curves since the C-fig. value is always less than 1·0.

We have also analysed the geomagnetic sequence associated with a most pronounced u.m.-region of 1953 and discussed by SIMPSON *et al.* (1955) by selecting zero day as the c.m.p. of this u.m. region. We failed to obtain any significant increases of cosmic ray intensity at Huancayo and Cheltenham around the c.m.p. of the u.m. region as were obtained by them. Fig. 2, however, shows a decrease of about 0·3 per cent in cosmic ray intensity on day $+5$ and a peak of geomagnetic activity on day $+4$, thus showing an inverse correlation between cosmic ray intensity and geomagnetic activity. From the above analysis we conclude that the cosmic ray intensity increase found by them around zero day is inconclusive.

The trapped particles of the solar ion streams in the radiation belt may be responsible for the cosmic ray increases associated with quiet M-storms. The low energy particles

moving along the solar-ion stream reach the Earth's geomagnetic field and become trapped in the radiation belts. These particles, on subsequent acceleration by magneto-hydrodynamic waves or by other processes in the local environment of the Earth, may be responsible for the observed increase of 0·3–0·4 per cent in cosmic ray intensity after the magnetic

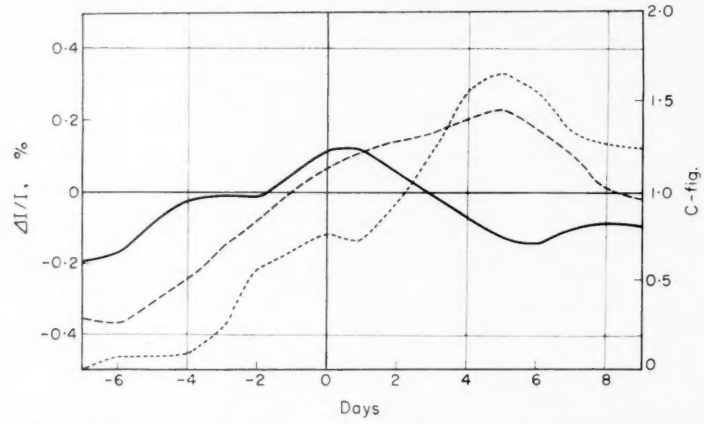

Fig. 1. The association of sequence *A* with cosmic ray variation. The full curve represents geomagnetic variations; dashed and dotted curves represent the departure of cosmic ray intensity from the mean intensity at Huancayo and Cheltenham respectively.

VOL. 21 1961

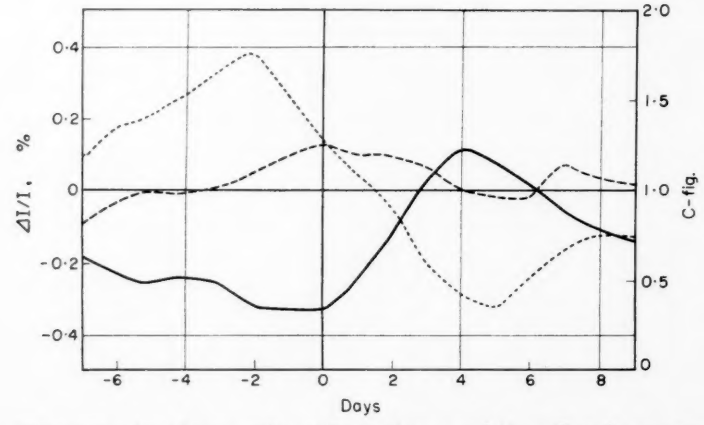

Fig. 2. The association of u.m.-region with cosmic ray variation. Zero day represents the c.m.p. of the u.m.-region. The full curve represents geomagnetic variation; dashed and dotted curves represent the departure of cosmic ray intensity from the mean intensity at Huancayo and Cheltenham respectively.

storm is over. In this way the radiation belt acts as the secondary source of cosmic ray particles. During the sunspot maximum period, these increases of cosmic ray intensity will get masked on account of very many solar-ion streams of large "frozen-in" magnetic fields. Hence one should not expect to observe such increases in cosmic rays during the high sunspot activity period. As far as the writer is aware no such increases at the time of maximum sunspot activity have been reported in the literature.

In conclusion, may we emphasize that a more detailed study of these phenomena in equatorial and other latitudes at the time of future sunspot minima would help to make the picture of the basic mechanism clearer.

J. N. TANDON

Department of Physics, University of Delhi
Delhi 6, India

REFERENCES

LANGE I. and FORBUSH S. E.	1957	Carnegie Institution of Washington Publication No. 175.
SIMPSON J. A., BABCOCK H. W. and BABCOCK H. D.	1955	*Phys. Rev.* **98,** 1402
TANDON J. N.	1956	*Ind. J. Phys.* **30,** 153.
TANDON J. N.	1957	Thesis, Delhi University.

Sporadic-*E* phenomena associated with the high altitude nuclear explosions over Johnston Island

(*Received* 3 *February* 1961)

Two nuclear bombs, in the megaton range, were exploded over Johnston Island (16.7°N, 169.4°W) in August 1958. The first explosion took place near 60 km height at 1050.05 U.T. on 1 August and the second near 30 km height at 1030.08 U.T. on 12 August (ATOMIC ENERGY COMMISSION, 1959a, b).

MATSUSHITA (1959) has noted increases in sporadic-*E* (E_s) ionization at certain medium latitude stations around the explosion points but he doubts whether any real association is implied. THOMAS (1960), however, has reported large increases at relatively higher latitudes. This note summarizes the results of a wide-world investigation using the published values of f_0E_s, or fE_s, supplemented by more frequent ionogram data available from many stations for 12 August.

Analyses of the incidence of dense E_s at high latitudes under normal conditions show that it seldom occurs simultaneously at more than two widely spaced stations. After both explosions, however, dense E_s occurred simultaneously at four or five such stations out of six in North America. In order to make an estimate of how improbable these E_s events would be under normal conditions, the incidence of high values of f_0E_s at 1200 U.T. at these six stations has been studied for all days, except 1 and 12 August, in the 50 day period centred on 7 August. A value of f_0E_s was designated high if it exceeded approximately twice the average median value for the chosen hour in July and August 1958. The probabilities (p_1, p_2, . . . p_6) of finding such a high value by chance at each station could be calculated from the number of high values which occurred in the period considered. The probability of simultaneous occurrence of dense E_s at two stations (r, s) on a given day is p_rp_s, provided there is no association between the occurrence of E_s at the two stations; a brief study over a much longer period has confirmed that the statistics based on 50 days are representative. For this pair of stations, the number of coincidences expected by chance is then $(p_rp_s)N_{rs}$, N_{rs} being the number of days for which numerical values of f_0E_s were available for both stations; on some days measurements were prevented because of excessive absorption or instrumental failure. The expected number of coincidences at pairs of stations is $\Sigma(p_rp_s)N_{rs} = 5$, as compared with the number of observed coincidences, four.

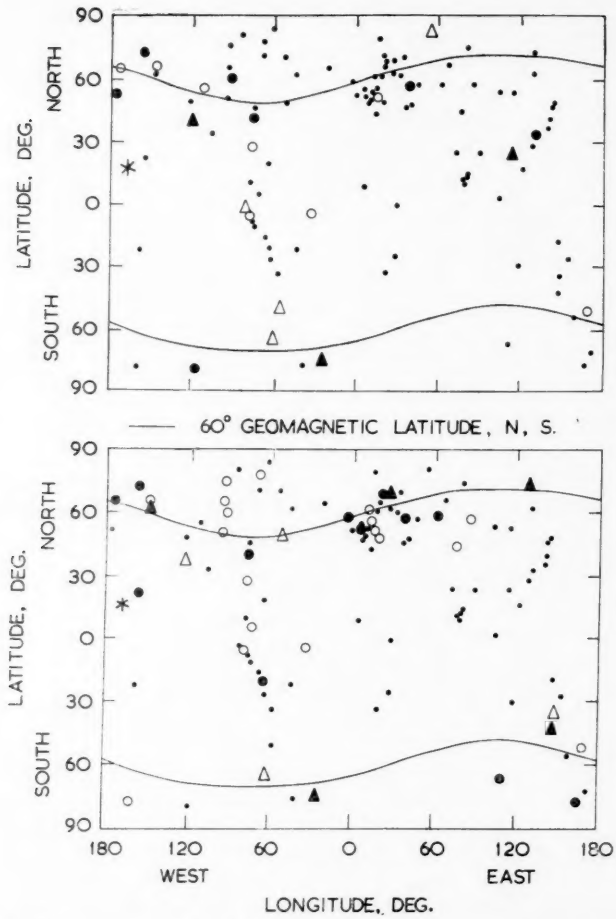

Fig. 1. The occurrence of sudden increases in f_0E_s between 1100 and 1900 U.T. on (a) 1 August and (b) 12 August 1958.

* Johnston Island.
● Stations showing outstanding effects before 1400 U.T.
○ Stations showing less significant effects before 1400 U.T.
▲ Stations showing outstanding effects between 1400 and 1900 U.T.
△ Stations showing less significant effects between 1400 and 1900 U.T.
• Stations showing no effect detectable.

Since the number of coincidences observed agrees with the number expected by chance, we conclude that there is no association between the occurrence of dense E_s at the stations considered.

On 1 August, dense E_s occurred simultaneously at five stations. Since there is no normal association between such events for the stations studied, the probability that an event occurred by chance at five stations out of six has been calculated to be only $1{\cdot}0 \times 10^{-5}$. It seems reasonable to conclude that this multiple coincidence must have been due in some way to the explosion of the bomb. On 12 August, dense E_s occurred simultaneously at four of the six stations and since the probability of such an event is only $8{\cdot}7 \times 10^{-4}$, it is again concluded that the bomb was responsible.

VOL. 21 1961

It might be suggested that the multiple events noted on 1 and 12 August were due to some unusual characteristic of these days, unconnected with the explosions, but a check on the occurrence of dense E_s at 0800 U.T., that is before the explosions, shows that there was no tendency to an abnormally high number of multiple occurrences on either day.

Thus there is very strong statistical evidence for assuming that the occurrence of high values of f_0E_s over an abnormally wide area at high latitudes on 1 and 12 August was due to the explosions.

The world-wide data are now examined for sudden increases in $f_0E_s(\Delta f)$ occurring in the period 1100–1900 U.T. on 1 and 12 August. Events shown before 1400 U.T. will be called "early" and those starting at, or after, 1400 U.T. will be referred to as "late". A change observed on either of these days is compared in magnitude with those found in the corresponding time interval during the 59 remaining days of July and August 1958. The Δf on the bomb day is denoted "outstanding" if no comparable Δf is found. Such a change has a statistical probability of less than 0·02 for each occasion. Any other Δf, the deduced statistical probability of which is not greater than 0·1, is described as "less significant". The results of this analysis are summarized in Fig. 1. The stations marked "no effect detectable" include both those with negligible increases and those where no decision could be made on the evidence available.

The most striking feature of the patterns is the marked concentration of both "outstanding" and "less significant" effects about geomagnetic latitudes 60°N and 60°S. The absence of abnormal ionization at some high latitude stations, however, implies considerable localization. Furthermore, almost all the early effects shown at high latitudes had occurred by 1100 U.T., i.e. within 30 min of the explosions, but marked discontinuities in the occurrence of the dense E_s with time were generally observed. A possible explanation of these results is in terms of leakage of radiation from the outer Van Allen radiation belt but the mechanism whereby particles are released by the explosions is not obvious.

No evidence of the existence of significant increases (Δf) before 1400 U.T. has been found at the stations showing the late effects, even when using the more numerous data on 12 August. The times of occurrence of these late effects are not consistent with a simple explanation such as the propagation of a sonic or shock wave from the explosion point (Cummack and King, 1959; Matsushita, 1959).

It may be noted that both explosions occurred during periods when magnetic and ionospheric activity were fairly low. The E_s effects were, however, clearly more marked after the second explosion than after the first.

At several stations the E_s associated with the explosions occurred at abnormally low heights, 90 km. While E_s at such heights is usually associated with meteoric activity (Naismith, 1954), the present phenomenon is quite different because the space and time variations are unlike those associated with meteoric E_s. Furthermore, multiple reflections were often observed whereas meteoric E_s gives one weak scattered reflection only.

The present investigation has demonstrated marked increases in E_s ionization associated with the explosions. Further studies show analogous perturbations in other ionospheric and geomagnetic variations. A full interpretation must await the completion of these studies.

Acknowledgements—The work described above was carried out as part of the programme of the Radio Research Board. The paper is published by permission of the Director of Radio Research of the Department of Scientific and Industrial Research.

L. Thomas
R. E. Taylor

*D.S.I.R. Radio Research Station**
Ditton Park, Slough, Bucks.

* Official communication.

References

Atomic Energy Commission	1959a	AEC Release B-39, March 10.
Atomic Energy Commission	1959b	AEC Release B-94, June 15.
Cummack C. H. and King G. A. M.	1959	*N.Z. J. Geol. Geophys.* **2**, 634.
Matsushita S.	1959	*J. Geophys. Res.* **64**, 1149.
Naismith R.	1954	*J. Atmosph. Terr. Phys.* **5**, 73.
Thomas L.	1960	*Some Ionospheric Results of the I.G.Y.* (Ed. by W. J. G. Beynon) p. 172. Elsevier, Amsterdam.

A new type of ionospheric drift recorder

(*Received* 9 *February* 1961)

The spaced receiver method developed by Mitra (1949) has been used extensively by several investigators for measurement of horizontal drifts in the ionosphere as it has the main advantage that it can be used practically all the time. The method is, however, laborious particularly as it involves photographic recording of the fading signals and analysis of records. The need has been long felt for the development of an instrument in which the time displacements are directly recorded. The Phillips recorder (1955), developed with this end in view, has the major advantage over signal recording methods that the time delay is recorded with its proper sign as a deflection on a pen recorder. Although the Philips recorder is decidedly an improvement over the usual method, it has the drawback that the recorder does not work reliably at all times and further considerable calculation is involved in order to obtain average time displacements. In this communication the authors present a brief description of a new type of drift recorder developed by them which gives the average time difference between any two fading records from spaced aerials.

While all the previous methods for ionospheric drift measurements are concerned with measuring time displacements by comparing the actual fading patterns and recording time differences between maxima or minima, the present method is based on the principle of introducing a time delay into one of the pair of time varying fading signals such that there is no net average time difference between them. In other words the delay introduced will be such as to compensate the average time difference originally existing between the two signals. This variable time delay is introduced by using a magnetic tape recorder with a continuously driven endless tape and a manually variable record–reproduce head separation. The block diagram of the entire experimental set-up is shown in Fig. 1.

Signals from aerials A_1, A_2 and A_3 situated at the three corners of a right-angled triangle are fed into three identical BC 348 receivers converted for pulse operation. A one-pole two-way switch S_1 permits the comparison of fading of signals from either aerials A_1–A_2 or A_2–A_3. The amplified and detected signals from either of these pairs of aerials is fed into gated integrators I and II to isolate one of the required signals from the ionosphere and integrate the pulses (which have a repetition frequency of 50 c/s) to give a smoothed d.c. output signal whose variation is a true replica of the original signal. The output from the gated integrator I is fed into a frequency modulator, which generates square waves the frequency of which vary from 4·2 to 9·8 kc/s as the input signal varies from minimum to maximum, the range of input signal variation being 24 V. The frequency modulated

VOL. 21 1961

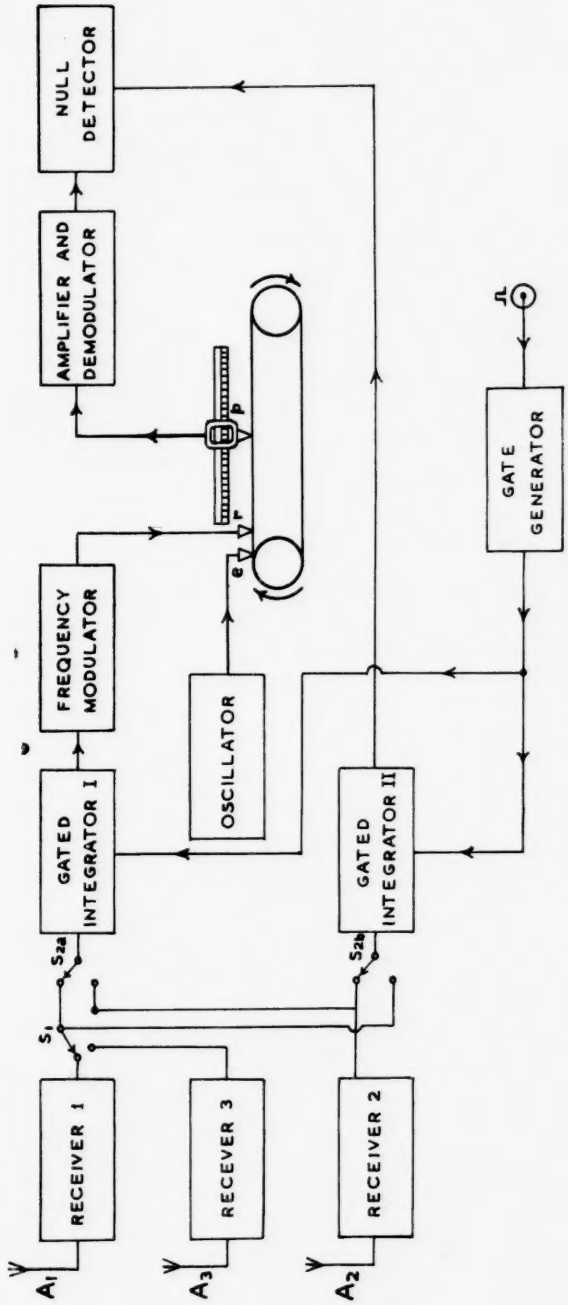

Fig. 1. Schematic diagram of magnetic delay ionospheric drift recorder.

signals from this unit are fed into a magnetic recording head which is in contact with a magnetic tape driven at a speed of 7·5 in/sec. The signals recorded on the magnetic tape are received by a reproducing head and the distance between it and the recording head can be varied continuously, so that a known time delay is introduced in the signal. It is found that the maximum separation required does not exceed 10 in., corresponding to a delay of about $1\frac{1}{2}$ sec. The signal from the reproducing head is fed into an amplifier and demodulator stage, the output of which is a true replica of the original signals but with a time delay. The outputs from the demodulator and the gated integrator II are adjusted to be equal and are fed into a double triode balanced cathode follower amplifier between the cathodes of which is placed an a.c. milliammeter. The deflection in the detector, due to the a.c. voltage between the cathodes, is a function of the time delay between the almost similar input signals. When the time delay between the signals is adjusted on the average to be zero, the deflection in the a.c. milliammeter will be a minimum. By manually varying the reproducing head position to give minimum output in the a.c. detector, and noting the distance between the record and reproduce heads and the speed of the tape, the time delay T is obtained. This minimum is observed only if the signal output of receiver 2 is delayed with respect to that of receiver 1. In cases in which the time delay is the other way, the receivers connected to the gated integrators are inter-changed by a double-pole double-throw switch S_2 so that the signal whose phase is ahead is fed into the tape delay system following the gated integrator I.

The main advantage of this method is the simplicity in obtaining average time delay without having recourse to taking fading records. The accuracy of delay control setting for minimum in the detector is not high, but the overall accuracy can be improved by taking the average of several observations. The recorder has the limitation that it can record a minimum time delay of 0·07 sec. A detailed paper giving all the technical details will shortly be published elsewhere. We are indebted to the Council of Scientific and Industrial Research for financial support of this research project.

B. Ramachandra Rao
R. Raghava Rao

Ionosphere Research Laboratories
Andhra University
Waltair, India

References

Mitra S. N. 1949 *Proc. Instn Elect. Engrs* III **96**, 441.
Phillips G. J. 1955 *J. Atmosph. Terr. Phys.* **6**, 124.

The anisotropy of turbulence at the meteor level

(*Received* 13 *February* 1961)

Recently it has been realized that the irregular motions that have been observed at the meteor level of the ionosphere (say 90 km in height) cannot be regarded as "turbulence" of the kind studied in the laboratory; nor can the theory of isotropic turbulence be applied. Both the observational and theoretical aspects were discussed at length in the International Symposium on Fluid Mechanics in the Ionosphere (*Journal of Geophysical Research*, 1959, Vol. 64, pp. 2037–2238).

Greenhow and Neufeld (1959a, b) reported "large eddies" with a vertical scale of 6 km and a horizontal scale of the order of 150 km. Greenhow (1959) also mentions that

estimates of the parameters describing the small eddies (i.e. the eddies in which most of the turbulent dissipation is taking place) can be obtained from the rate of expansion of a meteor trail during the early stages of its life. BOOKER (1959) has pointed out that if the latter data are used to estimate the rate of turbulent dissipation per unit mass, ε, the value obtained is quite inconsistent with the data for the large eddies, if the ordinary formulae are applied. BOLGIANO (1959, 1960) has outlined a theory in which the smaller eddies (the dissipation range and part of the inertial range if it exists) are isotropic, while larger eddies are anisotropic because of the buoyancy forces.

The purpose of this note is to present a simple way of estimating very roughly the size at which anisotropy should begin (the change does not take place abruptly, of course) and discuss the numerical results so obtained, using GREENHOW's data. The basic idea was given by STEWART (1959) during a discussion at the International Symposium mentioned above (see p. 2070). One supposes, for reasons which will be apparent shortly, that at sufficiently small sclaes, i.e. sufficiently large wave-number, k, the ordinary theory of isotropic turbulence holds and buoyancy effects are negligible. Thus in the inertial range the energy spectrum function (per unit mass per unit interval of wave number) is

$$E(k) \propto \varepsilon^{2/3} k^{-5/3} \tag{1}$$

where a numerical factor of order unity is omitted. The energy in a band of width k (say from $\frac{1}{2}k$ to $\frac{3}{2}k$) is therefore of order

$$(\varepsilon/k)^{2/3}. \tag{2}$$

This is a rough measure of the turbulent kinetic energy per unit mass due to motions at a scale $L = k^{-1}$.

This must be compared with the potential energy associated with such motions, which is simply the work done in raising unit mass adiabatically through a height L, namely

$$\frac{1}{2}\frac{g}{\theta_0}\frac{d\theta_0}{dz}L^2 \tag{3}$$

(BRUNT, 1944, Chap. II). Here $\theta_0(z)$ is the potential temperature in the unperturbed atmosphere, defined by

$$\frac{1}{\theta_0}\frac{d\theta_0}{dz} = \frac{1}{T}\left(\frac{dT}{dz} + \Gamma\right) \tag{4}$$

$T(z)$ is the actual temperature and $\Gamma = g/c_p$ is the adiabatic lapse rate. So, neglecting the factor $\frac{1}{2}$, we define a Richardson number for an eddy, with respect to the unperturbed density distribution, by the ratio of (2) to (3), namely

$$R_i(k) = \frac{g}{\theta_0}\frac{d\theta_0}{dz}\varepsilon^{-2/3}k^{-4/3} = \left(\frac{k}{k_0}\right)^{-4/3} \tag{5}$$

where k_0 is a critical wave number

$$k_0 = \varepsilon^{-1/2}\left(\frac{g}{\theta_0}\frac{d\theta_0}{dz}\right)^{3/4}. \tag{6}$$

As anticipated (5) shows that for very large k the buoyancy forces are negligible, since R_i is small. In addition, (6) provides an estimate of the wave number at which buoyancy cannot be neglected. Because of the resulting tendency to supress vertical motion the spectrum becomes anisotropic at about this point, and (1) presumably ceases to hold.

All this assumes that $L_0 = k_0^{-1}$ is greater than the scale of the smallest eddies,

$$L_2 = (\nu^3/\varepsilon)^{1/4} \tag{7}$$

where ν is the kinematic viscosity. If, on the other hand, $L_2 > L_0$, there is no inertial range in the usual sense.

BOLGIANO (1959, 1960) proposes that the inertial range be divided into a small-scale part, in which (1) applies, and a large-scale part which he calls the "buoyancy subrange". For the latter, a dimensional argument leads to a $k^{-11/5}$ law to replace (1). The two subranges are separated by a wave number k_B, and it may well be asked why k_B differs from the k_0 as defined in (6). The reason for this lies in the choice of parameters assumed to be relevant in the dimensional argument. BOLGIANO chooses a "rate of production of mean square density fluctuations" as his parameter. He shows that at $k = k_B$, the Richardson number characterizing an eddy is unity, provided this Richardson number is calculated with respect to the typical gradient in θ arising from the fluctuations at all scales greater than the eddy itself, rather than with respect to the unperturbed gradient, as at (5). Since the turbulent gradients are greater than the mean gradient, we expect $k_B > k_0$, i.e. $L_B < L_0$, where $L_B = k_B^{-1}$.

It seems to the present writer that the difference between these two results is less important than might at first be thought. It is true that in the case of mixing of a passive scalar, the root mean square gradients developed may be greatly in excess of the original gradient (BATCHELOR, 1959). For our purpose, however, it is only the *vertical* gradient of θ that is relevant, and the suppression of vertical motion at scales greater than that at which anisotropy becomes appreciable suggests that enhanced vertical gradients at such scales are not built up. If this is so, L_0 will not exceed L_B by a very large factor. Clearly both arguments involve unknown numerical factors and can do no more than suggest order-of-magnitude results. In addition, the use of dimensional methods can be criticized in the present situation, on the grounds that a simple power law may be inadequate to represent fields whose horizontal and vertical structures may depend on different parameters.

It is of great interest to consider the numerical consequences of these ideas. To calculate the critical size L_0 we need only GREENHOW's (1959) estimate $\varepsilon \approx 70$ cm^2 sec^{-3} at a height of 90 km, together with $T \approx 200°$K, $\Gamma \approx 10°$km^{-1} and $dT/dz \approx -2°$km^{-1}. Then (6) yields

$$L_0 = k_0^{-1} = 30 \text{ m}.$$

Taking $\nu = 4 \times 10^4$ cm^2 sec^{-1}, (7) yields

$$L_2 = 10 \text{ m}.$$

Thus the isotropic inertial range barely exists at all. Presumably any reasonable estimate of BOLGIANO's $L_B = k_B^{-1}$ would merely strengthen this conclusion. For comparison, we recall that the energy-containing motions have vertical scale

$$L_1 \approx 6 \text{ km}$$

and horizontal scale still bigger. Clearly only a trivial proportion of the total kinetic energy resides in the isotropic part of the spectrum.

This leaves unanswered the question of what *is* the nature of the large-scale energy containing "eddies" observed by GREENHOW and NEUFELD, and others. All we have shown is that they cannot be regarded as ordinary turbulence with buoyancy effects as a mere perturbation. In particular, the formula $\varepsilon \approx V_1^3/L_1$, where $V_1 \approx 25$ m sec^{-1} is a representative velocity, grossly overestimates ε, indicating that the flow has a more ordered structure than it would have if it were an ordinary turbulent one. I have remarked elsewhere (DOUGHERTY, 1960) that by regarding the "large eddies" as internal gravity waves of the kind considered by HINES (1960) and restricting the ideas of turbulence to the small eddies, a satisfactory qualitative picture of the whole motion emerges.

At heights greater than 90 km, the rapid increase in ν, which is unlikely to be matched by a corresponding increase in ε, means that

$$\frac{L_0}{L_2} = \left(\frac{\nu}{\varepsilon}\frac{g}{\theta_0}\frac{d\theta_0}{dz}\right)^{-3/4}$$

decreases still further. When its value falls below about unity, no inertial range exists at all. STEWART (1959, p. 2084) has mentioned that considerations of Reynold's and Richardson's numbers indicate that turbulence should cease altogether at a height of the order of 120 km. These various arguments suggest that the temptation to invoke turbulence as the cause of many of the ionospheric scattering phenomena (spread-F, radio star scintillation, etc.) should be avoided.

HOWELLS (1959, 1960) and DOUGHERTY (1960) have considered the production and propagation of irregularities in the electron density in the presence of a turbulent flow of neutral air, and a magnetic field. The main point of interest at that time was the effect of the magnetic field, and for simplicity isotropic turbulence was assumed. The considerations of the present note show that the results so obtained are relevant only over a rather small range of wave number; however, scattering theory indicates that this may well be the important range for fading experiments since the half-wavelength for reflection from the E-layer is around 50 m.

Acknowledgements—I am grateful to Dr G. K. BATCHELOR for a helpful discussion. This note was written during the tenure of a D.S.I.R. Research Studentship. My attendance at the International Symposium on Fluid Mechanics in the Ionosphere, at Cornell University, was made possible by the United States Office of Naval Research.

Cavendish Laboratory, Cambridge J. P. DOUGHERTY

REFERENCES

BATCHELOR G. K.	1959	*J. Fluid Mech.* **5,** 113.
BOLGIANO R., Jr.*	1959	*J. Geophys. Res.* **64,** 2226.
BOLGIANO R., Jr.	1960	*J. Res. Nat. Bur. Stand.* **64D,** 231.
BOOKER H. G.*	1959	*J. Geophys. Res.* **64,** 2074.
BRUNT D.	1944	*Physical and Dynamical Meteorology* (2nd Ed.), Cambridge University Press.
DOUGHERTY J. P.	1960	*Phil. Mag.* **5,** 553.
GREENHOW J. S.*	1959	*J. Geophys. Res.* **64,** 2208.
GREENHOW J. S. and NEUFELD E. L.*	1959a	*J. Geophys. Res.* **64,** 2129.
GREENHOW J. S. and NEUFELD E. L.	1959b	*Proc. Phys. Soc. Lond.* **74,** 1.
HINES C. O.	1960	*Canad. J. Phys.* **38,** 1441.
HOWELLS I. D.*	1959	*J. Geophys. Res.* **64,** 2198.
HOWELLS I. D.	1960	*J. Fluid Mech.* **8,** 545.
STEWART R. W.*	1959	*J. Geophys. Res.* **64,** 2070, 2084.

* Contributions to the International Symposium on Fluid Mechanics in the Ionosphere. Cornell University, July 1959.

The λ2763 Å (0,9) band of the O_2 Schumann-Runge system

(*Received* 6 *March* 1961)

THE SCHUMANN–RUNGE band system of O_2 and its associated photo-dissociation continuum are important constituents of the absorption spectrum of the atmosphere (GOLDBERG, 1954). The continuum ($X^3\Sigma_g^-$, $(v = 0) \rightarrow B^3\Sigma_u^-$ above dissociation limit) lies between 1300 and 1750 Å while bands of the $X^3\Sigma_g^-$, $v = 0$ progression lie between 1750·8 and 2025·2 Å. They are the absorption spectrum in this range of cold oxygen. Bands of higher wavelengths occur in the absorption spectrum of hot oxygen and in the emission spectrum.

Bands have been observed, mainly in emission, between 1750·8 Å and 4400 Å for the complete system whose primary Condon "parabola" is very wide, one limb of which lies along the $v' = 0$ sequence, $v'' > 11$ (NICHOLLS, 1960).

Vibrational and rotational analyses have been made for sufficient bands (LOCHTE-HOLTGREVEN and DIEKE, 1929; CURRY and HERZBERG, 1934; KNAUSS and BALLARD, 1935, FEAST, 1948, 1949, 1950; BRIX and HERZBERG, 1954) to establish vibrational and rotational constants and the dissociation energy definitively.

Many of the bands in emission in the $v' = 0, 1, 2, 3$ sequences are easily excited in a high voltage atmospheric pressure arc (FEAST, 1948, 1949, 1950) and also have been observed in absorption through shock-heated oxygen (TREANOR and WURSTER, 1960). GARTON and FEAST (1950) also report photography of the (4,5), (5; 3,4), (5,6), (6; 2,3), (7,3) bands in absorption through heated oxygen.

Table 1. The Schumann–Runge (0,9) band

P branch					*R* branch				
K	λ (air)	cm^{-1}	I_e*	I_p†	K	λ (air)	cm^{-1}	I_e*	I_p†
5	—	—	—	—	5	2763·04	36,181·3	1	15
7	2765·59	36,148·0	3	29	7	2763·77	171·8	1	25
9	2767·12	128·0	3	18	9	2764·82	158·0	5	39
11	2768·96	104·0	4	65	11	2766·22	139·8	4	54
13	2771·10	76·2	3	48	13	2767·85	118·5	7	51
15	2773·56	44·2	3	100	15	2769·78	93·3	6	76
17	2776·32	8·3	4	67	17	2771·99	64·6	4	60
19	2779·37	35,968·8	7	61	19	2774·49	32·0	4	28
21	2782·68	926·0	4	67	21	2777·29	35,995·7	5	83
23	2786·31	879·1	1	94	23	2780·43	955·1	3	47
25	2790·26	828·5	5	51	25	2783·76	912·1	3	43
27	2794·51	773·9	5	73	27	2787·50	863·9	4	59
29	2799·07	715·7	4	37	29	2791·53	812·5	4	42
31	2803·94	653·6	5	38	31	2796·00	754·9	3	44
33	2809·15	587·5	4	39	33	2800·66	695·3	3	51
35	2814·66	517·8	4	38	35	2805·67	631·7	4	44
37	2820·52	444·1	4	57	37	2810·99	564·4	2	35
39	2826·72	366·3	7	75	39	2816·63	492·9	7	58
41	2833·24	286·0	4	46	41	2822·63	417·5	4	32
					43	2828·94	338·5	4	32
					45	2835·62	255·4	5	40

* I_e: eye estimate of line intensity. † I_p: relative photoelectric intensity.

In a recent experimental study, photoelectric intensity measurements were made in emission upon thirty bands ($v' = 0$, $v'' = 9$–19; $v' = 1$, $v'' = 8$–12, 16–20; $v' = 0$, $v'' = 7$–9, 15, 16, 19–21) of the system (HÉBERT and NICHOLLS, 1961). The 0,9 band at 2763 Å which was measured has not previously been reported. Its rotational analysis is straightforward and is presented in Table 1. MOORE and BROIDA (1959a,b) have emphasized the importance of such detailed analyses for positive identification of features in complex solar and stellar spectra. Table 1 may thus be of some use in the interpretation of emission and absorption spectra of hot oxygen and hot air, and when available, spectra of high altitude nuclear explosions (GRIGGS and PRESS, 1961).

Acknowledgements—This work was made possible by research grants from the National Research Council of Canada. It was also supported in part by research grants from the

VOL. 21 1961

Defence Research Board of Canada and the Ontario Research Foundation and from contracts with the Air Force Cambridge Research Center, The Air Force Office of Scientific Research, The Office of Naval Research and The Department of Defence Production of Canada. One of us (G. R. H.) gratefully acknowledges the financial support of The Ontario Research Foundation by awards of Studentships and a Fellowship.

G. R. HÉBERT*
R. W. NICHOLLS

Department of Physics
University of Western Ontario
London, Ontario

REFERENCES

BRIX D. and HERZBERG G.	1954	*Canad. J. Phys.* **32**, 110.
CURRY J. and HERZBERG G.	1934	*Ann. Phys., Lpz.* **19**, 800.
FEAST M. W.	1948	*Nature, Lond.* **162**, 214.
FEAST M. W.	1949	*Proc. Phys. Soc. Lond.* A **62**, 114.
FEAST M. V.	1950	*Proc. Phys. Soc. Lond.* A **63**, 549.
GARTON W. R. S. and FEAST M. W.	1950	*Nature, Lond.* **165**, 281.
GOLDBERG L.	1954	*The Earth as a Planet* (Ed. by G. KUIPER) p. 441. University of Chicago Press.
GRIGGS D. T. and PRESS F.	1961	*J. Geophys. Res.* **66**, 237.
HÉBERT G. R. and NICHOLLS R. W.	1961	In preparation.
KNAUSS H. P. and BALLARD S. S.	1935	*Phys. Rev.* **48**, 796.
LOCHTE-HOLTGREVEN W. and DIEKE G. H.	1929	*Ann. Phys., Lpz.* **3**, 937.
MOORE C. E. and BROIDA H. P.	1959a	*J. Res. Nat. Bur. Stand.* **63** A, 19.
MOORE C. E. and BROIDA H. P.	1959b	*J. Res. Nat. Bur. Stand.* **63** A, 279.
NICHOLLS R. W.	1960	*Canad. J. Phys.* **38**, 1705.
TREANOR C. E. and WURSTER W. H.	1960	*J. Chem. Phys.* **32**, 758.

* Now at St. Francis Xavier University, Antigonish, Nova Scotia.

Year-to-year changes in the winter anomaly in ionospheric absorption

(*Received* 16 *March* 1961)

THE anomalous and large increases in ionospheric absorption in winter months at middle latitudes was first observed by APPLETON (1937). Subsequent studies have revealed no short-term correlation between this anomalous absorption and solar or magnetic activity (LANGE–HESSE, 1953; APPLETON and PIGGOTT, 1954). An examination of the absorption data for several stations during the I.G.Y. has confirmed these results.

In this note we examine the year-to-year changes in the anomaly and its association with the incidence of solar or magnetic activity. The absorption data for Slough for the period 1943–1954 are used. These data are conveniently summarized by the Slough "A" figure (PIGGOTT, 1953) which represents the non-deviative absorption on an equivalent frequency of 1 Mc/s, after correcting for deviative losses near f_0E.

The mean absorption in summer months is closely correlated with the changes in solar activity as represented by sunspot number and, in particular, it shows a maximum in 1947 and minima in 1942 and 1954. The winter data also show minima in years of low solar activity 1944–1945, 1954–1955 but a broad maximum occurs in the years of high magnetic

activity 1948–1952, when solar activity was already past its peak level. Thus the correlation of the mean winter absorption with sunspot number is much weaker than in summer.

We examine the year-to-year changes in the anomaly by considering for each year the ratio of the observed mean value to the computed value for the normal absorption in winter. This is calculated from the summer value by assuming that the seasonal changes in normal absorption are always proportional to $\cos \chi^{0.75}$ (APPLETON and PIGGOTT, 1954).

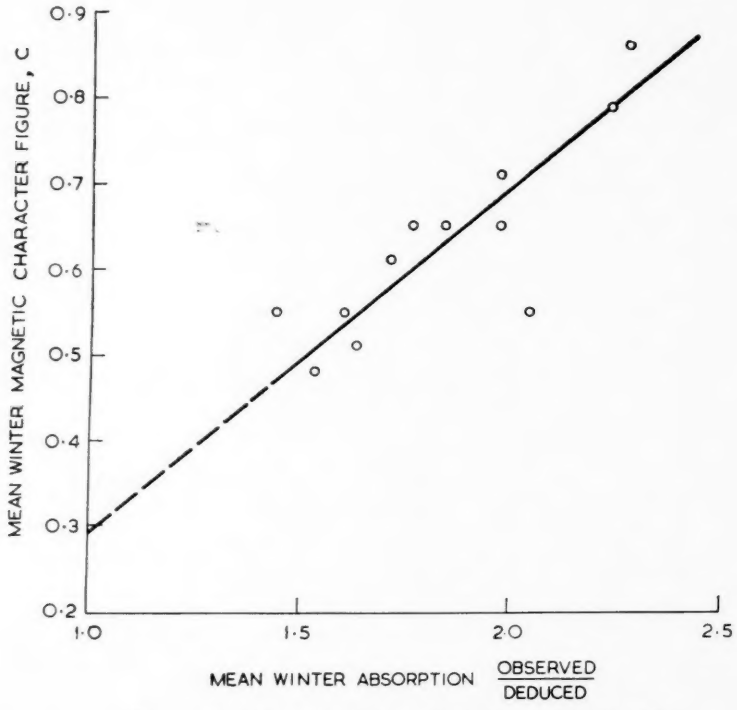

Fig. 1. Variation of anomalous absorption at Slough with magnetic activity 1943–1954.

Allowance is also made for any changes between the mean levels of solar activity in the summer and winter months (PIGGOTT, 1959). The resultant ratios show no significant correlation with the year-to-year changes in mean sunspot number. The ratios are, however, associated with C the mean International Magnetic Character Figure (Fig. 1). There is little correlation between sunspot number and magnetic activity themselves since the magnetic activity continues to increase during the decline of sunspot activity after its peak. The line of best fit suggests that the anomaly would disappear at a very low but finite value of mean magnetic activity. The correlation coefficient is 0·84 and is significant at the 0·1 per cent level.

Thus our analysis shows that the average absorption in winter may be expressed as the product of two terms:

(a) a normal absorption which varies with solar cycle and solar zenith angle only;
(b) a factor, representing the anomaly, which is proportional to the year-to-year changes in magnetic activity.

VOL. 21 1961

Acknowledgements—The work described was carried out as part of the programme of the Radio Research Board. This paper is published by permission of the Director of Radio Research of the Department of Scientific and Industrial Research.

L. Thomas

*D.S.I.R. Radio Research Station**
Ditton Park, Slough, Bucks.

References

Appleton E. V.	1937	*Proc. Roy. Soc.* A **162,** 451.
Appleton E. V. and Piggott W. R.	1954	*J. Atmosph. Terr. Phys.* **5,** 141.
Lange-Hesse G.	1953	*J. Atmosph. Terr. Phys.* **3,** 153.
Piggott W. R.	1953	*Proc. Instn. Elect. Engrs* III **100,** 61.
Piggott W. R.	1959	D.S.I.R. Radio Research Station, Spec. Rep. No. 27.

* Official communication.

Journal of Atmospheric and Terrestrial Physics, 1961, Vol. 21, pp. 218 to 219. Pergamon Press Ltd. Printed in Northern Ireland

BOOK REVIEWS

G. R. BURBIDGE, F. D. KAHN, R. EBERT, S. v. HOERNER and St. TEMESVARY: **Die Entstehung von Sternen.** Springer, Berlin, 1960. 330 pp., 38 DM.

IN ORDER to stimulate a thorough investigation into the basis of present day theories of stellar evolution, the Gesellschaft Deutscher Naturforscher und Ärzte announced in 1956 that they would award a special prize for a treatise containing a critical survey of recent work on "The Formation of Stars by Condensation of Diffuse Matter." The Society received twelve papers as the result of this announcement. Three of these were judged to be of the very highest and equal merit, and it is these which are collected in the present book. They were written, the first two in English, the third one in German, by G. R. BURBIDGE of Chicago, F. D. KAHN of Manchester, and R. EBERT, S. v. HOERNER and St. TEMESVARY of Hamburg, Heidelberg and Munich. It is fortunate that the competition attracted contributors from such distinguished workers in the field.

Each of the three papers examines in more or less detail the same fundamental questions: the problem of the original formation of stars, possible theoretical ways of stellar evolution, and the interplay between theory and observation in the study of the evolution of stellar associations, star clusters, and stellar populations. However, each of the authors naturally emphasizes what seems to him or to the school he comes from of particular importance. As a result, the sum of these three papers presents a pleasantly balanced and therefore particularly instructive survey of this very complex field. One must be grateful to the German Society and its president, Professor O. HECKMANN, not only for arranging this very topical competition, but also for publishing its results in the form of this book.

Since stellar evolution represents a rapidly developing field, much new work has been done since the essays of this book were submitted in 1958. Nevertheless, this volume is bound to remain for some time to come a splendid introduction into a problem which is at the heart of present astrophysics. It can be strongly recommended to physicists and research students, and, in the reviewer's opinion, might best be read in the sequence: KAHN, BURBIDGE, and the German group.

It is perhaps a pity that—unlike the case of the new *Handbuch der Physik*—the title of so valuable a book has been given in German only, which may possibly deter some non-German readers.

H. A. BRÜCK

G. FRANCIS: **Ionization Phenomena in Gases.** Butterworths, London, 1960. 300 pp., £3.

WHEN Professor A. VON ENGEL published his well-known treatise, *Ionized Gases*, in 1955, he recorded his gratitude to his pupils who had worked and argued with him on the subject over many years. Foremost among the pupils mentioned was Dr. GORDON FRANCIS, the author of the volume under review, who, in his turn, now gracefully acknowledges the inspiration and encouragement he received from his old teacher.

Dr. FRANCIS expressly states that his book is intended to be complementary to the various treatises on ionized gases published in recent years. For that reason he has avoided repeating accounts of the more well-known discharge processes such as the arc, the spark and the glow.

VOL. 21 1961

Instead he has concentrated on the physics of atomic processes in ionized media and discussed its application in a number of examples of up-to-date interest. Such examples include alternating and high-frequency discharges, upper-atmospheric ionization, high-current discharges and thermonuclear effects, as well as plasma oscillations and waves.

In the task he has set himself, Dr. FRANCIS succeeds admirably. His book has a unity which derives from the ambit of the scientific territory selected. He also writes with enviable lucidity. The volume can be recommended with confidence to students about to begin research in this important field of modern science.

Dr. FRANCIS is no convert to the metre-kilogram-second system of electrical units. Instead, he is an unrepentant believer in "the usual mixture of units". A Cambridge reviewer may feel that he can detect the influence of the Oxford Physics School, here and there, in Dr. FRANCIS' attractive volume. But he is sufficiently old-fashioned to note, with warm approval, that the author has resisted the influence of that famous Oxford teacher, F. B. PIDDUCK, a latter-day convert to the use of m.k.s. units.

E. V. APPLETON

H. BONDI, W. B. BONNOR, R. A. LYTTLETON and G. J. WHITROW: **Rival Theories of Cosmology.** Oxford University Press, 1960. 64 pp., 9s. 6d.

THIS LITTLE BOOK contains, in a slightly amplified version, the text of three broadcast talks on present day cosmology which were given in the Spring of 1959. Dr. BONNOR introduces relativistic theories, Professor BONDI writes on the steady-state theory, and Dr. LYTTLETON explains the effects on cosmology of a possible charge-excess in the proton over the electron. These chapters are followed by the text of the broadcast discussion of the rival theories which was held at the end of 1959 between the same three speakers under the chairmanship of Dr. WHITROW.

It would be difficult to explain in a more simple and lucid way than has been done here the essential points of these three theories and the reasons for their proposition. The stimulating discussion helps to clarify points which may have remained obscure in the chapters on individual theories, though—as would be expected by anybody familiar with the complexity of the problem—the discussion does not lead to any definite conclusion. In view of dogmatic attitudes adopted occasionally by other cosmologists, it is pleasing to hear Dr. LYTTLETON remind his readers that theories of cosmology "are still at a preliminary stage, waiting on observational evidence for their disproval or their precarious survival."

Issuing the talks in book form has enabled the authors to illustrate their discussion with a series of excellent representative photographs of galaxies taken with the 200 in. telescope on Mount Palomar.

H. A. BRÜCK

Journal of Atmospheric and Terrestrial Physics, 1961, Vol. 21, p. 220. Pergamon Press Ltd. Printed in Northern Ireland

Papers to be published in future issues

H. J. A. CHIVERS: A statistical study of ionospheric drifts measured by the radio star scintillation technique

H. UNZ: On vertical drift velocities of the *F2*-layer

U. HAUG: Zur Statistik der räumlichen Helligkeitsschwankungen der [OI]-Linie 5577 Å im Nachthimmelsleuchten

W. STOFFREGEN: The east–west drift of auroral forms determined from all-sky camera films

J. S. GREENHOW and J. E. HALL: Attachment processes in meteor trails

K. V. V. RAMANA and B. RAMACHANDRA RAO: Investigation of ionospheric absorption on 5·65 Mc/s at Waltair

S. N. GHOSH and V. MALAVIYA: Microwave absorption in the earth's atmosphere

M. S. V. GOPALA RAO and B. RAMACHANDRA RAO: Nocturnal and seasonal variations of equatorial spread-*F*

A. F. EL NADI and N. FARAG: The effect of light on the mobility and concentration of large ions in air mixed with N_2O gas

G. F. FOOKS: The fading of radio waves reflected vertically from the ionosphere during magnetic storms

O. K. GARRIOTT and A. W. NICHOL: Ionospheric information deduced from the Doppler shifts of harmonic frequencies from earth satellites

S. A. BOWHILL: Rocket measurements of *F*-layer electron density and their interpretation

D. VAN SABBEN: Ionospheric current systems of ten IGY-solar flare effects

J. S. GREENHOW: Head echoes from meteor trails

H. UNZ: The effect of small values of $Z = \nu/\omega$ on the complex refractive index in the magneto-ionic theory

VOL. 21 1961

ERRATA

J. Atmosph. Terr. Phys. **20** (1961)

J. K. HARGREAVES: Random fluctuations in very low frequency signals reflected obliquely from the ionosphere

Page 155, Abstract, line 5: for "1·02" read "0·12".

Page 164, Table 3, $\phi^2/\mathscr{A}^2$ for Night: for 0·8 ± 3·2" read "8·0 ± 3·2".

Journal of Atmospheric and Terrestrial Physics, 1961, Vol. 21, pp. 221 to 224. Pergamon Press Ltd. Printed in Northern Ireland

A statistical study of ionospheric drifts measured by the radio star scintillation technique

H. J. A. CHIVERS*
Nuffield Radio Astronomy Laboratories, Jodrell Bank, University of Manchester

(*Received* 22 *December* 1960)

Abstract—Ionospheric drifts have been measured by the radio-star scintillation spaced receiver technique and histograms are presented showing the magnitudes and directions of the drifts observed. The direction of drift is commonly found to reverse suddenly near 2300 hours local time, but the complementary reversal occurs at a less definite time during the following day.

EARLY MEASUREMENTS of ionospheric drifts determined by observing radio star scintillations at spaced receiving sites could only be made during night hours because of the lack of scintillations during the day (MAXWELL and DAGG, 1954). Drift speeds of the order of hundreds of metres per second were measured and the drift direction was nearly along an east–west line. The drifts were almost predominately westerly during the evening hours, but near midnight the drift direction commonly reversed quite suddenly so that the drifting was in an easterly direction.

The explanation of the fact that the drifting was always approximately along an east–west line has been furnished by SPENCER (1955). Since the irregularities causing scintillation are elongated along the lines of force of the earth's magnetic field, then the diffraction pattern projected onto the surface of the earth is similarly highly elongated. Because of this, only the component of the drift motion in or near the direction of the minor axis of the elongated blobs can be measured by a straightforward three-station technique (JONES, 1957), and this direction is very near east–west.

In spite of the limitations of the method for measuring either the magnitude or true direction of drift, the sudden reversals in direction can still be observed and it is the main purpose of this note to report on the diurnal variations of this phenomenon.

During the International Geophysical Year, regular drift observations were made on 80 Mc/s from Jodrell Bank with three stations spaced by about 1 km. The Cygnus (19N4A) radio source was observed for at least several days each month when near lower culmination. Scintillation of the source was always present for a period of about 5 hr centered on lower culmination regardless of the time of day at which the observations had to be made (LITTLE and MAXWELL, 1952). Thus the situation was different from that in the 1954 measurements when the source was observed at high elevations only and scintillations were only present at night.

In the course of the 18 months of the IGY, 627 determinations of drift motion were made. The drift directions are plotted in histogram form in Fig. 1 where the angles refer to the direction which the irregularities were approaching. It can be seen that most of the directions measured came within the range of directions

* Now with the National Bureau of Standards, Boulder, Colorado, U.S.A.

expected assuming the irregularities are elongated along the magnetic field direction (SPENCER, 1955). The drift speeds measured are shown in Fig. 2. The values observed ranged from 50 to 3700 m/sec and it can be seen from the histogram that the most common speed was between 200 and 300 m/sec.

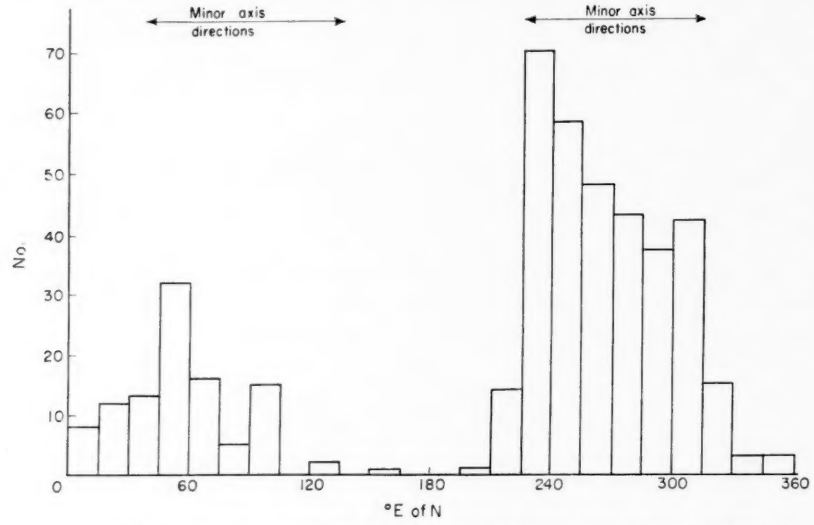

Fig. 1. Histogram of drift directions using Cygnus near lower culmination.

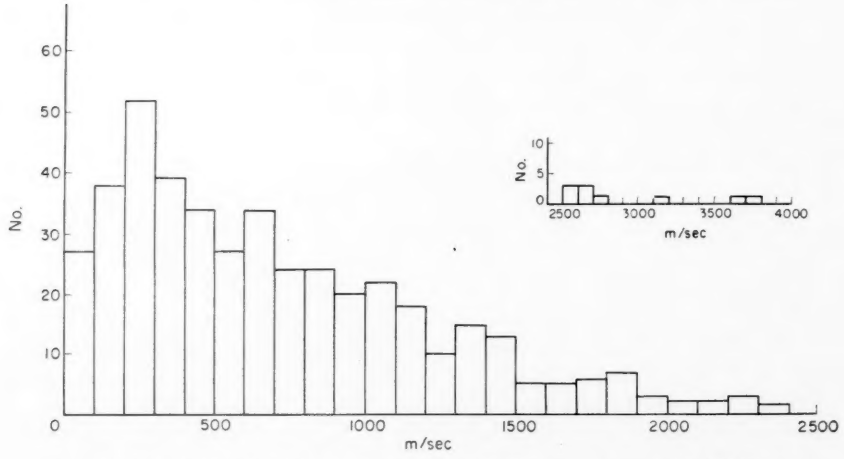

Fig. 2. Histogram of drift speeds using Cygnus near lower culmination.

To examine the "reversal" problem, the percentage of westerly drifts for each hour of the average solar day has been determined. In order to weight the percentages obtained according to the number of determinations in each hour, a 4 hr weighted running mean has been determined and is shown by the solid line in Fig. 3(a). It can be seen that near 1800 U.T., 96 per cent of the measured drifts were in a westerly direction, and that this value falls steadily to reach a minimum of 42 per

VOL. 21 1961

cent at 0300 U.T. On this evidence, drifts would be in a westerly direction almost every day and there would be just over a 50 per cent probability of a reversal in direction occurring during the night hours.

During actual observing periods, which usually lasted for several hours, sudden reversals were sometimes recorded, but these were few compared with the total number of vectors measured. Accordingly, to examine the diurnal distribution of reversals the diurnal distribution of westerly vectors has been used in the following

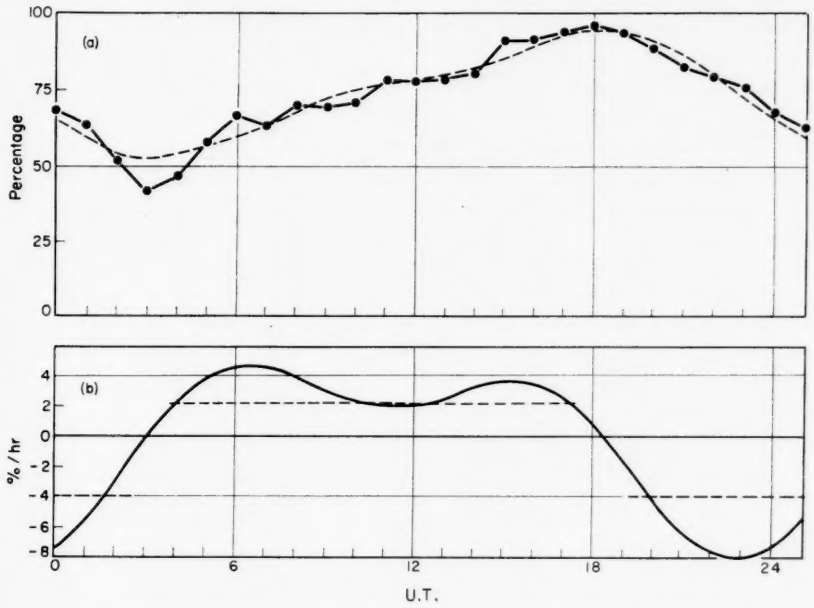

Fig. 3. (a) Percentage occurrence of westerly drifts. (b) Differential of harmonic curve.

way. A smooth curve has been fitted to the experimental points by harmonic analysis, and if y is the percentage of westerly drifts, and t is the time in hours, the equation obtained can be written:

$$y = 74{\cdot}5 - 19{\cdot}0 \sin 15(t + 0{\cdot}5) - 6{\cdot}0 \sin 30(t + 0{\cdot}07) + 3{\cdot}0 \sin 45(t + 2{\cdot}0)$$

including terms to the third harmonic only. Since the amplitude of the third harmonic curve is about the same as the probable error in the experimental value of y, it is not considered significant. The calculated points using terms to the second harmonic are plotted in Fig. 3(a) and are connected by the dashed line. Since the best estimate of the most probable time for the occurrence of a reversal is the time at which this curve has the greatest slope, its first differential has been derived and is reproduced in Fig. 3(b). The differential has a distinct negative value at 2300 hours but the two positive maxima are not so distinctive. It can be seen that the half amplitude width of the negative excursion is 6 hr while that of the positive excursion is 14 hr. The interpretation of this curve is that the most probable time

for the observation of a reversal from westerly to easterly drifting is near 2300 hours but that there is no definite time for the occurrence of the complementary reversal.

The information on reversals which has just been presented, can be compared with the MAXWELL and DAGG work of 1954 who found that drift measurements referring to temperate latitudes indicated a reversal from westerly to easterly drifting occurring near midnight. A few observations made by these authors on the Cygnus source when at low elevation (i.e. at high latitudes) indicated that the reversal occurred near 2100 hours local time. DAGG (1956) suggested that the time of reversal would be near 0100 hours under quiet magnetic conditions, but occurred earlier under disturbed conditions. For the most intense storms, the time would be 2100 hours which would coincide with the time quoted for the reversal in drift direction of auroral radio-echo regions (BULLOUGH *et al.*, 1957).

The present results have not been analysed to establish if there was any dependence on the prevailing magnetic conditions because of the lack of observations of actual reversals. However, the fact that the most probable time of a westerly to easterly reversal was near 2300 hours local time, is in accordance with the results quoted above for both scintillation and magnetic field reversals. The indication that the most probable time of an easterly to westerly reversal occurred between 0300 and 1800 hours is compatible with the observation that the average time in the second reversal of the magnetic field during magnetic storms occurred near midday (WATKINS, 1959). As MEINEL (1955) has pointed out for magnetic storms, the time of reversal varies from storm to storm but the average effect is that of a current system which changes from westward to eastward near midnight and from eastward to westward near midday . The present result showing the occurrence of reversals by the scintillation technique throughout the day, agrees with this statement.

Acknowledgements—This work formed a part of the programme of the British National Committee for the International Geophysical Year. I am grateful to Professor A. C. B. LOVELL who made the research facilities at Jodrell Bank available to me.

REFERENCES

BULLOUGH K., DAVIDSON T. W., KAISER T. R. and WATKINS C. D.	1957	*J. Atmosph. Terr. Phys.* **11,** 237.
DAGG M.	1956	Ph.D. thesis, University of Manchester.
JONES I. L.	1957	*J. Atmosph. Terr. Phys.* Special Supplement on Polar Atmospherics Symposium, p. 3.
LITTLE C. G. and MAXWELL A.	1952	*Phil. Mag.* **42,** 267.
MAXWELL A. and DAGG M.	1954	*Phil. Mag.* **45,** 551.
MEINEL A. B.	1955	*Astrophys. J.* **122,** 206.
SPENCER M.	1955	*Proc. Phys. Soc. Lond.* B **68,** 493.
WATKINS C. D.	1959	Ph.D. thesis, University of Manchester.

VOL. 21 1961

Journal of Atmospheric and Terrestrial Physics, 1961, Vol. 21, pp. 225 to 236. Pergamon Press Ltd. Printed in Northern Ireland

Zur Statistik der räumlichen Helligkeitsschwankungen der [OI]-Linie 5577 Å im Nachthimmelsleuchten*

U. Haug
Astronomisches Institut der Universität Tübingen

(*Received* 7 *January* 1961)

Abstract—Photoelectrical records of the [OI] 5577 Å line in the nightglow from the Hochalpine Forschungsstation Jungfraujoch/Switzerland have been analysed under the assumption that the emitting layer lies near 100 km. The brightness variations are mostly below 25 per cent of the mean intensity and exceed 50 per cent in only 5 per cent of all cases. The variations could be classified either as "local enhancements" or as "gradients of brightness". A simple model calculation shows that the mean diameter of the bright patches is generally not much larger than 1000 km whereas Roach *et al.* (1958b) consider airglow cells with diameters of approximately 2500 km.

Einleitung

Im Winter 1957/58 und 1958/59 wurden im Rahmen des A.G.I. auf der Hochalpinen Forschungsstation Jungfraujoch (Schweiz) lichtelektrische Messungen der grünen Sauerstofflinie [OI] 5577 Å im Airglow durchgeführt. Diese werden im folgenden dazu verwendet, statistische Angaben über Helligkeitsunterschiede an verschiedenen Stellen der Emissionsschicht zu machen. Im Teil I wird zunächst auf die Schwierigkeiten und Unsicherheiten hingewiesen, denen die Gewinnung solcher Aussagen von nur einem Beobachtungsort aus unterworfen ist. Die Behandlung der Messanordnung und Reduktionsmethode (Teil II) kann sehr kurz gehalten werden, da diese von den allgemein üblichen kaum abweichen (vgl. insbesondere Elsässer und Siedentopf, 1956, sowie Roach, 1957). Die statistischen Ergebnisse werden im Teil III dargestellt und besonders im Zusammenhang mit den Resultaten von Roach *et al.* (1958b) über die charakteristische Grösse von "Airglow-Zellen" diskutiert.

I. Beobachtung einer Emissionsschicht von einem Beobachtungsort aus

Die Verhältnisse bei der Beobachtung der Emission einer Schicht in der Höhe h über dem Erdboden, deren Dicke Δh klein verglichen mit h ist, sind in Abb. 1 vergröbert dargestellt. Man hat bei der Beobachtung in der Zenitdistanz ζ folgende Effekte:

(a) Die emittierende Schicht wird schräg angeschnitten; die wirksame Weglänge und damit die Emission wird vergrössert. Die Umrechnung der emittierten Intensität I_e in die Emission senkrecht zur Schicht $I_{e,s}$ nach der van Rhijnschen Beziehung

$$I_{e,s}:I_e = \cos\phi = \sqrt{\left[1 - \left(\frac{R}{R+h}\right)^2 \sin^2\zeta\right]} = V(h,\zeta) \qquad (1)$$

—R ist der Erdradius—liefert vergleichbare Helligkeiten für alle Zenitdistanzen.

* Mitteilungen des Astronomischen Instituts der Universität Tübingen Nr. 55.

(b) Die wachsende Entfernung des Beobachters von der Schicht mit der Zenitdistanz geht in die Korrektur der gemessenen Helligkeiten wegen Absorption und Streuung in der Atmosphäre unterhalb der Schicht ein. Unsicherheiten im Extinktionskoeffizienten und bei der Berechnung des gestreuten Anteils können zu systematischen Fehlern in Abhängigkeit von der Zenitdistanz führen. Die

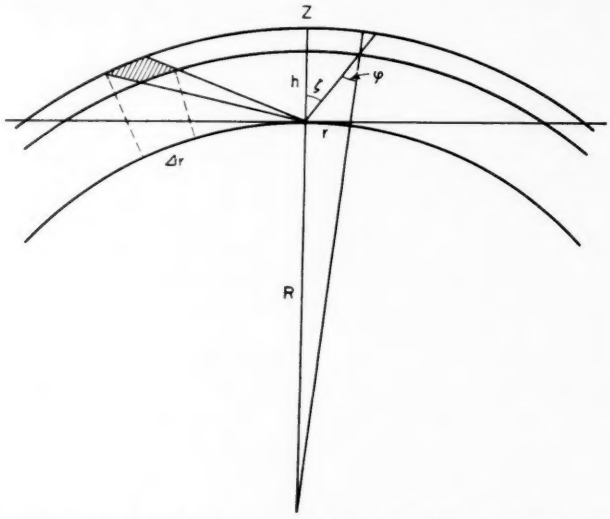

Abb. 1. Schematische Darstellung der geometrischen Verhältnisse bei der Beobachtung einer Emissionsschicht.

Betrachtung von zwei Extremfällen zeigt jedoch—vgl. Abschnitt II.3 und Tab. 1—dass merkliche Fehler (>1 Prozent) höchstens bei den grössten Zenitdistanzen ($\geq 80°$) zu befürchten sind.

(c) Je schiefer der Sehstrahl die Schicht durchstösst (und je dicker diese ist), desto weniger ist es möglich, die reduzierte Helligkeit als Zenithelligkeit eines

Tabelle 1. Zenitdistanz der Messpunkte, wirksamer Beobachtungsbereich, Umrechnungsfaktoren

Zenitdistanz (°)	0	20	40	50	60	70	75	80	85
Entfernung r (km)	0	36	83	117	167	258	338	466	694
Beobachtungsbereich Δr (km)	3	5	9	13	20	38	53	85	147
Faktor K: Modell I	1,008	0,948	0,796	0,686	0,564	0,437	0,377	0,335	0,349
Modell II	1,013	0,955	0,802	0,690	0,568	0,437	0,375	0,324	0,290

bestimmten Ortes (dessen Abstand r vom Beobachtungsort von der mittl. Schichthöhe h abhängt) anzusehen. Man erhält eine mittlere Zenithelligkeit für ein gewisses Entfernungsintervall.

(d) Dieser Effekt wird verstärkt durch den Öffnungswinkel der Gesichtsfeldblende, der mit wachsender Zenitdistanz immer grössere Stücke der Schicht einschliesst.

Für ein Modell der Schicht ($h = 100$ km, $\Delta h = 15$ km; vgl. II.3) und für den Öffnungswinkel der verwendeten Apparatur von 2° senkrecht zum Horizont ist

VOL. 21 1961

in Tabelle 1 der gesamte wirksame Entfernungsbereich Δr in Abhängigkeit von der Zenitdistanz angegeben. Obwohl der Effekt bei unseren Messungen durch Verwendung einer rechteckigen Gesichtsfeldblende mit der langen Seite parallel zum Horizont klein gehalten wird, beträgt Δr am Horizont das 50-fache des Zenitwertes und ist damit rund das 4-fache des Abstandes zweier Messpunkte bei kleinen Zenitdistanzen.

II. Die Beobachtungen und ihre Reduktion

1. Das azimutal montierte *Photometer* (vgl. auch Siedentopf, 1959) wurde in der Werkstatt des Astronomischen Instituts gebaut; dabei wurden Erfahrungen mit ähnlichen Photometern (vgl. Elsässer und Siedentopf, 1956) berücksichtigt. Durch automatische Richtungsumkehr der Höhenbewegung und selbsttätigen Filterwechsel am Horizont kann die Messung von einem Beobachter ohne Verlust von Beobachtungszeit durchgeführt werden. Eine Linse von 74 mm Öffnung und 205 mm Brennweite bildet ein Feld von 5,0° × 2,1° auf die rechteckige Gesichtsfeldblende (18,0 mm × 7,5 mm) ab. Ein Schott-Interferenzbandfilter für die Linie 5577 Å (max. Durchlässigkeit 67 Prozent bei 553 mμ, Halbwertsbreite 20 mμ) und ein gleichartiges für den linienarmen Vergleichsbereich bei 519 mμ (max. Durchlässigkeit 55 Prozent, Halbwertsbreite 19 mμ) werden abwechselnd in den Strahlengang gebracht. Dicht hinter der Gesichtsfeldblende folgt ohne Feldlinse als Empfänger ein Multiplier vom Typ RCA 1 P 21, dessen Anodenspannung von 850 V einem stabilisierten Netzgerät der Firma Knott/München entnommen wird. Über einen Gleichspannungsverstärker zur Anpassung, der nach dem gleichen Prinzip aufgebaut ist wie der von Elsässer und Siedentopf (1956) beschriebene, wird der Anodenstrom auf einen Stromschreiber von Siemens und Halske gegeben (Typ SD 12 K, Drehspulmesswerk von 7,4 kΩ Innenwiderstand, ca. 120 mm Endausschlag bei 1 mA, 0,5 sec Einstellzeit). Vom Photometer werden ausserdem über ein Markierwerk des Schreibers Höhenmarken für alle vollen 10°-Werte auf die Registrierung gebracht. Eine Registrierung von Horizont zu Horizont und mit dem zweiten Filter zurück dauert rund 7 min.

Die Konstanz der Empfindlichkeit der ganzen Apparatur wird mit einer radioaktiven Leuchtfolie geprüft, die vor und nach jeder Beobachtungsreihe auf die Taukappe des Photometers aufgesteckt wird.

2. Das *Beobachtungsmaterial* wurde während sechs bzw. vier Neumondperioden im Winter 1957/58 bzw. 1958/59 gewonnen. Das Photometer war auf der obersten Terrasse des Sphinx-Observatoriums (3575 m über N.N.) der Hochalpinen Forschungsstation Jungfraujoch aufgebaut. Der Beobachtungsort ist günstig wegen der photometrischen Qualität der klaren Nächte, wegen der Lage zwischen Jungfrau und Mönch liegt jedoch nach SW bzw. NO der natürliche Horizont in 10° bis 20° Höhe. Deshalb wurden vor allem Meridian- und OW-Beobachtungen gemacht. Das im folgenden diskutierte Material besteht nur aus solchen und zwar insgesamt aus 336 Registrierungen (vgl. auch Tabelle 4).

3. *Reduktion.* Die Registrierungen wurden bei den in Tabelle 1 angegebenen Zenitdistanzen abgelesen, wobei die Spitzen durch hellere Einzelsterne weggelassen wurden, und auf einheitliche Empfängerempfindlichkeit und einheitlichen Arbeitswiderstand (10 MΩ) umgerechnet. Aus den Messwerten bei Linienfilter I_L und

denen bei Vergleichsfilter I_V wurde die Intensität der grünen Nordlichtlinie I_{5577} nach der Beziehung

$$I_{5577} = I_L - kI_V \tag{2}$$

berechnet. Die Konstante $k = 0{,}735$ wurde mit der üblichen Annahme, dass das Kontinuum (Sternstrahlung, Zodiakallicht und schwache Banden bzw. Kontinuum des Airglows) in beiden Spektralbereichen gleich stark ist, als Verhältnis der Integrale über die Durchlässigkeitskurven der Interferenzfilter bestimmt.

Dem Ziel der Untersuchung entsprechend ist nun die Emission $I_{e,s}$ senkrecht zur Schicht zu berechnen. Dazu muss die beobachtete Intensität I_{5577} wegen Absorption und Streuung in der Atmosphäre korrigiert und dann die Emissionsrichtung nach Gl. (1) berücksichtigt werden. Bezeichnet Δm die Zenitextinktion bei $\lambda = 5577$ Å in Grössenklassen, $M(\zeta)$ die Luftmasse, $S(\zeta)$ den in die Richtung ζ geworfenen Streulichtanteil und $A(\zeta)$ den nach Reflexion am Erdboden aus der Atmosphäre wieder in die Richtung ζ gestreuten Anteil, so gilt:

$$\begin{aligned} I_{e,s} &= I_{5577}[V^{-1}(h, \zeta)\, e^{-0{,}921\Delta m} + S(\zeta) + A(\zeta)]^{-1} \\ &= I_{5577} \cdot K(h, \Delta m, \zeta). \end{aligned} \tag{3}$$

Durch Messungen der Linie bei Raketenaufstiegen (vgl. insbes. Heppner und Meredith, 1958) scheint gesichert, dass die Emissionshöhe stets zwischen 90 und 120 km liegt, nicht nur im statistischen Mittel, wie schon Messungen vom Boden aus ergeben hatten (vgl. Elsässer und Siedentopf, 1956; Roach *et al.*, 1958a). Deshalb wird angenommen, dass die mittlere Emissionshöhe 100 km ist, und dass Änderungen im Charakter der Zenitdistanzkurven auf Intensitätsschwankungen in der Schicht beruhen. Bezüglich Δm wurden für K zwei Modelle gerechnet. Nach Extinktionsmessungen von Elsässer (1954) auf dem Jungfraujoch ist dort häufig der Fall reiner Rayleighstreuung verwirklicht. Bei $\lambda = 5577$ Å ist dann $\Delta m = 0^m.095$, wobei $0^m.061$ auf die Rayleighstreuung, der Rest auf die Ozonabsorption entfällt. Diese Werte wurden dem Modell I zugrunde gelegt. Unter ungünstigen Bedingungen können bis zu $0^m.04$ Dunststreuung hinzukommen; dem Extremfall von $0^m.135$ Gesamtextinktion entspricht Modell II. Dabei wurden $S(\zeta)$ und $A(\zeta)$ für die Rayleighstreuung den Tabellen von Ashburn (1954) entnommen; das Albedo der schneebedeckten Erdoberfläche rings um die Beobachtungsstation wurde zu 0,5 angesetzt. Für die Dunststreuung wurde als Näherung

$$S_D = \alpha V^{-1}(1 - e^{-0{,}921\Delta m_D M(\zeta)}) \tag{4}$$

mit $\alpha = 0{,}75$ benützt, d.h. 75 Prozent der vom Dunst gestreuten Strahlung werden nach vorne gestreut und tragen ebenfalls zur Flächenhelligkeit bei.

Der Vergleich beider Modelle in Tabelle 1 zeigt, dass bis zu Zenitdistanzen von 80° die Unterschiede der Reduktionsfaktoren kleiner als 1 Prozent sind. Da keine individuellen Extinktionsmessungen verfügbar waren, wurde die ganze Auswertung nach Modell I (reine Rayleigh-Atmosphäre) vorgenommen.

Zur *Eichung* der gemessenen Intensitäsen wurden wiederholte Registrierungen von α UMi mit dem Nachthimmelsphotometer benützt. Tabelle 2 gibt die Ausschläge für die Normalempfindlichkeit, auf die alle Messungen umgerechnet wurden—der Stern wurde bei wesentlich höherer Empfindlichkeit gemessen!—und die

VOL. 21 1961

daraus abgeleiteten Umrechnungsfaktoren der Messwerte in Rayleigh. Der systematische Unterschied des Wertes in beiden Wintern ist vermutlich auf eine Helligkeitsänderung der Leuchtfolie zurückzuführen. Die angegebenen Unsicherheitsgrenzen beziehen sich nur auf die Schwankungen der Messwerte des Sterns. In die Umrechnungsfaktoren gehen die effektive Öffnung des Photometers und die Durchlasskurve des Linienfilters ein und können Anlass zu systematischen Fehlern geben.

Tabelle 2. Eichung des Photometers

	Sternausschlag (mm)	Umrechnungsfaktor (Rayleigh/mm)
Winter 1957/58	9,4 ± 0,5	14,9 ± 0,8
Winter 1958/59	11,2 ± 0,5	12,6 ± 0,6

Die Registrierungen wurden auf 0,5 mm genau abgelesen. Wird für die Schreibereinstellung ein Fehler gleicher Grösse angesetzt und berücksichtigt, dass in jeden Wert für die Linie 5577 Å ein Linien- und ein Vergleichsfilterwert eingeht, so folgt als mittl. Fehler eines Wertes 1 mm oder rund 14 Rayleigh.

III. Die Ergebnisse und ihre Diskussion

1. Nur rund 20 Prozent aller Registrierungen liefern nach der Bearbeitung im Rahmen der Messgenauigkeit konstante Intensität über den ganzen beobachtbaren Bereich der Schicht hinweg. Die gefundenen Schwankungen lassen sich zwanglos in zwei Klassen einordnen: A. Einer deutlich ausgeprägten "Normalintensität" überlagern sich begrenzte Helligkeitsschwankungen und zwar fast ausschliesslich in der Form von *Aufhellungen*. Ein Zusammenhang solcher Aufhellungen mit der Lage der Milchstrasse bzw. der Ekliptik (Zodiakallicht!) wurde nicht gefunden, sodass diese nicht durch systematische Reduktionsfehler vorgetäuscht sein können. B. Die Helligkeit ändert sich monoton im ganzen erfassbaren Ausschnitt der Schicht (*Helligkeitsgradienten*). Abb. 2 zeigt charakteristische Beispiele. Die Aufhellungen werden charakterisiert durch ihre Amplitude in Rayleigh gegenüber dem Normalniveau und ihre Ausdehnung in km zwischen den Punkten halber Amplitude. Eine Aufhellung wird als reell betrachtet, wenn das Normalniveau durch mindestens 2 Punkte auf beiden Seiten festgelegt ist und wenn sie durch mindestens 3 Messpunkte angedeutet ist. Amplituden kleiner als 25 Rayleigh wurden nicht berücksichtigt. Die Gradienten werden im folgenden beschrieben durch die Helligkeitsänderung in Rayleigh auf 1000 km.

Abb. 3 gibt zunächst einen Überblick über alle Aufhellungen. Besonders bezüglich der Ausdehnungen ist das Ergebnis im wesentlichen bestimmt durch den beschränkten Beobachtungsbereich: wegen der oben angegebenen Vorschrift liegen die kleinsten erkennbaren Aufhellungen bei 100, die grössten bei 700 km. Die Amplituden-Häufigkeit nimmt mit wachsender Amplitude stark ab. Setzt man im Amplitudenintervall 0 bis 30 Rayleigh die Häufigkeit der Registrierungen ohne Aufhellung ein, so lässt sich der Amplitudenabfall in erster Näherung durch eine Normalverteilung mit der Streuung $\sigma = 60$ Rayleigh darstellen. Daher ist

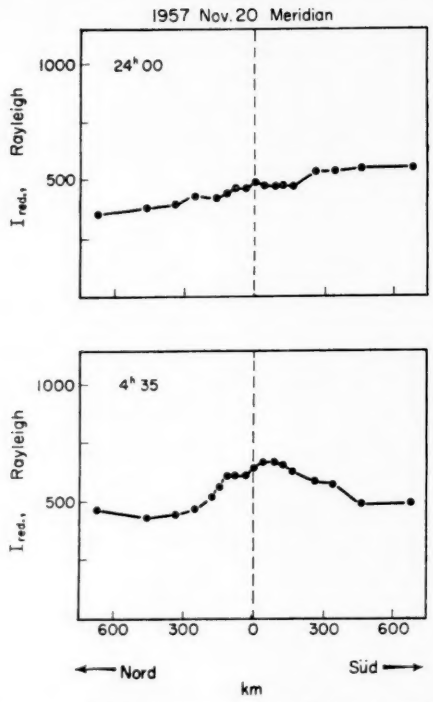

Abb. 2. Beispiel für einen "Helligkeitsgradienten" (oben) und für eine "Aufhellung". Die Messpunkte sind durch ausgefüllte Kreise markiert.

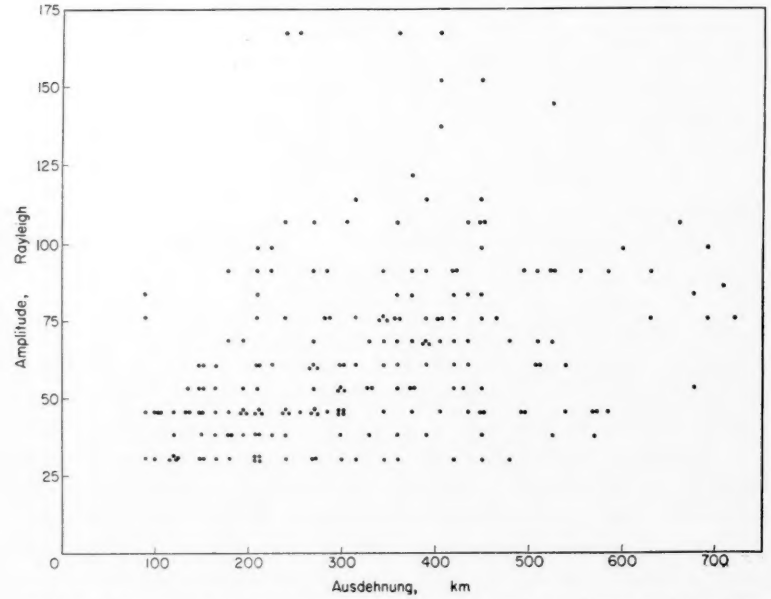

Abb. 3. Verteilung aller gefundenen Aufhellungen nach Amplitude und Ausdehnung.

VOL. 21 1961

ausgeschlossen, dass es sich bei den gefundenen Schwankungen nur um Beobachtungsfehler handelt. Im Hinblick auf den Vergleich mit anderen Ergebnissen scheint es wichtig, die relativen Amplituden, d.h. die Amplituden in Einheiten der Höhe des jeweiligen Normalniveaus, zu betrachten. Ihre Verteilung ist in

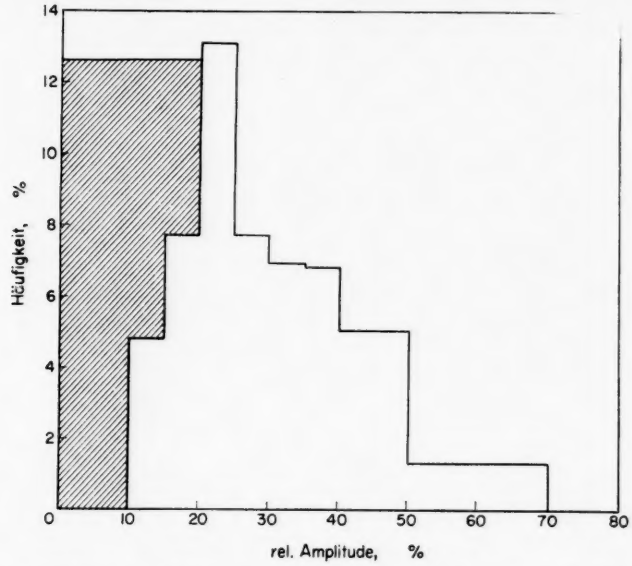

Abb. 4. Prozentuale Häufigkeit der relativen Amplituden der Aufhellungen. Gleichmässig auf die kleinen Amplituden verteilt und schraffiert eingezeichnet ist die Häufigkeit der Registrierungen, bei denen nach der gegebenen Messvorschrift keine Aufhellung vorhanden war.

Tabelle 3. Beobachtungen von Gradienten

Gradient (Rayleigh/1000 km)	0 bis 20	20 bis 40	40 bis 60	60 bis 80	80 bis 100	100 bis 120	120 bis 140	140 bis 160	160 bis 180	180 bis 200	200 bis 220	220 bis 240
Winter 1957/58 >0	3	7	6	4	4	1	1	1		1		1
<0	1	8	4	1	2		2		1			
OW/WO	6	7	3	3	1		1					
Winter 1958/59 >0	1	4	4	2	3	1	1	1	3		1	2
<0		1		1								
OW/WO	2	4	2			1						

Abb. 4 dargestellt. Danach fallen 50 Prozent aller Fälle in den Bereich 0 bis 25 Prozent rel. Amplitude, Schwankungen von mehr als 50 Prozent kommen nur bei rund 5 Prozent aller Registrierungen vor. Tabelle 3 gibt die Daten über die gefundenen Helligkeitsgradienten. Dabei wurde bei den Meridianregistrierungen unterschieden zwischen Helligkeitsabfall von N nach S (positive Gradienten) und von S nach N. Während die Verteilung der Gradientengrössen für die verschiedenen

Fälle statistisch nicht wesentlich verschieden ist und ganz allgemein durch den starken Abfall zu hohen Gradienten hin charakterisiert ist, fällt auf, dass im Winter 1958/59 die negativen Gradienten fast völlig fehlen, während sie im Winter 1957/58 kaum seltener waren als die positiven. Da die Gradienten mit der grossräumigen Struktur der Emissionsschicht zusammenhängen und somit hier amehesten Beziehungen zu den Nordlichtern zu erwarten sind, liegt vielleicht ein mit dem Sonnenfleckenzyklus zusammenhängender Effekt vor, der mit dem vorliegenden Material nicht näher untersucht und auch noch nicht als gesichert betrachtet werden kann.

In Tabelle 4 werden die Daten nochmals zusammengefasst: Etwa 60 Prozent aller Registrierungen zeigen Aufhellungen, 30 Prozent Gradienten (in 10 Prozent aller Fälle tritt eine Überschneidung der beiden Erscheinungen auf) das Verhältnis

Tabelle 4. Zusammenfassung der Beobachtungsdaten

	Registrierungen	Aufhellungen		Gradienten		Aufh./Grad.
		Anzahl	%	Anzahl	%	
Winter 57/58 Meridian	172	106	62	48	28	2,2
O–W	76	51	67	21	28	1,8
Winter 58/59 Meridian	54	29	54	25	46	1,2
O–W	34	24	71	9	26	3,8
	336	210	62	103	31	2,0

beider, das nachher zur Diskussion der mittleren Ausdehnung der Helligkeitsschwankungen herangezogen wird, liegt bei 2.

2. Roach *et al.* (1958a,b) haben die Vorstellung einer gleichmässig emittierenden Schicht mit gewissen Schwankungen oder Störungen ganz aufgegeben zugunsten der von einzelnen leuchtenden Zellen. Bei ihren Verfahren zur Bestimmung der Zellengrösse kommt dies jeweils in einer charakteristischen Voraussetzung zum Ausdruck. So wird bei der Korrelation der zeitlichen Helligkeitsschwankungen verschieden weit voneinander entfernter Schichtpunkte ausgeschlossen, dass eine positive Korrelation auch noch bei weit auseinander liegenden Schichtpunkten daher rühren kann, dass zur betreffenden Zeit keine Störungen des normalen Leuchtens auftreten. Lässt man diesen Fall zu, so ergibt die Korrelationsmethode, dass an Punkten in einigen hundert Kilometer Entfernung die Helligkeitsschwankungen gelegentlich voneinander unabhängig erfolgen; im Falle einer Korrelation der Schwankungen über den ganzen Beobachtungsbereich hinweg ist jedoch dann keine Aussage möglich.

Bei der Untersuchung der Helligkeitsgradienten wird vorausgesetzt, dass die räumliche Gesamtänderung der Helligkeit in einer Zelle gleich der mittleren Airglowintensität ist. Nach unserem oben beschriebenen Ergebnis, dass die relativen Amplituden innerhalb des von einer Station aus beobachtbaren Bereichs durchschnittlich 20 Prozent betragen, ist es klar, dass diese Annahme zu Airglowzellen führt, deren Grösse ein mehrfaches dieses Bereiches beträgt. Betrachtet

VOL. 21 1961

man die Gradienten wiederum als Störungen eines normalen Leuchtens mit einer mittleren Amplitude von rund 20 Prozent der mittleren Airglowhelligkeit, so liefert die Gradientenmethode von ROACH Ausdehnungen von rund 500 km anstatt 2500 km.

3. Bisher wurden nur andere Lösungs*möglichkeiten* als die Zellenvorstellung von ROACH *et al.* (1958b) angedeutet. Es ist jetzt die Frage, wie weit die hier betriebene Statistik der räumlichen Helligkeitsschwankungen gewisse Aussagen über die Ausdehnung von Airglowstörungen gibt. Sicher ist, dass Aussagen nur auf dem Wege über Modellrechnungen möglich sind, da sich jede Helligkeitsschwankung, je nach ihrer Lage zum Beobachtungsort, durch Aufhellungen verschiedener Ausdehnung oder auch durch Gradienten zeigen kann.

Da die beobachteten Helligkeitsschwankungen bei Aufhellungen und Gradienten von gleicher Grössenordnung sind, scheint es richtig, für ein einfaches Modell die Amplituden überhaupt ausser Acht zu lassen. Betrachtet werden kreisförmige Störungen, in denen die Helligkeit vom Zentrum bis zum Grenzradius r monoton abnimmt. Bei der Beobachtung werden durch solche Störungen parallele Schnitte der Länge b gelegt. Liegen beide Endpunkte ausserhalb der Störung, so hat man eine Aufhellung, liegen beide Endpunkte in einer Hälfte einer Störung, so erhält man einen Gradienten. Daneben ergeben sich noch Fälle mit Helligkeitsschwankungen, die sich nach dem angenommenen Schema nicht klassifizieren lassen, wie sie auch im Beobachtungsmaterial auftreten.

Störungen vom Radius r liefern Aufhellungen der Ausdehnung $a + (da/2)$ bis $a - (da/2)$, wenn der Abstand des Schnittes vom Störungszentrum zwischen $x + (dx/2)$ und $x - (dx/2)$ liegt, wobei

$$|dx\,(r, a, da)| = \frac{a\,da}{2\sqrt{[r^2 - (a/2)^2]}} \tag{5}$$

ist. Damit die Aufhellung ganz innerhalb des Schnittes liegt, muss das Zenit gleichzeitig in den Bereich $(b - a)$ symmetrisch zum Lot vom Zentrum auf den Schnitt fallen. Ist $h(r)dr$ die Häufigkeit der Störungen vom Radius $r + (dr/2)$ bis $r - (dr/2)$, so erhält man Aufhellungen a mit einer Häufigkeit proportional

$$2(b - a)\,dx \cdot h(r)\,dr.$$

Die Häufigkeit der Aufhellungen der Ausdehnung a folgt durch Integration über r zu

$$N_A(a)\,da = a(b - a)\,da \int_{r=\frac{a}{2}}^{\infty} \frac{h(r)\,dr}{\sqrt{[r^2 - (a/2)^2]}}\,. \tag{6}$$

Eine Integration über alle möglichen a liefert schliesslich ein Mass für die Gesamthäufigkeit der Aufhellungen:

$$A = \int_0^{b_{\max}} N_A(a)\,da. \tag{7}$$

Bei den Gradienten geht die Rechnung ganz analog. Die Häufigkeit der Gradienten, die von Schnitten herrühren, welche von den Störungen mit Radius r bei Verlängerung von b die Strecke a abschneiden würden, ist proportional

$$4\left(\frac{a}{2} - b\right)dx\,h(r)\,dr.$$

Durch Integration über r folgt unter Verwendung von Gl. (5)

$$N_G(a)\,da = a(a - 2b)\,da \int_{r=\frac{a}{2}}^{\infty} \frac{h(r)\,dr}{\sqrt{[r^2 - (a/2)^2]}}, \tag{8}$$

und für die Gesamthäufigkeit der Gradienten ergibt sich daraus

$$G = \int_{a=2b}^{\infty} N_G(a)\,da. \tag{9}$$

Aus (7) und (9) erhält man zum Vergleich mit den Werten der Tabelle 4 das Verhältnis von Aufhellungen zu Gradienten in Abhängigkeit von der Häufigkeitsverteilung. Es ist noch zu beachten, dass b für kleine a ebenfalls eine Funktion von a ist: unterhalb von $a = 100$ km ist es Null, da eine Aufhellung durch mindestens 3 Messpunkte angedeutet sein sollte, und erreicht bei 300 km seinen Normalwert von rund 800 km. Für die Rechnung wurde b mit den aus Tabelle 1 zu

Tabelle 5. Zahlenangaben für 2 Modelle der Radienverteilung

	Modell 1	Modell 2
s (km)	0	250
t (km)	500	500
$2\bar{r}$ (km)	886	1132
σ (km)	460	530
A/G	2,0	0,6

entnehmenden Abständen der Messpunkte für den vorliegenden Spezialfall abgeschätzt.

Physikalisch und nach den oben entwickelten Formeln erscheinen Modelle mit einer von Null verschiedenen Häufigkeit der Störungen bei $r = 0$ nicht sinnvoll. Es wurden deshalb einige Modelle der Form

$$h(r) = r\,e^{-\left(\frac{r-s}{t}\right)^2} \tag{10}$$

betrachtet, wobei die Parameter s und t eine Variation von mittlerem Radius $\bar{r}$ und Streuung σ der Radienverteilung erlauben.

Tabelle 5 gibt einige Zahlen für zwei in Abb. 5 dargestellte Modelle, die zeigen, dass die Resultate der hier verwendeten Methode des Häufigkeitsvergleichs von Aufhellungen und Gradienten gegenüber der Radienverteilung recht empfindlich ist. Auch wenn man die Unsicherheiten bei der Klassifikation der Helligkeitsschwankungen, bei der Abschätzung der in die Rechnung eingehenden Eigentümlichkeiten der Beobachtungsmethode, insbesondere der Grösse b, und durch die Vernachlässigung der Amplituden bei der auch sonst stark schematisierten Rechnung berücksichtigt, scheinen doch Werte des mittleren Durchmessers wesentlich grösser als 1000 km ausgeschlossen. Es ist nur eine Aussage über die Verteilung nach grossen Durchmessern hin möglich, weil die untere Grenze der Ausdehnung von Aufhellungen vom Beobachtungsverfahren bestimmt wird.

VOL. 21 1961

Eine wesentliche Annahme der Modellrechnung ist ausserdem, dass die Schwankungen durch Störungen mit einem einheitlichen Radienverteilungsgesetz hervorgerufen werden. Es wäre aber auch möglich, dass die Emissionsschicht statistische Helligkeitsschwankungen mit Ausdehnungen von einigen hundert Kilometern einerseits und grossräumige Helligkeitsgradienten über mehr als 1000 km andererseits zeigt. Dies kann wohl nur durch Beobachtungen entschieden werden, die

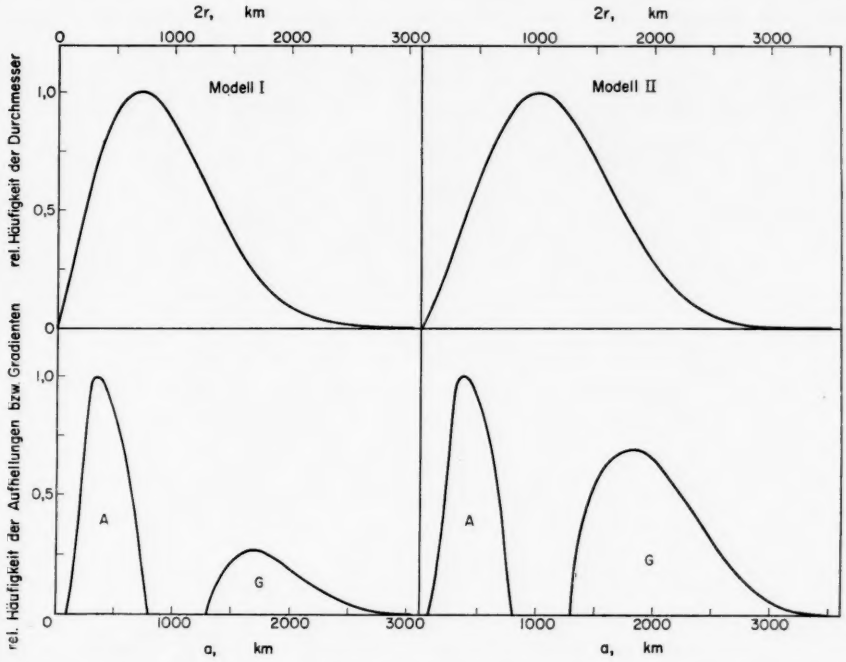

Abb. 5. Zwei Verteilungsgesetze der Durchmesser von Störungen (oben; vgl. Tabelle 5) und die ihnen entsprechenden Beiträge der Sehnenlänge a zur Gesamthäufigkeit der Aufhellungen A nach Gl. (6) bzw. der Gradienten G nach Gl. (8).

gleichzeitig mehr physikalische Informationen über das Nachthimmelsleuchten liefern als die bisherigen.

Bei der Durchführung der Arbeit wurde mir von vielen Seiten Hilfe zuteil: Herr Professor SIEDENTOPF regte die Beschäftigung mit dem behandelten Problem an und gab viele förderliche Ratschläge. Von ihm stammt auch die Konstruktion der benutzten Apparatur, die dann unter der Leitung von Herrn Dr. W. HERMANN in der Institutswerkstatt gebaut wurde. Die Deutsche Forschungsgemeinschaft schuf durch Sachbeihilfen die finanzielle Grundlage. Die Verwaltung der Hochalpinen Forschungsstation stellte Arbeitsplätze auf dem Jungfraujoch zur Verfügung und zeigte Verständnis für alle Anliegen. Fräulein Dr. U. MAYER machte rd. ein Drittel der Beobachtungen am Jungfraujoch. Frau U. JENSBACH, Fräulein S. VETTER und Fraülein I. WEISERT leisteten ausdauernde Rechenarbeit bei der Bearbeitung der Messungen. Ihnen allen gilt mein herzlicher Dank.

Literatur

Ashburn E. V.	1954	*J. Atmosph. Terr. Phys.* **5,** 83.
Elsässer H.	1954	*Z. Astrophys.* **35,** 36.
Elsässer H. und Siedentopf H.	1956	*J. Atmosph. Terr. Phys.* **8,** 222.
Heppner J. P. und Meredith L. H.	1958	*J. Geophys. Res.* **63,** 51.
Roach F. E.	1957	*Ann. I.G.Y.* IV, 115.
Roach F. E., Megill L. R., Rees M. H. und Marovich E.	1958a	*J. Atmosph. Terr. Phys.* **12,** 171.
Roach F. E., Tandberg-Hanssen E. und Megill L. R.	1958b	*J. Atmosph. Terr. Phys.* **13,** 113.
Siedentopf H.	1959	*Naturwissenschaften* **46,** 309.

VOL.
21
1961

Journal of Atmospheric and Terrestrial Physics, 1961, Vol. 21, pp. 237 to 242. Pergamon Press Ltd. Printed in Northern Ireland

On vertical drift velocities of the *F2*-layer

H. UNZ
Electrical Engineering Department, University of Kansas, Lawrence, Kansas

(*Received* 9 *January* 1961)

Abstract—The vertical drift velocities of the *F2*-layer are calculated approximately from the $N(z,t)$ measured curves. A correlation between the calculated velocities and the velocity of the position of the $0{\cdot}9N_{max}$ is shown and discussed.

1. INTRODUCTION

IN AN ATTEMPT to account for the peculiar behaviour of the *F2*-layer MARTYN (1959) has introduced the concept of ionozation transport by writing the continuity equation as:

$$\frac{\partial N}{\partial t} = Q - \beta N - \nabla \cdot (\bar{v} N) \tag{1}$$

where N = electron density,
β = recombination coefficient (decay) (attachment-like effect),
$\bar{v}$ = transport velocity of the electrons,
Q = rate of production of electrons.

The last term of equation (1) has been introduced by MARTYN (1947) who discussed the reasons for the transport velocities of the electrons in the ionosphere: the solar tide (MARTYN, 1947a, 1948), the lunar tide (MARTYN, 1947b), winds and electric fields (MARTYN, 1953a) and magnetic storms (MARTYN, 1953b). The dynamo current theory and the variations associated with the geomagnetic variations has been discussed in detail by K. MAEDA (1950, 1951, 1952a, b, 1954) and by H. MAEDA (1952, 1953, 1955, 1956). The effect of solar tides has been also discussed by WEISS (1952) and by MITRA (1951). The effect of gravity has been discussed by DUNCAN (1956) and by HIRANO (1955). Atmospheric oscillations which might explain the vertical drift have been discussed by PEKERIS (1936, 1937, 1950). Summaries about the existing knowledge of the movements in the ionosphere have been given by RATCLIFFE (1954, 1956), MARTYN (1956, 1959), MITRA (1952), HINES (1959) and CHANDRA (1960).

2. THE CONTINUITY EQUATION

Let us assign a coordinate system (x,y,z) to the *F2*-layer such that z is the vertical direction and x,y are in the horizontal plane. Let us assume that the quantities in equation (1) vary only in the vertical z direction such that we have horizontal layers:

$$N = N(z,t), \quad Q = Q(z,t), \quad \beta = \beta(z). \tag{2}$$

Let us also assume that the motion of the layers in the horizontal direction is uniform such that:

$$\bar{v} = v(z,t)\bar{\imath}_x + v_y(z,t)\bar{\imath}_y + v(z,t)\bar{\imath}_z. \tag{3}$$

This is true for the horizontal distances which we are considering. Substituting (3) and (2) into (1) we get:

$$\frac{\partial N}{\partial t} = Q(z,t) - \beta(z)N - \frac{\partial}{\partial z}[v(z,t)N] \tag{4}$$

where $N = N(z,t)$. (4) may be rewritten as:

$$\frac{\partial N}{\partial t} = Q - \beta N - N\frac{\partial v}{\partial z} - v\frac{\partial N}{\partial z} \tag{5}$$

and using the well-known relationship (APPLETON and LYON, 1954):

$$\frac{dN}{dt} = \frac{\partial N}{\partial t} + \frac{\partial N}{\partial z}\frac{dz}{dt} = \frac{\partial N}{\partial t} + v\frac{\partial N}{\partial z}. \tag{6}$$

Substituting (6) into (5) we can get:

$$\frac{dN}{dt} = Q - \left(\beta + \frac{\partial v}{\partial z}\right)N. \tag{7}$$

Let us assume that a layer of the ionosphere of a certain finite width is moving vertically with constant velocity v_0. Let us assume that the electrons have a vertical velocity v_1 with reference to the moving layer. The total velocity of the electrons v will be then:

$$v = v_0 + v_1. \tag{8}$$

Let us assume now that the velocity of the layer is much greater than the velocity of each electron compared to the layer:

$$v_0 \gg v_1. \tag{9}$$

Obviously (9) will not hold when the layer is stationary. Let us also assume that the layer has almost a uniform velocity:

$$\frac{\partial v_0}{\partial z} \ll \frac{\partial v_1}{\partial z}. \tag{10}$$

(10) will hold in general since the velocity of the layer is the average velocity of the electrons, so it does not change as much as the velocity of the individual electrons. Substituting (8), (9) and (10) in (5) we get:

$$\frac{\partial N}{\partial t} = Q - \beta N - N\frac{\partial v_1}{\partial z} - v_0\frac{\partial N}{\partial z}. \tag{11}$$

Let us now assume that:

$$N\frac{\partial v_1}{\partial z} \ll v_0\frac{\partial N}{\partial z} \tag{12}$$

and we get from (11):

$$\frac{\partial N}{\partial t} = Q - \beta N - v_0\frac{\partial N}{\partial z} \tag{13}$$

VOL. 21 1961

and since we know $N(z,t)$ from measurement of the ionosphere we can write (13) as:

$$v_0 = \frac{Q - \beta N - (\partial N/\partial t)}{\partial N/\partial z} \tag{14}$$

where v_0 will be the velocity of the layer at each height.

3. Discussion of the Results

It has been accepted (Ratcliffe *et al.*, 1956) that $\beta(z)$ varies with height according to the formula:

$$\beta = \beta(z) = 10^{-4} \exp\left[\frac{300 - z(\text{km})}{50}\right] 1/\text{sec} \tag{15}$$

and that according to Mitra (1952, p. 280):

$$Q = Q(z,t) = Q_0 \exp\left[1 - z - e^{-z} \sec \chi(t)\right] \tag{16}$$

where $\chi(t)$ represents the position of the sun.

Since $N(z,t)$ is known quite well from measurements, by using (15), (16) and the values measured for $N(z, t)$ we can find v_0 from (14). However, β in (15) is known only within a factor of 3 and Q in (16) is known only within a factor of 2, and the inaccuracies can be in both cases as high as within a factor of 10. Therefore the calculated result of v_0 in (14) will not be very accurate and will depend on the error factors of Q and β. We will have to take this later into account in the final results.

In Figs. 1–4 we have drawn the height of the *F2*-layer in the ionosphere for the $0{\cdot}9N_{\max}$ position. The graphs are for 22–23 December 1957 for four stations: Panama, Talara, Washington, and Huancayo. We have calculated in the graph the value of the derivatives of the curve dh/dt in m/sec at each particular point. Since the measurements were made every hour, the values of the derivatives at the maximum and the minimum points are not known. Those values of dh/dt represent the velocity by which $0{\cdot}9N_{\max}$ of the layer moves in a vertical direction due to all effects (Martyn, 1954); ionization production, decay, diffusion and vertical drift (we have included the last two together in v_0).

Then we have compared the values of v_0 calculated in (14) with the values of dh/dt calculated from the curves in Figs. 1–4. At some positions the values of v_0 and dh/dt were of the same order of magnitude (a difference of about ± 60 per cent), and of the same sign. We have denoted those positions by $\times$ on top of the curve.

Looking at those curves we see that there is quite a remarkable correlation between calculated v_0 and measured dh/dt. The points where we do not have correlation are mainly at the maximum and minimum points of h, where dh/dt is unknown and varies very fast from positive to negative values. At those points the layer changes direction of motion and conditions (9) and (12) do not hold. We see that there is quite a good correlation when the slope is constant for a period of time, i.e. when the velocity dh/dt is constant.

The only place where there is no correlation is in Washington. It has been pointed out to the author that at these times the value of Q in Washington is not very good, and it might be the source for the unagreement.

In the light of those results the author proposes the hypothesis that the movement of the maximum of the *F2*-layer vertically is mostly due to vertical drift velocities or transportation of the electrons. While at the maximum and minimum

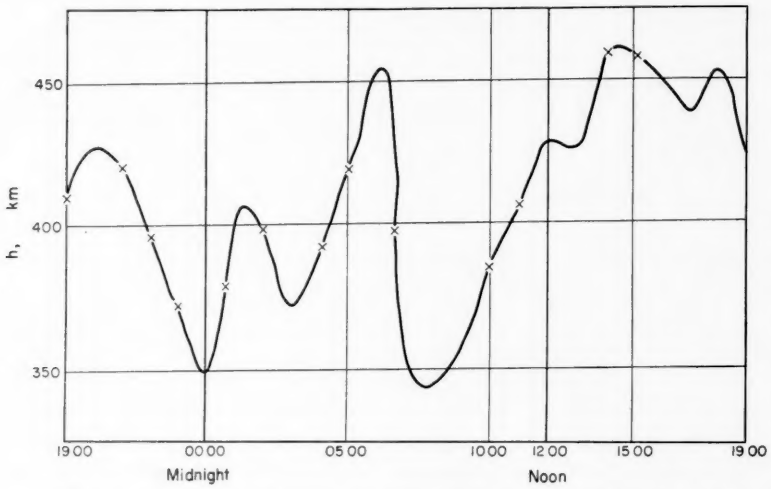

Fig. 1. Panama, 22–23 December 1957, *F2*-layer, $h = (0{\cdot}9\ N_{max})$, 9·4°N.

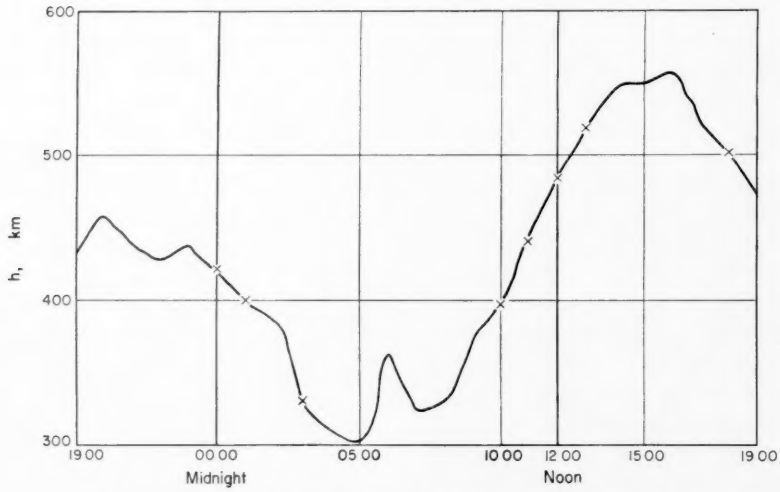

Fig. 2. Talara, 22–23 December 1957, *F2*-layer, $h = (0{\cdot}9N_{max})$, 4·0°S.

positions, decay and production could be dominant, it is clearly shown by the curves that the effect of transportation of the electrons is rather large and dominant in most cases. The correlation of the results is rather amazing if we realize the inaccuracies in the factors Q and β used to calculate v_0 in (14).

It has been found that v_0 varies in the maximum mainly around 7 m/sec but

VOL. 21 1961

sometimes goes as high as 12 m/sec. Those values are about 25 km/hr and 43 km/hr. While MITRA (1951) found vertical drift velocities of about 12–17 km/hr, other authors calculated theoretically vertical drift velocities of larger values.

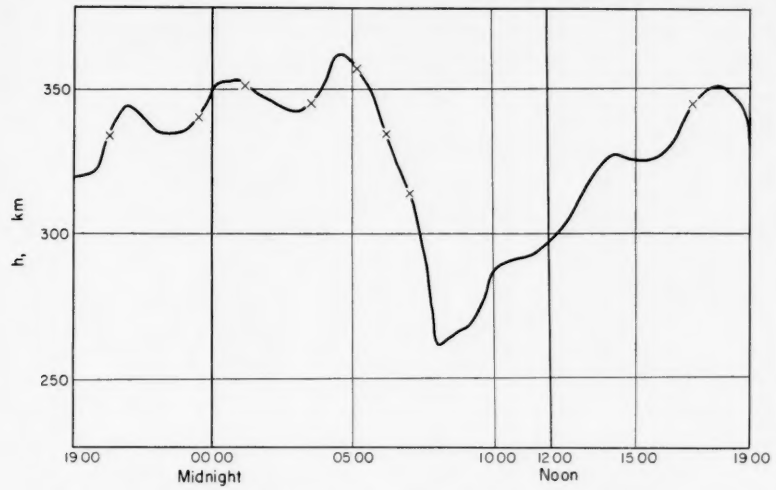

Fig. 3. Washington, 22–23 December 1957, *F2*-layer, $L = (0{\cdot}9\ N_{max})$, 38·7°N.

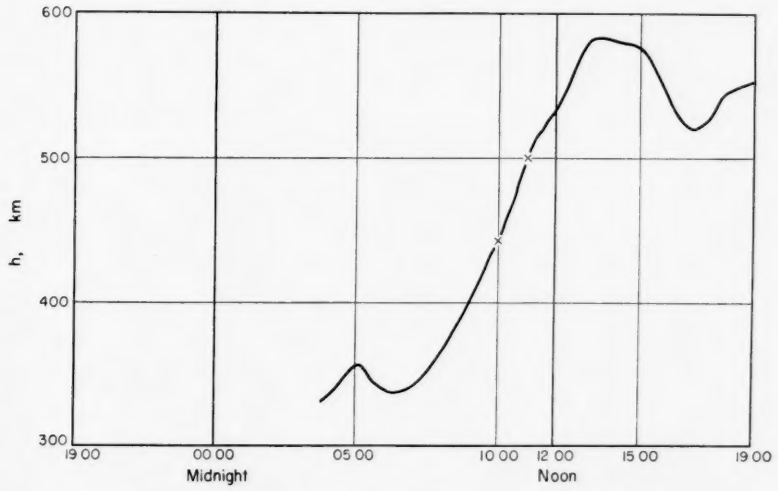

Fig. 4. Huancayo, 23 December 1957, *F2*-layer, $h = (0{\cdot}9\ N_{max})$, 12·0°S.

KIRKPATRICK (quoted by MARTYN, 1948) found maximum vertical velocities of about 22 km/hr and MAEDA (1955) discusses vertical drift velocities as high as 16 m/sec.

The vertical drift velocity v has been discussed theoretically in detail by MARTYN (1954, 1959) who found that near the magnetic equator the vertical transport velocity is of the order of 12 m/sec, directed down during the night and up during the day. This is about what we get in the case of Talara.

It is suggested therefore that v_0 will be calculated by (14), since Q and β are known only within a factor of 10, and it will be compared with dh/dt. By comparing the two curves we can see in what part the vertical drift velocity of transportation of the electrons is responsible for the *F2*-layer movement.

Although we have used here only the most limited data in order to show correlation on which we have based the hypothesis, it is hoped that analysis of further data in the light of the above will be done in the near future.

REFERENCES

APPLETON E. and LYON A. J.	1954	*The Physics of the Ionosphere*, p. 20. Physical Society, London.
CHANDRA S., GIBBONS J. J. and SCHMERLING E. R.	1960	*J. Geophys. Res.* **65,** 1159.
DUNCAN R. A.	1956	*Aust. J. Phys.* **9,** 436.
HINES C. O.	1959	*Proc. I.R.E.* **47,** 176.
HIRANO M.	1955	*Rep. Ionos. Res. Japan* **9,** 95.
MAEDA H.	1952	*Rep. Ionos. Res. Japan* **6,** 155.
MAEDA H.	1953	*J. Geomagn. Geoelect. Kyoto* **5,** No. 3.
MAEDA H.	1955	*Rep. Ionos. Res. Japan* **9,** No. 2.
MAEDA H.	1956	*Rep. Ionos. Res. Japan* **10,** No. 2.
MAEDA K.	1950	*J. Geomagn. Geoelect. Kyoto* **2,** No. 2.
MAEDA K.	1951	*J. Geomagn. Geoelect. Kyoto* **3,** Nos. 3/4.
MAEDA K.	1952a	*J. Geomagn. Geoelect. Kyoto* **4,** No. 2.
MAEDA K.	1952b	*J. Geomagn. Geoelect. Kyoto* **4,** Nos. 3/4
MAEDA K.	1954	*Rep. Ionos. Res. Japan* **8,** No. 4.
MAEDA K.	1955	*Rep. Ionos. Res. Japan* **9,** 71.
MARTYN D. F.	1947a	*Proc. Roy. Soc.* A **189,** 241.
MARTYN D. F.	1947b	*Proc. Roy. Soc.* A **190,** 273.
MARTYN D. F.	1948	*Proc. Roy. Soc.* A **194,** 445.
MARTYN D. F.	1953a	*Phil. Trans.* A **246,** 306.
MARTYN D. F.	1953b	*Proc. Roy. Soc.* A **218,** 1.
MARTYN D. F.	1954	*The Physics of the Ionosphere*, p. 254. Physical Society, London.
MARTYN D. F.	1956	*Aust. J. Phys.* **9,** 161.
MARTYN D. F.	1959	*Proc. I.R.E.* **47,** 147.
MITRA A. P.	1951	*J. Atmosph. Terr. Phys.* **1,** 286.
MITRA S. K.	1952	*The Upper Atmosphere.* The Asiatic Society, Calcutta.
PEKERIS C. L.	1936	*Nature, Lond.* **138,** 642.
PEKERIS C. L.	1937	*Proc. Roy. Soc.* **158,** 650.
PEKERIS C. L.	1950	Techn. Note 2209. National Advisory Committee for Aeronautics, Washington.
RATCLIFFE J. A.	1954	*Physics of the Ionosphere.* Physical Society, London.
RATCLIFFE J. A.	1956	*Nature, Lond.* **177,** 307.
RATCLIFFE J. A., SCHMERLING E. R., SETTY C. S. G. K. and THOMAS J. O.	1956	*Phil Trans.* A **248,** 621
WEISS A. A.	1952	*J. Atmosph. Terr. Phys.* **3,** 30.

VOL. 21 1961

Journal of Atmospheric and Terrestrial Physics, 1961. Vol. 21, pp. 243 to 256. Pergamon Press, Ltd. Printed in Northern Ireland

Microwave absorption in the earth's atmosphere

S. N. Ghosh and V. Malaviya
J. K. Institute of Applied Physics, University of Allahabad, Allahabad, India

(*Received* 28 *January* 1961)

Abstract—In this paper the microwave absorption has been calculated for different layers of the earth's atmosphere around peak resonance frequencies for each constituent gas. The total absorption for the whole atmosphere is then obtained. For such calculations, it is necessary to know the peak absorption at the centre of the absorption line and its half-width. It has been shown that for atmospheric gases the peak absorption is pressure-independent and that it varies as $(3 - x)_{\text{th}}$ power of absolute temperature for diatomic (O_2) and linear polyatomic (N_2O) molecules and as $(7/2 - x)_{\text{th}}$ power of absolute temperature for symmetric (H_2O) and asymmetric top (O_3) molecules. The half-widths of the absorption lines have been calculated after assuming the temperature from ARDC Model Atmosphere and the vertical distribution of atmospheric constituents as given by Miller.

Three sets of curves are also presented whereby the amount of absorption at an operating frequency can be calculated for different atmospheric layers.

1. Introduction

For intercommunication between planets and satellites by radiations in the microwave region, it is necessary to know their absorption by atmospheric gases. The main atmospheric gases which absorb microwaves are oxygen, water vapour, ozone and nitrous oxide. The useful frequency range for this purpose in the microwave region is 10,000–100,000 Mc/s, where it is possible to generate waves at high power level. In this frequency range, the spectrum of microwave absorption coefficients, given by Ghosh and Edwards (1956) (Fig. 1), shows that a large number of absorption lines cluster in different frequency ranges, namely, at 10–11, 22–25, 50–52 and 59–70 kMc/s, with windows in between them.

In this paper, we shall calculate microwave absorption for different atmospheric layers around peak resonance frequencies of each constituent, and then shall obtain the total absorption for the whole atmosphere. Finally, three sets of curves will be presented, whereby microwave absorption for a gas at any frequency can be calculated for different atmospheric layers.

2. Formula for Microwave Absorption

The microwave absorption coefficient of a gas for a radiation of frequency ν is given by the relation (Townes and Schawlow, 1955),

$$\alpha_\nu = \frac{8\pi^2\nu^2 Nf}{3ckT} \cdot (\mu_{ij})^2 \cdot \left[\frac{\Delta\nu}{(\nu_0 - \nu)^2 + \Delta\nu^2} + \frac{\Delta\nu}{(\nu_0 + \nu)^2 + \Delta\nu^2}\right] \tag{1}$$

where

N = total number of molecules per ml,
f = fraction of the total molecules present in the lower state,
μ_{ij} = matrix element of the components of the dipole moment μ, which gives rise to the transition from i to j states,
$\Delta\nu$ = half-width of the absorption line, and
ν_0 = peak resonance frequency of the absorption line.

Other symbols have their usual significance.

For all absorbing gases in the atmosphere, ν_0 is considerably higher than $\Delta\nu$. Hence, the second expression of the above formula can be neglected. The formula then reduces to the form

$$\alpha_\nu = \frac{8\pi^2\nu^2 Nf}{3ckT} \cdot (\mu_{ij})^2 \cdot \frac{\Delta\nu}{(\nu_0 - \nu)^2 + \Delta\nu^2}. \tag{2}$$

At $\nu = \nu_0$ we have,

$$\alpha_\nu = \alpha_0 = \frac{8\pi^2 {\nu_0}^2 Nf}{3ckT} \cdot (\mu_{ij})^2 \cdot \frac{1}{\Delta\nu} \tag{3}$$

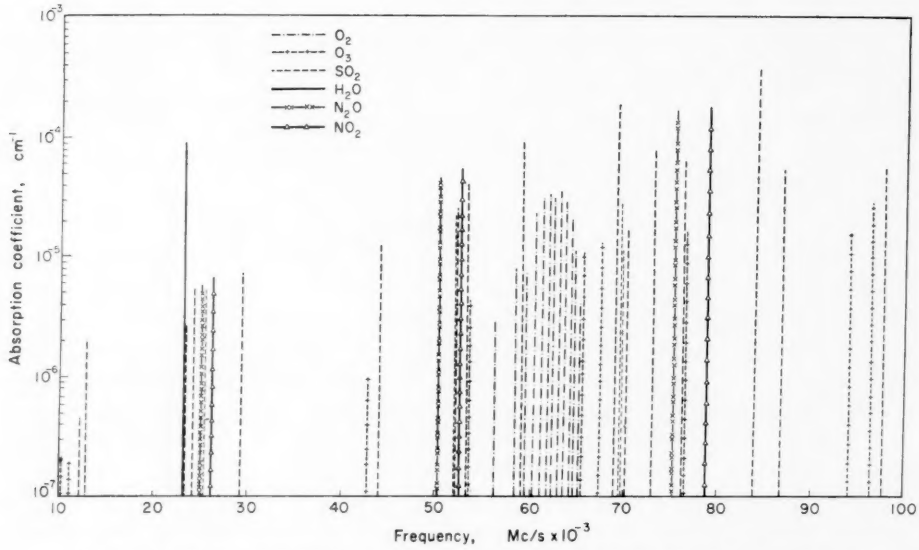

Fig. 1. Microwave absorption coefficients of atmospheric gases given by Ghosh and Edwards (1956) in the frequency range 10–100 kMc/s.

where α_0 is the absorption coefficient at the peak resonance frequency. Therefore, in terms of α_0 the expression for α_ν becomes,

$$\alpha_\nu = \alpha_0 \cdot \frac{\Delta\nu^2}{(\nu_0 - \nu)^2 + \Delta\nu^2} \cdot \frac{\nu^2}{{\nu_0}^2}. \tag{4}$$

Therefore, the amount of absorption in dB/km at a frequency ν is given by

$$\gamma = 10 \,.\, \log_{10} e \cdot \alpha_\nu \cdot 10^5$$
$$= 10^6 \log_{10} e \; \alpha_0 \cdot \frac{\Delta\nu^2}{(\nu_0 - \nu)^2 + \Delta\nu^2} \cdot \frac{\nu^2}{{\nu_0}^2}$$

or

$$\gamma = \gamma_0 \cdot \frac{\Delta\nu^2}{(\nu_0 - \nu)^2 + \Delta\nu^2} \cdot \frac{\nu^2}{{\nu_0}^2} \tag{5}$$

where $\gamma_0 = 10^6 \alpha_0 \log_{10} e$.

From the above relation it follows that for the calculation of microwave absorption by atmospheric gases, a knowledge of γ_0 and $\Delta\nu$ for each constituent gas

VOL. 21 1961

of the atmosphere at different altitudes is required. Since temperature and pressure vary with altitude, we shall first obtain the variation of γ_0 with these parameters. In the subsequent section we shall calculate $\Delta\nu$ for atmospheric constituents.

3. Variation of γ_0 with Pressure and Temperature

It has been found experimentally that for all microwave absorbing gases, the value of $\Delta\nu$ varies linearly with pressure (i.e. with the number density of absorbing gas molecules) over a wide range of low pressures (Gordy *et al.*, 1953, p. 190). It, therefore, follows from expressions (3) and (5) that the peak absorption at the centre of the line, γ_0, is independent of pressure. The extent of low pressure up to which the above condition is valid, is determined by the collisional diameter of the absorbing gas molecule. (Even at a high pressure of 1 atm, this condition may be valid if the collisional diameter is small enough to obey considerations of kinetic theory.) For O_2, the above condition holds up to atmospheric pressure (Strandberg *et al.*, 1949). Even for bigger molecules like O_3, H_2O and N_2O, this condition holds at every altitude of the atmosphere because of low concentration. Therefore for calculating microwave absorption in the atmosphere, γ_0 is independent of pressure.

Remembering (Herzberg, 1947)

$f \propto \dfrac{1}{T}$, for diatomic molecules and linear polyatomic molecules (in our case for O_2 and N_2O)

and $f \propto \dfrac{1}{T^{3/2}}$, for symmetric and asymmetric top molecules (in our case for H_2O and O_3)

and substituting $N = P/kT$, where P is the partial pressure of the absorbing gas, we obtain, for O_2 and N_2O

$$\left.\begin{aligned} \alpha_0 &= \frac{8\pi^2 {\nu_0}^2 \,.\, (\mu_{ij})^2 P}{\text{const.} \times 3ckT^3} \cdot \frac{1}{\Delta\nu} \\ \text{and for } H_2O \text{ and } O_3 \qquad \alpha_0 &= \frac{8\pi^2 {\nu_0}^2 \,.\, (\mu_{ij})^2 P}{\text{const.} \times 3ck^2T^{7/2}} \cdot \frac{1}{\Delta\nu}. \end{aligned}\right\} \tag{6}$$

The variation of $\Delta\nu$ with temperature and pressure is given (Gordy *et al.*, 1953, p. 196) by

$$\Delta\nu = (\Delta\nu)_1 \cdot P_{mm} \left(\frac{300}{T}\right)^x \tag{7}$$

where $(\Delta\nu)_1$ = half-width at 300°K and at 1 mm pressure. Substituting expression (7) in (6), we obtain (i) for O_2 and N_2O

$$\alpha_0 \propto \frac{1}{T^{3-x}}$$

and for H_2O and O_3

$$\alpha_0 \propto \frac{1}{T^{7/2-x}}.$$

The value of x for oxygen has been found experimentally by TINKHAM and STRADBERG (1956) to be 3/4. For ozone, water vapour and nitrous oxide the value of x has been assumed to be unity (GORDY *et al.*, 1953, p. 196).

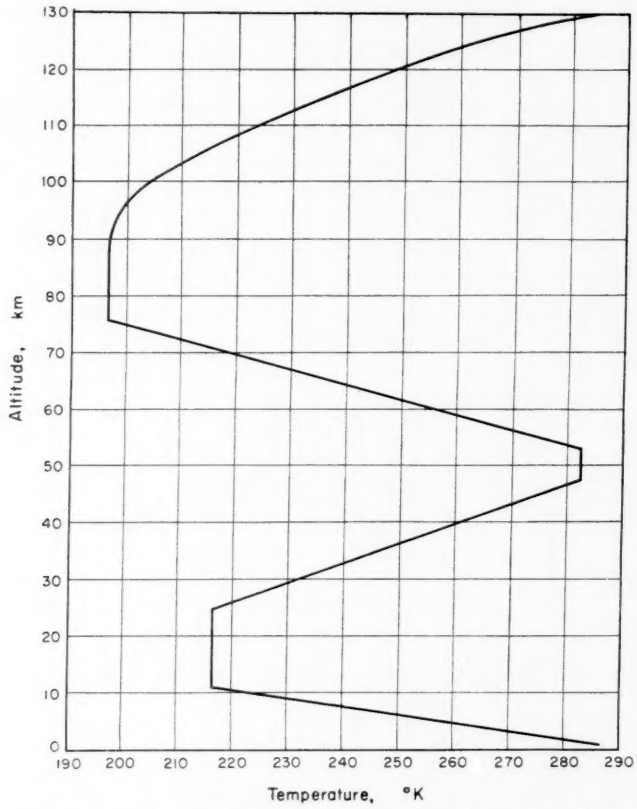

Fig. 2. Idealized temperature distribution of the atmosphere.

Since $\gamma_0 = 10^6 \alpha_0 \log_{10} e$, we obtain

$$\left.\begin{aligned} \gamma_0 &\propto \frac{1}{T^{9/4}} && \text{for } O_2 \\ \gamma_0 &\propto \frac{1}{T^2} && \text{for } N_2O \\ \gamma_0 &\propto \frac{1}{T^{5/2}} && \text{for } H_2O \\ \gamma_0 &\propto \frac{1}{T^{5/2}} && \text{for } O_3 \end{aligned}\right\} \qquad (8)$$

To calculate γ_0 for the atmosphere, an idealized temperatute distribution given in Fig. 2 has been assumed (MINZER and RIPLEY, 1956). The atmosphere below 100 km has been divided into segments of layers as shown in the Table 1. Above

VOL. 21 1961

Table 1. The values in dB/km of γ_0 for oxygen, water vapour, ozone and nitrous oxide, and the division of atmospheric column according to the temperature variation which has been assumed for calculating γ_0

Height (km)	Av. temperature (°K)	Oxygen			Water vapour	Ozone			Nitrous oxide	
		γ_0 62,998 Mc/s	γ_0 65,222·6 Mc/s	γ_0 58,446·7 Mc/s	γ_0 22,235·7 Mc/s	γ_0 65,471·1 Mc/s	γ_0 42,832·0 Mc/s	γ_0 11,075·9 Mc/s	γ_0 25,123·4 Mc/s	γ_0 50,246·6 Mc/s
0–11	253·5	22·25	2·54	4.82	59·48	6·61	0·661	0·139	3·47	27·37
11–25	216·66	31·57	3·6	6·85	88·13	9·79	0·979	0·206	4·75	37·45
25–35	231·3	25·76	2·94	5·59	74·93	8·32	0·832	0·175	4·16	32·87
35–47	263·86	20·24	2·32	4·4	53·88	5·99	0·599	0·126	3·20	25·30
47–53	282·66	16·87	1·93	3·66	44·35	5·03	0·503	0·106	2·79	22·01
53–64	262·45	20·52	2·34	4·46	54·58	6·06	0·606	0·127	3·23	25·54
64–76	219·5	30·75	3·51	6·67	85·39	9·49	0·949	0·199	4·62	36·50
76–91	196·86	39·16	4·48	8·52	112·05	12·44	1·244	0·248	5·75	45·40
91–100	201·93	36·77	4·21	7·99	105·13	11·69	1·169	0·245	5·47	43·14
100–120	229·6	27·74	3·17	6·04	76·28	8·48	0·849	0·178	4·22	33·37
120–140	307·45	14·38	1·64	3·11	36·75	4·08	0·408	0·086	2·36	18·60
140–160	439·75	6·42	0·74	1·40	14·98	1·67	0·167	0·035	1·15	9·09
160–180	592·95	3·28	0·38	0·71	7·12	0·79	0·079	0·017	0·63	5·00
180–200	390·65	2·32	0·27	0·50	4·86	0·54	0·054	0·011	0·47	3·69
200–220	734·4	2·03	0·23	0·44	4·17	0·46	0·046	0·010	0·44	3·26
220–240	779·15	1·8	0·20	0·39	3·60	0·40	0·040	0·008	0·37	2·89
240–260	824·55	1·56	0·18	0·34	3·12	0·35	0·035	0·007	0·33	2·59
260–280	875·35	1·36	1·16	0·30	2·69	0·29	0·029	0·0065	0·29	2·29
280–300	916·3	1·23	0·14	0·27	2·4	0·27	0·027	0·006	0·27	2·10
300–350	996·7	1·02	0·12	0·22	1·94	0·21	0·021	0·0045	0·22	1·77
350–400	1111·5	0·8	0·09	0·17	1·48	0·16	0·016	0·0035	0·18	1·42
400–450	1225·5	0·64	0·07	0·14	1·16	0·13	0·013	0·003	0·15	1·17
450–500	1338·0	0·52	0·06	0·11	0·73	0·102	0·010	0·002	0·12	0·98

Table 2. The values of half-widths of absorption lines of oxygen, water vapour, ozone and nitrous oxide at different altitudes of the earth's atmosphere

Altitude (km)	$\Delta\nu$ for oxygen (kc/s)	$\Delta\nu$ for water vapour (kc/s)	Altitude (km)	$\Delta\nu$ for ozone (c/s)	Altitude (km)	$\Delta\nu$ for nitrous oxide (c/s)
0–2	$1093{\cdot}7 \times 10^3$	97,030·0			0–5	1304·0
2–4	$884{\cdot}7 \times 10^3$	25,940·0			5–10	747·6
4–6	$708{\cdot}3 \times 10^3$	6673·0			10–15	365·9
6–8	$561{\cdot}4 \times 10^3$	1696·0			15–20	165·4
8–10	$438{\cdot}0 \times 10^3$	408·3			20–25	73·3
10–12	$337{\cdot}6 \times 10^3$	84·12			25–30	31·22
12–14	$253{\cdot}4 \times 10^3$	27·86			30–35	13·82
14–16	$196{\cdot}3 \times 10^3$	22·32	15–17	90·9	35–40	7·75
16–18	$131{\cdot}9 \times 10^3$	24·18	17–19	266·1	40–45	3·66
18–20	$95{\cdot}6 \times 10^3$	26·79	19–21	685·5	45–50	1·98
20–25	$59{\cdot}1 \times 10^3$	31·99	21–23	1462·0	50–55	1·11
25–30	$26{\cdot}7 \times 10^3$	40·08	23–25	2228·0		
30–35	9620·0	14·89	25–27	2193·0		
35–40	5780·0	3·87	27–29	2188·0		
40–45	2890·0	1·04	29–31	1807·0		
45–50	1510·0	0·24	31–33	1406·0		
50–55	823·0	0·06	33–35	1023·0		
55–60	467·0	0·02	35–40	547·0		
60–65	271·6		40–45	181·0		
65–70	136·9		45–50	59·7		
70–75	69·2					
75–80	32·4					
80–85	13·9					
85–90	5·9					

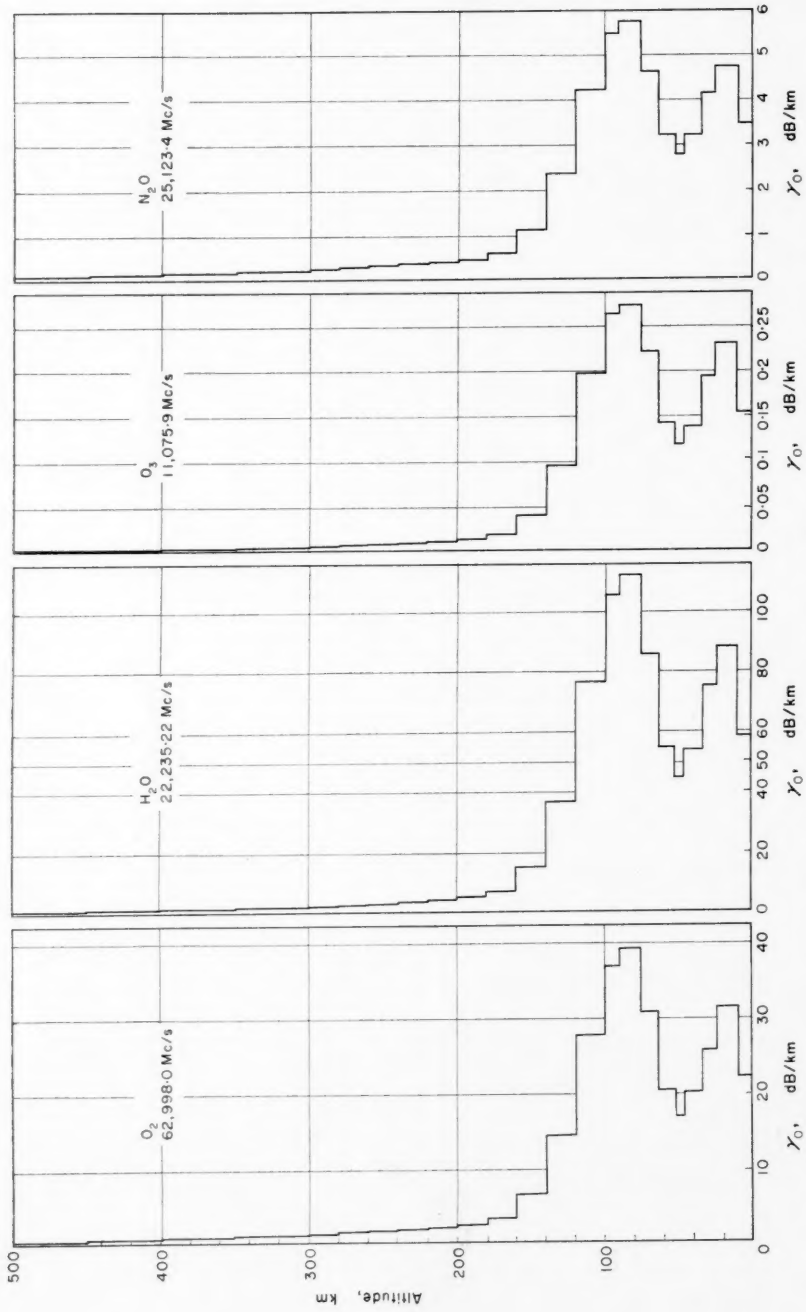

Fig. 3. Histograms showing the variations of peak absorption of different atmospheric gases with altitude.

VOL. 21 1961

100 km, due to the regular variation of temperature with altitude, the atmosphere has been divided into layers each 20 km thick. The value of γ_0 at different altitudes are calculated and tabulated in Table 2. The corresponding histograms are shown in Fig. 3.

4. Calculation of $\Delta\nu$

For oxygen it has been found experimentally that the concentration of nitrogen molecules also affects the collisional broadening of the absorption line (Artman, 1957). If, therefore, a factor β is defined as the ratio of O_2–N_2 to O_2–O_2 broadenings, the half-width of the oxygen absorption line in O_2–N_2 mixture becomes

$$(\Delta\nu)_{\text{mix}} = (\Delta\nu)_1 \cdot \left(\frac{300}{T}\right)^x \cdot \left[P_{O_2} + \beta P_{N_2}\right] \tag{9}$$

where P_{O_2} and P_{N_2} are the partial pressures due to oxygen and nitrogen molecules respectively. Artman (1953) has found $\beta = 0{\cdot}75$ and $(\Delta\nu)_1 = 1{\cdot}94$ Mc/s per mm at 300°K. Hence for oxygen molecules we get

$$(\Delta\nu)_{\text{mix}} = (1{\cdot}94) \cdot \left(\frac{300}{T}\right)^{3/4} \cdot \left[P_{O_2} + 0{\cdot}75 P_{N_2}\right]. \tag{10}$$

Using the above formula, the values of $\Delta\nu$ for oxygen absorption line at different altitudes have been calculated and are tabulated in Table 2.

For ozone, water vapour and nitrous oxide the collisional broadenings due to foreign molecules have not been taken into account due to lack of proper data. The value of x for these gases has been taken to be unity. Hence the expression for $\Delta\nu$ becomes

$$(\Delta\nu) = (\Delta\nu)_1 \cdot P_{mm} \cdot \left(\frac{300}{T}\right). \tag{11}$$

For these gases the half-width has been calculated after assuming the value of $(\Delta\nu)_1$ for ozone, water vapour and nitrous oxide as 25, 14 and 4·2 Mc/s per mm respectively (Ghosh and Edwards, 1956).

The vertical distribution of atmospheric constituents has been obtained after Miller (1957) and that of temperature from ARDC Model Atmosphere Data (Minzer and Ripley, 1956).

The values of $\Delta\nu$ for ozone, water vapour and nitrous oxide are also tabulated in Table 2.

The amount of absorption γ has been calculated, using formula (5), for a set of values of $(\nu_0 - \nu)$ in a given layer of the atmosphere. This value is then plotted against $\pm(\nu_0 - \nu)$. Finally, corresponding to each value of $(\nu_0 - \nu)$, values of γ for each segmented division of the atmosphere are added, thereby giving the total absorption for the whole atmosphere. This is shown in Figs. 4 and 5.

The absorption at high altitudes becomes very small owing to the low concentration of the absorbing gases and is neglected.

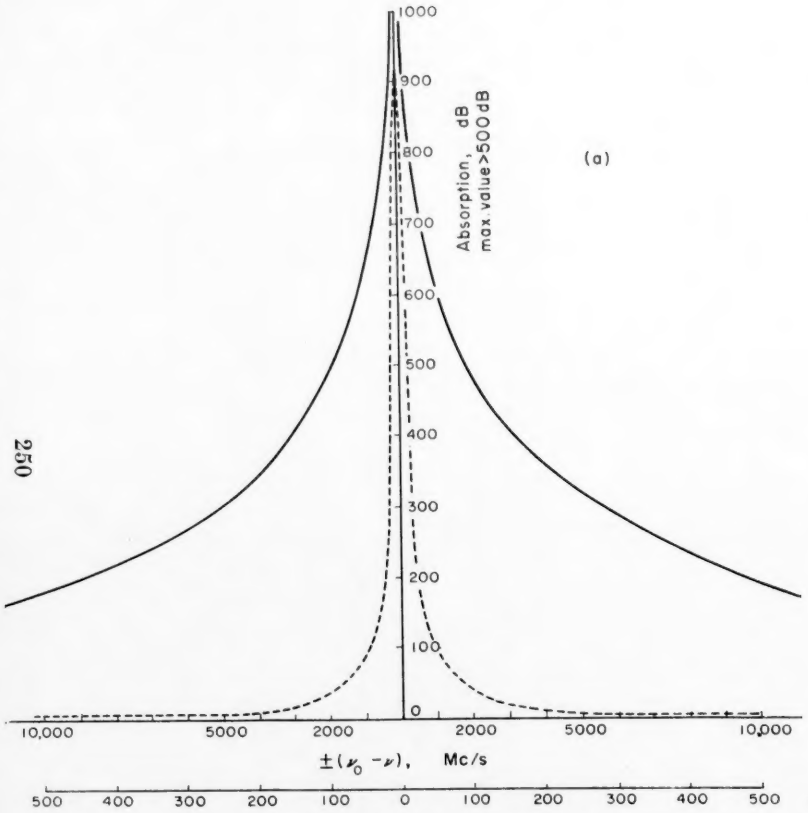

Fig. 4(a). Total absorption around peak resonance frequencies for oxygen, $\nu_0 = 62{\cdot}998$ Mc/s.

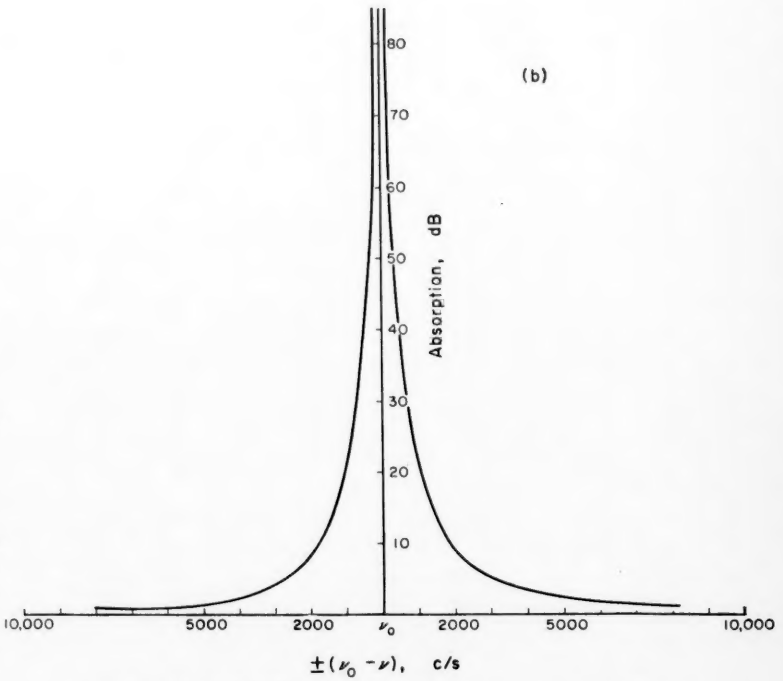

Fig. 4(b). Total absorption around peak resonance frequencies for nitrous oxide, $\nu_0 = 25{,}123{\cdot}4$ Mc/s.

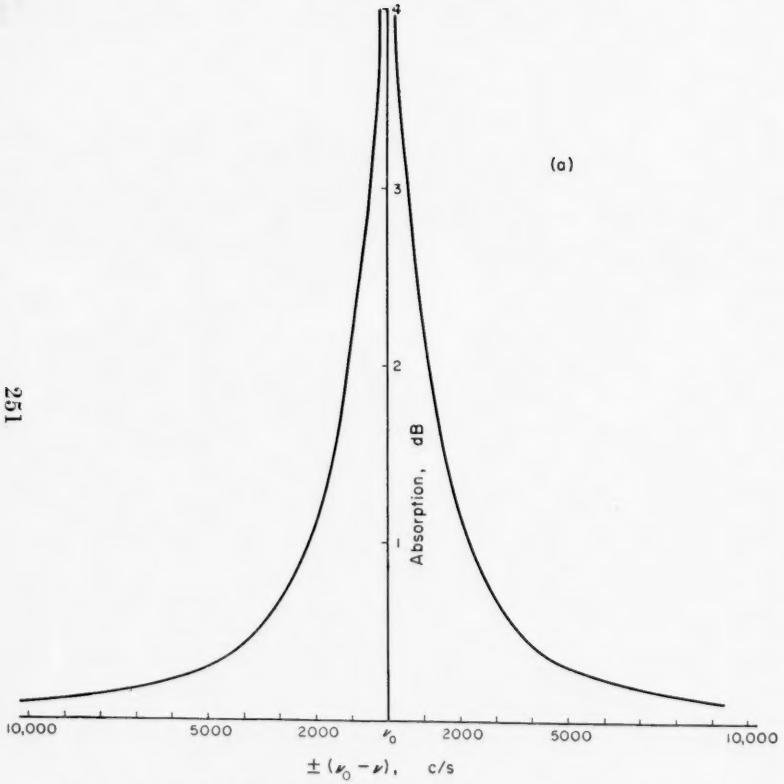

Fig. 5(a). Total absorption around peak resonance frequencies for ozone, $\nu_0 = 11{,}075{\cdot}9$ Mc/s.

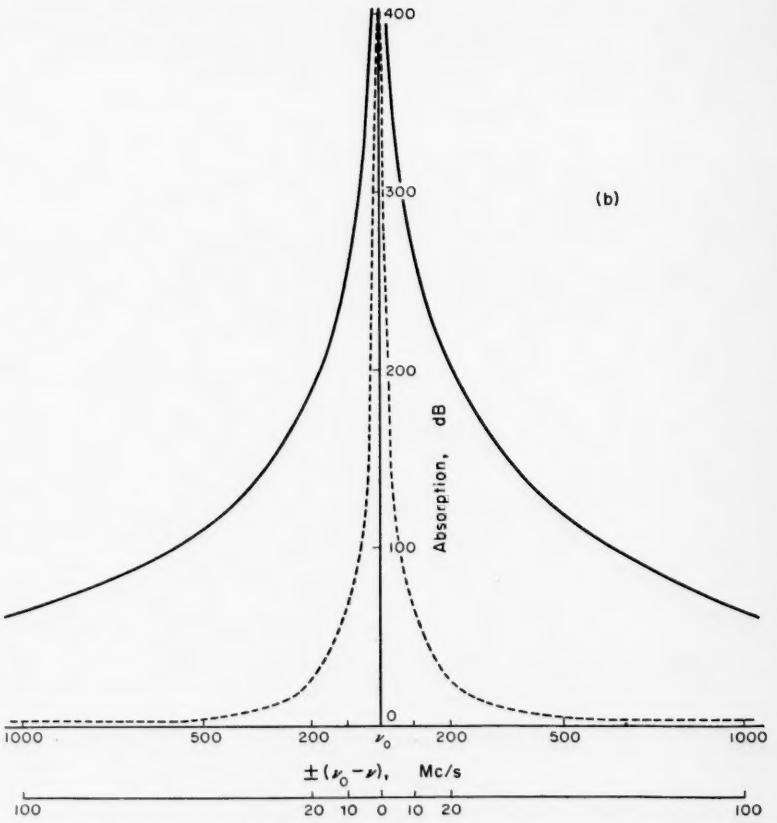

Fig. 5(b). Total absorption around peak resonance frequencies for water vapour, $\nu_0 = 22{,}235{\cdot}22$ Mc/s.

5. General Curves for Calculating Microwave Absorption in the Atmosphere

Rewriting formula (5) in the form

$$\gamma = \gamma_0 \cdot \frac{1}{1 + [(\nu_0 - \nu)/\Delta\nu]^2} \cdot \frac{\nu^2}{\nu_0^2} \tag{12}$$

we find that for determining absorption of microwaves in the atmosphere, the values of γ_0 and $1/[1 + (\nu_0 - \nu)^2/\Delta\nu^2]$ should be known and are given in the general curves. Multiplying their values with that of ν^2/ν_0^2, one will obtain the amount of absorption in dB/km at an operating frequency ν.

In order to obtain the values of γ_0 and $1/[1 + (\nu_0 - \nu)^2/\Delta\nu^2]$, three sets of curves relating the variations of (i) γ_0 with altitude, (ii) $\Delta\nu$ with altitude and (iii) $1/[1 + (\nu_0 - \nu)^2/\Delta\nu^2]$ with $\Delta\nu$ are required. These curves are obtained as follows.

Regarding the first set of curves, it should be noted from Section 3, that for O_2 and N_2O

$$\gamma_0 \propto \alpha_0 \propto \frac{1}{T^{3-x}}.$$

Therefore

$$\frac{\alpha_0(T)}{\alpha_0(300)} = \left(\frac{300}{T}\right)^{3-x}$$

where $\alpha_0(T)$ and $\alpha_0(300)$ represent values of α_0 at $T°$K and at 300°K respectively. Hence $\gamma_0(T)$, the value of γ_0 at $T°$K can be written as

$$\gamma_0(T) = 10^6 \,.\, \alpha_0(T) \,.\, \log_{10} e = 10^6 \,.\, \alpha_0(300) \,.\, \left(\frac{300}{T}\right)^{3-x} \,.\, \log_{10} e$$

or $$\frac{\gamma_0(T)}{\alpha_0(300)} = 10^6 \,.\, \log_{10} e \,.\, \left(\frac{300}{T}\right)^{3-x}.$$

Similarly for H_2O and O_3 for which

$$\gamma_0 \propto \alpha_0 \propto \frac{1}{T^{7/2-x}}$$

we obtain

$$\frac{\gamma_0(T)}{\alpha_0(300)} = 10^6 \log_{10} e \,.\, \left(\frac{300}{T}\right)^{7/2-x}.$$

Since, as already mentioned in Section 3, $x = 3/4$ for oxygen and unity for other atmospheric gases, three curves have been plotted corresponding to three variations of γ_0 with temperature, namely

(i) T^{3-x} for $x = 3/4$,

(ii) T^{3-x} for $x = 1$ and

(iii) $T^{7/2-x}$ for $x = 1$.

VOL. 21 1961

All these curves are shown in Fig. 6. From these curves, the values of $\gamma_0(T)$ for atmospheric gases at any altitude can be obtained, provided their absorption coefficients at 300°K at the peak resonance frequencies are known. These coefficients are given by GHOSH and EDWARDS (1956).

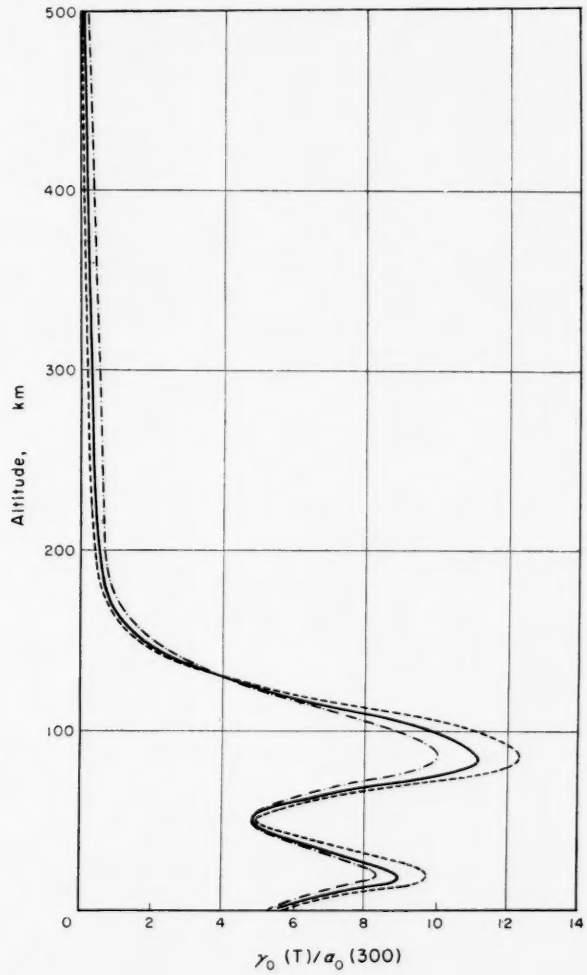

Fig. 6. Variation of $\gamma_0(T)/\alpha_0(300)$ with altitude for oxygen and other atmospheric gases.
——— Corresponding to $T^{9/4}$ (for O_2); – – – – Corresponding to $T^{-5/2}$ (for H_2O and O_3);
—·—·— Corresponding to T^{-2} (for N_2O).

Regarding the second set of curves, relating the variation of $\Delta\nu$ with altitude, it should be noted from expression (7), that the values of $\Delta\nu$ depend on only pressure and temperature and it is independent of either the peak resonance frequency or the absorption coefficient of the gas. Therefore, for obtaining the second set of curves,

only the values of $\Delta\nu$ at different altitudes are required. These curves are plotted from data given in Table 2 and are shown in Figs. 7 and 8.

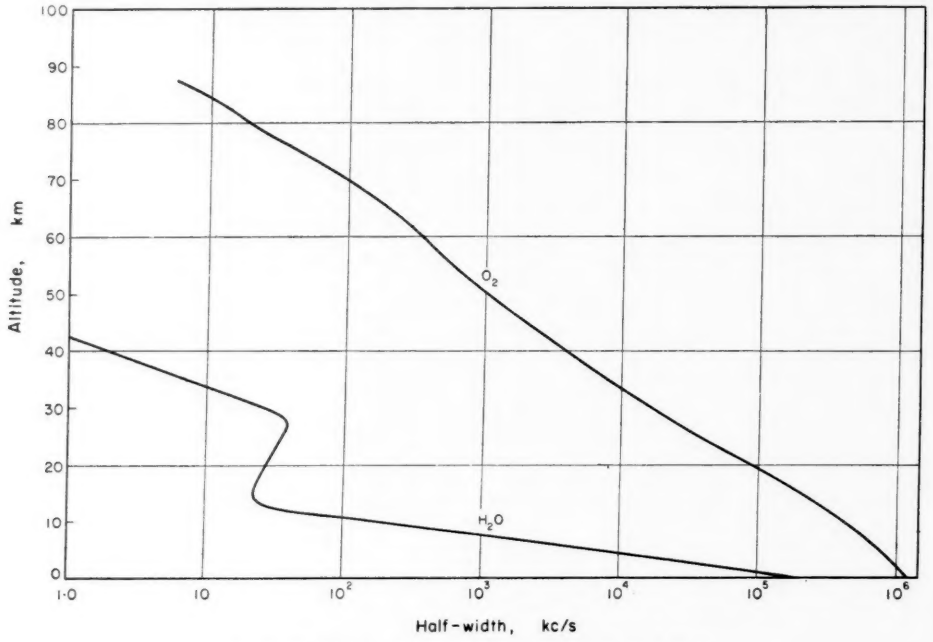

Fig. 7. Variation of $\Delta\nu$ with altitude for O_2 and H_2O.

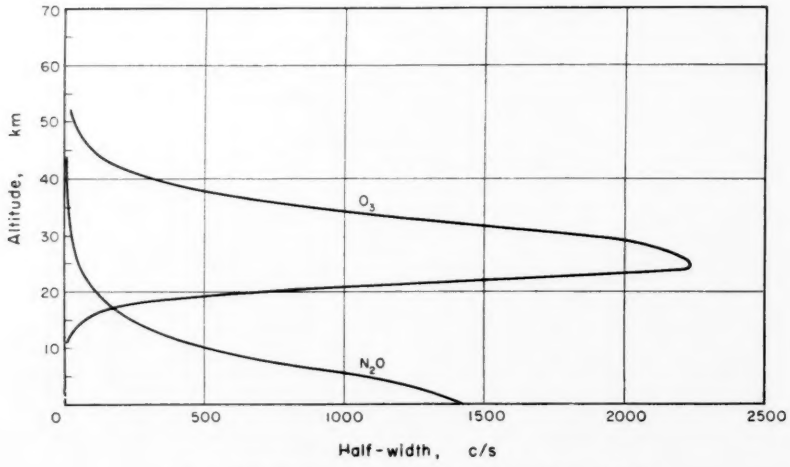

Fig. 8. Variation of $\Delta\nu$ with altitude for O_3 and N_2O.

For obtaining the last set of curves, a particular value of $\Delta\nu$ is first chosen and then the values of the expression $1/[1 + (\nu_0 - \nu)^2/\Delta\nu^2]$ are calculated for different

VOL. 21 1961

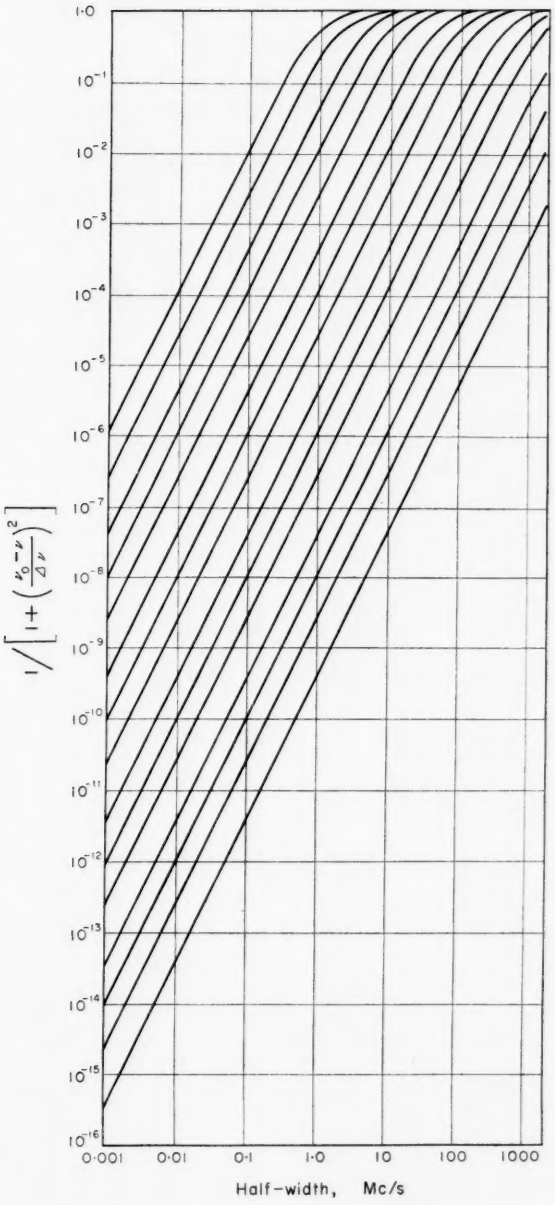

Fig. 9. Variation of $1\Big/\left[1+\left(\frac{\nu_0-\nu}{\Delta\nu}\right)^2\right]$ with $\Delta\nu$ for different values of $(\nu_0 - \nu)$.

values of $(\nu_0 - \nu)$. The values of the expression $1/[1 + (\nu_0 - \nu)^2/\Delta\nu^2]$ are then plotted against $\Delta\nu$ and are shown in Fig. 9.

To calculate the microwave absorption due to a particular gas at any altitude, the value of $\gamma_0(T)/\alpha_0(300)$ should be obtained, which in turn will give $\gamma_0(T)$ because $\alpha_0(300)$ is known. The half-width $\Delta\nu$ is then obtained from Figs. 7 and 8.

Finally, the value of $(\nu_0 - \nu)$ is calculated from the peak resonance frequency and the operating frequency. For the above values of $(\nu_0 - \nu)$ and $\Delta\nu$, the value of $1/[1 + (\nu_0 - \nu)^2/\Delta\nu^2]$ is obtained from Fig. 9. The product of γ_0, $1/[1 + (\nu_0 - \nu)^2/\Delta\nu^2]$ and ν^2/ν_0^2 gives the absorption in terms of dB/km at the desired height.

For calculating absorption for the whole atmosphere at a particular frequency, the amount of absorption for different layers (shown in Table 1) should be first calculated in the manner described above. The absorption for the whole atmosphere is the sum total of all these absorptions.

References

Artman J. O.	1953	*Absorption of Microwaves by Oxygen in the Millimeter Wavelength Region.* Columbia Radiation Laboratory Report.
Ghosh S. N. and Edwards H. D.	1956	Report No. 82, Geophysics Research Directorate, Air Force Cambridge Research Center.
Gordy W., Smith W. V. and Trambarulo R. F.	1953	*Microwave Spectroscopy.* John Wiley, New York.
Herzberg G.	1947	*Molecular Spectra and Molecular Structure,* Vol. 2. Van Nostrand, New York.
Miller L. E.	1957	*J. Geophys. Res.* **62,** 351.
Minzer R. A. and Ripley W. S.	1956	Report No. 86, Geophysics Research Directorate, Air Force Cambridge Research Center.
Strandberg M. W. P., Meng C. Y. and Ingersoll J. G.	1949	*Phys. Rev.* **75,** 1524.
Tinkham M. and Strandberg M. W. P.	1956	*Phys. Rev.* **99,** 537.
Townes C. H. and Schawlow A. L.	1955	*Microwave Spectroscopy.* McGraw-Hill, New York.

VOL. 21 1961

Journal of Atmospheric and Terrestrial Physics, 1961, Vol. 21, pp. 257 to 260. Pergamon Press Ltd. Printed in Northern Ireland

The east–west drift of auroral forms determined from all-sky camera films

W. STOFFREGEN
Uppsala Ionospheric Observatory, Research Institute of National Defence, Sweden

(*Received* 1 *February* 1961)

Abstract—Using all-sky camera observations from a chain of stations lying in a N–S direction from Spitzbergen along the Scandinavian peninsula and crossing the auroral zone, the E–W motions of the auroral forms have been studied. It is shown that at stations lying to the south of the auroral zone there is a mean drift towards W before midnight and a mean drift towards E after midnight. At stations lying to the north of the auroral zone the diurnal variation in the drift direction is reversed. A station ~5° south of the auroral zone (Lycksele) shows E–W motions more often than stations in or north of the auroral zone. The close resemblance between the mean diurnal drift directions of auroral forms deduced from all-sky films and the drifts of ionized areas determined from studies of auroral echoes is stressed.

THE AURORAL FORMS generally show two distinct and different types of motions: (a) a general N–S displacement of the whole auroral display, and (b) E–W motions of the individual forms or features within the display. These latter movements seem often to be directed along the geomagnetic parallels of latitude. In the present paper only the latter type of motions will be discussed.

The material used is the IGY all-sky camera films obtained during the winter 1957–1958 from the Scandinavian chain of recording stations lying in a S–N direction and crossing the auroral zone extending from 60° N to 80° N. In addition, the Arctic station Godhavn, lying to the north of the auroral zone, has been included. In Table 1 are listed the stations and their geographic and geomagnetic co-ordinates.

Table 1

Station	φ	λ	Φ	Approximate time for reversal of auroral motion (hours, L.T.)
Uppsala	59·8°	17·6°	58·4°	—
Lycksele	64·7°	18·8°	62·5°	2300–0000
Kristineberg	65·1°	18·6°	63·0°	2300–0000
Kiruna	67·9°	20·5°	65·4°	2300–0000
Tromsö	69·7°	19·0°	67·0°	0000–0100
Murchison Bay	80·1°	18·3°	75·1°	0200–0300
Godhavn	69·3°	306·5°	79·9°	0300–0400

The all-sky films were inspected and the cases where distinct E–W motions appeared were noted. It is apparent that E–W motions can only be noticed for certain types of forms as curved bands, draperies and rays, whereas diffuse bands and arcs cannot be used for E–W drift determinations. There is a distinct change in the occurrence frequency of various auroral forms with latitude. Close to the auroral zone, strong diffuse arcs and bands are most frequent and these forms

cannot be used for E–W movement determinations. In the drift statistics this type effect appears. Thus the station Lycksele, which lies about 600 km to the south of the auroral zone and where draperies and rays are frequent, shows the E–W motions very distinctly, whereas the auroral station Tromsö, lying close to the auroral zone, shows a comparatively low number of drift determinations in spite of the far greater numbers of auroral displays occurring at Tromsö compared with Lycksele.

From the all-sky camera films the number of quarter-hours where E–W drift motions appear, n, have been counted and in Fig. 1(a) this frequency of occurrence

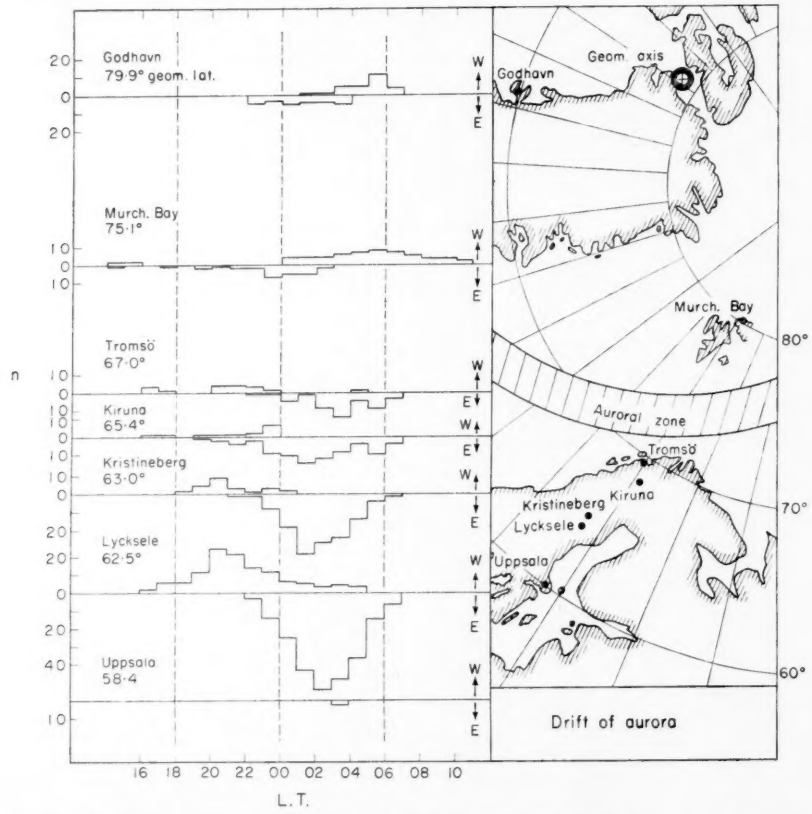

Fig. 1(a). Frequency of occurrence n of drift motions in E–W direction of auroral forms determined from all-sky films, versus local time (L.T.).

n has been arranged according to local time (L.T.) for each station. As a comparison the drift motions of the ionized areas determined from studies of auroral echoes in the v.h.f.-band are given in the lower part of the figure, together with the horizontal geomagnetic perturbing vector S_D. These measurements were made at the two stations Kjeller and Tromsö by HARANG and TRÖIM (1961).

The diurnal curves in Fig. 1 indicate the following characteristic features of the E–W motions of the auroral luminosities:

VOL. 21 1961

1. South of the auroral zone there is a motion towards W before midnight and a motion towards E after midnight;
2. North of the auroral zone the directions of motions are reversed;
3. There seems to be a gradual change with geomagnetic latitude in the time of reversal of drift from W- to E-directions, the time of reversal appearing later at high geomagnetic latitude (see Table 1);

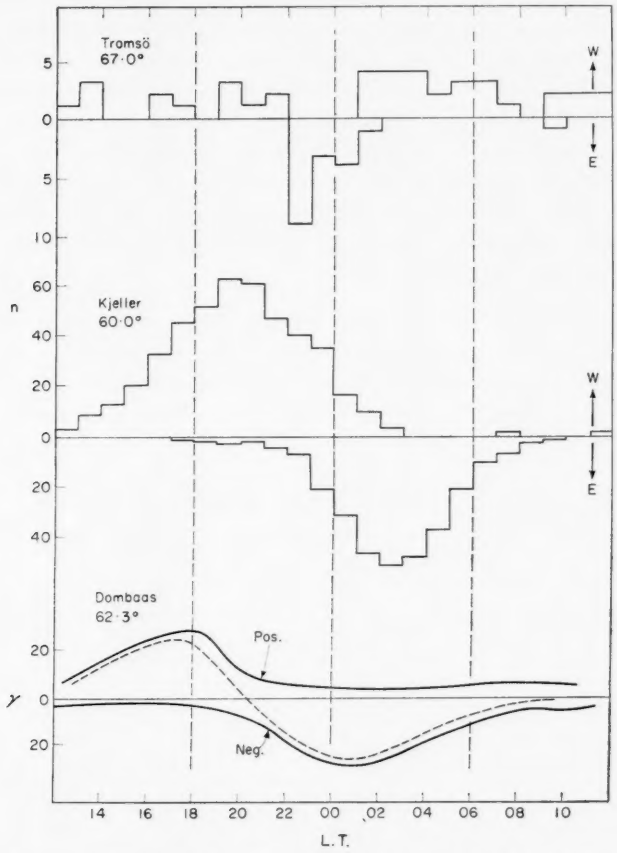

Fig. 1(b). Drift motions of ionized areas at Tromsö and Kjeller (Oslo) determined by auroral echoes according to HARANG and TRÖIM (1961), and the mean values of the horizontal perturbing geomagnetic vector, S_D at Dombaas (~300 km north of Oslo).

4. There is a similar diurnal variation in the mean drift motions of the optical auroral forms, the drift of ionized areas, and the mean current system producing the geomagnetic disturbance.

Several of the effects here discussed which are appearing along the Scandinavian chain of stations have been noticed from recordings at other stations. Thus KIM and CURRIE (1958) have stated that auroral motions deduced from all-sky films over Canada show a similar diurnal motion, with drifts towards W before local midnight and towards E after midnight. The E–W drifts of the ionized areas

recorded by means of auroral echoes have been extensively studied on the northern hemisphere by BULLOUGH and KAISER (1954, 1955) in Great Britain, and in Alaska by NICHOLS (1957); all stations showing the same characteristic diurnal change in the mean drift directions from W to E.

Studies of the mean drift direction of the ionized areas north of the auroral zone have not hitherto been published. If the close parallelism between mean drift directions of optical auroral forms and ionized areas are also maintained north of the auroral zone, for the ionized areas one should also expect a reversal in the mean drift directions to occur when crossing the auroral zone.

A study of the direction of auroral forms at eight stations in Alaska has been made by DAVIES (1960), who has deduced a pattern of auroral forms which is centred in the geomagnetic pole and fixed with respect to the sun. This pattern explains the reversal of E–W motions north of the auroral zone, but the gradual change of the time of reversal at high geomagnetic latitudes as shown in Table 1 indicates rather that the pattern should be somewhat asymmetric with respect to the geomagnetic midnight meridian.

Acknowledgements—The author wishes to express his thanks to Dr J. OLSEN for kindly putting at his disposal the auroral films from Godhavn, Mr H. DERBLOM and Mr. L. O. GUSTAFSON for assisting in the analysis of a great number of all-sky films, and Professor L. HARANG for valuable discussions in connexion with this paper.

VOL.
21
1961

REFERENCES

BULLOUGH K. and KAISER T. R.	1954	*J. Atmosph. Terr. Phys.* **5**, 189.
BULLOUGH K. and KAISER T. R.	1955	*J. Atmosph. Terr. Phys.* **6**, 198.
DAVIES T. N.	1960	*J. Geophys. Res.* **65**, 3497.
HARANG L. and TRÖIM J.	1961	*Planet. Space Sci.* **5**, 33.
KIM J. S. and CURRIE B. W.	1958	*Canad. J. Phys.* **36**, 160.
NICHOLS B.	1957	Scientific Report No. 1, Geophysical Institute, University of Alaska.

Journal of Atmospheric and Terrestrial Physics, 1961, Vol. 21, pp. 261 to 271. Pergamon Press Ltd. Printed in Northern Ireland

Attachment processes in meteor trails

J. S. GREENHOW and J. E. HALL*
Royal Radar Establishment, Malvern

(*Received* 8 *February* 1961)

Abstract—The effects of the loss of electrons by attachment to neutral particles on the characteristics of long duration meteor echoes are considered. In a previous paper some properties of enduring echoes were explained using a two-body attachment process, with an attachment time constant of 40 sec at a height of 95 km. This mechanism does not explain satisfactorily the rapid fall off in echo duration below 95 km, and in this paper the effects of two-body and three-body attachment processes are compared. It is concluded that a three-body reaction with a time constant of 70 sec at 95 km gives a better explanation of the rapid decay in electron density at lower heights. This view is supported by the very short durations of visual meteor trains between altitudes of 80 and 90 km.

1. INTRODUCTION

THE IONIZATION produced by bright meteors at heights of 80–100 km can be sufficiently dense to exceed the critical electron density at frequencies of a few megacycles/sec to several hundred megacycles/sec, and the radar echo duration obtained from these trails is limited to the time for which the electron density remains greater than the critical value (GREENHOW, 1952; KAISER and CLOSS, 1952).

For heights greater than about 90 km and meteor trails with linear electron densities less than 10^{14} electrons/cm, diffusion is the predominant factor in determining echo duration. At lower heights and greater electron densities the loss of electrons by attachment to neutral particles predominates.

The attachment of electrons to oxygen molecules or atoms can take place in several ways:

(i) With the emission of a photon;
(ii) In the presence of a third body which takes up the excess energy;
(iii) With the production of vibrational excitation of the ion, which is subsequently stabilized by collision;
(iv) Accompanied by dissociation of the molecule.

Processes (i) and (iv) are two-body reactions, with the rate of fall of electron density given by

$$\frac{dn_e}{dt} = -(\beta n_0)n_e \tag{1}$$

whereas (ii) and (iii) are three-body mechanisms, with

$$\frac{dn_e}{dt} = -(\gamma n_0 n_a)n_e. \tag{2}$$

β and γ are the two and three-body attachment coefficients respectively, n_0 is the negative ion forming particle density, and n_a is the density of particles taking part in the collision processes.

* Present address: D.S.I.R. Radio Research Station, Slough.

Laboratory measurements of β and γ have been made by a number of authors (CHANIN *et al.*, 1959), using pure oxygen molecules, but it is not obvious that these values will apply at the atmospheric pressures, electron energies and with the constituents appropriate to meteor trails.

In two previous papers (DAVIS *et al.*, 1959a,b), which will be referred to as Paper I and Paper II respectively, the effect of attachment on echo duration has been considered assuming a two-body process. This mechanism, however, does not explain the very rapid disappearance of free electrons at heights near 80 km, as the attachment time constant $T_\beta = 1/\beta n_0$ does not vary sufficiently rapidly with height. This difficulty can be overcome if three-body attachment with a time constant $T_\gamma = 1/\gamma n_0 n_a$ which varies as the square of the atmospheric density, is predominant.

As a number of echo characteristics have been satisfactorily explained by a two-body reaction, it is therefore important to compare the predicted effects of the two mechanisms with the experimental observations, in order to determine whether the differences between theory and experiment enable the appropriate reaction to be identified. Further evidence for the extremely rapid decay of ionization at low heights, given by the photographic observations of the decay in luminosity of a meteor train, will also be considered.

2. THE ATTACHMENT TIME CONSTANTS

Following the procedure of Paper I, we have for the echo duration t_β or t_γ from part of a meteor trail of linear electron density α, in the presence of two or three-body attachment

$$\log_e t_D = \log_e t_{\beta,\gamma} + \frac{t_{\beta,\gamma}}{T_{\beta,\gamma}}. \tag{3}$$

$t_D = \alpha/4\pi D n_e$ is the echo duration in the presence of diffusion alone, where D is the diffusion coefficient and n_e the critical electron density.

In Paper I the variation of electron density along the trail of a bright meteor was deduced from the photographic light curve. Using (3) the variation of t_β along the trail was then calculated for various values of T_β, until a value of T_β was found which explained the height and duration of the observed echo. A value of $T_\beta = 40$ sec at a height of 95 km was deduced. A similar procedure can be adopted for a three-body attachment process, and the best value of T_γ is found to be 70 sec at 95 km. The relative effects of the two mechanisms can now be compared, assuming height variations of T_β and T_γ of the form

$$T_\beta = 40 \exp -\left(\frac{h - 95}{H}\right) \tag{4}$$

and

$$T_\gamma = 70 \exp -2\left(\frac{h - 95}{H}\right). \tag{5}$$

H is the atmospheric scale height. These height variations are plotted in Fig. 1, assuming a constant value of $H = 6{\cdot}5$ km between 60 km and 110 km.

VOL. 21 1961

3. Comparison of the Effects of Two and Three-Body Attachment on Long Duration Meteor Echoes

(a) *Trails following the theoretical ionization curve*

Consider a meteor trail in which the ionization α along its length varies according to the theoretical relationship

$$\frac{\alpha}{\alpha_{max}} = \frac{9}{4}\frac{\rho}{\rho_{max}}\left(1 - \frac{\rho}{3\rho_{max}}\right)^2 \tag{6}$$

(Herlofson, 1948). ρ is the air density, α_{max} the maximum linear electron density and ρ_{max} the air density at the height of α_{max}. As an example a meteor with $\alpha_{max} = 10^{15}$ cm^{-1}, producing its maximum ionization at a height of 80 km will be

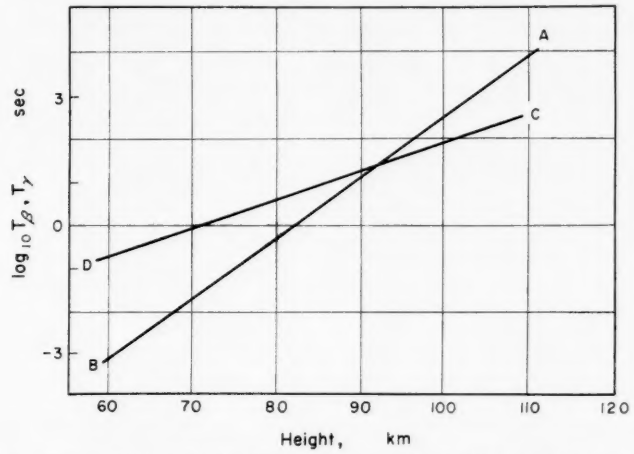

Fig. 1. The variation of attachment time constant with height AB, three-body attachment; CD, two-body attachment.

considered. An isothermal atmosphere with a scale height $H = 6{\cdot}5$ km will be assumed. At any frequency the value of t_D can be calculated for all points on the trail, using the known variation of D and ρ with height (Greenhow and Neufeld, 1955). The height variations of t_β and t_γ can then be deduced using (3). The curves of t_D, t_β and t_γ for a wavelength of $\lambda = 9$ m are shown in Fig. 2. It can be seen that the maximum durations for the two types of attachment, 25 sec and 22 sec, are not significantly different, although both are about two orders of magnitude less than the value of $t_D = 1300$ sec. There is also a small difference in the heights of the enduring echoes, but in both cases the echo is obtained from a height approximately $2H$ above the point of maximum t_D. These results are in agreement with observation. An important difference is, however, that in the case of two-body attachment the echo duration at the point of t_D(max) is still as high as 12 sec; about half the duration of the final echo at a height of 90 km. Thus enduring echo components should often be observed from comparatively low heights. There is no record of such long duration echoes being obtained from 80 km, indeed the majority of enduring echoes are observed above 90 km, irrespective

of the height of maximum ionization. When three-body attachment is considered the predicted duration at the point of maximum t_D is reduced from 12 sec to 2 sec, in better agreement with observation.

In the case of the Geminid meteor discussed in Paper I, the final echo lasting 46 sec was obtained from a height of 95 km, although the maximum ionization

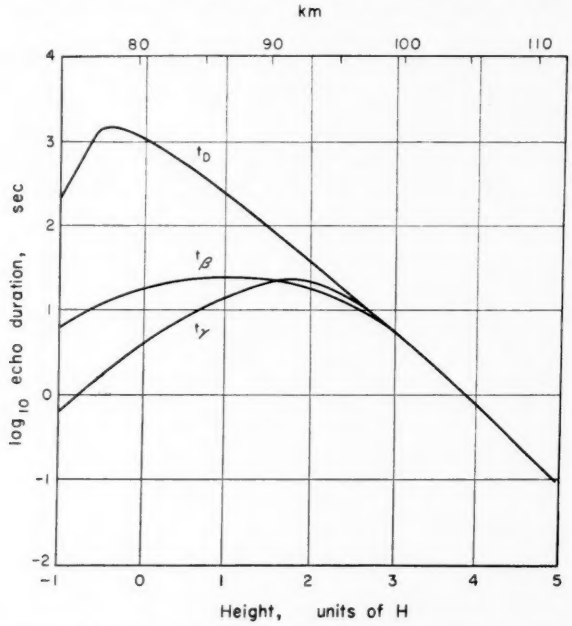

Fig. 2. The variation of t_D, t_β and t_γ with height for a meteor with $\alpha_{max} = 10^{15}$ electrons/cm at a height of 80 km, observed at a wavelength of 9 m.

was produced at 79 km. With two-body attachment an echo of 20 sec duration should still have been obtained from near 79 km, and it is very difficult to accept that irregular winds would not have distorted the trail sufficiently to give an echo from the ionization maximum in this time. With three-body attachment the expected duration at the point of maximum ionization is reduced to only 4 sec, and it is quite probable that an initially linear meteor trail at some angle off specular would not distort sufficiently to give an echo in this period (MCKINLEY and MILLMAN, 1949). Thus the absence of enduring echoes at heights below 80 km is best explained by a three-body attachment process. As some characteristics of enduring echoes have been explained previously using a two-body reaction (Paper II), it is therefore important to re-examine the results with a view to comparing the effects of two and three-body processes.

(b) *The theoretical variation of echo heights and durations for two and three-body attachment*

The previous Section shows that the effects of both two and three-body attachment are to reduce the echo duration below that expected for diffusion alone, and

VOL. 21 1961

to cause the most enduring echo to be obtained from a region above the point of maximum ionization. Large departures from the λ^2 dependence of echo duration, predicted by diffusion theory, also occur. As the heights of occurrence and the electron line densities for meteors of various brightness and velocity are known

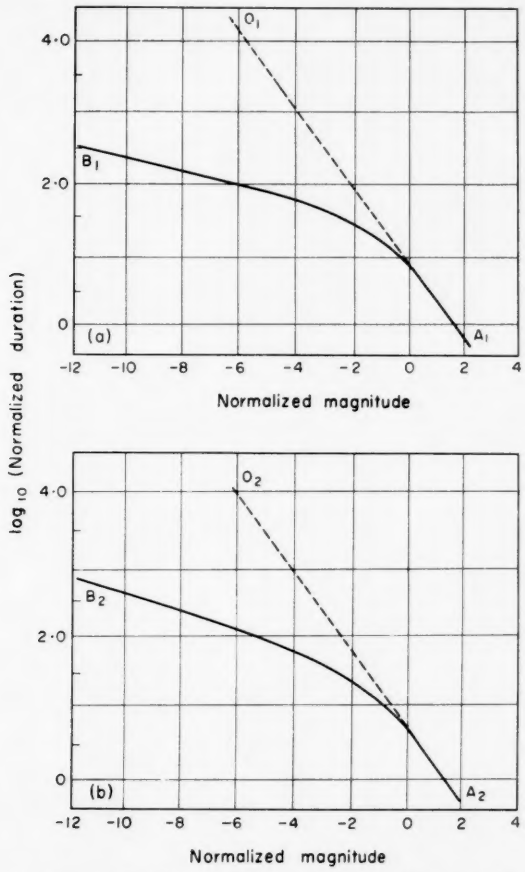

Fig. 3. Theoretical curves for the variation of echo duration with absolute visual meteor magnitude (M_V) for any wavelength λ (metres) and velocity V (km/sec).
(a) A_1B_1—for two-body attachment.
Ordinates: $\log_{10} t_\beta + 1{\cdot}8 \log_{10} V/60 + 0{\cdot}4 \log_{10} \lambda/8$ (sec).
Abscissae: $M_V - 9 \log_{10} V/60 + 3 \log_{10} \lambda/8$.
(b) A_2B_2—for three-body attachment.
Ordinates: $\log_{10} t_\gamma + 3 \log_{10} V/60 + 0{\cdot}6 \log_{10} \lambda/8$ (sec).
Abscissae: $M_V - 11{\cdot}25 \log_{10} V/60 + 3 \log_{10} \lambda/8$.
Curves A_1O_1 and A_2O_2 are for no attachment.

(Paper I), the heights and durations of the enduring echoes can be predicted in the manner described in Section 3(a). General curves giving the predicted durations as a function of visual magnitude M_V are shown in Fig. 3, and the expected heights of the echoes, compared with the heights of maximum t_D, are given in Fig. 4. The coordinates are normalized for any wavelength λ and meteor velocity V. The

wavelength dependence of echo duration can be derived from the curves in Fig. 3, by varying λ with fixed V and M_V.

(c) *Comparison of the theoretical curves with experimental observations*

The theoretical results are compared with various experimental observations in Figs. 5–7. Figs. 5(a) and (b) show the radio echo duration–visual meteor

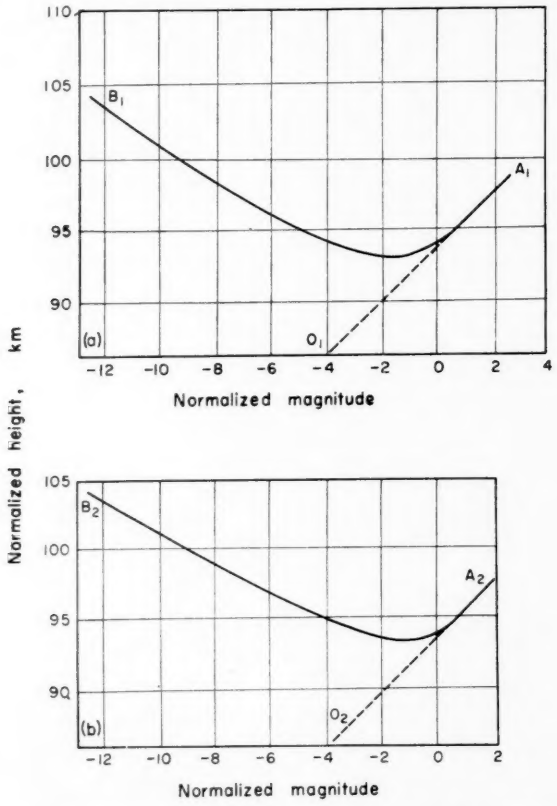

Fig. 4. Theoretical curves showing the height from which the most enduring echo is obtained for meteors of absolute visual magnitude M_V, velocity V(km/sec) and wavelength λ (metres).

(a) A_1B_1—for two-body attachment.
Ordinates: Height (km) $- 4 \log_{10} \lambda/8 - 25 \log_{10} V/60$.
Abscissae: $M_V - 2 \log_{10} \lambda/8 + 8{\cdot}3 \log V/60$.

(b) A_2B_2—for three-body attachment.
Ordinates: Height (km) $- 8 \log_{10} \lambda/8 - 20 \log_{10} V/60$.
Abscissae: $M_V - 4 \log_{10} \lambda/8 + 10 \log_{10} V/60$.
Curves A_1O_1 and A_2O_2 are for no attachment.

magnitude correlations of MILLMAN and MCKINLEY (1956), for meteors of velocity 60 km/sec and 37 km/sec. The straight lines A_1B_1, A_2B_2 are the expected variations of echo duration with magnitude for diffusion alone. A_1C_1, A_2C_2 are the curves for two-body attachment discussed in Paper II, and A_1D_1, A_2D_2 the

curves for a three-body mechanism. It can be seen that the theoretical curves for both two and three-body attachment processes give equally good fits to the experimental results.

The final heights of enduring echoes, in relation to the heights of maximum t_D are illustrated in Fig. 6 (MILLMAN, 1958). It can be seen that the echoes from very

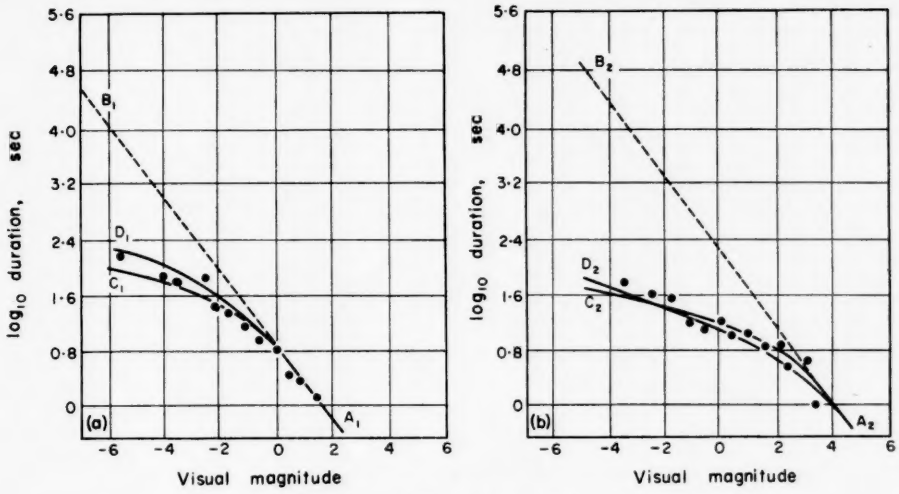

Fig. 5. The variation of echo duration with meteor magnitude.
(a) For Perseid meteors (Velocity 60 km/sec).
(b) For Geminid meteors (Velocity 37 km/sec).
A_1B_1, A_2B_2 predicted variations in the absence of attachment.
A_1C_1, A_2C_2 show the effect of two-body attachment.
A_1D_1, A_2D_2 show the effect of three-body attachment.
●—Experimental points based on the observations of MILLMAN and MCKINLEY (1956).

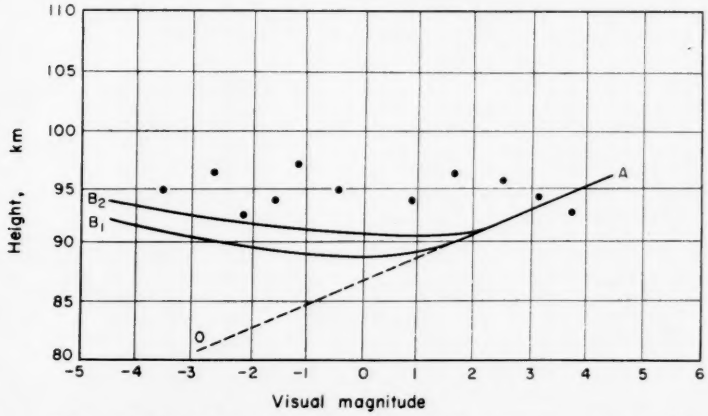

Fig. 6. The heights of enduring echoes as a function of meteor magnitude.
●—Experimental observations of MILLMAN (1958) at a wavelength of 9 m.
AO—the predicted curve in the absence of attachment.
AB_1—with two-body attachment, for meteors of velocity 45 km/sec observed at a wavelength of 9 m.
AB_2—with three-body attachment for meteors of velocity 45 km/sec observed at a wavelength of 9 m.

bright meteor trails are obtained from heights considerably above the points of maximum t_D. Once again, however, it is difficult to distinguish between the effects of the two attachment processes which both account for the observations reasonably well.

A similar situation exists when the wavelength dependence of echo duration is examined. The variation of echo duration between wavelengths of 8 m and 4 m, for meteors of velocity 60 km/sec, is shown in Fig. 7 (GREENHOW, 1952). The exponent n is derived assuming a wavelength–duration relationship of the form

$$\frac{T_1}{T_2} = \left(\frac{\lambda_1}{\lambda_2}\right)^n$$

and n is plotted as a function of T_2. (The suffixes 1 and 2 refer to wavelengths of 8 m and 4 m respectively.)

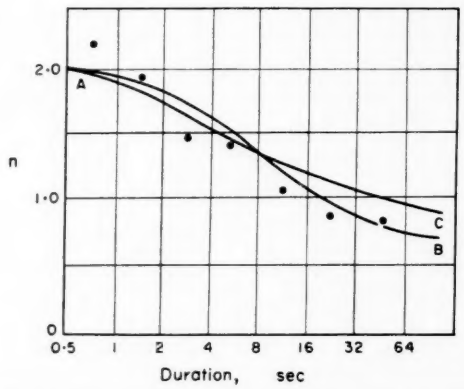

Fig. 7. The variation of echo duration with wavelength.
●—Experimental points
AB shows the effect of two-body attachment.
CD shows the effect of three-body attachment.

The theoretical variation of n for two-body attachment (Paper II), is compared with the three-body variation derived from Fig. 3(b), and it can be seen that there is little difference between the two results.

Thus the echo characteristics discussed above cannot be used to distinguish between two or three-body attachment processes. They do confirm that the attachment time constant is of the order 40–70 sec at a height of 95 km, but it is not known whether this time constant varies with ρ^{-1} or ρ^{-2}.

Evidence favouring the more rapid height variation is given by observation of the decay of luminous trains left behind by meteors, and this effect will now be considered.

4. PERSISTENT METEOR TRAINS

Very bright meteors leave behind a luminous train which may persist many seconds. The cause of this luminosity is uncertain, as the train durations are much

VOL. 21 1961

greater than the lifetimes of excited atoms. It is very probable, however, that the light emission is produced as the positive or negative ions recombine in some way as the lifetime of meteor ionization is of the order required to explain the train durations.

LILLER and WHIPPLE (1954) have published the results of the photographic observation of a train, where successive exposures enabled the decay of luminosity with height to be determined. It was found that the rate of decay was a minimum near 92 km, the decay time decreasing rapidly above this height, and even more

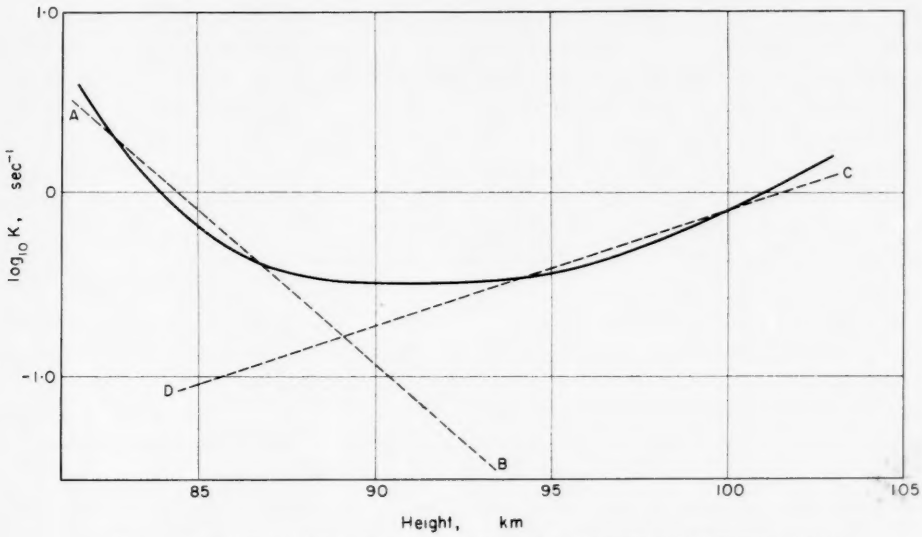

Fig. 8. The decay in luminosity of a meteor train (LILLER and WHIPPLE, 1954).
AB—a line corresponding to $K \propto \rho^{2 \cdot 5}$.
CD—a line corresponding to $K \propto \rho^{-1}$.

rapidly at lower heights. LILLER and WHIPPLE suggest that diffusion and recombination are responsible for the rapid decays above and below 92 km. A decay constant K was determined, on the assumption that the luminosity falls with time in the manner $(1 + Kt)^{-2}$. Their curve of K vs. height, replotted on a log scale, is shown in Fig. 8. Any decay constant due to diffusion is likely to vary with height in the manner $K \propto \rho^{-1}$, and a line of slope corresponding to a scale height of 7·0 km is fitted to the upper part of the curve. There is a reasonable fit with the experimental curve above 95 km.

Below 90 km a true recombination process involving only positive ions and electrons would be independent of air density. In fact K increases very rapidly with decreasing height, consistent with the attachment mechanisms discussed previously. The slope of the straight line fitted to the decay curve below 90 km corresponds to $K \propto \rho^{2 \cdot 5}$ for $H = 6 \cdot 5$ km. This is an extremely rapid variation with ρ, and clearly favours a three-body process with $K \propto \rho^2$. If the light is emitted during the attachment process, or during the subsequent recombination of the negative ions $1/K$ may be identified approximately with the attachment

time constant T_γ. T_γ is found to increase from only 0·4 sec at 82 km to 2·5 sec at 87 km. Above this height the decay time no longer increases. If, however, the line AB is extrapolated to 95 km, it is found that $1/K \sim 70$ sec. This is of the same order as the attachment time constant determined from the radio observations.

5. Discussion

The decay of the ionization in meteor trails has been considered in relation to two and three-body attachment processes. Previously a two-body reaction has been assumed to be appropriate, but the height variation of this mechanism is not sufficiently rapid to explain the absence of long duration echoes from heights near 80 km. Thus, whereas either process will explain some other echo characteristics equally well, only three-body attachment will remove free electrons from near the ionization maxima with sufficient rapidity. Decay times of about 50 sec at a height of 95 km are deduced, and for three-body attachment this leads to a decay time of less than 1 sec at 80 km. Evidence for such rapid decays in ionization at this height is given by the observation of a luminous train, from which a decay time of only 0·3 sec at 83 km is determined.

If it is assumed that oxygen molecules are the only negative ion forming particles at a height of 95 km, we have for a particle density of $2 \times 10^{13}/\text{cm}^3$, $\beta \sim 5 \times 10^{-15}$ cm^3/sec or $\gamma = 2 \times 10^{-28}$ cm^6/sec. These figures may be compared with the measurements of Chanin *et al.* (1959), who found that β varied from 2×10^{-11} cm^3/sec to 2×10^{-13} cm^3/sec for electron energies of 3·5–1·5 eV. No measurements are available for electrons of thermal velocity. The value of γ was found to be 3×10^{-30} cm^6/sec for thermal electrons. There is, therefore, considerable disagreement between the laboratory measurements and the values of β and γ required to explain the decay of meteor ionization.

The laboratory measurements were made using pure molecular oxygen at pressures above 7 mm of mercury, and it may be that the differences arise because of detachment processes which occur at these relatively high pressures. In a meteor trail we are concerned with pressures of 10^{-2}–10^{-3} mm of mercury, so that the effects of collision detachment would be much reduced. Further, at meteor heights, molecular oxygen begins to dissociate into atomic oxygen, which may have very different attachment cross-sections. On the other hand the relevant process in a meteor trail may not be one of simple attachment to neutral oxygen; for example, attachment to the dust particles which are thought to be present at D-region heights is a possible process. It is therefore important to carry out further measurements of the decay of ionization in meteor trails, in order to resolve the various recombination processes which are effective in ionized trails at heights of 80–100 km.

Acknowledgement—Acknowledgement is made to the Controller, H.M. Stationery Office, for permission to publish this paper.

References

Chanin L. M., Phelps A. V. and Biondi M. A. 1959 *Phys. Rev. Letters* **2**, 8.

Davis J., Greenhow J. S. and Hall J. E. 1959a *Proc. Roy. Soc.* A **253**, 121.

Davis J., Greenhow J. S. and Hall J. E.	1959b	*Proc. Roy. Soc.* A **253**, 130.
Greenhow J. S.	1952	*Proc. Phys. Soc. Lond.* B **65**, 169.
Greenhow J. S. and Neufeld E. L.	1955	*J. Atmosph. Terr. Phys.* **6**, 100.
Herlofson N.	1948	*Rep. Progr. Phys.* **11**, 444.
Kaiser T. R. and Closs R. L.	1952	*Phil. Mag.* **43**, 1.
Liller W. and Whipple F. L.	1954	*J. Atmosph. Terr. Phys.* Suppl. **1**, 112.
McKinley D. W. R. and Millman P. M.	1949	*Proc. Inst. Radio Engrs* **37**, 364.
Millman P. M.	1958	*J. R. Astr. Soc. Can.* **52**, 230.
Millman P. M. and McKinley D. W. R.	1956	*Canad. J. Phys.* **34**, 50.

Journal of Atmospheric and Terrestrial Physics, 1961, Vol. 21, pp. 272 to 283. Pergamon Press Ltd. Printed in Northern Ireland

Rocket measurements of *F*-layer electron density and their interpretation*

S. A. Bowhill
Ionosphere Research Laboratory, The Pennsylvania State University, University Park, Pennsylvania

(*Received* 8 *April* 1961)

Abstract—Solutions of the continuity equation for ionospheric electron density including the effects of ambipolar diffusion, near the peak of the *F*-layer, indicate that the width of the peak is determined by the atmospheric scale height at night, but is less during photo-equilibrium conditions during the day. This conclusion is borne out by rocket electron density measurements. Evidence is found supporting measurements of diurnal atmospheric heating deduced from satellite drag data, and a thermopause temperature is found of about 1100°K at night and 1490°K during the day. Assuming the classical form for the ambipolar diffusion coefficient, a value of the loss coefficient β is found of about 5×10^{-4} sec^{-1}, at 300 km height, which falls within the range measured by other methods.

1. Introduction

Though radio methods have been used for at least 30 years in the determination of the electron density of the *F*-layer of the ionosphere, it is only within the last 5 years that its mechanism of formation has been resolved with reasonable certainty. This is principally due to a drawback of the radio sounding technique, namely that electron density measurements are possible only below the peak of the layer. This has concentrated attention on the lower edge of the layer, where the interpretation is complicated by the presence of the *F1*-layer, and the little-understood processes which form it.

The essence of the formation of the *F*-layer was arrived at by Ratcliffe *et al.* (1956), in their discovery of the "attachment-like" loss process applying for heights of about 300 km, and their suggestion that the *F2*-peak occurred due to a diffusion process. Yonezawa (1955) showed that, if the loss coefficient were independent of height, the night-time *F*-layer would assume a Chapman form, and move downwards due to diffusion. Other workers (Martyn, 1956; Duncan, 1956; Dungey, 1956) showed that the effect of a height-dependent loss coefficient is to stabilize the *F*-layer at night at an equilibrium height, at which it will decay without change of shape at a rate determined by the loss coefficient at the peak of the layer.

The more difficult problem of the shape of the *F*-layer during the day has been studied by Yonezawa (1958), who showed that the lower edge of the layer corresponds approximately to photo-equilibrium conditions, while the part above the maximum is effectively in hydrostatic equilibrium due to diffusion. Further studies by Rishbeth and Barron (1960) have essentially confirmed these conclusions.

Theoretical work of this kind is handicapped by the lack of even reasonably accurate data concerning the chemical composition of the upper atmosphere. Earth satellite drag data, while satisfactory in themselves, do not give information about

* The work described in this paper was supported in part by the National Science Foundation under contract NSF-G14246, and in part by the Guidance and Control Laboratory of the Army Ballistic Missile Agency under contract DA-36-061-ORD-577.

VOL. 21 1961

the temperature of the atmosphere, but only about the variation of density with height. Since the temperature and the scale height are connected by the mean molecular mass of the total atmosphere, no assistance can be obtained from these data in determining the chemical composition of the atmosphere. All theoretical attempts so far made to determine the electron distribution have therefore depended on rather speculative atmospheric models.

It is the intent of this paper to use some recent rocket measurements of F-layer electron density, obtained by NISBET and BOWHILL (1960), to put limits on some unknown parameters governing the production of the F-layer, making only a minimum of assumptions concerning the mechanisms involved. The measurements concerned are given in Section 2, and the necessary theory developed in Section 3. The theory is compared with the experimental data in Section 4, and discussed in Section 5.

2. Measured Height and Density Parameters

Using either the Faraday rotation of the plane of polarization of a radio wave or the ionospheric dispersion of two radio waves of differing frequencies, it is possible without too much difficulty to measure the electron density in the ionosphere as a function of height, if rockets are available to carry the needed radio transmitters to sufficient heights. Only recently have rockets been available which would penetrate beyond the maximum of the $F2$-layer. Seven measurements of this kind, spread over several years, have recently been described by NISBET and BOWHILL (1960). The experimental arrangement and data reduction techniques will not be further discussed here.

In comparing these observed electron density–height profiles with theory it has been found convenient to follow a suggestion made, in connexion with vertical incidence pulsed ionosphere sounding, by SCHMERLING (1960). Five heights were measured on each profile: the height h_m of the maximum electron density N_m; the heights $h_{+0\cdot9}$ and $h_{-0\cdot9}$, where the electron density is $0\cdot9\ N_m$, respectively above and below h_m; and the heights $h_{+0\cdot5}$ and $h_{-0\cdot5}$, where the electron density is $0\cdot5\ N_m$. These six parameters effectively describe the electron density–height profile in the region not too far from the peak.

These data are given in Table 1, together with data from two flights, in October and December 1959, not previously reported, and communicated by Dr. J. S. NISBET.

It has been found convenient to use these data to determine a quantity d, defined as the height difference between h_m and its intersection with the height axis of the parabolic profile which best fits the observed profile in the region immediately adjacent to the maximum. This parabola is represented by the equation

$$N = N_m\left[1 - \left(\frac{h - h_m}{d}\right)^2\right] \tag{1}$$

N being the electron density and h the height. It can easily be shown that, provided the derivatives of a function $N(h)$ higher than the second are not too large, d is given by

$$d = 1\cdot581(h_{+0\cdot9} - h_{-0\cdot9}). \tag{2}$$

Values of d are given in Table 1. This parameter, though similar in its definition to the quantity y_m used in the past for characterizing the thickness of the $F2$-layer, refers only to the parabola which best fits the layer profile near its peak.

It is evident that the value of d is systematically smaller for the daytime flights than for the night-time flights. An explanation for this phenomenon is developed in the next section.

Table 1

Date	Time (E.S.T.)	$10^{-6} N_m$ (cm^{-3})	$h_{-0.5}$ (km)	$h_{-0.9}$ (km)	h_m (km)	$h_{+0.9}$ (km)	$h_{+0.5}$ (km)	d (km)
3/17/58	0715	2·03	253	285	306	336	416	81
2/17/59	1100	2·50	240	268	300	323	440	90
5/6/59	2047	1·24	308	326	344	—	—	—
5/14/59	0057	0·85	285	330	368	416	505	136
5/28/59	0235	0·67	235	315	350	384	475	109
7/9/59	2001	0·90	285	330	365	435	—	166
10/13/59	1030	1·76	221	272	300	328	426	89
12/9/59	1908	1·25	210	298	330	383	(490)	131

3. Theoretical Width of the F-Layer Peak

In a horizontally stratified ionospheric layer in which gravity is the only externally applied force, the electron density N is determined by the continuity equation

$$q - \beta N - \frac{d}{dh}(N w_D) = \frac{dN}{dt} \tag{3}$$

where q is the rate of electron production, β the loss coefficient, and w_D the upward ambipolar diffusion velocity of the ionization relative to the neutral gas. Part of the difficulty in applying this equation arises because there are essentially five parameters, each having dimensions of reciprocal distance, which characterize the height variations of the important atmospheric processes. Four of these are defined by the equation

$$a_r = \frac{m_r g}{kT} \quad (r = 1, 2, 3, 4) \tag{4}$$

where k is Boltzmann's constant, T the absolute temperature, g the acceleration due to gravity, and m_r the mean molecular mass. The mass m_1 refers to the ionizable gas, the distribution of which determines the height variation of q, while m_2 refers to the (presumably molecular) constituent entering into β, m_3 to the total atmosphere at the given height, and m_4 to the plasma (assumed electrically neutral). In addition, the temperature variation with height is characterized by a quantity b,

$$b = \frac{1}{T}\frac{dT}{dh}. \tag{5}$$

It is understood that all the above quantities may vary with height in the general case.

VOL. 21 1961

Following RISHBETH and BARRON (1960), the upward diffusion velocity w_D can be written

$$w_D = -D\left[\frac{1}{N}\frac{dN}{dh} + a_4 + b\right] \tag{6}$$

if the density of the plasma is small compared with that of the neutral atmosphere; D is the ambipolar coefficient. Before substituting in equation (3), it should be noted that

$$\frac{dD}{dh} = -\frac{D}{n_3}\frac{dn_3}{dh} = D(a_3 + b) \tag{7}$$

for a non-isothermal atmosphere where n_3 is the number density of the total neutral atmosphere. Equations (6) and (7) then give

$$-\frac{1}{D}\frac{d(Nw_D)}{dh} = \frac{d^2N}{dh^2} + (a_3 + a_4 + 2b)\frac{dN}{dh} + \left(a_3 a_4 + a_3 b + b^2 + \frac{db}{dh}\right)N \tag{8}$$

for an atmosphere in which the composition and temperature may vary in an arbitrary manner with height. For an isothermal atmosphere, equation (8) reduces to

$$-\frac{1}{D}\frac{d(Nw_D)}{dh} = \frac{d^2N}{dh^2} + (a_3 + a_4)\frac{dN}{dh} + a_3 a_4 N. \tag{9}$$

The form of the diffusion equation used by RISHBETH and BARRON (1960) in their calculations assumes, in addition

$$a_1 = a_3 = 2a_4 = \text{constant}.$$

In view of the known change in composition of the atmosphere with height in the neighbourhood of the *F2*-peak, this assumption will not be followed. However, it is useful to ask whether the simplifying assumption of an isothermal atmosphere may be made. Assuming, for convenience, a constant value of b (though this may not represent the temperature variation over a large range of heights), the temperature gradient may be neglected provided

$$2b \ll a_3 + a_4$$

$$a_3 b + b^2 \ll a_3 a_4$$

in equation (8). Both of these conditions are fulfilled in

$$b \ll a_4.$$

The question of a temperature gradient in the thermosphere has been extensively discussed by NICOLET (1961). His evidence suggests that no temperature gradient is present at night, and that the magnitude of the temperature gradient in the day is uncertain, but may be small also. A contrasting viewpoint has been expressed by KALLMAN (1959), who attributed the variation of scale height of the atmosphere with height to a temperature gradient rather than to a change of chemical composition. Her model A, which may be taken to represent an extreme

value for the temperature gradient, has

$$\left.\begin{aligned} T_{300} &= 1499^\circ\mathrm{K} \\ T_{500} &= 1993^\circ\mathrm{K} \end{aligned}\right\} b = 0{\cdot}00142\ \mathrm{km}^{-1}$$

In contrast, one may take approximate figures for a_4, assuming that the plasma consists entirely of ionized atomic oxygen, of about $0{\cdot}008\ \mathrm{km}^{-1}$ at 300 km and $0{\cdot}006\ \mathrm{km}^{-1}$ at 500 km. One may therefore conclude that, even if a temperature gradient is present, its effect will not be large, and in the present state of knowledge of upper atmosphere parameters, one may assume it equal to zero, as Kallman does in a later paper (1961).

The electron density continuity equation can therefore be written, combining equations (3) and (9), as

$$q - \beta N + D\left[\frac{d^2N}{dh^2} + (a_3 + a_3)\frac{dN}{dh} + a_3 a_4 N\right] = \frac{dN}{dt}. \tag{10}$$

In order to compare this equation with the experimental results derived in the previous Section, all of the quantities in equation (10) will be taken at their values at the peak of the layer denoting these values by the suffix m,

$$q_m - \beta_m N_m + D_m\left[\left(\frac{d^2N}{dh^2}\right)_m + a_3 a_4 N_m\right] = \frac{dN_m}{dt}. \tag{11}$$

From equation (1)

$$\left(\frac{d^2N}{dh^2}\right)_m = -\frac{2N_m}{d^2} \tag{12}$$

giving

$$d^{-2} = \frac{a_3 a_4}{2} + \frac{q_m}{2D_m N_m} - \frac{\beta_m}{2D_m} - \frac{1}{2D_m N_m}\frac{dN_m}{dt}. \tag{13}$$

The value of the electron production q_m may conveniently be expressed in terms of the photochemical equilibrium value N_{me} which would be obtained at the height h_m in the absence of diffusion;

$$q_m = \beta_m N_{me}. \tag{14}$$

With this substitution (13) becomes

$$d^{-2} = \frac{a_3 a_4}{2} + \frac{\beta_m}{2D_m}\left(\frac{N_{me}}{N_m} - 1\right) - \frac{1}{2D_m N_m}\frac{dN_m}{dt}. \tag{15}$$

Two special cases of this equation are important: firstly, in the day, when photo-equilibrium conditions are attained, the final term in the equation becomes zero and

$$d^{-2} = \frac{a_3 a_4}{2} + \frac{\beta_m}{2D_m}\left(\frac{N_{me}}{N_m} - 1\right). \tag{15a}$$

Secondly, in the night, after the diffusion–loss equilibrium has set in, $N_{me} = 0$, and the peak electron density decays according to the equation

$$N_m \propto \exp(-\beta_m t). \tag{16}$$

On substituting into equation (15),

$$d^{-2} = a_3 a_4/2. \tag{15b}$$

Equations (15a) and (15b) will be compared with the experimental evidence in the next Section. Two features of them are of immediate interest: firstly, the night equation (15b) does not contain the diffusion coefficient, and so measurements of the width of the night $F2$-peak cannot give a measure of D_m. Secondly, comparison of equations (15a) and (15b) indicate that, since $N_{me} > N_m$, the peak of the layer is narrower in the day than at night.

The equations (15) do not contain the height variation of q or β in any explicit form. For comparison with the day observations, the equilibrium form of equation (11) may be differentiated with respect to height, to give

$$\frac{dq}{dh} - \beta\frac{dN}{dh} - N\frac{d\beta}{dh} + D\left[\frac{d^3N}{dh^3} + (2a_3 + a_4)\frac{d^2N}{dh^2} + \left(2a_3a_4 + a_3^2 + \frac{da_1}{dh} + \frac{da_3}{dh}\right)\frac{dN}{dh} + \left(a_3^2a_4 + \frac{d(a_3a_4)}{dh}\right)N\right] = 0. \tag{17}$$

Since the vertical temperature gradient has been neglected, one may take

$$\frac{dq}{dh} = -a_1 q$$

$$\frac{d\beta}{dh} = -a_2\beta$$

giving, near the peak of the layer, for quasi-equilibrium conditions,

$$-a_1q_m + N_m a_2\beta_m + D_m\left\{\left(\frac{d^3N}{dh^3}\right)_m + (2a_3 + a_4)\left(\frac{d^2N}{dh^2}\right)_m + \left[a_3^2a_4 + a_4\left(\frac{da_3}{dh}\right)_m\right]N_m\right\} = 0. \tag{18}$$

If the peak of the layer coincides with the point of greatest curvature of the electron density–height profile, the third derivative will vanish at the peak of the layer. One may test the validity of this reasonable assumption as follows: the third derivative may be neglected provided

$$\left(\frac{d^3N}{dh^3}\right)_m \ll a_3^2a_4N_m. \tag{19}$$

In terms of the parameters observed in the previous Section,

$$\frac{d^3N_m}{dh^3} = \frac{0{\cdot}6N_m(h_{+0{\cdot}9} + h_{-0{\cdot}9} - 2h_m)}{(h_{+0{\cdot}9} - h_m)^2(h_m - h_{-0{\cdot}9})^2} \tag{20}$$

while from (2)

$$h_{+0{\cdot}9} - h_m = h_m - h_{-0{\cdot}9} = 0{\cdot}316d$$

giving

$$\frac{1}{N_m}\frac{d^3N_m}{dh^3} \simeq \frac{120}{d^4}(\tfrac{1}{2}h_{+0{\cdot}9} + \tfrac{1}{2}h_{-0{\cdot}9} - h_m). \tag{21}$$

Using the value for d, only approximately true during the day, given by equation (15b), the inequality (19) becomes

$$\tfrac{1}{2}h_{+0\cdot9} + \tfrac{1}{2}h_{-0\cdot9} - h_m \ll \frac{4}{a_4}. \tag{22}$$

For the three day observations reported in the previous Section, the left hand side of (22) is respectively 0, $-4{\cdot}5$ and $4{\cdot}5$ km, while $4/a_4 = 490$ km approximately. Evidently, therefore, the third derivative of N may be neglected in equation (18).

Making the further assumption that the mean molecular mass of the plasma is half that of the constituent ionized, namely $a_4 = a_1/2$, one may solve equation (18) for the ratio a_3/a_1, giving

$$\frac{a_3}{a_1} = \frac{d^2}{4}\left[\tfrac{1}{2}{a_3}^2 + \tfrac{1}{2}\frac{da_3}{dh} - \frac{\beta_m}{D_m}\left(\frac{N_{me}}{N_m} - \frac{a_2}{a_1}\right)\right]. \tag{23}$$

4. Comparison with Experiment

4.1. *Night measurements*

In order to decide whether the night measurements in Table 1 are in accord with the equation (15b) for conditions of diffusion–loss equilibrium, it is necessary to establish an atmospheric model which can be used to calculate values for a_3 and a_4. While a_3 can be derived directly from satellite drag data, as recapitulated by Nicolet (1961) and by Kallman-Bijl (1961), it is necessary to make some assumption about the atmospheric composition in order to find a value for a_4. Inspection of Fig. 3 of Nicolet's paper (1961) shows that the night models of Jacchia and of King-Hele and Walker are very closely fitted, in the region 300–400 km, by an atmosphere at a constant temperature of 1190°K. Substantially this model (but with $T = 1180$°K) was previously given by Nicolet as Tableau 3 of another paper (Nicolet, 1960). Values of the scale height H and the relative mean molecular mass M, related to the parameters of this paper by

$$H = {a_3}^{-1}, \qquad M = 16m_1/m_3 \tag{24}$$

are given in Table 2.

Theoretical values for d can be calculated by transforming equation (15b) into the form

$$d = \sqrt{\left(\frac{2}{a_3 a_4}\right)} = 2H\sqrt{\left(\frac{m_3}{m_1}\right)} \tag{25}$$

the assumption here being made that the molecular mass m_1 is that of atomic oxygen. The night-time experimental data of Section 2 are presented again in Table 3, in order of increasing elapsed time after local ground sunset (sun's upper limb). The final column should be constant and equal to unity if equation (15b) applies with the given atmospheric model.

It will be noted that the two profiles measured in the middle of the night have values of d which accord very closely to the theoretical prediction. However, the earlier profiles have a broader peak, in one case by as much as 34 per cent, than is predicted by theory. This cannot be explained by the layer not yet having reached the diffusion–loss equilibrium condition; for, as shown by equation (15a), the

VOL. 21 1961

daytime layer peak would be expected to be narrower than the night-time peak. Rather, it is suggested that the difference arises from a diurnal fluctuation of thermopause temperature of the kind discussed in detail by NICOLET (1961) and by KALLMAN-BIJL (1961).

To investigate this possibility, the results of JACCHIA (1960) were investigated in detail. From the formulae given by him for the variation with time of the total atmospheric density at various heights, it is possible to find the diurnal variation of the scale height. The atmospheric density ρ at some height h above a reference level

Table 2. Adopted night model (NICOLET, 1960)

h (km)	H (km)	M (0 = 16)
250	43·00	25·24
300	46·57	23·66
350	51·04	21·92
400	55·97	20·28

Table 3

Time (E.S.T.)	Time after local sunset (hr)	h_m (km)	a_3^{-1} (km)	$\frac{m_3}{m_1}$	$\sqrt{\left(\frac{2}{a_3 a_4}\right)}$ (km)	d (km)	$d\sqrt{\left(\frac{a_3 a_4}{2}\right)}$
2001	1·02	365	52·52	1·344	122	166	1·34
1908	2·05	330	49·19	1·415	117	131	1·12
0057	6·23	368	53·82	1·332	124	136	1·10
0235	7·70	350	51·04	1·370	119	109	0·92

is related to the night density ρ_n, and to the corresponding densities ρ_0 and ρ_{0n} at the reference level, by the equation

$$\frac{\rho}{\rho_n} = \frac{\rho_0}{\rho_{0n}} \exp\left[h(a_{3n} - a_3)\right] \tag{26}$$

if the composition of the atmosphere and its temperature are constant over the range of heights considered. JACCHIA gives formulae for the diurnal variation with height, which can be expressed in the form

$$\frac{\rho}{\rho_n}\sqrt{\left(\frac{a_{3n}}{a_3}\right)} = 1 + f_1(h)\cos^6(\psi/2) \tag{27}$$

where ψ is the geocentric angular distance between the point of observation and a point having the same latitude as the subsolar point, but lagging 30° in longitude behind it. The function $f_1(h)$, as tabulated by JACCHIA, is reproduced in Table 4.

Assuming the composition of the atmosphere as constant between day and night between the heights of 562 and 655 km, the application of the hydrostatic equation gives $a_{3n} = 0{\cdot}0119\ \mathrm{km}^{-1}$, at a height of about 600 km. Combining

equations (26) and (27) the value of a_3 at 600 km height may be found at any time for any point on the surface of the earth from the equation

$$a_3 = a_{3n} - 0{\cdot}01075 \ln \left[\frac{1 + 9 \cos^6 (\psi/2)}{1 + 4{\cdot}9 \cos^6 (\psi/2)} \sqrt{\left(\frac{a_{3n}}{a_3}\right)} \right]. \tag{28}$$

This procedure has been carried out for all the results in Table 3, as shown in Table 5. The fifth column in this table represents the anticipated change in a_3/a_{3n},

Table 4

	h (km)			
	210	353	562	655
$f_1(h)$	~0·3	1·2	4·9	9·0

the slight effects of composition change having been allowed for. The final column shows the ratios from Table 3, after allowance for the effect of varying atmospheric temperature. It will be noted that the variation is almost completely accounted for, the mean ratio of d to its expected value being $1{\cdot}02 \pm 0{\cdot}04$.

4.2. *Daytime measurements*

In interpreting daytime measurements of the width of the *F2*-peak, in the light of equations (15a) and (23), no attempt will be made to develop a model and

Table 5

Time (E.S.T.)	ψ	$\cos^6 (\psi/2)$	a_3 at 600 km (km^{-1})	$\frac{a_3}{a_{3n}}$	$d\sqrt{\left(\frac{a_3 a_4}{2}\right)}$
2001	79·9°	0·2022	0·0094	1·22	1·10
1908	89·8	0·1262	0·0099	1·17	0·96
0057	~180	0	0·0119	1·00	1·10
0235	~180	0	0·0119	1·00	0·92

apply it to all times of day indiscriminately. The model of Nicolet (1960) used in the interpretation of the night data is again used in Table 6; also included as the fourth result in Table 6 is a rocket flight, recently reported by Berning (1960), made near Wallops Island, Virginia.

The values of N_{me}/N_m were derived in the following way. It was known from previous work (e.g. Rishbeth and Barron, 1960) that the lower edge of the F-layer corresponded to photo-equilibrium conditions. Confirmation of this was found in the increasing exponential form with height of the electron density–height profile below the maximum, which would be expected if the variation of q and of β were exponential with height. The exponential curve fitted to the profile below the peak was then extrapolated to the height of the maximum, and the value of N_{me} read off. In the case of the third profile, it was not sufficiently exponential in form for the extrapolation to be made with confidence.

VOL. 21 1961

The correction of the data for diurnal heating is carried out in Table 7. The average of the first three ratios in the final column of Table 7 is 0·62, compared with 0·61 found from BERNING's rocket data, the fourth ratio, using the same analysis technique. Taking an average value of N_{me}/N_m of 1·20 from Table 6, equation (15a) gives a value for β_m/D_m of $8{\cdot}2 \times 10^{-14}$ cm^{-2}.

A check on the theory may be obtained by calculating the ratio a_3/a_1 from equation (23). This quantity gives a measure of the degree of dissociation of the

Table 6. Day results

Time (E.S.T.)	h_m (km)	a_3^{-1} (km)	$\frac{m_3}{m_1}$	$\sqrt{\left(\frac{2}{a_3 a_4}\right)}$ (km)	d (km)	$d\sqrt{\left(\frac{a_3 a_4}{2}\right)}$	$\frac{N_{me}}{N_m}$
0715	306	47·11	1·468	114	81	0·71	1·17
1100	300	46·57	1·480	113	90	0·80	1·22
1030	300	46·57	1·480	113	89	0·79	—
0700	263	43·93	1·553	109	71	0·65	

molecular constituents of the atmosphere. The calculated values are to be compared with the values pertaining to the particular model of the atmosphere used in the calculation. In order to perform this calculation, it is necessary to know the ratio a_2/a_1, representing the relative height variation of q and β. Most workers (RISHBETH and BARRON, 1960; VAN ZANDT *et al.*, 1960) have assumed that electrons disappear by a process involving a molecular species, such as molecular nitrogen or oxygen. If the ionized species is atomic oxygen, this implies a ratio a_2/a_1 of 1·75 in the former case and 2·0 in the latter.

Table 7

Time (E.S.T.)	ψ	$\cos^6(\psi/2)$	a_3 at 600 km (km^{-1})	$\frac{a_3}{a_{3n}}$	$d\sqrt{\left(\frac{a_3 a_4}{2}\right)}$
0715	110·1°	0·0356	0·0111	1·07	0·66
1100	48·2	0·5786	0·0084	1·33	0·60
1030	62·0	0·3968	0·0088	1·30	0·61
0700	112·0	0·0306	0·0112	1·06	0·61

Using an average value for the atmospheric heating in the three day observations relative to the night, a value is obtained for a_3 of 0·0175 km^{-1}, and a corresponding height gradient of a_3 of $-3{\cdot}9 \times 10^{-5}$ km^{-2}. The assumptions of molecular nitrogen and molecular oxygen in the recombination process then lead, through equation (23), to values for a_3/a_1 of 1·10 and 1·42 respectively. This compares with an average of 1·49 from Table 6. The calculation is therefore found to be reasonably self-consistent, considering the errors involved, and suggests that molecular oxygen may be the more important molecular constituent in the recombination process.

5. Discussion

It is interesting to compare the values measured for β_m/D_m, from the daytime rocket measurements, with accepted formulae for the ambipolar diffusion coefficient. The following formula was suggested by Shimizaki (1957):

$$D = 4{\cdot}5 \times 10^{17}\, T^{1/2} \sin^2 I/n(M) \tag{29}$$

where I is the geomagnetic dip angle, and $n(M)$ the total number density of all atmospheric constituents at the given height. Using Jacchia's data from Table 4, the three experimental daytime profiles give mean increases of a factor of 1·44 and 1·26 in the atmospheric density and temperature respectively, relative to night conditions, corresponding to a mean total number density of $1{\cdot}34 \times 10^9$ cm^{-3} and a temperature of 1490°K at about 300 km height, the dip angle being 59·9°. The diffusion coefficient from equation (29) gives $D_m = 6{\cdot}5 \times 10^9$ cm^2 sec^{-1}; combining this with the β_m/D_m from Section 4.2 gives $\beta_m = 5{\cdot}3 \times 10^{-4}$ sec^{-1}. This value of β_m, obtained for a height of 300 km, compares with values of 10^{-4} sec^{-1} found by Ratcliffe *et al.* (1956), and $6{\cdot}8 \times 10^{-4}$ sec^{-1} found by van Zandt *et al.* (1960) from eclipse observations.

While part of the variation in β_m may be attributable to variations of atmospheric density with time of day or time of year, a considerable discrepancy nevertheless remains. It may be remarked that, in determining β from electron density–height profiles measured with vertical incidence ionosphere sounders, it is hard to be absolutely certain that all effects of diffusion of ionization have been eliminated.

A possible explanation for the discrepancy may be found in the work of Dalgarno (1958), who suggested that the case of the diffusion of atomic oxygen ions in an atmosphere composed of atomic oxygen is a very special problem in which the simple formula, appropriate to differing gases, does not apply. His suggestions give a diffusion coefficient

$$D = 2 \times 10^{18} \sin^2 I/n(\mathrm{O}) \tag{30}$$

where $n(\mathrm{O})$ is the number density of atomic oxygen at the given height. Repeating the previous calculation with this formula, one obtains $n(\mathrm{O}) = 4{\cdot}45 \times 10^8$ cm^{-3}, $D_m = 2{\cdot}2 \times 10^9$ cm^2 sec^{-1}, and $\beta_m = 1{\cdot}8 \times 10^{-4}$ sec^{-1}, in better agreement with the result of Ratcliffe *et al.* However, this necessitates using values of a_3 appropriate to atomic oxygen in Table 3, introducing a factor of about 0·86 in the ratio of observed to expected F-layer peak width; on the whole, the observations do not support this hypothesis.

A further check on the preceding theory may be obtained from a consideration of the height at which the peak of the night diffusion–loss equilibrium layer settles. From Table 3, this averages 359 km for the two cases near the middle of the night. For the case

$$a_1 = a_3 = 2a_4 \text{ constant} \tag{31}$$

Martyn (1956) has shown that the height of the maximum is given by

$$\beta_m = \tfrac{1}{4} a_3^2 D_m. \tag{32}$$

Assuming the night model, Nicolet (1960) gives $n(M)$ as $2{\cdot}83 \times 10^8$ cm^{-3} at 359 km, and a_3 as 0·0193 km^{-1}. Substitution in equations (29) and (32) gives

VOL. 21 1961

$D_m = 2{\cdot}73 \times 10^{10}\ \mathrm{cm^2\,sec^{-1}}$, and $\beta_m = 2{\cdot}6 \times 10^{-4}\ \mathrm{sec^{-1}}$. This is reasonably consistent with the daytime value deduced previously, having regard to the differing height, and the crude nature of the assumptions (31) involved in the derivation of equation (32).

One final point concerns the value of the ratio N_{me}/N_m, which should be deducible from theoretical considerations. RISHBETH and BARRON (1960), in their Fig. 2, plot the reciprocal of this ratio, which they call $\beta N/q$. They find values lying between about 1·0 and 1·5, depending on the particular parameters of the model they employed. In a more recent paper, BRIGGS and RISHBETH (1961) have studied the non-equilibrium electron density–height profile of the F-layer by an analogue computer method. They confirm the theoretical statements in Section 3, that the night peak of the F-layer is wider than the day peak.

6. CONCLUSIONS

It has been shown that experimental measurements of the width of the peak of the *F2*-layer are consistent with its being formed by a process of diffusion. The observations are in agreement with satellite measurements of scale height and density. A model with a thermopause temperature of about 1180°K in the night, and about 1490°K in the day, gives agreement with the data. The observations further support the classical value of diffusion coefficient, and suggest a value for the loss coefficient β at 300 km which lies between values found by other workers.

More data concerning the width of the F-layer peak, particularly at other geomagnetic latitudes, are needed to confirm these conclusions. Ground ionospheric soundings or "topside sounder" results may be used to supplement further rocket measurements.

REFERENCES

BERNING W. W.	1960	*J. Geophys. Res.* **65,** 2589.
BRIGGS B. H. and RISHBETH R.	1961	*Proc. Phys. Soc. Lond.* In press.
DALGARNO A.	1958	*J. Atmosph. Terr. Phys.* **12,** 219.
DUNCAN R. A.	1956	*Aust. J. Phys.* **9,** 436.
DUNGEY J. W.	1956	*J. Atmosph. Terr. Phys.* **9,** 90.
JACCHIA L. G.	1960	*J. Geophys. Res.* **65,** 2775.
KALLMAN H. K.	1959	*J. Geophys. Res.* **64,** 615.
KALLMAN-BIJL H. K.	1961	*J. Geophys. Res.* **66,** 787.
MARTYN D. F.	1956	*Aust. J. Phys.* **9,** 161.
NICOLET M.	1960	*Space Research*, p. 46. North-Holland Publishing Co., Amsterdam.
NICOLET M.	1961	*Planet. Space Sci.* **5,** 1.
NISBET J. S. and BOWHILL S. A.	1960	*J. Geophys. Res.* **65,** 3609.
RATCLIFFE J. A., SCHMERLING E. R., SETTY C. S. G. K. and THOMAS J. O.	1956	*Phil. Trans.* A **248,** 621.
RISHBETH H. and BARRON D. W.	1960	*J. Atmosph. Terr. Phys.* **18,** 234.
SCHMERLING E. R.	1960	*J. Geophys. Res.* **65,** 1072.
SHIMIZAKI T.	1957	*J. Radio Res. Lab.* **4,** 309.
VAN ZANDT T. E., NORTON R. B. and STONEHOCKER G. H.	1960	*J. Geophys. Res.* **65,** 2003.
YONEZAWA T.	1955	*J. Radio Res. Lab.* **2,** 125.
YONEZAWA T.	1958	*J. Radio Res. Lab.* **5,** 165.

Journal of Atmospheric and Terrestial Physics, 1961, Vol. 21, pp. 284 to 295. Pergamon Press Ltd. Printed in Northern Ireland

RESEARCH NOTES

A possible explanation of *sc** observed at high geomagnetic latitudes

(*Received* 21 *March* 1961)

FOR the purpose of interpreting positive *sc* phenomena, the ray paths and transit times for hydromagnetic waves propagating in the geomagnetic equatorial plane have been calculated in accordance with Fermat's principle by DESSLER *et al.* (1960).

They have considered that hydromagnetic waves will be generated over the broad front-surface by the impact of the solar plasma on the geomagnetic field, and the effects of the impact will be carried obliquely or perpendicular to the geomagnetic line of force to the earth's surface by the modified Alfvén waves. In these situations we can also expect that Alfvén waves generated by the impact of the solar plasma on the geomagnetic field will propagate along geomagnetic lines of force to the earth's surface and the effects of these waves will be observed as positive sudden impulses at high geomagnetic latitudes.

In consideration of the transit times for charged particles and above mentioned Alfvén waves propagating along the geomagnetic line of force from the geomagnetic equatorial plane to the high geomagnetic latitudes on the earth's surface, we try to interpret *sc** observed at high geomagnetic latitudes in this paper.

Results obtained by many investigators (NEWTON, 1948; WATSON and MCINTOSH, 1950; NAGATA, 1952; NAGATA and ABE, 1955) have indicated that *sc** (negative *sc*) is recorded at least somewhere over the world in most cases of the sudden commencements of geomagnetic storms (ABE, 1959).

NAGATA (1952) has found that the preliminary reverse impulse precedes by 1–2 min the main impulse of *sc**, which takes place almost simultaneously with the ordinary *sc* in the low geomagnetic latitude zone. Recently WILLIAMS (1960) has indicated that the sudden commencements have been registered at high geomagnetic latitudes first.

We regard the geomagnetic field as a well-known centred dipole. Then the equation of geomagnetic line of force is given by $r = r_e \cdot \cos^2\theta$ in a spherical co-ordinate system with origin at the centre of the earth, where r_e is the distance from the origin of the point where the geomagnetic line of force intersects the geomagnetic equatorial plane ($\theta = 0$). The length L of the geomagnetic line of force from the geomagnetic equatorial plane to the geomagnetic latitude of θ_0 on the earth's surface is expressed as

$$L = r_e \int_0^{\theta_0} \cos\theta\,(1 + 3\sin^2\theta)^{\frac{1}{2}}\,d\theta$$

$$= \frac{r_e}{2\sqrt{3}}\left[\sqrt{3}\sin\theta \cdot \sqrt{(1 + 3\sin^2\theta)} + \log\left|\sqrt{3}\sin\theta + \sqrt{(1 + 3\sin^2\theta)}\right|\right]_0^{\theta_0}.$$

Calculated values of L for $r_e = 6r_0$ ($\theta = 65°53'$) and $r_e = 4r_0$ ($\theta = 60°$) are 51,800 km and 28,700 km respectively, where r_0 is the earth's radius. Therefore charged particles having velocity of the order of 10^4 km/sec could travel along the geomagnetic line of force within several seconds from the geomagnetic equatorial plane to high geomagnetic latitudes on the earth's surface.

VOL. 21 1961

Although sudden commencements (including *sc* and *sc**) take place more frequently in the afternoon with a maximum around 1300 hours local time (ABE, 1959), we consider conveniently the propagation of charged particles and hydromagnetic waves on the noon meridian plane. When the source of generation of hydromagnetic waves lies at $6r_0$ and $4r_0$ of the noon meridian on the geomagnetic equatorial plane, the transit time T_m for hydromagnetic waves propagating perpendicular to the geomagnetic line of force from the outer boundary to the geomagnetic equator on the earth's surface is calculated as 67·1 sec and 19·1 sec respectively by DESSLER *et al.* (1960). In the meanwhile the transit time T_a for hydromagnetic waves propagating along the geomagnetic line of force from θ_i to θ_j is expressed as

$$T_a = \int_{s(\theta_i)}^{s(\theta_j)} \frac{ds}{V} = \frac{\sqrt{(4\pi)} \cdot {r_e}^4}{H_0 {r_0}^3} \int_{\theta_i}^{\theta_j} \sqrt{\rho} \cos^7 \theta \, d\theta$$

where V is the Alfvén velocity, H_0 the geomagnetic field strength at the geomagnetic equator on the earth's surface, and ρ the mass density of the ions in the earth's exosphere.

When we calculate T_a, we neglect the effect of neutral particles on V in the lower ionosphere for comparison with results calculated by DESSLER *et al.* and we use the average value of ρ in the part from θ_i to θ_j instead of $\rho(\theta)$.

Thus we have

$$T_a = \frac{\sqrt{(4\pi)} \cdot {r_e}^4}{105 H_0 {r_0}^3} \sqrt{\rho} \, [(15 \cos^6 \theta + 18 \cos^4 \theta + 24 \cos^2 \theta + 48) \sin \theta]_{\theta_i}^{\theta_j}.$$

The integral path along the geomagnetic line of force is divided into six parts corresponding to the altitude as given in Table 1. This ion distribution is calculated from one used by DESSLER *et al.* (JOHNSON, 1960). When the source of generation of hydromagnetic waves lies at $6r_0$ and $4r_0$ on the geomagnetic equatorial plane, the transit time T_a for hydromagnetic waves propagating along the geomagnetic line of force from the geomagnetic

Table 1

Altitude (km)	Density (g/cm^3)
100–600	$1{\cdot}92 \times 10^{-17}$
600–1000	$4{\cdot}71 \times 10^{-18}$
1000–1500	$3{\cdot}96 \times 10^{-19}$
1500–2300	$3{\cdot}42 \times 10^{-20}$
2300–10,000	$2{\cdot}43 \times 10^{-21}$
>10,000	$8{\cdot}84 \times 10^{-22}$ (when $r_e = 4r_0$)
	$7{\cdot}32 \times 10^{-22}$ (when $r_e = 6r_0$)

equatorial plane to the earth's surface is calculated as 116·6 sec and 28·9 sec respectively. Here we compare the above calculated results with each other. Table 2 shows the calculated values.

It is generally considered that the source causing hydromagnetic waves may lie from $6r_0$ to $4r_0$ on the geomagnetic equatorial plane. From the above calculated results, we can deduce that the preliminary reverse impulse of *sc** is generated by a dynamo action of ionization due to high speed charged particles (10^4 km/sec) impinging upon the high latitude ionosphere (OBAYASHI and JACOBS, 1957) or an initial diamagnetic effect due to such charged particles spiraling about the geomagnetic line of force (SINGER, 1960), and that hydromagnetic waves propagating along the geomagnetic line of force from the geomagnetic equatorial plane to the earth's surface cause the main impulse of *sc** at high

latitudes, and other hydromagnetic waves propagating obliquely or perpendicular to the geomagnetic line of force cause the sudden increase of the geomagnetic field at low latitudes.

The above model can explain the observed fact that sudden commencements have been registered earlier at high latitudes than low latitudes and the preliminary reverse impulse has preceded by 1–2 min the main impulse of *sc**, which has taken place almost simultaneously with the ordinary *sc* in low latitude zones.

Table 2

Position of the source on the equatorial plane	Transit time of charged particles	T_a (sec)	T_m (sec)
$4r_0$	Within several seconds	28·9	19·1
$6r_0$	Within several seconds	116·6	67·1

But this model requires that the ordinary *sc* at low latitudes should occur earlier than the main impulse of *sc** at high latitudes by about several tens of seconds. In this argument we do not consider the distortion of the geomagnetic field by the impact of solar plasma on it. It seems likely from the above results that the transit times of modified Alfvén waves from the geomagnetic equatorial plane to high latitudes on the earth's surface will give more hopeful values to explain *sc** phenomena.

T. Ondoh

Geophysical Institute
Kyoto University, Japan

References

Abe S.	1959	*J. Geomagn. Geoelect.* **10,** 153.
Dessler A. J., Francis W. E. and Parker E. N.	1960	*J. Geophys. Res.* **65,** 2715.
Johnson F. S.	1960	*J. Geophys. Res.* **65,** 577.
Nagata T.	1952	*Rep. Ionos. Res. Japan* **6,** 13.
Nagata T. and Abe S.	1955	*Rep. Ionos. Res. Japan* **9,** 39.
Newton H. W.	1948	*Mon. Not. R. Astr. Soc., Geophys. Suppl.* **5,** 159.
Obayashi T. and Jacobs J. A.	1957	*J. Geophys. Res.* **62,** 589.
Singer S. F.	1960	*Planet. Space Sci.* **2,** 165.
Watson R. A. and McIntosh D. H.	1950	*Nature, Lond.* **165,** 1018.
Williams V. L.	1960	*J. Geophys. Res.* **65,** 85.

VOL. 21 1961

Rate of ion–atom interchange

(*Received* 4 *April* 1961)

Bates and Nicolet (1960) have deduced that ion–atom interchange processes like

$$O^+ + O_2 \rightarrow O_2^+ + O \quad (1)$$

$$O^+ + N_2 \rightarrow NO^+ + N \quad (2)$$

and

$$O_2^+ + N \rightarrow NO^+ + O \quad (3)$$

must be very much slower than some aeronomers have supposed since otherwise almost all the O^+ ions in the upper atmosphere would be replaced by NO^+ ions within a few seconds of sunset. HERTZBERG (1961) has recently questioned the deduction. Though DICKINSON and SAYERS (1960) have reported laboratory measurements which indicate that the rate coefficient for process (1) is about $2{\cdot}5 \times 10^{-11}$ cm^3/sec HERTZBERG believes that neither steric hindrance nor activation energy is likely to enter and therefore that the rate coefficients for exothermic ion–atom interchange processes are of the order of 10^{-9} cm^3/sec. He argues that this is not inconsistent with the O^+ ions persisting long after sunset since they may be reformed through

$$O_2^+ + N \rightarrow NO + O^+ \qquad (4)$$

(which is only slightly endothermic). There is however a difficulty. HERTZBERG lists all the ion–atom interchange processes which might conceivably be important in the upper atmosphere. The only one which leads to the conversion of NO^+ ions into another species of positive ion is

$$NO^+ + N(^2D) \rightarrow N_2 + O^+. \qquad (5)$$

This can safely be ignored: thus it requires an electronic transition so that its rate coefficient would be expected to be very much less than that for a simple ion–atom interchange process (cf. BATES, 1955); and furthermore metastable atoms of nitrogen are rare compared with other atoms and molecules. The conversion of other positive ions into NO^+ is effectively irreversible under upper atmospheric conditions. Hence NO^+ would be the dominant species of positive ion in ion–atom interchange equilibrium. If the rate coefficients for ion–atom interchange were indeed of order 10^{-9}cm^3/sec this equilibrium would be reached shortly after sunset in contradiction to the observations of rocket scientists (JOHNSON *et al.*, 1958; POLOSKOV, 1960).

Department of Applied Mathematics
The Queen's University of Belfast
Belfast 7

D. R. BATES

Department of Radiation
R. Meteorological Institute
Brussels 18

M. NICOLET

REFERENCES

BATES D. R. 1955 *Proc. Phys. Soc. Lond. A* **68,** 344.
BATES D. R. and NICOLET M. 1960 *J. Atmosph. Terr. Phys.* **18,** 65.
DICKINSON P. H. G. and SAYERS J. 1960 *Proc. Phys. Soc. Lond.* A **76,** 137.
HERTZBERG M. 1961 *J. Atmosph. Terr. Phys.* **20,** 177.
JOHNSON C. Y., MEADOWS E. B. and HOLMES J. C. 1958 *J. Geophys. Res.* **63,** 443.
POLOSKOV S. M. 1960 *Space Research* (Ed. by H. K. KALLMAN BIJL), p. 95. North Holland Publ. Co., Amsterdam.

Thickness of an active auroral curtain

(*Received* 7 *April* 1961)

ONE of the most remarkable characteristics of the polar aurora is its thin curtain structure. In a homogeneous arc, the thickness may be of the order of a few kilometers. In the active

phase the bottom edge of the arc is often well defined and the thickness is much less than that of a homogeneous arc.

ELVEY (1957), by visually comparing an arc passing through the magnetic zenith with the adjacent moon, estimated the thickness to be not more than 250 m. The thickness has not hitherto been determined photographically. This is rather difficult, because of the extremely rapid changes of auroral arcs in their active phase.

The thickness can best be determined at the moment when an arc is sweeping across the magnetic zenith and shows a corona structure. At this time, only the bottom edge of the arc can be seen, because the arc has the form of a sheet parallel to the local magnetic lines of force. At College (geographic lat., 64° 51′; dip angle, + 77°), the declination δ of the magnetic zenith is given by

$$64^\circ\,51' - (90^\circ - 77^\circ) = 51^\circ\,51'.$$

In most cases, however, because of irregular motions in the curtain, the bottom edge is often changing very rapidly.

During this winter a series of photographic studies* of the aurora has been made at the Geophysical Institute. Two colour photographs of an active corona were unusually suitable for the determination of the auroral thickness. Because of the limitation of sensitivity of the film, the exposure time was 1 sec, although a shorter time would be preferable if possible.

The photographs were taken at 0245 hours (150° WMT), 19 February 1961 with a time difference of about 5 sec between them. Black and white versions of them are shown as Figs. 1 and 2. For such an active aurora, the height of the bottom edge may reasonably be taken to be 95 (±5) km. The thickness is determined at the points A and B in Figs. 1 and 2 respectively. There were no two bright stars with optimum angular separation, so that the distance (5° 30′) between the stars α and β of Ursa Major is used for scale from the photograph taken separately a few minutes later. The mean declination δ of these two stars is 59° 30′. No correction was made for variations of scale on different points of the film.

The thickness at the points A and B are respectively 336 m and 144 m. This may be taken to be an upper limit for each case, because the aurora was moving rapidly while the films were exposed. At the time, the active rayed arc stretched across the sky from horizon to horizon. Thus its length was of the order of at least 1500 km. This may be contrasted with the thickness of the order of 300 m. It must be noticed that the distance of two lines of force separated by 300 m in the corona is of the same order as the radius of gyration of auroral electrons (~30 keV) in the equatorial plane. An auroral electron beam must be extremely thin. This has been discussed by AKASOFU and CHAPMAN (1961) in connexion with a new theory of the aurora.

Acknowledgements—The writer is indebted to Dr. S. CHAPMAN, Dr. C. T. ELVEY and Mr. W. B. MURCRAY for their suggestions and discussions. The study reported here was supported by the National Science Foundation under Grant NSF–G6030.

Geophysical Institute
University of Alaska
College, Alaska

S.-I. AKASOFU

REFERENCES

AKASOFU S.-I. and CHAPMAN S. 1961 *Phil. Trans.* A **253,** 359.
ELVEY C. T. 1957 *Proc. Nat. Acad. Sci., Wash.* **43,** 63.

* Lens: $f = 1{\cdot}5$ wide angle; Film: High-speed Ektachrome (ASA 160).

VOL. 21 1961

1

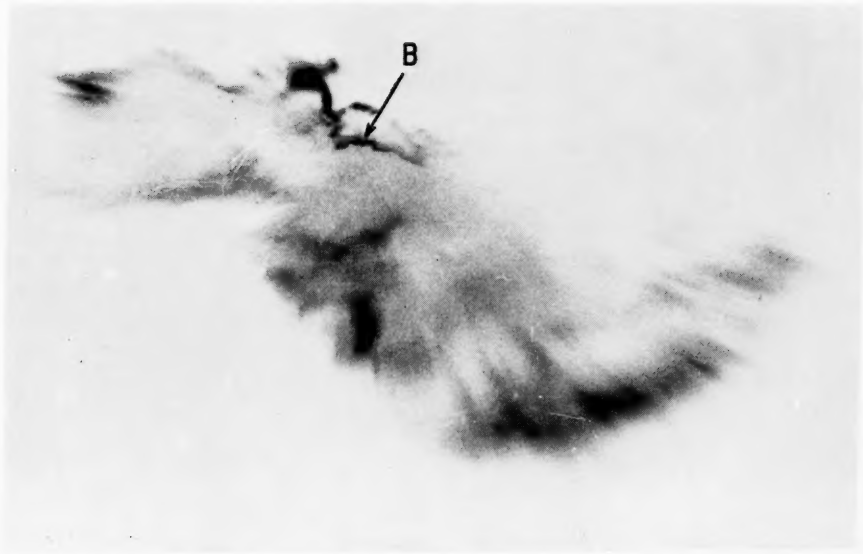

2

Figs. 1 and 2. Photographs of an active corona taken at College (Alaska) at 0245 hours on 19 February 1961. They were taken with a time difference of about 5 sec.

VOL.
21
1961

Geomagnetic crochet of 15 November 1960

(*Received* 17 *April* 1961)

On 15 November 1960 a very strong solar flare was observed, and the accompanying geomagnetic crochet (or s.f.e.) was an unusually great one. The time of occurrence was about noon in Japan, Australia, and their neighbouring countries, where many geomagnetic stations were in operation, and so this strong flare offered us a good chance to study the properties of geomagnetic crochet.

The position of the flare on the solar disk was 26°N 33°W, and its importance was class 3+. It commenced at 0207 hours (U.T.) and reached maximum at 0221 hours. The ionogram at Yamagawa Radio Wave Observatory, Japan, showed a strong short-wave fade-out which commenced between 0215 and 0230 hours; meanwhile the receiving stations of solar radio emission at Tokyo and Toyokawa, Japan, recorded a predominant outburst of type IV beginning at 0221 hours (i.e. the time of maximum activity of the flare) as shown in Fig. 1.

Figs. 2(a) and 2(b) show, respectively, the geomagnetic crochet recorded at Me, Ka, Ss, As, Ky, Ho, Gm and Mu in the northern hemisphere, and at Ap, Gn, To, Am and Mc in the southern hemisphere. The crochet commenced at 0220 hours and reached its maximum development at 0224 hours at many stations. Here we had some doubt as to whether or not the foregoing increase in H-trace which started at about 0208 hours was an effect of the flare. This variation, however, was omitted from the effect of the solar flare we are concerned with, because of the following reasons: (1) No distinct changes were noticeable until 0215 hours on the ionogram, and until 0221 hours on the dynamic spectrum of the solar radio outburst; (2) As the records from stations in the dark hemisphere showed another disturbance commencing before 0200 hours, this would also affect the sunlit hemisphere.

Fig. 3 shows the pattern of the electric currents flowing in the ionosphere, which are necessary to produce the horizontal component of the crochet at the time of its maximum development, where the arrows denote the geomagnetic disturbance vector at each station. As for Brisbane, on account of a lack of D-trace, and for Macquarie Island, because of the superposition of another disturbance owing to the locality in the auroral zone, the data of these two stations were only referred to. It is clear from the figure that the electric currents responsible for the crochet were unusually strong, roughly estimated as 250,000 A, and that the centre of vortex of the northern current was considerably shifted southwards. Although, because of the continuity of severe disturbances in November, it is not easy to deduce the normal S_q variation of the day concerned, yet, as compared with the standard S_q current system (Chapman and Bartels, 1940) it seems very likely that the electric currents responsible for the geomagnetic crochet should not be a simple augmentation of the S_q currents, as suggested by many workers hitherto (e.g. Grafe, 1958; Volland and Taubenheim, 1958; Veldkamp and van Sabben, 1960). Moreover, the following facts convince us that the geomagnetic crochet may be caused by the currents flowing mainly in the D-region.

Hachenberg and Krüger (1959) pointed out a close correlation between bursts of solar radio emission in the centimetre range with flares and sudden ionospheric disturbances (s.i.d.). On the other hand, it is now generally accepted that the s.i.d. is caused by an abnormal increase of ionization in the D-region by solar X-rays, and Chubb *et al.* (1957) actually observed the penetration of X-rays of $1 \sim 8$ Å wavelength into the lower part of the D-region at the time of s.i.d. From these facts, a good correlation is also expected between solar radio outbursts in the centimetre range and abnormal increase in the radiation

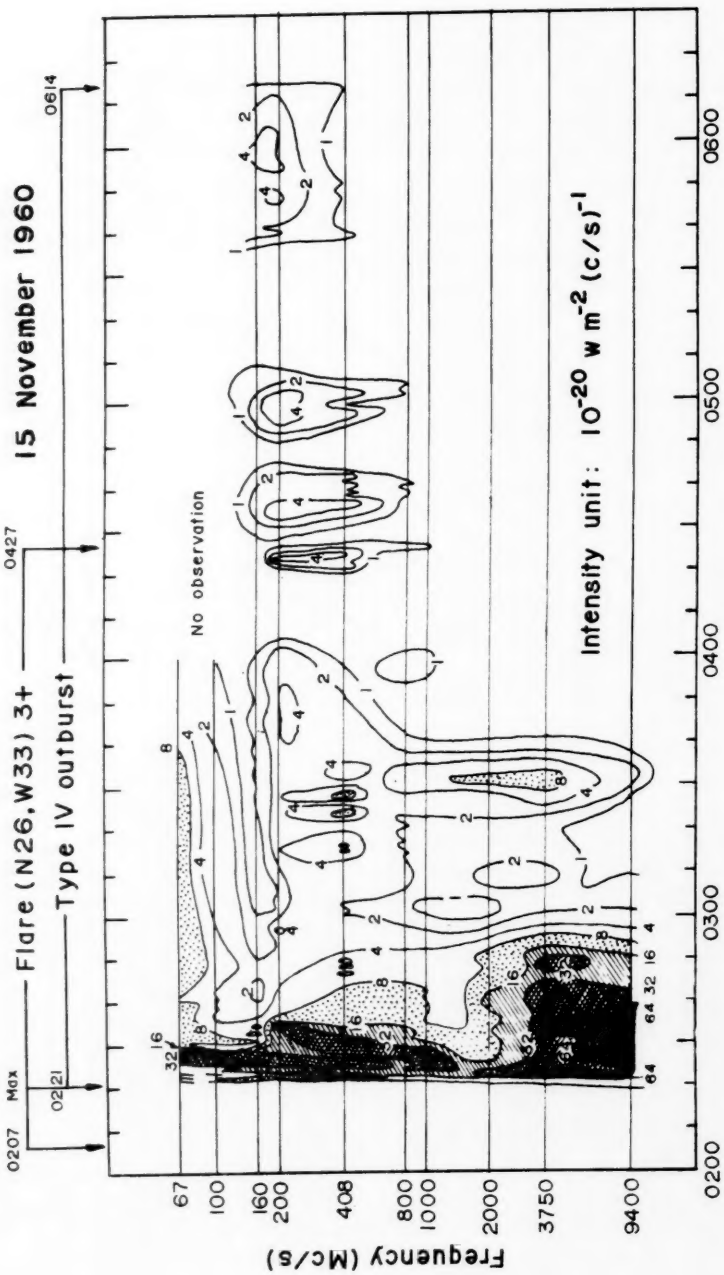

Fig. 1. Dynamic spectrum of type IV solar radio outburst of 15 November 1960. (Based on the data from Tokyo Astronomical Observatory, Tokyo University, and Research Institute of Atmospheries, Nagoya University).

VOL.
21
1961

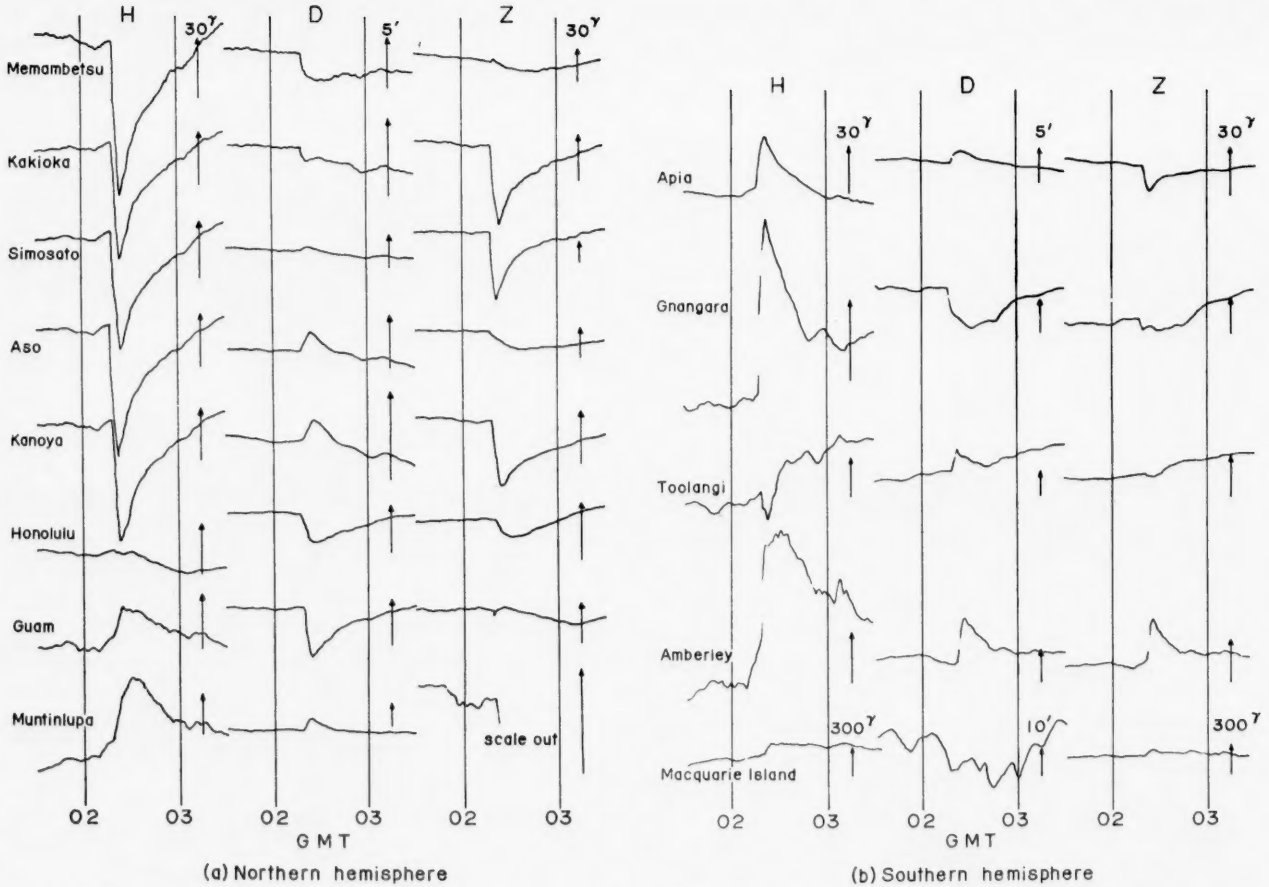

Fig. 2. Magnetograms from the stations Me, Ka, Ss, As, Ky, Ho, Gm and Mu in the northern hemisphere (a) and Ap, Gn, To, Am and Mc in the southern hemisphere (b), showing the geomagnetic crochet of 15 November 1960. The length of arrows corresponds to 30 gammas for H and Z, and 5 min for D, except for Macquarie Island, and the direction of arrows indicates: Increase for H; Downward for Z; Clockwise for D.

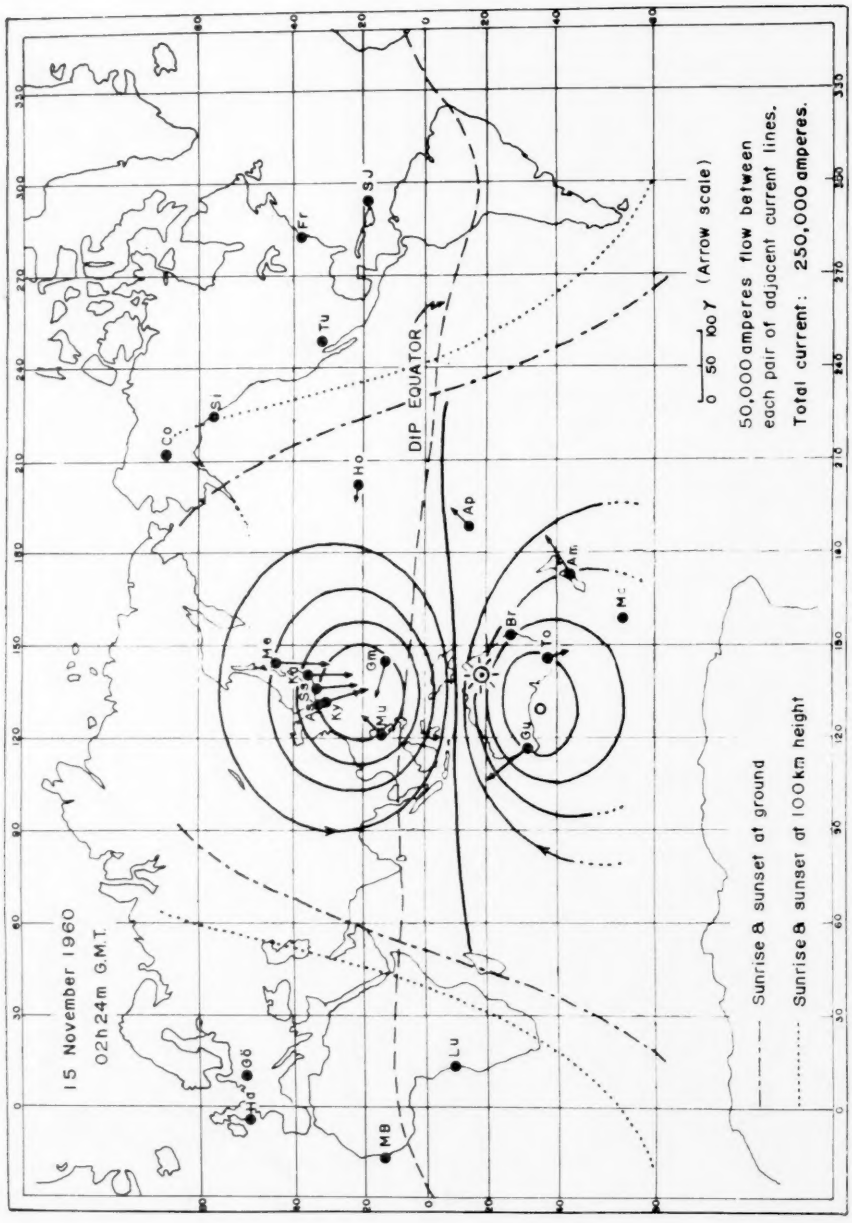

Fig. 3. Current pattern of geomagnetic crochet of 15 November 1960, 0224 hours U.T.

VOL. 21 1961

of solar X-rays. Fig. 1 shows a greater flux intensity in the centimetre range than in the metre range of solar radio emission. Thus it may be concluded that the considerably stronger penetration of solar X-rays into the ionospheric *D*-region had to exist at the time of maximum development of the solar flare, and it played an important role in the occurrence of s.i.d. and such a great geomagnetic crochet as dealt with here.

Now, from Fig. 3 we feel that it is difficult to agree with a view, which was emphasized by VELDKAMP and VAN SABBEN (1960), that the current pattern for geomagnetic crochets should be controlled by the magnetic (or dip) equator. However, further study of similar cases would give a clearer solution for this problem.

Acknowledgements—Copies of magnetograms were received from the following observatories: Amberley (Am), Apia (Ap), Aso (As), Brisbane (Br), College (Co), Fredericksburg (Fr), Göttingen (Gö), Guam (Gm), Gnangara (Gn), Hartland (Ha), Honolulu (Ho), Kakioka (Ka), Kanoya (Ky), Luanda (Lu), Macquarie Island (Mc), M'Bour (MB), Memambetsu (Me), Muntinlupa (Mu), San Juan (SJ), Simosato (Ss), Sitka (Si), Toolangi (To), Tucson (Tu).

Solar and ionospheric data from: Astronomical Observatory (Tokyo), CRPL (Boulder), CSIRO (Sydney), Dr. Neher Laboratory (Leidschendam), Radio Wave Observatory (Hiraiso and Yamagawa), Research Institute of Atmospherics (Toyokawa).

The authors are greatly indebted to the directors of these observatories, who supplied us with the necessary data to complete this study.

Geophysical Institute
Kyoto University
Kyoto, Japan

M. YASUHARA
H. MAEDA

REFERENCES

CHAPMAN S. and BARTELS J. 1940 *Geomagnetism.* Oxford University Press.
CHUBB T. A., FRIEDMAN H., KREPLIN R. W. and KUPPERIAN J. E. 1957 *J. Geophys. Res.* **62,** 389.
GRAFE A. 1958 *Geofis. Pur. Appl.* **40,** 172.
HACHENBERG O. and KRÜGER A. 1959 *J. Atmosph. Terr. Phys.* **17,** 20.
VELDKAMP J. and VAN SABBEN D. 1960 *J. Atmosph. Terr. Phys.* **18,** 192.
VOLLAND H. and TAUBENHEIM J. 1958 *J. Atmosph. Terr. Phys.* **12,** 258.

A note on non-equilibrium species concentrations in air*

(*Received* 28 *April* 1961)

THE RATE equations governing the species change in hot rarefied air ($\rho/\rho < 10^{-5}$, $1000°\text{K} < T < 10{,}000°\text{K}$) are highly non-linear. It is difficult to rigorously state which reactions are fast and which are slow. However, inspection of both the rate constants of the important reactions and the number densities of the dominant species indicates that, generally speaking, particle-conserving two-body reactions like dissociative recombination and charge exchange are the fast reactions, while three-body reactions and two-body radiative recombination reactions are much slower reactions.

* This work was supported by the Geophysics Research Directorate, Air Force Cambridge Research Laboratories, Bedford, Massachusetts, under Contract AF 19(604)-6140.

If, then, a sample of air, through some mechanism such as hydrodynamic expansion, is forced out of thermodynamic equilibrium and allowed to return to a new equilibrium state, the first reactions that would be operative in changing the species concentration would be the two-body particle-conserving reactions.

Now when a gas is disturbed from a state of thermodynamic equilibrium, in general, the total number of particles/cm^3 changes as the gas approaches a new equilibrium state. (A typical example is the lowering of the kinetic temperature of the gas to a new value at constant mass density.) Thus, the fast two-body reactions alone cannot return a gas to equilibrium except in the special case when the total number of particles/cm^3 is the same in both the initial and final equilibrium states. These reactions alone will drive the gas to some metastable state. A non particle-conserving reaction is necessary, in general, to return the gas to equilibrium.

One notes, though, that air at 10^{-5} atmospheric density has only about four times as many particles/cm^3 at 10,000°K as at 1000°K, while various species concentrations change by over ten orders of magnitude as the air passes from the lower to the higher temperature. Thus, one asks if perhaps in this region the conservation of particles by the fast two-body reactions is a minor effect and that, consequently, the fast two-body reactions alone drive the gas reasonably close to equilibrium if the air changes from one kinetic temperature in this range to another.

The principal purpose of this note is to show, by stating the results of a numerical calculation, that the effect of particle conservation is not small. It is shown here that the necessity for a minor (10 per cent) change in the number of total particles/cm^3 as the air changes from one equilibrium state (6000°K) to another (5000°K) at constant mass density prevents the two-body particle conserving reactions from driving the air to even the vicinity of the new equilibrium state.

Consider the air to be a nitrogen–oxygen mixture at 10^{-5} atmospheric density. Assume it to be initially at 6000°K in thermodynamic equilibrium. Then suppose that the kinetic and excitation temperatures are quickly reduced to 5000°K, keeping the species concentration appropriate to the initial 6000°K equilibrium state. The total number of particles/cm^3 at equilibrium at 6000°K is $0{\cdot}535 \times 10^{15}$, while the total number of particles/cm^3 if the air reached equilibrium at 5000°K would be $0{\cdot}478 \times 10^{15}$; this is only about a 10 per cent reduction.

To determine the state to which the air would be driven by the particle-conserving two-body reactions, we have set up and numerically solved the rate equations, assuming the kinetic and excitation temperature remains at 5000°K. Only the dominant species, N_2, N_2^+, NO, NO^+, e, N, N^+, O, O^+, have been included. The reactions included and the exothermic rate constants assumed are given in Table 1. The rate constants for the charge exchange reactions are poorly known, and a matter of some controversy (Bates and Nicolet, 1960) (see also Papers of International Symposium on Chemical Reactions in the Lower and Upper Atmosphere, Stanford Research Institute, 1961). Since there are no experimental data at 5000°K, we have chosen the theoretically estimated values. However, the nature of the results are not particularly dependent on the values chosen as long as they are correct within one or two orders of magnitude.

The initial conditions are found in Gilmore (1955). An asymptotic solution is reached in $\sim$0·02 sec and these values, the initial conditions, and the equilibrium species concentrations at 5000°K are shown in Table 2. The values of most of the species obtained differ from the equilibrium values at 5000°K by an order of magnitude. Further, it can be shown analytically that, for these conditions, at least one species concentration must differ from the 5000°K equilibrium values by an order of magnitude.

If the three-body reaction $N + N + M \rightarrow N_2 + M$ is included in the rate equations,

Table 1. Particle-conserving two-body reactions

Reactions	Rate constant (α cm^3/sec)	Reference
(1) $N_2^+ + e \rightarrow N + N$	5×10^{-8}	(1)
(2) $NO^+ + e \rightarrow N + O$	10^{-8}	(1)
(3) $N^+ + NO \rightarrow NO^+ + N$	10^{-9}	(2)
(4) $N + N_2^+ \rightarrow N^+ + N_2$	10^{-9}	(2)
(5) $NO + N_2^+ \rightarrow NO^+ + N_2$	10^{-9}	(2)
(6) $O^+ + NO \rightarrow O + NO^+$	10^{-9}	(2)
(7) $O + N^+ \rightarrow O^+ + N$	10^{-9}	(2)
(8) $O + N_2^+ \rightarrow O^+ + N_2$	10^{-9}	(2)
(9) $N + NO \rightarrow O + N_2$	10^{-10}	(3)
(10) $N_2 + O^+ \rightarrow NO^+ + N$	10^{-9}	(2)
(11) $N^+ + NO \rightarrow N_2^+ + O$	10^{-9}	(2)
(12) $NO + N^+ \rightarrow N_2 + O$	10^{-9}	(2)
(13) $N_2^+ + O \rightarrow NO^+ + N$	10^{-9}	(2)
(14) $N_2^+ + O^+ \rightarrow NO^+ + N^+$	10^{-9}	(2)

(1) Hammerling P. *et al.*, *Proceedings of Fourth International Conference on Ionization Phenomena in Gases*, Uppsala, 1959 (Ed. by N. Nilsson), Vol. 2. North Holland Publishing Co., Amsterdam, 1960.
(2) These are the theoretically estimated values. For convenience α_{14} has been given the same value as the other charge exchange reactions.
(3) Glick H., Klein J. and Squire W., *J. Chem. Phys.* **27**, 850 (1957).

Table 2. Species concentrations vs. time

t (sec)	Particles (cm^{-3})								
	N_2	N_2^+	NO	NO^+	e	N	N^+	O	O^+
0·000000	0·253E 13	0·115E 10	0·590E 10	0·358E 11	0·132E 13	0·417E 15	0·962E 12*	0·113E 15	0·319E 12
0·020051	0·180E 13	0·197E 09	0·117E 10	0·215E 11	0·567E 12	0·419E 15	0·365E 12	0·113E 15	0·178E 12
(Equilibrium at 5000°K)	0·583E 14	0·515E 09	0·520E 11	0·774E 11	0·116E 12	0·306E 15	0·216E 11	0·113E 15	0·144E 11

* Value changed from 0·940E 12 to insure charge neutrality, which was destroyed by omitting minor species.

the species concentration eventually assumes the values appropriate to equilibrium at 5000°K, but the time to equilibrium is >1 sec.

As a practical matter, we conclude from the above that, in estimating a characteristic time for approaching the neighbourhood of equilibrium in hot rarefied air, one must not, in general, use the time constants appropriate for attaining the state reached by fast particle-conserving two-body reactions alone. The rate is governed by the fastest non particle-conserving reaction.

It is noted that this situation does not apply only to air but its counterpart should be found in many hot rarefied gas mixtures.

M. J. Beran

Technical Operations, Inc.
Burlington, Massachusetts

References

Bates D. R. and Nicolet M. 1960 *J. Atmosph. Terr. Phys.* **18**, 65.
Gilmore F. 1955 Rand Report RM1513.

Journal of Atmospheric and Terrestrial Physics, 1961, Vol. 21, p. 296. Pergamon Press Ltd. Printed in Northern Ireland

BOOK REVIEWS

V. A. KAZINSKII: **Mathematical Tables for the Approximation of Geophysical Anomalies.** Pergamon Press, Oxford, 1960. 93 pp., 35s.

THIS is a book of tables, chiefly designed for ground gravimetry, densities of strata and mass anomalies.

After a brief description of principle, which is simply the approximation of a volume integral by numerical integration, using bivariate differences as far as the second order, the tables proceed to the anomalies and reductions of various bodies, homogeneous and non-homogeneous. The formula of numerical integration is almost exclusively a double Simpson formula taken over many subdivisions, with perhaps a weight or density function superimposed on the ordinates. The kind of function tabulated may be exemplified by Supplement I, which gives values of $(x^2 + y^2 + z^2)^{-\frac{1}{2}} . 10^{-3}$, over the trivariate range of (x, y, z) from (0, 0, 0) to (500, 200, 500), first by fine steps, finally by broad ones. Other tabulated functions are for use in determining the gravitational elements due to irregularities in walls, roof or floor of underground workings, or for finding magnetic field components of bodies of any shape and magnetization.

The eleven supplements, set up by non-letterpress and photolithographed, are clear enough for practical use, though not of the highest elegance; and the translation reads well.

The section (pp. 1–27) on the principles underlying the tables is well illustrated by good numerical examples. Appeal is constantly made to the theorem which the Russian author naturally attributes to OSTROGRADSKII and which we are apt to call GREEN's theorem. It would seem that the name should be shared, since OSTROGRADSKII read his paper and GREEN published his privately subscribed book in the same year, 1828.

A. C. AITKEN

R. L. F. BOYD: **Space Research by Rocket and Satellite.** Arrow Science Series, Arrow Books Ltd., London, 1960. 128 pp., Library Edition 10s. 6d., Popular Edition 5s.

THIS is an admirable little volume; and, in its cheaper, popular form, should sell in its hundreds of thousands. Dr. BOYD, himself a distinguished worker in the field of space research, writes with authority and lucidity and tells the serious student what he really wants to know about this fascinating field of scientific exploration. There is, first of all, a chapter on "Near Space", dealing with the upper atmosphere. This is followed by a chapter entitled "Deep Space" with a brief survey of the outer universe. We then come to two chapters on space technology, headed, respectively, "Rockets" and "Electronics and Basic Instrumentation"; while the final two chapters are devoted to actual "Space Experiments" in their wide variety.

The publishers claim for their Arrow Science series, of which this volume is a member, that each subject "is covered concisely but fully in 128 pages and well illustrated". The claim is amply justified in the case of Dr. BOYD's short book, for rarely can anyone have conveyed, so simply, so much information in so few words. It is refreshing to meet a volume of this kind after seeing all the pseudo-scientific rubbish which has been written on the subject of space research in the past.

E. V. APPLETON

VOL. 21 1961

Journal of Atmospheric and Terrestrial Physics, 1961, Vol. 21, pp. 297 to 300. Pergamon Press Ltd. Printed in Northern Ireland

Indices of geomagnetic activity

of the Observatories HARTLAND (*Ha*), ESKDALEMUIR (*Es*) and LERWICK (*Le*) January–April 1961

The figures given on pages 297 to 300 represent the K-indices for three-hour intervals, beginning with 00–03 hrs for the first and ending with 21–24 hrs for the eighth figure.

January 1961

Day	*Ha* Range for $K = 9 : 500\gamma$			*Es* Range for $K = 9 : 750\gamma$			*Le* Range for $K = 9 : 1000\gamma$			*Day*
	K-Indices		*Sum*	*K-Indices*		*Sum*	*K-Indices*		*Sum*	
1	2231	2201	13	2332	1101	13	2221	1101	10	1
2	0001	1012	5	0112	2112	10	0001	1112	6	2
3	1110	1100	5	1121	1112	10	1111	1111	8	3
4	0000	1001	2	0011	1111	6	0011	1111	6	4
5	0010	0032	6	0011	1132	9	0001	1022	6	5
6	1201	2011	8	1222	2111	12	0221	2111	10	6
7	3311	2113	15	3211	2113	14	3211	2112	13	7
8	4333	3443	27	3332	3333	23	3322	2563	26	8
9	3333	2355	27	2333	3445	27	2333	3565	30	9
10	2001	1111	7	2011	2112	10	3001	1102	8	10
11	0000	0000	0	1110	1000	4	1100	0001	3	11
12	0211	1132	11	0221	1232	13	0210	0133	10	12
13	2012	2132	13	2022	2132	14	2022	2223	15	13
14	1010	0113	7	1101	1213	10	1100	0123	8	14
15	3232	2206	20	3233	2216	22	2222	2205	17	15
16	3330	0033	15	3331	1133	18	3331	0021	13	16
17	2112	2123	14	2212	2222	15	2111	1212	11	17
18	3122	4343	22	3122	4343	22	3122	3243	20	18
19	3221	3465	26	3221	3455	25	3311	2566	27	19
20	5433	3442	28	5533	3442	29	7643	4642	36	20
21	2333	3411	20	2332	3421	20	1322	3432	20	21
22	1234	3443	24	1224	3444	24	1133	3433	21	22
23	2111	1212	11	2222	1222	15	2211	1211	11	23
24	3233	2354	25	3233	2354	25	3232	2353	23	24
25	4423	3222	22	4323	3222	21	3323	3221	19	25
26	1222	3223	17	1222	3233	18	1112	2323	15	26
27	2112	2121	12	2222	2221	15	2122	2121	13	27
28	4212	2352	21	4112	3342	20	3112	2342	18	28
29	2211	3232	16	2221	2232	16	2111	2232	14	29
30	2202	0001	7	1212	1101	9	2211	0001	7	30
31	2110	1010	6	2211	1111	10	2100	0010	4	31

February 1961

Day	*Ha* Range for $K = 9{:}500\gamma$		*Sum*	*Es* Range for $K = 9{:}750\gamma$		*Sum*	*Le* Range for $K = 9{:}1000\gamma$		*Sum*	*Day*
	K-Indices			*K-Indices*			*K-Indices*			
1	1000	1121	6	2011	1221	10	1101	1121	8	1
2	0100	1000	2	2111	1101	8	0000	1001	2	2
3	1003	4322	15	0102	4322	14	0012	3222	12	3
4	1211	4366	24	1121	4466	25	1111	3678	28	4
5	5442	1200	18	5443	2211	22	6643	2211	25	5
6	2233	3433	23	2233	2233	20	2232	2433	21	6
7	3321	2124	18	3322	2124	19	3321	2114	17	7
8	2211	2233	16	2110	1133	12	3111	1233	15	8
9	3222	2102	14	3222	2202	15	3221	2102	13	9
10	2000	0022	6	2021	0022	9	2010	1022	8	10
11	3323	1022	16	3312	2022	15	2212	1122	13	11
12	0001	0101	3	0111	1101	6	0101	1001	4	12
13	1134	3542	23	1133	3442	21	1033	3642	22	13
14	2112	1133	14	1122	1133	14	1011	1133	11	14
15	2112	2111	11	2112	2111	11	3112	1111	11	15
16	3334	3322	23	3343	4323	25	3333	3333	24	16
17	2023	4345	23	2023	4344	22	2013	3347	23	17
18	5444	4652	34	5444	4652	34	8533	3642	34	18
19	3222	4442	23	3223	3442	23	2222	3342	20	19
20	3233	4544	28	3233	4544	28	3333	4544	29	20
21	2233	3534	25	2233	3544	26	2222	3534	23	21
22	3322	2324	21	3323	2424	23	2322	2324	20	22
23	3222	2242	19	2122	2242	17	3221	2242	18	23
24	2331	2100	12	2331	2200	13	2331	1111	13	24
25	0001	0023	6	0012	1122	9	0001	0023	6	25
26	2100	1110	6	2111	2111	10	1101	1121	8	26
27	0321	2310	12	1321	3321	16	1322	2310	14	27
28	2222	2132	16	2322	2232	18	2212	2233	17	28

March 1961

1	0212	3023	13	1221	3123	15	1211	2023	12	1
2	2321	0013	12	2222	1113	14	2222	1223	16	2
3	3110	1110	8	3110	2211	11	3110	1101	8	3
4	0001	2001	4	0111	3101	8	0011	3101	7	4
5	1211	1145	16	1211	1245	17	1211	1237	18	5
6	5533	3110	21	6434	3221	25	7643	3211	27	6
7	0001	1123	8	0011	1223	10	1012	1123	11	7
8	2110	1123	11	2111	2223	14	2100	1222	10	8
9	2220	3334	19	2221	3333	19	2221	3333	19	9
10	4455	4310	26	4454	4321	27	4445	5211	26	10
11	1112	2131	12	1122	2231	14	1111	2121	10	11
12	3011	2102	10	3112	2112	13	3111	2102	11	12
13	3121	1322	15	3221	2322	17	3121	2312	15	13
14	4433	3442	27	3333	3343	25	5433	3442	28	14
15	2323	4235	24	1323	4225	22	2323	4335	25	15

VOL. 21 1961

March 1961 (*contd.*)

Day	*Ha* Range for $K = 9{:}500\gamma$		*Sum*	*Es* Range for $K = 9{:}750\gamma$		*Sum*	*Le* Range for $K = 9{:}1000\gamma$		*Sum*	*Day*
	K-Indices			*K-Indices*			*K-Indices*			
16	4242	3310	19	4243	3311	21	4342	2311	20	16
17	2243	2211	17	2243	3311	19	2232	2211	15	17
18	2121	2443	19	2122	3343	20	2111	2343	17	18
19	1553	4543	30	2453	4444	30	1452	4554	30	19
20	3223	3242	21	3223	3342	22	4223	3242	22	20
21	3322	1331	18	2312	2331	17	3311	1231	15	21
22	2333	2200	15	2333	2210	16	2232	1210	13	22
23	1222	3221	15	0222	3221	14	0222	3322	16	23
24	1123	2213	15	1113	3223	16	1112	2213	13	24
25	2011	2112	10	2001	3212	11	2001	2112	9	25
26	0222	3213	15	1222	3213	16	1112	2103	11	26
27	1222	3542	21	2222	3532	21	2112	2543	20	27
28	3333	3221	20	3323	3321	20	3332	3321	20	28
29	0112	3231	13	1122	3222	15	1111	2132	12	29
30	2331	2220	15	2331	2221	16	3332	2111	16	30
31	0011	2322	11	1011	2422	13	1011	1311	9	31
	April 1961									
1	5332	1123	20	4231	2223	19	5432	2222	22	1
2	2232	2233	19	1221	2233	16	1222	2233	17	2
3	3433	2223	22	3433	2223	22	3543	3343	28	3
4	3120	1111	10	2122	1120	11	3111	1110	9	4
5	3311	1100	10	3312	1210	13	2311	1210	11	5
6	2111	2244	17	2112	2243	17	2111	1344	17	6
7	4311	1111	13	3312	2111	14	3211	1111	11	7
8	1123	1122	13	1123	1122	13	0112	1111	8	8
9	2225	4333	24	1225	4333	23	1214	3322	18	9
10	4323	3333	24	4333	3433	26	4222	3332	21	10
11	4422	3532	25	3322	3542	24	3332	2531	22	11
12	2121	3333	18	2122	3333	19	2121	3223	16	12
13	1221	3432	18	1222	4432	20	1222	3421	17	13
14	3223	3566	30	2223	4466	29	2223	4588	34	14
15	7542	3333	30	8552	3432	32	9753	3433	37	15
16	3222	3334	22	3222	3334	22	3212	3334	21	16
17	1221	2110	10	1212	2210	11	2111	2110	9	17
18	1121	1101	8	1221	1111	10	1111	2101	8	18
19	2221	1333	17	1221	2333	17	1221	2223	15	19
20	4121	1121	13	4121	1121	13	3221	1122	14	20
21	0000	1111	4	0001	2111	6	1011	2112	9	21
22	0011	3233	13	1011	3333	15	1012	2323	14	22
23	0111	2223	12	1111	3232	14	1112	3233	16	23
24	3112	2333	18	3112	3333	19	3412	2333	21	24
25	3210	1222	13	3110	2221	12	4311	1222	16	25
26	2322	3440	20	2322	3441	21	2322	3441	21	26
27	2233	3322	20	2233	3322	20	2322	2223	18	27
28	3221	1122	14	3222	1221	15	3231	1222	16	28
29	3002	2113	12	2002	1223	12	2002	1113	10	29
30	2111	3323	16	2112	3313	16	2112	3313	16	30

Journal of Atmospheric and Terrestrial Physics, 1961, Vol. 21, p. 300. Pergamon Press Ltd. Printed in Northern Ireland

Papers to be published in future issues

K. V. V. Ramana and B. Ramachandra Rao: Investigation of ionospheric absorption on 5·65 Mc/s at Waltair

M. S. V. Gopal Rao and B. Ramachandra Rao: Nocturnal and seasonal variations of equatorial spread-F

A. F. El Nadi and N. Farag: The effect of light on the mobility and concentration of large ions in air mixed with N_2O gas

G. F. Fooks: The fading of radio waves reflected vertically from the ionosphere during magnetic storms

O. K. Garriott and A. W. Nichol: Ionospheric information deduced from the Doppler shifts of harmonic frequencies from earth satellites

D. van Sabben: Ionospheric current systems of ten IGY-solar flare effects

J. S. Greenhow: Head echoes from meteor trails

H. Unz: The effect of small values of $Z = \nu/\omega$ on the complex refractive index in the magneto-ionic theory

R. Raghava Rao and B. Ramachandra Rao: Study of horizontal drifts in the E-region at Waltair

Elizabeth Cooper: The properties of low frequency radio waves reflected from the ionosphere, calculated by the phase-integral method

M. Gadsden: The relative intensities of some nitrogen bands in auroral spectra

A. R. Thompson: Sweep frequency observations of meteor scatter bursts

S. Chapman and P. C. Kendall: An idealized problem of plasma dynamics that bears on geomagnetic storm theory; Oblique projection

D. E. Shemansky and A. Vallance Jones: New measurements of the night airglow spectrum in the 1·5 μ region.

J. Wolfe: 20 Mc/s w.w.v. bursts during the last few periods of 1958 $\delta 2$

VOL.
21
1961

L.
1
61